United States
Environmental Protection
Agency

Industrial Environmental Research
Laboratory
Research Triangle Park NC 27711

EPA-600/7-79-065
February 1979

EPA

# Proceedings: Advances in Particle Sampling and Measurement

(Asheville, NC, May 1978)

## Interagency Energy/Environment R&D Program Report

## RESEARCH REPORTING SERIES

Research reports of the Office of Research and Development, U.S. Environmental Protection Agency, have been grouped into nine series. These nine broad categories were established to facilitate further development and application of environmental technology. Elimination of traditional grouping was consciously planned to foster technology transfer and a maximum interface in related fields. The nine series are:

1. Environmental Health Effects Research
2. Environmental Protection Technology
3. Ecological Research
4. Environmental Monitoring
5. Socioeconomic Environmental Studies
6. Scientific and Technical Assessment Reports (STAR)
7. Interagency Energy-Environment Research and Development
8. "Special" Reports
9. Miscellaneous Reports

This report has been assigned to the INTERAGENCY ENERGY-ENVIRONMENT RESEARCH AND DEVELOPMENT series. Reports in this series result from the effort funded under the 17-agency Federal Energy/Environment Research and Development Program. These studies relate to EPA's mission to protect the public health and welfare from adverse effects of pollutants associated with energy systems. The goal of the Program is to assure the rapid development of domestic energy supplies in an environmentally-compatible manner by providing the necessary environmental data and control technology. Investigations include analyses of the transport of energy-related pollutants and their health and ecological effects; assessments of, and development of, control technologies for energy systems; and integrated assessments of a wide range of energy-related environmental issues.

## EPA REVIEW NOTICE

This report has been reviewed by the participating Federal Agencies, and approved for publication. Approval does not signify that the contents necessarily reflect the views and policies of the Government, nor does mention of trade names or commercial products constitute endorsement or recommendation for use.

This document is available to the public through the National Technical Information Service, Springfield, Virginia 22161.

EPA-600/7-79-065

February 1979

# Proceedings: Advances in Particle Sampling and Measurement
## (Asheville, NC, May 1978)

W.B. Smith, Compiler

Southern Research Institute
2000 Ninth Avenue, South
Birmingham, Alabama 35205

Contract No. 68-02-2131
Task No. 21306
Program Element No. INE623

EPA Project Officer: D. Bruce Harris

Industrial Environmental Research Laboratory
Office of Energy, Minerals, and Industry
Research Triangle Park, NC 27711

Prepared for

U.S. ENVIRONMENTAL PROTECTION AGENCY
Office of Research and Development
Washington, DC 20460

# PREFACE

The Symposium on Advances in Particle Sampling and Measurement held in Asheville, NC, May 15-17, 1978, was sponsored by the Process Measurement Branch, Industrial Environmental Research Laboratory, U.S. Environmental Protection Agency. D. Bruce Harris, EPA, served as symposium chairman. Session chairmen were A.R. MacFarland, Texas A&M University; Dale Lundgren, University of Florida; W.B. Kuykendal, EPA; T.T. Mercer, University of Rochester; and G.B. Nichols, Southern Research Institute.

A list of reports on the research supported by the Process Measurements Branch can be obtained from Mrs. Judy Ford, MD-62, Process Measurements Branch, Industrial Environmental Research Laboratory, U.S. Environmental Protection Agency, Research Triangle Park, NC 27711.

## ABSTRACT

The proceedings consist of 17 papers on improved instruments and techniques for sampling and measurement of particulate emissions and aerosols. Cascade impactors are described with low-pressure stages that extend the useful range of these sampling devices down to 0.02 μm; their use in measuring particle size distribution of fly ash from coal-fired boilers and in testing a smoke suppressant in a gas turbine is described. A new empirical equation simplifies calibration of cyclone collectors used for sampling aerosols. Diffusion battery-nuclei counter combinations can be used for automatic monitoring of particle-size distribution and number concentration of ambient aerosols. Transmissometers and instruments for measuring scattered light were compared over a one-year period for continuous monitoring of stack emissions at a secondary lead smelter. Instruments for measuring electrical charge transfer and beta radiation attenuation were less reliable in this use. A laser light back-scattering instrument was compared in pulp and paper mills against a transmissometer in continuous monitoring of emissions from a wood-waste fired power boiler, a kraft recovery furnace, and a lime kiln. Other papers discussed a computer-based, data reduction method for plotting curves of particle size distribution; techniques and equipment for generating monodisperse aerosols and their use in calibrating instruments; guidelines in selecting laboratory methods for particle sizing; minimizing weight changes in impactor collection substrates due to heat and sulfur oxides; spectroscopic methods for determination of trace elements in fly ash and their valence states; and sampling errors due to aerodynamic effects. Applications of improved sampling and measurement techniques to the evaluation of emission control devices include a wet impingement technique for measuring particle sizes in wet scrubbers; the use of real-time aerosol instruments in studying the dynamic behavior of baghouses; and the measurement of fractional collection efficiency of electrostatic precipitators for particles 0.01-10 μm in diameter, enabling the detection of transient fluctuations such as rapping reentrainment of fly ash.

CONTENTS

Preface . . . . . iii
Abstract. . . . . iv
List of Speakers and Chairmen . . . . . vii

Paper 1. Inertia Effects in Sampling Aerosols
C.N. Davies and M. Subari . . . . . 1

Paper 2. Cyclone Sampler Performance
Morton Lippmann and Tai L. Chan . . . . . 30

Paper 3. Research on Dust Sampling and Measurement in our Laboratory
Koichi Iinoya . . . . . 52

Paper 4. Sizing Submicron Particles With a Cascade Impactor
Michael J. Pilat. . . . . 74

Paper 5. Experience in Sampling Urban Aerosols With the Sinclair Diffusion Battery and Nucleus Counter
Earl O. Knutson and David Sinclair. . . . . 98

Paper 6. Selecting Laboratory Methods for Particle Sizing
Ronald G. Draftz. . . . . 121

Paper 7. Long Term Field Evaluation of Continuous Particulate Monitors
A.W. Gnyp, S.J.W. Price, C.C. St. Pierre, and D.S. Smith. . . 122

Paper 8. An In-Stack Fine Particle Size Spectrometer: A Discussion of its Design and Development
Robert G. Knollenberg . . . . . 169

Paper 9. Optical Measurements of Particulate Size in Stationary Source Emissions
A.L. Wertheimer, M.N. Trainer, and W.H. Hart. . . . . 195

Paper 10. Studies on Relating Plume Appearance to Emission Rate and Continuous Particulate Mass Emission Monitoring
K.T. Hood and H.S. Oglesby. . . . . 211

Paper 11. A Data Reduction System for Cascade Impactors
J.D. McCain, G. Clinard, L.G. Felix, and J. Johnson . . . . . 228

Paper 12. Aerosol Generation and Calibration of Instruments
David Y.H. Pui and Benjamin Y.H. Liu. . . . . 260

Paper 13. Substrate Collectors for Impactors - An Evaluation
D. Bruce Harris, G. Clinard, L.G. Felix, G. Lacey, and J.D. McCain . . . . . 293

Paper 14. Particle Size Measurement for the Evaluation of Wet Scrubbers
Seymour Calvert, Richard Chmielewski, and Shui-Chow Yung. . . 301

Paper 15. Evaluation of Performance and Particle Size Dependent Efficiency of Baghouses
D.S. Ensor, R.G. Hooper, G. Markowski, and R.C. Carr. . . . . 314

Paper 16. Evaluation of the Efficiency of Electrostatic Precipitators
Wallace B. Smith, John P. Gooch, Joseph D. McCain, and James E. McCormack. . . . . 337

Paper 17. Some Studies of Chemical Species in Fly Ash
L.D. Hulett, J.F. Emery, J.M. Dale, A.J. Weinberger, H.W. Dunn, C. Feldman, E. Ricci, and J.O. Thomson . . . . . 355

Summary. Advances in Particle Sampling and Measurement
William Farthing. . . . . 372

Metric Conversion Factors . . . . . 380

## SPEAKERS AND CHAIRMEN

Mr. Richard Chmielewski
APT, Incorporated
4901 Morena Boulevard
Suite 402
San Diego, CA 92117
Phone: 714/272-0050

Dr. C.N. Davies
Department of Chemistry
University of Essex
Wivenhoe Park
Colchester CO4 3SQ
ENGLAND
Phone: Colchester 44144
(STD Code 020 6)

Mr. R.G. Draftz
IIT Research Institute
10 West 35th Street
Chicago, IL 60616
Phone: 312/567-4291

Dr. David S. Ensor
Meteorology Research, Inc.
464 West Woodbury Road
Altadena, CA 91009
Phone: 213/791-1901

Dr. Alec Gnyp
Department of Chemical
Engineering
University of Windsor
Windsor, Ontario N9B3P4
CANADA
Phone: 519/253-4232

Mr. D. Bruce Harris
Environmental Protection
Agency
Industrial Environmental
Research Laboratory
Mail Stop MD-62
Research Triangle Park, NC
27711
Phone: 919/541-2557-8

Mr. Kenneth T. Hood
NCASI, Engineering Experiment
Station
Oregon State University
Corvallis, OR 97331
Phone: 503/754-2015

Dr. Lester D. Hulett
Oak Ridge National Lab
4500 North E-10
Oak Ridge, TN 37830
Phone: 615/483-0155

Dr. Koichi Iinoya
Department of Chemical
Engineering
Kyoto University
Kyoto
JAPAN

Dr. Robert G. Knollenberg
Particle Measurement Systems
1855 South 57th Court
Boulder, CO 80301
Phone: 303/443-7100

Dr. Earl Knutson
Health & Safety Lab
U.S. ERDA
376 Hudson Street
New York, NY 10014
Phone: 212/620-3655

Mr. W.B. Kuykendal
Environmental Protection Agency
Industrial Environmental
Research Laboratory
Mail Stop MD-62
Research Triangle Park, NC
27711
Phone: 919/541-2557

Dr. Morton Lippmann
Institute of Environmental
Medicine
New York University Medical
Center
New York, NY 10016
Phone: 212/679-3200

Dr. Dale Lundgren
Environmental Engineering
Department
University of Florida
410 Black Hall
Gainesville, FL 32611
Phone: 904/392-0846

Mr. Joseph D. McCain
Southern Research Institute
2000 Ninth Avenue, South
Birmingham, AL 35205
Phone: 205/323-6592,
extension 278

Dr. Andrew R. McFarland
Civil Engineering Department
Texas A&M University
College Station, TX 77843
Phone: 713/845-2241

Dr. Thomas T. Mercer
University of Rochester
Rochester, NY 14642
Phone: 716/275-3821

Mr. Grady B. Nichols
Southern Research Institute
2000 Ninth Avenue, South
Birmingham, AL 35205
Phone: 205/323-6592,
extension 361

Dr. Michael Pilat
Air Resources Engineering
University of Washington
Seattle, WA 98195
Phone: 206/543-4789

Dr. David Pui
Mechanical Engineering
Department
University of Minnesota
Minneapolis, MN 55455
Phone: 612/323-2815

Dr. Wallace B. Smith
Southern Research Institute
2000 Ninth Avenue, South
Birmingham, AL 35205
Phone: 205/323-6592,
extension 520

Dr. Allen Wertheimer
Leeds & Northrup Company
Dickerson Road
North Wales, PA 19454
Phone: 215/643-2000,
extension 493

PAPER 1

# INERTIA EFFECTS IN SAMPLING AEROSOLS

C.N. DAVIES
M. SUBARI
DEPARTMENT OF CHEMISTRY
UNIVERSITY OF ESSEX

## ABSTRACT

A study is made of the aspiration coefficient of orifices sampling aerosols, starting with a point sink and proceeding to a tube of finite diameter. A critical analysis is made of previous work and new experimental results are presented for sampling at 90° yaw with a sharp-edged tube.

## INERTIALESS PARTICLES

The trajectories of particles suspended in moving air may differ from the streamlines of air flow either if their rate of fall due to gravity is appreciable, compared with the air velocity, or if the particles are sufficiently heavy to persist in their original direction to some extent when the air flow changes direction (Albrecht,[1] Sell [2]). Measurements of the concentration of particles, by sucking a known volume of aerosol and assessing the particles in it, are liable to error because of these gravitational and inertial effects.

Consider, first, inertialess particles. These can be defined as having a stop-distance, $d_s$, at the local air velocity, u, which is small compared with the distance, $\ell$, from any bounding solid surface. That is

$$d_s = \tau u << \ell \tag{1}$$

where $\tau$ is the relaxation time of a particle and is equal to the mass divided by the aerodynamic drag at unit velocity. Such particles can still fall at an appreciable velocity, this being

$$v_s = \tau g. \tag{2}$$

Inertialess particle systems therefore have small $\tau u$ and large $\ell$, but the limiting size of the Stokes number of the systems,

$$St_u = \tau u/\ell << 1 \tag{3}$$

depends on the value of $St_u$, being lower for high values of $v_s/u$, hence both $St_u$ and $v_s/u$ need to be considered in deciding whether a particle is inertialess and, of course, since u varies from point to point in a flow field the particle may be inertialess while it is in some parts of the field but not so in others.

The sampling of inertialess particles with an isolated small tube yields accurate results (Davies[3]). When the airflow approximates to ideal flow (potential or irrotational) the particles themselves trace out a potential flow pattern, the concentration of particles is the same at all points along a particle trajectory and trajectories do not intersect (Walton[4]; Robinson[5]; Levin[6]).

There are two reasons why this does not mean that a sampling orifice will always take a perfect sample of inertialess particles.

Firstly, the velocity of the particles entering the orifice may not be the same as the air velocity, V, in the orifice. Suppose that the normal to the plane of the sampling orifice makes an angle $\psi$ with the vertical. Then the velocity with which particles enter the orifice, resolved along the normal is

$$V + v_s \cos \psi \tag{4}$$

Hence the concentration, c, calculated from the catch of particles (including those stuck on the internal surface of the orifice) and the volume of air sampled, is related to the true concentration, $c_0$, by

$$cV = c_0 (V + v_s \cos \psi) \tag{5}$$

The efficiency of sampling or the aspiration coefficient of the orifice is then, for inertialess particles,

$$A = c/c_0 = (V + v_s \cos \psi)/V \tag{6}$$

Hence when $\psi = 0$ and the orifice faces upwards, $A = 1 + v_s/V$ and when $\psi = \pi$, with the orifice facing downwards, $A = 1 - v_s/V$. Only when the plane of the orifice is vertical and $\psi = \pi/2$ is a true sample obtained.

The other factor causing error in the sampling of inertialess particles is the existence of dust shadows. These regions

free from particles exist below and downwind of objects placed in an aerosol. The effects are negligible in the case of a small tube, but a bulky sampling head creates a shadow which sometimes reduces the aspiration coefficient of its sampling orifice. The writer has described the general effects (Davies[7,8,9]).

When the orifice in an isolated head faces upwards it always has $A \geq 1$; at low rates of suction in calm air a dust shadow exists below the head and particles settle upon the top, around the orifice. With increasing aspiration rate the shadow region climbs up over the top of the head so that particles settle only upon a decreasing area around the orifice.

With an orifice in the under side of the head, in calm air, no particles enter until a certain rate of aspiration is attained; increasing above this value gradually raises the value of A until it reaches unity at an infinite rate of suction. As A increases there is no change in the deposition of particles on top of the head. In a cross wind particles enter the head at a lower suction rate than is the case for calm air. The value of A remains higher than the value for calm air, as suction is increased, but the difference decreases until they become the same at a fairly high rate of suction.

Dust shadows can reduce A when the orifice is not isolated, even when its plane is vertical, if it is in the lee of an obstacle; they may also affect the sampling of particles with inertia (Davies[10]).

Since the concentration of inertialess particles is constant along all trajectories, the values of A which are less than unity result not from the aspiration of reduced concentrations but because some of the particle trajectories which enter the orifice originate from boundaries inside dust shadows and therefore have zero concentration at all points along their lengths. This was shown clearly by Walton[4] who considered tubes of flow of inertialess particles, particularly in elutriators.

## PARTICLES WITH INERTIA; POINT SINK

The trajectories of particles with inertia do not form a system with a velocity potential; the concentration may vary along a trajectory and trajectories may intersect (Voloshchuk and Levin[11]). A true sample can still be obtained, when particles exhibit unlimited inertia, if their rate of fall under gravity is negligible and if the air movement is solely due to aspiration into a point sink. The concentration builds up as the orifice is approached, due to the particles lagging behind the air flow, and the analogue of a space charge around the orifice is formed. Particles enter the orifice with a reduced velocity which compensates for the excess concentration and a true sample with $A = 1$ results (Davies [12]).

If the symmetry of this "space charge" is sufficiently destroyed by wind, or by the settlement of particles under gravity, the aspiration coefficient of the sampling orifice is reduced.

Levin[6] has shown how particles which have very limited inertia behave when approaching a point sink when they are sedimenting under gravity and there is a wind.

In order to understand his paper it is best to start with the equations for inertialess particles. His equations are similar to those of Davies[3] but are in polar coordinates. A great simplification of the equations was achieved by using as x-axis the direction of the vector sum of the wind velocity, W, and the sedimentation velocity of the particles, $v_s$. This sum has magnitude

$$u_0 = (W^2 + v_s^2 + 2Wv_s \cos \phi)^{\frac{1}{2}} \tag{7}$$

where $\phi$ is the angle between W and $v_s$.

Since the particles are inertialess, the equations for the trajectories are the same as those for the streamlines of flow. The sink sucks with flow Q and creates radial velocities $- Q/4\pi r^2$ to which must be added the radial resolutes of $u_0$. Hence the equations for radial and tangential resolutes of a trajectory are

$$\left.\begin{aligned} u_r &= - Q/4\pi r^2 + u_0 \cos \theta \\ u_\theta &= - u_0 \sin \theta \end{aligned}\right\} \tag{8}$$

By putting

$$\ell_0^2 = Q/4\pi u_0 \tag{9}$$

these are rendered dimensionless,

$$\left.\begin{aligned} u_r/u_0 &= - \ell_0^2/r^2 + \cos \theta \\ u_\theta/u_0 &= - \sin \theta \end{aligned}\right\} \tag{10}$$

The solution of these equations is

$$\left(r^2/2\ell_0^2\right) \sin^2 \theta + \cos \theta = K \tag{11}$$

where K is constant along a streamline or an inertialess trajectory.

The formulation of these equations is shown in Figure 1. Note the direction of the x-axis about which all trajectories

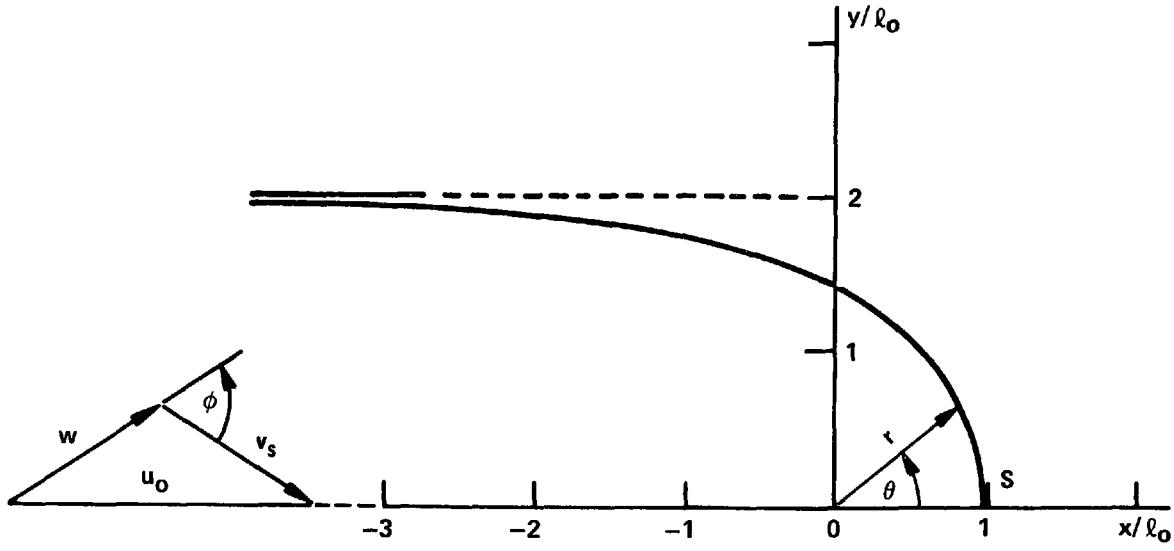


*Figure 1. The coordinate system. A sink at O draws a flow Q. The curve with asymptote 2 at $x/\ell_0 = -\infty$ is a critical trajectory with stagnation point of both air flow and particle motion at S.*

are symmetrical. The figure shows a meridian section and the critical trajectory through the stagnation point, S, where

$$u_r = u_\theta = 0 \tag{12}$$

It is necessary to locate the critical trajectory for the calculation of the aspiration coefficient (Davies[3]). The equation of the critical trajectory is

$$\left.\begin{aligned} &\left(r^2/2\ell_0^{\,2}\right) \sin^2\theta + \cos\theta = 1 \\ \text{or} \quad &r/\ell_0 = 1/\cos\left(\theta/2\right) \end{aligned}\right\} \tag{13}$$

All particles with trajectories between the critical trajectory and the x-axis enter the orifice; none of those outside do so. The critical trajectory has the asymptote at $x = -\infty$ ($\theta = \pi$, $y = y_\infty$)

$$y_\infty/\ell_0 = 2, \tag{14}$$

hence, the rate of entry of particles into the sink is

$$\pi\,(4\ell^2)\,c_0 u_0 = Qc_0 \tag{15}$$

by equation (9), so that A = 1.

The critical trajectory meets the x-axis at the stagnation point, S, where $\theta = 0$, $y = 0$, $r = x$ and

$$x_s/\ell_0 = 1 \tag{16}$$

When the particles have inertia it is necessary to consider their acceleration in order to write down the dynamic equations:

$$\left.\begin{aligned} m\,(dv_r/dt - v_\theta\, d\theta/dt) &= 6\pi a\eta\,(-Q/4\pi r^2 + u_0 \cos\theta - v_r) \\ m\,(dv_\theta/dt + v_r\, d\theta/dt) &= 6\pi a\eta\,(-u_0 \sin\theta + v_\theta) \end{aligned}\right\} \tag{17}$$

where $v_r$ and $v_\theta$ are the radial and tangential resolutes of particle velocity. The equations are rendered dimensionless by dividing through by $6\pi a\eta \cdot u_0$ and reducing t to dimensionless t' and r to dimensionless r', so that

$$t = t'\,\ell_0/u_0 \text{ and } r = r'\,\ell_0 \tag{18}$$

Since $\tau = m/6\pi a\eta$, equations (17) in dimensionless form become

$$\left.\begin{aligned} (\tau u_0/\ell_0)\left(dv_r'/dt' - v_\theta' \cdot d\theta/dt'\right) &= -1/r'^2 + \cos\theta - v_r' \\ (\tau u_0/\ell_0)\left(dv_\theta'/dt' - v_r' \cdot d\theta/dt'\right) &= -\sin\theta + v_\theta' \end{aligned}\right\} \tag{19}$$

where equation (9) shows that the dimensionless scale factor,

$$\tau u_0/\ell_0 = \tau u_0 \sqrt{4\pi u_0/Q} = \tau \sqrt{4\pi u_0^3/Q} = k \tag{20}$$

By integrating these equations the particle velocity ($v_r$, $v_\theta$) can be obtained at all points along a trajectory. Levin[6] succeeded in obtaining solutions as series of rising powers of k, for small values of k, by assuming that a particle stagnation point existed at S, in the same position as the air velocity stagnation point. At S, and nowhere else, both particles and air have zero velocity. This is justifiable for small values of k, since continuity must exist between air streamlines and particle trajectories as k tends to zero. When k = 0 equation (19) reduces to equation (10).

His solutions are

$$\begin{aligned} v_r' &= \cos\theta - 1/r'^2 + k\left\{\frac{2(1-r'^2\cos\theta)}{r'^5}\right\} \\ &\quad + k^2\left\{\frac{3(1-3\cos^2\theta)}{r'^4} + \frac{20\cos\theta}{r'^6} - 14/r'^8\right\} + \ldots \\ v_\theta' &= -\sin\theta - k\,\frac{\sin\theta}{r'^3} - k^2\left\{\frac{6\sin\theta\cos\theta}{r'^4} - \frac{4\sin\theta}{r'^6}\right\} + \ldots \end{aligned} \tag{21}$$

When $k = 0$ these equations reduce to equation (10). They include powers of $1/r' = \ell_0/r$ up to the sixth; since $\ell_0/r = 1$ at the stagnation point, the trajectories are increasingly accurate for greater distances from the sink. This is important since the calculation of the aspiration coefficient, A, depends on the value of y at $r = \infty$, $\theta = \pi$ (equations (14), (15)).

In order to obtain the trajectory equations it is necessary, as in integrating equation (10), to substitute in

$$dr/rd\theta = v_r/v_\theta \tag{22}$$

from equation (21) and perform the integration. It is not clear how Levin proceeded at this point but he obtained the asymptote ($r = \infty$) of the critical trajectory by successive approximation, starting with the equation (13) for $k = 0$. This gave, in place of (14), the formula

$$\left(y_\infty/\ell_0\right)^2 = 4 - 3.2\ k + 0.32\ k^2 \tag{23}$$

Hence, since

$$A = \pi y_\infty{}^2 u_0/Q\ ,$$

then, using (9)

$$A = 1 - 0.8\ k + 0.08\ k^2 \tag{24}$$

By comparing this with the results of numerical integrations of equations (19), Levin[6] concluded that the error in A, as given by (24) was not more than 1% when $k = 0.25$ and not more than 2.5% when $k = 0.5$. It will be seen, later, that equation (24) is not valid up to such large values of k as Levin claimed.

The writer (Davies[12]) made an analysis of the behavior of particles with inertia approaching a point sink in otherwise calm air. In the absence of appreciable rate of fall, series solutions of the dynamic equations were obtained for large and small inertia and connected by interpolation. This gave the distribution of concentration in the spherical "space charge" region near the orifice. Stepwise solutions, when the particles were also falling under gravity, showed that some particles described orbits about the sink. The calculations were made for the condition

$$v_s/V_0 = 1 \tag{25}$$

where

$$V_0 = 1/\tau\ (Q\tau/4\pi)^{1/3} \tag{26}$$

was later defined as the dynamic sampling velocity (Davies,[14] 1968). This particular formulation arose because the dynamical equations were rendered dimensionless by measuring lengths in

units of the stop distance at velocity $V_0$, and times in units of the particle relaxation time, $\tau$; hence

$$V_0 = d_s/\tau \tag{27}$$

In order to compare these results with those of Levin it is necessary to convert from Davies' system to Levin's. This is easily done. Since $u_0 = v_s$ $(W = 0)$, we have from (26), (29) and (20)

$$v_s/V_0 = \tau u_0(Q\tau/4\pi)^{-1/3} = (\tau u_0/\ell)^{2/3} = k^{2/3} \tag{28}$$

Hence the condition (25) also means that $k = 1$.

This of course is far outside the limit for Levin's results and explains why his particles did not execute orbits around the sink.

Davies found that the limiting trajectory failed to complete an orbit while trajectories outside the limiting one did not orbit at all. On this limiting trajectory the aspiration coefficient was estimated to be 0.37. For $k = 1$, Levin's series (24) gives $A = 0.28$; naturally, this is not the correct value, since k is too large; in fact, for slightly larger values of k the series (24) gives negative values of A.

The value $A = 0.37$ for $v_s/V_0 = k = 1$ would be correct if all particles inside the critical trajectory entered the orifice, even after orbiting. However, it is not yet clear whether this is true. Davies found that a group of trajectories, inside the critical trajectories, completed closed orbits and then escaped from the sink. If this is correct, the value of A is reduced from 0.37 to 0.23. However, ter Kuile[13] believes that all trajectories which execute orbits, these being inside the critical trajectory, must enter the sink. He found that in order to plot accurate trajectories, a large number of very short steps had to be taken as the sink was approached and his computer program was designed to do this. It is possible that the writer's escaping particles only did so because too few steps were taken along the trajectories and that they should really have been caught. To settle the point, either more trajectories need to be computed or recourse made to the theory of central orbits. Ter Kuile and the writer agree, when calculated on the nearest non-orbiting trajectory to the axis of symmetry through the sink, on the assumption that all orbiting particles enter, that for $v_s/V_0 = k = 1$, then $A \simeq 0.37$.

For heavy particles there is no stagnation point on the x-axis, as was assumed by Levin for $k < 0.5$.

It is important to notice that Levin's equation (24) is derived by a theory in which the effect of the inertia of the particles is dominated by their velocity of approach to the vicinity of the point sink; this velocity is $u_0$. In limiting the result to low values of k, he has eliminated the influence upon the value of A of the concentration "space charge" around the sink and of particles with enough inertia to describe orbits around the sink. Because of this limitation, it will be seen that decreasing the rate of suction, Q, increases the value of k, equation (20), so that the aspiration coefficient, A, decreases. Obviously this is because, when Q is small, more particles can shoot past the sink, due to their inertia upon the wind and sedimentation velocities. This dependence of A on Q was noted by Kaslow and Emrich,[21] but its significance was not realized and some confusion was created.

When inertia effects are larger, inside Levin's range, those due to the aspiration velocity may preponderate and cause a reversal of the effect on A, so that increasing Q increases the sampling error.

Confusion has also been caused by a failure to realize that particles with unlimited inertia have A = 1 if the wind and sedimentation velocities are both negligible. Examples of error on this account are seen in the work of Kaslow and Emrich,[21] Kim,[22] Pickett and Sansone,[17] Breslin and Stein,[15] Agarwal,[19] Gibson and Ogden,[16] and, no doubt, others.

PARTICLES WITH INERTIA; FINITE ORIFICE

Levin's equation (24) applies to a point orifice. He thought that it could be used for orifices of finite diameter, D, as long as

$$D < 2\ell_0. \tag{29}$$

This means that the radius is less than the distance, OS, between the orifice and the stagnation point (16).

A point sink has no orientation; on replacing it by a finite orifice the direction of the normal to the plane of the orifice introduces an additional variable. For simplicity, this will be referred to as the direction of the sampling tube, $\psi$, as shown in Figure 2 relative to $v_S$. An independent yaw angle, relative to W, will be considered later.

Let W be the wind velocity, which is usually horizontal. V is the mean air velocity in the sampling orifice and has the direction of the sampling tube. Then

$$V = 4Q/\pi D^2 \tag{30}$$

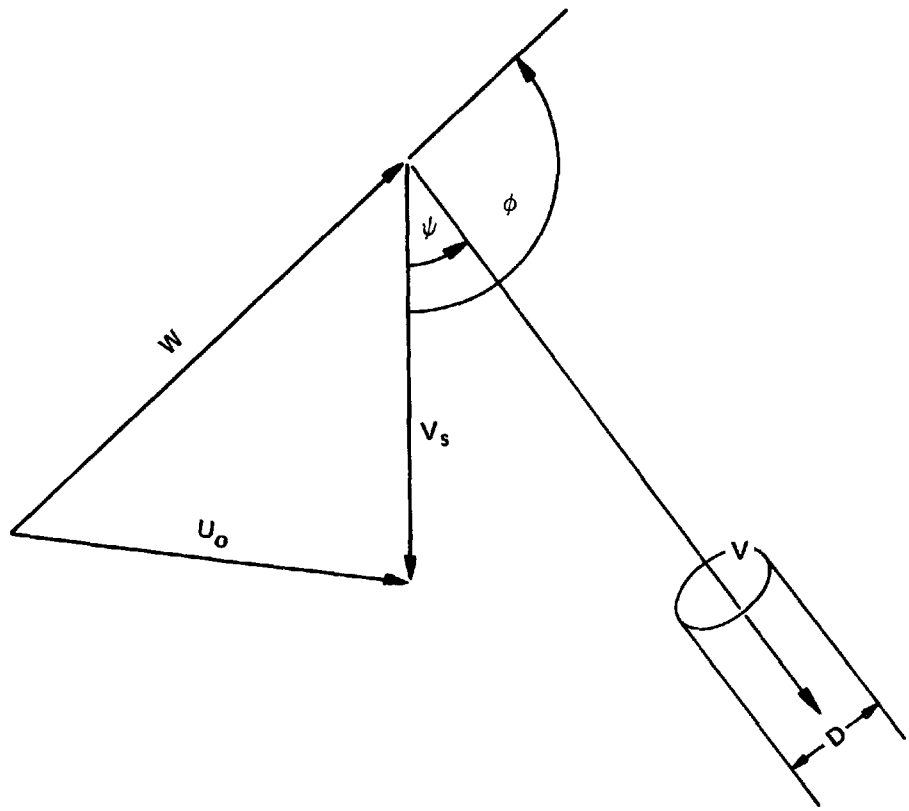


*Figure 2. The additional angle, $\psi$, which is necessary in proceeding from a point sink to a sampling tube of diameter D. Note that the angles $\psi$ and $\phi$ are not necessarily in the same plane. The angle of yaw between V and W is not shown.*

Two Stokes' numbers are involved, that on the wind velocity

$$St_W = \tau W/D, \tag{31}$$

and that on the sampling velocity

$$St_V = \tau V/D \tag{32}$$

The magnitude of the sum of the wind and sedimentation velocity vectors is $u_0$ (equation 7), as before, but, from (9) and (30)

$$\ell_0 = \left(D/4\right) \sqrt{V/u_0} \tag{33}$$

and, by (20), (31), (32), (33), and (7)

$$\begin{aligned} k = \tau u_0/\ell_0 &= \left(4\tau u_0/D\right) \sqrt{u_0/V} \\ &= 4St_W \ (W/V)^{\frac{1}{2}} \left\{1 + \left(v_s/W\right)^2 + 2\ v_s/W \cos\phi\right\}^{3/4} \end{aligned} \tag{34}$$

$$= 4St_V\left\{(W/V)^2 + (v_s/V)^2 + 2(W/V)\cdot(v_s/V)\cos\phi\right\}^{3/4} \tag{35}$$

Equation (35) is used when the wind velocity, W, is small.

Substitution of these values of k in equation (24) gives

$$A = 1 - 3.2\ St_W\left(\frac{W}{V}\right)^{\frac{1}{2}}\left\{1 + \left(\frac{v_s}{W}\right)^2 + 2\frac{v_s}{W}\cos\phi\right\}^{3/4} + 1.28\ St_W{}^2\left(\frac{W}{V}\right)\left\{1 + \left(\frac{v_s}{W}\right)^2 + 2\frac{v_s}{W}\cos\phi\right\}^{3/2} \tag{36}$$

or

$$A = 1 - 3.2\ St_V\left\{\left(\frac{W}{V}\right)^2 + \left(\frac{v_s}{V}\right)^2 + 2\frac{Wv_s}{V^2}\cos\phi\right\}^{3/4} + 1.28\ St_V{}^2\left\{\left(\frac{W}{V}\right)^2 + \left(\frac{v_s}{V}\right)^2 + 2\frac{Wv_s}{V^2}\cos\phi\right\}^{3/2}. \tag{37}$$

According to Levin, the limits of validity of these equations, which in fact are overestimated, are

within 1% for $k = 0.25$, $A = 0.805$ (38)

within 2.5% for $k = 0.5$, $A = 0.62$ (39)

It must not be forgotten that another angle, that between the sampling tube and the vertical, $\psi$, also has to be allowed for. The values of A in equations (36) and (37) therefore need to be multiplied by the factor of equation (6) (see Figure 2). The final value becomes

$$A\left\{1 + (v_s/V)\cos\psi\right\} \tag{40}$$

Note that the terms containing $v_s$ in equations (36) and (37) express the loss of particles by the effect of sedimentation in causing them to shoot past the orifice, whereas the $v_s$ in (40) expresses the loss or gain due to sedimentation in the plane of the orifice. These equations do not include losses due to distortion of the symmetry of the concentration "space charge" or to orbiting which come into operation at higher values of k.

The value of A for a sampling tube of finite diameter depends upon the yaw angle between V and W. This is not expressed by equations (34) to (37) which hold only for very small values of

k. When V and W have the same or opposite directions, yaw is 0° or 180° and the concentration "space charge" is symmetrical about the sampling tube. Changing the yaw to 90° destroys this symmetry and will be accompanied by a decrease in the value of A. Some experimental results at 90° yaw are described below. When the sampling tube is large there is a possibility of the dust shadow reducing A at 180° yaw.

## THE DAVIES SAMPLING CRITERION

The writer (Davies[14]) proposed that accurate samples in calm air would be obtained with an isolated small tube, the words "small tube" meaning that the aspiration coefficient is independent of the orientation of the tube, provided that

$$5(Q\tau/4\pi)^{1/3} \leq D/2 \leq 0.2(Q/\pi g\tau)^{\frac{1}{2}} \tag{41}$$

The right hand term represents a maximum error of ±4% under the worst conditions, with the tube facing up or down ($\psi = 0$ or $\pi$, equation (5)), due to sedimentation.

The left hand term is derived from the excess concentration in the "space charge" region being 1.6% at a distance of $5d_s$ from the center of the orifice (Davies[12]), where, by (26) and (27)

$$d_s = (Q\tau/4\pi)^{1/3}$$

Considering the gravitational condition, use of equations (2) and (30) shows that it makes

$$v_s/V < 0.04 \tag{42}$$

The inertia condition reduces as follows, by (30) and (32),

$$5(D^2V\tau/16)^{1/3} \leq D/2$$

or

$$5D/2\left(St_V/2\right)^{1/3} \leq D/2 \tag{43}$$

or

$$St_V \leq 0.016$$

When W = 0 and these values are inserted in equation (37) we obtain

$$A = 0.9996$$

Hence, in absolutely calm air, the theoretical sampling error, according to Levin, is only 0.04% which is obviously too strict a criterion. However, the important effect of a low wind velocity needs to be looked at. Davies[14] suggested that calm air be defined as

$$W/V < 0.2 \tag{44}$$

Note that the limited size of orifice imposed by (29) reduces, by (33) to

$$\left(u_0/V\right)^2 < 0.25 \tag{45}$$

and that the value of $u_0/V$ defined by (42) and (44) for all values of $\phi$ has

$$\left(u_0/V\right)^2 \leq 0.0576$$

so that Davies' "small tube" is well inside Levin's maximum size, (29). Putting W/V = 0.2 into equation (37) gives (W horizontal, $\phi = 90°$)

$$A = 1 - 3.2\ (0.016)\ (0.20^2 + 0.04^2)^{3/4} + \ldots$$

$$= 0.995$$

showing an error of 0.5% due to a slight ambient wind. Great care needs to be taken before relaxing the criterion too much since the wind error increases rapidly. For example, if W/V = 0.5,

$$A = 0.982$$

and the error has increased nearly four times for a two and half times increase in wind speed.

If a 2.5% error is accepted as tolerable in "calm air", that is for W/V = 0.2, then

$$0.975 = 1 - 3.2\ St_V\ (0.2^2 + 0.04^2)^{3/4}$$

and

$$St_V = 0.085$$

Substituting this value in (41) changes the original Davies criterion to

$$2.87\ (Q\tau/4\pi)^{1/3} \leq D/2 \leq 0.2(Q/\pi g\tau)^{\frac{1}{2}} \tag{46}$$

For a 4% inertial error at W/V = 0.2, $St_V = 0.136$. This matches the sedimentation error and the criterion becomes

$$2.45\ (Q\tau/4\pi)^{1/3} \leq D/2 \leq 0.2(Q/\pi g\tau)^{\frac{1}{2}} \tag{47}$$

In this case, the error when W = V is 41%. When W = 0.2V and $v_s = 0.04V$, with St = 0.136, the criterion (47) makes A = 0.95.

The limit of W/V to which this can be extended while still remaining within Levin's criterion (29) requires

$$W/V < 0.5$$

With this value, and the factor 2.45 of (47) instead of 5, calculating as in (43) gives

$$(St_V/2)^{1/3} = 1/2.45 \text{ or } St_V = 0.136$$

Hence, by (35)

$$k = 0.193$$

and by (24)

$$A = 0.85$$

which is within Levin's other limit of 1% error at k = 0.25, (38). When the wind is not horizontal, the value of A is raised. However, the experiments described below indicate that Levin's estimate of 1% error at k = 0.25 is far too low when applied to a finite tube diameter.

There are thus grounds for considering a change in the factor 5 of the inertial term of the Davies criterion to 2.45 so that the new criterion is as in (47), but lower values than this will certainly involve larger errors. (Figure 3)

Several papers have been published in which the original criterion is criticized as too severe. The experimental technique in some has been inadequate and in all the importance of the reaction of the wind speed and the sedimentation speed of the particles upon the inertia effect has been entirely overlooked, although it was emphasized by the writer[12] and is implicit in Levin's equations (Figure 3).

EXPERIMENTAL RESULTS; CALM AIR

A very careful series of experimental measurements is due to Breslin and Stein[15] (1975). They measured aspiration coefficients with 398 < V < 5968 cm/sec and 0.04 < D < 0.4 cm, using particles of coal dust with aerodynamic diameters between 2.9 and 41 μm. By means of a Coulter counter, the dust counts were broken down into 14 size ranges so that the disadvantages of employing an aerosol of wide size distribution were overcome. Sampling was carried out with horizontal and vertical (facing upwards) tubes; in most of the latter experiments the gravitational error due to settlement into the orifice was small. Many experiments resulted in low values of A, down to 0.4. The extraordinary thing about these results is that Breslin and Stein operated with an ambient wind velocity averaging 20 cm/sec near

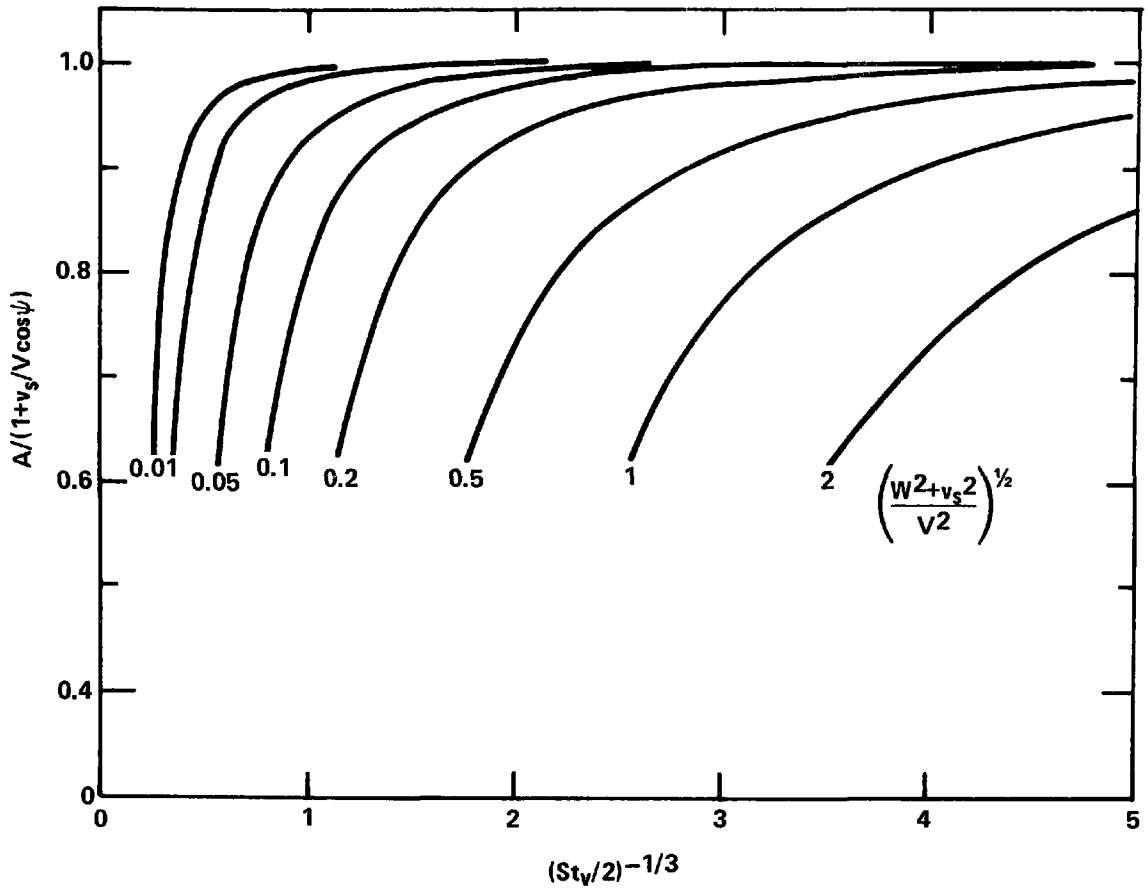


*Figure 3. $A/[1 + (v_S/V)] \cos \psi$ as a function of $[(W^2 + v_S^2)/V^2]^{1/2}$ and $(St_V/2)^{-1/3}$ according to equation (37) for horizontal wind. The units on the axis of abscissae are $(St_V/2)^{-1/3}$ since this is the value of the constant multiplying the inertia term of the Davies sampling criterion. The graphs enable the sampling error to be read off, for various values of $(W^2 + v_S^2)/V^2$ and $v_S/V$, according to the value chosen for the constant, assuming that equation (37) is correct.*

the sampling points without realizing that this contributed very much to their values of A; in fact, they actually wrote that the spread in their results "may indicate that the inertial parameter alone is not completely adequate to characterize aerodynamic effects at sampling inlets".

Their experimental data are plotted on Figure 4, the aspiration coefficient, as ordinate, against $(St_V/2)^{-1/3}$. This quantity is chosen since it is equal to the numerical factor multiplying the left hand term of the Davies criterion, namely 5 in the original expression (41) and now, perhaps, reduced to 2.87 (46) or 2.45 (47). How this comes about can easily be seen from (43). In these experiments $v_S/V$ was negligibly small but W/V ranged from about 0.05 to 0.004. By inserting these values in equations (37) the two curves, according to Levin, of A against

$(St_V/2)^{-1/3}$ have been plotted on Figure 4. Most of the experimental points fall between these curves and it is evident that the spread of the values of A as well as the low values are entirely due to the 20 cm/sec ambient wind. If $W = v_S = 0$ then $A = 1$. In these experiments $W >> v_S$ so that the reduction of A below unity was due to W. Once again, it is the effect of W and $v_S$ upon particles with appreciable inertia, which causes a reduction in A. Particle inertia alone does not affect A for isolated orifices, as long as the tube is reasonably sharp-edged and particles deposited on the inner tube wall are included in the sample. Note that Breslin and Stein use $r_0/d_S$, which is the same as $(St_V/2)^{-1/3}$, and is the radius of the sampling tube divided by the stop distance of the particles from velocity $V_0$, equations (26) and (27).

Some experiments have been performed by Gibson and Ogden;[16] they did not attempt to measure absolute concentrations but

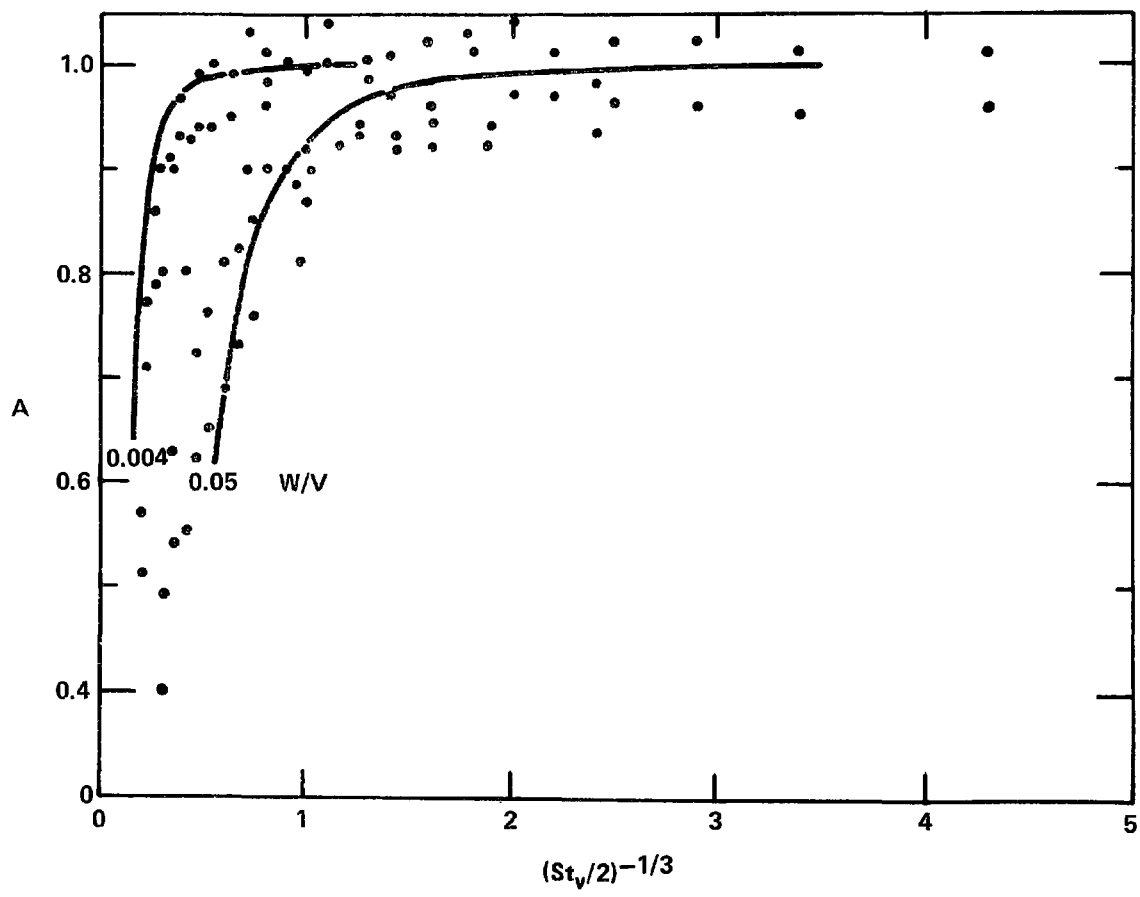


*Figure 4. The experimental points of Breslin and Stein.[15] The two curves correspond to W/V = 0.004 and 0.05. They illustrate the importance of the low ambient wind velocity of 20 cm/sec when the sampling velocity was 6000 and 400 cm/sec, respectively; $v_S/V$ was very small.*

merely compared individual pairs of samples taken at differing values of $St_V$. Sampling was carried out with $\psi = \phi = 0$, and W rarely exceeded 5 cm/sec. Particle aerodynamic diameters were 9 to 39 μm. Unfortunately the experiments were incorrectly planned, the authors falling into the old trap of failing to recognize that the influences of particle inertia and of wind plus sedimentation are complementary. In some pairs of samples the inertia ratio was high and the wind plus sedimentation ratio was low; in others, the reverse was true. In fact, without exception, the relative values of each ratio were such that the defect of the aspiration coefficient, A, in one member of a pair, due to one cause, was almost exactly balanced by the defect in the other member of the pair, due to the other cause. Calculation of the ratio of the values of A for every pair by equations (37) and (40) shows that it should be within 1% of unity in each of the 26 pairs. The experimental ratios were between 0.51 and 1.15 and averaged 0.93, the differences from unity being due to experimental error.

Pickett and Sansone[17] carried out some experiments on sampling coal dust, comparing the distributions of mass with particle size in samples taken with nozzles 0.2 cm square and 1.3 cm diameter. They failed to detect any difference between the mass distributions because most of the mass of particles collected was in sizes too small for the sampling error of the small orifice to be revealed; this was pointed out by Davies.[18] Their criticism of the Davies criterion is invalidated by inadequate experimental technique and for the same reason no conclusions can be drawn, as was done from the data of Breslin and Stein,[15] about the influence of the ambient wind velocity.

Agarwal[19] also criticized the criterion but failed to realize that the aspiration coefficient is a function of $v_s$ of specific form, for horizontal wind, namely

$$A = f\left\{St_V\left[\left(W^2 + v_s^2\right)/V^2\right]^{3/4},\ v_s/V\right\} \qquad (48)$$

by equations (37) and (6). Instead, he took the product

$$St_V \cdot v_s/V = \tau v_s/D$$

which is independent of V and is obviously incorrect.

## EXPERIMENTAL RESULTS — SAMPLING IN A WIND AT 90° YAW ANGLE

Some experiments have been carried out in a small wind tunnel with the sampling tube at right angles to the wind direction; in some of the experiments the wind was vertically downwards so that $\phi = 0$ and $\psi = 90°$. In others, the wind was horizontal, making $\phi = 90°$, and the sampling tube sucked vertically upwards so that $\psi = 180°$.

According to equations (6) and (37), for values of A near to unity, the aspiration coefficients can be calculated from the experimental data as follows, for comparison with the actual measured values of A.

When $\phi = 0$, $\psi = 90°$:

$$A = 1 - 3.2\ St_V \left(\frac{W + v_s}{V}\right)^{3/2} + 1.28\ St_V^{\ 2}\left(\frac{W + v_s}{V}\right)^3 \tag{49}$$

and when $\phi = 90°$, $\psi = 180°$,

$$A = \left(1 - \frac{v_s}{V}\right)\left[1 - 3.2\ St_V \left(\frac{W^2+v_s^{\ 2}}{V^2}\right)^{3/4} + 1.28\ St_V^{\ 2}\left(\frac{W^2+v_s^{\ 2}}{V^2}\right)^{3/2}\right] \tag{50}$$

Provided that both $v_s/W$ and $v_s/V$ are small, each case reduces to the same formula, namely

$$A = 1 - 3.2\ St_V\left(\frac{W}{V}\right)^{3/2} + 1.25\ St_V^{\ 2}\left(\frac{W}{V}\right)^3 \tag{51}$$

Levin's equation (24) relates to a point sink. The object of the experiments was to find out whether its adaption to a finite sampling tube in a given orientation, expressed by equations (36) and (37), was accurate.

Nearly uniform particles of di-2-ethylhexyl sebacate (density 0.92 g/cm$^3$) were produced by a spinning disc generator and had diameters between 15 and 30 μm. The wind speed, W, could be varied from 74 to 306 cm/sec and the suction speed, V, from 188 to 2090 cm/sec. The sampling tubes had parallel bores with thin walls tapering finely to a sharp edge at the orifice. Belyaev and Levin[20] have shown that the use of a thick-walled tube reduces A when sampling with $\phi = \psi = 90°$ at zero yaw.

The experiments were difficult to perform accurately because of fluctuations in the concentration of particles. $v_s/W$ never exceeded 1.8% and $v_s/V$ 0.72%, hence equation (51) applies for each of the orientations with an error which is barely perceptible in comparison with the scatter of the results. The best way of displaying the data is to plot the aspiration coefficient, A, as a function of $St_V\ (W/V)^{3/2}$; according to equation (51), A should be a unique function of this variable. The experimental points are shown in this way on Figure 5.

Each sampling tube was attached to the second stage of a standard cascade impactor. The particles deposited partly on the inside of the sampling tube and partly on the cascade impactor plate, the aspiration coefficient being calculated from

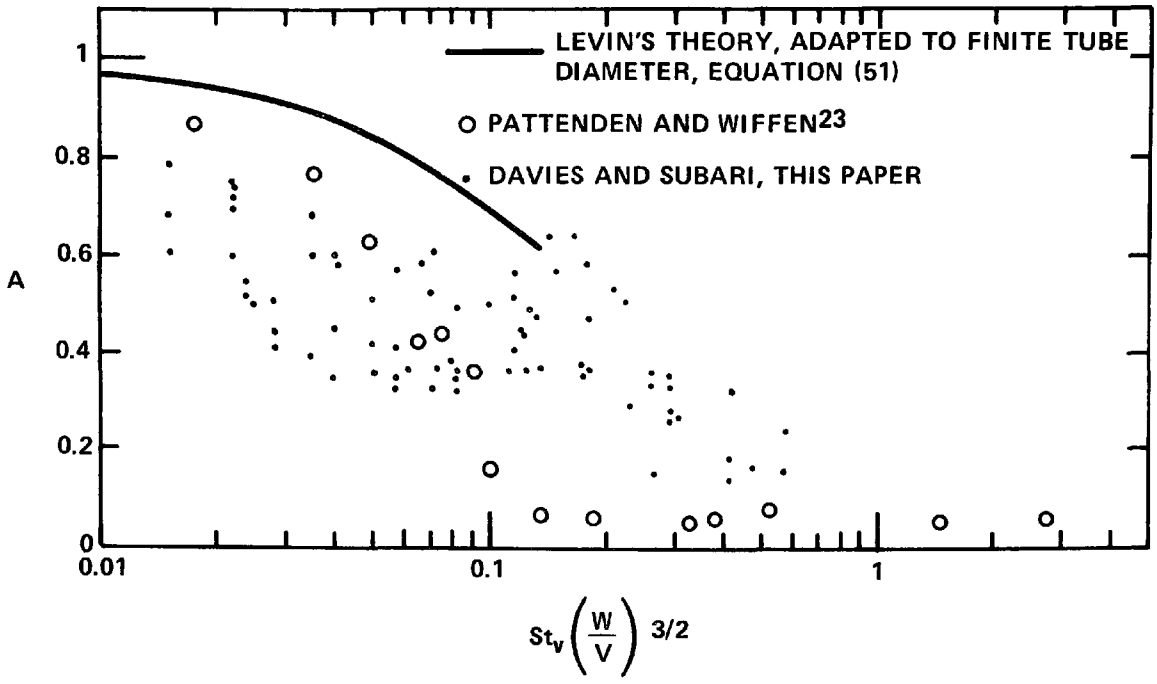


*Figure 5. Experimental results for A as a function of $St_V(W/V)^{3/2}$, sampling at 90° yaw angle with $v_S$ very small.*

the sum of those in the tube plus those on the plate, divided by the volume of air sampled. The particles inside the tube were estimated either by weighing the tube before and after deposition or by lining it with thin metal foil coated with a film of magnesium oxide. The airborne concentration was measured with a small isokinetic impactor, facing the wind, with a sharp-edged slit orifice.

It is essential, when measuring the concentration of aerosols, to include particles deposited inside the sampling tube with particles collected on the impactor plate or filter. Liquid particles will usually adhere to the tube wall, on impact, but some solid particles, especially at high rates of suction may bounce off. In the experiments now described the liquid droplets of di-2-ethylhexyl sebacate adhered to the metal tube, but particles which struck the magnesium oxide layer at glancing incidence often rebounded and reached the sampling plate.

$F_t$ is defined as the fraction of the total particles entering the sampling tube which were found adhering to the wall of the tube. The experimental results are shown in Table 1. $F_t$ could be calculated by the empirical formula

$$F_t = \frac{1}{2}\left[1 + \mathrm{erf}\left\{2\ln \frac{St_W\,(W/V)^{0.2}}{0.15}\right\}\right] \qquad (52)$$

TABLE 1. FRACTION $F_t$ OF PARTICLES ENTERING THE SAMPLING TUBE WHICH DEPOSITS ON THE WALL OF THE TUBE

| Method | $St_W$ | W/V | $F_t$ | |
|---|---|---|---|---|
| | | | Calculated | Experimental |
| MgO | 0.065 | 0.093 | 0 | 0 |
| | .065 | .093 | 0 | 0 |
| | .077 | .110 | 0.001 | 0 |
| | .077 | .110 | .001 | 0 |
| | .078 | .400 | .009 | 0 |
| | .078 | .400 | .009 | 0 |
| | .089 | .400 | .023 | 0 |
| | .089 | .400 | .023 | 0 |
| | .100 | .150 | .013 | 0 |
| | .100 | .300 | .034 | 0 |
| | .100 | .400 | .048 | 0.10 |
| | .100 | .610 | .077 | .14 |
| | .113 | .400 | .094 | 0 |
| | .160 | .060 | .080 | .05 |
| | .160 | .120 | .155 | .17 |
| | .160 | .232 | .260 | .18 |
| | .160 | .470 | .404 | .25 |
| | .178 | .400 | .489 | .29 |
| | .178 | .400 | .489 | .31 |
| | .178 | .400 | .489 | .27 |
| | .190 | .070 | .202 | .36 |
| | .190 | .140 | .329 | .31 |
| | .190 | .270 | .472 | .31 |
| | .190 | .400 | .560 | .58 |
| | .190 | .530 | .622 | .64 |
| | .204 | .400 | .638 | .53 |
| | .204 | .400 | .638 | .44 |
| | .220 | .080 | .365 | .43 |
| | .220 | .170 | .532 | .58 |
| | .220 | .310 | .644 | .61 |

(continued)

TABLE 1 (continued)

| Method | $St_W$ | W/V | $F_t$ | |
|---|---|---|---|---|
| | | | Calculated | Experimental |
| MgO | 0.240 | 0.351 | 0.770 | 0.75 |
| | .240 | .351 | .770 | .78 |
| | .256 | .400 | .839 | .81 |
| | .278 | .200 | .798 | .50 |
| | .278 | .400 | .891 | .54 |
| | .278 | .400 | .891 | .54 |
| | .290 | .475 | .926 | .92 |
| | .290 | .475 | .926 | .89 |
| | .346 | .400 | .968 | .85 |
| | .377 | .200 | .955 | .46 |
| | .377 | .200 | .955 | .57 |
| | .397 | .400 | .987 | 1 |
| | .397 | .400 | .987 | 1 |
| | .403 | .400 | .989 | .89 |
| | .462 | .400 | .996 | .87 |
| | .630 | .400 | .999 | 1 |
| Weighing | .630 | .200 | .998 | 1 |
| | .630 | .200 | .998 | 1 |
| | .630 | .400 | .999 | 1 |
| | .722 | .200 | 1.000 | 1 |
| | .722 | .400 | 1.000 | 1 |
| | .856 | .400 | 1.000 | 1 |
| | .856 | .400 | 1.000 | 1 |
| | .895 | .400 | 1.000 | 1 |
| | .895 | .400 | 1.000 | 1 |

and Table 1 shows that this agrees quite well with the experimental measurements which cover the ranges $0.068 < St_W < 0.3$ and $0.05 < W/V < 0.53$. Equation (52) is graphed in Figure 6 and has been extrapolated beyond the experimental values to give the curves up to W/V = 2. This was done, as an interim measure, to give warning of losses that can occur upon the tube wall.

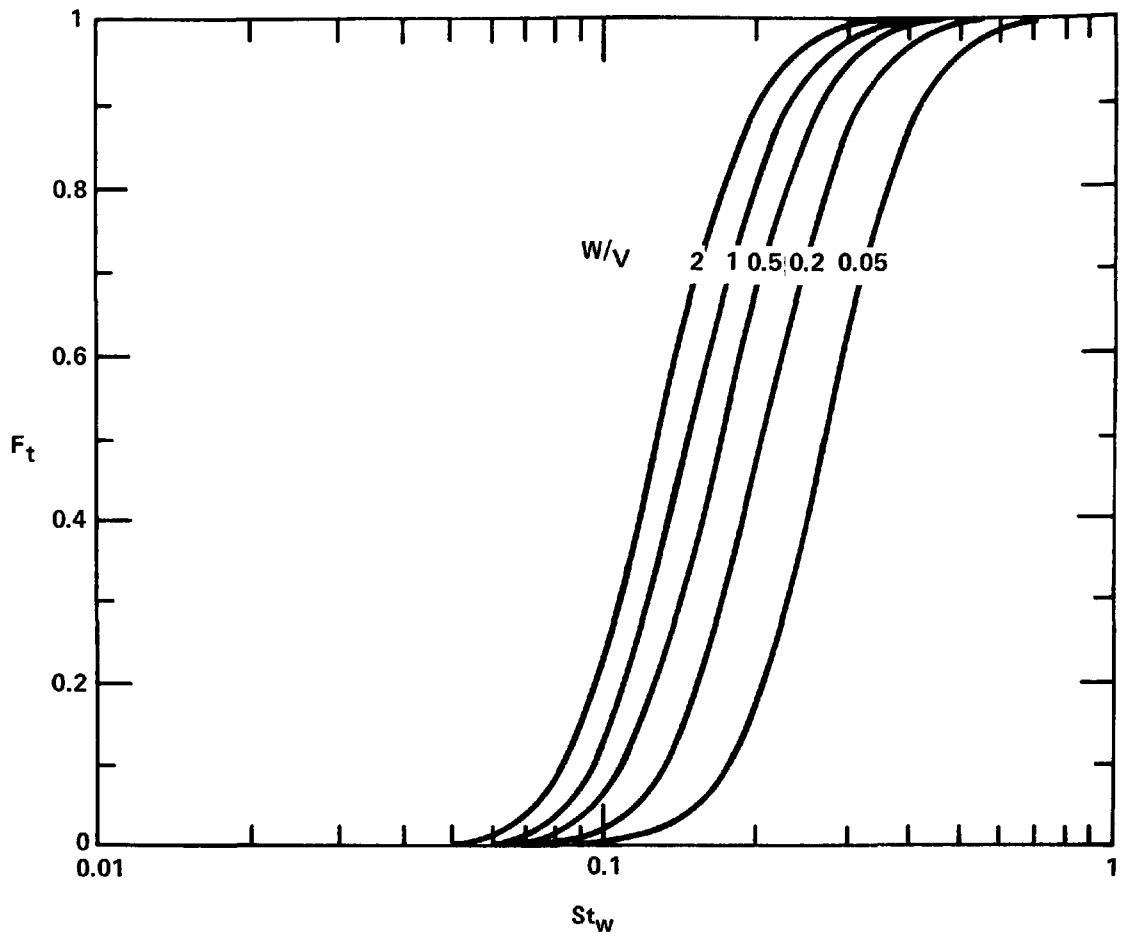


*Figure 6. The fraction, $F_t$, of particles entering the sampling tube which deposits upon the inside of the tube (experimental data in Table 1).*

The experimental data, for each value of A measured, are given in Table 2 and the results are plotted in Figure 5, with a separate point for each experiment. Also shown in Figure 5 are 14 points calculated from Table 2 of Pattenden and Wiffen's paper[23]; each is the mean of about four measurements in a wind tunnel at wind speeds between 2 and 6 m/sec, using solid particles with aerodynamic diameters from 4.5 to 25 μm. The sampling tube was vertical, in a horizontal wind, and it made no difference whether the tube pointed upwards or downwards, hence $v_s$ was negligible; the tube diameter was 1.25 cm, its end was cut off square and the wall thickness was about 0.2 cm. The mean inlet velocity was 70 cm/sec. Only their experiments with a tube without a cover are discussed here. They found that with a cylindrical rain cover over the tube there was a substantial increase in the aspiration coefficient; this is an example of May's stagnation point sampling,[24] an important idea which is not directly relevant to the present work.

TABLE 2. EXPERIMENTAL RESULTS

| Series | Orientation | $St_V$ | W/V | $v_s/V$ | A | $St_V\left(\frac{W+v_s}{V}\right)^{3/2}$ |
|---|---|---|---|---|---|---|
| $A_1$ | V | 0.70 | 0.110 | 0.001 | 0.498 | 0.026 |
| $A_1$ | V | .70 | .110 | .001 | .515 | .026 |
| $A_1$ | V | .70 | .093 | .001 | .425 | .020 |
| $A_1$ | V | .70 | .310 | .001 | .433 | .121 |
| $A_1$ | V | .70 | .232 | .001 | .378 | .079 |
| $A_1$ | V | .70 | .270 | .001 | .500 | .099 |
| $A_1$ | V | .70 | .150 | .001 | .580 | .041 |
| $A_1$ | V | .70 | .475 | .001 | .287 | .230 |
| $A_1$ | V | .70 | .475 | .001 | .556 | .230 |
| $A_1$ | V | .70 | .351 | .001 | .566 | .146 |
| $A_1$ | V | .70 | .351 | .001 | .504 | .146 |
| $A_2$ | V | 1.35 | .17 | .001 | .346 | .095 |
| $A_2$ | V | 2.7 | .08 | .000 | .365 | .061 |
| $A_2$ | V | 1.35 | .14 | .001 | .324 | .071 |
| $A_2$ | V | 1.35 | .14 | .001 | .390 | .071 |
| $A_2$ | V | 2.7 | .07 | .000 | .358 | .050 |
| $A_2$ | V | .36 | .53 | .002 | .638 | .140 |
| $A_2$ | V | .47 | .40 | .002 | .446 | .120 |
| $A_2$ | V | 1.35 | .12 | .001 | .343 | .057 |
| $A_2$ | V | .35 | .47 | .002 | .361 | .113 |
| $A_2$ | V | .17 | .61 | .003 | .493 | .082 |
| $A_2$ | V | .26 | .40 | .002 | .586 | .066 |
| $A_2$ | V | .35 | .30 | .001 | .570 | .058 |
| $B_1$ | V | .17 | .2 | .0018 | .786 | .015 |
| $B_1$ | V | .17 | .2 | .0018 | .609 | .015 |
| $B_1$ | V | .17 | .2 | .0018 | .687 | .015 |
| $B_1$ | V | .27 | .2 | .0018 | .516 | .024 |
| $B_1$ | V | .27 | .2 | .0018 | .547 | .024 |
| $B_1$ | V | .31 | .2 | .0018 | .448 | .028 |
| $B_1$ | V | .31 | .2 | .0018 | .507 | .028 |
| $B_1$ | V | .31 | .2 | .0018 | .408 | .028 |
| $B_3$ | V | .89 | .2 | .0034 | .354 | .082 |
| $B_3$ | V | 1.02 | .2 | .0034 | .364 | .094 |

(continued)

TABLE 2 (continued)

| Series | Orientation | $St_V$ | W/V | $v_s/V$ | A | $St_V \left(\frac{W+v_s}{V}\right)^{3/2}$ |
|---|---|---|---|---|---|---|
| $C_1$ | V | 0.086 | 0.4 | 0.0034 | 0.602 | 0.022 |
| $C_2$ | V | .28 | .4 | .0068 | .368 | .073 |
| $C_3$ | V | 1.43 | .4 | .0021 | .135 | .365 |
| $C_4$ | V | 1.43 | .4 | .0021 | .178 | .365 |
| $C_4$ | V | 1.64 | .4 | .0021 | .139 | .418 |
| $C_4$ | V | 1.64 | .4 | .0021 | .32 | .418 |
| $C_4$ | V | 2.234 | .4 | .0021 | .154 | .571 |
| $C_4$ | V | 2.238 | .4 | .0021 | .238 | .571 |
| $B_3$ | H | .89 | .2 | .0034 | .342 | .082 |
| $B_3$ | H | .89 | .2 | .0034 | .310 | .082 |
| $B_3$ | H | 1.02 | .2 | .0034 | .337 | .094 |
| $B_3$ | H | 1.02 | .2 | .0034 | .334 | .094 |
| $B_3$ | H | 1.39 | .2 | .0034 | .364 | .128 |
| $B_3$ | H | 1.39 | .2 | .0034 | .488 | .128 |
| $B_3$ | H | 1.89 | .2 | .0034 | .371 | .173 |
| $B_3$ | H | 1.89 | .2 | .0034 | .359 | .173 |
| $B_4$ | H | 3.15 | .2 | .0036 | .259 | .289 |
| $B_4$ | H | 3.15 | .2 | .0036 | .349 | .289 |
| $B_4$ | H | 3.6 | .2 | .0036 | .326 | .289 |
| $B_4$ | H | 3.6 | .2 | .0036 | .274 | .289 |
| $C_1$ | H | .086 | .4 | .0034 | .747 | .022 |
| $C_1$ | H | .086 | .4 | .0034 | .600 | .022 |
| $C_1$ | H | .086 | .4 | .0034 | .690 | .022 |
| $C_1$ | H | .086 | .4 | .0034 | .718 | .022 |
| $C_1$ | H | .086 | .4 | .0034 | .744 | .022 |
| $C_1$ | H | .136 | .4 | .0034 | .390 | .035 |
| $C_1$ | H | .136 | .4 | .0034 | .600 | .035 |
| $C_1$ | H | .136 | .4 | .0034 | .686 | .035 |
| $C_1$ | H | .136 | .4 | .0034 | .686 | .035 |
| $C_1$ | H | .155 | .4 | .0034 | .346 | .040 |
| $C_1$ | H | .155 | .4 | .0034 | .450 | .040 |
| $C_1$ | H | .155 | .4 | .0034 | .600 | .040 |
| $C_2$ | H | .195 | .4 | .0023 | .509 | .050 |
| $C_2$ | H | .195 | .4 | .0023 | .417 | .050 |
| $C_2$ | H | .22 | .4 | .0023 | .403 | .057 |
| $C_2$ | H | .22 | .4 | .0023 | .306 | .057 |

(continued)

TABLE 2 (continued)

| Series | Orientation | $St_V$ | W/V | $v_s/V$ | A | $St_V\left(\frac{W+v_s}{V}\right)^{3/2}$ |
|---|---|---|---|---|---|---|
| $C_3$ | H | 0.445 | 0.4 | 0.0068 | 0.570 | 0.115 |
| $C_3$ | H | .445 | .4 | .0068 | .512 | .115 |
| $C_3$ | H | .445 | .4 | .0068 | .400 | .115 |
| $C_3$ | H | .51 | .4 | .0068 | .475 | .132 |
| $C_3$ | H | .51 | .4 | .0068 | .468 | .132 |
| $C_3$ | H | .69 | .4 | .0068 | .581 | .180 |
| $C_3$ | H | .69 | .4 | .0068 | .468 | .180 |
| $C_3$ | H | .28 | .4 | .0068 | .520 | .073 |
| $C_3$ | H | .28 | .4 | .0068 | .610 | .073 |
| $C_5$ | H | .64 | .4 | .0047 | .645 | .165 |
| $C_6$ | H | .865 | .4 | .0062 | .500 | .224 |
| $C_6$ | H | .99 | .4 | .0062 | .331 | .256 |
| $C_6$ | H | .99 | .4 | .0062 | .360 | .256 |
| $C_7$ | H | 1.01 | .4 | .0072 | .151 | .262 |
| $C_7$ | H | 1.16 | .4 | .0072 | .263 | .300 |
| $C_7$ | H | 1.58 | .4 | .0072 | .183 | .409 |
| $C_7$ | H | 1.58 | .4 | .0072 | .130 | .409 |
| $C_7$ | H | 1.81 | .4 | .0072 | .160 | .469 |

Also shown in Figure 5 is the line of equation (51) as far as A = 0.62, which is Levin's limit for 2.5% error and k = 0.5. It is clear that this equation makes the value of A too large compared with the experimental results at 90° yaw.

The results of Pattenden and Wiffen are in rough agreement with ours up to $St_V(W/V)^{3/2} \simeq 0.9$. At this point their values of A fall abruptly and maintain a low level, 0.05 to 0.08 for $0.13\ St\ (W/V)^{3/2} < 3$.

Since

$$St_V(W/V)^{3/2} = St_W(W/V)^{\frac{1}{2}} \tag{53}$$

the lower limit, 0.13, corresponds to

$$St_W = 0.13\ (2.9)^{-\frac{1}{2}} = 0.08$$

and the higher to

$$St_W = 3\ (8.6)^{-\frac{1}{2}} = 1.02$$

where their range of W/V was from 2.9 to 8.6.

Looking at Figure 6, it is clear that all their measurements which give the low values of A were made under conditions such that a large proportion of the particles would be likely to stick to the tube wall and fail to reach the filter. It is possible that their employment of a thick-walled, blunt tube had something to do with this.

Instead of A falling at an initial rate corresponding to

$$A = 1 - 3.2\ St_V(W/V)^{3/2} + \ldots \tag{51}$$

it seems that the equation should be more like

$$A = 1 - 10\ St_V(W/V)^{3/2} + \ldots \tag{54}$$

There are signs of minimum and maximum values of A at the abscissae 0.8 and 0.16, respectively. The temporary reversal of the trend of A, between these values, must be due to a change in the mechanism of inertia effect, which was referred to above. Bearing equation (53) in mind, the initial, Levin effect is due to particles being whisked past the orifice and A is increased if V is increased; however, at higher values of $St_V$ the "space charge" effect comes in and A increases as V is decreased, by enough to give the small rise in A between the minimum and maximum.

At still higher values of $St_W$ and W/V the wind stream flow tube has to expand considerably on entering the sampling tube so that many particles shoot out of the flow tube, due to their inertia, and A becomes small. This, actually, is a return towards the point sink approximation. An increase in W lowers the ratio of the cross section of the wind stream flow tube to that of the orifice and A falls; an increase in V has the opposite effect and A rises.

Of course, the tube diameter has to be constant during the above changes, but this is looked after by the Stokes numbers.

## CONCLUSIONS

Levin's equation for a point sink in a wind (24) can be adapted for use with sampling tubes of finite diameter by including as variables the angle between the tube axis and the vertical (36, 37, 40) and the angle of yaw between the tube axis and the wind direction.

His limits (38, 39) overestimate the accuracy of his equation, when adapted to finite tubes, because his theory takes account neither of the ratio of the sedimentation velocity of the particles to the mean sampling velocity, nor of the effect of inertial build-up of concentration near the orifice, or "space charge" which, in the presence of wind or sedimentation, may

reduce A. Levin's assumption that a quadratic function of k can represent A down to 0.62 (2.5% error) does not hold; a more complicated expression, at least a cubic, is necessary in the case of sampling at 90° yaw angle.

Quite low wind and sedimentation velocities have a substantial effect in reducing A according to Levin's theory. That they must be taken account of in assessing sampling error is clear from the work of Breslin and Stein[15] and from our own experiments. Arguing from Levin's equation (24) adapted to a finite orifice (36, 37), it is shown that the Davies sampling criterion might be made slightly less restrictive for small tube sampling with $W/V < 0.2$ by using, instead of the original form (41),

$$2.45\ (Q\tau/4\pi)^{1/3} \leq D/2 \leq 0.2\ (Q/\pi g\tau)^{\frac{1}{2}}, \qquad (55)$$

which gives a maximum error of about 5% when both terms have the most unfavorable values.

However, caution is necessary because the inertial term is based on the adaptation (finite orifice) of Levin's equation, which tends to

$$A = 1 - 3.2\ f(St_V,\ W/V,\ v_s/V),$$

as in equation (37), whereas the experiments suggest, at 90° yaw, that the factor is 10 rather than 3.2. It is possible, when $St_V(W/V)^{3/2}$ is less than 0.01, that the curve actually decreases its slope and approaches ($A = 1$, $St_V(W/V)^{3/2} = 0$) with the factor 3.2, in which case the criterion (55) is correct. Were the factor to be greater than 3.2 the original form of (55), namely (41) might be better. Unfortunately, it is very difficult to do experiments at small values of $St_V$ and neither our own nor those of Breslin and Stein[15] are sufficiently accurate and numerous to enable a decision to be taken. In place of the 2.45 in the criterion (55) they suggest 1.5 at which value their own values of A range from 0.92 to 1.01 and an average error of 5% might be anticipated. In any practical sampling system, though, the wind is certainly not zero. The writer's view is that $W/V = 0.2$ is a practical figure for a "calm air" situation and it is on this that (55) was based.

Our work shows that when $St_W$ exceeds 0.08 an increasing deposition takes place on the inner surface of the sampling tube, and with $St_W > 0.3$ almost all the sample will strike the tube wall. This effect needs to be looked after in practical sampling.

It is possible that impact on the inside of the tube is affected to some extent by turbulence in the wind stream. A study is being made of the way in which the density of the deposit is distributed in the tube. The Reynolds number of the wind

tunnel, which was a smooth circular duct 10 cm in diameter, ranged from 5000 to 20,000. The stop distance of the particles on the wind velocity varied from 0.052 cm to 0.85 cm.

Clearly the particles with the larger values of stop-distance would be little affected by turbulence and at low wind speeds there would not have been strong turbulence. In the intermediate ranges of particle size and wind speed some enhancement of deposition in the tube is possible but an appreciable effect on the aspiration coefficient seems unlikely.

ACKNOWLEDGEMENTS

The apparatus was built by Sarah Weedon and M.J. Farncombe with the aid of a grant from the National Coal Board. Mr. M. Subari developed the apparatus and performed all the experiments. He is grateful for financial support from the University of Technology Malaysia, at Kuala Lumpur.

The apparatus is designed for experiments on the deposition of particles between 2.5 and 15 μm aerodynamic diameter in the human respiratory tract. Before this work could be started it was necessary to study the entry of particles into a breathing tube at 90° yaw angle to the moving stream of aerosol. Applications for a grant to support the inhalation experiments were made to the Medical Research Council and to the Directorate-General, Employment and Social Affairs, of the Commission of the European Communities but were rejected, the latter on the grounds that no funds were to be provided for basic research.

REFERENCES

1. Albrecht, F. Physik. Z. 32:48, 1931.

2. Sell, W. VDI-Forschungsh. 347: 1, 1931.

3. Davies, C.N. Trans. Inst. Chem. Eng. Suppl. 25:36, 1947.

4. Walton, W.H. Br. J. Appl. Phys. Suppl. No. 3, S29, 1954.

5. Robinson, A. Commun. Pure Appl. Math. 9:69, 1956.

6. Levin, L.M. Izv. Akad. Nauk SSSR Ser. Geofiz. 7:914, 1957.

7. Davies, C.N., and V. Peetz. Br. J. Appl. Phys. Suppl. No. 3, S17, 1954.

8. Davies, C.N. Br. J. Appl. Phys. 18:653, 1967.

9. Davies, C.N. Br. J. Appl. Phys. 18:1787, 1967.

10. Davies, C.N. Br. J. Appl. Phys. 11:535, 1960.

11. Voloshchuk, V.M., and L.M. Levin. Izv. Akad. Nauk SSSR Fiz. Atmos. Okeana 4(7):734, 1968.

12. Davies, C.N. Proc. R. Soc. London Ser. A 279:413, 1964.

13. ter Kuile, W.M. Rep. F. 1582. Inst. Milieuhygiene Gezondheidstechniek. IG-TNO, Delft, 1977.

14. Davies, C.N. Br. J. Appl. Phys. (J. Phys. D), Ser. 2, 1:921, 1968.

15. Breslin, J.A., and R.L. Stein. J. Am. Ind. Hyg. Assoc. 36:576, 1975.

16. Gibson, H., and T.L. Ogden. J. Aerosol Sci. 8:361, 1977.

17. Pickett, W.E., and E.B. Sansone. J. Am. Ind. Hyg. Assoc. 34:421, 1973.

18. Davies, C.N. J. Am. Ind. Hyg. Assoc. 36(9):714, 1975.

19. Agarwal, J.K. Particle Technology Lab. Publication 265, Univ. of Minnesota, 1975.

20. Belyaev, S.P., and L.M. Levin. J. Aerosol Sci. 3:127, 1972.

21. Kaslow, D.E., and R.J. Emrich. Lehigh Univ., Bethlehem, PA. Dept. Physics Tech. Rep. 23, 1973; Tech. Rep. 25, 1974.

22. Kim, Y.W. Lehigh Univ. Dept. Physics Tech. Rep. 24, 1974.

23. Pattenden, N.J., and R.D. Wiffen. Atmos. Environ. 11:677, 1977.

24. May, K.R. Physical Aspects of Sampling. In: Airborne Microbes, P.H. Gregory and J.L. Monteith, eds. Cambridge Univ. Press, London, 1967. pp. 60-80.

PAPER 2

# CYCLONE SAMPLER PERFORMANCE

MORTON LIPPMANN
NEW YORK UNIVERSITY
INSTITUTE OF ENVIRONMENTAL MEDICINE

AND

TAI L. CHAN
GENERAL MOTORS RESEARCH LABORATORIES

## ABSTRACT

Cyclones are finding increasing application in air sampling both as pre-collectors in two-stage samplers and as stages in multi-stage samplers for size-mass distribution determinations. They are well suited for both applications because of their relatively low cost, compact size, and independence of orientation and loading conditions. Their applications have been limited primarily because they have required extensive empirical calibrations. A new predictive relation for cyclone collection efficiency has been developed which permits extrapolation from a limited experimental data base to a wide variety of operating conditions. Constants for the equation are presented for eleven small cyclones ranging in diameter from 10 to 152 mm.

## INTRODUCTION

Cyclones are devices which remove particles from fluid streams as the stream is caused to rotate within a cylindrical and/or conical cross section. A conventional cyclone design is illustrated in Figure 1. Particles with sufficient momentum to cross the flow streamlines and reach the outer wall are arrested, and are either retained at the wall or migrate along the wall to a collection zone at the bottom. In hydroclones, which are cyclones for separating particles from aqueous suspensions, a small percentage of the liquid effluent is withdrawn at the bottom with the collected particles. The bulk of the liquid and the undersized particles exit through the axial pipe at the top. In air cleaning and air sampling cyclones, all of the air exits at the top.

Cyclones are widely used for removing particles of relatively large size from fluids because of their relative simplicity and relatively low costs in terms of construction, operation, and energy consumption. They are frequently used as a first stage or pre-collector upstream of a particle collector with a high collection efficiency for the small particles not removed by the cyclone.

Most of the literature on cyclones and their performance relates to cyclones used in cleaning of fluid streams, and has proven to be, unfortunately, of relatively little use in describing the performance of cyclones used in air sampling applications. The flow patterns and dust loading in the small cyclones

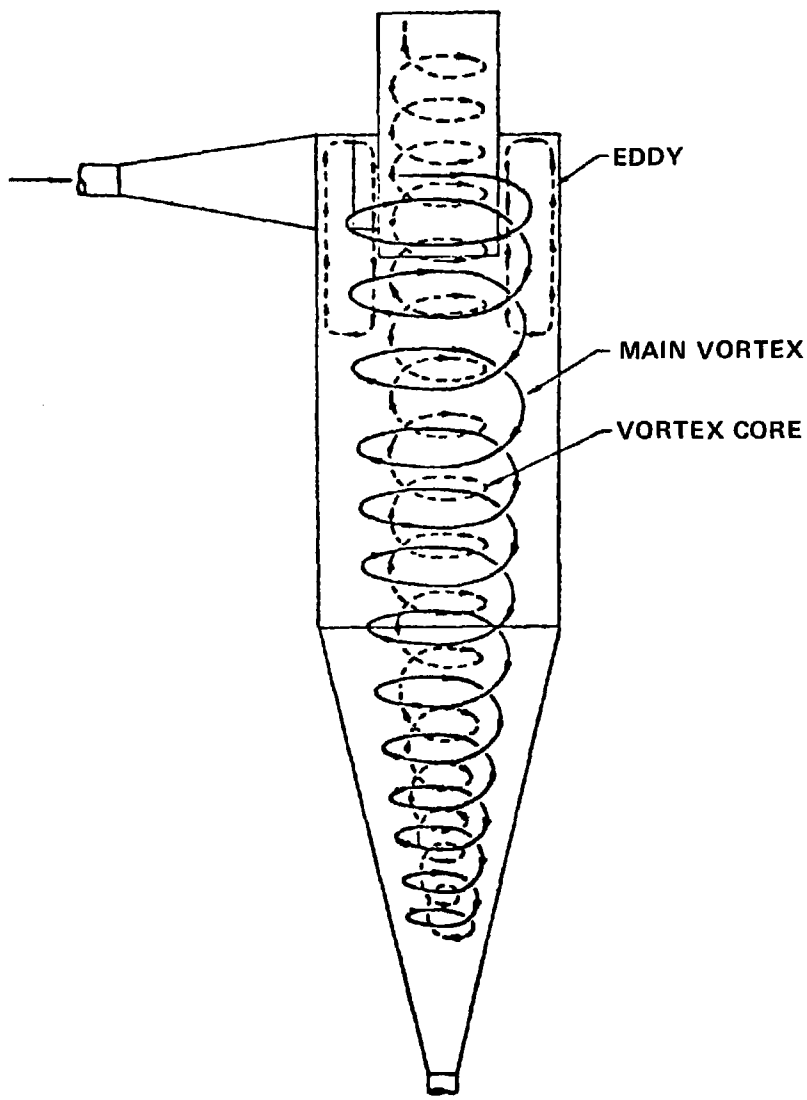


*Figure 1. Conventional double vortex flow pattern found in air cleaning cyclones (from Hochstrasser[24]).*

used in sampling are generally quite different from those found in air cleaning cyclones and hydroclones.

## APPLICATIONS OF CYCLONES IN AIR SAMPLING

### "Respirable" Dust Sampling

By far the greatest usage of small cyclones in aerosol sampling has been as the first stage of a two-stage sampler. In most cases, they have been operated at flow rates which were believed to permit cyclone penetrations equivalent to the penetration of inhaled dust to the non-ciliated deep lung spaces in humans. Such applications have been called "respirable" dust sampling, and their rationale has previously been discussed.[1,2,3]

In "respirable" dust sampling, it is essential that the cyclone cut-off characteristics be known and constant, and that each cyclone be operated at a flow rate which produces the desired cut-off. In the absence of a usable theory, it has been necessary to design and calibrate air sampling cyclones empirically. Unfortunately, dependence on an empirical calibration can lead to controversy and errors. The original calibration of the Dorr-Oliver 10-mm nylon cyclone[4] failed to include an appropriate aerodynamic shape factor. With Kotrappa's[5] shape factor correction, the recommended sampling rate was reduced to 1.8 ℓ/min, which is in good agreement with most of the more recent empirical calibrations,[6,7,8,9,10] which recommend either 1.7 or 1.8 ℓ/min. However, the Mine Safety and Health Administration, which specifies acceptable samplers and their operating characteristics in mine dust evaluations, still insists that the 10-mm cyclone be operated at 2.0 ℓ/min, on the basis of its own calibration by Tomb and Raymond.[11]

There are conflicting calibration data for several of the 12.5 to 50-mm diameter stainless steel cyclones which have also been used for size-selective sampling. Some of the differences can be attributed to the same causes as for the 10-mm cyclone, i.e., differences in calibration techniques, data interpretation, and failure to use appropriate particle shape corrections. Another factor is the dimensional variations between nominally identical samplers which were documented by Lippmann and Chan.[12] The steel cyclones are individually assembled, and the quality control exercised by the manufacturers has not always been adequate. The 10-mm nylon cyclones, which are injection molded, have not been observed or reported to vary significantly from one to another.

The use of cyclones as the first stage in two-stage samplers for "respirable" dust sampling received its first major impetus in the atomic industry when, in January 1961, the U.S. Atomic Energy Commission's Office of Health and Safety defined "respirable" dust as that portion of the inhaled dust which penetrates

to the non-ciliated portions of the lung. Further, they defined "respirable" dust specifically as follows:

| Aerodynamic Diameter (μm): | ≥10. | 5. | 3.5 | 2.5 | ≤2.0 |
|---|---|---|---|---|---|
| % Respirable: | 0 | 25 | 50 | 75 | 100 |

A variety of commercially available small cyclones were found to have collection characteristics at appropriate flow rates which were close to those of the AEC specification,[4] and some of them were used extensively in sampling programs by AEC contractors.

More widespread application followed the decision of the American Conference of Governmental Industrial Hygienists (ACGIH) in 1968 to issue a Notice of Intended Change in the threshold limit value (TLV) for quartz, cristobalite, and tridymite (three forms of crystalline free silica).[13] The size-selection characteristics for the first stage collector defined by ACGIH were identical to those of AEC, except that they specified that at ≤ 2.0 μm, the % "respirable" would be 90% rather than 100%. For all practical purposes, the two specifications are essentially the same.

In 1969, the Federal Coal Mine Health and Safety Act specified a "respirable" dust limit for coal mine dust, and all compliance sampling in the mines has been on "respirable" dust sampling, with most samples collected with a sampler including a 10-mm nylon cyclone.

Cyclone Samplers with Other Cut Sizes

The ambient atmospheric aerosol has two major mass modes. The so-called "accumulation mode" contains some primary submicron combustion-related particles, (from stationary and mobile sources), and also the secondary particles which are formed in the atmosphere from gaseous precursors by gas phase chemical and photochemical reactions. The mass median diameter of this mode is generally between 0.3 and 0.5 μm, and little of the mass is in particles smaller than 1.0 μm or larger than 2 to 3 μm. The larger particles found in the ambient air, which form the so-called coarse mode, are generally released by mechanical processes, and differ substantially in chemical characteristics and physical properties from the accumulation mode particles. A variety of samplers designed to aerodynamically sort the ambient particles into the two major mass modes have used cyclones to collect the larger particles. There is no general agreement on the appropriate cut size for this application, or whether the cut-off characteristic should be sharp or broad. Some prefer

a sharp cut at an aerodynamic diameter of 2, 2.5, or 3.5 μm. Others prefer a 3.5 μm aerodynamic mass median with the ACGIH respirable cut characteristic. Their rationale is that there will be little practical difference in the size of the two mass fractions for most atmospheric aerosols, and, therefore, little justification for introducing a different sampler acceptance standard.

A cyclone with a sharp cut-off characteristic and intended for two-stage ambient air sampling has been described by John, et al.[14] The EPA has used some of the cyclone samplers developed for "respirable" dust sampling for two-stage ambient air sampling, primarily the 1/2-in. HASL cyclone described by Lippmann and Harris.[4]

Several instrument vendors market cyclone preseparators for either source-test cascade impactors or high volume samplers. While there are no data on their performance in the literature, calibration data on the Sierra Model 220CP cyclone have been made available to us by Dr. John Olin of Sierra Instruments, and they have been utilized in our analyses.

Virtual dichotomous samplers have been widely used in recent years for two-stage sampling. The precise balance of the two different parallel flow streams in such samplers makes them much more expensive than cyclones. On the other hand, they put both mass fractions on filters, and this is often advantageous in terms of subsequent analyses of the large particle fractions.

Size-Mass Distribution Determinations

Size-mass distribution analyses of aerosol constituents have been made using cascade impactor samplers for more than thirty years, beginning with the original May impactor,[15] and the Laskin[16] University of Rochester modification. They have also been performed with aerosol centrifuges which deposit particles on a collection foil according to their aerodynamic size. However, both types of sample collectors have significant limitations when used for such applications. Solid particles tend to bounce off or be re-entrained from impaction surfaces which lack an adhesive layer, or whose adhesive becomes saturated. Unfortunately, saturation usually is reached either before the investigator is aware of it, or before the accumulated sample is large enough for the subsequent analysis. Applications of centrifuges are limited by their low sampling rates and large physical size and cost.

The limitations of the other inertial classifiers for compositional analysis by particle-size fraction have led to the development of samplers using cyclones in either parallel or series arrays. The first development of a portable sampler using a parallel array of cyclone-filter series samplers was described

by Lippmann and Kydonieus.[7] Each cyclone had a different cut size and the overall size-mass distribution of the total aerosol, or of any of its chemical constitutents, could be determined from analyses of the collection on the filter following each cyclone and a parallel filter sampler operated without a cyclone precollector. The performance characteristics of an improved version of this sampler were described by Blachman and Lippmann.[9] Individual cyclones could be operated at flow rates of ∿ 1 to 22.5 ℓ/min, giving cut points ranging from ∿ 6 μm to 0.25 μm. A much larger version of this sampler for fixed-station ambient air pollution sampling was described by Bernstein, et al.,[17] having cut points at 3.5, 2.5, 1.5 and 0.5 μm. A parallel multi-cyclone sampling train for stack sampling applications was described by Chang,[18] but sufficient calibration data were not provided to characterize the cyclone's performance.

A series array of cyclones for in-stack sampling through an eight-inch port was described by Rusanov[19] in 1969. A more compact series sampler which fit within a six-inch port and sampled at 1 $ft^3$/min was described by Smith, et al.[20] in 1975. It consisted of three cyclones and a back-up filter. The first cyclone, with a reported cut point of 2.6 μm, was the T2A cyclone used by Chang[18] in his parallel array. The other two cyclones, with nominal cut points of 1 μm and 0.5 μm, were designed and constructed by Southern Research Institute (SRI) for this sampler. A later development from SRI[21] is a six-stage in-stack series sampler which operates at 1 $ft^3$/min and fits through a 10-cm sampling port. The five cyclones were reported to have cut points at aerodynamic diameters of 5.4, 2.1, 1.4, 0.65, and 0.32 μm. The collection characteristics of the cyclones in this train are notable in that their cut off characteristics are quite sharp, as shown in Figure 2. For the SRI II cyclone, with a cut size of 2.1 μm, the ratio of the particle sizes with 90% and 10% removal, respectively, is 1.5. By comparison, for the Andersen Stage 4 impactor, with a cut size of ∿ 2.3 μm, the corresponding ratio is also 1.5 (Figure 3).

Data processing to determine the particle size distribution for these multi-stage samplers can be treated in a similar manner as the cascade impactor.[22] An alternate approach is the iteration scheme that has been developed by Sinclair and Knutson based on the approach of Twomey.[23] It will be presented later in this symposium.

## AERODYNAMIC FLOW AND PARTICLE COLLECTION IN CYCLONES

### Air Cleaning Cyclones

The conventional view of flow within a cyclone shown in Figure 1 appears to be realistic for air cleaning cyclones. There is a double vortex, with the air stream spiralling downward near the outer wall and then upward in a tighter spiral and out

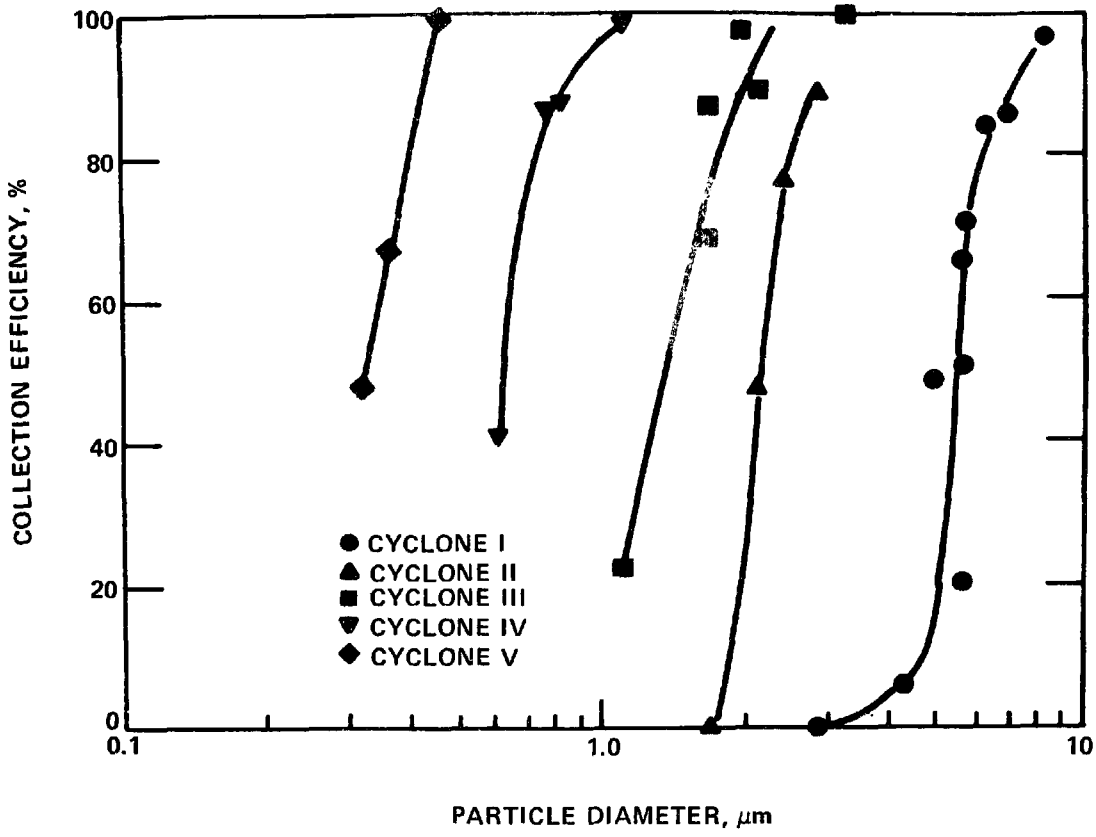


*Figure 2. Collection efficiencies of Southern Research Institute cyclones for a sampling rate of 28.3 ℓ/min, a temperature of 25°C, and a particle density of 1.0 g/cm³ (from Smith and Wilson[21]).*

through the axial exit tube. The particles may initially deposit on the wall in a well-defined spiral pattern. With continued operation, a dust layer will form and migrate along the wall to a collection hopper in a still-air zone at the bottom of the conical section. The concentration of particles in an air cleaning cyclone is usually quite high, which favors particle coagulation while they are still airborne. Since collection probability increases with increasing particle size, the collection efficiency increases with increasing particle concentration.

Tangential inlet cyclones used in air cleaning are generally at least six inches in diameter, have inlet velocities of 2500 ft/min or greater, and Reynolds numbers in the inlets of about 100,000 or more. Thus, the flow will be highly turbulent. Particles of about 5 μm and larger can be collected with relatively low energy consumption. However, the energy input required to capture smaller particles increases rapidly with decreasing size and is rarely worthwhile economically, except when using plenum housings containing large numbers of small diameter cyclones operating in parallel. Particles as small as 2 μm can be collected efficiently with cyclones of 2-inch diameter when operated with a flow rate of about 900 ℓ/min through each cyclone.

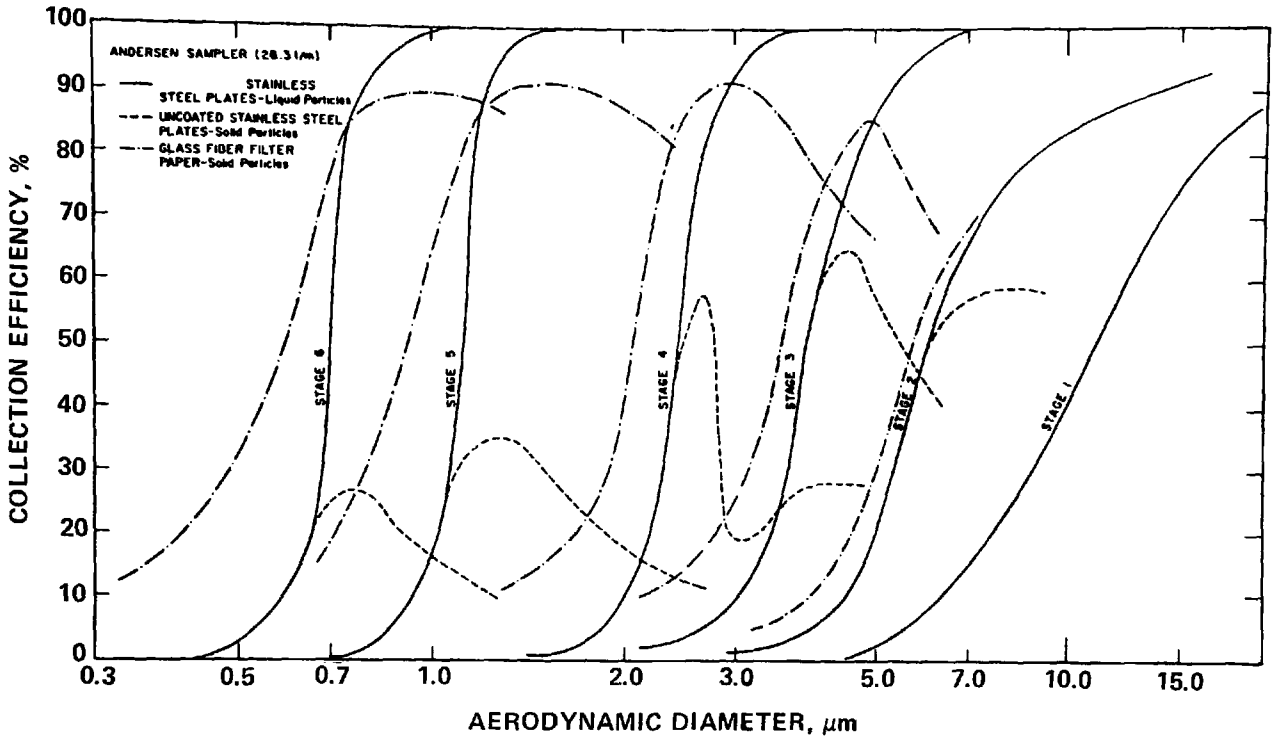


*Figure 3. Collection efficiencies for Andersen cascade impactor stages at a sampling rate of 28.3 ℓ/min (from Marple and Willeke[22]).*

## Air Sampling Cyclones

Inertial separation efficiency in cyclones increases with decreasing body diameter because of the tighter turns of the air path and the greater relative radial acceleration of the airborne particles. As a result, the same collection efficiency can be achieved with lower air velocities. With lower air velocities, the flow regime will change from highly turbulent to partially turbulent. The flow is predominantly laminar in the small cyclones used in personal "respirable" dust samplers. However, when these same cyclones are used at higher sampling rates in multi-stage particle size samplers, a flow transition occurs and the flow patterns are affected by turbulence. The change in the nature of the flow pattern within the cyclones with changing flow rate makes it difficult to develop a general description or predictive relationship for cyclone performance, and makes extrapolation from one operating condition to another somewhat questionable.

Direct evidence for a change in airflow pattern with a change in flow rate is provided by the abrupt changes in the pressure-flow relations. Figure 4 shows pressure-flow data of Hochstrasser[24] for three different 19-mm diameter long-cone cyclones. As the

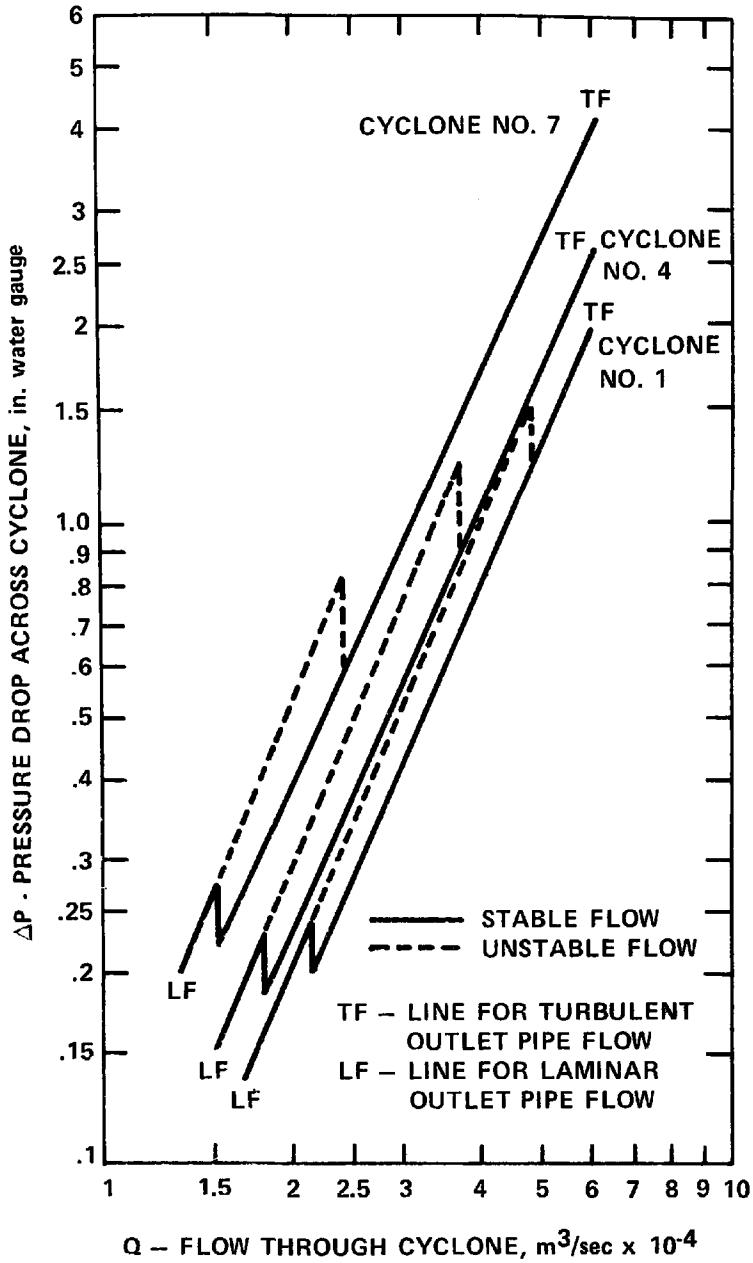


*Figure 4. Pressure-flow relationships for three 19-mm diameter long-cone cyclones (from Hochstrasser[24]).*

flow increases, a point is reached where there is an abrupt reduction in pressure drop. With increasing flow thereafter, the pressure drop increases again, but the slope of the curve is lower. The same phenomenon was observed by Blachman and Lippmann for the widely used 10-mm nylon cyclone of Dorr-Oliver.

Blachman and Lippmann[9] presented indirect evidence for a change in flow pattern within the cyclone in terms of an abrupt change in the collection efficiency characteristic at a critical

flow rate. Figure 5 shows that there is an abrupt change in the collection characteristic between 5.0 and 5.8 ℓ/min. They further reported that locations at which the particles were deposited within the cyclone change for the different flow regimes.

Since the iron oxide in their test aerosol was reddish in color, it was possible to observe the pattern of particle collection along the walls of the white nylon cyclones. For flows below 5 ℓ/min, the collection was essentially all close to the cyclone inlet, with no visible collection in the lower part of the cyclone body. For higher flow rates and small particles, the inlet deposit extended into a spiral along the tapered inner wall. In addition, there was another separate "ring" deposit in the lower part of the cyclone. At a higher sampling rate, the location of the ring deposit was lower. Since the lower portion of the cyclone is tapered, the particles forming the ring were depositing in a region with a smaller diameter, and this presents a complication in attempts to fit the data into generalized models. The number of turns that particles traversed before the cyclone's collection was completed was dependent on the flow rate and varied from 1 at 0.9 ℓ/min to 5 at 9.2 ℓ/min. For higher flow rates, it was not possible to visualize the numbers of turns.

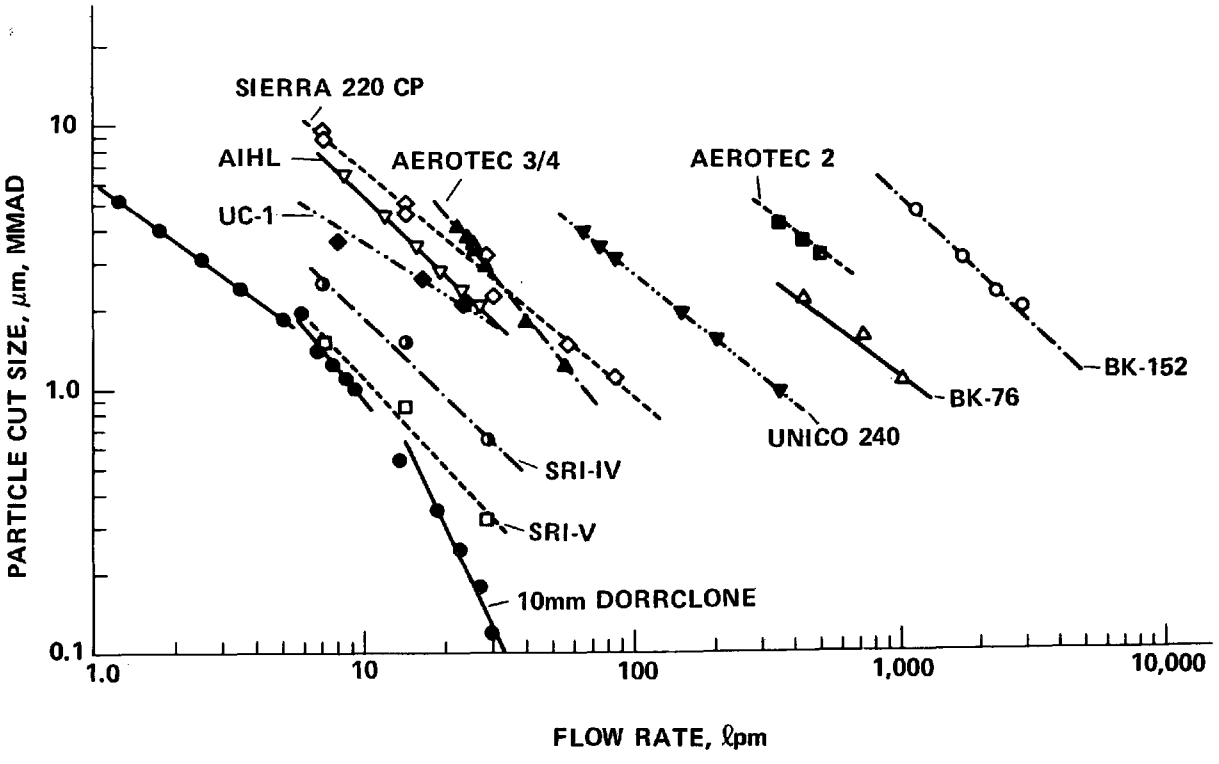


*Figure 5. Particle cut size, i.e., aerodynamic particle size for 50% cyclone retention, as a function of flow rate through cyclone for eleven small cyclones.*

Ring deposits in small cyclones have also been observed by others[24,25] and have been associated with a uniform radial motion of the airstream. Hochstrasser[24] found ring deposits only when there was a flow rate below the critical pressure drop transition point. He then inserted a pressure probe into the lower cone portions of his cyclones and demonstrated that there was a stagnant air zone present when flow conditions produced ring deposits, but not when conventional vortex flow existed. The height of the stagnant zone appeared to be proportional to the height of the ring deposit. Hochstrasser associates the ring deposit mode of cyclone operation with a laminar flow condition in the outlet pipe of the cyclone, as illustrated in Figure 6.

Since the flow pattern in the outlet pipe appears to critically affect the performance of the cyclone, Hochstrasser suggests that restrictions in the outlet flow imposed by couplings to the downstream filter or other second stage collector may alter the removal characteristics of the cyclone itself, and that lack of standardization of such couplings may account for some of the reported discrepancies of small cyclone sampler calibration and field performance.

Hochstrasser noted that the laminar outlet pipe flow condition could only be produced in long-cone cyclones, i.e., having a cone length of 5 cm in relation to his cyclone diameter of 1.9 cm. When the cone lengths were changed to 2.7 or 1.6 cm, only the turbulent flow condition was observed.

John, et al.[14] confirmed that abrupt flow pattern changes cannot be produced in short-cone cyclones. Their cyclone has a body diameter of 3.7 cm and a cone length of 4.6 cm. There was a vortex in the outlet pipe under all test conditions.

John, et al. also studied the patterns of deposition and retention of both liquid and solid particles within the cyclone. They noted the following features:

1. An impaction spot on the wall of the cyclone body opposite the inlet, but slightly off a direct line.

2. A spiral trace of 1.25 to 1.5 turns.

3. A diffuse deposit on the cone walls increasing in density toward the bottom.

4. Large aggregates of particles in the collection cup at the bottom.

5. A spiral trace in the outlet tube.

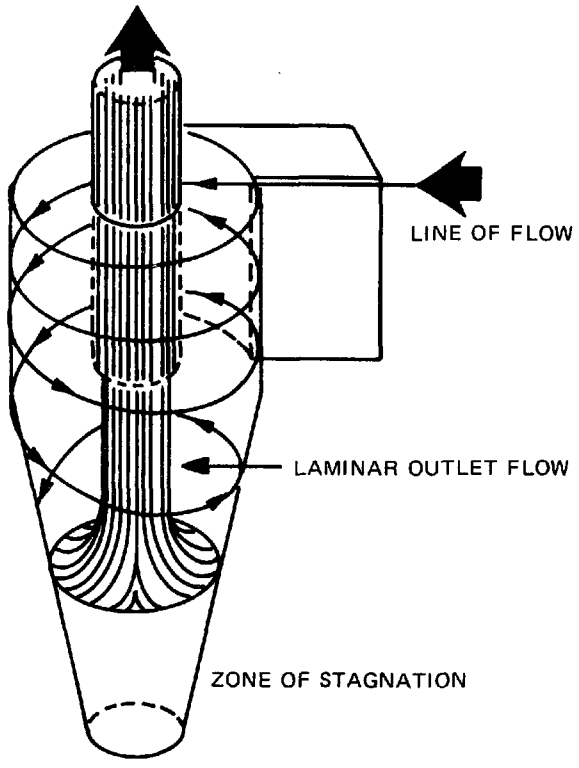


NEW THEORETICAL CYCLONE
LAMINAR FLOW PATTERN

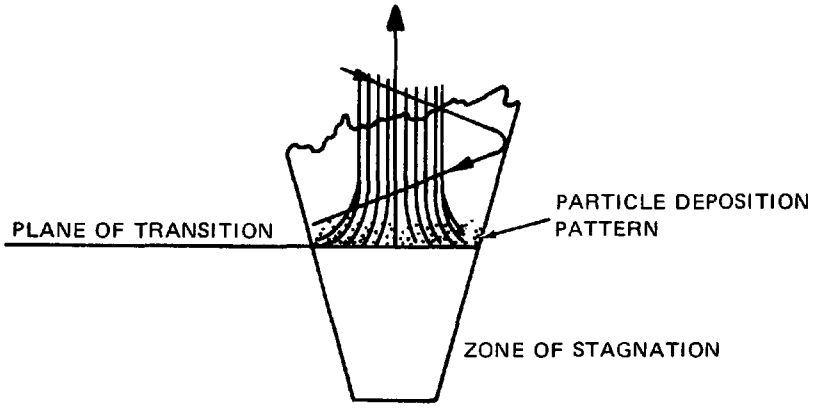


PARTICLE DEPOSITION PATTERN
( LAMINAR FLOW CYCLONE )

*Figure 6. Flow pattern and particle deposition in long-cone cyclones operating in laminar outlet pipe flow condition (from Hochstrasser[24]).*

6. No measurable differences in the percentage of the aerosol penetrating to the back-up filter between liquid and solid particles of the same aerodynamic size.

They also tested the cyclone for re-entrainment losses. It was loaded with the equivalent of several days of expected collection and then clean air was drawn through. The material transferred from the cyclone walls to the outlet filter was about 1% per day or less.

The insensitivity to sample loading and the nature of the sampled material gives the cyclone significant advantages over the impactor for long-period sampling. Figure 3 shows that uncoated impaction plates do not retain solid particles efficiently, and that the use of filters as impaction surfaces may result in even greater losses. Cyclones do not suffer from such limitations and, as shown in Figure 2, the collection characteristics can be as sharp as those of impactors.

In multi-stage samplers used for size-mass distribution analyses, it is desirable to have the sharpest possible cut-off characteristics for each stage. The work of Mercer[26] and Marple and Willeke[22] has led to considerable refinement in the design of jet impactors and characterization of their performance. While comparable definitive work has yet to be performed on cyclones, recent work, such as that illustrated in Figure 2, has shown that it is possible to achieve relatively sharp cut-off characteristics in properly designed cyclones. The sharpness of the cut-off can be compared for cyclones of different sizes by plotting cyclone retention as a function of a normalized particle diameter $(D_p-D_{50})/D_{50}$, where $D_p$ is the aerodynamic diameter of the test aerosol and $D_{50}$ is the diameter at which the cyclone retention is 50%. Figure 7 shows calibration data for 5 Stairmand-type cyclones which have been developed and calibrated in recent years. The sharpest cuts are produced by the SRI-V cyclone of Smith and Wilson.[21]

The particle collection characteristics of the conductive airways of the respiratory tract are not sharp. Hence, it is desirable that pre-collectors used for "respirable" dust sampling should have similar collection characteristics. In this sense, the 10-mm nylon cyclone, which is widely used for this purpose, is less than ideal in that it has a relatively sharp cut-off characteristic. For cyclones designed specifically for "respirable" dust sampling, such as the 1/2-inch and 1-inch diameter dual-inlet stainless steel cyclones developed by the Health and Safety Laboratory of the U.S. Atomic Energy Commission, the potentially sharp performance characteristics of cyclones were deliberately degraded in order to produce samplers with appropriately coarse cut-off characteristics.[4]

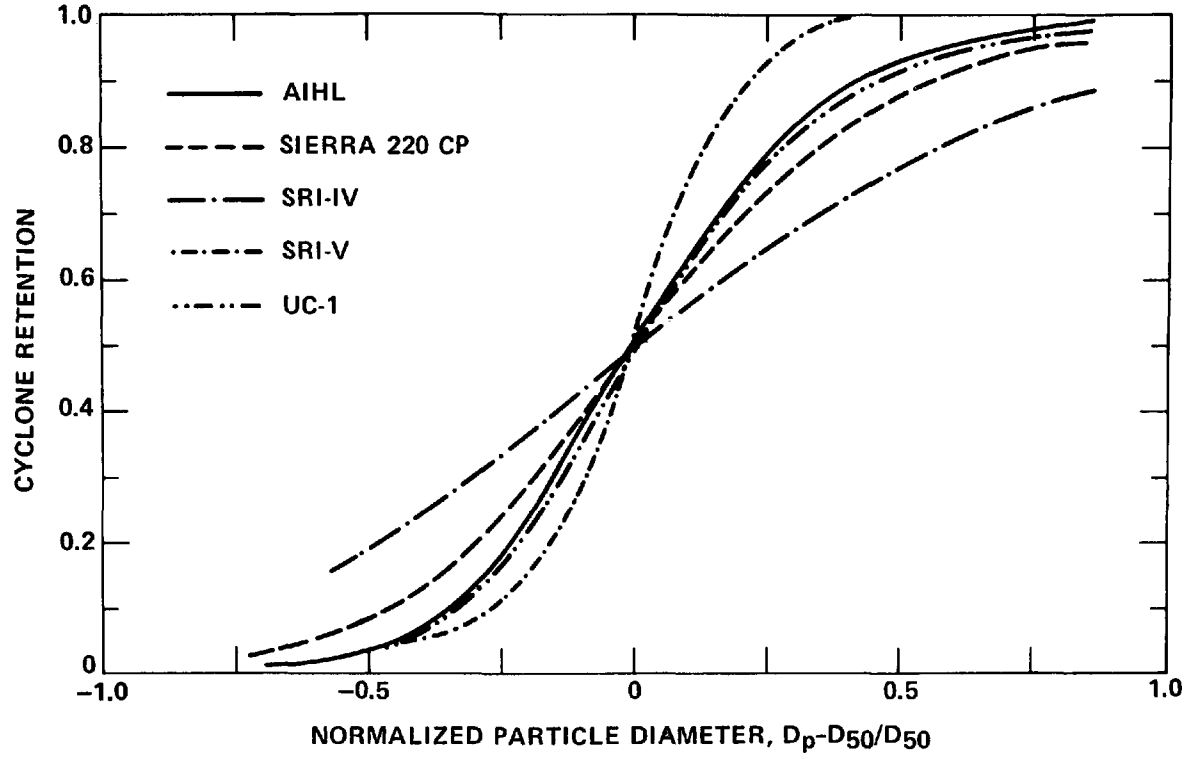


*Figure 7. Cyclone retention as a function of normalized particle diameter for five small cyclones which have recently been calibrated. $D_p$ is the aerodynamic particle size of the test aerosol and $D_{50}$ is the aerodynamic size for 50% cyclone retention.*

The variation of experimentally determined particle cut sizes with sampling rate is illustrated in Figure 5 for a variety of sampling cyclones. For each cyclone, there are characteristic relations between cut size and sampling rate. Most of the calibration data are for aerodynamic particle sizes between 1 and 10 μm. Some of the cyclones, specifically the 10-mm Dorr-Oliver and the SRI-V, have calibrations for cut sizes extending to 0.5 μm and below. Furthermore, as shown in Figure 7, the SRI-V has a relatively sharp cut-off characteristic for such small particles. Thus, it is particularly well suited for use as the final inertial stage in a multi-stage size-mass sampling instrument.

## PREDICTIVE RELATIONS

Chan and Lippmann[27] showed that previously proposed predictive relations for cyclone efficiency (Rosin, et al.,[28] Lapple,[29] Leith and Licht,[31] and Beeckmans[32]) are inconsistent with experimental observations in tests using low concentrations of monodisperse test aerosols. Using a hyperbolic tangent relation

for cyclone performance first developed by Blachman and Lippmann,[9] they also described the empirical constants of this equation for four commercially available small cyclones which have been used in air sampling and for several Stairmand-type cyclones. It should be noted that the previous predictive theories were developed from test data on, and have primarily been applied to, cyclones used for air cleaning applications.

Hochstrasser[24] and John, et al.[14] also attempted to adapt available predictive relations to their experimental data. Figure 8 shows the comparison of Hochstrasser's experimental data with the predicted values for one of the cyclones he tested. He concluded that for operational conditions where there was turbulent flow in the outlet pipe, either the Barth equation or the hyperbolic tangent formulation provided consistently good predictions. On the other hand, for operational conditions where the flow in the outlet pipe was laminar, only the Blachman and Lippmann formulation was consistently reliable. Both the Leith and Licht and the Lapple equations were unreliable for all cases.

John, et al.[14] compared their data to predictions based on the theoretical formulations of Lapple,[29] Sproull,[33] Leith and Licht,[31] and Barth.[30] They found that none of them fit the data, although the predicted slope of the efficiency curve from the Barth relation was closer to that observed than were any of the others. They did not attempt to fit their data to the hyperbolic tangent relation of Blachman and Lippmann.[9]

The discrepancies between the conventional predictive theories and experimental performance could be due to any or all of the following differences between the conditions within cyclones used in air cleaning as opposed to cyclones used in air sampling: (1) in air cleaning, the concentrations are much higher than the ambient aerosols; (2) in air sampling cyclones, the particles usually remain on the wall where they were initially deposited, while in air cleaning cyclones, deposited particles are continually scoured from the initial deposition sites and migrate to the collecting hopper; (3) the flow patterns in air cleaning cyclones are always turbulent, while in the smaller cyclones used in air sampling, the flows may be completely or partially laminar.

The various cyclone theories are summarized in Table 1. The complete expression for the hyperbolic tangent equation as developed by Chan and Lippmann[27] is:

$$\eta = 0.5 + 0.5 \tanh\left[B\left(\frac{D_p}{KQ^n}\right)^2 + (A - 2B)\frac{D_p}{KQ^n} + B - A\right]$$

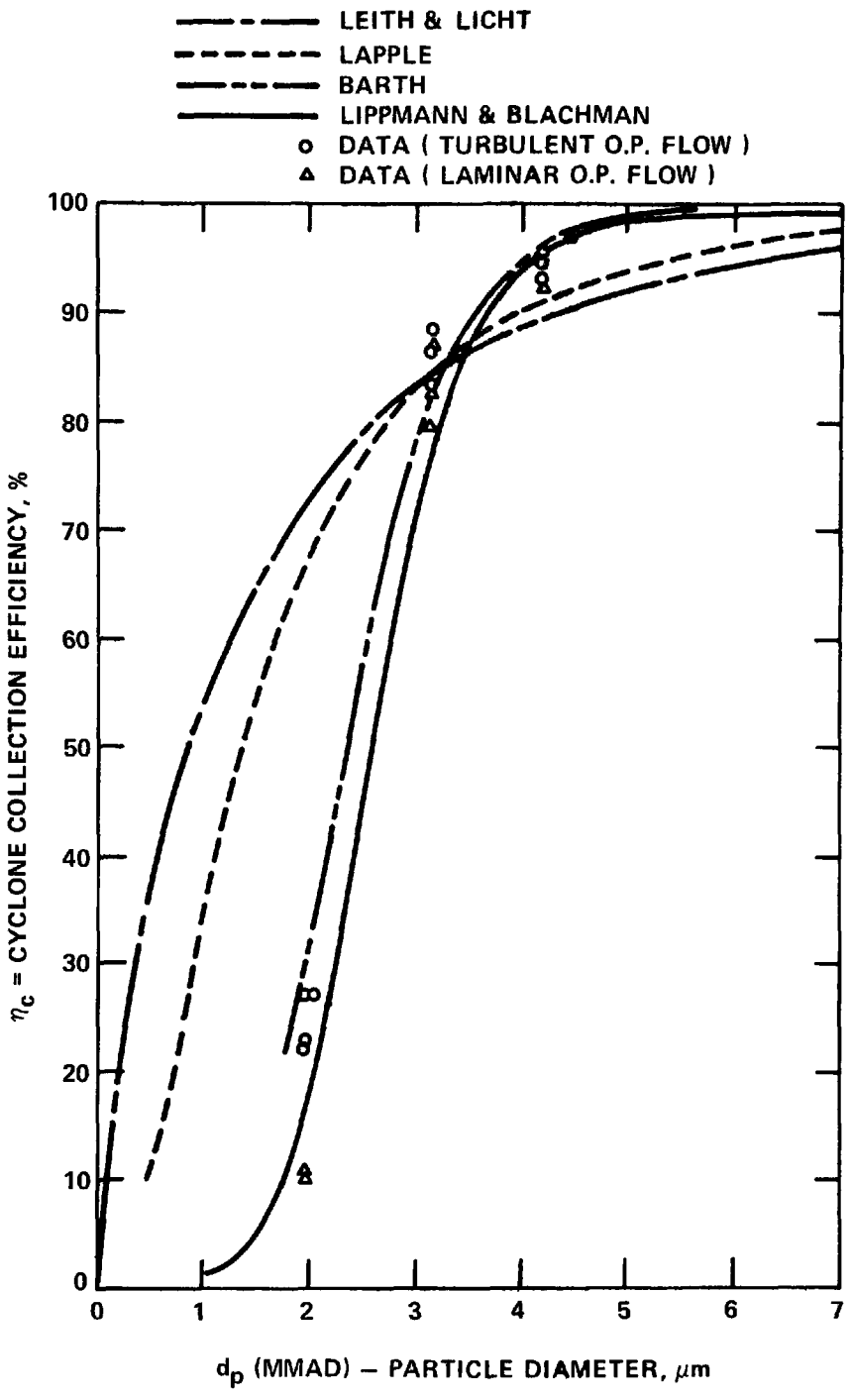


*Figure 8. Experimental cyclone collection data of Hochstrasser in comparison with predictions based on various predictive relations (from Hochstrasser[24]).*

The constants K and n are obtained from a plot of the experimentally determined particle cut sizes at several sampling rates. The constants A and B are determined using a least-squares fitting program for all of the pertinent experimental efficiency data.

A summary of the four empirical constants and the ranges of particle size and flow rate over which they apply is presented in Table 2 for eleven small cyclones for which a sufficient calibration data base exists.

## SUMMARY

Cyclones have many advantages over other inertial-type particle separators for the in-situ classification of sampled aerosols. They are much smaller, more easily portable, and less dependent on orientation than elutriators or centrifuges; they are much less subject to errors by misclassification due to particle bounce or overloading of collection surfaces than conventional jet impactors; and they are much simpler than virtual dichotomous samplers. On the other hand, the performance characteristics of properly designed and operated elutriators, centrifuges, jet impactors, and dichotomous samplers are predictable from first principles, while the prediction of cyclone performance is dependent on empirical calibration data. Therefore, better predictive relations for cyclone collection efficiency are needed in order to exploit the inherent advantages of cyclones for air sampling. A generalized predictive empirical relationship for cyclone performance has been developed and described. It has been applied to the available calibration data for the eleven small cyclones for which reliable calibrations exist, and the four characteristic constants have been determined for each. The equation permits the calculation of cyclone collection efficiency for any aerodynamic particle size and flow rate within the range established by the original calibration.

The cyclones evaluated vary considerably in their sharpness of cut. Some have coarse cut-off characteristics which match those of the ACGIH cut-off for "respirable" dust. Others have much sharper cut-off curves, comparable to those of jet impactors, and are, therefore, useful for multi-stage samplers for determining size-mass distributions.

TABLE 1. SUMMARY OF CYCLONE COLLECTION THEORIES

| | Category | Theory | Form of Equation | Reference |
|---|---|---|---|---|
| I. | Conventional | Rosin (1932) | $D_{50} = kQ^{-0.5}$ | 28 |
| | | Lapple (1951) | | 29 |
| | | Davies (1952) | | 34 |
| | | Barth (1956) | | 30 |
| II. | Semi-empirical | Sproull (1970) | $\eta = 1 - e^{f(D,Q)}$ | 33 |
| | | Leith and Licht (1972) | | 31 |
| III. | Theoretical | Beeckmans (1973) | $\eta = 1 -$ (infinite series with algebraic and exponential terms) | 32 |
| | | Soo (1973) | | 35 |
| IV. | Empirical | Wagner and Murphy (1971) | $D_{50} = kQ^{-n}$ | 36 |
| | | Lippman and Chan (1974) | $\eta = F\{\mathrm{Tanh}[f(D,D_{50})]\}$ | 12 |
| | | Chan and Lippmann (1977) | $\eta = F\{\mathrm{Tanh}[f(Q,D)]\}$ | 27 |
| | | Beeckmans and Kim (1978) | $\eta = F(St,Re)$ | 37 |

TABLE 2. EMPIRICAL CONSTANTS FOR CYCLONE EFFICIENCY CALCULATIONS

| Cyclone | $D_{pc}$, μm, AED | Q, ℓ/min | K | n | A | B | Reference |
|---|---|---|---|---|---|---|---|
| Aerotec 2 | 2.5-4.0 | 350-500 | 468.01 | -0.80 | 2.02 | -0.68 | 12 |
| UNICO 240 | 1.0-5.0 | 65-350 | 123.68 | -0.83 | 1.76 | -0.82 | |
| Aerotec 3/4 | 1.0-5.0 | 22-65 | 214.17 | -1.29 | 2.04 | -0.77 | |
| 10-mm nylon | 1.8-7.0 | 0.9-5.0 | 6.17 | -0.75 | 3.07 | -0.93 | 4 |
| | 1.0-1.8 | 5.8-9.2 | 16.10 | -1.25 | 1.19 | -0.59 | |
| | 0.1-1.0 | 18.5-29.6 | 178.52 | -2.13 | 0.74 | -0.07 | |
| BK-152 | 2.0-5.0 | 1150-2700 | 4591.0 | -0.98 | 0.914 | -0.111 | 37 |
| BK-76 | 1.0-3.0 | 400-1100 | 221.48 | -0.77 | 0.507 | -0.026 | |
| 19-mm UC-1 | 2.0-5.0 | 6-25 | 15.46 | -0.636 | 2.927 | -0.849 | 24 |
| AIHL | 2.0-7.0 | 8-27 | 52.48 | -0.99 | 2.906 | -0.547 | 14 |
| Sierra 220 CP | 1.0-10.0 | 7-85 | 48.08 | -0.86 | 2.163 | -0.370 | -- |
| SRI IV | 0.5-3.0 | 7-28 | 17.60 | -0.98 | 1.580 | -0.202 | 21 |
| SRI V | 0.3-2.0 | 7-28 | 14.00 | -1.11 | 4.928 | 3.347 | |

ACKNOWLEDGEMENT

This study was part of a center program supported by Grant No. ES-00260 from the National Institute of Environmental Health Sciences.

REFERENCES

1. AIHA Aerosol Technology Committee. Guide for Respirable Mass Sampling. J. Am. Ind. Hyg. Assoc. 31:133-137, 1970.

2. Lippmann, M. "Respirable" Dust Sampling. J. Am. Ind. Hyg. Assoc. 31:138-159, 1970.

3. Lippmann, M. Size-Selective Sampling for Inhalation Hazard Evaluations. In: Fine Particles, B.Y.H. Liu, ed. Academic Press, New York, 1976. pp. 287-310.

4. Lippmann, M., and W.B. Harris. Size-Selective Samplers for Estimating "Respirable" Dust Concentrations. Health Phys. 8:155-163, 1962.

5. Kotrappa, P. Revision of Lippmann-Harris Calibration for Two-Stage Sampler Using Shape Factor. Health Phys. 20:350-351, 1971.

6. Ettinger, H.J., J.E. Partridge, and G.W. Royer. Calibration of Two-Stage Air Samplers. J. Am. Ind. Hyg. Assoc. 31:537-545, 1970.

7. Lippmann, M., and A. Kydonieus. A Multi-Stage Aerosol Sampler for Extended Sampling Intervals. J. Am. Ind. Hyg. Assoc. 31:730-738, 1970.

8. Seltzer, D.F., W. Bernaski, and J.R. Lynch. Evaluation of Size-Selective Presamplers. II. Efficiency of the 10-mm Nylon Cyclone. J. Am. Ind. Hyg. Assoc. 32:441-446, 1971.

9. Blachman, M.W., and M. Lippmann. Performance Characteristics of the Multi-Cyclone Aerosol Sampler. J. Am. Ind. Hyg. Assoc. 35:311-316, 1974.

10. Caplan, K.J., L.J. Doemeny, and S.D. Sorenson. Performance Characteristics of the 10-mm Cyclone Respirable Mass Sampler. Part I. Monodisperse Studies. J. Am. Ind. Hyg. Assoc. 38:83-95, 1977.

11. Tomb, T.F., and L.D. Raymond. Evaluation of Collecting Characteristic of Horizontal Elutriator and 10-mm Nylon Cyclone Gravimetric Dust Samplers. Presented at 1969 Annual Meeting, American Industrial Hygiene Association, Denver, May, 1969.

12. Lippmann, M., and T.L. Chan. Calibration of Dual-Inlet Cyclones for "Respirable" Mass Sampling. J. Am. Ind. Hyg. Assoc. 35:189-200, 1974.

13. Threshold Limits Committee. Threshold Limit Values of Airborne Contaminants for 1968. American Conference of Governmental Industrial Hygienists, Cincinnati, 1968.

14. John, W., G.P. Reisehl, and J.J. Wesolowski. Final Report, California Air Resources Board Contract No. A5-00487, February 1978.

15. May, K.R. The Cascade Impactor, an Instrument for Sampling Coarse Aerosols. J. Sci. Instrum. 22:187-195, 1945.

16. Laskin, S. The Modified Cascade Impactor. UR-129, University of Rochester Atomic Energy Project, Rochester, NY, August, 1950.

17. Bernstein, D., M.T. Kleinman, T.J. Kneip, T.L. Chan, and M. Lippmann. Development of a High-Volume Sampler for the Determination of Particle Size Distribution in Ambient Air. J. Air Pollut. Control Assoc. 26:1069-1072, 1976.

18. Chang, H.C. A Parallel Multicyclone Size-Selective Particulate Sampling Train. J. Am. Ind. Hyg. Assoc. 35:538-545, 1974.

19. Rusanov, A.A. Determination of the Basic Properties of Dust and Gases. In: Ochistka Dymovykh Gasov v Promyshlennoy Energetike, A.A. Rusanov, I.I. Urbakh, and A.P. Anastasiadi, eds. "Energiya". Moscow, 1969.

20. Smith, W.B., K.M. Cushing, G.E. Lacey, and J.D. McCain. Particulate Sizing Techniques for Control Device Evaluation. EPA-650/2-74-102a, U.S. Environmental Protection Agency, Research Triangle Park, NC, 1975. 132 pp.

21. Smith, W.B., and R.R. Wilson. Development and Laboratory Evaluation of a Five-Stage Cyclone System. EPA-600/7-78-008, U.S. Environmental Protection Agency, Research Triangle Park, NC, 1978. 66 pp.

22. Marple, V.A., and K. Willeke. Inertial Impactors: Theory, Design and Use. In: Fine Particles, B.Y.H. Liu, ed. Academic Press, New York, 1976. pp. 411-446.

23. Twomey, S. Comparison of Constrained Linear Inversion and an Iterative Nonlinear Algorithm Applied to the Indirect Estimation of Particle Size Distributions. J. Comput. Phys. 18:188-200, 1975.

24. Hochstrasser, J.M. The Investigation and Development of Cyclone Dust Collector Theories for Application to Miniature Cyclone Presamplers. Ph.D. Thesis, Department of Environmental Health, College of Medicine, Univ. of Cincinnati, 1976.

25. Löffler, F. The Calculation of Centrifugal Separators. Staub Reinhalt. Luft (in English) 30:1-5, Dec. 1970.

26. Mercer, T.T. Aerosol Technology in Hazard Evaluation. Academic Press, New York, 1973. pp. 297-304.

27. Chan, T.L., and M. Lippmann. Particle Collection Efficiencies of Air Sampling Cyclones: an Empirical Theory. Environ. Sci. Technol. 11:377-382, 1977.

28. Rosin, P., E. Rammler, and W. Intelman. Principles and Limits of Cyclone Dust Removal. Z. Ver. Deut. Ing. 76:433-437, 1932.

29. Lapple, C.E. Dust and Mist Collection. In: Chemical Engineers' Handbook, J.H. Perry, ed. McGraw-Hill, New York, 1963.

30. Barth, W. Calculation and Design of Cyclones on the Basis of Recent Tests. Brennst. Waerme Kraft 8:1-9, 1956.

31. Leith, D., and W. Licht. The Collection Efficiency of Cyclone Type Particle Collectors--A New Theoretical Approach. AIChE Symp. Ser. No. 126, 68:196-206, 1972.

32. Beeckmans, J.M. A Two-Dimensional Turbulent Diffusion Model of the Reverse Flow Cyclone. J. Aerosol Sci. 4:329-336, 1973.

33. Sproull, W.T. Air Pollution and Its Control. Exposition Press. NY, 1970.

34. Davies, C.N. The Separation of Airborne Dust and Particles. Proc. Inst. Mech. Eng. London B (1):185-198, 1952.

35. Soo, S.L. Particle-Gas Surface Interactions in Collection Devices. Int. J. Multiphase Flow 1:89-101, 1973.

36. Wagner, J., and R.S. Murphy. Miniature Liquid Cyclones—Effects of Fluid Properties on Performance. Ind. Eng. Chem. Process Des. Dev. 10:346-352, 1971.

37. Beeckmans, J.M., and C.J. Kim. Analysis of the Efficiency of Reverse Flow Cyclones. Can. J. Chem. Eng., in press.

PAPER 3

# RESEARCH ON DUST SAMPLING AND MEASUREMENT IN OUR LABORATORY

KOICHI IINOYA
DEPARTMENT OF CHEMICAL ENGINEERING
KYOTO UNIVERSITY

## ABSTRACT

The presentation includes four topics of particle sampling and measurement studied in our laboratory during the last few years.

1. Anisokinetic sampling errors by round and slit probes for wide ranges of Reynolds number and inertia parameter.

2. Sampling efficiency for particles by a ribbon which has various inclination angles to the flow direction for wide ranges of Reynolds number.

3. Fractional efficiency of impactor, taking into account velocity distributions in the boundary layer at nozzle outlet.

4. Effect of probe diameter on isokinetic sampling error in experiments.

Details of the four research topics are given in the following sections.

## ANISOKINETIC SAMPLING ERRORS OF PARTICLE CONCENTRATION BY ROUND AND SLIT PROBES

In order to examine the errors in measuring particle concentration due to anisokinetic sampling over a wide range of inertia parameters, theoretical and experimental studies have been conducted.[1,2] In the experiments, a monodisperse methylene blue-uranine aerosol generated by a spinning disc and lycopodium

spores were sampled by a round and a slit type probe respectively as shown in Figures 1 and 2. Figure 3 shows the details of these two kinds of test probes. The experimental conditions are given in Table 1.

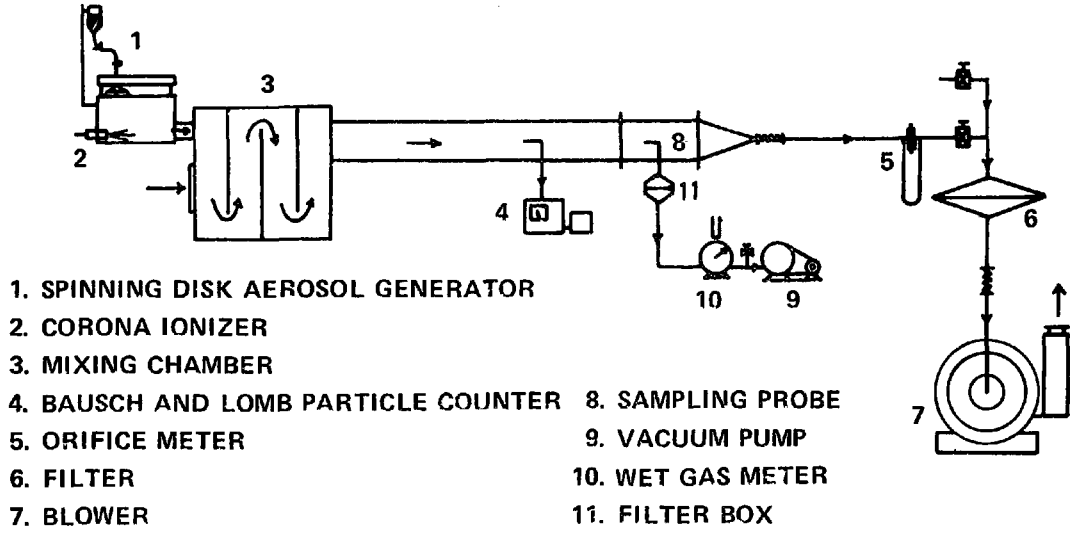


*Figure 1. Schematic diagram of horizontal experimental apparatus for methylene blue-uranine aerosol by spinning disc generator.*

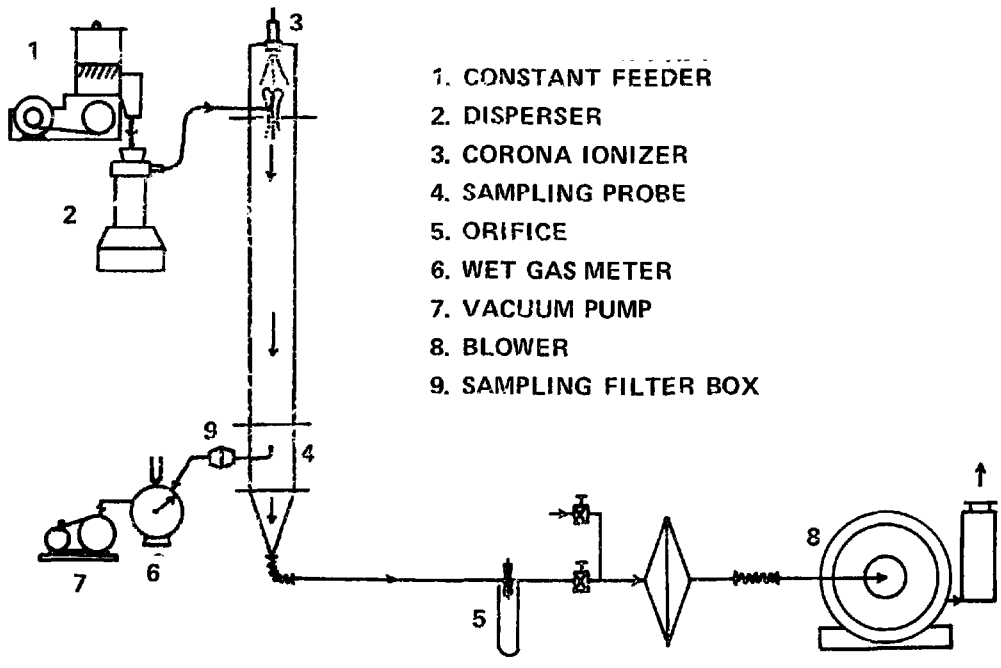


*Figure 2. Schematic diagram of vertical experimental apparatus for lycopodium spores.*

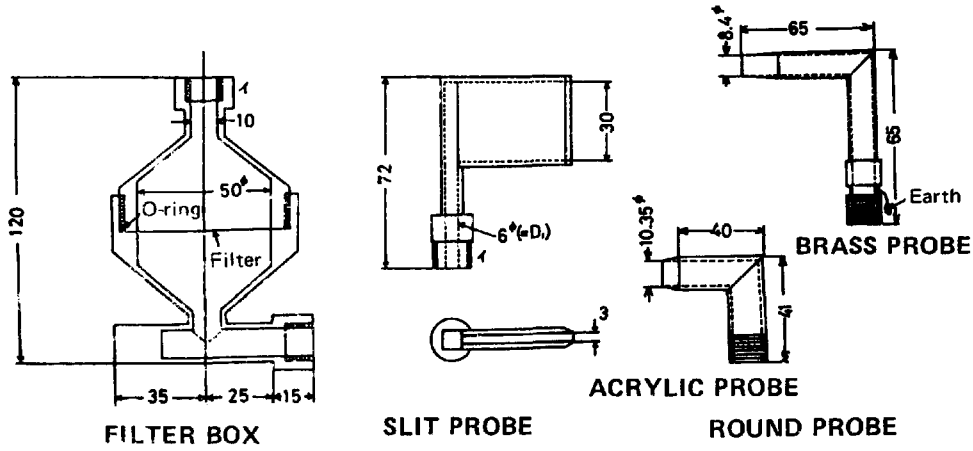


*Figure 3. Sampling probes and filter box.*

TABLE 1. EXPERIMENTAL CONDITIONS

| Particles | Particle size, $D_{p50}$ (μm) | Geometric standard deviation, $\sigma_g$ | Particle density, $\rho_p$ (g/cm$^3$) | Concentration in liquid (wt %) |
|---|---|---|---|---|
| Lycopodium spores | 33 (24) | 1.09 | 1.05 | - |
| Methylene blue-uranine | 3.5 | 1.07 | 1.42 | 0.21 |
| Methylene blue-uranine | 4.3 | 1.07 | 1.42 | 0.5 |
| Air Velocity, $u_0$ (m/sec) | | 0.2 - 15.0 | | |
| Inertia Parameter, P | | 0.05 - 3.4 | | |
| Flow Reynolds Number | | (1.1 - 81) x $10^3$ | | |

Theoretical results obtained under the assumption of potential flow are mostly in good agreement with experimental data for both types of probe, as shown in Figures 4, 5 and 6. However, the anisokinetic sampling errors obtained from experiments with the slit probe are smaller than the calculated values in the large inertia region (lycopodium), as shown in Figure 7. In general, it is possible to use these figures to estimate

anisokinetic sampling errors. It is also recognized that the concentration errors become smaller as the sampling velocity (u) becomes extremely high. Therefore, the super high speed sampling may be a practically simple method for particulate sampling without the tedious procedure of isokinetic sampling.

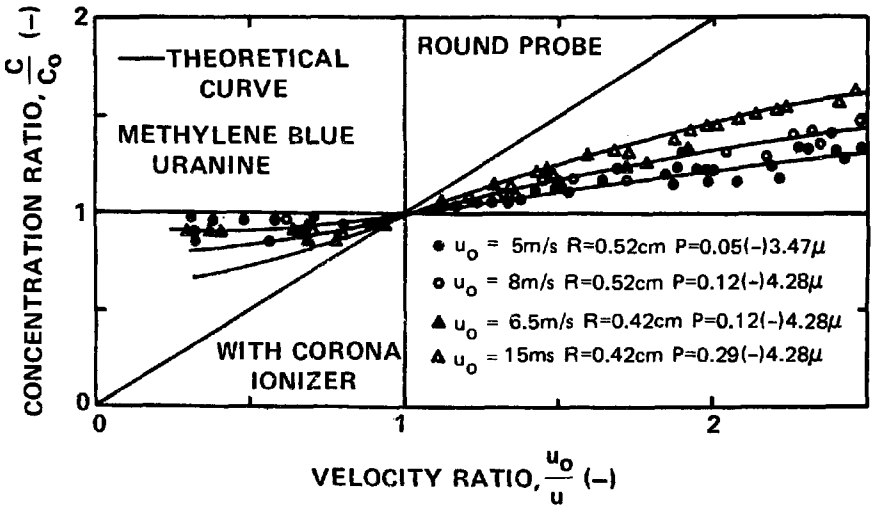


*Figure 4. Anisokinetic sampling errors of round probe for smaller particles (methylene blue-uranine particles).*

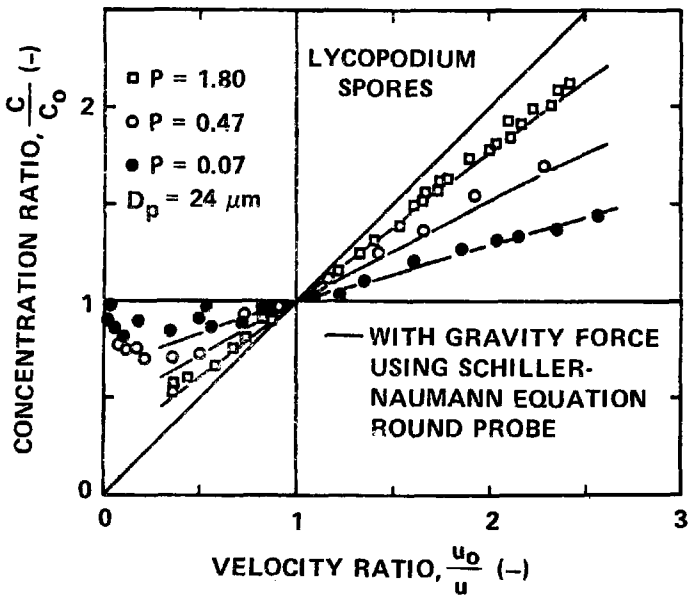


*Figure 5. Anisokinetic sampling errors of round probe for larger particles (lycopodium spores).*

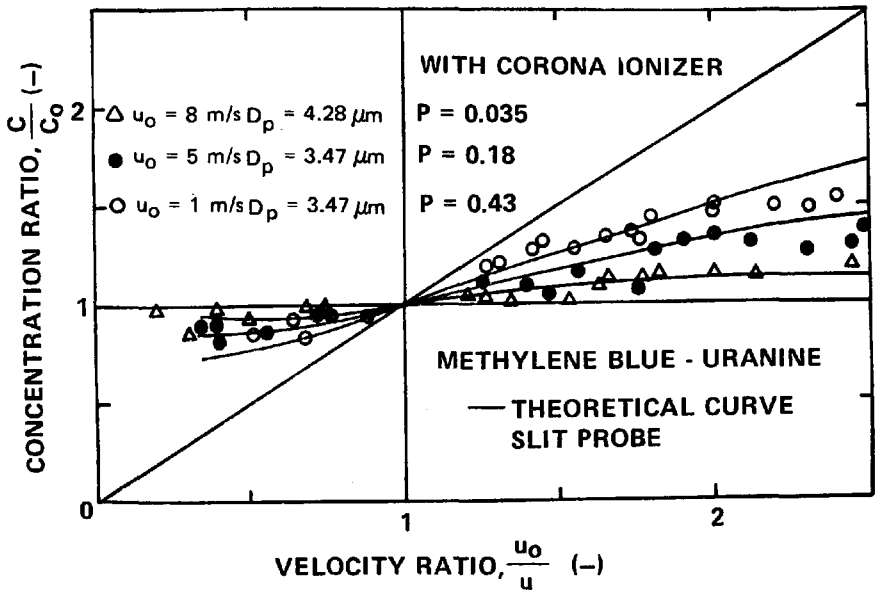


*Figure 6. Anisokinetic sampling errors of slit probe for smaller particles (methylene blue-uranine particles).*

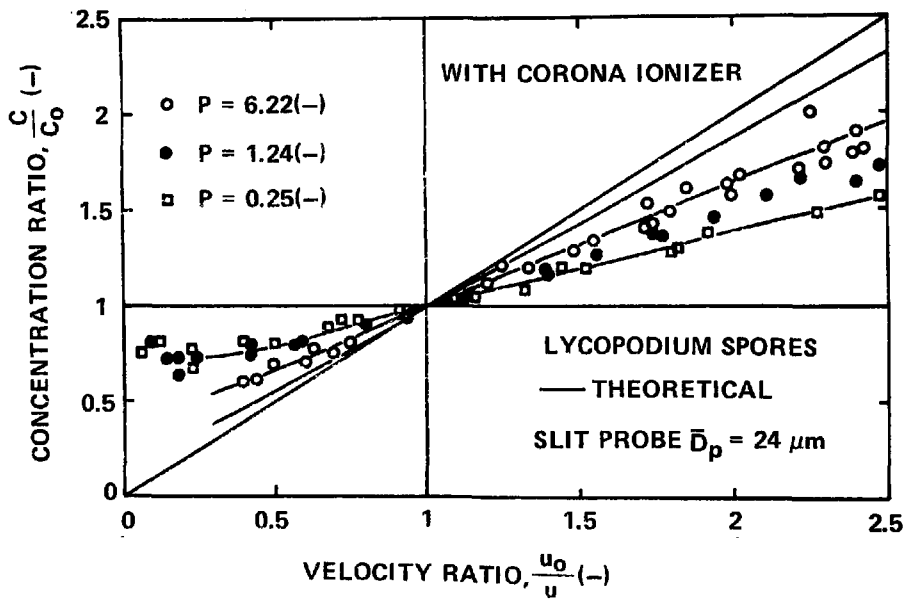


*Figure 7. Anisokinetic sampling errors of slit probe for larger particles (lycopodium spores).*

The amounts of particulate deposited in the probe and the sampling tube are also examined. It is found that the deposit shows a minimum value at Reynolds numbers of 2000 to 3000 for

both probes, as shown in Figures 8 and 9, and that the amount of deposit in an acrylic probe is much more than that in a brass one, as shown in Figure 8.

Nomenclature

$c$ : measured concentration

$c_0$ : mainflow concentration

$D_p$ : particle diameter

$M_p$ : deposited mass in the probe and sampling tube

$M_f$ : collected mass on the filter

$P$ : inertia parameter = $\rho_p D_p^2 u_0/(18\mu R) = 2\Psi$

$R$ : probe radius

$u$ : sampling velocity

$u_0$ : main gas velocity

Re : Reynolds number in sampling probe

$\rho$ : gas density

$\rho_p$ : particle density

$\mu$ : gas viscosity

SAMPLING EFFICIENCY FOR PARTICULATES BY RIBBON

Average and local impaction efficiencies for a ribbon, at various angles of inclination to the flow direction, have been calculated for a wide range of particle Reynolds numbers from the Stokes to Newton regions.[3] The calculations were based on a discontinuous potential flow model[4-10], which is in good agreement with the observation of paraffin mist streamlines around the ribbon as shown in Figure 10.

The experimental apparatus is shown in Figure 11. The calculated sampling efficiencies agree well with the experimental results of lycopodium spores, which have a settling velocity of 1.76 cm/sec in air, as shown in Figures 12 and 13. The efficiency decreases as the particle Reynolds number increases for the region beyond the Stokes one. The smaller the inclination angle of a ribbon, the higher the sampling efficiency. This tendency is also observed beyond the Stokes region as shown in Figure 14. Local impaction efficiencies are higher at the

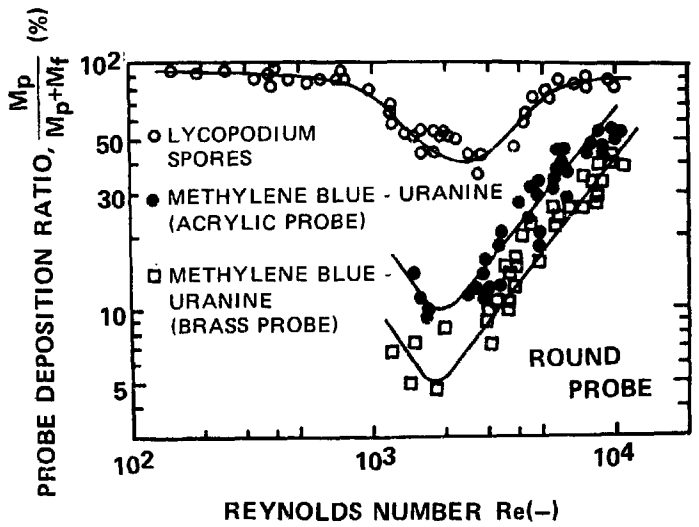


*Figure 8. Relationship between deposition ratio and Reynolds number in round probe.*

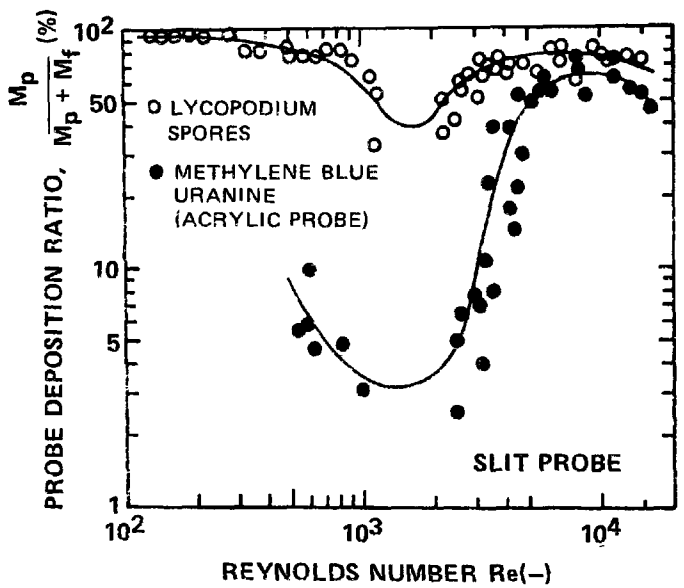


*Figure 9. Relationship between deposition ratio and Reynolds number in slit probe.*

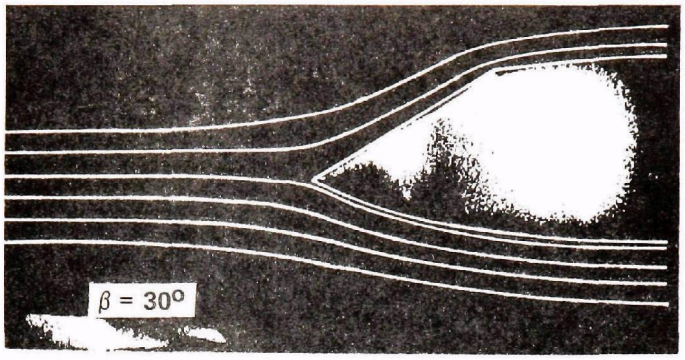


*Figure 10. Calculated streamlines superimposed on photograph of wake.*

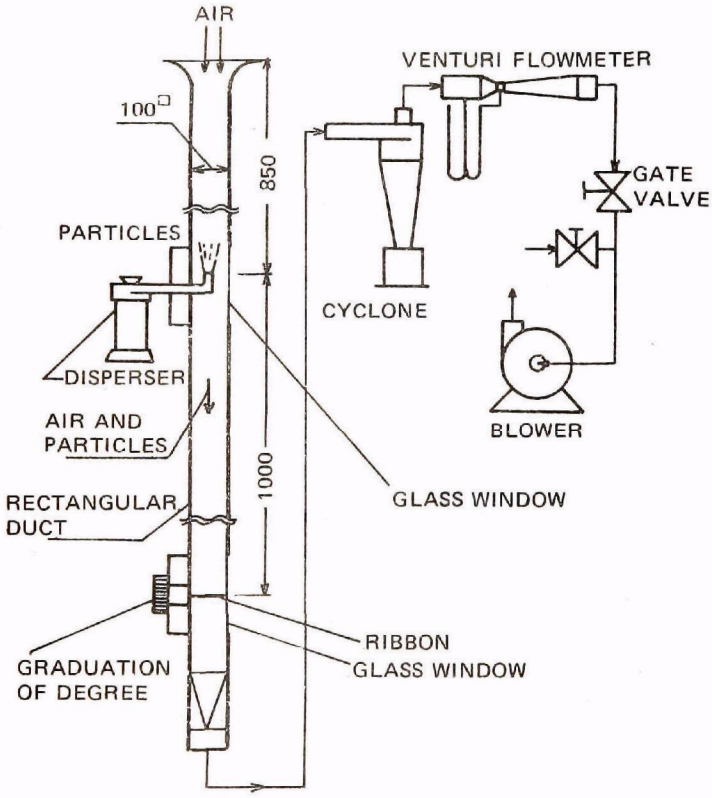


*Figure 11. Schematic diagram of experimental apparatus.*

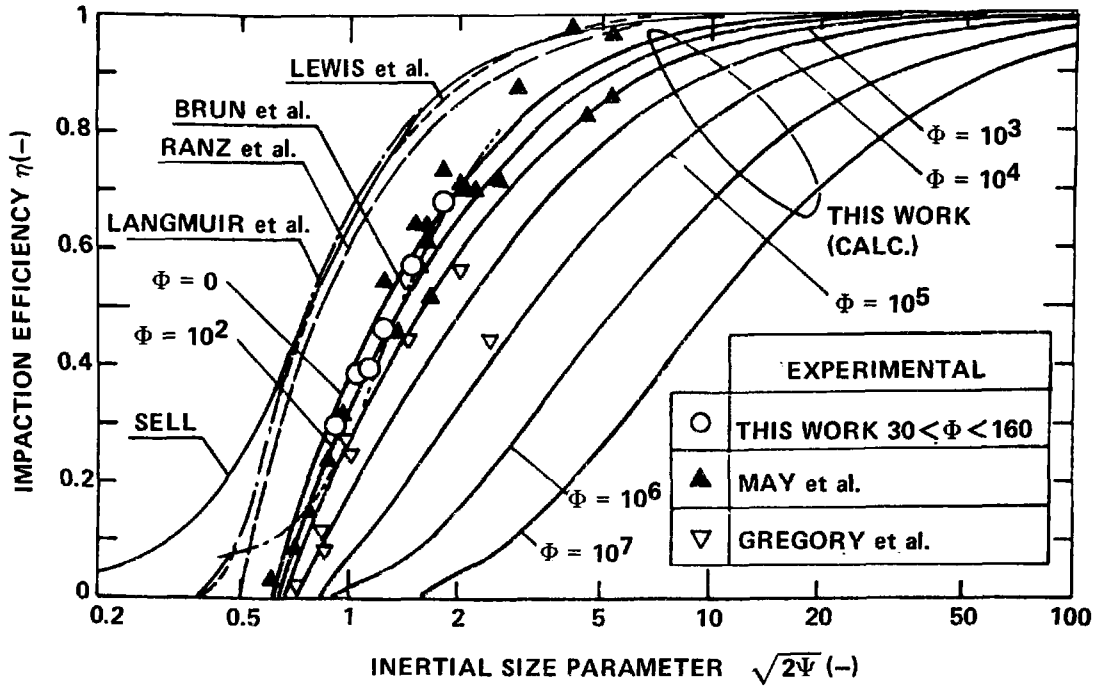


*Figure 12. Relation between impaction efficiency and inertia parameter for a ribbon perpendicular to the flow.*

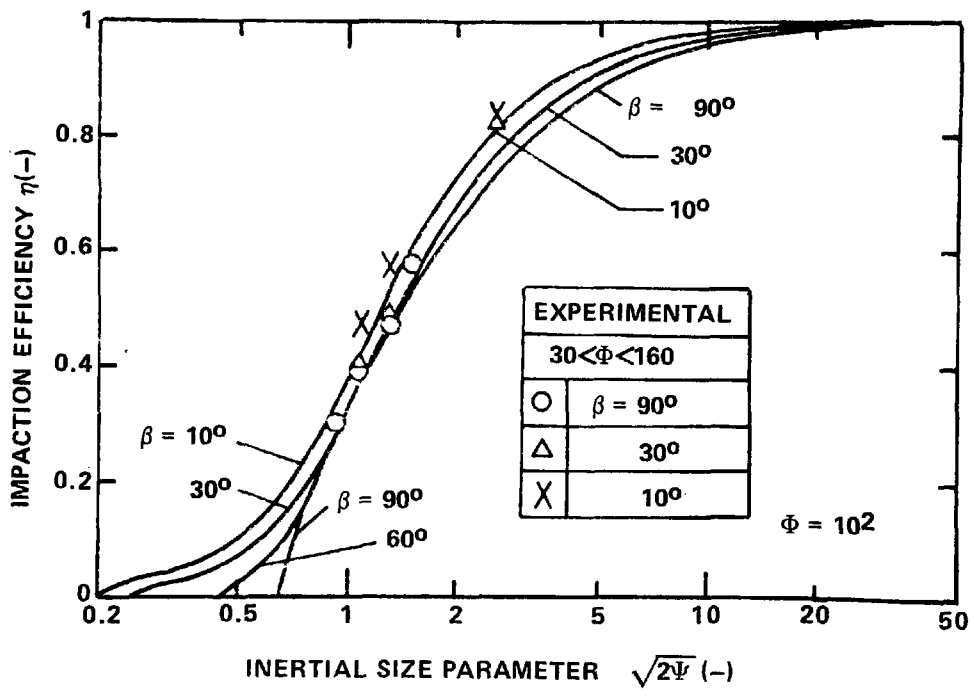


*Figure 13. Relation between impaction efficiency and inertia parameter for a ribbon inclined to the flow at $\phi = 10^2$.*

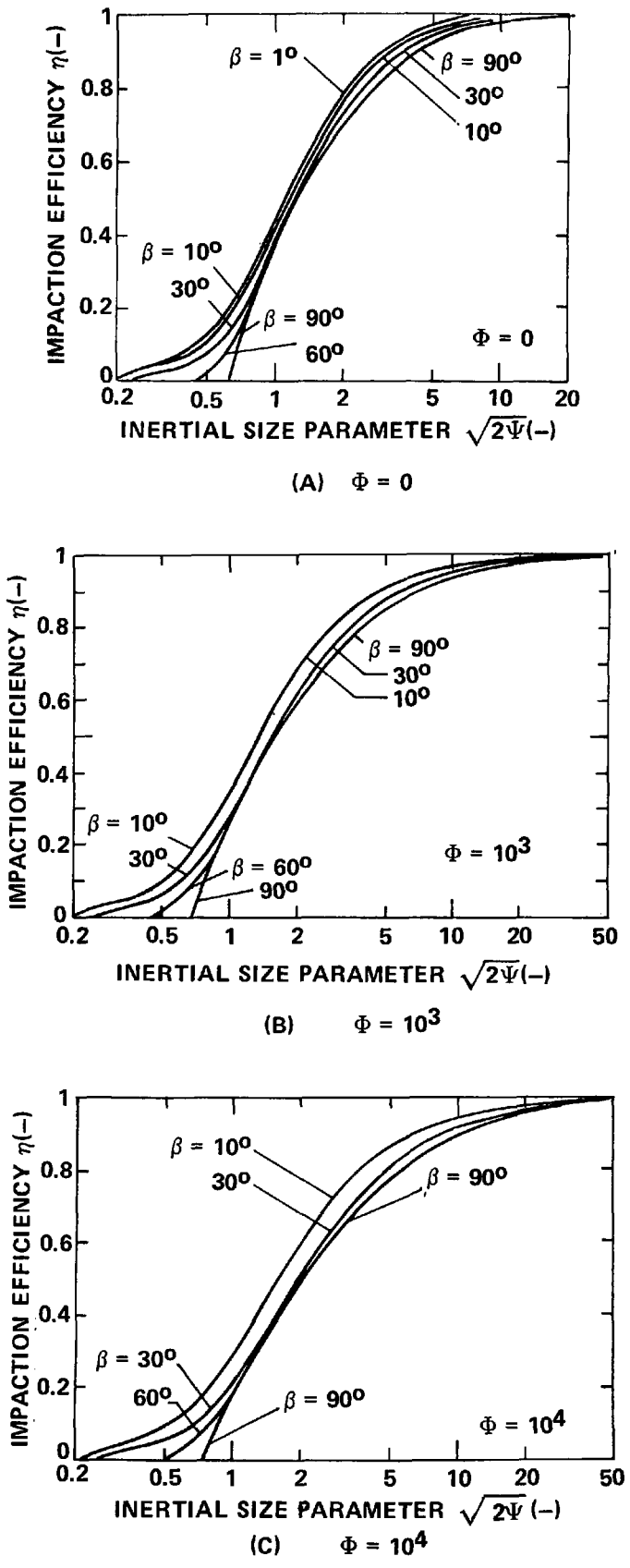


*Figure 14. Relations between impaction efficiency and inertia parameter for a ribbon inclined to the flow at $\phi = 0$ (Stokes flow), $10^3$, and $10^4$.*

leading edge ($\bar{x}$=1) than those at the trailing edge ($\bar{x}$=-1) of an inclined ribbon. The average sampling efficiencies are determined along the transverse line at a distance of 20% of ribbon width from the leading edge, as shown in Figure 15A. Therefore, the microscopic observation of sampled particles should be conducted along this line. Experimental local impaction efficiencies are generally in good agreement with the theoretical results as shown in Figures 15 A and C. As the inclination angle becomes smaller than 90 degrees, the local impaction efficiencies are higher at the leading edge and lower at the trailing edge of the ribbon than those of 90 degrees, and the efficiencies of the inclined ribbons change little at the center line of ribbon, compared with those of 90 degrees, as shown in Figures 15 A, B, C.

Nomenclature

$D_p$ : particle diameter

$r$ : half width of ribbon

$Re_{p0}$ : particle Reynolds number for main gas velocity ($=D_p\rho u_0/\mu$)

$u_0$ : main air velocity

$x$ : distance from the center line of ribbon

$\beta$ : inclination angle of ribbon to flow direction

$\eta$ : impaction (sampling) efficiency

$\eta_x$ : local impaction efficiency

$\rho$ : air density

$\rho_p$ : particle density

$\mu$ : air viscosity

$\Phi$ : parameter which accounts for particle motion beyond Stokes' law = $Re_{p0}^2/(2\Psi)$

$\Psi$ : inertia parameter for Stokes' law = $D_p^2\rho_p u_0/(36\mu r)$

FRACTIONAL EFFICIENCIES OF ROUND AND SLIT NOZZLE IMPACTORS

Separation mechanisms of an impactor have usually been studied by use of a potential flow model. However, there is some discrepancy between such theoretical results and the experimental data. In the present study, the theoretical impaction efficiencies have been calculated, taking into account the velocity

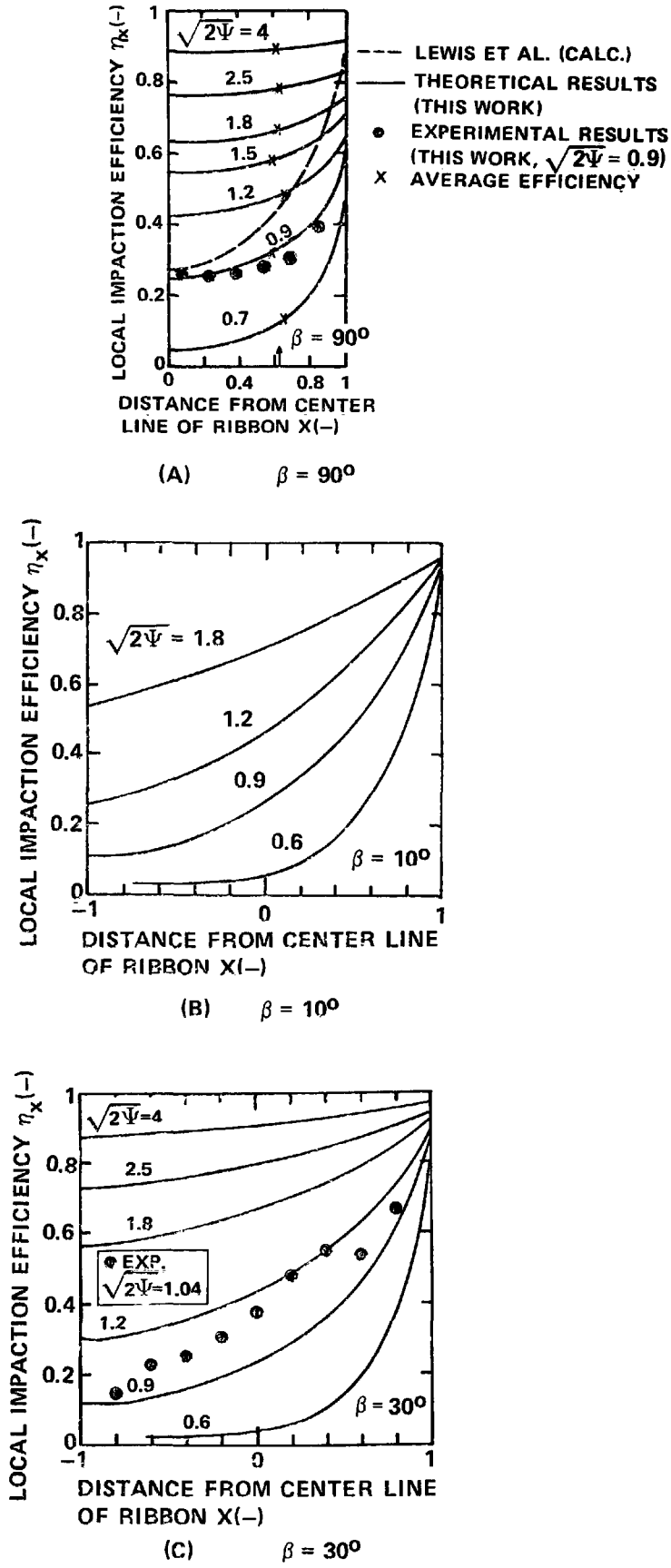


*Figure 15. Local impaction efficiencies for a ribbon of various inclined angles at $\Phi$ = 0 (Stokes flow).*

boundary layer of incompressible gas at the nozzle outlets. The theoretical results are in good agreement with the experimental values for a round[11,12] and a slit nozzle impactor, respectively. Figure 16 shows the fractional efficiency of a slit nozzle impactor as an example.

Effect of the clearance ratio ($R_C$), which is defined as the ratio of the distance between nozzle and impaction plate to the nozzle diameter, on the fractional efficiency has been calculated by use of a potential flow model[13] for a round nozzle impactor, as shown in Figure 17.[14] The calculated efficiencies are in good agreement with experimental results for the ratios of 2, 1, 0.5, 0.33 and 0.25 as shown in Figure 18 as an example. Table 2 gives the approximate straight line equations of these fractional curves.

Particle precipitating efficiencies on the inner wall of a slit nozzle impactor have also been theoretically calculated by use of a velocity distribution[15] in the region where the motion of a particle is mainly influenced by gravitational and inertia forces. The nozzle and the calculated efficiencies are shown in Figures 19 to 23.[16] The experimental results obtained by use of lycopodium spores and ragweed pollens are in good agreement with the calculated precipitating efficiencies, as shown in Figure 24.

TABLE 2. APPROXIMATE EQUATIONS OF FRACTIONAL EFFICIENCIES FOR VARIOUS CLEARANCE RATIOS OF ROUND NOZZLE IMPACTOR

| Clearance ratio, $R_C$ | Approximate equations of fractional efficiency, $\eta_T$ |
|---|---|
| 5 | $2.34\sqrt{\Psi} - 0.427$ |
| 3 | $3.17\sqrt{\Psi} - 0.649$ |
| 1-3 | $3.80\sqrt{\Psi} - 0.954$ (Ranz) |
| 1 | $4.74\sqrt{\Psi} - 1.05$ |
| 0.5 | $5.63\sqrt{\Psi} - 1.26$ |

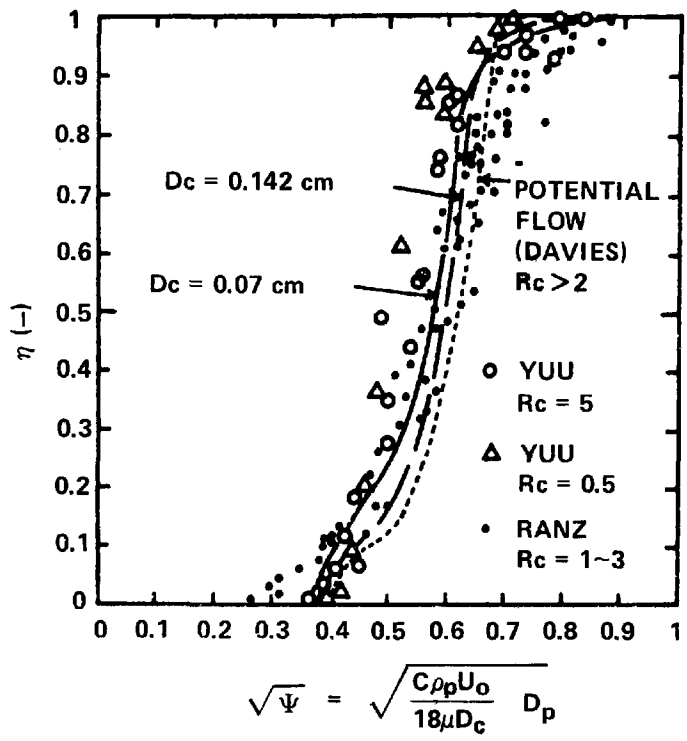


*Figure 16. Relation between fractional efficiency and inertia parameter for a slit nozzle impactor (S. Yuu).*

Nomenclature

- $C$ : Cunningham slip correction factor
- $D_c$ : nozzle diameter or width at outlet
- $G$ : gravitational parameter or dimensionless settling velocity = $C\rho_p D_p^2 g/(18\mu u_0)$
- $L$ : distance from nozzle outlet to impaction plate
- $\bar{L}$ : dimensionless nozzle length = $\ell/D_c$
- $\ell$ : length of converging part of nozzle
- $R_c$ : clearance ratio = $L/D_c$
- $Re_j$ : Reynolds number based on nozzle outlet
- $u_0$ : gas velocity at nozzle outlet
- $\alpha$ : half-angle of converging nozzle
- $\eta$ : impaction (target or fractional) efficiency

$\eta_{wc}$ : calculated precipitating efficiency on the inner nozzle wall

$\Psi$ : inertia parameter = $CD_p^2\rho_p u_0/(18\mu D_c)$

EFFECT OF PROBE DIAMETER ON ISOKINETIC SAMPLING ERRORS

In order to examine the effect of probe diameter on isokinetic sampling errors, experimental studies have been conducted using methylene blue-uranine aerosol and lycopodium spores in the small and large inertia regions respectively.[17] It is found that the standard deviation of concentration ratio, defined as the concentration measured by a probe of any diameter divided by that of a 1-cm diameter probe, becomes larger as the probe diameter decreases. The following empirical equations are obtained by use of the method of least squares, assuming that the standard deviation is inversely proportional to the square root of sampling amount W.

$$\sigma = 9.19 \times 10^{-3}\ W^{-0.5}\ d^{-0.31};\ \text{for lycopodium} \quad (1)$$

$$\sigma = 7.25 \times 10^{-4}\ W^{-0.5}\ d^{-0.28};\ \text{for methylene blue-uranine} \quad (2)$$

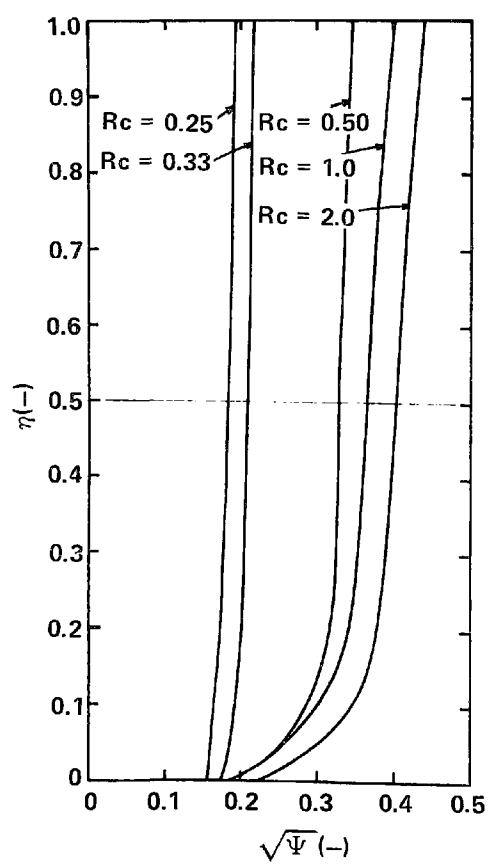


*Figure 17. Relation between fractional efficiency and inertia parameter for various clearance ratios of a round nozzle impactor.*

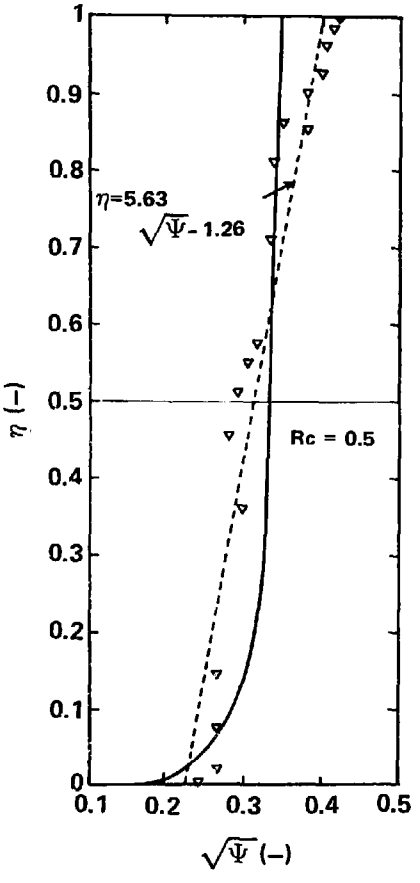


*Figure 18. Relation between fractional efficiency and inertia parameter for clearance ratio $R_c$ = 0.5 of a round nozzle impactor.*

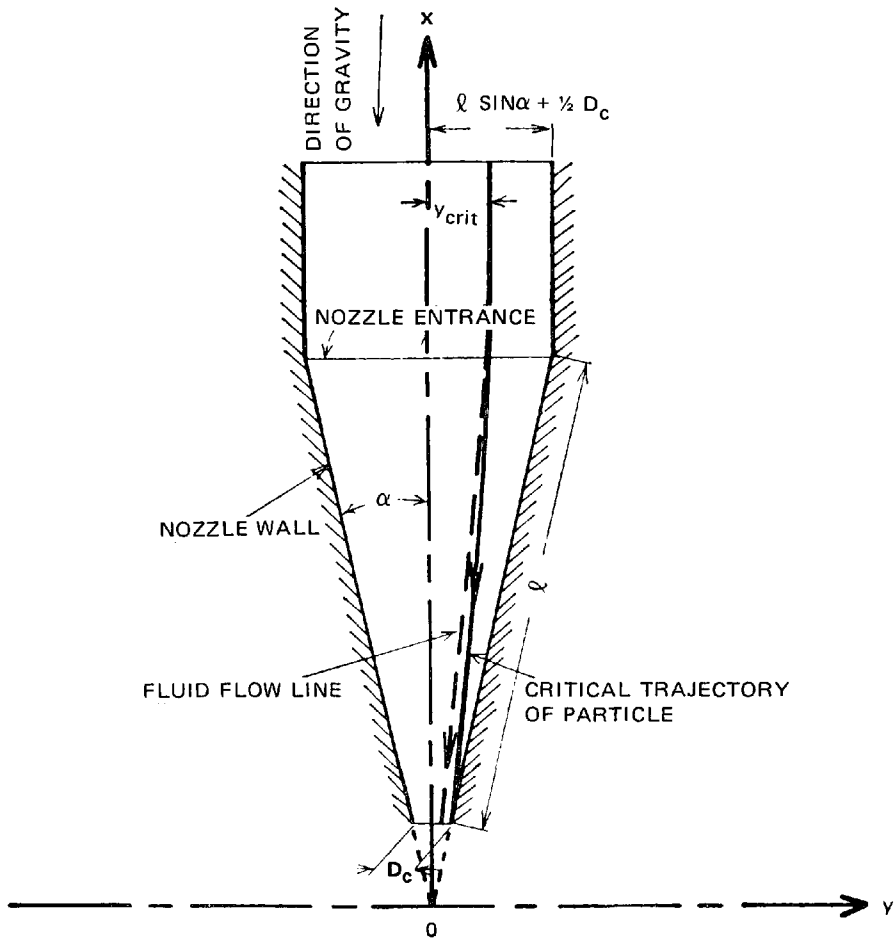


*Figure 19. Schematic diagram of two-dimensional nozzle.*

A comparison of experimental data with the results calculated by the above equations is shown in Figure 25.

It is also found in the small inertia region that the mean values of concentration ratio measured by smaller diameter probes differ with each other and significantly deviate from unity in some cases, as shown in Figure 26.

$c$ : mean measured concentration ($g/m^3$)

$c_0$ : mean measured concentration for 1-cm reference probe diameter ($g/m^3$)

$d$ : inner probe diameter (cm)

$n$ : number of trial

$u_0$ : main flow velocity far upstream of probe (m/sec)

W : amount of sample (g)

$\sigma$ : nondimensional standard deviation of sample

$\sigma_1$ : nondimensional standard deviation by reference probe of 1 cm diameter

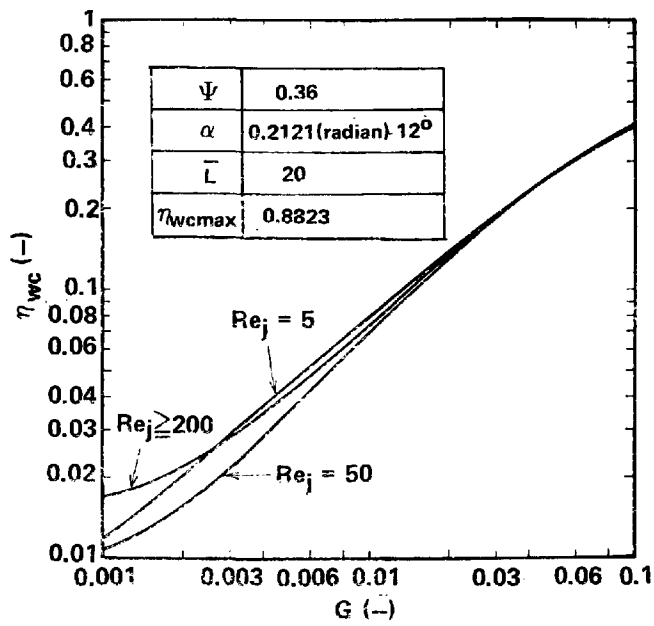


*Figure 20. Calculated settling efficiencies for different Reynolds numbers, taking account of air velocity distribution at nozzle entrance.*

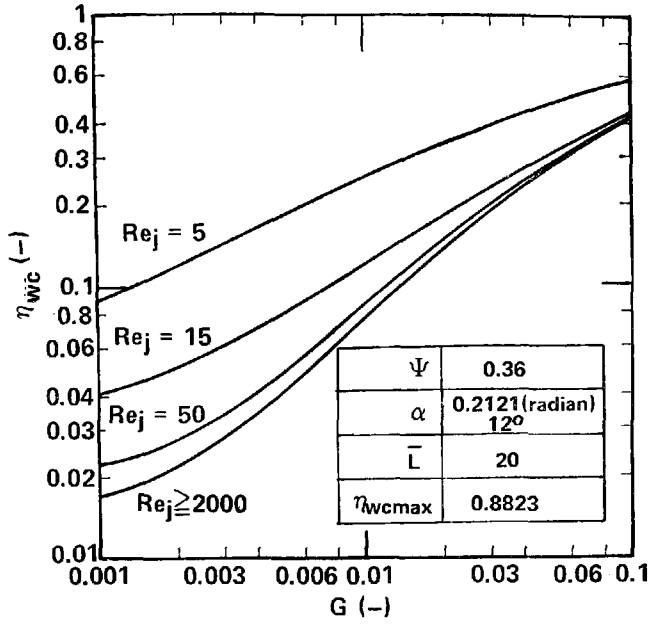


*Figure 21. Calculated settling efficiencies for different Reynolds numbers with uniform air velocity at nozzle entrance.*

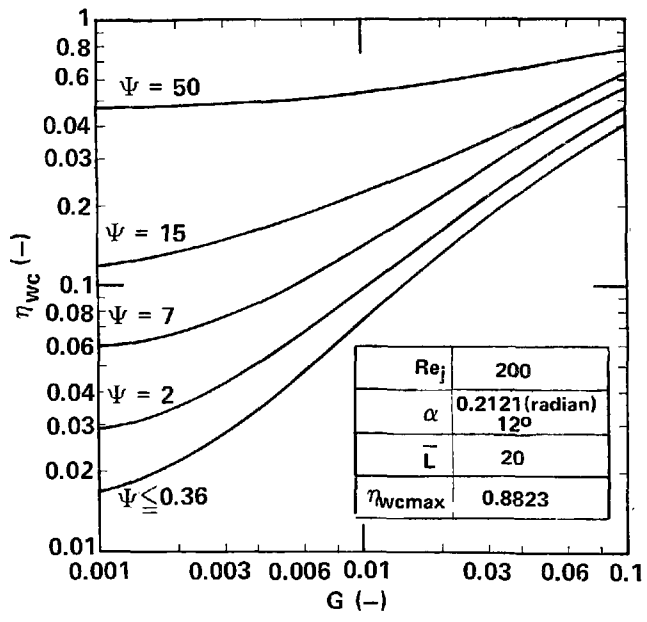


*Figure 22. Calculated settling efficiencies for various inertia parameters, taking account of air velocity distribution at nozzle entrance.*

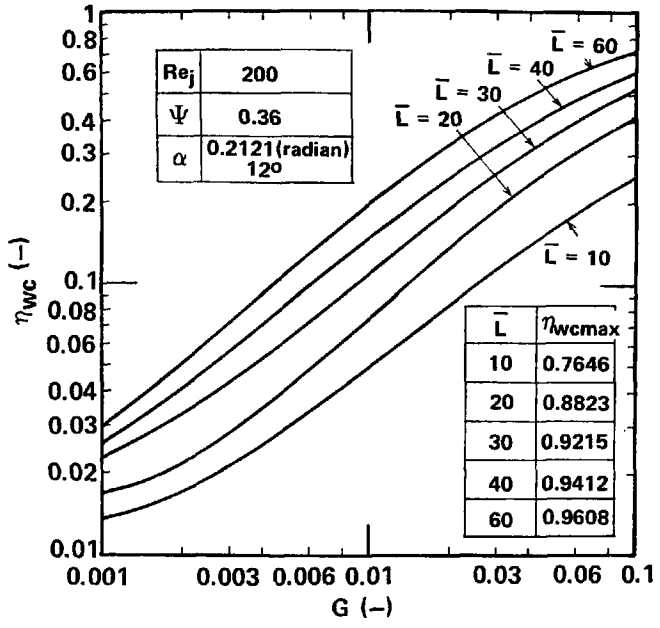


*Figure 23. Calculated settling efficiencies for various nozzle lengths, taking account of air velocity distribution at nozzle entrance.*

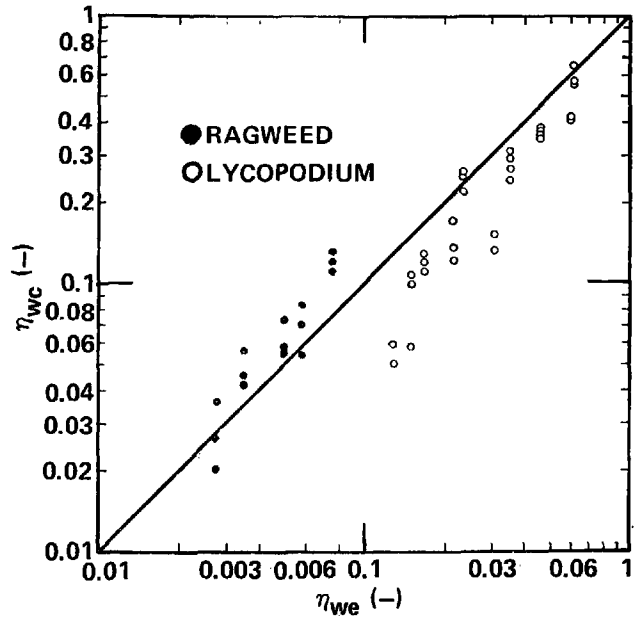


*Figure 24. Comparison of experimental settling efficiencies with calculated ones.*

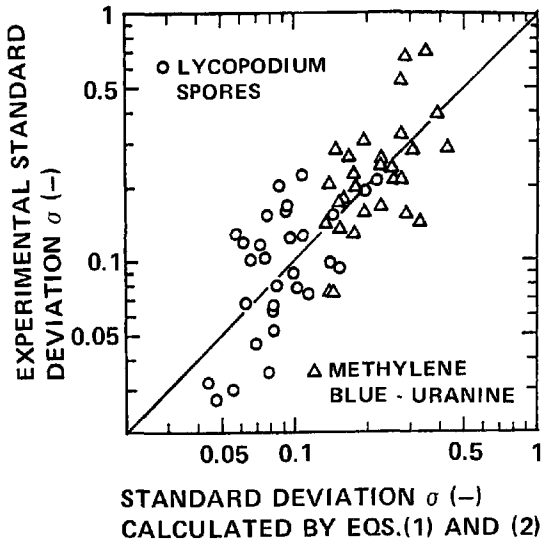


*Figure 25. Comparison of experimental and calculated standard deviations of concentration ratio.*

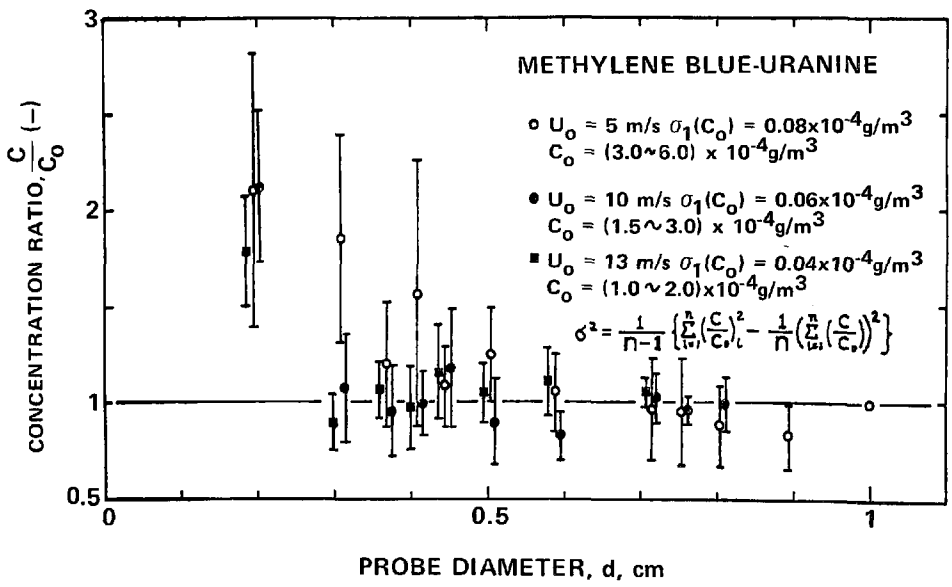


*Figure 26. Experimental relation between concentration ratio and probe diameter for methylene blue-uranine aerosol.*

REFERENCES


1. Yoshida, H., T. Osugi, H. Masuda, S. Yuu, and K. Iinoya. Kagaku Kogaku Ronbunshu 2:336, 1976.

2. Yoshida, H., T. Osugi, H. Masuda, and K. Iinoya. Zairyo: J. Soc. Material Sci. Japan. 25:667, 1976.

3. Ushiki, K., K. Kubo, and K. Iinoya. Kagaku Kogaku Ronbunshu 3:172, 1977.

4. Hess, J.L. J. Fluid Mech. 60:225, 1973.

5. Lewis, W., and R.J. Brun. NACA Tech. Note 3658, 1955.

6. Langmuir, I., and K.B. Blodgett. U.S. Army Air Force Tech. Rep. No. 548, 1946.

7. Brun, L.D., and M. Vasseur. Rech. Aeronaut. 15:1, 1948.

8. Ranz, W.E., and J.B. Wong. Ind. Eng. Chem. 44:1371, 1952.

9. May, K.R., and R. Clifford. Ann. Occup. Hyg. 10:83, 1967.

10. Gregory, P.H., and Q.J. Stedman. Ann. Appl. Biol., 40:651, 1953.

11. Iinoya, K. In: Fine Particles, B.Y.Liu, ed. Academic Press, New York, 1976. p 24.

12. Yuu, S., N. Miyake, and K. Iinoya. Kagaku Kogaku Ronbunshu 1:115, 1975.

13. Strand, T. J. Aircr. 4:466, 1967.

14. Yuu, S., and K. Iinoya. Kagaku Kogaku 34:427, 1970.

15. Rosenhead, H. Laminar Boundary Layers. Oxford Press, 1963. p. 114.

16. Yuu, S., and K. Iinoya. Kagaku Kogaku 35:1251, 1971.

17. Yoshida, H., et al. J. Chem. Eng. Japan 11:48, 1978.

PAPER 4

# SIZING SUBMICRON PARTICLES WITH A CASCADE IMPACTOR

MICHAEL J. PILAT
DEPARTMENT OF CIVIL ENGINEERING
UNIVERSITY OF WASHINGTON

## ABSTRACT

The UW Mark 3-4 Source Test Cascade Impactors and associated sampling train have been designed, constructed, and used for measuring the size distribution over the approximately 0.02 to 20 μm aerodynamic range. The UW Mark 4 Cascade Impactor utilizes low absolute gas pressure which results in large Cunningham correction factors and accordingly enables sizing of particles of 0.02 to 0.2 μm diameter. The Mark 3-4 sampling train includes the UW Mark 3 and Mark 4 Cascade Impactors followed by a 90 mm diameter filter, a low pressure drop tabular coiled condenser, a two-stage high vacuum pump, and an instrumental control box for pressure and temperature gauges, heater controls, and valves. The UW Mark 3-4C Cascade Impactors operate around 0.4 to 0.5 acfm whereas the UW Mark 3-4D model has a gas sampling flow rate in the 1.6 to 1.8 acfm (stack conditions) range. Particle size distributions measured at emission sources including the J.E. Corette Power Plant (pulverized coal-fired boiler), UW Power Plant (pulverized coal-fired boiler), and Kearny Power Plant (Pratt and Whitney oil-fired gas turbine) are presented.

## INTRODUCTION

Cascade impactors have been used since about 1968 to measure the in-stack distribution (in the 0.2 to 20 μm diameter range) emitted from stationary sources. Research at the University of Washington has resulted in the development of the University of Washington Source Test Cascade Impactor (models Mark 1, 2, 3, 4, 5, 10, and 20) which have been or are being patented by Pilat[1] and licensed out by the University of Washington (to Pollution Control Systems Corporation of Renton, WA) for manufacture and commercial sale.

This paper reports on the Mark 3-4 Source Test Cascade Impactor sampling train and its application for sizing particles emitted from electric utility power plants. Pilat, Ensor, and Bosch[2] reported on the development and use of the Mark 1 and 2 UW Source Test Cascade Impactors. The Mark 1, 2, 3, and 5 models size particles in the general range of 0.2 to 20 μm aerodynamic diameter. The Mark 5 model has 11 stages followed by a filter and is designed for use at high particle concentrations such as exist at the inlet to control equipment. Pilat[3] described the earlier development work on the Mark 4 impactor. Pilat, Fioretti, and Powell[4] reported on the sizing of particles (in the 0.02 to 20 μm diameter range) emitted from coal-fired power boilers using the Mark 3-4 cascade impactor sampling train.

## THEORY OF CASCADE IMPACTORS

Cascade impactors fractionate the particulate matter from an emission source into size increments by inertial impaction of the particles on a collection surface. This occurs at successive stages within the impactor. The resulting index of particle size is traditionally expressed by the particle size collected with 50% collection efficiency for each stage, $d_{50}$. The particle diameter has been related to the Stokes inertial impaction parameter $\Psi$ which is defined by Ranz and Wong[5] as

$$\Psi = \left[\frac{C\rho d_p^2 V_j}{18\mu D_j}\right] \tag{1}$$

where C is the Cunningham correction factor, $\rho$ the particle density, $d_p$ the particle diameter, $V_j$ the gas velocity in the jet, $\mu$ the gas viscosity and $D_j$ the jet diameter. Solutions of the equation of particle motion at various magnitudes of $\Psi$ and experimental studies have shown that the Stokes inertial impaction parameter at 50% collection efficiency ($\Psi_{50}$) for a particular diameter ($d_{50}$) ranges between 0.12 and 0.17 for circular jets. These values were originally reported by Ranz and Wong[5] and later confirmed by McFarland and Zeller.[6] Solving for the particle diameter from equation (1) gives

$$d_p = \left[\frac{18\mu D_j \Psi}{C\rho_p V_j}\right]^{\frac{1}{2}} \tag{2}$$

Substituting an average value of 0.145 for $\Psi_{50}$ provides an equation for $d_{50}$,

$$d_{50} = \left[\frac{2.61\mu\ D_j}{C\rho_p\ V_j}\right]^{\frac{1}{2}} \tag{3}$$

Equation (3) provides an expression which relates the cascade impactor stage $d_{50}$ and the impactor parameters. These parameters can be appropriately altered to provide an even distribution of $d_{50}$'s throughout the impactor stages. For sizing of submicron particles, the Cunningham correction factor becomes of particular significance due to the physical limitations in further altering the other impactor parameters. The Cunningham correction factor C is defined by an equation reported by Davies[7]

$$C = 1 + \frac{2\lambda}{d_{50}}\left[1.275 + 0.40\ \exp\left(-1.10\ \frac{d_{50}}{\lambda}\right)\right] \tag{4}$$

where $\lambda$ is the gas mean free path. Thus, it can be seen by examination of equations (3) and (4) that it is possible to select the appropriate magnitudes of the impactor parameters necessary to provide a stage $d_{50}$ as low as 0.02 μm. Assuming a particle density $\rho$ of 1 g/cm$^3$ and substituting into equation (3) provides an equation for the aerodynamic cut diameter $da_{50}$

$$da_{50} = \left[\frac{2.61\mu\ D_j}{C\ V_j}\right]^{\frac{1}{2}} \tag{5}$$

UW MARK 3-4 CASCADE IMPACTOR INSTRUMENTATION

Sampling Train

The UW Mark 3-4 Cascade Impactor sampling train is shown in Figures 1 and 2. Figure 1 illustrates the Mark 4D and 90 mm filter located inside the stack, whereas Figure 2 shows them external of the stack. Heaters can be used to maintain the Mark 4D and filter holder at the desired temperatures. The Mark 4C cascade impactor can also be used with the Mark 3-4D sampling train. The UW Mark 3-4 Cascade Impactor sampling train includes a UW Mark 3 impactor, a UW Mark 4 impactor, a filter holder, a condenser, a leakless vacuum pump, a dry gas meter, and a control box. The train can also be used with a BCURA cyclone upstream of the Mark 3 impactor. When physical constraints such as too small a diameter of the sampling port exist, the sampling train can be arranged with the Mark 4 located outside the stack. External heaters can be used to maintain the Mark 4 and filter holder temperature above the dew point.

The control unit contains the instruments for measuring the temperature and gas pressures, heater control, and pressure tap valves. Pyrometers are used for the temperature readouts measured by type J (iron-constantan) thermocouples. Thermocouples

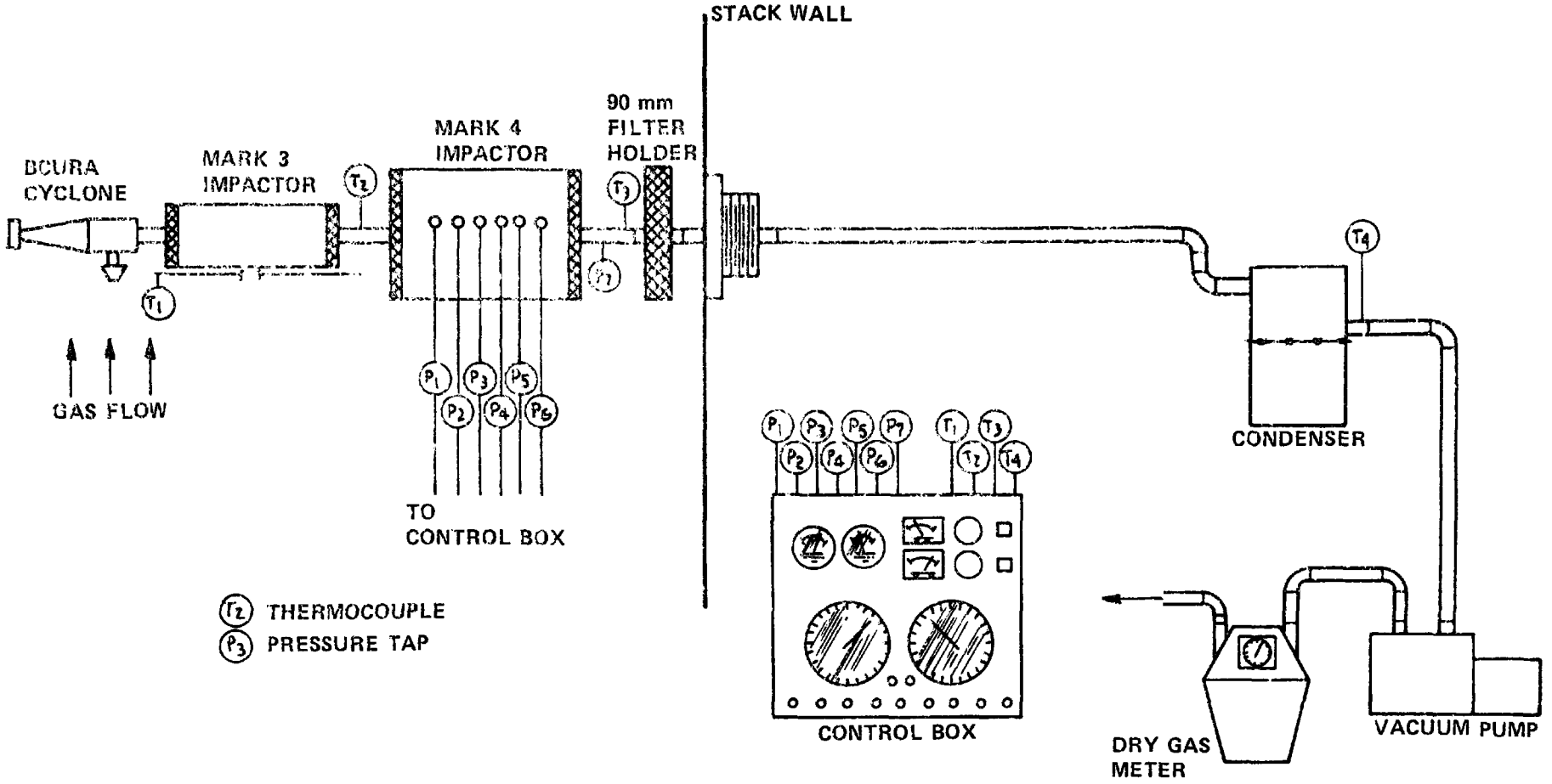


*Figure 1. U. of W. Mark 3-4D cascade impactor sampling train schematic.*

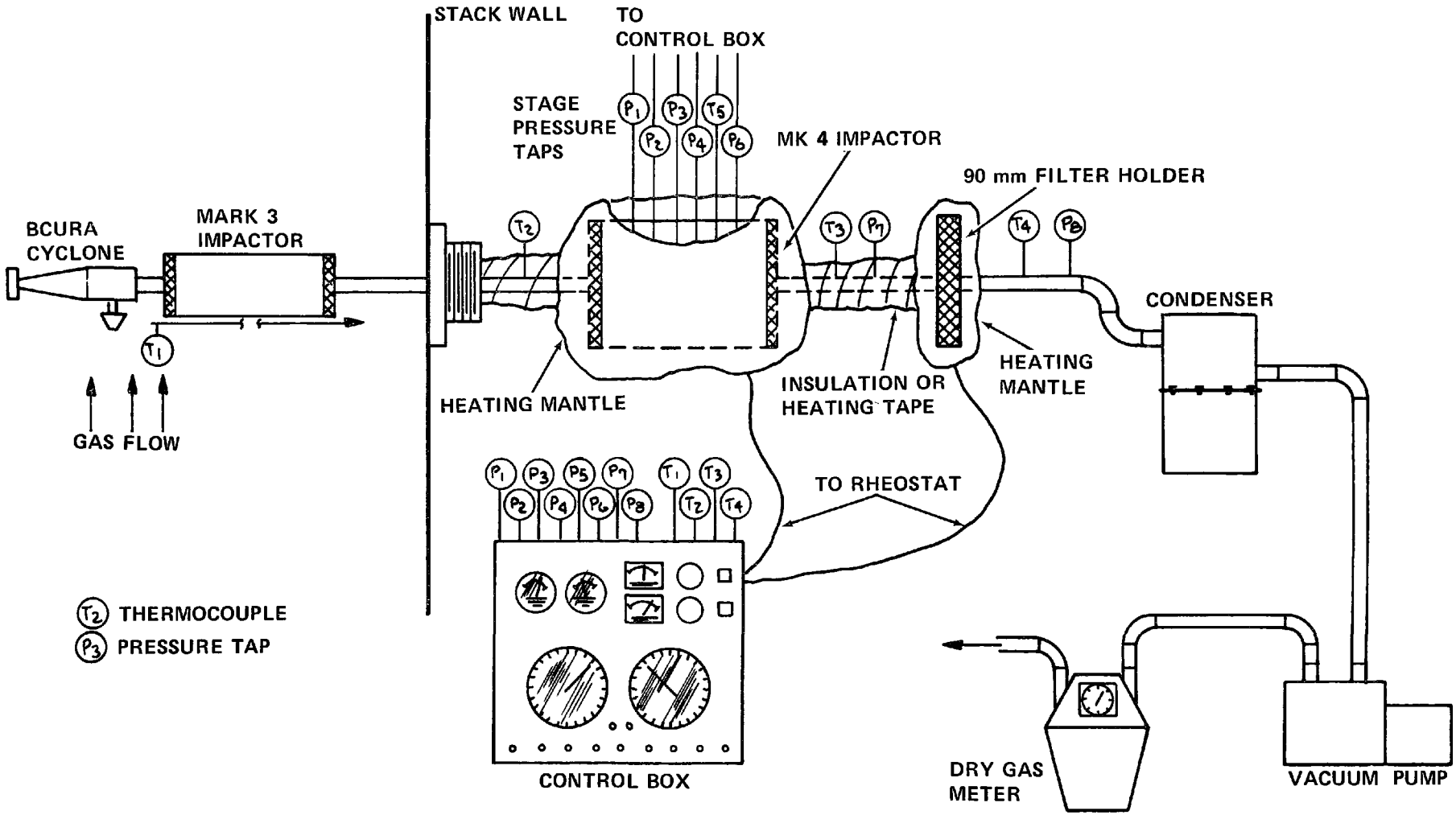


*Figure 2. Mark 3-4D sampling strain with Mark 4D located outside the stack.*

are located for measurement of the gas temperature inside the stack, at the Mark 4 inlet, Mark 4 outlet and filter outlet. Gas pressures are measured at all Mark 4 jet stages, the filter inlet, and the filter outlet. The gas velocity and static pressures are indicated by Dwyer Magnahelic gauges. The external heaters for the cascade impactors and/or filter holder are controlled by rheostats housed in the control unit.

UW Mark 3 Cascade Impactor

The UW Mark 3 Cascade Impactor has 7 stages followed by a filter holder (47 mm diameter filters). Figure 3 presents a graph of the Mark stage $da_{50}$'s (calculated) as a function of the gas volumetric gas sampling rate at stack conditions (assuming a gas pressure of 29.92 in. mercury). The number of jets per stage and the stage jet diameters are presented in Figure 3.

UW Mark 4C Cascade Impactor

The UW Mark 4C Cascade Impactor has jet stage and collection plate dimensions similar to the Mark 3 model such that the cylindrical casing diameter is about 2.9 in. (will fit through 4 in. diameter pipe sampling port). However, the Mark 4C has gas pressure taps on the jet stages. Also the Mark 4C has a unique arrangement of jet hole diameters and numbers per stage such that the gas velocity does not reach Mach 1 (sonic velocity) on any one stage until an upper limit gas sampling rate is reached. This upper limit gas sampling rate is about 0.5 cfm for the Mark 4C. With this lower gas sampling rate, a 47 mm diameter filter holder can be used.

UW Mark 4D Cascade Impactor

The Mark 4D Cascade Impactor model was designed in 1974 to have approximately 2 to 3 times the gas sampling flow rates of the Mark 4C (or about 1 to 1.8 cfm at stack conditions). The Mark 4D has a jet stage of about 3.55 in. diameter and a cylindrical casing of 3.95 in. diameter and thus requires a minimum 5 in. diameter pipe sampling port. Copper tubing of 1/8-in. diameter is connected to the pressure taps on each jet stage. This pressure tubing is connected to the pressure gauges in the control box.

For collecting those particles passing the last stage of the Mark 4D, a 90 mm filter holder is used. This 90 mm filter holder was designed and constructed at the UW. The condenser is connected to the sampling probe by a Teflon lined flex hose. The condenser is to condense and collect water vapor and other condensable vapors. The condenser is a 3/4-in. diameter stainless steel tube coil with a built-in water trap. It employs dry ice as a coolant and is capable of handling a 5.0 scfm gas

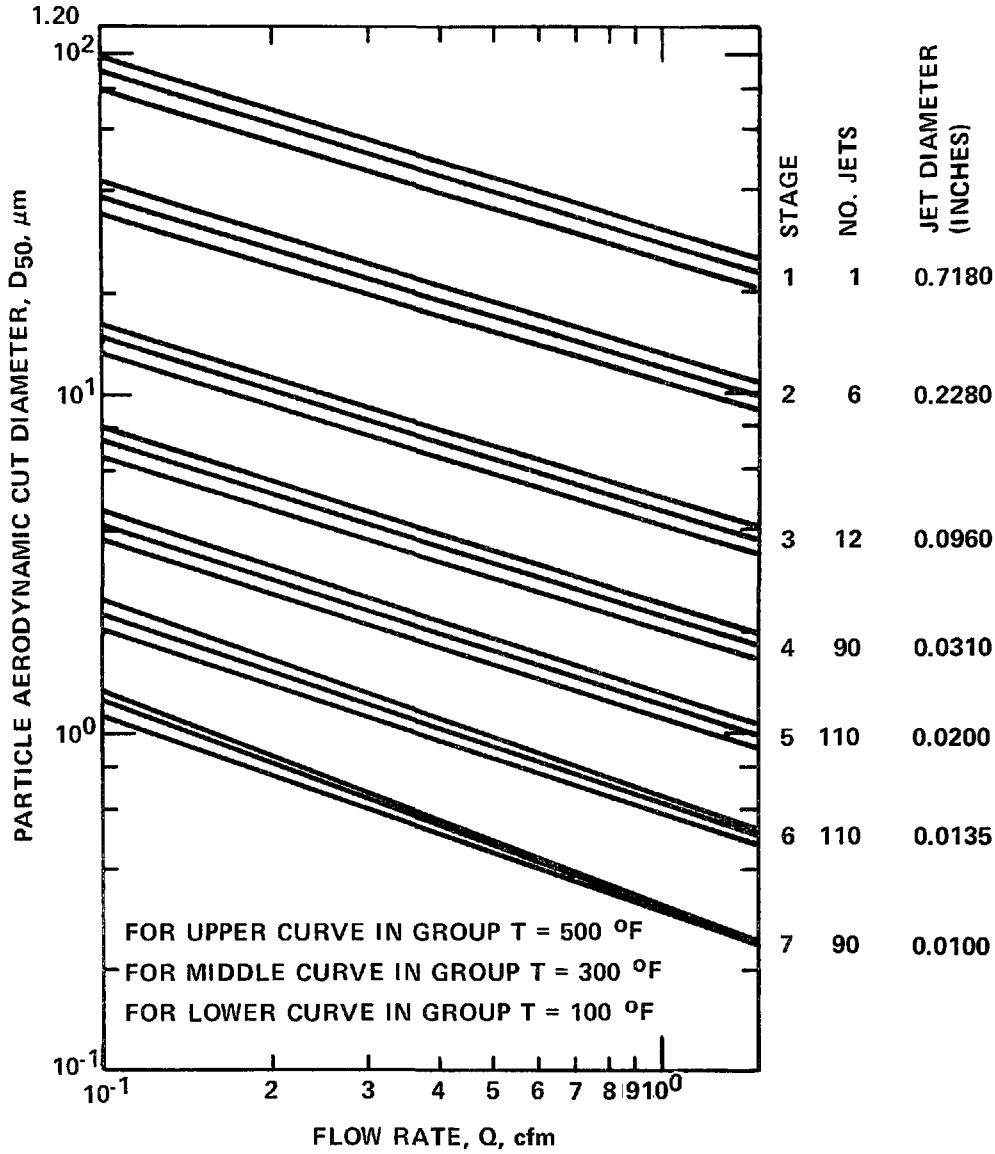


*Figure 3. Calculated aerodynamic cut diameters for U. of W. Mark 3 stages.*

flow rate. A two-stage, leakless vacuum pump is used with the Mark 3-4D sampling train. A Rockwell Model 250 dry gas meter with temperature compensation to 70°F is used to measure the volume of gas sampled and the gas sampling flow rate.

BCURA Cyclone

A BCURA (British Coal Utilization Research Association) Cyclone is used to collect the larger sized particles which at the higher particle concentrations can overload the inlet particle collection plates of the Mark 3 impactor. The BCURA Cyclone is located at the inlet of the Mark 3 impactor, as illustrated in Figure 1. The particulate sample is collected in the hopper.

When physical constraints hinder the use of a 90° angle probe, the BCURA Cyclone offers a convenient approach for enabling the sampling nozzle to be faced upstream. The BCURA Cyclone (as commercially available from Pollution Control Systems Corporation, Renton, WA) can be used in sampling ports of 4 in. or larger diameter (this commercially available model is slightly modified from the British model).

The equation for calculating the aerodynamic cut diameter $da_{50}$ of the BCURA Cyclone has been reported by Hawksley, et al.,[8]

$$da_{50} = \left[\frac{18\ K_c a_i \mu\ D}{\rho\ Q}\right]^{\frac{1}{2}} \tag{6}$$

where $a_i$ is the cross-sectional area of the cyclone inlet, D the cyclone body diameter, $\mu$ the gas viscosity, $\rho$ the particle density (assumed to be unity), Q the gas volumetric flow rate through the impactor, and $K_c$ a dimensionless cyclone constant. $K_c$ is defined by the equation

$$K_c = \lambda/L \tag{7}$$

where L is the cyclone length and $\lambda$ is the "range" of the particles. The variable $\lambda$ is defined by the equation

$$\lambda = \upsilon\ V/g \tag{8}$$

where $\upsilon$ is the Stokes velocity of the particle, V is the fluid velocity and g the acceleration of gravity.

The aerodynamic cut diameter $da_{50}$ for the BCURA Cyclone as a function of the gas sampling flow rate at stack conditions is presented in Figure 4.

## UW MARK 3-4 CASCADE IMPACTOR SAMPLING PROCEDURE

### Pre-Test Preparation

Prior to a particulate source test, certain information about the emission source should be known. Since the aerodynamic particle diameters ($d_{50}$'s) of the impactor stages are dependent upon the gas flow rate through the impactor, approximate values for the exhaust gas temperature and volumetric flow rate should be known. From this information, a jet stage sequence can be chosen to provide an even distribution of particles throughout the impactors for the particle size range expected.

To reduce the tare weight for the particulate collection plates, 0.002 in. thick stainless steel inserts are cut and formed for the impactor plates. The inserts must be conditioned for

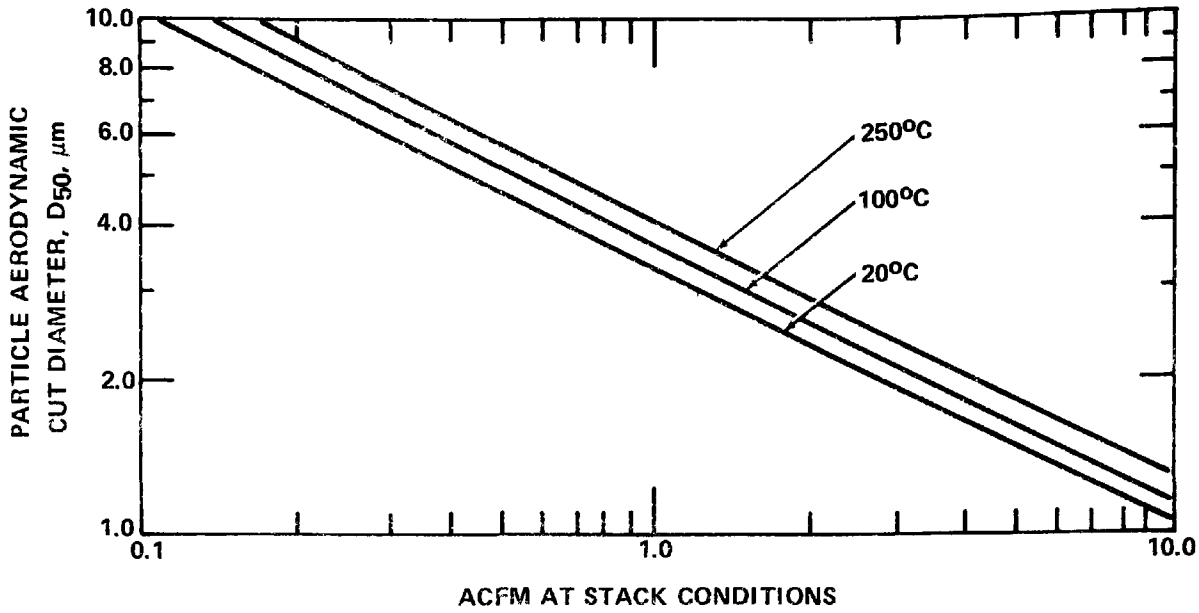


*Figure 4. BCURA cyclone aerodynamic cut diameter versus gas sampling rate.*

the particular emission source. They are first baked at a temperature slightly higher than the expected exhaust gas temperature to alleviate the possibility of weight loss due to evaporation of surface impurities. If the particulate matter to be sized is of a non-adhesive nature (e.g., coal dust) the collection inserts can be greased with a thin layer of an adhesive such as Dow Corning High Vacuum Grease prior to baking. This minimizes bounce off and re-entrainment of particles within the impactor. After the baking process the inserts and filters are desiccated for at least 12 hours and weighed with an accuracy of ± 0.01 mg. They are then stored in marked petri dishes and are ready for shipment to the sampling site. Blank inserts are prepared in order to identify weight changes caused by reasons such as weighing balance out of calibration or grease volatilization.

Certain consideration must also be given to the physical restrictions of the sampling site. A probe length must be chosen to be compatible with the particular stack or exhaust duct to be tested. The size and location of the actual sampling platform can also affect the lengths of reinforced flex hose required to connect the components of the sampling train.

Prior to testing, it is important to thoroughly clean the particulate sizing components of the train. An ultrasonic cleaner is recommended for cleaning the impactor jet stages.

## Test Procedures

With the impactors cleaned and loaded, the sampling train is assembled as described above. Temperature measurements are performed and the gas humidity is calculated by the wet bulb-dry bulb method. A type S pitot tube is used for velocity head and stack static pressure measurements. A velocity profile across the duct is selected for isokinetic sampling.

When the test parameters have been measured and calculated, the probe is inserted inside the stack with the nozzle facing downstream. Sufficient time (at least 15 minutes) is allowed to pre-heat the impactors and filters to stack temperature. The probe is then rotated so that the nozzle faces upstream and the test is started.

After an isokinetic sampling rate has been established, pressure measurements for the various stages of the Mark 4 impactor are made and recorded. After all pressure readings have been recorded, the pressure at the filter inlet is monitored in order to detect an overloading of the filter. The temperature in the stack and at the impactor outlets is also monitored and recorded on the data sheet.

Upon completion of the test the probe is removed from the stack and allowed to cool. The impactors and filter holder are disassembled and the collection inserts and filter are carefully removed and stored in the appropriate petri dishes. The cyclone catch is stored in a marked petri dish and the cyclone is washed with acetone. The wash liquid is also stored in a sample bottle.

## Post-Test Procedures

The collected samples (inserts and filters) are first baked at 250°F to drive off any moisture which might have been collected in return shipment. The wash solutions are evaporated at slightly elevated temperatures in cleaned and tared aluminum dishes. They are then desiccated for at least 12 hours and weighed. The particle weights are then recorded and used in the computer program for data reduction.

The data reduction computer program RASS is used to calculate size distributions, mass concentrations and other pertinent data to be used in the final analysis. It also generates input information to be used in a particle collection efficiency program which calculates the collection efficiency as a function of particle size using data from simultaneous inlet and outlet tests. Figure 5 presents a computer flow diagram for the data reduction program which illustrates the calculation procedures.

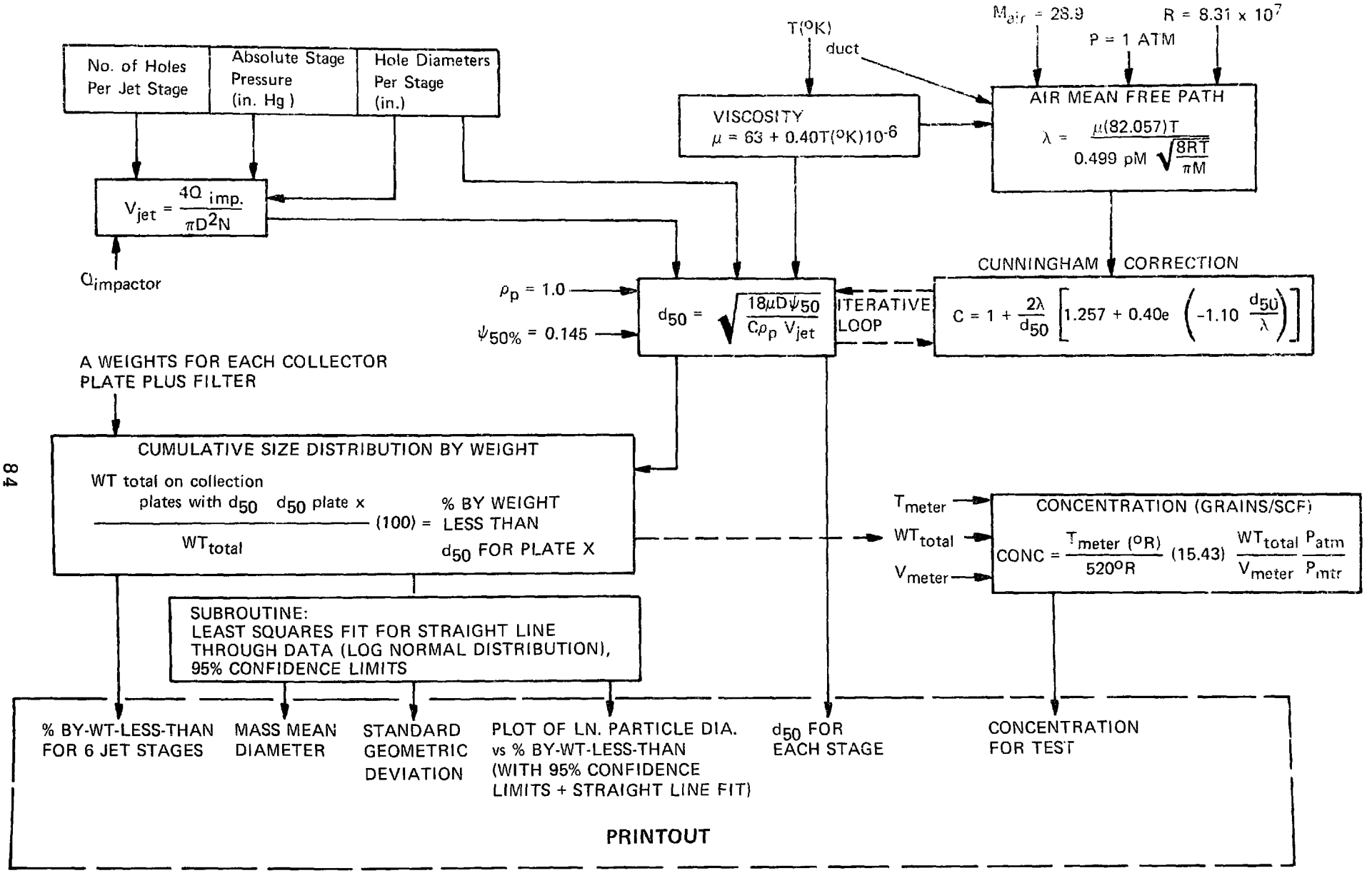


*Figure 5. Computer flow diagram for reduction of U. of W. Mark 3 and Mark 4 cascade impactor test data.*

## PARTICLE SIZE DISTRIBUTION RESULTS

### J.E. Corette Power Plant

Boiler and Electrostatic Precipitator Description--

Unit No. 2 at the J.E. Corette Power Plant, Billings, MT, burns pulverized coal in a Combustion Engineering boiler rated at 163 MW electrical output. Sub-bituminous Grade C coal having a gross heating value of 8,600 Btu/lb and a sulfur content of 0.7% is introduced in a tangential firing (swirling) pattern from 16 burners located at four elevations in the boiler corners. Combustion gases leaving the unit typically contain 80% of the total ash load and pass through a regenerative air preheater before entering a Research-Cottrell electrostatic precipitator. The precipitator is designed for 600,000 acfm gas flow at 300°F and 96% by weight particulate collection efficiency.

Sampling Site Description--

The inlet sampling site was located on the top of a short horizontal section of duct connecting the air preheater and the precipitator. The 4 in. diameter sampling port used was located about 0.34 equivalent duct diameters downstream and less than 0.1 diameters upstream from major gas flow disturbances. The arrangement of this port necessitated vertical insertion of the sampling equipment.

Sampling Technique--

The Mark 3-4D Cascade Impactor sampling train was used for the tests. Due to certain physical constraints at the sampling ports, the Mark 4D impactor and the absolute filter were located outside the stack as illustrated in Figure 2. Efforts were made through thermostatically controlled heating tape and insulation to maintain the Mark 4D and the filter at stack temperatures.

Due to the nature of the aerosol to be tested, the collection inserts were greased with Dow Corning High Vacuum Grease, conditioned at 350°F and weighed. All other pre-test and testing procedures as well as the post test analysis were performed in the same manner as described above in this paper.

Five tests (A through E, Tables 1 and 2) were conducted at the site during September 29 and October 8, 1975. The first four were performed at the outlet sampling port while the last (Test E) was at the inlet to the precipitator. All of the tests were conducted under normal operating conditions with the exception of tests C and D in which the soot blowers in the superheater section were curtailed.

Test Results--

The distribution of particulate matter collected by the various components of the Mark 3-4 sampling train is presented in Table 1. The source test results are listed in Table 2. The Pearson Correlation Coefficient, listed in Table 2, is a measure of the degree of fit between the log normal approximation (a linear regression) and the actual particulate size distributions. The Pearson Correlation Coefficient is more precisely defined as the ratio of the covariance to the square root

TABLE 1. DISTRIBUTION OF PARTICULATE WEIGHT COLLECTED BY THE UW MARK 3-4 IMPACTOR SAMPLING TRAIN FOR J.E. CORETTE TESTS

| | Particulate weight, g | | | | | |
|---|---|---|---|---|---|---|
| Test | BCURA cyclone hopper & wash | Mark III | Mark IV | Filter | Condenser trap & wash | Total weight excluding condenser |
| A | 0.0514 | 0.0559 | 0.0015 | 0.0006 | 0.2142 | 0.1094 |
| B | 0.0332 | 0.0617 | 0.0032 | 0.0007 | 0.0298 | 0.0978 |
| C | 0.1182 | 0.0888 | 0.0023 | 0.0007 | 0.0348 | 0.2100 |
| D | 0.1850 | 0.0883 | 0.0045 | 0.0018 | 0.0018 | 0.2796 |
| E | 0.9984 | 0.1808 | 0.0024 | 0.0029 | 0.0076 | 1.1845 |

TABLE 2. SOURCE TEST RESULTS FOR J.E. CORETTE TESTS

| Test | Mass mean diameter, μm | Standard geometric deviation | Pearson Correlation Coefficient | Solid particle concentration, gr/dscf | Condensed particle concentration, gr/dscf |
|---|---|---|---|---|---|
| A | 4.9 | 5.17 | 0.985 | 0.064 | 0.126 |
| B | 3.5 | 5.32 | 0.974 | 0.052 | 0.016 |
| C | 10.4 | 5.10 | 0.967 | 0.110 | 0.018 |
| D | 35.7 | 12.97 | 0.953 | 0.192 | 0.001 |
| E | 210.6 | 12.73 | 0.910 | 3.151 | 0.033 |

of the product of squares of the variation in X and the variation in Y. The actual particulate size distributions for each test are illustrated in Figure 6.

Discussion--

The average size distribution for the four tests conducted at the outlet of the precipitator (Tests A-D) shows that 13.4% of the particle mass is less than 1.0 μm in diameter.

The actual size distribution for the inlet, Test E, shows a marked skew to the right for particles greater than about 0.8 μm in diameter indicating a decreasing concentration of large particles. The mass mean diameter for this test, calculated from the log-normal approximation, is indicated as 210 μm. The lack of additional actual data points for particles greater than 4.0 μm has skewed the log-normal approximation to the left and given it a greater relative slope. Extrapolation of this curve from the last actual data point of 7.5% of the cumulative weight to the 50% points results in the unreasonably high mass mean diameter. A further breakdown of the mass which was consolidated in the last data point (approximately 90% of the total mass) would eliminate the necessity of extrapolating the curve to 50% of the cumulative weight and result in a more reasonable mass mean diameter. For this particular test the BCURA cyclone has a cut point diameter which was too small, thus collecting and consolidating too much data into one point.

The vertical insertion of the sampling train into both the inlet and outlet sampling ports meant that the UW Mark 3 and 4D impactors were oriented in an upside-down position. Disassembly of the impactors after each test showed that some particles had fallen off the collection plates onto the preceding jet stages. These jet stages were cleaned by washing with distilled water and the particle weights were determined (after evaporation to dryness) and added to appropriate collection stages. However, the extra lab work caused by the vertical sampling probe alignment could be obviated by either a horizontal or a right-side up positioning of the impactors.

## UW Power Plant

Description of Source--

UW Power Plant Boiler No. 5 is a Riley Stoker Corporation pulverized coal-fired boiler. It has a rated steam capacity of 120,000 lb/hr with outlet steam conditions of 400 psig and 600°F. The exhaust gases from Boiler No. 5 pass through a Research-Cottrell electrostatic precipitator with an overall design efficiency of 94% for particulate matter. The precipitator is designed for a volumetric flow rate of 50,000 acfm at 400°F.

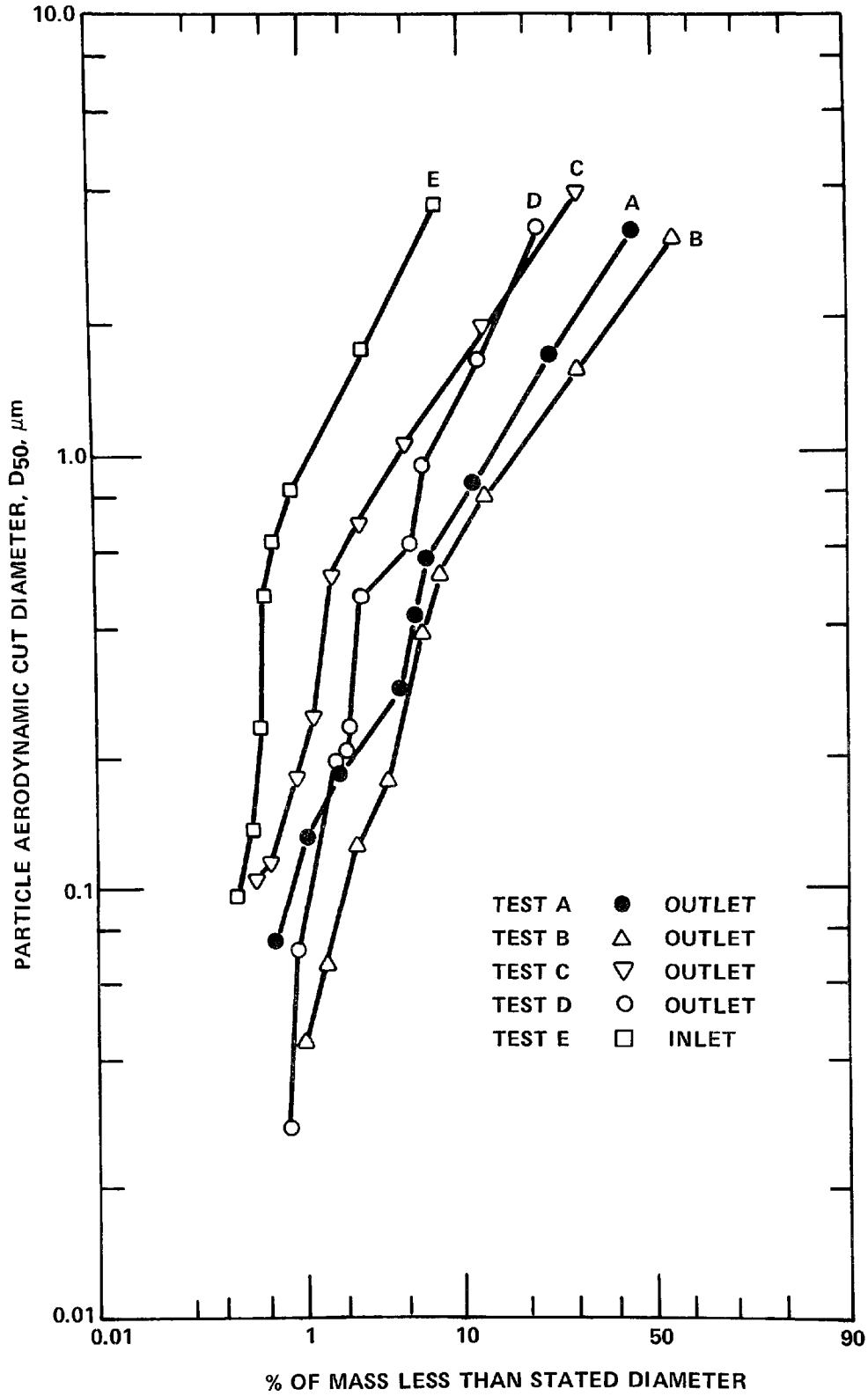


*Figure 6. Particle size distributions for tests A-E, J. E. Corette Power Plant.*

The simultaneous samples were taken at the inlet and outlet of the precipitator. The inlet sampling port is located at the No. 5 Boiler exhaust duct prior to entrance into the precipitator. The exhaust gases flow vertically upwards at the sampling point.

Sampling Technique--

The UW Mark 3-4 Cascade Impactor Sampling Train used was identical to the one described above. The BCURA Cyclone, the Mark 3 and Mark 4 Impactors and the 90 mm glass fiber filter were inserted inside the duct. A Mark 4C was used at the precipitator inlet and a Mark 4D was used at the precipitator outlet.

The pre-test preparation, the testing procedures and the post-test analyses were conducted in the same manner as described above. All pre and post test tasks were performed at the UW Air Resources Lab since the UW power plant is directly adjacent to the Civil Engineering Building. The two tests reported (A and B) were simultaneous source tests performed at the inlet and outlet of the electrostatic precipitator.

Test Results--

The size distribution and collection efficiency results are summarized in Table 3. The overall collection efficiency, including solid and condensible matter, was found to be 94.4% and 90.3% for the two tests performed. The particle size distributions are presented in Figure 7.

Discussion--

These tests demonstrated that the Mark 3-4 impactor trains were capable of simultaneous particle sizing (during the same time period) at the inlet and outlet of particulate control devices. Testing was performed at the inlet and outlet of the control device at considerably different gas sampling rates providing particle collection efficiency data as a function of particle size over a 0.07 to 3.5 μm size range.

Kearny Generating Station

Test Site Information--

The primary objective of the source tests at the Public Service Electric and Gas Company Generating Station, Kearny, NJ, was to determine the effect of three different fuel additives upon the particulate size distribution in the exhaust gas from an FT4C-1LF Pratt and Whitney gas turbine engine. The three different smoke suppressing fuel additives injected into the turbine fuel supply are listed in Table 4. To avoid any conflict as to the industrial designation of the additives, they

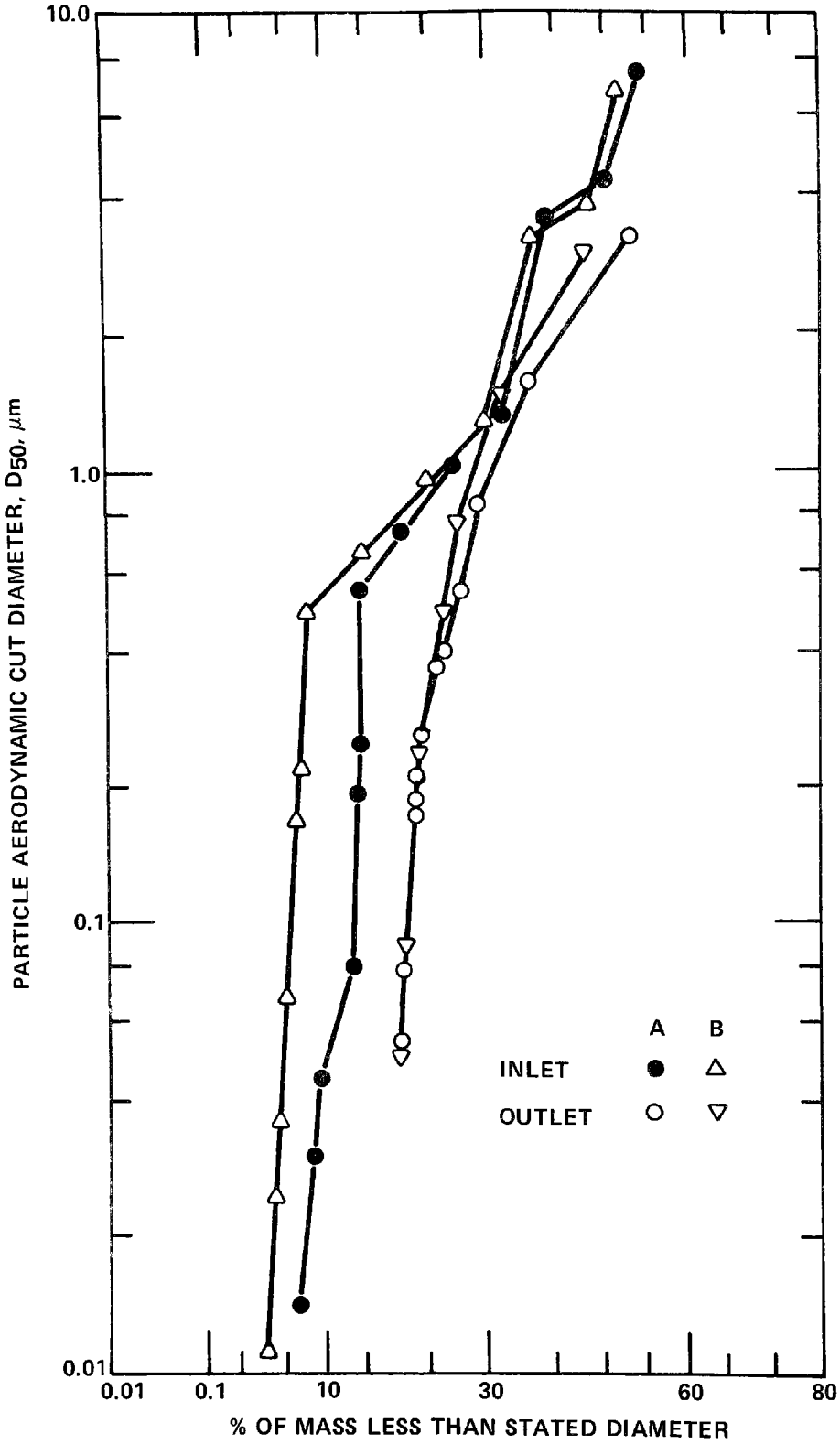


*Figure 7. Particle size distributions for U. of W. Power Plant.*

TABLE 3. SOURCE TEST RESULTS OF UW POWER BOILER TESTS

| Test | Mass mean diameter, μm | Standard geometric deviation | Pearson Correlation Coefficient | Particle mass concentration, gr/dscf | | Overall particle collection efficiency, % |
|---|---|---|---|---|---|---|
| | | | | Solids | Condensibles | |
| A-Inlet | 25 | 12 | 0.92 | 0.708 | 0.010 | 94.4 |
| A-Outlet | 12 | 12 | 0.91 | 0.033 | 0.007 | |
| B-Inlet | 23 | 9 | 0.91 | 0.784 | 0.000 | 90.3 |
| B-Outlet | 34 | 21 | 0.90 | 0.050 | 0.026 | |

TABLE 4. DESCRIPTION OF FUEL ADDITIVES USED FOR KEARNEY TESTS

| Test | Additive designation | Additive metal content, % by weight |
|---|---|---|
| A | None | --- |
| B | I | 6.75 Fe |
| C | I | 6.75 Fe |
| D | II | 5.34 Mn<br>1.48 Ba |
| E | III | 24.7 Mn |

are defined as additives I, II and III. Additive I was an iron based substance, additive II was an organic manganese-barium compound and additive III was an organic manganese compound. All additives were mixed with the fuel at a concentration of approximately 50 ppm.

The FT4C-1LF Pratt and Whitney gas turbine which was tested at the Kearney Power Plant is one of two engines included in a TP4-2LF Twin Pac gas turbine installation. The two turbines are located in opposite directions and simultaneously drive the generator. The generator is also capable of operation at approximately half power with one turbine either windmilling or decoupled from the generator. For all tests performed, turbine B was decoupled.

Test Schedule and Sampling Conditions--

The tests were performed January 21-27, 1976. The UW Mark 3-4 Cascade Impactor sampling train was arranged as shown in Figure 2 with the BCURA Cyclone and Mark 3 Impactor located inside the stack and the Mark 4D Impactor and 90 mm diameter filter holder outside the stack. The overall test preparation and procedures were the same as described above with certain considerations given to the extreme conditions to be faced in this test. To alleviate any problem with weight changes in the stainless steel collection inserts due to the extreme temperatures, pretest temperature experiments were performed. Type 304 stainless steel was found to exhibit a significant weight change due to intergranular corrosion when baked at 950°F for a 2 hour period. Type 316 ELC (extra low carbon) stainless steel showed negligible weight change due to the elevated temperature and was chosen for the collection insert material. All inserts were prebaked at 950°F for 2 hours, desiccated, and weighed, then packed in marked petri dishes.

Test Results--

The results from the five particulate source tests are presented in Table 5. The mass mean diameters are shown to vary from 0.13 to 0.21 μm. Figure 8 illustrates the actual particle size distribution for each test. The particles sized in all five tests ranged from 0.03 μm to 3.7 μm in diameter. Excellent correlation between the straight line approximation and the actual size distribution is demonstrated by the Pearson Correlation Coefficients listed in Table 5.

Discussion--

The source test results indicate that the turbine fuel additives have a small effect upon the size distribution by mass of the particulate emissions. The most apparent variation is observed for the larger particles. The injection of additives, particularly the organic manganese and the manganese-barium additives, created a greater percentage of larger particles (greater than 0.3 μm diameter). The additives had only a slight effect upon mass mean diameter, the greatest change being for the two manganese additives. The convergence of the size distributions in the 0.1 and 0.2 μm diameter range indicates an insensitivity for particles of this size to the additives. Reduction from the industrial load schedule to the minimum load schedule for the turbine, with the injection of iron based additive in both cases, resulted in a very negligible change in the size distribution.

Due to the particularly high exhaust gas temperatures (about 800°F), the Mark 4D Impactor was situated outside the stack. The impactor and the exposed portion of the probe were maintained at an elevated temperature by external heating. Despite these efforts, a substantial amount of weight was obtained from the probe washes. This weight is labeled as probe wash and not included in the particulate size distribution since the exact nature of this weight is not certain.

To alleviate such problems it is recommended that the connecting probe section between the Mark 3 and Mark 4 Impactors be minimized and both impactors plus any connecting probes be held at stack temperatures.

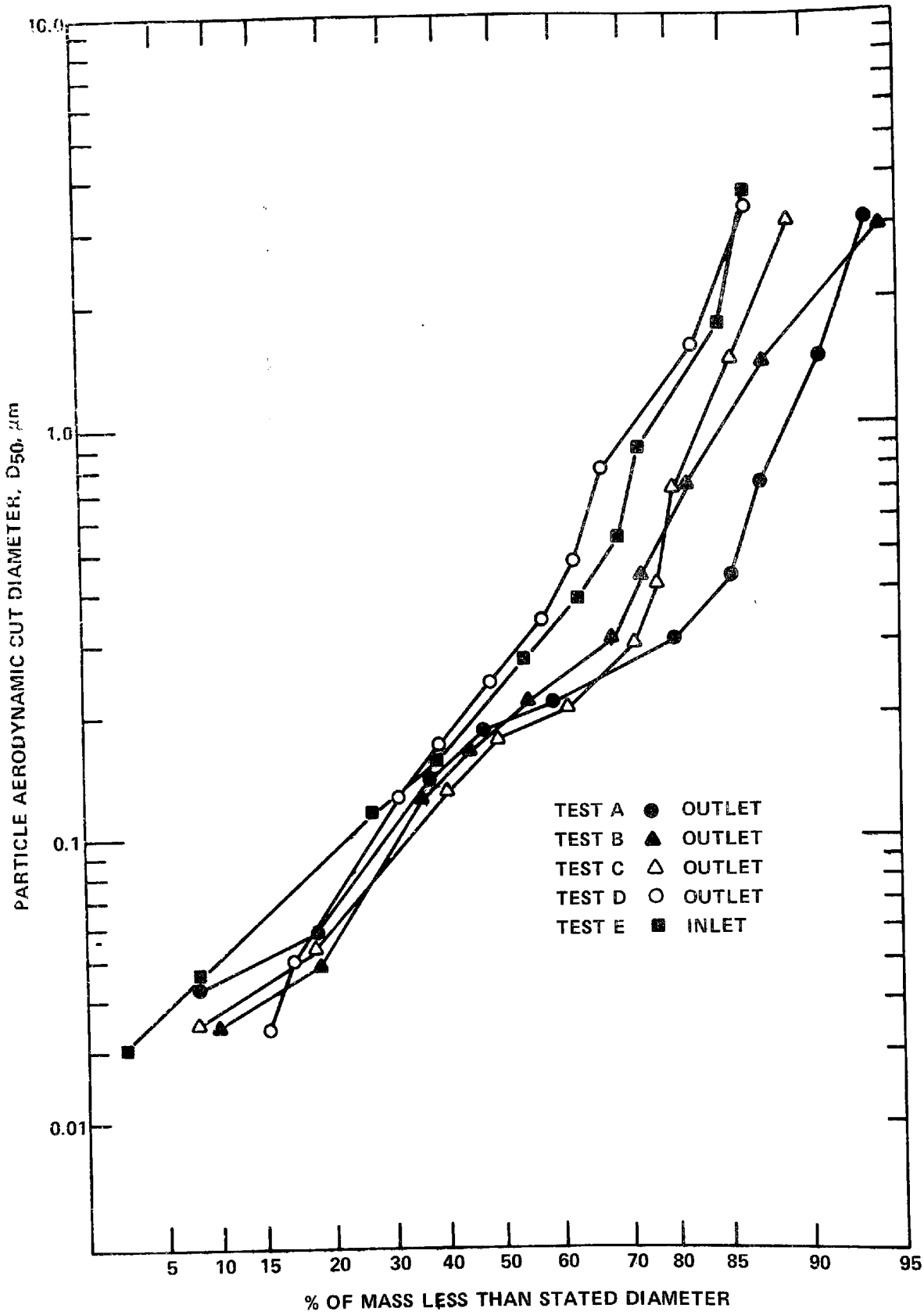


*Figure 8. Particle size distributions, tests A-E, Kearney Generating Station.*

TABLE 5. SOURCE TEST RESULTS FOR KEARNY TESTS

| Test | Turbine load | Fuel additive | Mass mean diameter, μm | Standard geometric deviation | Pearson Correlation Coefficient | Particle mass concentration, gr/dscf | | |
|---|---|---|---|---|---|---|---|---|
| | | | | | | Solids | Condensibles | Probe wash |
| A | Ind. | None | 0.14 | 3.5 | 0.96 | 0.0033 | 0.0025 | -- |
| B | Ind. | I | 0.13 | 4.5 | 0.99 | 0.0023 | 0.0162 | 0.0027 |
| C | Min. | I | 0.13 | 4.7 | 0.96 | 0.0027 | 0.0039 | 0.0052 |
| D | Ind. | II | 0.17 | 7.1 | 0.99 | 0.0014 | 0.0043 | 0.0010 |
| E | Ind. | III | 0.21 | 4.6 | 0.97 | 0.0014 | 0.0040 | 0.0021 |

## CONCLUSIONS

An improved particulate sampling train was constructed to size particles emitted from coal-fired power boilers in the range of 0.02 to 20.0 μm in diameter. The new components were designed and assembled to accompany the UW Mark 3 and Mark 4 Impactors. It has been demonstrated that this equipment and technique is capable of in-stack particulate sizing for the 0.02 to 20 μm diameter range.

Two source test programs were performed on coal-fired power boilers at the J.E. Corette Power Plant, Billings, MT, and at the University of Washington Power Plant, Seattle, WA. A particulate source test was also performed on an oil fired turbine at the Kearny Generating Station, Kearny, NJ. It has been shown that the new sampling train is capable of sizing particles at both the inlet and outlet of particulate control devices. It was also demonstrated that two such sampling trains can be simultaneously operated at the inlet and outlet of a particle control device on a coal fired power boiler during the same sampling period to evaluate the collection efficiency as a function of particle size.

## ACKNOWLEDGEMENTS

This research was supported by the Electric Power Research Institute, Palo Alto, CA. The assistance of G. Fioretti, G. Raemhild, A. Thoreen, and E.B. Powell with the field testing is appreciated.

## REFERENCES

1. Pilat, M.J. Source Test Cascade Impactor. U.S. Patent 3,963,457, 1972.

2. Pilat, M.J., D.S. Ensor, and J.C. Bosch. Source Test Cascade Impactor. Atmos. Environ. 4:671-679, 1970.

3. Pilat, M.J. Submicron Particle Sampling with a Cascade Impactor. Paper No. 73-284, presented at APCA Annual Meeting, Chicago, IL, 1973.

4. Pilat, M.J., G.M. Fioretti, and E.B. Powell. Sizing of 0.02 to 20 Micron Diameter Particles Emitted from Coal-Fired Power Boiler with Cascade Impactors. Presented at APCA Annual Meeting, Vancouver, B.C., 1975.

5. Ranz, W.E., and J.B. Wong. Jet Impactors for Determining the Particle Size Distribution of Aerosols. AMA Arch. Ind. Hyg. Occup. Med. 5:464-477, 1952.

6. McFarland, A.R., and H.W. Zeller. Study of Large Volume Impactor for High Altitude Aerosol Collection. USAEC TLD 18624, 1963.

7. Davies, C.N. Definitive Equations for the Fluid Resistance of Spheres. Proc. Phys. Soc. London 57:259-270, 1945.

8. Hawksley, P.G.W., S. Badzioch, and J.H. Blackett. Measurement of Solids in Flue Gases. British Coal Utilization Research Association, Leatherhead, Surrey, 1961. 214 p.

PAPER 5

# EXPERIENCE IN SAMPLING URBAN AEROSOLS WITH THE SINCLAIR DIFFUSION BATTERY AND NUCLEUS COUNTER

EARL O. KNUTSON
DAVID SINCLAIR
ENVIRONMENTAL MEASUREMENTS LABORATORY
U.S. DEPARTMENT OF ENERGY

## ABSTRACT

The Sinclair diffusion battery and nucleus counter have been coupled to a data acquisition and control system for automated monitoring of ambient aerosol size distribution and number concentration in New York City. Previous versions of this equipment required recording of data manually or by strip chart. The present version also incorporates a newly-designed rotary sequencing valve and a nucleus counter with increased cooling capacity and continuous alcohol feed. Unattended operation for three days or more is possible.

Diffusion battery penetration data are obtained on computer-compatible punched tape at 10, 20, 60 or 120-minute intervals. Our standard practice is to resolve these data into an eight-class particle size histogram spanning the diameter range 32 to 322 nm. Twomey's nonlinear iterative algorithm is used for this calculation.

Approximately 1000 size spectra of the New York City urban aerosol have been obtained with the present system in addition to 233 spectra that were obtained with an earlier version. Typically, the geometric mean diameter and geometric standard deviation are in the ranges 25 to 40 nm and 1.8 to 2.0 nm, respectively. The spectra typically show a slight positive skew relative to the log normal.

## INTRODUCTION

This paper is a report on the status of the Sinclair diffusion battery and nucleus counter and an account of our experience with this apparatus. Several events of significance have

occurred since the last status report, given over two years ago:[1] fourteen replicas of the diffusion battery were manufactured by a commercial firm and distributed to subscribers worldwide; the screen version of the diffusion battery is now commercially available (Thermo-Systems, Inc., St. Paul, MN); we have made approximately 1000 measurements of urban aerosol size distributions and have made a number of changes in the apparatus based on that experience.

The bulk of the information in the earlier report,[1] including calibration data, remains valid. The reader is referred to that report and its references for descriptions of the basic components of the system. Some additional information concerning the system will appear in a forthcoming article on the New York summer aerosol.[2] The present paper will describe the modifications made to date, new peripheral equipment added for control and data acquisition, data processing including the calculation of size distributions from observed diffusion battery penetrations, and the use of the system.

## MODIFICATIONS TO PREVIOUSLY-DESCRIBED EQUIPMENT

### Principal Dimensions of the Diffusion Battery

There now exist two manufacturing runs of the Sinclair diffusion battery and these differ significantly in their principal dimensions. The first sets of diffusion batteries were made using diffusional separating elements supplied by the Brunswick Corp. of Chicago. Brunswick used the term "Collimated Holes Structures" to identify these elements. Each element consisted of a circular disk, 4.44 cm in diameter, containing 14,500 holes of 230 micrometers diameter. Eighteen disks of various thicknesses were used in the batteries.[3]

The second manufacturing run, which included the 14 batteries distributed to subscribers, made use of diffusional elements manufactured by Nuclear Metals of Concord, MA. The elements were referred to as "Honeycomb Structures" by the manufacturer. These elements were disks, also 4.44 cm in diameter, but they differed from the Brunswick version in the number and size of holes in each disk. The Nuclear Metals disks contain 9,750 parallel holes of 380 micrometers diameter.

Table 1 shows the principal dimensions of the original and recently manufactured diffusion batteries.

### Sequencing Valve

In the previous version of the automated Sinclair diffusion battery, air flow through the various stages of the battery was controlled by a bank of 13 solenoid valves which were opened in sequence by means of a cam and microswitch assembly. The

TABLE 1. PRINCIPAL DIMENSIONS OF THE CHS AND HS SINCLAIR DIFFUSION BATTERIES

| Segment No. | Tap* No. | Segment Thickness (cm) CHS** | HS |
|---|---|---|---|
| 1 | 1 | 0.343 | 0.318 |
| 2 | 2 | 0.310 | 0.318 |
| 3 | 3 | 0.640 | 0.635 |
| 4 | 4 | 1.029 | 0.952 |
| 5 | 5 | 1.313 | 1.270 |
| 6 | 6 | 1.880 | 1.905 |
| 7 | 7 | 2.57 | 2.54 |
| 8 | | 2.61 | 2.54 |
| 9 | 8 | 1.228 | 1.270 |
| 10 | | 2.56 | 2.54 |
| 11 | 9 | 2.55 | 2.54 |
| 12 | | 2.60 | 2.54 |
| 13 | | 2.58 | 2.54 |
| 14 | 10 | 2.56 | 2.54 |
| 15 | | 2.58 | 2.54 |
| 16 | | 2.56 | 2.54 |
| 17 | | 2.62 | 2.54 |
| 18 | 11 | 2.57 | 2.54 |

CHS: "Collimated Holes Structures" manufactured by Brunswick Corp.

HS: "Honeycomb Structures" manufactured by Nuclear Metals.

* Indicated tap follows the corresponding segment in the left column.

** The CHS version was used in all measurements described in this paper.

valves were noisy, both acoustically and electrically. The electrical noise was troublesome, since it caused spurious signals in the digital circuitry used to record data. A second disadvantage of the arrangement was that it was not amenable to external control, such as timing signals for synchronization purposes.

Based on our experience, specifications were drawn up for a new sequencing valve. Particular attention was given to the requirements of aerosol mechanics and to compatibility with digital data-handling circuitry. The valve was designed and constructed by the Instrumentation Division at EML.

The new valve is shown in Figure 1. A configuration is used in which 15 ports are arranged in a circular pattern. A drive motor, which runs continuously, is coupled to the valve rotor through a gear train and an electromechanical clutch. Each actuation of the clutch causes the rotor to advance 1/15 of a revolution, stepping the valve to the next port.

To minimize aerosol losses, the valve was designed with relatively large flow passages and a minimum number of changes in flow direction. The smallest passage is the straight passage through the rotor which has diameter of 0.64 cm. Downstream of the rotor, the 15 ports are connected to a toroidal manifold, with relatively large internal dimensions.

The time required to step the valve is one second so that the interruption of flow is negligible. The clutch is activated by momentarily (1/20 to 1/4 second) grounding a line from the clutch solenoid, which is powered by an on-board 24 V DC power supply. The solenoid current is only 220 mA and no interference with digital data circuitry has been noted.

The fifteen ports include three spares, which are used to obtain clean air readings (through an absolute filter) at the beginning and end of each measurement cycle and to obtain a redundant reading of the diffusion battery inlet concentration. Table 2 shows the valve sequence used in the present system. Port O is used as a "home" position, where the valve starts and ends each measurement cycle.

Continuous Flow Nucleus Counter

As described elsewhere,[4] the continuous flow nucleus counter utilizes ethyl alcohol as the working fluid which condenses on the aerosol particles. During the first extended outdoor test of the nucleus counter, in August of 1976, we found that the alcohol also served as a good desiccant. As long as the alcohol is fresh, it dehumidifies the air sample stream. However, after two to three days in humid weather, the alcohol becomes so diluted with water that it is no longer an effective desiccant. Atmospheric water vapor then enters the cold tube, where it forms frost and blocks the light beam.

To counter the formation of frost, fresh alcohol is continuously supplied to the alcohol tube of the nucleus counter. The alcohol flows under gravity through a needle valve adjusted to 150 $cm^3$/day. The alcohol tube overflow is collected in another receptacle, closed to the atmosphere.

A second difficulty encountered in August 1976, was that of maintaining sufficiently low temperature in the cold tube of the nucleus counter. We have found that it is necessary to

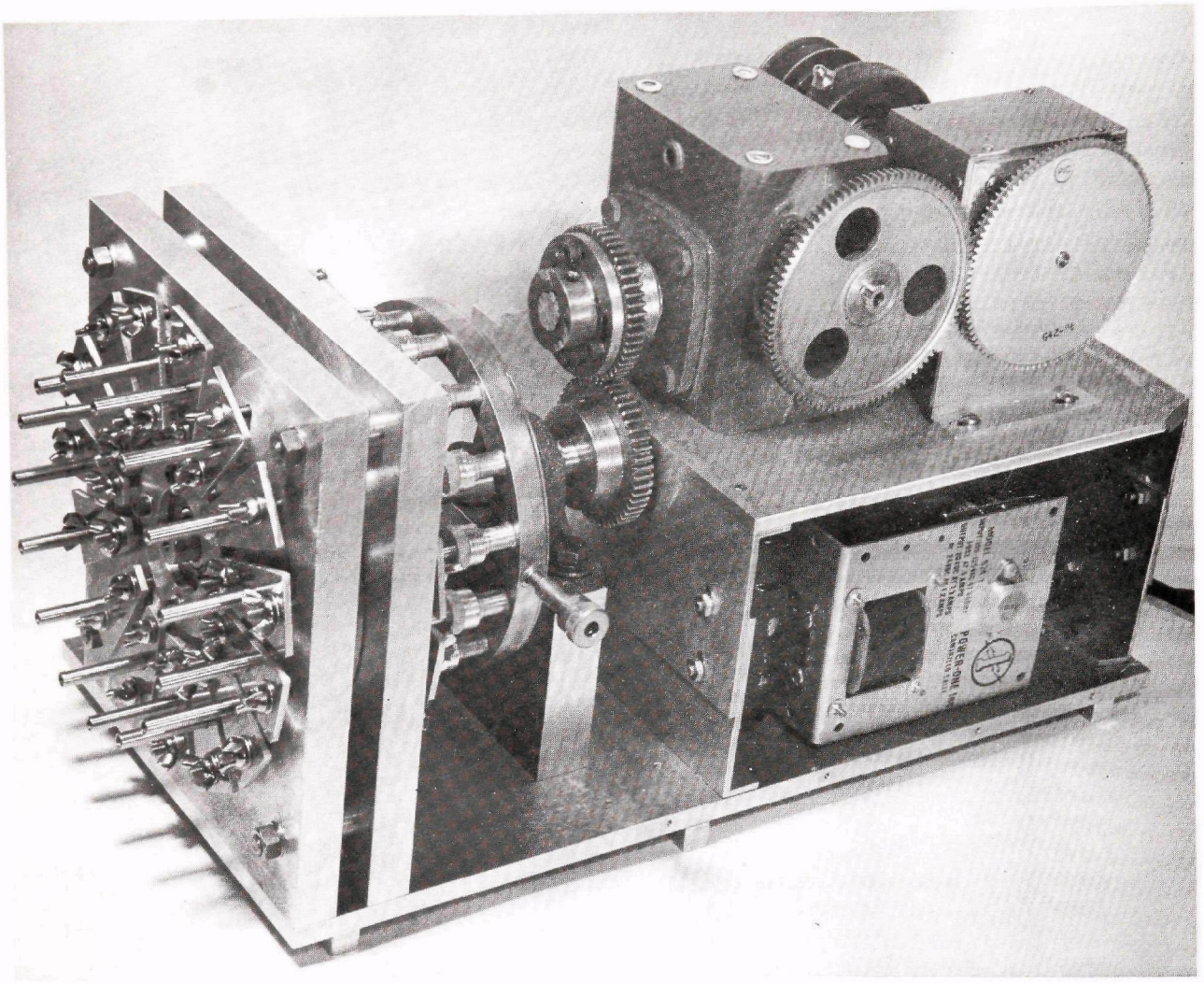

*Figure 1. Sequential multiport sampling valve.*

TABLE 2. VALVE PORT ASSIGNMENTS

| Valve Port | Connection |
|---|---|
| 0 | Absolute Filter |
| 1 | Absolute Filter |
| 2 | Diffusion Battery inlet |
| 3 | Diffusion Battery inlet |
| 4 | Diffusion Battery tap no. 1 |
| 5 | tap no. 2 |
| 6 | tap no. 3 |
| 7 | tap no. 4 |
| 8 | tap no. 5 |
| 9 | tap no. 6 |
| 10 | tap no. 7 |
| 11 | tap no. 8 |
| 12 | tap no. 9 |
| 13 | tap no. 10 |
| 14 | tap no. 11 |

maintain -15°C in the cold tube for proper nucleus counter operation. In the August sampling session, the temperature in the equipment shed often reached 35°C and we had to supply additional cooling by means of an air conditioner. Since then, a Model 2 nucleus counter has been built incorporating additional cooling capacity. This version was found to be marginally adequate in hot weather. To provide a reserve of cooling power, Model 3 (now in preparation) will incorporate two-stage thermoelectric elements to increase the attainable temperature differential.

## NEW PERIPHERAL EQUIPMENT

### Timing and Control Circuit

Continuous cycling through the diffusion battery taps produce more data than is needed in most applications. Single cycles initiated periodically give the preferred mode of operation. To facilitate correlating aerosol data from the diffusion battery with other information, such as meteorological variables, it is convenient to have these single cycles initiated on the hour.

The Instrumentation Division at EML has devised a timing and control circuit which provides the desired control signals to the rotary valve. As indicated in the functional diagram, Figure 2, all timing is based on counting pulses derived from the 60 Hz power main. Counting commences from zero at the time

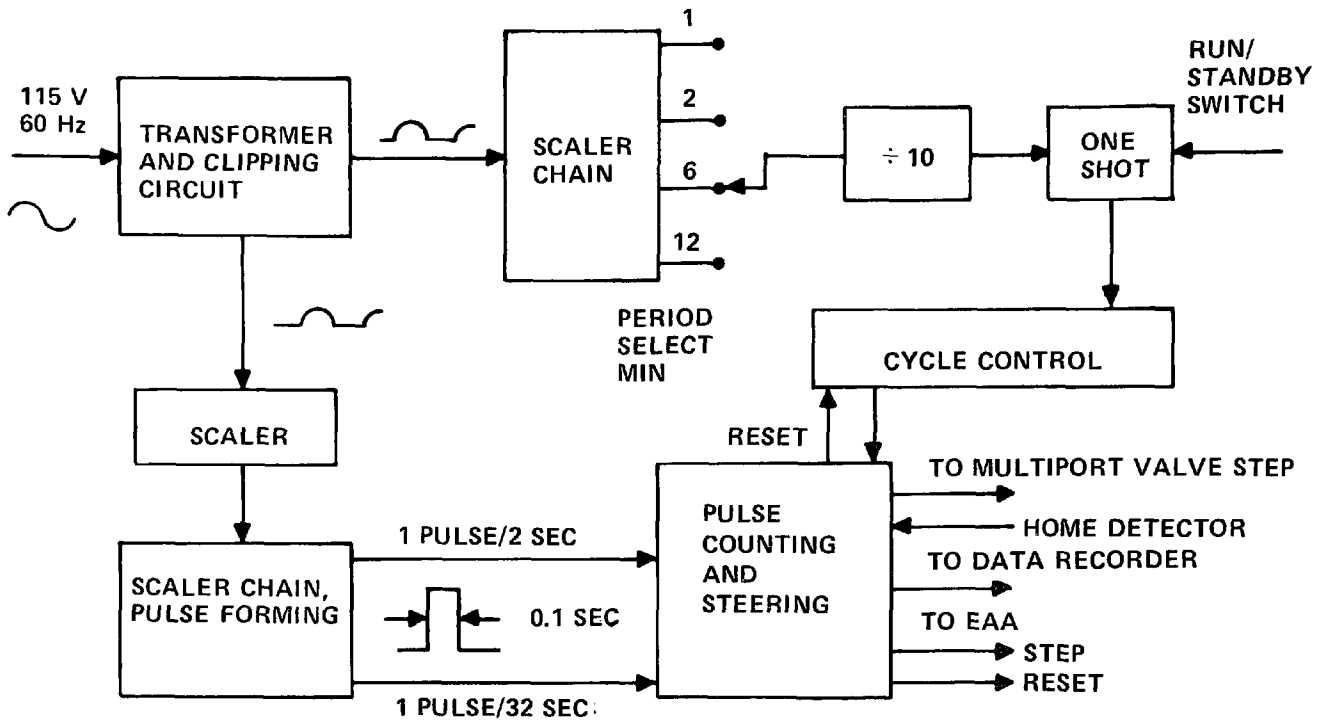


*Figure 2. Functional diagram of timing and control circuit.*

when the Run/Standby control is switched to Run. Cycles consisting of fifteen 0.1-second pulses spaced 32 seconds apart are started at one-hour intervals to step the multiport valve. A provision is made to insure that the valve stops at home position (port 0) after each cycle.

The same circuit also controls the data acquisition equipment and an electrical aerosol analyzer (Thermo-Systems Model 3030). The latter is often run in conjunction with the diffusion battery/nucleus counter for comparison.

The timing and control circuit has proved to be reliable in two separate four-week periods of continuous operation. The maximum observed error in cycle initiation time, using the telephone company time as a standard, was 5 seconds. The important point here is that the timing errors are not cumulative, since the power company apparently adjusts its generators periodically to keep the cumulative number of cycles on schedule.

In addition to the hourly schedule, the timing and control circuit can be set to initiate cycles at 10, 20 and 120-minute intervals.

## Data Recording Apparatus

The Sinclair diffusion battery and nucleus counter generate a large volume of data, even when operated on hourly cycles.

Extended operation is feasible only in conjunction with apparatus for reliable recording data in machine-readable form. We presently use a system assembled by the EML Instrumentation Division, using some commercial components and some components which are standard within our Laboratory. It is likely that this system will change considerably in the near future to take advantage of the rapid developments in commercial data handling electronics.

The main components of the present data recording apparatus are two analog-to-digital conversion circuits, a time-of-year clock, a teletype interface and a teletypewriter. The electronic modules are housed in a standard full-width NIM bin, which also houses the timing and control circuit.

The analog signal from the nucleus counter is converted to digital form by means of a voltage controlled oscillator connected to a scaler. A gating circuit keyed to the timing and control circuit (described earlier) gates pulses from the oscillator into the scaler during a five second period starting 17 seconds after each step of the rotary valve. The 17-second period allows for the response time of the nucleus counter and the five-second period provides signal averaging. The accumulated count, which is directly proportional to the five-second averaged analog voltage, is sent out to the teletypewriter on the next step signal from the timing and control circuit. A second analog channel is normally used to record data from the electrical aerosol analyzer.

The data are recorded in the form of six-digit integers. The teletype produces both a printed and a punched tape record of the data. Due to a local convention in data handling, the punched tape approach is the most direct method for us to enter data into our main computer.

Teletype systems are widely used for data recording in our Laboratory, mostly in temperature and humidity-controlled indoor environments. We have logged about 2,500 hours of operation in uncontrolled outdoor equipment sheds and we find that the reliability of recording data varies with the weather. In cool weather, the error rate is of the order of one mispunched bit per day (1 bit in $\sim$100,000). In hot weather, the error rate may increase 1000-fold. We have found, however, that the punching errors are of such a nature that the actual numerical values are seldom affected. By reprogramming our tape reading routine, we find that even badly mispunched tapes can be read with good reliability.

The main disadvantage of the teletype is that it is cumbersome in field use. It is planned to replace the teletype in the near future with a magnetic tape cassette system.

## DATA PROCESSING

A fully mechanized procedure has been developed for processing the data from the Sinclair diffusion battery and nucleus counter. The input is punched paper tape from the teletype and the output is computer cards, one for each measurement cycle. Each card is encoded with year-month-date-hour and eight values of $\Delta N/\Delta(\log_{10} d_p)$ from that hour's measurement. The cards are suitable for filing and subsequent statistical studies. The procedure also produces a printed summary, including a bar-graph histogram, of each hour's results.

A flow chart of the computer program used for data processing is shown in Figure 3. All elements of the program are straightforward, with the exception of the size distribution calculation.

For analyzing diffusion battery data, we sought an algorithm which would be well suited for automatic calculations on large volumes of data. Simplicity and speed of execution were important. Other criteria were that the algorithm should be directly applicable to field-grade data, without screening or smoothing, and that it should have sensitivity and resolution sufficient to bring out the main features of the size distribution.

Our criteria tended to rule out elaborate, mathematically proper approaches such as that of Maigné[5] and those based on linear programming[6] or nonlinear least squares.[7] Four algorithms were examined in detail and one of these, Twomey's nonlinear iterative algorithm,[8] was selected as the best compromise.

### Twomey's Nonlinear Iterative Algorithm

The nonlinear iterative algorithm described by Twomey[8] in 1975 was intended for the calculation of the aerosol size distribution from measurements of penetration through Nuclepore filters. As described below, this algorithm adapted readily to analysis of data from the Sinclair diffusion battery.

The diffusion battery taps 1 through 11 will be designated by the index i. It is convenient to define two additional taps: Tap 0, sampling the aerosol at the diffusion battery inlet and tap 12, sampling the aerosol through an absolute filter. Thus, the data from the diffusion battery consist of a set of 13 decreasing aerosol concentrations $C_i$, i=0, 12. The last of these is zero and is used primarily to check the zero reading of the nucleus counter.

Determination of the aerosol size distribution involves comparison of the 13 observed concentrations, $C_i$, to the corresponding trial concentrations, $C_i^*$. The latter are given by the integral expression:

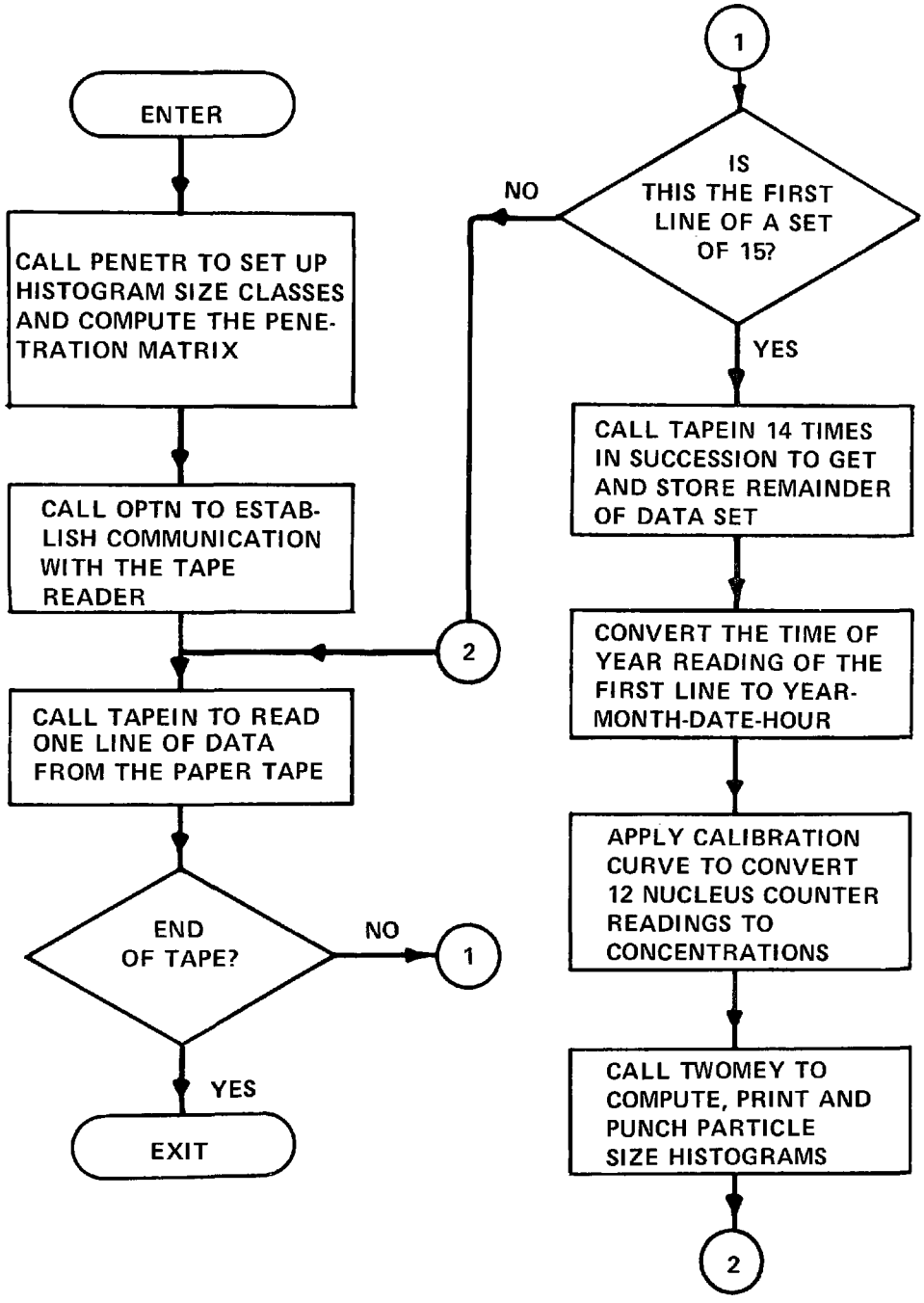


*Figure 3. Flow chart of data processing program.*

$$C^*_i = N \int_0^\infty \phi_i(x) f(x) dx \tag{1}$$

where

$N$ = the aerosol number concentration

$f(x)$ = the (unknown) differential size distribution

$x$ = the particle diameter

$\phi_i(x)$ = the fractional penetration of aerosol particles of diameter x through the diffusion battery segments preceding the i-th tap. Note that $\phi_0(x) = 1$ and $\phi_{12}(x) = 0$.

The penetration functions $\phi_i(x)$ are calculated as the product of penetration expressions for each of the diffusion battery segments preceding the i-th tap. For the latter, we use Thomas' expression,[9] which is simple and sufficiently accurate. Plots of $\phi_i(x)$ may be seen in reference 3 and, in an alternative form, in Figure 4.

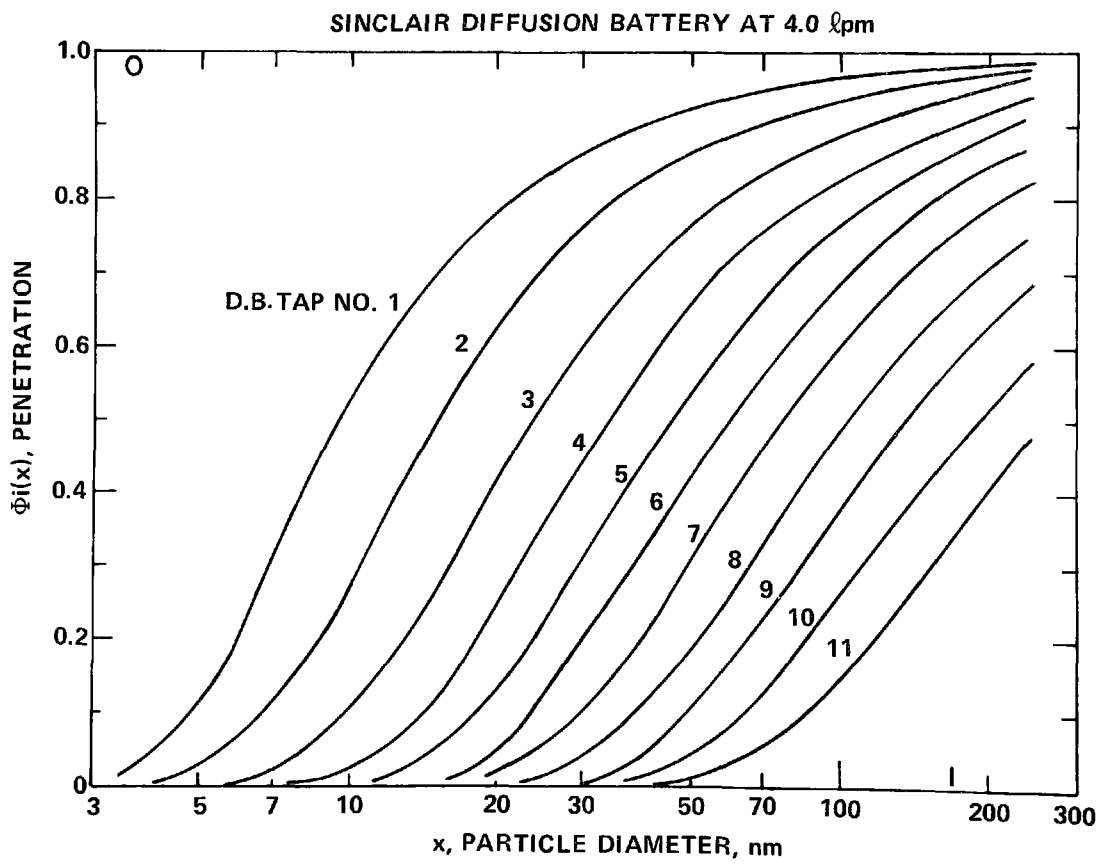


*Figure 4. Penetration functions for the Sinclair diffusion battery.*

Although the algorithm can be applied to the observed diffusion concentrations directly, we find that convergence is speeded by taking their first differences, $D_i$, which are the depositions in the corresponding diffusion battery segments:

$$D_i = C_{i-1} - C_i, \quad \text{for } i = 1, 12. \tag{2}$$

The corresponding trial differences are:

$$D^*_i = N \int_0^\infty \Omega_i(x) f(x) dx, \quad \text{for } i = 1, 12. \tag{3}$$

where

$$\Omega_i(x) = \phi_{i-1}(x) - \phi_i(x), \quad i = 1, 12.$$

The functions $\Omega_i(x)$, which represent the deposition in the diffusion battery segments between taps i-1 and i, are shown in Figure 5. The function $\Omega_{12}(x)$ represents deposition in the absolute filter.

Twomey's algorithm requires preselection of a number of discrete sizes to represent the continuous size distribution. There are no fixed rules for selecting the number and spacing of these sizes. The number and spacing should be such as to reproduce the major features of the deposition curves, Figure 5, but using a larger number and smaller spacing is permissible. The computation time, however, increases in proportion to the number of discrete sizes selected.

We commonly use a set of eight discrete sizes, starting with 42.2 nm and increasing to 237 in a geometric progression with a common ratio of $10^{0.25}$. Figure 5 suggests that it might be possible to add one or two larger sizes, since $\Omega_{12}(x)$ is still changing beyond 237 nm. However, this part of the curve is uncertain due to the unknown effects of gravitational settling. Furthermore, many aerosols have relatively few particles larger than 250 nm diameter, which makes extension to larger sizes unnecessary.

In terms of the discrete sizes, the trial depositions are:

$$D^*_i = \sum_{j=1}^{n} \Omega_{ij} N_j \tag{4}$$

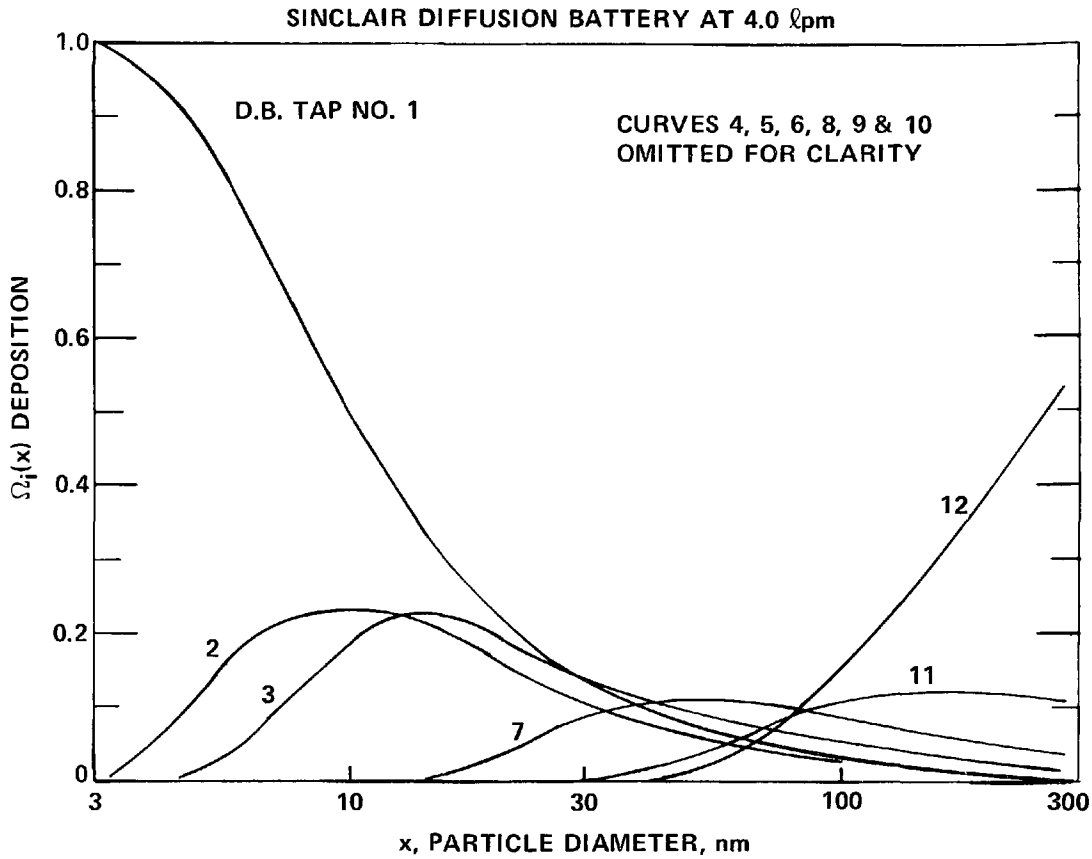


*Figure 5. Deposition curves for the Sinclair diffusion battery.*

where

$\Omega_{ij}$ = $\Omega_i(x_j)$

$x_j$ = the j-th discrete size

$N_j$ = the particle concentration at the j-th discrete size

n = the number of discrete sizes.

Twomey's algorithm starts with an initial guess for the size distribution, then refines this guess by a series of small changes to improve the fit to the observed depositions. For the initial guess, we assume that each of the discrete sizes has a concentration equal to 1/n times the observed concentration at tap 0: $N_j = C_0/n$, $j = 1,n$. The refined values, denoted by $N_j'$, are obtained by applying Twomey's nonlinear iteration formula:

$$N_j' = N_j \cdot \left[1 + \left(D_i/D_i^* - 1\right)\Omega_{ij}\right] \tag{5}$$

There are no fixed rules concerning the sequence in which the subscripts i and j in the formula are to be varied. We use the following scheme:

1. The index i is varied in the sequence 1,2,3,...,12,1,2,3,..., 12,1,2,3,....

2. At each step of the index i, $D_i^*$ is computed from equation 4 using the most recent values of $N_j$.

3. For each i, a complete cycle through the index j is performed using equation 5 to obtain refined estimates of $N_j$.

This procedure is continued until there is satisfactory agreement between $D_i^*$ and $D_i$.

The rationale of Twomey's algorithm may be seen as follows. Suppose, that for a particular value of i, the computed $D_i^*$ is smaller than $D_i$. Equation (5), which is a sum of positive terms, shows that the only way to close the gap is to increase at least one of the $N_j$ terms. The strategy used is to increase all the $N_j$ terms, each in proportion to the impact it has on $D_i^*$. Similar reasoning applies if $D_i^*$ is larger than $D_i$. By cycling through the subscripts as previously indicated, the $N_j$ values are continually adjusted so as to bring each $D_i^*$ closer to the corresponding $D_i$.

Two further steps were taken in the computer program to increase execution speed:

1. The factor $\Omega_{ij}$ in equation 5 was replaced by $0.8\ \Omega_{ij}/\Omega_{imax}$, where $\Omega_{imax}$ is the largest $\Omega_{ij}$ for the given value of i. This increases the size of the step made in each iteration.

2. No test is made for convergence. Experience has shown that 30 cycles through the double loop (i = 1,12; j = 1,n) is sufficient to achieve reasonable agreement between $D_i^*$ and $D_i$. Therefore, 30 cycles of iteration are used for each data set.

## Computational Speed and Accuracy

The data processing just described is done in our Laboratory using an IBM 360/30 computer and peripheral IBM equipment, such as the paper tape reader, card punch and line printer. The throughput is about four diffusion battery data sets per minute. The calculation itself (the algorithm) requires eight seconds per data set and the balance of the time is used in reading the paper tape and the printout. This throughput is adequate for our needs, but could probably be increased five or ten fold by using faster equipment.

All computations are done using single-precision IBM FORTRAN (32 bit words). We think that the entire procedure could also be done with a field microcomputer programmed in BASIC.

A convenient check on the internal consistency of the data is provided by comparing the calculated concentrations, $C_i^*$, to the observed concentrations, $C_i$. With either field or laboratory data, we find that the root mean square relative difference between these two is usually in the range 2 to 3%, which is believed to be comparable to the random perturbances in the measured concentrations. When larger relative differences occur, they can often be traced to errors in data transmission or to apparatus malfunctions.

The Twomey algorithm itself has been tested with simulated data. It was found that simulated data from monodisperse aerosols calculates to a unimodal distribution with geometric standard deviation $\sim$1.3. Simulated data from a mixture of two monodisperse aerosols calculates to a bimodal distribution provided that the two sizes are separated by a factor of four or more. This resolution cannot be improved by increasing the number of size classes.

The algorithm also was tested with simulated data perturbed by random errors. It was found that random relative errors of 2% had little effect, but that 5% errors produced obvious distortions in the computed size distribution. This shows that data of good quality are required to obtain reliable size distributions.

A more comprehensive test of the algorithm was carried out by analyzing real data obtained with near-monodisperse aerosols. The body of data used in this test was obtained in a cooperative project with personnel of the University of Minnesota Particle Technology Laboratory, who generated the test aerosols using their electrical aerosol generator. The two separate sessions of this project are described in references 1 and 10.

Twenty-one of the sets of diffusion battery penetration readings from the cooperative project were analyzed by means of the Twomey algorithm. These data sets include several for which the Pollak counter, General Electric counter, or an electrical aerosol detector was used to measure diffusion battery penetration.

The results of those tests for which the Sinclair nucleus counter was used as the detector are summarized in Table 3. It is seen that the geometric mean particle diameter extracted by the algorithm agrees well with the size expected from the electrical aerosol generator. The geometric standard deviations are larger than expected, but this is a measure of the limited

TABLE 3. RESULTS OF TWOMEY CALCULATION APPLIED TO DATA FROM NEAR-MONODISPERSE NaCl AEROSOLS

| Test No. | Aerosol Size From EAG (nm) | Calculated Results "Old" CFC Calibration $d_g$ (nm) | $\sigma_g$ | fit (%) | "New" CFC Calibration $d_g$ (nm) | $\sigma_g$ | fit (%) |
|---|---|---|---|---|---|---|---|
| 2 | 42 | 36 | 1.67 | 6.6 | 31 | 1.49 | 12.2 |
| 3A | 42 | 47 | 1.27 | 10.2 | 43 | 1.11 | 10.3 |
| 14+15 | 42 | 49 | 1.43 | 17.2 | 46 | 1.27 | 5.0 |
| 17 | 75 | 80 | 1.48 | 2.3 | 85 | 1.35 | 3.6 |
| 19A | 24 | 23 | 1.41 | 4.9 | 25 | 1.18 | 18.3 |
| 19B | 24 | 24 | 1.38 | 2.6 | 25 | 1.20 | 8.0 |

CFC: Continuous flow condensation nucleus counter (Sinclair nucleus counter)

EAG: Electrical aerosol generator

$d_g$: Geometric mean diameter

$\sigma_g$: Geometric standard deviation

Fit: Root mean square relative difference between the observed and trial values of aerosol concentration at the diffusion battery taps.

resolution of the algorithm. The table also lists results obtained using two calibration curves for the nucleus counter. Although the curves were somewhat different, the calculated particle size is nearly the same.

OVERALL SYSTEM: SERVICE AND MAINTENANCE

A block diagram of the complete aerosol measurement system is shown in Figure 6, while a photograph showing the system installed in a roof-top air sampling station is shown in Figure 7.

The ballast tank shown in Figure 6 is necessary to damp out the wide and frequent excursions of aerosol concentration which occur in urban aerosols. Normally, the flow rate through the tank is 8 ℓpm, providing a mean residence time of 7½ minutes. This has been found to be adequate. A penalty of using this

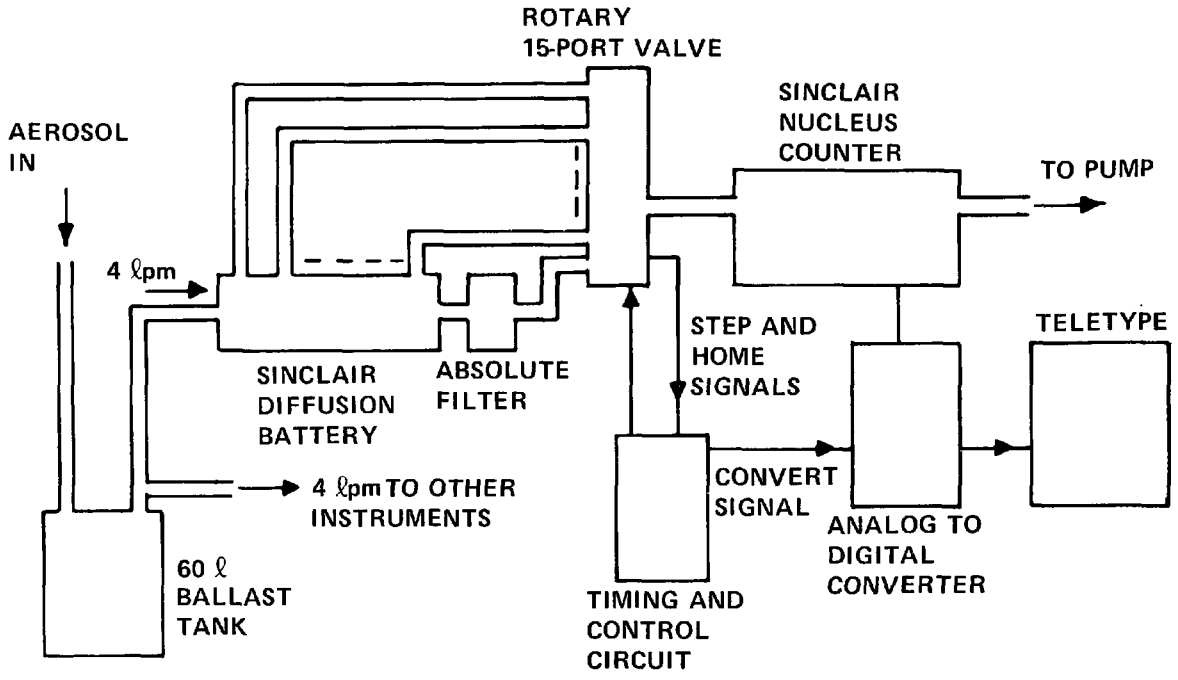


*Figure 6. Block diagram of aerosol measurement system.*

tank is that some modification of the size distribution is incurred by losses and by coagulation. We have estimated mathematically that losses by diffusion do not change the size distribution significantly, but coagulation (assuming a typical urban aerosol concentration at the ballast tank inlet) causes a 40% reduction in the concentration of 5 nm particles. For particles larger than 10 nm, the loss (or gain) is insignificant.

Routine Service Schedule

When the system is in use for hourly sampling of the outdoor aerosol, it is serviced once each weekday. On weekends, the system operates unattended for 72 hours. Our recent experience indicates that in cool or cold weather, the service interval could be extended to one week.

The parameters which are checked during each visit are the temperature in the nucleus counter cold tube and the alcohol supply and flow rate. Other parameters, such as the nucleus counter lamp intensity and the aerosol flow rate have been found to be very stable. The cycle initiation time is also checked each visit and has been found to be reliable. The punched tape is removed twice a week to avoid handling awkwardly long tapes, but this interval could be extended to one week if desired.

## Maintenance

A provisional maintenance schedule has been established for the Sinclair diffusion battery and nucleus counter in which the apparatus is disassembled and thoroughly inspected at approximate 1000 hour intervals of running time. Particular areas of concern in the inspection are the diffusion battery segments, the rotary valve seals and the lenses in the nucleus counter. The segments should be inspected for discoloration or debris on the upstream surfaces. (A slight accumulation of debris is usually found on the first segment.) The segments should be inspected for blocked holes by holding them up to a strong light.

If required, the diffusion battery segments are cleaned by soaking in ethanol, acetone or a 20% solution of phosphoric acid. The solvent treatment should not exceed one hour, since the solvents may attack the aluminum and epoxy used to mount the segments. The organic solvents are cleared from the segments by drawing air through them.

The rate of fouling of the diffusion battery segments is very low due to the low duty cycle used. In the normal one cycle per hour schedule, there is flow through the diffusion battery only 7.2 minutes per hour. The segments between taps 10 and 11, where the greatest mass deposition is expected, have a duty cycle of 1 minute per hour. The nucleus counter is to a large extent self-cleaning due to the continuous flow and condensation of alcohol in the cold tube.

Upon reassembly of the system, or after any move of the system, it is advisable to check for leaks. One convenient check is to place an absolute filter at the diffusion battery inlet, then go through a normal measurement cycle. Leaks which contribute 200 to 300 particles/$cm^3$ are detectable in this way.

## USE HISTORY AND FUTURE WORK

Three extended sampling sessions have been conducted to date with the Sinclair diffusion battery and nucleus counter. The first of these was in August 1976, on the roof of the dormitory at New York University Medical Center using an earlier version of the apparatus. Data transcription was done by hand and 233 hours of data were obtained. The results of this work, which was part of a multi-laboratory study of the New York aerosol under summer conditions, will be described in a forthcoming article.[2]

The second and third sampling sessions were conducted on the roof at EML during November 1977, and February 1978. The full complement of equipment, as described in this report, was used. The two sessions resulted in 966 hours of data. At this writing, all these data have been reduced to cards and a few statistical summaries have been done.

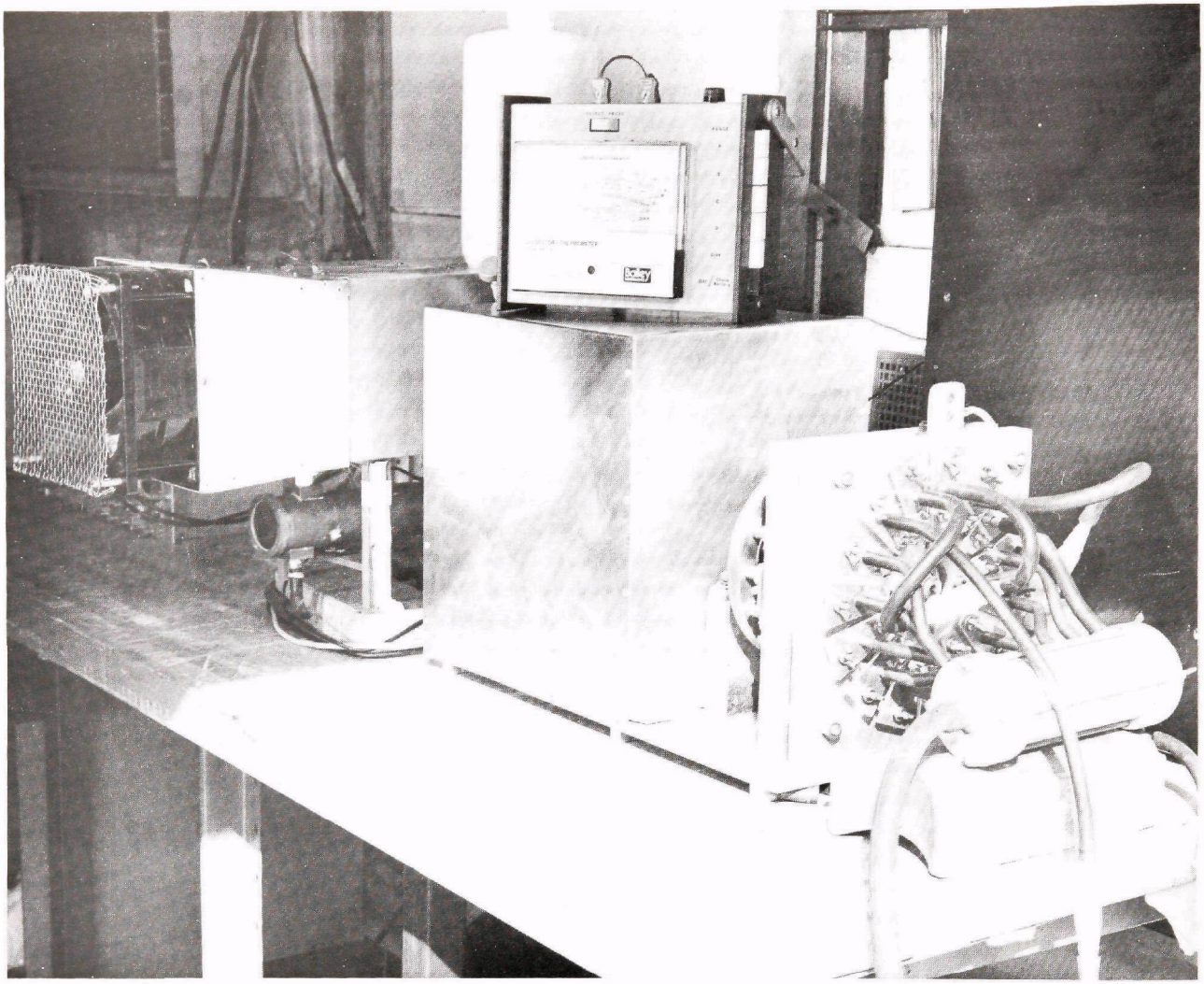

*Figure 7. Sinclair diffusion battery and nucleus counter mounted in the rooftop sampling station. (The rotary multiport valve is shown in the foreground and the nucleus counter is in the left background. Note that the screen battery, rather than the CHS or HS battery, is shown in this photograph).*

Figure 8 shows the grand average number-weighted aerosol size distribution based on 400 measurements made on the roof at EML during November and December 1977. The distribution is seen to be unimodal, with the modal diameter at 30 nm. The curve has a bell shape closely resembling that of a log-normal distribution. The grand average number concentration was 26,900 $cm^{-3}$.

Figure 9 shows the average diurnal pattern of concentration for 42 nm particles. It is seen that the minimum and maximum concentrations occur in the predawn hours and during the morning rush hours, respectively. A second maximum occurred during the afternoon rush hours. This latter maximum was not present in the earlier data taken during the summer.[2]

Additional sampling sessions are planned and further apparatus modifications are contemplated to make the system more convenient to use. We anticipate that in the near future a second system will become available so that sampling can be done simultaneously at two sites.

The most recent sampling session also indicated a need for further development or calibration work with the nucleus counter. This sampling was done during extremely cold weather. The concentrations measured with the nucleus counter were abnormally low, possibly due to the reduced amount of alcohol vapor available to condense on particles. We therefore plan to check the nucleus counter calibration over a wide range of temperatures in a laboratory environmental chamber.

## SUMMARY

The Sinclair diffusion battery and nucleus counter have been improved and modified to make them suitable for extended use in uncontrolled environments. A new sequencing valve, compatible with digital data recording circuitry and the requirements of aerosol mechanics, has been designed and constructed. An accurate timing and control circuit and a data recording device have been added to make up a system which operates unattended for three days or more.

Data processing techniques have been developed to conveniently handle data from the diffusion battery and nucleus counter. The processing is largely automatic and results in a computer card file of differential size distribution data.

Over 1000 hourly measurements of the urban aerosol in New York City have been made with the system. Operation in winter months has been found to be virtually trouble free. Operation in hot, humid weather is more difficult, but it is anticipated that the recent modification will prove to be adequate for sampling planned for this summer.

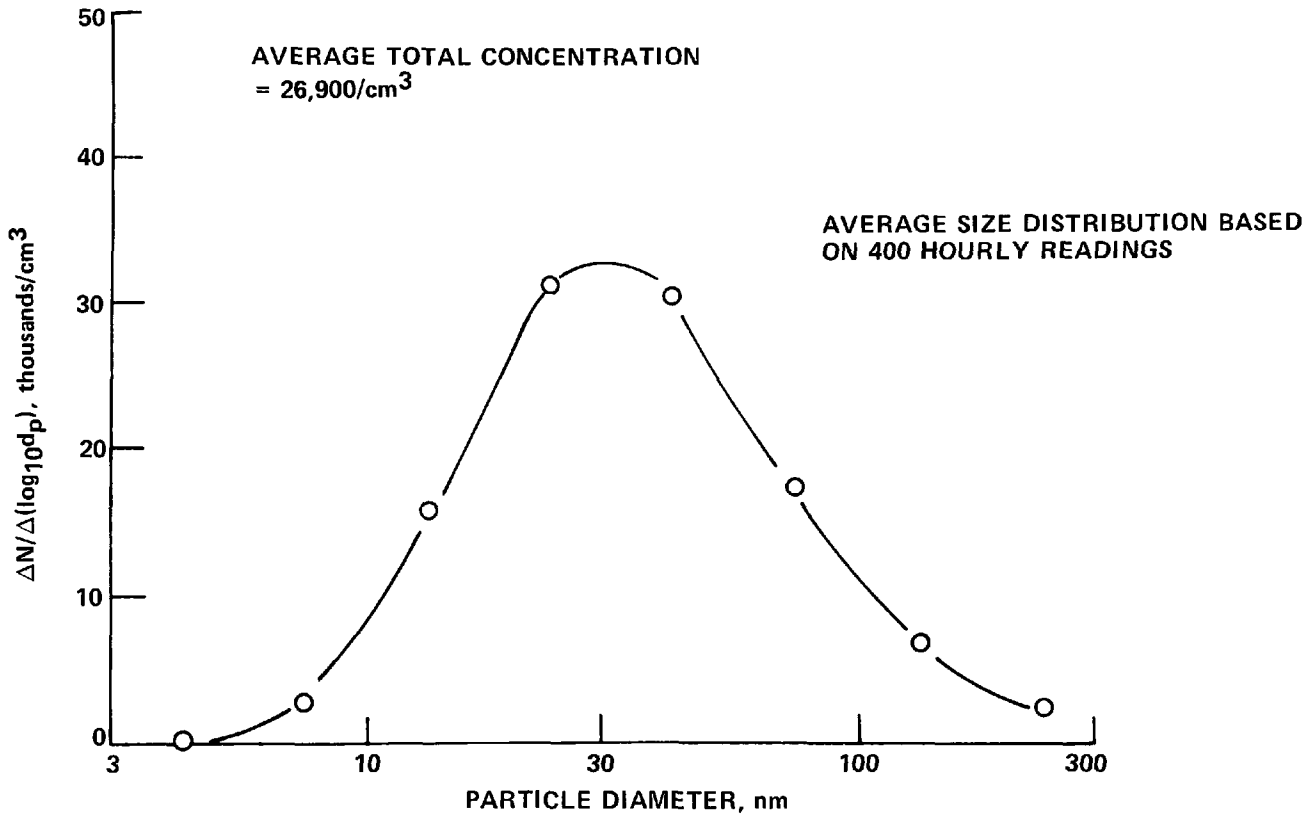


*Figure 8. Average number-weighted size distribution on EML roof, November-December, 1977.*

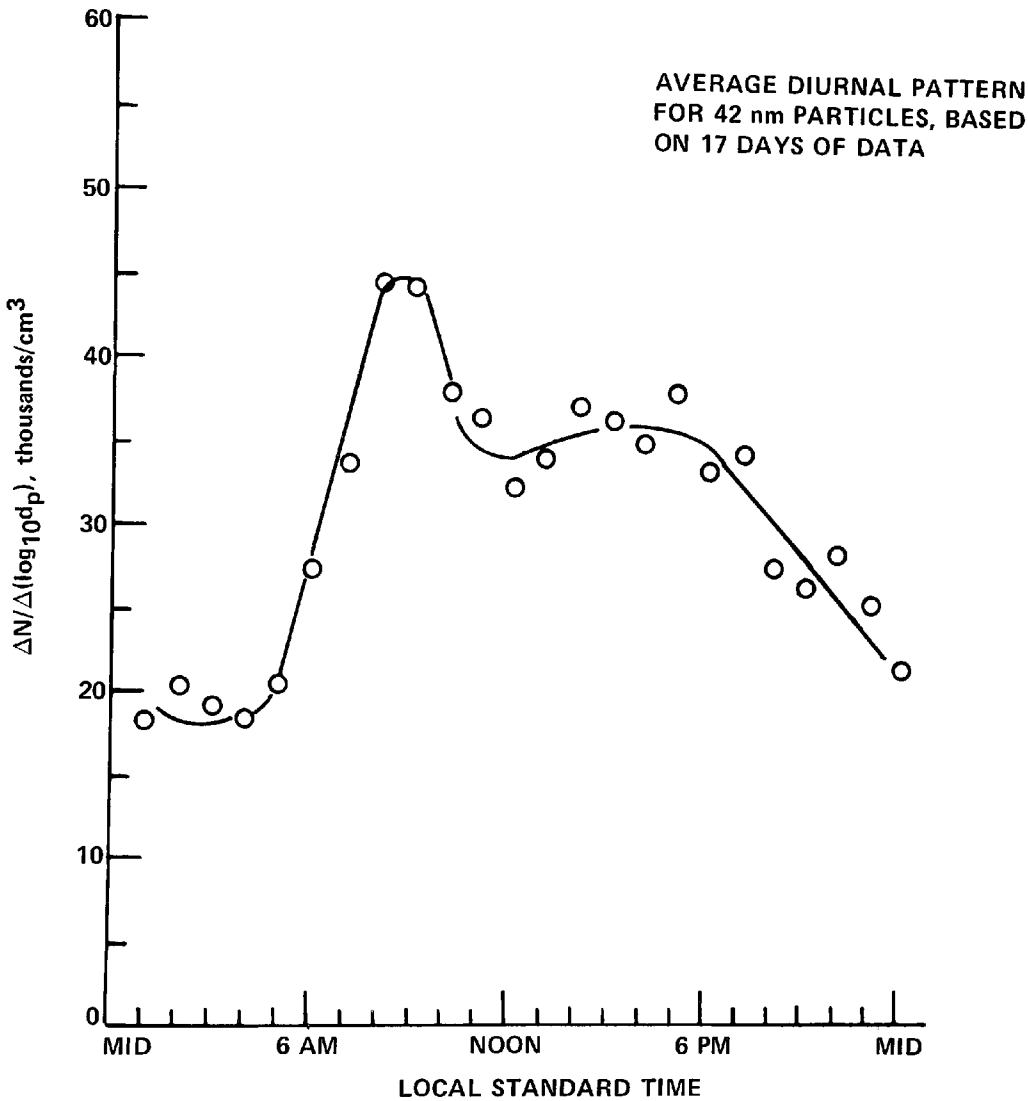


*Figure 9. Average diurnal pattern for 42 nm particles on EML roof.*

ACKNOWLEDGEMENT

F. Guggenheim and M. Cassidy, both of EML's Instrumentation Division, contributed the design and supervised the construction of the multiport rotary valve and the timing and control circuit, respectively.

REFERENCES

1. Sinclair, D., R.J. Countess, B.Y.H. Liu, and D.Y.H. Pui. Automatic Analysis of Submicron Aerosols. In: Aerosol Measurement. Proc. of Aerosol Measurement Workshop, March 24-26, 1976, to be published by University of Florida Press, 1978.

2. Knutson, E.O., D. Sinclair, and B. Leaderer. New York Summer Aerosol Study – Number Concentration and Size Distribution. New York Academy of Sciences, to be published, 1978.

3. Sinclair, D. A Portable Diffusion Battery – Its Application to Measuring Aerosol Size Characteristics. J. Am. Ind. Hyg. Assoc. 33:729-735, 1972.

4. Sinclair, D., and G.S. Hoopes. A Continuous Flow Condensation Nucleus Counter. J. Aerosol Sci. 6:1-7, 1975.

5. Maigné, J.P., P.-Y. Turpin, G. Madelaine, and J. Bricard. Nouvelle Methode de Determination de la Granulometrie d'un Aerosol au Moyen d'une Battery de Diffusion. [New Method for Determination of the Granulometry of an Aerosol by Means of a Diffusion Battery.] J. Aerosol Sci. 5:339-355, 1974.

6. Cooper, D.W., and L.A. Spielman. Data Inversion Using Nonlinear Programming with Physical Constraints: Aerosol Size Distribution Measurement by Impactors. Atmos. Environ. 10:723-729, 1976.

7. Mallove, E.F., and W.C. Hinds. Aerosol Measurement by Combined Light Scattering and Centrifugation. J. Aerosol Sci. 7:409-423, 1976.

8. Twomey, S. Comparison of Constrained Linear Inversion and an Iterative Nonlinear Algorithm Applied to the Indirect Estimation of Particle Size Distributions. J. Comput. Phys. 18:188-200, 1975.

9. Thomas, J.W. Particle Loss in Sampling Conduits. In: IAEA Symposium Proc. Vienna, 1967. pp. 701-712.

10. Sinclair, D., R.J. Countess, B.Y.H. Liu, and D.Y.H. Pui. Experimental Verification of Diffusion Battery Theory. J. Air Pollut. Control Assoc. 26:661-663, 1976.

PAPER 6

# SELECTING LABORATORY METHODS FOR PARTICLE SIZING

RONALD G. DRAFTZ
FINE PARTICLES RESEARCH LABORATORY
ILLINOIS INSTITUTE OF TECHNOLOGY RESEARCH INSTITUTE

ABSTRACT

In spite of continuing efforts to develop in-situ particle sizing methods for process streams, there still remain many instances when in-lab particle sizing is necessary or desirable. The analyst has many methods available for particle sizing and often faces the choice of which one is best.

This paper presented some general guidelines for selecting a particle sizing method based on sample size, instrument size range, analysis time, and measurement parameter and principle. Suggestions were given for sample preparation and microscopical methods for previewing samples to select the ideal sizing method.

PAPER 7

# LONG TERM FIELD EVALUATION OF CONTINUOUS PARTICULATE MONITORS

A. W. GNYP
S. J. W. PRICE
C. C. ST. PIERRE
D. S. SMITH
INDUSTRIAL RESEARCH INSTITUTE
UNIVERSITY OF WINDSOR

ABSTRACT

A critical field evaluation of five different particulate monitors representing four distinctly different principles of operation was carried out over a one year period at a secondary lead smelter. Instrument performance was rated on the basis of accuracy, reliability and maintenance as criterion variables.

The Lear Siegler RM41 and RAC transmissometer responses were primarily dependent on particle size when aerodynamic diameters exceeded 1 μm. Improvements in the long-term reliability of the Environmental Systems Corporation PILLS V backscattering device could make it potentially more useful than the best transmissometer because its calibration appears to be less sensitive to changes in particle size, color and refractive index. The Research Appliance Company transmissometer was adequate for monitoring emissions from the controlled reverberatory mode of operation but did not appear to be capable of detecting large particles whose diameters exceeded 25 μm during lead alloying kettle production. Very limited potential for application to either the reverberatory or lead alloying kettle modes of operation was exhibited by the charge transfer IKOR 2710 particulate monitor. Because of repeated mechanical failures in the sampling module of the Research Appliance Company beta radiation attenuating device supplied for the study, it was impossible to critically evaluate its monitoring capabilities.

Reliable continuous monitoring is possible in stacks exhausting gases that have passed through efficient control equipment and contain particulate matter having constant physical and chemical properties over long time periods. Continuous particulate monitors offer interesting possibilities for improving

surveillance capabilities, validating manual compliance testing and minimizing emissions from industrial sources on a 24-hour real-time basis.

## INTRODUCTION

Increasing awareness of the potential dangers arising from the discharge of toxic materials into the environment from industrial sources has prompted regulatory agencies to establish maximum emission levels. At the present time compliance is determined by periodic manual source testing programs that can provide data that are valid, at best, only for the short-term testing periods. Conventional manual stack sampling methods cannot provide records of any periodic excessive emissions resulting from faulty operation of installed abatement equipment or process upsets.

Assurance of long-term compliance with and enforcement of regulations requires the availability of reliable continuous monitoring capabilities. Although there are several promising particulate monitoring systems, their application has been restricted by the lack of information on their accuracy, precision and long-term reliability. In the absence of such data, it is not surprising that industries have been reluctant to commit significant capital outlays for the installation of large scale continuous monitoring systems.

This study concentrated on the evaluation of the performance characteristics of continuous particulate monitoring devices because, with the exception of transmissometer systems, there are no established performance specifications for any commercially available monitors. The principal objectives of this investigation were to assess the suitability, reliability, and accuracy of continuous particulate monitors for stationary sources on the basis of field experience at a secondary lead smelter.

### Site

The secondary lead processing plant selected for this study provided an opportunity for assessing the viability of using continuous instrumentation for real-time monitoring of lead, which had been designated as a hazardous pollutant by Environment Canada. From a practical viewpoint, the stack was of suitable size and construction to simultaneously accommodate five continuous monitors and three manual sampling trains. The two distinctly different operating modes:

i. uncontrolled lead alloying kettle

ii. baghouse equipped reverberatory furnace

provided a wider range of emission characteristics than normally obtainable from a time invariant process.

## Process Exhaust System

Reverberatory furnace gases, exhausted by means of an 18,000 scfm fan, were cleaned in a baghouse before entering the stack through horizontal breeching at the 55-foot level as illustrated in Figure 1. Gas temperatures to the bags were kept below 300°F by means of ambient air drawn through the intakes in the ducting from the reverberatory furnace. Cleaning of the baghouse was initiated manually at 15-20 minute intervals. Mechanical shaking of the bags in each of the three baghouse compartments for periods of 25-30 seconds set up well-defined vibrations in the stack. Pulses of particulate emissions were detected by all of the continuous monitors during bag cleaning.

Emissions from the lead alloying kettles by-passed the baghouse. They were removed from the top of the kettles by fume hoods located at the rear of each unit. These fume hoods were connected to a common 30-inch, round, duct which led to a 24,000 scfm fan located at the base of the stack. During reverberatory furnace processing both the baghouse and alloying kettle fans were operational; otherwise the baghouse fan was not used.

The test plant had several kettle units. They were used for remelting, alloying and refining purposes. Each consisted essentially of a hemispherical cast steel bowl mounted over burners fired with light industrial oil.

## Instrument Selection

Instruments commercially available in Canada at the inception of this investigation were limited to systems employing

i. light attenuation

ii. light scattering

iii. charge transfer

iv. beta-radiation attenuation.

Instrument selection was dependent, partly, on the cooperation of American and Canadian manufacturers and distributors. As a result, the final complement consisted of the five monitors listed in Table 1.

# TESTING PROGRAM

Figure 2 illustrates the relative locations of the twelve ports, installed at the enclosed sampling and exposed instrument platforms, with respect to the breeching from the baghouse.

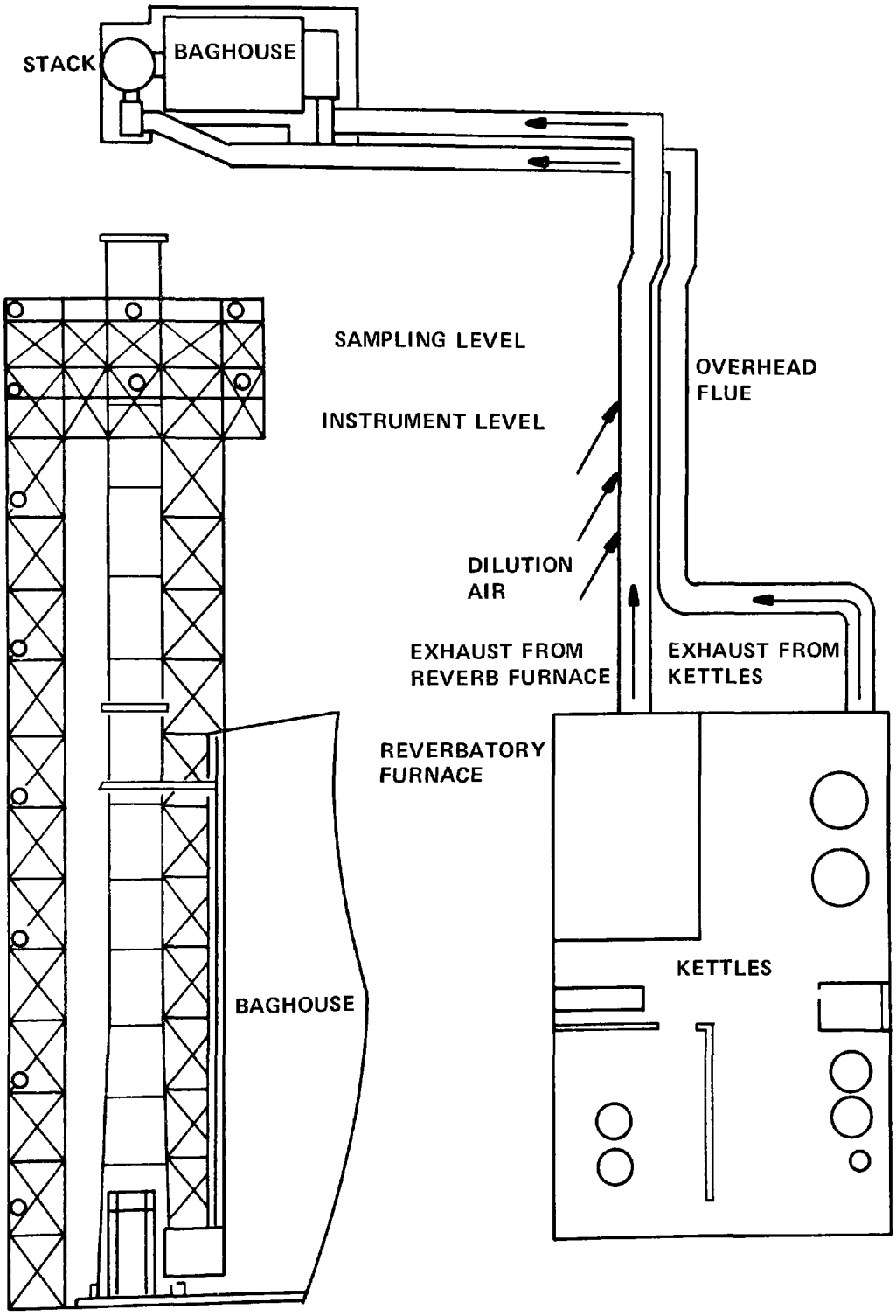


*Figure 1. Plan and elevation of secondary lead smelter.*

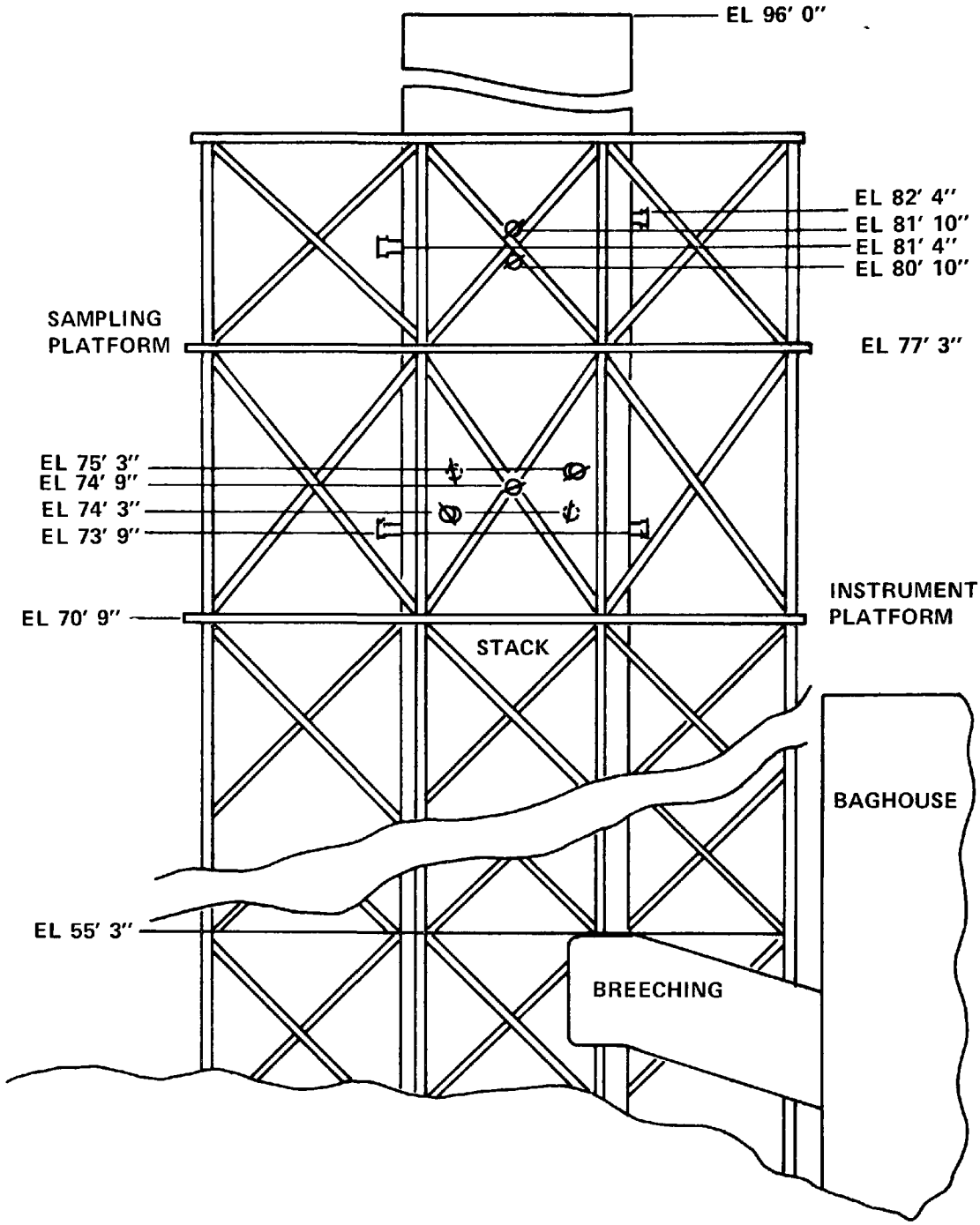


*Figure 2. Elevations of ports and instrument and sampling levels.*

TABLE 1. CONTINUOUS PARTICULATE MONITORS SUBJECTED TO FIELD EVALUATIONS

| Principle of operation | Instrument model | Manufacturer |
|---|---|---|
| Light Attenuation | RM 41 No. 275 | Lear Siegler Inc. Environmental Technology Div. |
| | RAC No. 2700 | Contraves Goertz Corp. with Research Appliance Co. |
| Light Scattering | PILLS V | Environmental Systems Corp. |
| Charge Transfer | 2710 | IKOR Incorporated |
| Beta Radiation Attenuation | Automatic Stack Monitor No. 2412 | Research Appliance Co. |

## Sampling Trains

The basic components of the particulate matter sampling trains, distributed by the Western Precipitation Division of Joy Manufacturing and sold under the trade name "Emission Parameter Analyzer", are represented schematically in Figure 3. Prior to use the S-type pitot tube, orifice rate meter and dry total gas meter were calibrated in the University of Windsor laboratories according to EPS standard procedures.[1]

Aerodynamic particle size determinations were carried out by means of an Andersen Stack Sampler in conjunction with a second Joy sampling train. The standard sampling probe-pitot tube arrangement was modified by extending the S-type pitot tube in order that velocity determinations could be made in the vicinity of the sampling nozzle. Figure 4 shows the arrangement of the extended S-type pitot tube, Andersen impactor and sampling nozzle.

In order to acquire samples for microscopic particle sizing and to test the validity of single point monitoring and sample acquisition a third sampling train was required. The arrangement of components, illustrated in Figure 5, also facilitated the acquisition of gas samples for on-site gas chromatographic analysis.

## Location of Ports

Because seven ports were required for the five particulate monitors and four ports were needed for the manual sampling

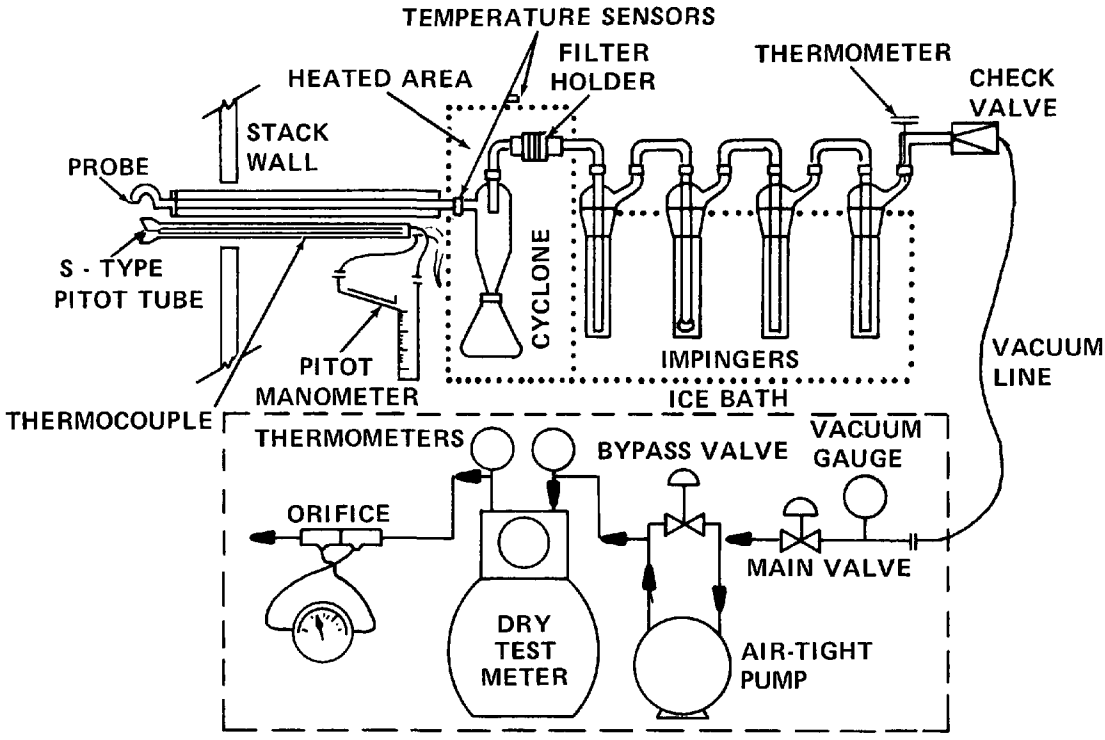


*Figure 3. Particulate matter sampling train.*[1]

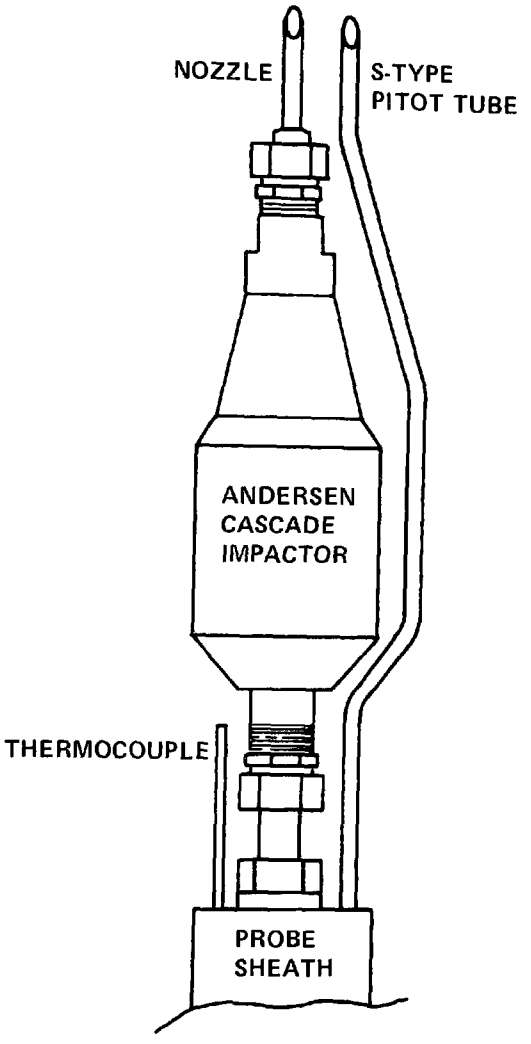


*Figure 4. Arrangement of extended S-type pitot tube with respect to Andersen cascade impactor and sampling nozzle.*

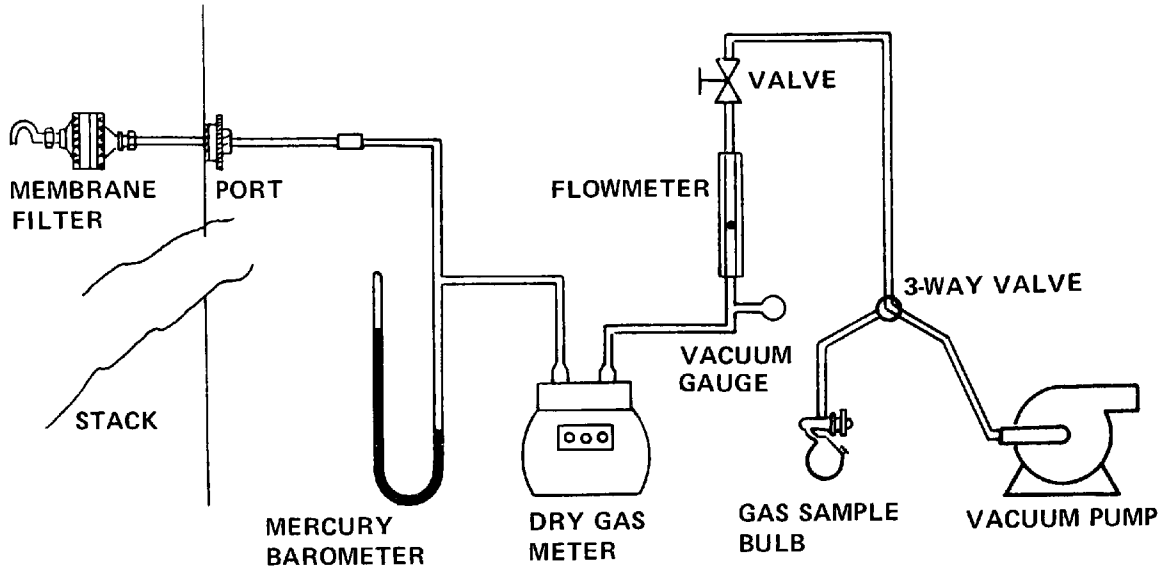


*Figure 5. Components of membrane sampling train.*

trains, it was not possible to locate all of them at one level on the stack. Limitations imposed by scaffolding dimensions and minimum requirements of the EPS source testing code[1] dictated that the manual sampling train ports be provided at the upper level as shown in Figure 2. The arrangement of the continuous monitoring instruments is shown in Figure 6. Under the test conditions all monitors were at least four stack diameters downstream from the flow disturbance created by the baghouse breeching. The manual sampling trains were 6 1/2 stack diameters from the same flow disturbance and 3 1/2 diameters upstream from the stack exit.

The placement of the instruments at the lower level was designed to minimize mutual interference. The proximity to the flow disturbance was not expected to handicap the sampling program because submicron particulate matter would predominate during the reverberatory furnace campaign. Introduction of exhaust gases at the base of the stack during the lead alloying kettle production mode provided more than 8 stack diameters of separation between the sampling sites and the exit from the induced draft fan.

Sampling Points

All particulate matter loading evaluations were determined from samples collected at 12 points along each of the two perpendicular traverses as shown in Figure 7.

Aerodynamic particle size determinations with the Andersen in-stack cascade sampler demand that isokinetic conditions be maintained at the nozzle for representative sample collection.

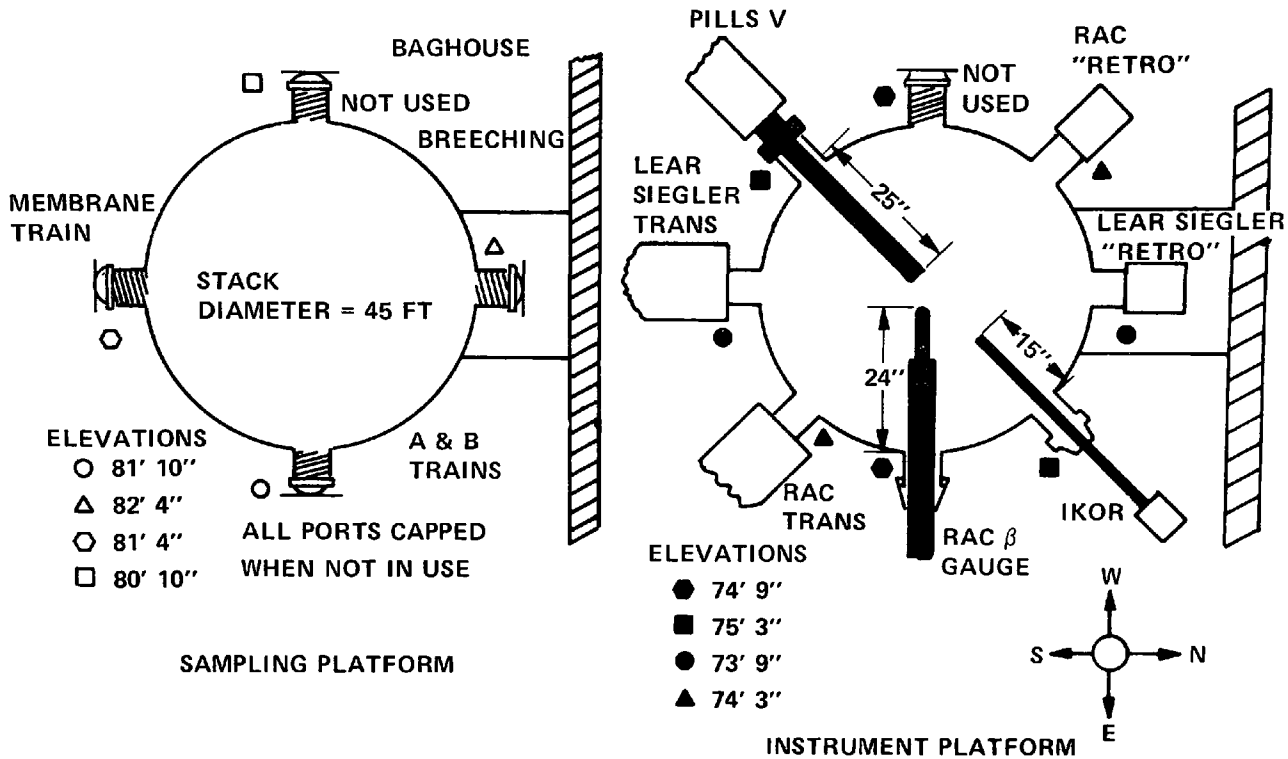


*Figure 6. Arrangement of ports at the sampling and instrument levels.*

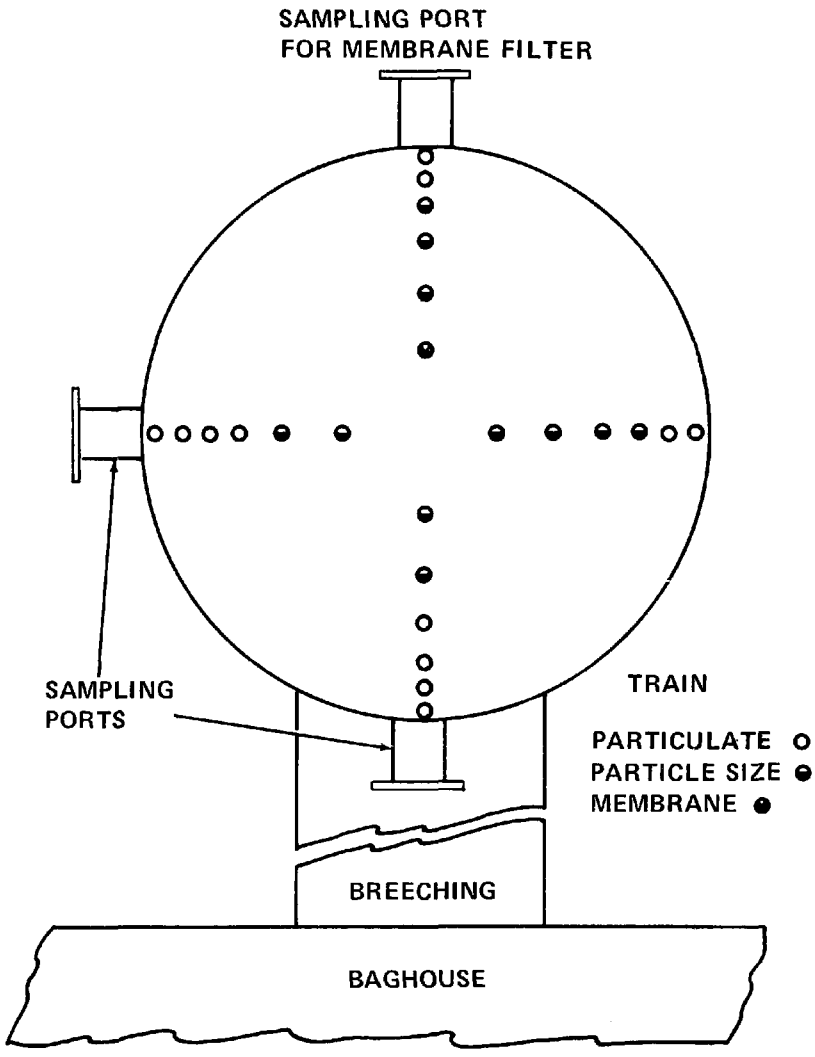


*Figure 7. Location of sampling points.*

In addition, a constant volumetric flow rate must be maintained through the device because the impaction efficiency of each collecting plate is a function of the gas flow rate. In order to satisfy both conditions, it was necessary to locate sampling points along both traverses where the stack conditions were such that a constant flow rate provided, essentially, isokinetic sampling conditions. Aerodynamic particle size sampling was carried out at the points shown in Figure 7. The cumulative method of sample collection was employed for both particulate loading and particle size determinations.

Initially, the membrane sampling train was to be used to collect particulate matter for microscopic particle sizing and gas samples for chromatographic analyses. In view of its limited traversing capabilities this train provided samples from a single fixed point only. Because two of the continuous particulate

monitors represented stack conditions in terms of measurements at a single point, it was useful to check the validity of their data with grain loading determinations derived from single point sample acquisition with the membrane train. The sampling probe on this train provided sample collection from the point ⊕ in Figure 7.

Sampling Time Per Point and Gas Sample Volume

Sampling times per point for particulate loading and particle size determinations were designed to provide readily measurable amounts of materials without overloading the filter or plates of the Andersen impactor. Consequently, gas sample volumes corresponded to about 150 $ft^3$ for particulate matter and approximately 125 $ft^3$ for particle sizing tests. The membrane train was kept at one point for the duration of any test.

CONTINUOUS PARTICULATE MONITOR DATA LOGGING

Although all the continuous particulate monitors were installed at the lower level, where they were exposed to adverse effects of the environment, the remote control and recording components had to be located in a protected area equivalent to an industrial control room. The sampling level was modified to control room specifications when it became apparent that location of the remote control and recording devices in the field office, at ground level, would not permit real time observation of monitor performance in conjunction with the manual sampling program. Before and after every test, each continuous particulate monitor system was zeroed and calibrated according to procedures outlined by the instrument manufacturers.

Optical Transmissometry

The electrical output from the optical head assembly of the RAC transmissometer passed to the remote control panel which provided:

i. direct readings for 0-100% opacity

ii. the operating mode selector switch (normal, span and zero calibration modes)

iii. electrical connections for both the data transmitting cable and 115-volt single-phase power input.

The two-speed strip chart recorder provided with the remote control panel was not used because its scale was inadequate for the scientific purposes of this study. Instead, the remote output signal was fed to a Hewlett-Packard, Model 7100B, strip chart recorder with a 17500 A multiple-span input module.

In the Lear Siegler RM 41 monitor, the electrical signal from the transducer unit was directed to the Optical Density/ Opacity Converter which provided, simultaneously, linear opacity and optical density outputs. The convertor unit also provided

i. manual controls for remote zero and span calibration checks

ii. a remote fault indicator for the transmissometer

iii. a shutter position indicator

iv. an over-range indicator for the selected measurement range

v. a filter air-purge flow restriction indicator

vi. an automatic compensation for zero drift and excessive compensation indicator

vii. an alarm level indicator and reset switches.

The four-inch strip chart recorder normally supplied with the RM 41 system as an optional unit was replaced with a Hewlett-Packard Model 7100B version, equipped with a 17500 A multiple-span input module, for improved accuracy when integrating optical density signals.

Backscattering

The ESC Particulate Mass Concentration Monitor was a completely self-contained unit with meter read-out and range selection located on the instrument panel at the monitoring level. For remote data logging at the sampling level control room, the output signal was fed to a Rikadenki B-161-361 Series multipen recorder with a 50 ohm resistor connected across its input terminals. The resulting 0-1 volt analog signal was integrated with a Monitor Lab Model 8640 Mean-Value Integrator. A second channel of the Rikadenki recorder produced a permanent record of the output from this integrator. On the model supplied for this investigation the manufacturer provided measurement ranges of 0.05, 0.2, 1.0 and 5.0 gr/acf.

Charge Transfer

The continuous output signal from the IKOR 2710 sensor probe was fed to a control unit consisting of

i. a power supply for the device

ii. a sensor output display

iii. an integrating totalizer

iv. a test set function switch that is used for checking sensor electronics.

The 0-10 volt output was fed to one of the Hewlett-Packard Model 7100B recorders located in the control room area. Five decades, varying from 0.1 to 1,000, provided sensitivity selection for mass flow sensing.

Beta Radiation Attenuation

The RAC Automatic Stack Monitor control console in association with a Monroe, Model 1810, programmable printing calculator regulated the entire operation of this system. Automatic governing of all system sequences, as well as individual component functions, was performed by the master control module. Input signals from the instrument subsystems were assimilated by the control module and then transmitted to the mini-computer for storage, calculation and printout.

The control console panel provided visual, digital readouts of

i. gas sample volumes

ii. beta counts for filter taring and loading

iii. time intervals

Tape printouts of the above parameters and particulate matter concentrations in appropriate units were obtained from the mini-computer.

RESULTS

Thirty-two particulate matter concentration, particle sizing, and membrane tests were carried out at the secondary lead smelter during the nine month period from 4 June, 1976 to 7 March, 1977. Twelve of these tests accounted for the reverberatory furnace mode of operation. The remaining tests were conducted while refining processes were in progress in the various lead alloying kettles.

The simultaneous evaluation of the five continuous particulate monitors ended on 15 October, 1976 after the completion of seventeen tests. A five month period of long-term reliability evaluations terminated on 7 March, 1977.

## Particulate Matter Concentrations

Since particulate concentrations in the stack gases were determined simultaneously with three different trains, it is possible to compare single point (membrane) and limited traversing (Andersen impactor) sample acquisition with the standard EPS source testing procedures.

Figure 8 illustrates the close agreement between the data obtained from the 24 point conventional grain loading tests and values based on particle size determinations using 12 sampling points. During some of the lead alloying kettle tests, a wide range of particulate loadings in the stack gases was obtained through the cooperation of the Smelter Supervisor, who provided conditions simulating undesirable upset episodes that could occur during normal processing.

With the exception of two tests during which obvious sampling train failure occurred as a result of glass breakage, a paired t-statistic test indicates a 92% level of confidence for the particulate concentrations measured.

According to Figure 9, particulate concentrations determined from the one point, membrane, sample acquisition technique are approximately 35% higher than the mean values determined from the 24 point and 12 point traversing tests. Deviations of this magnitude indicate that single point sampling with membrane filters can serve only as a semi-quantitative measure of continuous particulate monitor performance. It should be noted that the mode of plant operation did not significantly bias the particulate concentrations measured with the membrane filter.

## Aerodynamic Particle Size Distribution Data

The experimental data were plotted on logarithmic-probability (log-prob) paper as illustrated by Figure 10. Normal heating of a molten charge during lead alloying kettle processing produced particulate emissions corresponding to the linear plot exemplified by Test 24.

Disturbance of a kettle melt by the addition of sawdust or sulfur was conducive to the generation of particles whose cumulative log-probability size distribution plot showed two linear segments comparable to the Test 13 representation in Figure 10. The break in the linearity seems to be indicative of particulate production as a result of normal emissions from a hot melt plus charring of granular additives dumped on to the hot metal surface.

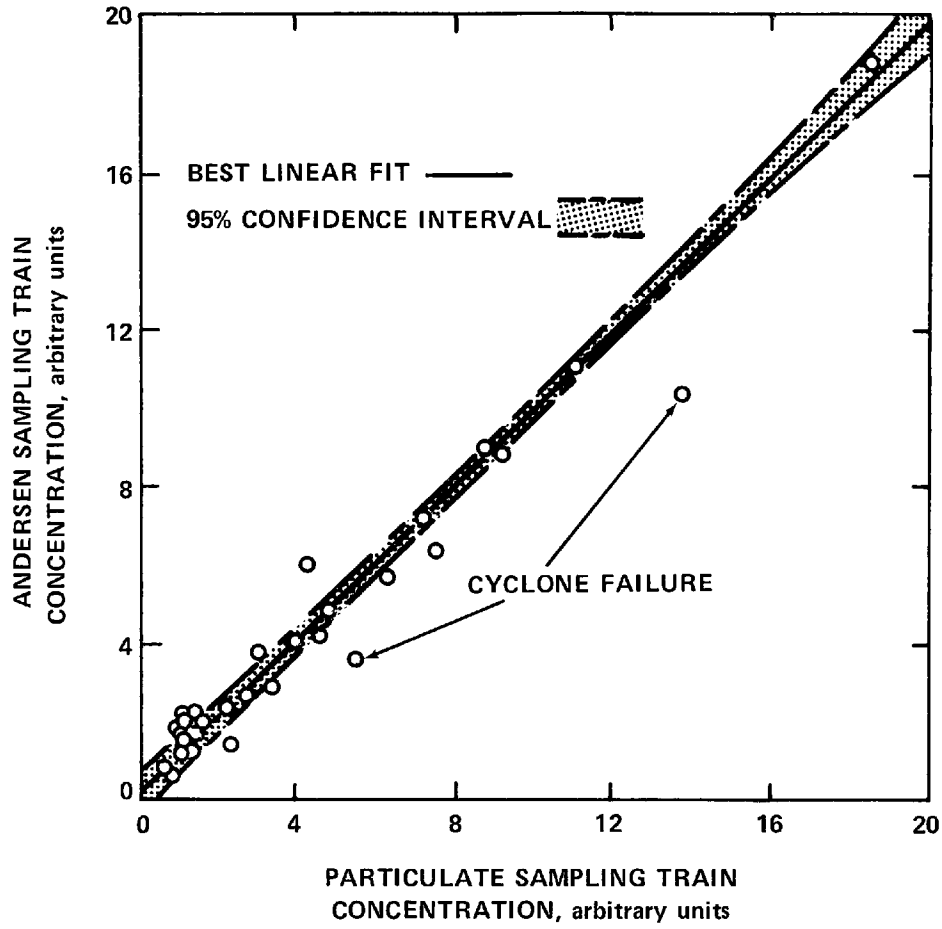


*Figure 8. Comparison of standard and particle sizing train data.*

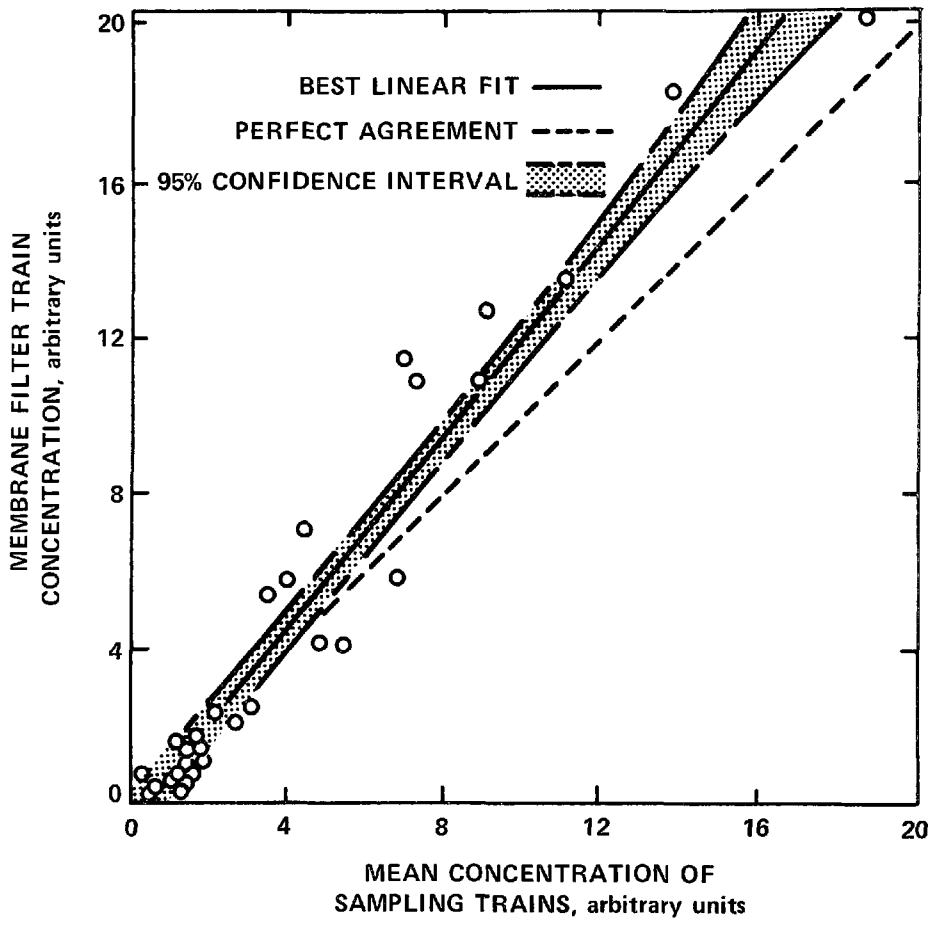


*Figure 9. Comparison of particulate concentration determinations from single point membrane and two traversing techniques.*

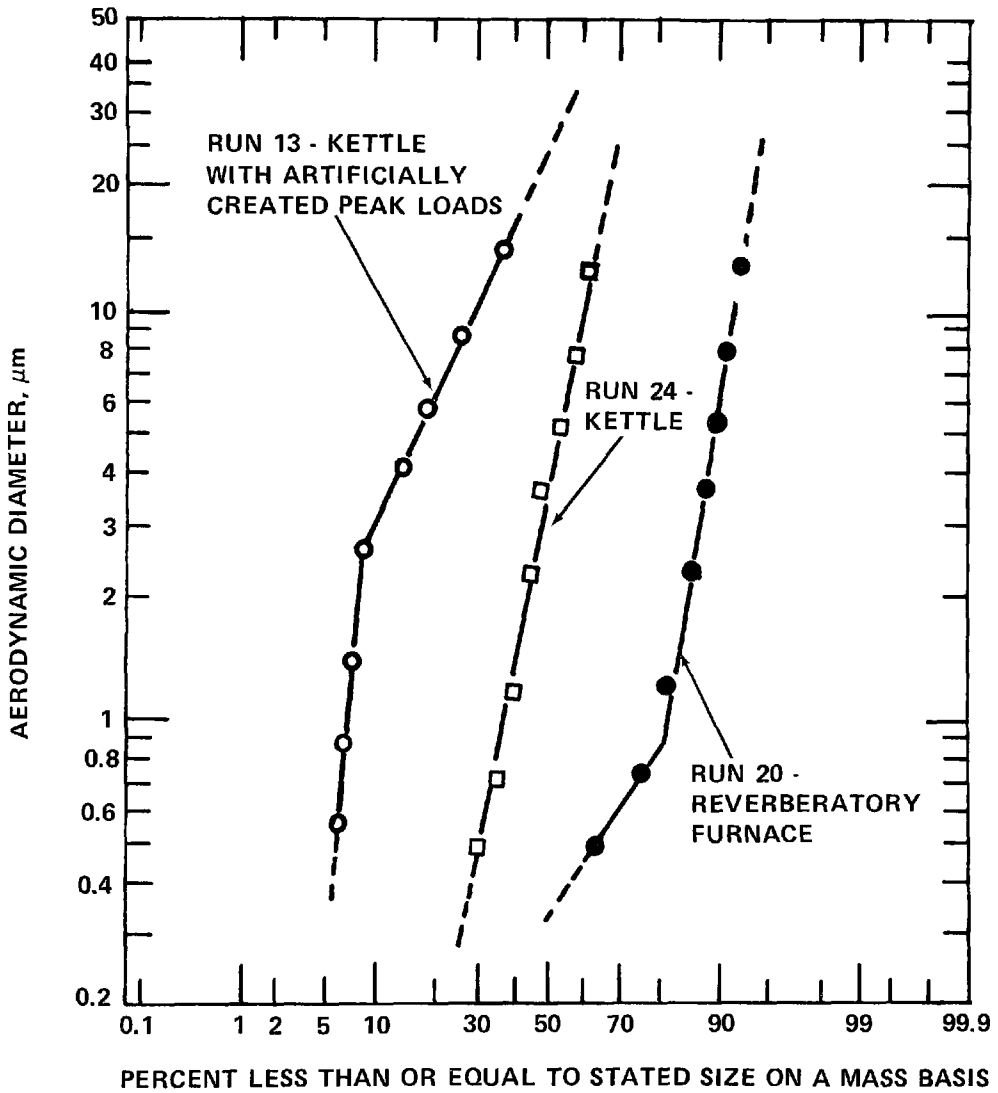


*Figure 10. Typical aerodynamic particle size distribution data.*

Test 20 illustrates the typical log-probability distribution of the particles collected during the reverberatory furnace mode of operation. The two linear portions of the resultant plot again suggest that the sample was a composite of emissions from two different processes. It must be remembered that during reverberatory furnace production the lead alloying kettles were normally operational. As a result, reverberatory furnace test samples really represent superimposition of baghouse emissions on conventional kettle particulate matter. When the data from Test 15 are excluded, on the basis of sample color and documentation of simultaneous lead-alloying kettle operation, from the eleven other reverberatory tests, the arithmetic mean of the aerodynamic particle diameters of the baghouse emissions is 0.43 μm with a standard deviation of 0.13 μm. The arithmetic mean of the aerodynamic particle diameters for the twenty lead alloying kettle tests is 18.9 μm for the approximate range from 0.05 to 150 μm.

## Particulate Matter Analysis

Identification of the major metallic components in the particulate emissions was required in order to determine whether continuous monitor performance characteristics could be related to particle compositions. A preliminary ESCA determination showed that lead, tin and zinc were the three principal metals in both the reverberatory furnace and lead alloying kettle stack emissions. No other metals were present, consistently, in excess of 0.5%.

The results of X-ray fluorescence analyses carried out in the EPA laboratories at Research Triangle Park, North Carolina, confirmed that lead, tin and zinc would be the predominant metallic species in all the samples.

Due to the presence of tin oxides in the collected solid materials, it was necessary to fuse the particulate matter before atomic absorption analyses were carried out on all samples. The data in Table 2 represent average values determined from the combination of particulate matter recovered from the nozzle, probe, cyclone, filter and impinger components of the sampling train.

## Continuous Particulate Monitor Performance

Figure 11 illustrates the Lear Siegler RM 41 instrument response. It is impossible to correlate the results of the 32 tests by a single curve. However, three distinctly different least square linear calibration plots can be recognized in terms of the aerodynamic particle size of the emissions. The behavior of the RAC instrument was essentially similar to the Lear Siegler RM 41 as shown in Figure 12.

TABLE 2. CHARACTERISTIC COLORS AND COMPOSITIONS OF PARTICULATE SAMPLES

| Test number | Color of particulate on membranes | Composition of particulate matter by atomic absorption analysis, weight % | | | |
|---|---|---|---|---|---|
| | | Pb | Sn | Zn | Total metal |
| 1 | grey white | 11 | 4 | 0.33 | 16 |
| 2 | blue grey grey | 31 | 22 | 2.0 | 55 |
| 3 | grey white | 27 | 18 | 2.6 | 47 |
| 4 | brown | 6.0 | 3.5 | 0.23 | 10 |
| 5 | black | 22 | 21 | .39 | 44 |
| 6 | brown | 11 | 6.7 | .95 | 18 |
| 7 | grey black | 30 | 12 | .95 | 42 |
| 8 | dark grey black | 27 | 4.3 | 12 | 43 |
| 9 | black | 50 | 5.8 | 1.2 | 57 |
| 10 | brownish grey black | 39 | 6.9 | 0.28 | 46 |
| 11 | brownish | 44 | 5.6 | .56 | 50 |
| 12 | membranes ruined | 14 | 5.1 | 3.3 | 22 |
| 13 | black | 45 | 7.0 | 0.75 | 53 |
| 14 | brown | 32 | 5.9 | .70 | 38 |
| 15 | brown | 47 | 15 | .75 | 63 |
| 16 | whitish grey | 36 | 14 | 2.5 | 52 |
| 17 | dirty grey yellowish | 11 | 3.6 | 0.30 | 15 |
| 18 | grey white yellowish | 23 | 30 | 2.1 | 56 |
| 19 | dark grey | 24 | 31 | 2.1 | 57 |
| 20 | grey | 16 | 33 | 1.9 | 51 |
| 21 | dark grey | 12 | 11 | 2.4 | 25 |
| 22 | brownish black | 9.6 | 9.4 | 1.5 | 20 |
| 23 | black light grey | 22 | 20 | 2.2 | 43 |
| 24 | black | 56 | 8.6 | 0.11 | 65 |
| 25 | silver grey black | 58 | 8.7 | .11 | 66 |
| 26 | dark grey brown | 40 | 3.0 | .13 | 43 |
| 27 | brown | 39 | 3.6 | .14 | 43 |

(continued)

TABLE 2 (continued)

| Test number | Color of particulate on membranes | Composition of particulate matter by atomic absorption analysis, weight % | | | |
|---|---|---|---|---|---|
| | | Pb | Sn | Zn | Total metal |
| 28 | brown light cream | 28 | 2.9 | 0.24 | 31 |
| 29 | membranes ruined | 16 | 2.4 | .11 | 18 |
| 30 | orange grey grey | 19 | 4.2 | .21 | 23 |
| 31 | black | 33 | 4.6 | .55 | 38 |
| 32 | black | 34 | 19 | .62 | 53 |

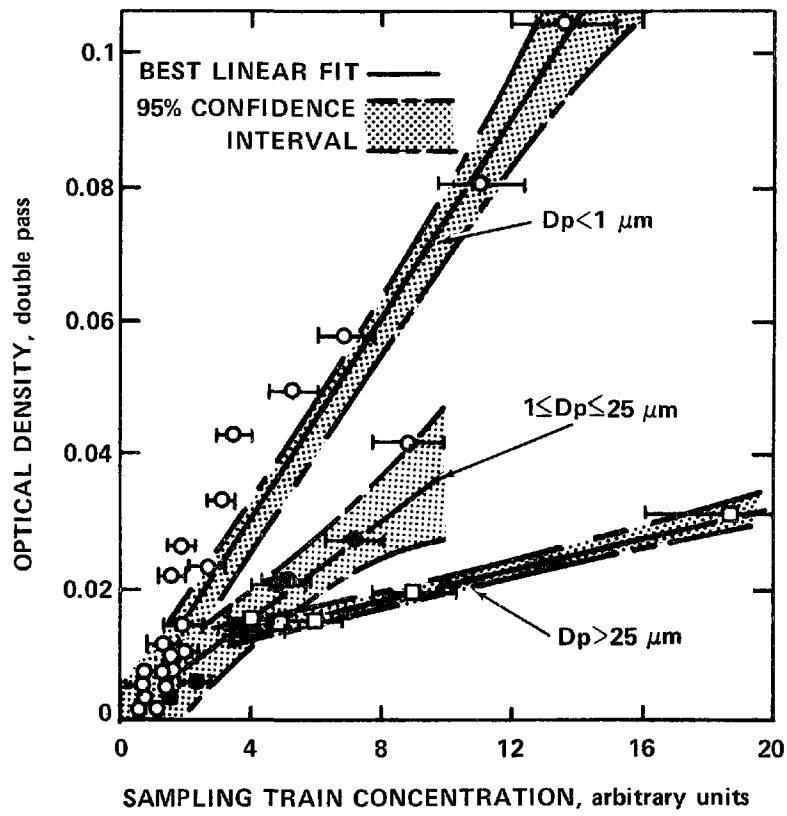


*Figure 11. Calibration data for Lear Siegler RM 4I transmissometer.*

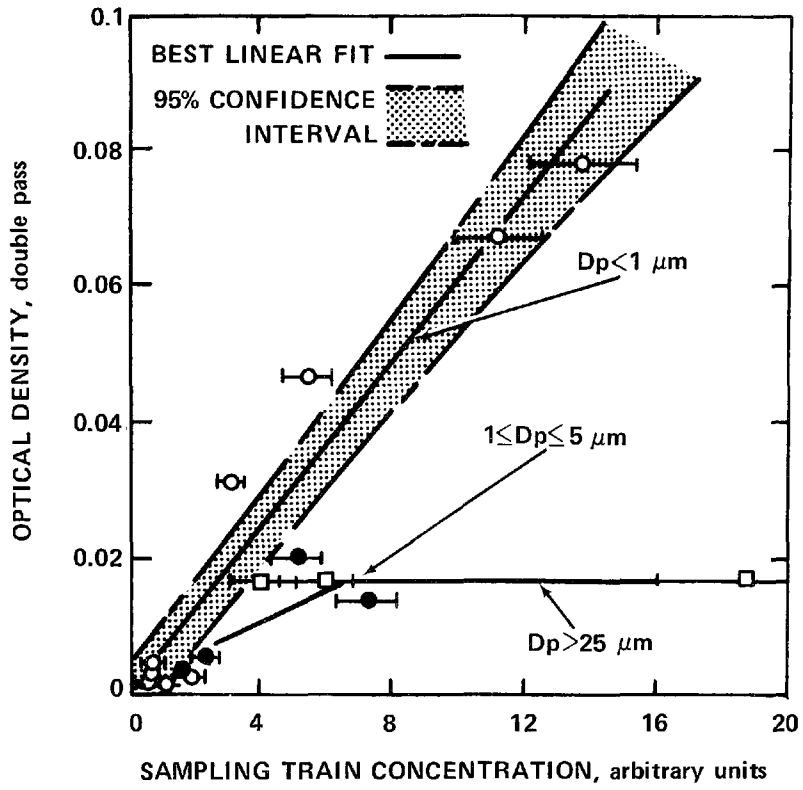


*Figure 12. Calibration data for RAC transmissometer.*

According to Figure 13, it would appear that there are two distinctly different calibrations for the PILLS V continuous particulate monitor. These lines correspond to periods following initial installation and extensive field servicing by personnel from ESC head office.

When the 31 test points during which the IKOR device was operational are plotted in Figure 14, particle size considerations once again provide a means of classifying instrument performance according to the two linear plots.

It was extremely difficult to derive reliable calibration curves for the RAC beta radiation attenuating device because of repeated mechanical failures in the tape drive and clamping systems. Figure 15 illustrates the instrument response during the 13 tests when data could be collected. The two calibration lines suggest that the performance of this continuous particulate monitor was also dependent on the size of the particulate matter being examined.

## Continuous Monitor Reliability

Figure 16 and Table 3 summarize the results of the long-term reliability evaluation of the five continuous particulate monitors used in this study.

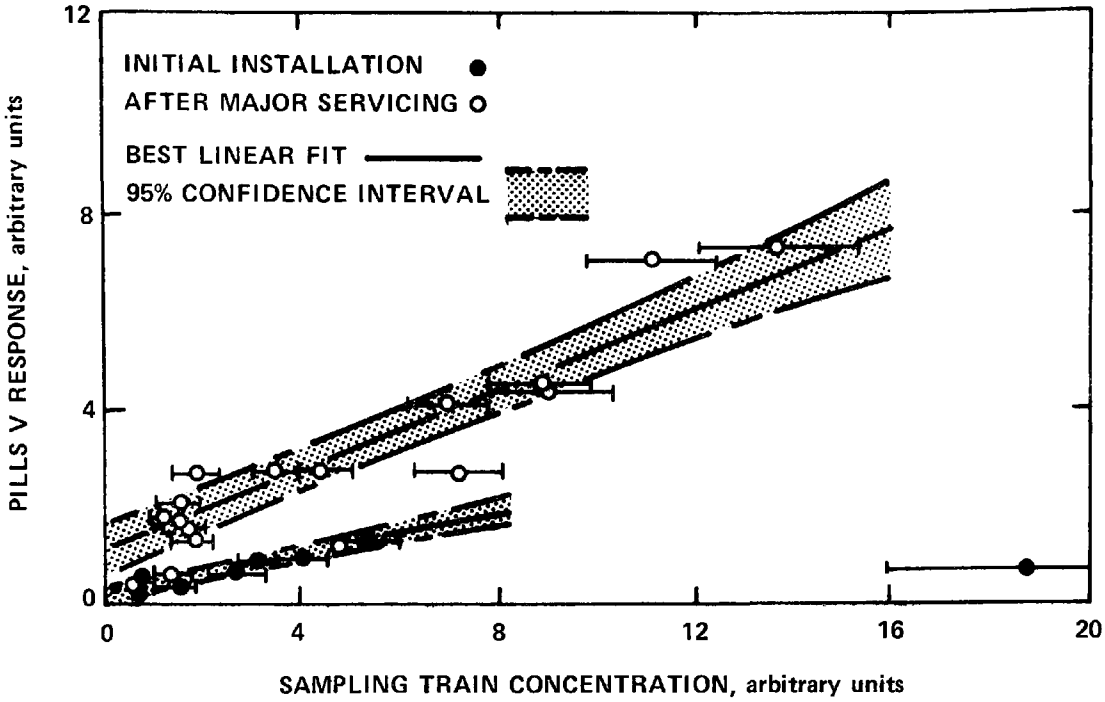


*Figure 13. Calibration data for ESC PILLS V monitor.*

It is clearly evident that the Lear Siegler RM 41 transmissometer operated throughout the entire testing period without any major servicing. Only routine cleaning of filters and retro-reflector and replacement of indicating bulbs were required.

The RAC transmissometer experienced a blower-motor failure after about five weeks of operation. However, the capacity of the retro-reflector blower provided sufficient purge air to permit the instrument to function satisfactorily until its removal from the stack.

The IKOR charge transfer device operated during the entire testing program but required regular removal from the stack for cleaning of the sensor. Although this was a relatively simple procedure requiring minimal time, the conditioning of the sensor following cleaning often took several hours.

Factory trained personnel were called to the site twice during the testing period to make appropriate adjustments to the ESC PILLS V backscattering monitor. Prior to Test 8, the optical interrupters and a printed circuit board were replaced in an effort to eliminate the excessive base line current signal which made zeroing and spanning of the instrument impossible. When the same problems reappeared after Test 14, the unit was overhauled completely. The amount of servicing was consistent with the field development of any new instrument. This was the fourth PILLS V manufactured and the first subjected to rigorous evaluation in an industrial stack.

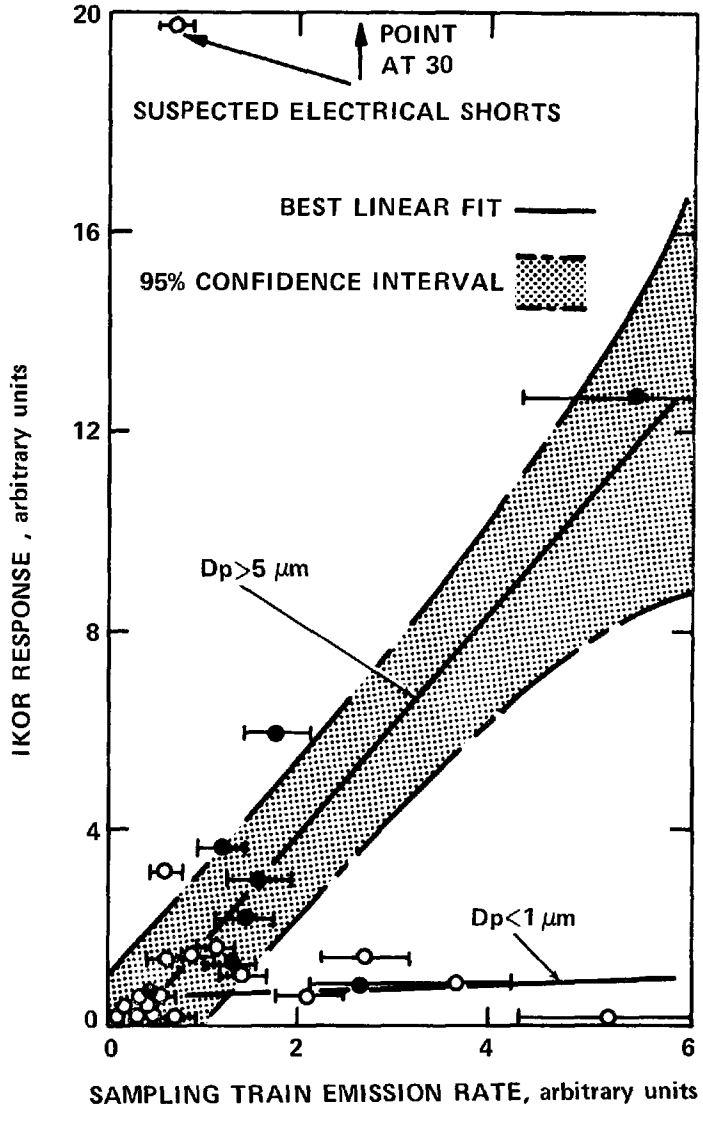


*Figure 14. Calibration data for IKOR monitor.*

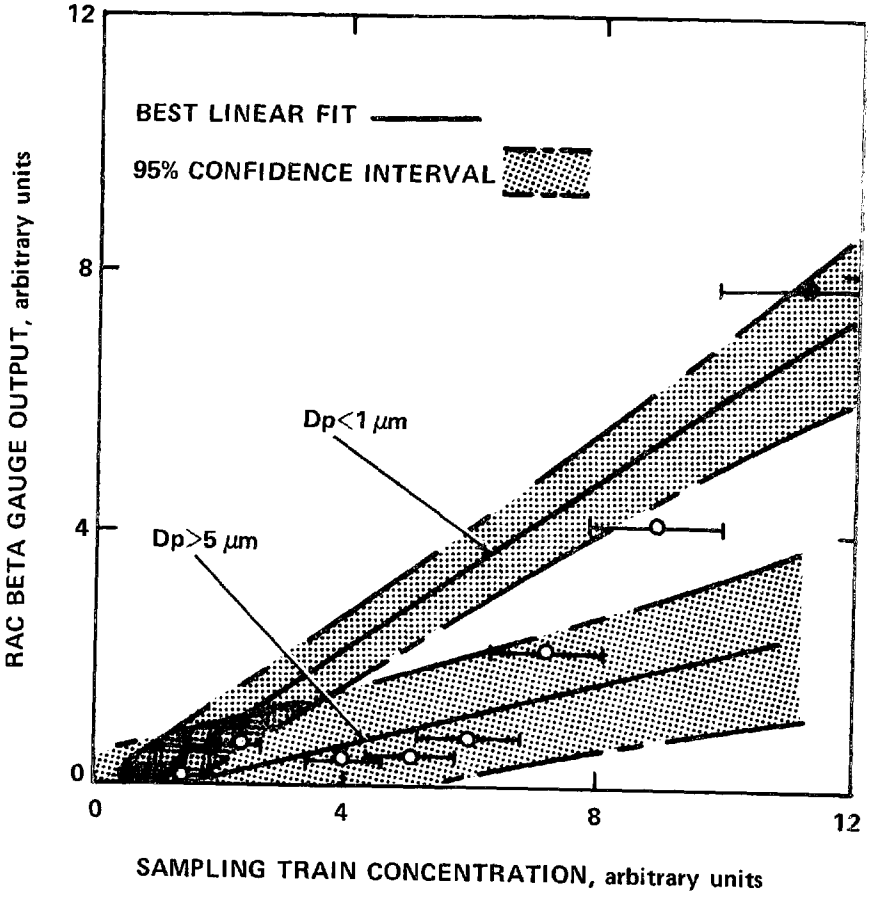


*Figure 15. Calibration data for RAC beta radiation monitor.*

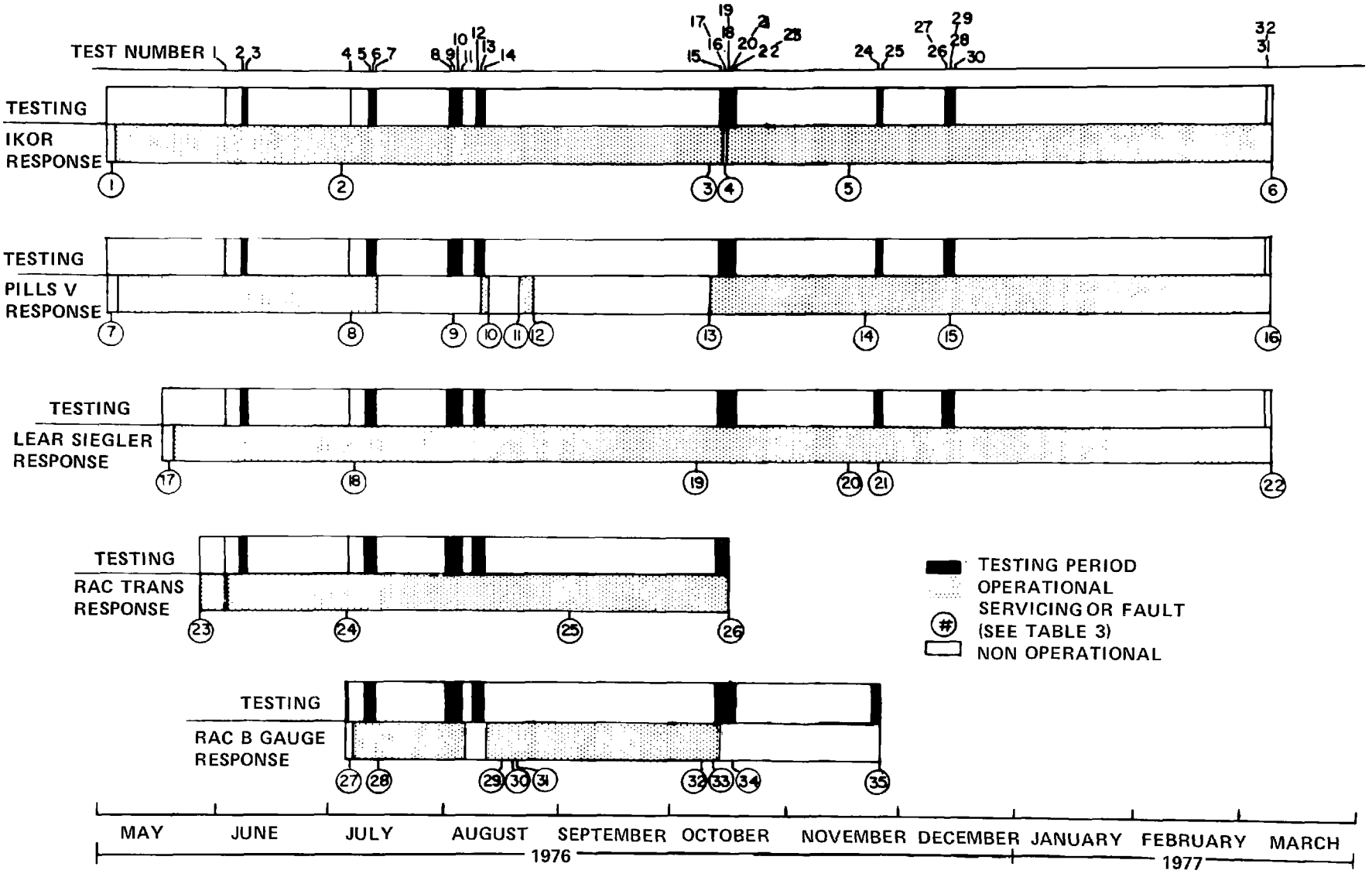


*Figure 16. Summary of servicing record and operational periods of continuous monitors over a one year period.*

TABLE 3. SERVICING RECORD OF CONTINUOUS MONITORS

| Instrument | Key | Servicing or fault |
|---|---|---|
| IKOR | 1. | Installation complete. |
| | 2. | Bullet sensor cleaned and turned horizontally and exposed at suggestion of Mr. A. Gruber. |
| | 3. | Reading high and erratic, probe cleaned. |
| | 4. | Additional cleanings required. Mr. A. Gruber and Mr. E. Allen visit site. |
| | 5. | Instrument functioning, however, showed signs of severe dust build-up. |
| | 6. | Instrument removed from stack. |
| PILLS V | 7. | Installation complete. |
| | 8. | Excessive base line current, manufacturer notified. |
| | 9. | Impossible to zero or span, serviced by Mr. B. Nuspliger. |
| | 10. | Full scale deflection. |
| | 11. | Returned to normal. |
| | 12. | Optical assembly retracts and blower fails. |
| | 13. | Major servicing by Mr. Nuspliger and Associate. |
| | 14. | Optical assembly retracts, fail safe switch placed in "on" position in order to keep optics in stack. |
| | 15. | Retracts in "auto" position, again left in fail safe "on" mode. |
| | 16. | Instrument removed from stack. |
| Lear Siegler RM 41 Transmissometer | 17. | Installation complete. |
| | 18. | Fault light, indicates dirty retro-reflector cleaned by Mr. T. Novak. |
| | 19. | Routine cleaning of filters and automatic compensation check performed by Mr. I. Kent. |
| | 20. | Operate light burned out. |
| | 21. | Light bulb replaced. |
| | 22. | Instrument removed from stack. |

(continued)

TABLE 3 (continued)

| Instrument | Key | Servicing or fault |
|---|---|---|
| RAC Transmissometer | 23. | Installation complete. |
| | 24. | Blower-motor failure,retro blower sufficient to provide air to both sides of transmissometer. |
| | 25. | New blower arrived (not installed). |
| | 26. | Instrument removed from stack. |
| RAC β-Gauge | 27. | Installation complete. |
| | 28. | Tape drive control failure. |
| | 29. | Tape drive fault causes "double spotting". |
| | 30. | Operational only when tape drive advanced and controlled manually. |
| | 31. | Low sample volumes. |
| | 32. | Tape drive advancing continuously, clamping device not sealing. |
| | 33. | Major servicing by Mr. D. Wetick. |
| | 34. | Tape drive malfunction. Clamping device fails. Instrument not operational. |
| | 35. | Instrument removed from stack. |

The RAC beta radiation attenuation monitor arrived after the completion of Test 3 because of problems experienced by the supplier during reconditioning after use at a potential site in the U.S.A. Although it functioned for 13 tests, manual assistance to the tape drive had to be provided for 6 of them. Extensive on-site servicing by a factory trained technician failed to correct the major faults. Because of the repeated failures in the Sampling Module the RAC β-gauge was eliminated from the program after Test 19.

Of the four remaining monitors the Lear Siegler RM 41 transmissometer, the ESC PILLS V and IKOR 2710 were retained for a long-term reliability evaluation because they represented three distinctly different classes of instrumentation. The RAC transmissometer was removed from the stack and further consideration due to the blower-motor failure and satisfactory performance of the alternate light attenuating instrument.

## DISCUSSION OF RESULTS

The interpretation of continuous particulate monitor performance depends on the reliability of the manual stack sampling data used as a standard of comparison. This means that a thorough appreciation of the errors and assumptions inherent in the determination of particulate concentrations, mass emission rates,

and aerodynamic and optical particle sizes is needed for a comprehensive analysis of instrument characteristics.

Random Error Analysis for Particulate Sampling Train

The acquisition of a truly representative sample from a source stack involves a careful step-by-step process using a sampling train consisting of several parts, each designed to perform a specific task. Determinations of particulate concentrations and mass emission rates require a series of calculations employing various measurements which leads to a compounding of errors. Systematic and random errors are compounded differently.

Systematic errors were minimized by:

i. calibrating the S-type pitot tube – sampling probe assembly, integrating dry test meter, orifice rate meter and stack temperature sensing element

ii. sampling isokinetically to within ± 10%

iii. following standard procedures outlined by the EPS source testing code[1]

iv. assigning specific responsibilities to individuals in the sampling team.

Random errors are inherent in any measurement. For any stack sampling program they can be attributed to

i. source condition variation

ii. equipment and personnel variations in field procedures

iii. equipment and personnel variations in the laboratory

In the calculation of mass loading, there will be compounding of 7 random errors involving

i. the variance in average stack gas velocity

ii. the variance in stack or duct cross-sectional area

iii. the variance in proportion by volume of water

iv. the variance in the average absolute stack gas temperature

v. the variance in the absolute stack gas pressure

vi. the variance in particulate matter collected

vii. the variance in total gas sample.

Table 4 summarizes the individual measurement variables along with their standard deviations used to calculate the relative random errors in particulate concentrations and mass emission rates.

In this error analysis the measurement of average stack gas velocity and total gas sample comprised approximately 85% of the total random errors in the determination of the mass emission rate except for tests involving particulate samples weighing less than 50 mg. For low loading tests, the measurement of the particulate catch was the principal source of random error.

Random error limits, corresponding to one standard deviation, for the manual sampling program have been defined in Figures 11-15.

Particulate Matter Analysis

Results of ESCA, X-ray fluorescence and atomic absorption analyses showed that lead, tin and zinc were the three most prominent metals encountered in the stack emissions.

Although the ESCA procedures provided measures of composition at particle surfaces only, the results are in reasonable agreement with the atomic absorption analyses.

It is difficult to comment on the X-ray fluorescence results provided by the U.S. EPA laboratories because the techniques employed in preparing and mounting membrane samples for analysis were not described. When raw data in terms of $\mu g/cm^2$ of filter area were recalculated to percent of mass reported, the levels of lead, tin and zinc were essentially comparable to those determined by atomic absorption. However, the compositions expressed on a weight per cent basis by the U.S. EPA laboratories are much lower than atomic absorption determinations. Because of the extreme variations in the sample characteristics it is suspected that matrix effects could be responsible for the discrepancies in the X-ray fluorescence analyses.

The metal composition data in Table 2 represent the results of replicate analyses of material recovered from the sampling nozzle, probe, cyclone, filter and impinger components of the sampling train. Each of these composite samples provided a measure of the average composition of the stack emissions during the period of any particulate matter concentration determination in terms of the entire spectrum of particle sizes. Examination of membrane samples by X-ray fluorescence neglected the significant portion of particulate matter that had been collected in the sampling nozzle ahead of the filter.

The recovery of material from dried beakers and filters for the fusion step in the atomic absorption procedure represented

TABLE 4. SUMMARY OF INDIVIDUAL MEASUREMENT VARIABLES AND THEIR CORRESPONDING STANDARD DEVIATIONS

| Error term | Individual measurements affecting error term | | |
|---|---|---|---|
| | Symbol | Description | Standard deviation, $\sigma$ |
| Cross-sectional flow area of duct, $A_s$ | $D_s$ | Stack diameter | 1/2 in. |
| Mass of particulate matter, $M_p$ | $W_g$ | Gross weights of filter and beakers including errors resulting from washing, drying, and weighing | 4 mg |
| | $W_t$ | Tare weights of filters and beakers | 1/2 mg |
| Average stack velocity, $(Us)_{avg}$ based on 24 local measurements | $C_p$ | S-type pitot tube coefficient (by calibration) | 0.005 |
| | $T_s$ | Absolute stack gas temperature | 5°R |
| | $\Delta_p$ | Stack gas velocity head (inclined manometer) | 0.01 in. $H_2O$ |
| | $P_s$ | Absolute stack gas pressure | 0.05 in. Hg |
| | $M_s$ | Molecular weight of stack gas on wet basis | 0.1 $lb_m$/lb-mole |
| Stack gas moisture content, $B_{wo}$ | $V_F$ | Final volume of impinger contents | 0.5 ml |
| | $V_i$ | Initial volume of impinger contents | 0.5 ml |

(continued)

TABLE 4 (continued)

| Error term | Individual measurements affecting error term | | |
|---|---|---|---|
| | Symbol | Description | Standard deviation, $\sigma$ |
| | $V_m$ | Dry gas metered volume | 0.02 $ft^3$ |
| | $P_m$ | Absolute pressure at the dry test meter | 0.05 in. Hg |
| | $T_m$ | Absolute temperature at dry gas meter | 2°R |
| Average stack gas temperature $(T_s)_{avg}$ | $T_s$ | Local stack gas temperature | 5°R |
| Absolute stack gas pressure, $P_s$ | $P_{bar}$ | Atmospheric pressure at sampling site | 0.05 in. Hg |
| | $P_{static}$ | Stack gas static pressure | 0.1 in. $H_2O$ |
| Total gas sample, $(V_m)_{ref}$, including errors in average stack velocity, $(U_s)_{avg}$ | $K_0$ | Calibration constant for orifice | $0.01 \frac{ft^3}{min} \left[\frac{lb_m}{lb\text{-}mole} \frac{in.\ Hg}{in.\ H_2O,\ °R}\right]^{\frac{1}{2}}$ |
| | $D_N$ | Nozzle diameter | 0.001 in. |
| | $M_d$ | Molecular weight of stack gas on dry basis | $0.1 \frac{lb_m}{lb\text{-}mole}$ |
| | $P_m$ | Absolute pressure upstream of the orifice | 0.05 in. Hg |
| | $T_m$ | Absolute temperature upstream of the orifice | 2°R |

(continued)

TABLE 4 (continued)

| Error term | Individual measurements affecting error term | | |
|---|---|---|---|
| | Symbol | Description | Standard deviation, $\sigma$ |
| | $\tau$ | Sampling time interval | 0.5 sec |
| | $(\Delta H)$ setting | Error associated with setting the required orifice pressure drop | 0.02 in. $H_2O$ |
| | $(1-B_{wo})$ | Proportion by volume of dry gas in stack gas stream | 0.01 |

80 to 92% of the particulate matter caught during any mass loading test. Trial runs with laboratory formulations of lead, tin and zinc compounds of compositions approximating those of collected samples showed that better than 90% of each metal was accounted for after the fusion process. On this basis it is believed that the atomic absorption procedure provided the most reliable evaluation of metal levels in stack emissions.

Particle Sizing Determinations

Because of the differences between theory and practice, aerodynamic particle sizes must be used with caution. In principle, cascade impactors provide discrete fractions as approximations to the true continuous particle size distributions that are sampled. The uncertainty in particle size is compounded by errors associated with wall losses, particle bounce and deviations from theoretical calibration curves. Evaluations of the severity of these errors are topics of current investigations.[2]

Particle bounce could have been significant during any test because the impactors used for particle size determinations employed no substrate material on the plates. It was decided to work with bare metal stages to minimize any potential weighing errors that could result from anomalous weight increases in glass fiber substrates as a result of sulfate formation in the presence of $SO_2$.[3] The use of unlined impactor plates facilitated quantitative recovery of collected particulate matter for future analytical purposes.

According to McCain et al.,[4] particle bounce can severely distort size distributions of aerosols having large mass mean diameters. As a result, the reported dimensions of distributions with large mass median diameters could be smaller than the true values. On the other hand, mass median diameters for small particle aerosols (whose mass median sizes are less than 10 μm) could be systematically larger than the true values because of the low resolution provided by cascade impactors.

Although it was recognized that sampling times as long as 4 hours could contribute to particle re-entrainment in the cascade impactor, the particle sizing train was operated as long as the particulate loading train

i. to provide a check on the mass concentrations which served as the primary standard for instrument evaluation

ii. to ensure a representative sample for the random smelter process over the sampling period.

Because of particle bounce and re-entrainment considerations, which cannot be readily evaluated, the aerodynamic diameters

are subject to an uncertainty approximated as ± 25% of the reported value. However, this accuracy is sufficient for the analysis of continuous particulate monitor performance characteristics.

Aerodynamic particle sizes affect the performance of the IKOR charge transfer and RAC β-attenuation devices because both instruments depend on particle capture from a flowing gas stream. The light attenuating Lear Siegler RM 41 and RAC transmissometers and backscattering PILLS V monitor respond to the optically projected sizes of particles.

In principle, it is possible to convert aerodynamic particle sizes to optical dimensions using the relationship between the true density of the particles under consideration and the theoretical 1 $g/cm^3$ standard. This conversion becomes virtually impossible when dealing with particulate matter whose composition could vary from test to test and during any specific test period. The problem is further complicated by the fact that the geometric standard deviation, $\sigma_g$, is required for computation of median diameters on a number basis.[5] Table 5 summarizes the lead, tin and zinc compounds that could be found in varying proportions in the stack emissions. The colors of the materials listed are consistent with the characteristic colors of the membrane samples reported in Table 2. Because of the additions of sulfur and sawdust to the lead alloying kettles, elemental sulfur and carbon also could have been present in substantial quantities in any sample. Without a detailed evaluation of the density of any test specimen it is not possible to derive reliable optical sizes from the aerodynamic data.

## Continuous Particulate Monitor Performance

For each instrument, calibration curves were expressed in terms of the best linear fits wherever justified by the statistical "F" test. Error variances for each calibration curve were evaluated and illustrated as 95% confidence intervals. Random error limits for each manual particulate matter concentration test have been indicated in Figures 11-15 in terms of one standard deviation, $\sigma$.

In Figures 11-15 particulate matter concentrations or mass emission rates have been used as independent variables because they were the primary standards against which instrument responses were compared.

## Transmissometers

Figures 11 and 12 indicate that the Lear Siegler RM 41 and RAC transmissometer responses are primarily dependent on particle size when aerodynamic diameters exceed one micron. This behavior is consistent with the theoretical predictions of Pilot and Ensor[5] and the experimental work of Uthe and Lapple.[7]

TABLE 5. SUMMARY OF PHYSICAL PROPERTIES OF METALLIC COMPOUNDS LIKELY TO BE EMITTED FROM A SECONDARY LEAD SMELTER[6]

| Compound | Molecular weight | Color | Refractive index | Specific gravity |
|---|---|---|---|---|
| Pb | 207.21 | cubic silver blue white | | 11.3 |
| $PbCl_2$ | 278.12 | rhombic white | 2.199<br>2.260 | 5.85 |
| $PbCl_2.3PbS$ | 995.95 | red | | |
| $Pb_2O$ | 430.42 | amorphous black | | 8.342 |
| PbO | 223.21 | tetragonal yellow | 2.665<br>2.535 | 9.53 |
| PbO | 223.21 | rhombic yellow | 2.51<br>2.61<br>2.71 | 8.0 |
| $Pb_3O_4$ | 685.63 | crystalline red amorphous powder | | 9.1 |
| $Pb_2O_3$ | 462.42 | amorphous yellow powder | | |
| $PbO_2$ | 239.2 | tetragonal brown | 2.3 | |
| $PbCl_2.Pb(OH)_2$ | 519.35 | tetragonal white | 2.04,2.15<br>2.15 | 7.21 |
| $PbCl_2.Pb(OH)_2$ | 519.35 | rhombic | | 6.24 |
| $PbCl_2.\ PbO.\ H_2O$ | 519.35 | monoclinic prism colorless to white | 2.146 | 6.05 |
| $PbCl_2.2PbO$ | 724.54 | rhombic yellow | 2.24, 2.27, 2.31 | 7.08 |
| $PbCl_2.3PbO$ | 947.75 | yellow | | |

(continued)

TABLE 5 (continued)

| Compound | Molecular weight | Color | Refractive index | Specific gravity |
|---|---|---|---|---|
| $PbCl_2 . 7PbO$ | 1840.59 | yellow crystal or powder | | |
| $PbSO_4$ | 303.28 | monoclinic or rhombic white | 1.877<br>1.882 | 6.2 |
| $PbSO_4 . PbO$ | 526.49 | monoclinic white | 1.93<br>1.99<br>2.02 | 6.92 |
| $PbS_2O_8 . 3H_2O$ | 453.39 | deliquescent | | |
| $Pb(HSO_4)_2 . H_2O$ | 419.37 | crystalline | | |
| PbS | 239.28 | cubic black metallic | 3.912 | 7.5 |
| Sn | 113.7 | α cubic gray<br>β tetragonal white metallic<br>γ rhombic white | | 5.75<br>7.28<br>6.54 |
| $SnCl_2$ | 139.61 | rhombic white | | 3.39 |
| $SnCl_2 . 2H_2O$ | 225.65 | white monoclinic | | 2.71 |
| $SnCl_4$ | 260.53 | colorless liquid | | 2.23 |
| $SnCl_4 . 3H_2O$ | 314.58 | monoclinic crystal | | |
| SnO | 134.70 | tetragonal (cubic) black | | 6.64 |
| $SnO . xH_2O$ | | white powder or yellow brown crystal | | |
| $SnO_2$ | 150.70 | tetragonal white, brown black | 1.997<br>2.093 | 6.95 |
| $SnO_2 . xH_2O$ α stannic acid | | amorphous or colorless precipitate | | |

(continued)

TABLE 5 (continued)

| Compound | Molecular weight | Color | Refractive index | Specific gravity |
|---|---|---|---|---|
| $SnO_2 \cdot xH_2O$ β stannic acid | | amorphous or gelatinous white | | |
| $SnSO_4$ | 214.77 | yellowish white crystalline powder | | |
| SnS | 150.77 | rhombic gray black | | 5.08 |
| $SnS_2$ | 182.83 | hexagonal gold yellow | | 4.5 |
| Zn | 65.38 | hexagonal bluish white metal | | 7.14 |
| $ZnCl_2$ | 136.29 | cubic white deliquescent | 1.687<br>1.713 | 2.91 |
| $Zn(OH)_2$ | 99.40 | rhombic colorless | | 3.05 |
| ZnO | 81.38 | white or yellowish amorphous powder | | 5.47 |
| ZnO | 81.38 | hexagonal white | 2.008<br>2.029 | 5.605 |
| $ZnO_2$ + ZnO | 178.76 | white yellow powder | | 1.571 |
| $ZnSO_4$ | 161.44 | rhombic colorless | 1.658<br>1.659<br>1.67 | 3.74 |
| $ZnSO_4 \cdot 6H_2O$ | 269.54 | monoclinic or tetragonal colorless | | 2.07 |
| $ZnSO_4 \cdot 7H_2O$ | 287.56 | rhombic colorless efflorescent | 1.457<br>1.480<br>1.484 | 1.97 |

(continued)

TABLE 5 (continued)

| Compound | Molecular weight | Color | Refractive index | Specific gravity |
|---|---|---|---|---|
| ZnS | 97.45 | hexagonal colorless | 2.356 | 4.087 |
| ZnS | 97.45 | cubic colorless | 2.368 | 4.102 |
| $ZnS \cdot H_2O$ | 115.46 | yellowish white powder | | 3.98 |
| $ZnSO_3 \cdot 2H_2O$ | 181.48 | white crystalline powder | | |

In principle, the sensitivity of a transmissometer shows a monotonic decrease with increasing particle size if particulate matter having an absorptive index of refraction is involved. However, a maximum in the response-particle size relationship is to be expected according to the classical Mie theory for particles having only a real index of refraction. Figure 17 illustrates the effect of the absorptive refractive index on the response-size relationship for a real refractive index of 1.5. Because of these size and refractive index effects, transmissometers should not be capable of detecting very small, non-absorbing particles, but would respond well to absorbing particles in the same size range.

Most theoretical discussions involve monodispersed particulate systems which are seldom encountered in real life situations. Figure 18 shows that as the polydispersivity of an aerosol increases, as evidenced by increasing values of $\sigma_g$, the effect of particle size on transmissometer response is diminished.

Because the stack emissions under investigation consisted of the black and/or opaque whitish particulate matter and particle size distributions were of a highly polydispersed nature, as indicated by the high slopes of the log-probability curves, the effects of particle size on instrument performance should have been minimized for particles smaller than about 1 μm and larger than 25 μm optical diameter. Consequently, the typical performance curves supplied by manufacturers showing the effect of particle size on light attenuation are virtually useless for the evaluation of the applicability of these instruments to any specific source.

Both the Lear Siegler and RAC transmissometers satisfy the U.S. EPA performance specifications.[10] According to the operating manual provided, the RAC instrument was designed with a smaller angle of view. On the basis of collimation considerations the RAC device should be better than the Lear Siegler RM 41 model. However, a comparison of Figures 11 and 12 shows that the Lear Siegler system exhibits higher sensitivities and provides calibration curves with lower error limits. In actual fact, the RAC transmissometer was incapable of detecting particles, during this testing program, when the aerodynamic diameters exceeded 25 μm.

Environmental Systems Corporation PILLS V

The PILLS V monitor provided two calibration curves that were relatively independent of particle size. The two data sets were due, most likely, to a change in the instrument calibration as a result of the replacement of the optics head and other adjustments made during the major overhauling of October 11, 1976.

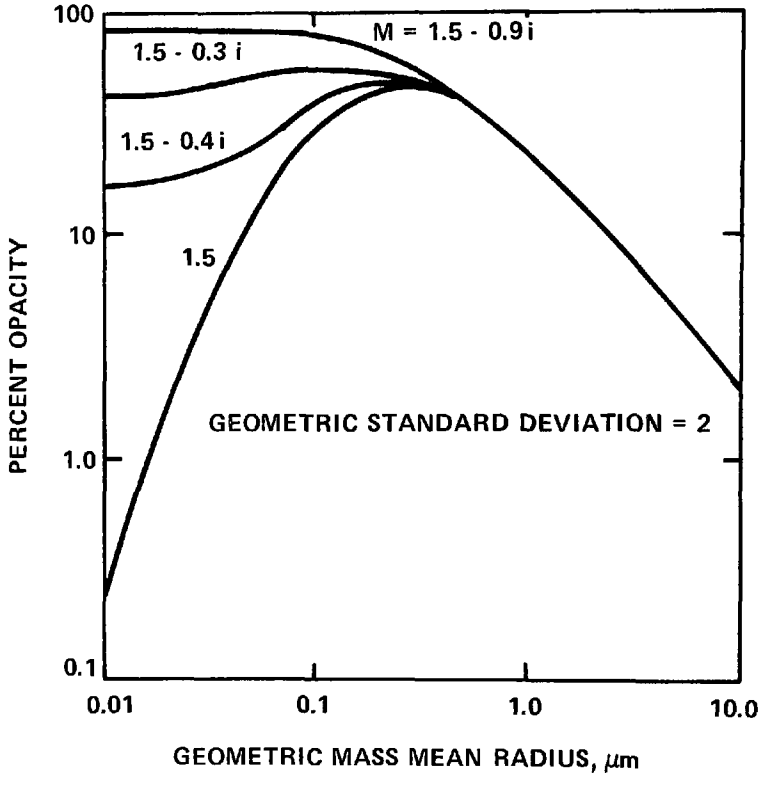


*Figure 17. Effect of absorptive refractive index on opacity-size relationship.*[8]

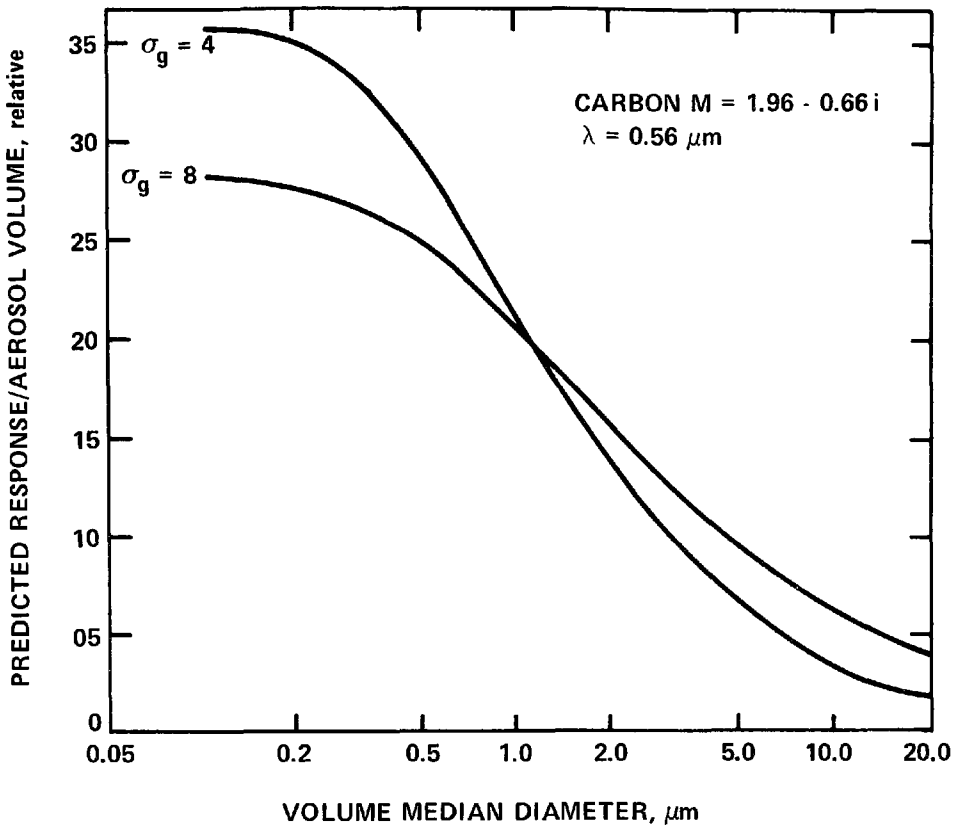


*Figure 18. Transmissometer response as a function of geometric standard deviation and volume mean diameter.*[9]

The calibration curve, corresponding to the data collected after major servicing, exhibits a zero off-set and an increase of approximately 2.3 in the "effective gain" or sensitivity. Discussions with H.W. Schmitt, President of Environmental Systems Corporation, confirmed that both of these effects could be attributed to the replacement of the optics head and adjustments made during the on-site reconditioning. The ESC personnel made no attempts to quantify or adjust for the instrument changes that could have resulted from their modifications.

Some of the scatter in the data collected after the major servicing can be attributed to changes in both the real and absorptive components of refractive indices. Figure 19 illustrates how a backscattering instrument would respond to particulate matter of varying refractive index. Additional scatter in the data can be attributed to mean diameters beyond the flat portion of the PILLS V response curve and the general backscattering response curves as shown in Figure 19.

IKOR Particulate Monitor

The data in Figure 14 show that the IKOR monitor has limited sensitivity to particles smaller than one micron in aerodynamic

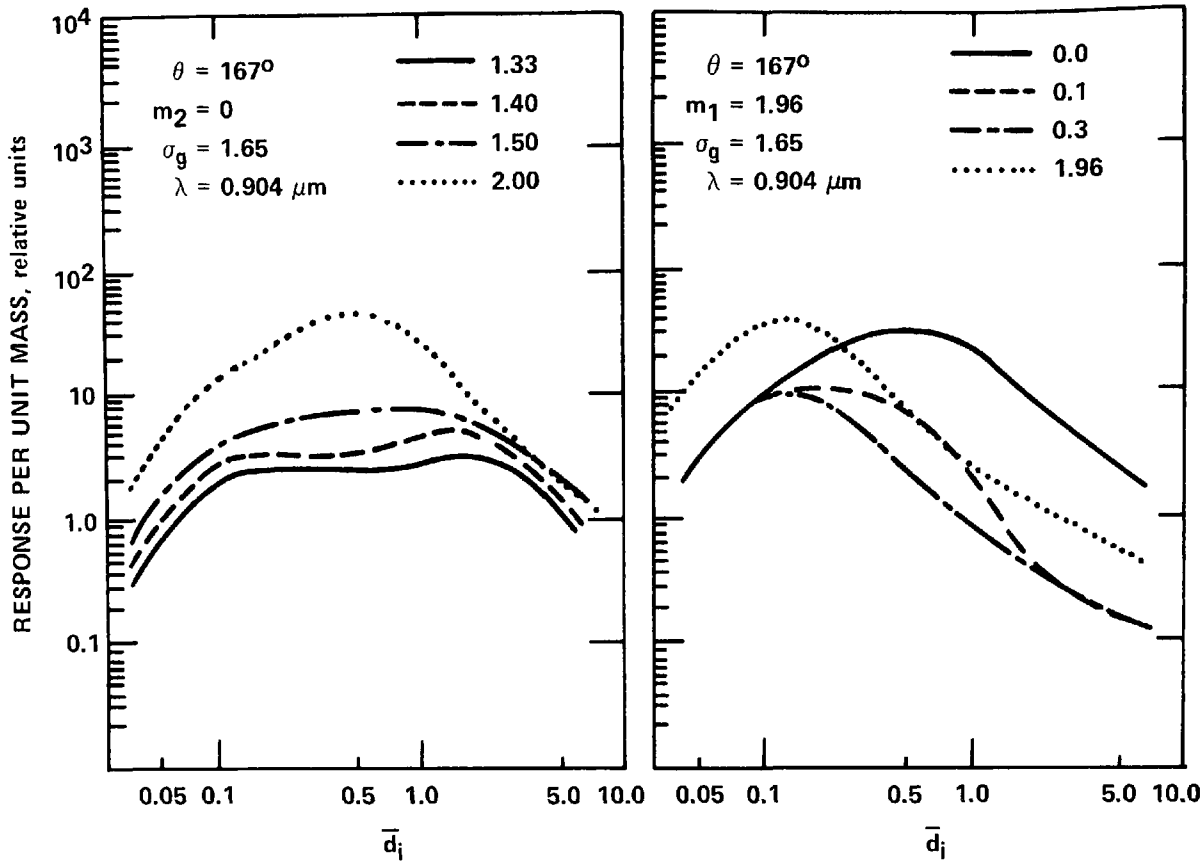


*Figure 19. Response per unit mass vs. $\bar{d}_i$, $m_1$ = 1.33, 1.40, 1.50, 2.0; $m_2$ = 0, 0.1, 0.3, 1.96 for backscattering.*[11]

diameter. This is not surprising in terms of its design principles. Charge transfer from particles to the sensor can occur only if particulate matter impinges on the collecting head. For the stack conditions encountered the impaction efficiencies were generally so low that only that fraction of the particulate matter with diameters exceeding 4 μm would make contact with the sensor surface.

When it became apparent during the testing program that particulate matter with diameters below one micron was being missed by the IKOR sensor, the recommendation was made by A. Gruber, Vice President, IKOR Inc., that the sensing element be exposed and oriented with its axis perpendicular to the stack gas stream. When this was done there did not appear to be any significant effect on the instrument performance.

The wide scatter about the calibration curve for particles whose diameters are larger than 5 μm can be due to variations in

i. electrical resistivity of the particulate matter

ii. stack gas humidity

iii. stack gas temperature

iv. particle precharge characteristics

v. probe surface conditions as a result of the accumulation of particles or cleaning with abrasive cleansers,

as suggested by John.[12]

RAC Beta Radiation Monitor

The RAC beta radiation attenuating instrument supplied for this program was a reconditioned unit which suffered from repeated mechanical failures in the tape drive, indexing and clamping components of the sampling module. Consequently, this monitor functioned during only 13 of 22 possible testing periods.

According to design principles, a single calibration curve should have been obtained. However, Figure 15 shows that this instrument was more sensitive to smaller particles whose aerodynamic diameters were less than one micron. This behavior suggests that the RAC β-gauge was affected by particulate deposition in the sampling nozzle and probe and the transport lines to the filter tape. Such deposition was confirmed at the conclusion of the testing program when substantial amounts of particulate matter were recovered from the nozzle, probe and boundary layer dilution screen.

Neither calibration curve passed through the origin. The observed shift in these curves would result from

i. the previously discussed particulate deposition in the lines

ii. in-leakage at the sampling head due to poor clamping

iii. filter tape losses as a result of de-fluffing under vacuum during the sampling interval after taring

iv. filter tape losses as a result of abrasion during tape transport between taring, sampling and final counting.

CONCLUSIONS AND RECOMMENDATIONS

The performance characteristics of 5 continuous particulate monitors were evaluated over a one-year period to assess their

i. suitability

ii. reliability

iii. accuracy

with respect to their substitution for manual methods as a means of ensuring long-term compliance with and enforcement of federal regulations pertaining to emissions from secondary lead smelters in the Canadian environment.

The Lear Siegler RM 41 transmissometer was more reliable than the other four monitors. The experimental data indicate that this device would be suitable for monitoring emissions from controlled sources provided that the particulate matter had appreciable absorptive indices of refraction. Its first order dependence on particle sizes exceeding one micron aerodynamic diameter makes it unsuitable for use where process variations result in the generation of particulate matter of varying sizes, colors and/or refractive indices. Transmissometer performance could not be related to changes in the chemical composition of the emissions.

The Environmental Systems Corporation PILLS V monitor performance was handicapped by its poor reliability and high maintenance requirements. These deficiencies were consistent with the difficulties experienced by prototype units undergoing long-term field evaluations for the first time. Improvements made to the optical interrupters, controlling the zero-span band, and provision of an external standard for referencing the band should eliminate many of the problems encountered during the reliability determinations. If the long-term reliability were improved, the PILLS V device could be potentially more useful than the best transmissometer because its calibration appears to be less sensitive to changes in particle size, color and refractive index. Variations in the metal content of the particulate matter could not be directly correlated to the calibration curve for this backscattering instrument.

Performance of the Research Appliance Company transmissometer was adequate for monitoring emissions from the controlled reverberatory mode of operation consistently producing particulate matter with median diameters approximating 0.5 μm. However, it does not appear to be capable of detecting large particles whose diameters exceed 25 μm.

The IKOR 2710 particulate monitor showed limited potential for application to either the reverberatory or lead alloying kettle processes. The particles passing through the baghouse were too small to impact effectively on the sensor. On the other hand, short, periodic bursts of high emissions during the uncontrolled refining operations necessitated frequent cleaning of the sensing element.

Because of the repeated mechanical failures in the sampling module of the Research Appliance Company beta radiation attenuating device supplied for the study, it is difficult to comment critically on its possible application to measurement of emissions from a secondary lead smelter.

Continuous particulate monitors have not been developed to the stage where particle size, shape, composition and color, which have pronounced effects on instrument performance, can be accounted for in the calibration curves for the instruments. Reliable continuous monitoring could be possible only if the physical and chemical properties of the emissions remained sufficiently constant over long time periods. These conditions are approximated in stacks exhausting gases that have passed through efficient control equipment.

REFERENCES


1. Standard Reference Methods for Source Testing: Measurement of Emissions of Particulates from Stationary Sources. EPS 1-AP-74-1, Air Pollution Control Directorate, Environmental Protection Service, Environment Canada, Ottawa, Ontario, 1974.

2. Harris, D.B. Procedures for Cascade Impactor Calibration and Operation in Process Streams. EPA-600/2-77-004, U.S. Environmental Protection Agency, Research Triangle Park, NC, 1977.

3. Hemeon, W.C.L., and A.W. Black. Stack Dust Sampling: In-Stack Filter or EPA Train. J. Air Pollut. Contr. Assoc. 22(7):516-518, 1972.

4. McCain, J.D., and J.E. McCormack. Non-Ideal Behavior in Cascade Impactors. APCA paper 77-35.3, presented at 70th Annual Meeting, Toronto, Ontario, June, 1977.

5. Pilat, M.J., and D.S. Ensor. Plume Opacity and Particulate Mass Concentraion. Atmos. Environ. 4:163-173, 1970.

6. Handbook of Chemistry and Physics, R.C. Weast, Editor, 49th Edition, The Chemical Rubber Co., Cleveland, OH, 1968-69.

7. Uthe, E.E., and C.E. Lapple. Study of Laser Backscatter by Particulates in Stack Emissions. SRI 8730, Stanford Research Institute, Menlo Park, CA, 1972. NTIS PB 212530.

8. Feldman, P.L., and D.W. Coy. Comparison of Computed and Measured Opacities: Lignite Fired Boilers. APCA paper 73-168, presented at 66th Annual Meeting, Chicago, IL, June, 1973.

9. Markowski, G.R., G.J. Woffinden, and D.S. Ensor. Optical Method for Measuring the Mass Concentration of Particulate Emissions. EPA-600/2-76-062, U.S. Environmental Protection Agency, Research Triangle Park, NC, 1976.

10. Nader, J.S., F. Jaye, and W. Connor. Performance Specifications for Stationary-Source Monitoring Systems for Gases and Visible Emissions. EPA-650/2-74-013, U.S. Environmental Protection Agency, Research Triangle Park, NC, 1974.

11. Miller, A.C. Theoretical Modelling and Calibration for a Particulate Mass Concentration Monitor. M.S. Thesis, The University of Tennessee, Knoxville, TN, August, 1977.

12. John, W. Investigation of Particulate Matter Monitoring Using Contact Electrification. EPA-650/2-75-043, U.S. Environmental Protection Agency, Research Triangle Park, NC, 1975.

PAPER 8

# AN IN-STACK FINE PARTICLE SIZE SPECTROMETER: A DISCUSSION OF ITS DESIGN AND DEVELOPMENT

ROBERT G. KNOLLENBERG
PARTICLE MEASURING SYSTEMS, INC.

## ABSTRACT

The development of an in-stack fine particle size measuring device for the EPA has been underway at PMS for the past several months. The instrument utilizes a laser fed optical system with detection by near-forward light scattering. Sample volume is established through the use of a high resolution imaging system using paired detectors viewing the sample plane through a masked beam splitter. The instrument covers a 0.3 to 10.0 μm size range with 60 channels resolution. Absolute theoretical accuracy is ±20% of size for completely unknown refractive index. The instrument is designed to operate continuously at in-stack temperatures up to 250°C at flow velocities up to 30 m/sec. Flow velocities are determined from measured particle transit times through the laser beam. Internal probe components are cooled by a water jacket and external heat exchanger. The heat exchanger, probe pulse processing electronics, data acquisition system and operating controls are housed in a central electronics console. The instrument is being tested on a local coal fired power plant. Its eventual use will be directed at the characterization of particulate emissions of stacks or other stationary sources and to qualitatively evaluate the performance and collection efficiencies of particulate control devices now in operation.

## INTRODUCTION

In September, 1977 Particle Measuring Systems, Inc. (hereafter PMS) was contracted by the Environmental Protection Agency (hereafter EPA) to design, fabricate, and evaluate an in situ Fine Particle Stack Spectrometer System (FPSSS). The FPSSS will

be used to characterize the particulate emissions of stacks and other stationary sources and to quantitatively evaluate the performance and collection efficiencies of particulate control devices now in use. The EPA design criteria that the FPSSS had to satisfy were to provide in situ high resolution particle sizing over a size range from 0.5 to 5.0 μm diameter with concentrations in this range above $10^4/cm^3$ and integrated particulate loading from 0.3 to 3.0 $g/m^3$. The FPSSS is also required to operate at temperatures from 20 to 250°C and at flow velocities from 1 to 30 m/sec. An operational prototype instrument has been designed and fabricated and initial performance testing begun. This paper describes the current status of this developmental effort.

The basic design approach followed in the FPSSS utilizes existing technology. There are three major areas of prior work which have provided the needed technology base upon which the underpinnings of the FPSSS design could be established. These are:

1) The PIONEER VENUS Large Probe Cloud Particle Size Spectrometer (LCPS),[1] development work with joint involvement of PMS and Ball Brothers Research Corporation (BBRC).

2) The recent experience by PMS in stack measurements using plumbed instruments.

3) The well developed PMS technique of utilizing high resolution imaging systems with light scattering to perform in situ single particle size measurements.

The current prototype FPSSS instrument would appear to meet the original EPA design objectives. It has a near-forward light scattering optical system with an expanded 60 channel 0.3 to 10.0 μm size range divided into four subranges of 15 size channels each. The instrument is capable of relatively accurate measurements at concentrations up to $10^5/cm^3$ without regard to refractive index. An optical velocimeter has also been designed into the FPSSS. The instrument operates continuously at 250°C temperatures utilizing a water-cooled head design and external heat exchanger. Extensive theoretical modeling of thermal as well as optical performance has been utilized in configuring the FPSSS Probe head. Wind tunnel facilities at PMS have played an extremely important role in measuring aerodynamic impacts of the FPSSS sampling section. Calibration has included laboratory and wind tunnel tests on particulates having known or independently verifiable size distributions. Field tests on an operating coal-fired power plant stack began in April, 1978 and some preliminary results are presented here.

## DESIGN APPROACH OF THE FINE PARTICLE STACK SPECTROMETER SYSTEM (FPSSS)

A hot stack environment may appear to present possibly too high concentrations for in situ single particle measuring devices; however, measurements with a standard laboratory aerosol spectrometer manufactured by PMS employing a ducted sample flow showed this not to be the case. Today most sources must comply with much more stringent emission controls. The standard compliance device for coal-fired power plants is an opacity monitor which measures total extinction. Permissible emissions generally compute to extinction coefficients less than $3 \times 10^{-4}$/cm. This would correspond to a visibility of approximately 120 meters and maximum concentrations around $5 \times 10^{3}/cm^{3}$ for 1 μm radius particles. Such concentrations are well within the range of standard aerosol spectrometers offered by PMS. The real problem is performing measurements in the hot environment. The stack is often well above boiling temperature and if continuous measurements are desired the instrument must be cooled to survive. Our approach was to provide a reasonable thermal environment for an existing PMS light scattering spectrometer electro-optical system using an active cooling system.

The FPSSS design involves a laser fed high resolution imaging optical system with particle detection and sizing by strong forward light scattering (see optical system in Figure 1). The imaging system provides accurate sample volume definition and enables accurate particle transit time measurements to extract flow velocity. The FPSSS sampling head design shown in Figure 2 reveals a water cooled insulated electro-optical system. The probe head communicates to a standard PMS Data Acquisition System (DAS) and thermal control system packaged in a control console (see Figure 3). The FPSSS Probe has now been fabricated much as shown in Figures 1 and 2; however, the subsystems within the control console are still evolving and will eventually be repackaged.

The development of the FPSSS was not considered a high risk task although it did require the application of diverse and demanding technology. The performance requirements are within the range of standard PMS instruments (with the exception of the high temperatures involved). Extensive use has been made of prior success in developing technology to perform measurements in even more severe environments. For instance, the Cloud Particle Size Spectrometer developed for NASA and the PIONEER VENUS payload must withstand 450°C.[1,2] This technology base has been applied to design the FPSSS. An 80 node thermal model for the probe head was developed by BBRC predicting cooling requirements, thermal gradients and mechanically induced changes in optical alignment. The design in Figures 1 and 2 primarily reflects efforts to minimize alignment error predicted by the model. The optical system design, scattering response, and thermal

design will be detailed here. The actual hardware description is deferred to the section in which the prototype is discussed, below.

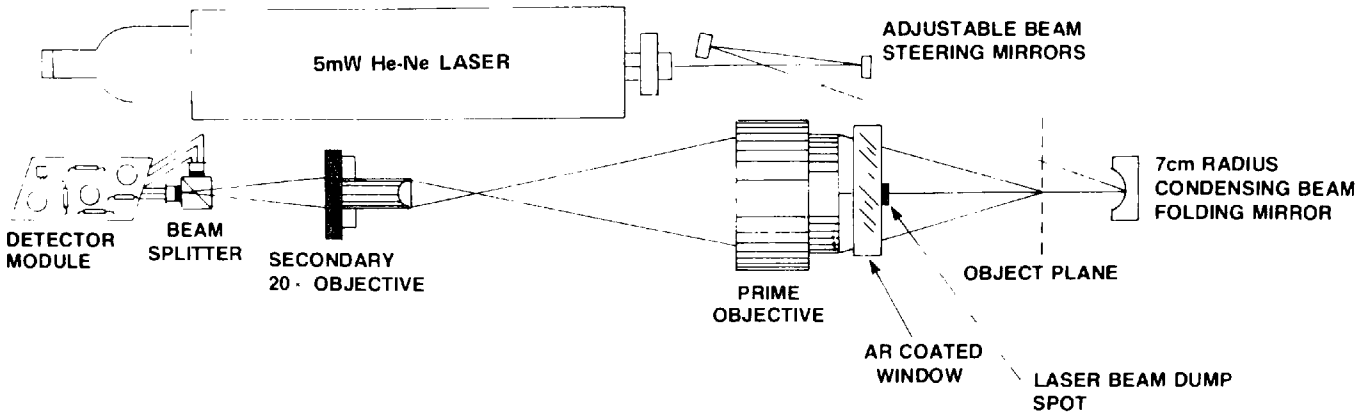


*Figure 1. Fine particle stack spectrometer probe optical system.*

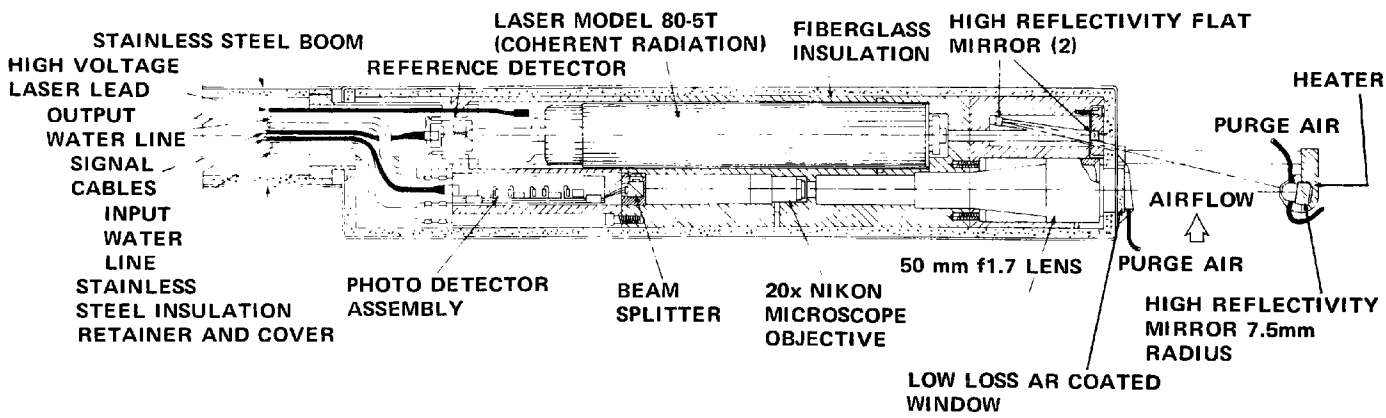


*Figure 2. Fine particle stack spectrometer probe head.*

## FPSSS Optical System Design

The optical system became the primary design driver in the FPSSS. Its alignment is the single most important optical parameter requiring control. The optical system shown in Figure 1 is essentially identical to that originally proposed to the EPA. The output of a 5 mW high order multimode laser is directed towards a 7 cm radius condensing mirror by a pair of plane mirrors. The condensing mirror focuses the laser beam down to approximately 125 μm diameter at the object plane of the light collecting/ imaging system. The laser beam then expands to approximately 3 mm diameter before being absorbed by a dump spot on

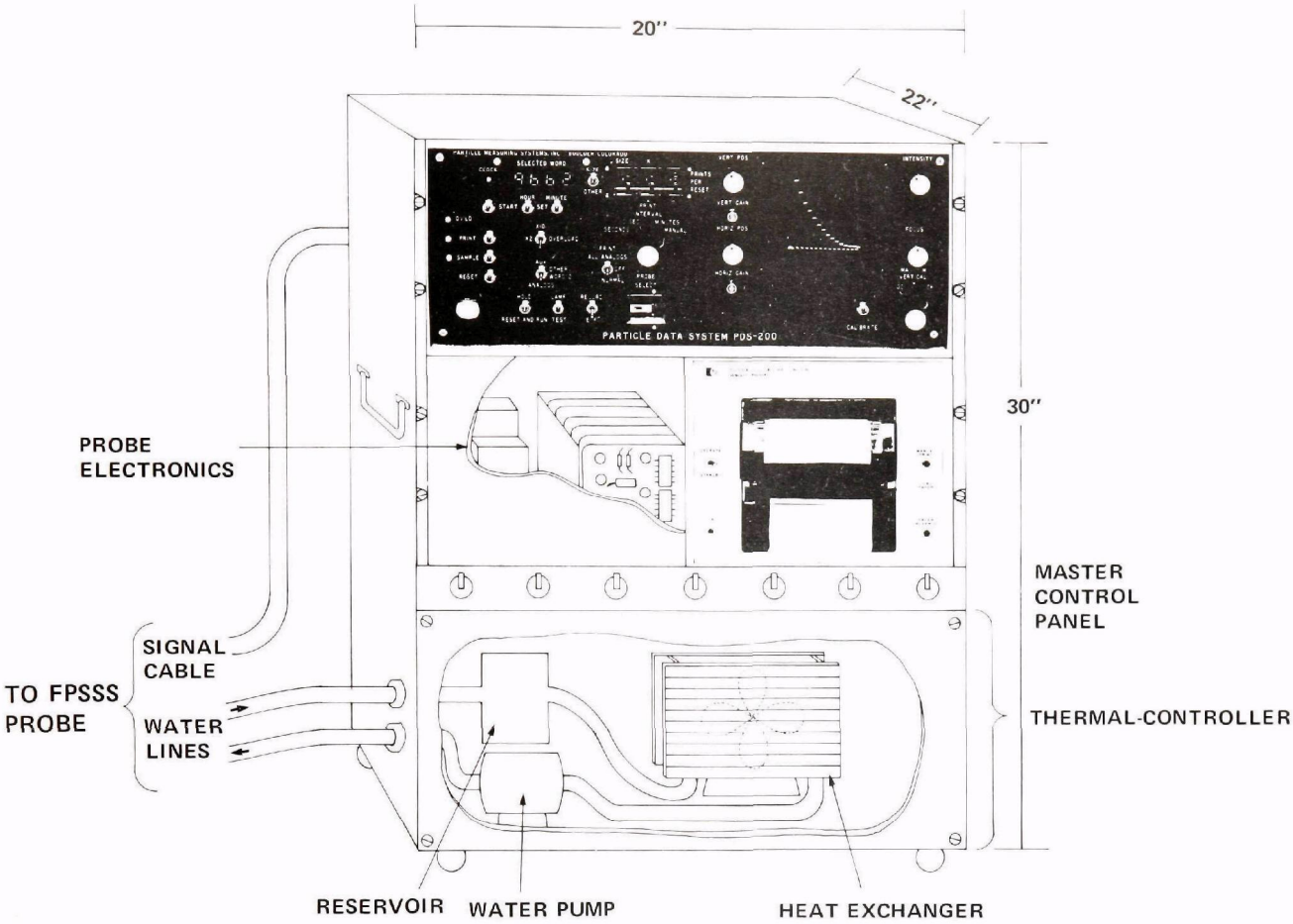


*Figure 3. FPSSS data/control console.*

the FPSSS window. Particles in the vicinity of the object plane scatter energy through the window which is collected by the prime objective (F/1.8, 50 mm f.l.) and relayed at 2:1 magnification to the secondary objective which is a 20X Nikon microscope objective operated at 10X. The total magnification is thus 20X. The final image is produced on a pair of exit faces of a beam splitter. The reflected image face is masked with a 0.78 mm wide vertical mask aligned in the direction of particle flow. The second transmission prism face is unmasked. A pair of photodiodes and their associated preamps view the particle images through each prism face.

The capabilities of this optical system are of a fundamental nature in that they provide a means of defining a desired sample volume effecting the in situ measurement capability.[3,4,5] The masked beam splitter derives two signals, which in conjunction with double pulse height analysis, provide a means of determining if a particle's position is in the desired sample volume. The relative size of the sample volume cross section with respect

to the laser beam is depicted in Figure 4. The sample volume includes only the region near the center of the laser beam. The sample volume cross section is noticeably diamond shaped. The center of this diamond cross section coincides with the object plane of the collecting optics. The points of this diamond cross section define the limiting depth-of-field of the FPSSS. Both the width of the cross section and the depth-of-field vary inversely with the magnification used in the collecting optics.

The diamond shaped sample cross section results from the accept/reject criteria used in comparing signals at the masked and unmasked detectors. The light transmitted on axis through the beam splitter is the signal used to size the particles. The light reflected at 90° forms its image on a circular aperture with the central opaque vertical mask. Shown in Figure 5 are the size and positions of images formed by particles at various positions in the illuminated volume. It is important to understand that for small particles (essentially point objects) the image size is only a function of its axial displacement from the object plane. The image size is linearly related to the numerical aperture of the collecting optics and is given approximately by:

Image size = N.A. x displacement from object plane.

It is apparent that only images that are near the object plane and the center of the sample volume form images with light concentrated on the opaque mask as illustrated in Figure 5. Thus, such images transmit little signal through the masked aperture. Particles whose pulse amplitudes, as seen by the masked aperture detector, are greater than those seen by the signal aperture detector are rejected. This defines the diamond shaped sample cross section and image relationships shown in Figure 6. We use a gain ratio of masked aperture detector to signal aperture detector of 4X for best noise immunity. The sample cross section area is the product of the sample volume width and one-half the depth-of-field.

One final aspect of the sample volume needs explanation. As we have defined it the sample volume is only the region of accepted measurements. The total view volume includes a much larger volume where both accepted and rejected particles are viewed. This view volume is as much as ten times larger than the sample volume, and must be used for coincidence error estimates. The ratio of the sample volume to view volume is a function of the inner numerical aperture of the collecting solid angle (2°, N.A. = 0.03). This presents an obvious trade-off between a design to collect very strong forward scattering and one which maximizes measurements at the highest concentrations.

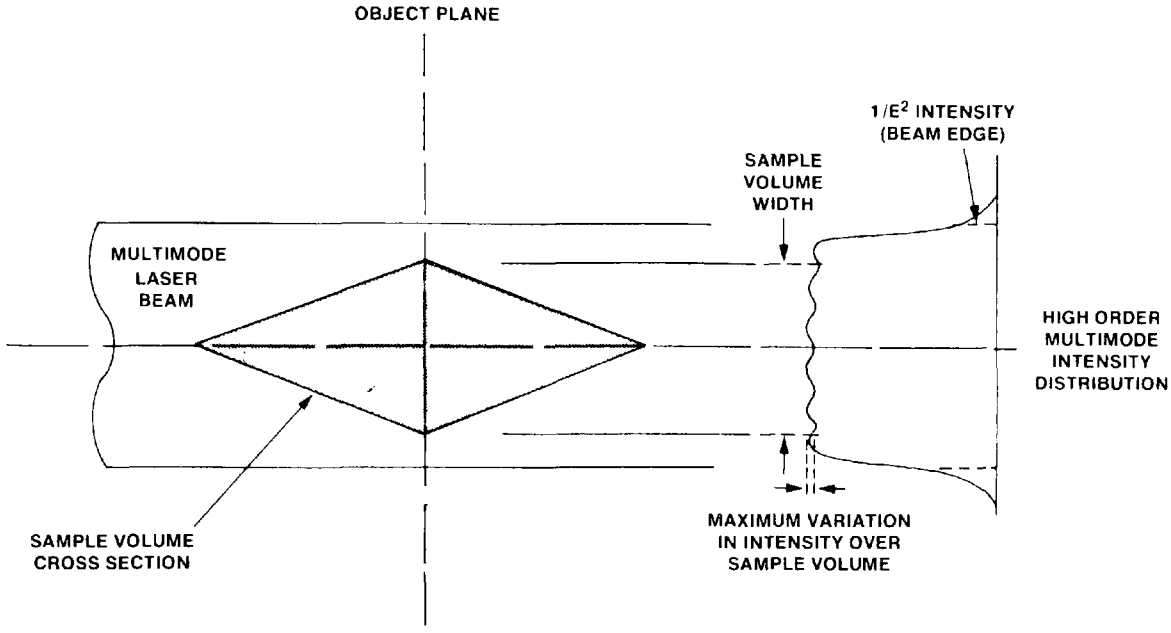


*Figure 4. Relative size and position of sample volume cross section.*

## Theoretical Optical Performance

The optical system discussed in the previous section was obviously constrained by several factors. The FPSSS collecting solid angle of 2 to 11° is smaller than that employed in standard aerosol spectrometers offered by PMS (4 to 22°). This collecting solid angle has primarily evolved from the alignment analysis incorporated in the thermal model. The 2° inner angle can be increased but the 11° outer angle cannot be increased without moving the object plane closer to the probe window or increasing the lens diameter. The latter choice may induce some flow errors. Wind tunnel results of flow through the present sample volume location insure sample flow velocities within 5% of free stream. The option of increasing the inner angle remains and more will be said in this regard in the section on future work; however, all theoretical computational work thus far has used the 2 to 11° collecting solid angle.

The computed optical response curves along with some experimental data points are presented in Figure 7. The oscillating curves presenting the results of Mie scattering computations for real indices should be viewed as worst case in that the effects of laser beam convergence and multimode characteristics have not been included and all particles are nonabsorbing (any

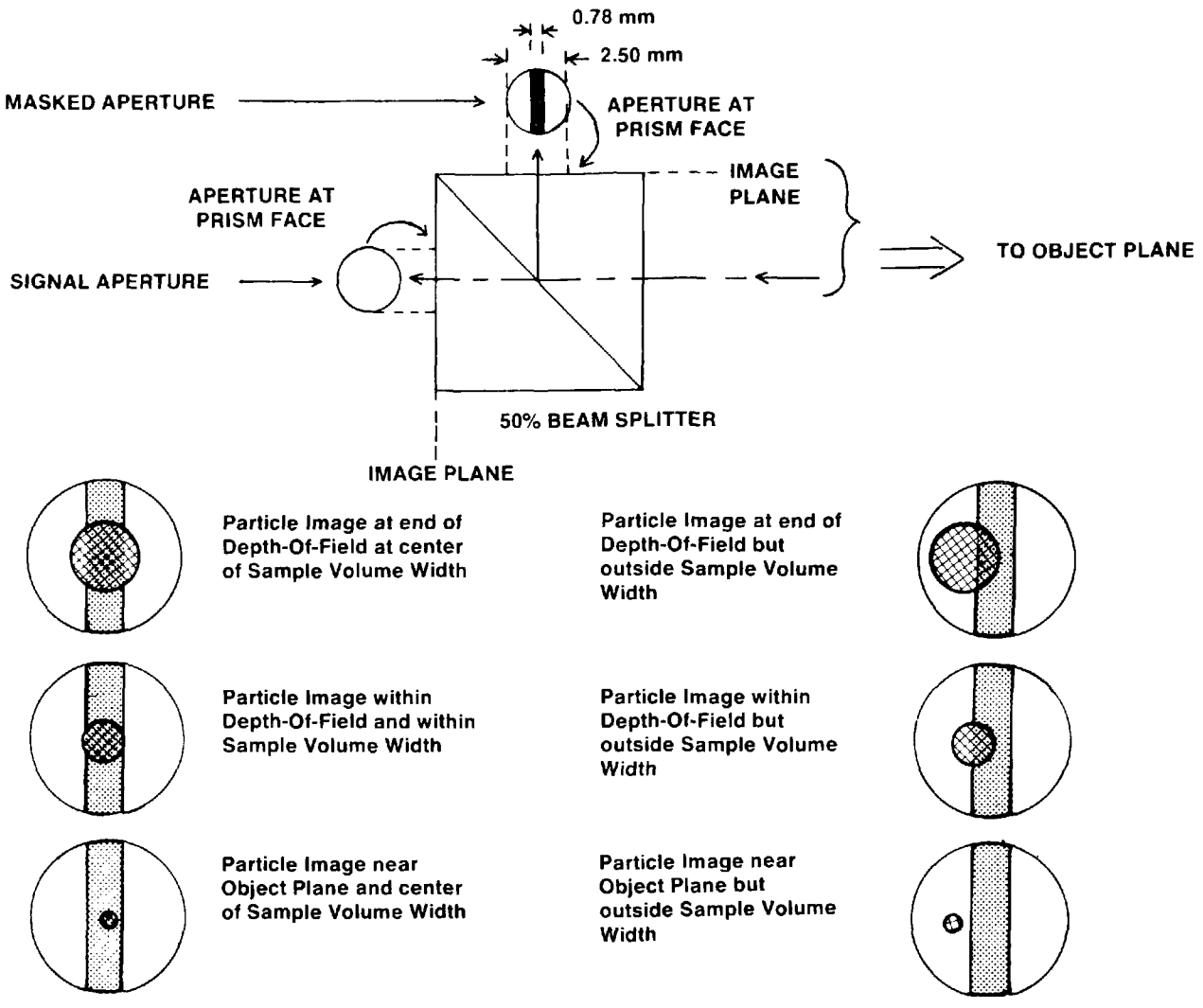


*Figure 5. Image sizes and positions on masked aperture detector.*

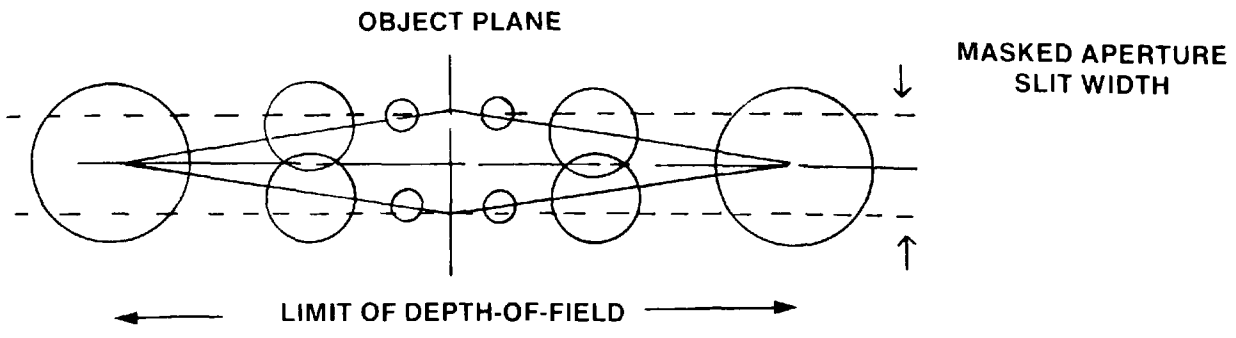


*Figure 6. Image size as a function of sample volume position for the case of 4X gain ratio of masked-to-signal aperture.*

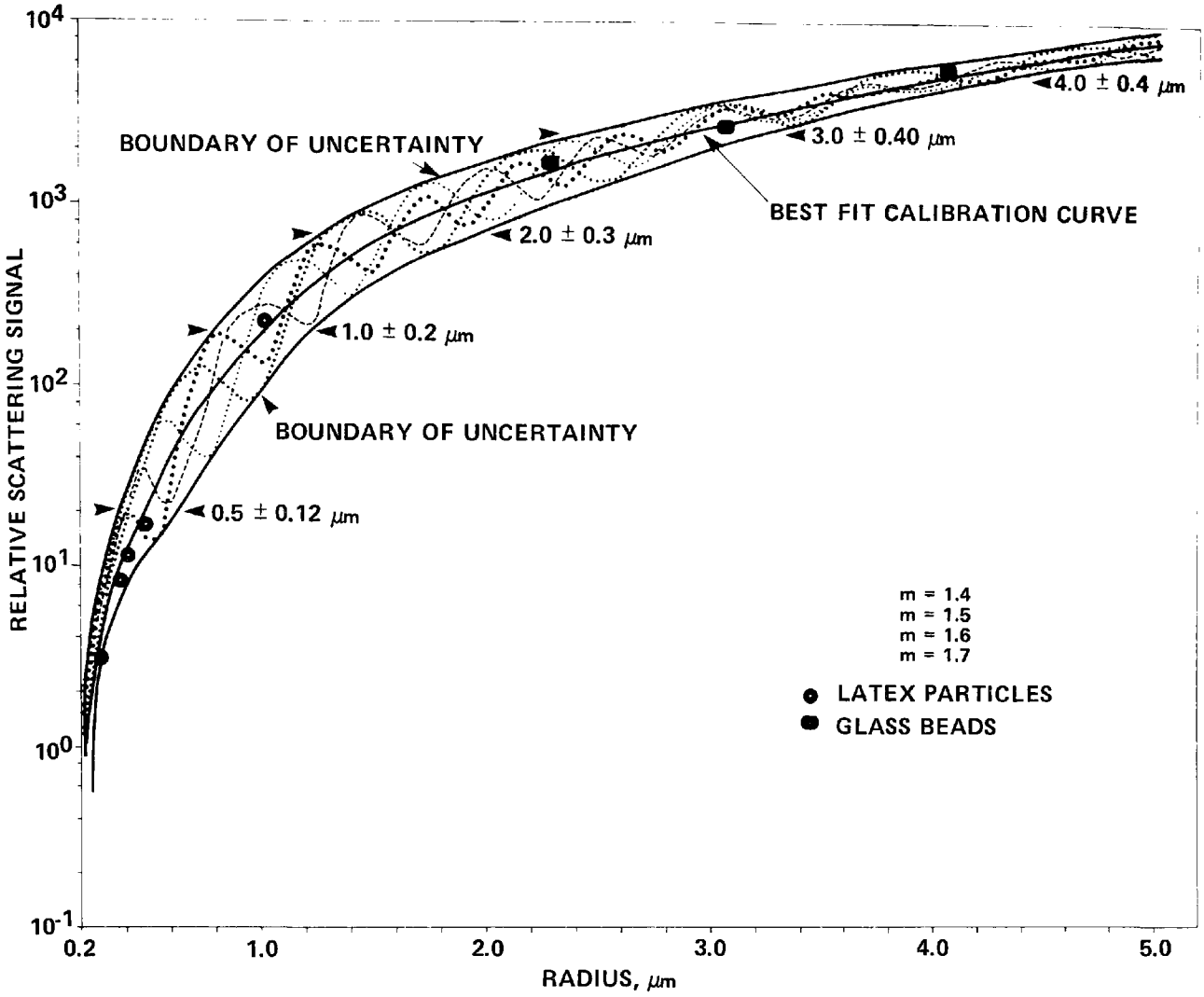


*Figure 7. Theoretical Mie scattering for 2-11° real indices 1.4, 1.5, 1.6, and 1.7.*

of these will reduce the amplitude of the oscillations). Thus, the error bounds apply to all indices. Small amounts of absorption simply reduce the amplitude of the oscillations, as well as the probable error, and few particles would be expected to be completely nonabsorbing. The effect of absorption is illustrated in Figure 8 for a single real index of 1.4 and complex index values of 0.001i, 0.005i, and 0.01i.

The bounded results presented in Figure 7 represent sizing tolerances for all particles, i.e., particles with higher and lower indices or absorbing particles will still fit within the envelope given. However, what we really desire is the average error expected. Using the best fit calibration curve presented this would be within 10% of actual size. The latex and glass

particles, in fact, show errors to be considerably less than that theoretically predicted. This is partially due to beam convergence and laser multimode properties as well as the polydispersion in the case of the glass beads. In general, the results are better than expected considering the many compromises involved in configuring such an instrument.

The choice of the collecting solid angle has been largely dictated by other design constraints; however, it is nearly as good a choice as any other set of angles. Strong forward scattering is quite insensitive to particle shape because the diffracted light contribution is itself a function only of cross sectional area. It also provided the greatest working distance for viewing particles and thus enabled more nearly in situ measurements.

## Thermal Analysis

Single particle size spectrometers designed to operate at high particle concentrations and at small size require an extremely small view volume. Ordinarily, the beam width must be small if the view volume is to be small. A laser is required to produce beam widths of 100 μm dimension if any useful energy density is to be achieved. In the FPSSS this beam must stay essentially fixed with respect to the imaging system if the beamsplitter detector set is to view particles in the same region of the laser beam cross section. Because of the high order multimode beam intensity profile a movement of ±25% of the beam width (25 μm or 0.001 in.) is tolerable. The essential thermal problem is thus to prevent a transverse beam movement of one mil over a 250°C temperature range. The general problem of cooling the laser electronics and optics to a tolerable temperature is trivial by comparison. Looking at the optical system in Figure 1 and the probe head in Figure 2 it can be seen that only two optical components see the high temperature environment --- the 7.5 cm radius mirror and the window. All other elements are within the insulated water-cooled regions. The window has zero power and thus cannot introduce alignment errors except by tilting, which produces a negligible beam offset as long as it is perpendicular to the optical axis to within a couple of degrees. The 7.5 cm mirror is thus the single element of concern.

The 80 node thermal model was used to predict the thermal effects on alignment as well as cooling requirements. First, the optical effects of thermal-mechanical movement of the laser, all mirrors and the windows were measured using an optical brassboard with x, y, z translation stages. The thermal model then provided the positional data for optical elements from which changes in alignment were calculated.

The most important results of the thermal analysis can be summarized as follows:

a) Maximum cooling load of 765 watts is developed at 250°C and 30 m/sec velocity with 20 feet of support boom (see below).

b) The internal head can be maintained to within 3°C of ambient outside air temperature (as seen by heat exchanger) at a 1 gpm coolant flow rate.

c) Internal head temperature gradients are less than 1°C.

d) The alignment is only sensitive to cross gradients between the two support arms holding the external 7.5 cm mirror mount.

The resulting FPSSS head design reflects these results in subtle ways. The internal head body must be fabricated from like material with high thermal conductivity and high thermal mass --- aluminum was selected. The external mirror support arms should have low thermal conductivity and coefficient of expansion --- stainless steel was found adequate. Since these support arms attach directly to the cooled aluminum inner head body they must withstand the nearly full temperature gradient from outside ambient to that inside the stack. It is always desirable to maintain maximum gradients in the most stable materials, thermally.

## DESCRIPTION OF THE PROTOTYPE FPSSS

At the time of this writing the FPSSS design is nearly complete but only certain subsystems have been fabricated and tested. The final FPSSS will contain a dedicated intelligent DAS instead of the standard DAS shown in Figure 3, which will be capable of real time computations of size and mass distributions, mass loading, and extinction coefficient (or opacity). However, it was found highly desirable to make preliminary in-stack measurements to determine the scope of the DAS requirements, as well as uncovering any probe problems early. For the preliminary test work an existing Model CSAS-100 Classical Scattering Aerosol Spectrometer electronics console satisfied the DAS requirements. Furthermore, because of the great similarity in the FPSSS electronics to standard PMS instruments preliminary measurements could be made with existing probe electronic subsystems as well. Pulse processing electronics and pulse height analyzers were fabricated and installed in the CSAS-100 electronics console. Other fabricated subsystems include the FPSSS head, support boom, thermal control system and port bearing assembly. These subsystems are shown in Figures 9 and 10.

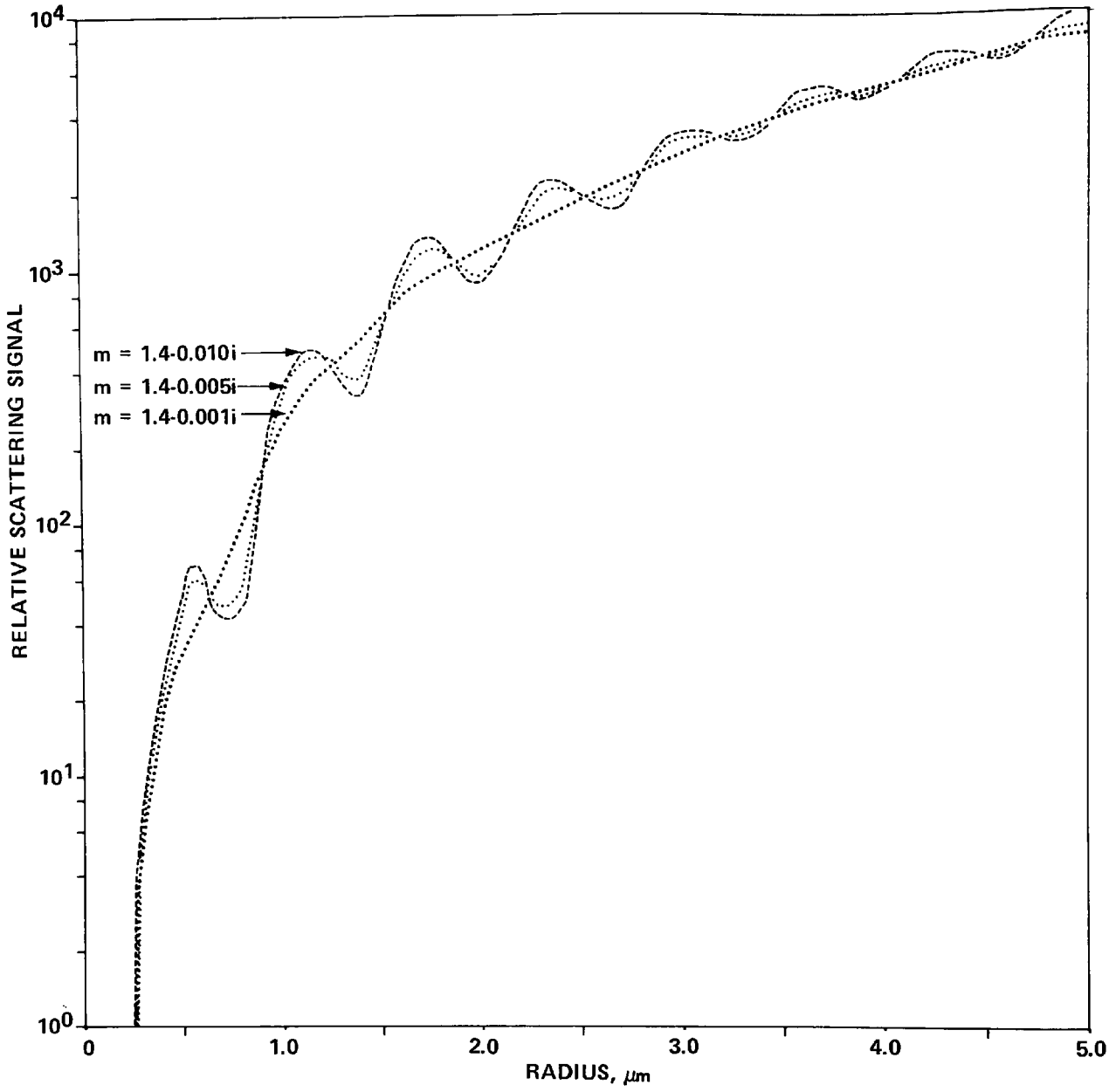


*Figure 8. Theoretical Mie scattering for 2-11$^{o}$ absorbing particles with 1.4 real index.*

FPSSS Head

The head of the prototype FPSSS illustrated in Figures 2 and 3 is shown in Figure 11 with the insulation retainer split. The head is approximately 20 in. long, has a 2.25 in. x 3.5 in. elliptical cross section and weighs seven pounds. The head body is fed by two water lines which have circuitous paths running the full length of the head body making several internal bends

before running back to the rear and exiting. Thus, four water lines are fed through the boom. Two high voltage laser leads, a multiconductor signal cable, and an air line also feed through the boom to the FPSSS head.

The optical system is identical to that described above. The laser is mounted on "O" rings without adjustments. The only adjustments are x-y adjustments on the first beam-folding mirror and the 7.5 cm mirror. The adjustment on the 7.5 cm mirror was not initially planned; however, it was found necessary when we discovered that adjustment using the beam folding mirror had near zero effect at the object plane by virtue of the object plane being centered at the focus of the 7.5 cm mirror.

The head body was constructed in three sections to gain access to the various optical element cells and for machineability. "O" ring seals are used for the water paths and sealing is positive up through 100 psi. The photodetector assembly loads from the rear end can be removed without splitting the head body.

Purge air was provided only for the 7.5 cm mirror initially. This element has a small aperture and is easily purged. Contamination on its surface is, however, more critical than on the window. We eventually plan to purge the window, as well, but did not initially in order to determine its potential exposure and rate of contamination.

FPSSS Support Beam and Port Bearing

The FPSSS is designed to permit installation on a stack port flange and penetrate into the stack to any desired length in order to sample continuously across the stack. This has been accomplished using a sectioned tubular support boom which can be fed through a lateral bearing mounted to a stack port flange. All water lines and electrical cables are continuous through all boom sections. To add a section it is merely necessary to screw it into the preceding one. The first boom section is normally left mounted to the probe head and all boom sections are of 5 feet length. The boom sections are constructed of thin-walled stainless steel tubing. Approximately 0.5 in. of fiber glass insulation and an inner 1.125 in. I.D. PVC sleeve allow sufficient room to slide the lines and cables when joining and separating sections. Each boom section adds about 6 pounds of suspended weight although the final section is slightly heavier due to a larger wall thickness required for the increasing loads.

The port bearing design is of a clamshell nature and is split to allow passage of the larger probe head. Once the head is by the bearing it is closed forming a snug fit to the 2.5 in. O.D. stainless steel walls of the boom sections. The lateral bearing has four sets of four concave stainless steel rollers.

## Thermal Control System

The thermal control system was rather simply constructed using a small centrifugal pump, an automotive type heater radiator, instrument blower and storage reservoir all packaged in a single housing. The purge air pump is also currently housed in the thermal control system. The water pump has a throughput of 1 gpm with 30 feet of line and a corresponding pressure drop of 7 psi. Quick disconnects are used on all lines.

## FPSSS Probe Electronics

A block diagram of the FPSSS Probe electronics is shown in Figure 12. The section enclosed in the box containing the preamps and photodiodes is a separate module housed inside the FPSSS Probe head. The amplifiers have a minimum bandwidth of 300 KHz. The second stage is a programmable amplifier used to gain switch between size ranges. The two diodes with their preamps provide the signals which make it capable of distinguishing whether a particle is within the proper sample volume and rejecting particles which are not. A reference detector constructed using a photodiode and an appropriate amplifier is also inside the FPSSS Probe head. This reference detector provides a reference signal proportional to the power output of the laser. Changes in laser output are thus cancelled when the signal is applied as the reference input of the pulse height analyzer.

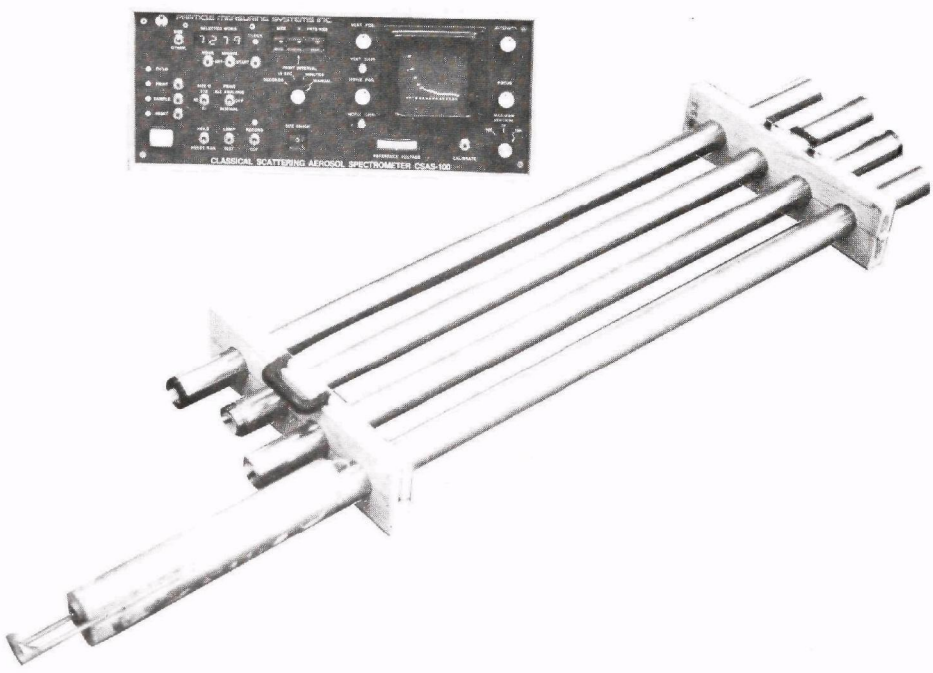


*Figure 9. Photograph showing the FPSSS head mounted to the sectional boom and CSAS-100 electronics console.*

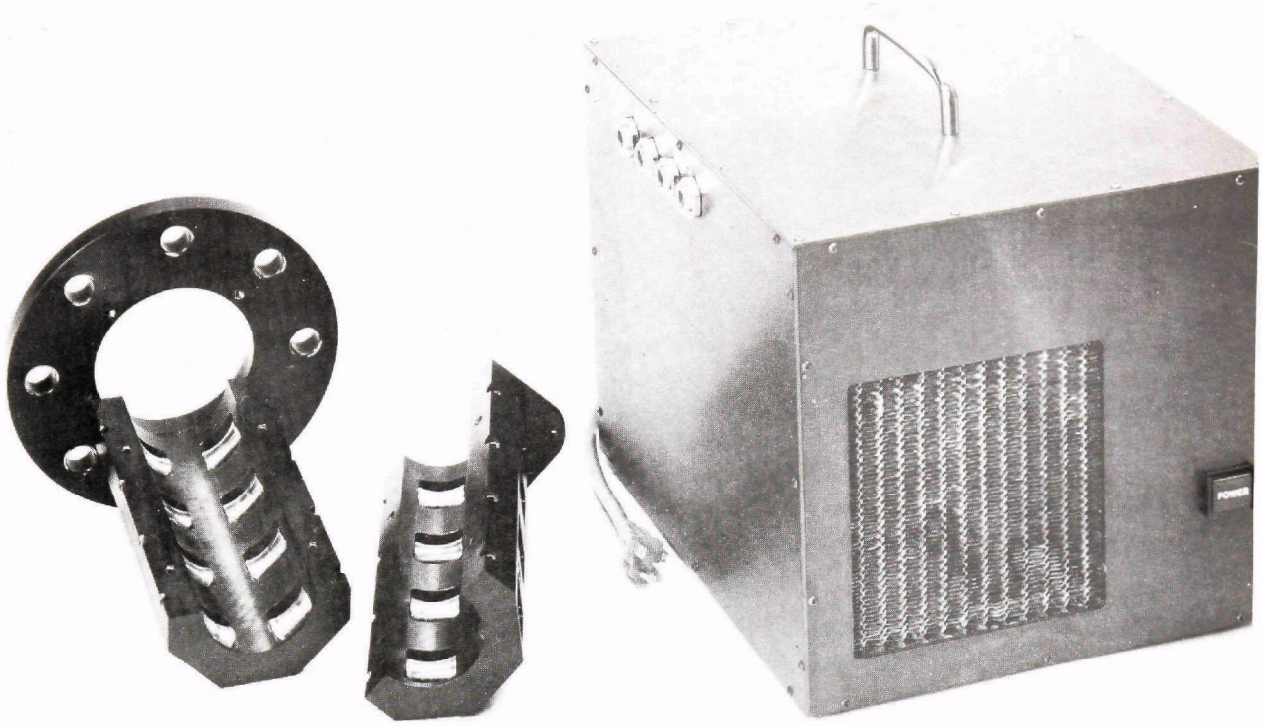

*Figure 10. Photograph of FPSSS port bearing assembly and heat exchanger.*

The remainder of the FPSSS electronics are contained in the CSAS-100 Electronics Console. The two signal pulse streams are first properly leveled with baseline restoration and DC offset circuitry. Dual peak readers then momentarily store the pulse heights from both the signal and masked aperture detectors. The peak readers are used to provide inputs to a comparator to determine which of the two pulse heights from the preamps is the greatest. This measurement determines when particles are in the accepted sample volume.

A pulse height analyzer sizes the signal pulses of all particles passing through the beam. The pulse height analyzer has a set of sixteen voltage comparators and latches. The reference voltage to the comparators provided by the reference detector is divided by resistive dividers. Because its reference voltage is derived from the source of illumination, the entire system has an effective automatic gain control (AGC).

The transmit time analyzer measures the half-width of delayed pulses that are found to be in the sample volume. The transit times are averaged over a great number of particles to provide a true statistical velocity average (note that velocity is actually the reciprocal of transit time).

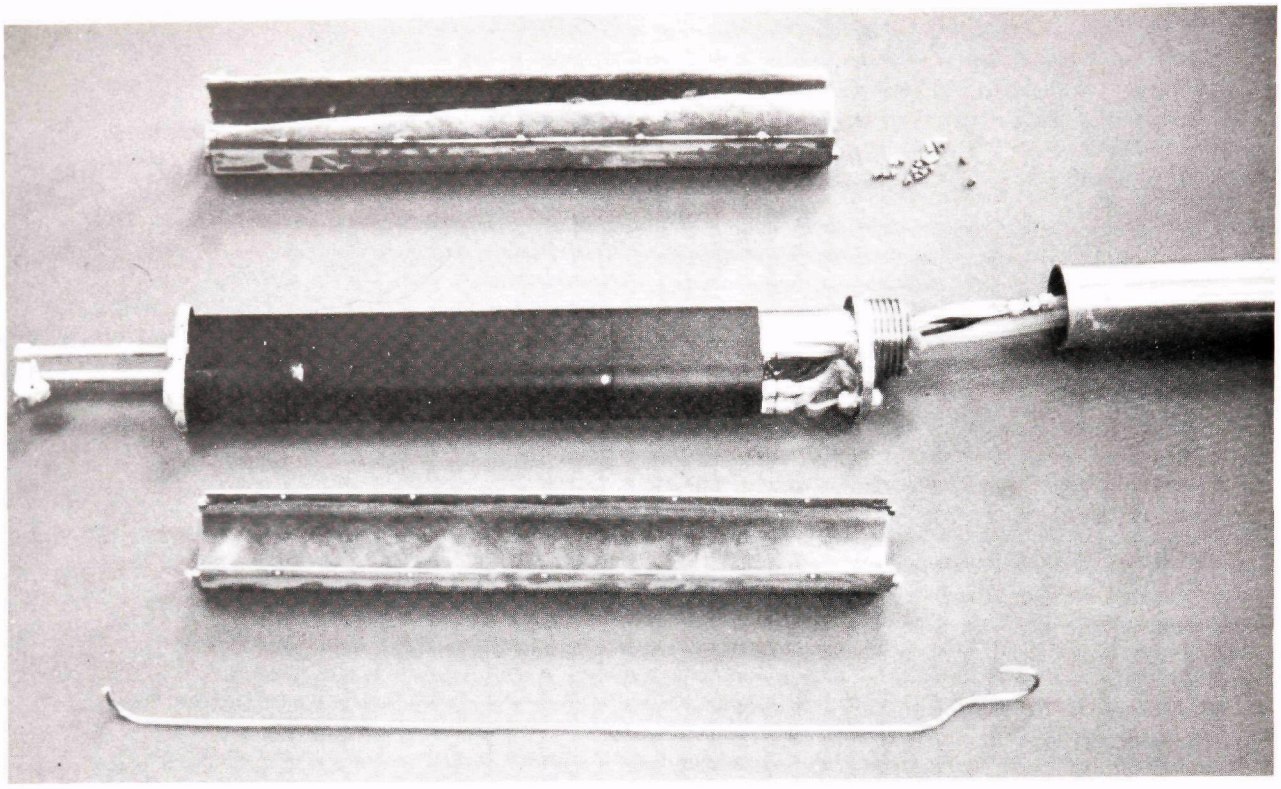

*Figure 11. Photograph of FPSSS partially disassembled revealing construction insulation details.*

The control (accept/reject) logic provides the proper delay between an event and the strobe and reset pulses. This logic also provides gating for valid and invalid strobes.

The pulse height analyzer is currently configured to provide four size ranges of 15 channels each as follows:

| | | |
|---|---|---|
| Range 0 | 2.5 - 10 | μm |
| Range 1 | 1 - 5.5 | μm |
| Range 2 | 0.5 - 2.0 | μm |
| Range 3 | 0.4 - 0.85 | μm |

All size intervals are linear with maximum resolution in Range 3 being 0.03 μm. The ability to switch ranges has been found to be particularly important in field measurements. Calibrations with particles of known size have been performed previously using latex spheres and glass beads with results shown in Figure 7.

## RESULTS OF INITIAL IN-STACK TESTS

The first tests of the FPSSS were conducted at the Valmont Power Plant owned and operated by the Public Service Company of Colorado on April 24, 1978. This is a coal-fired power plant

with general operation and control devices similar to that depicted in Figure 13. Measurements were performed at the 80 foot level on the stack which afforded good access and at which a Lear Siegler Model RM41 Opacity Monitor was also operating. These initial tests were limited to an hour of measurement time with the entire set-up, measurement, and pack-up completed in less than two hours.

Measurements were taken at two foot intervals from 3 to 17 feet in-stack penetration. The stack had an I.D. of 21 feet and we did not have sufficient boom to reach completely across. However, the measurements revealed a symmetric profile of particle flux and the lack of measurement over the final four feet was not regarded as significant.

The in-stack velocity profile revealed a greater amount of turbulence than anticipated with gusts of 5 m/sec common near the stack center. The mean flow varied from 5 to 12 m/sec with the highest values at the center. No regions of reverse flow could be identified.

The particle size distributions measured at 2 foot intervals were surprisingly uniform as viewed on the CRT spectral display of the CSAS-100 electronics console. In fact, once corrections for variations in flow rate were made the distributions revealed only minor spatial spectral differences which were of the same order as temporal changes at a fixed location. For this reason all measurements were integrated together to generate a single average particle size distribution representative of the entire stack (see Figure 14). The particle size distribution is seen to be highest in number at the smallest size (0.4 μm) although the slope is decreasing. The overall slope is quite steep. In fact, it is steeper than observed ambient background in many cases. A size distribution with such a steep slope is characteristic of air passed through coarse filters.

The computed average distribution of extinction cross section (2nd moment) as a function of particle size is given in Figure 15. The extinction cross section was computed for a wavelength of 5500Å in an effort to make comparisons with the opacity monitor operating with a white light source with its spectral maximum at this wavelength. The extinction cross section is seen to peak at sizes of 0.5 to 0.6 μm and has an integral value of $3.0 \times 10^4 \mu m^2/cm^3$. The integrated cross section over the 6 meter stack diameter provides a computed transmission of 0.83 or an opacity of 17%. The Lear Siegler RM41 had comparable opacity values of 14 to 16% during the period of measurement.

The close agreement between the Lear Siegler RM41 and the FPSSS opacities must be regarded as fortuitous at the present time. A certain amount of particle cross section also exists below the 0.4 μm lower limit of sensitivity although probably

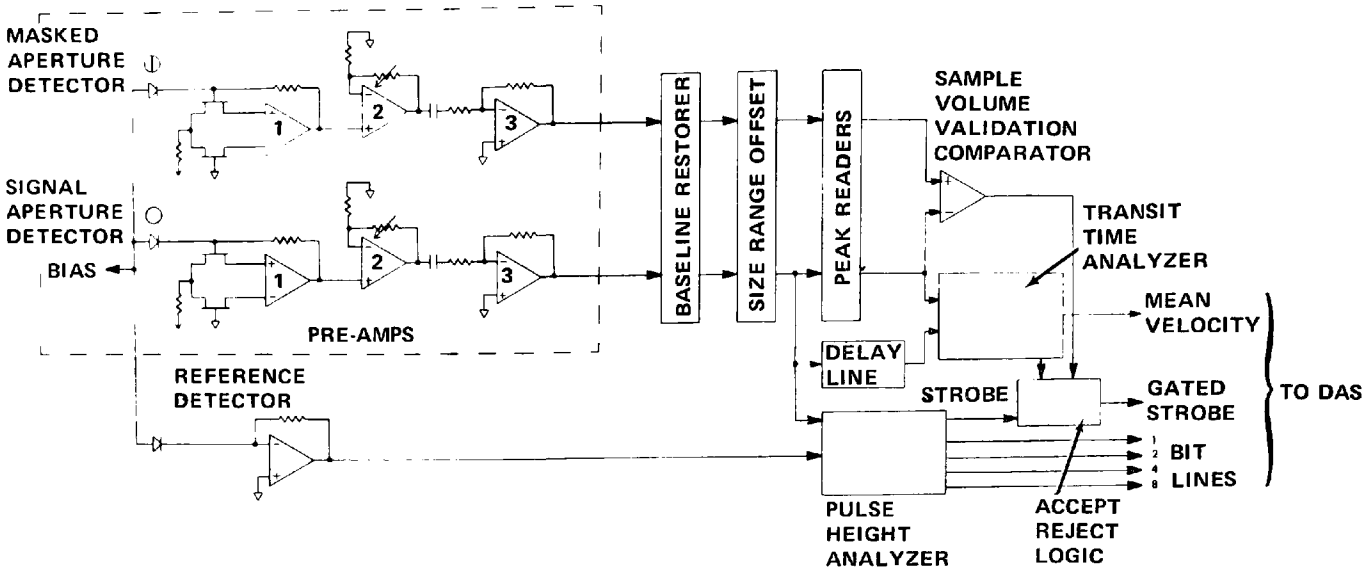


*Figure 12. FPSSS probe electronics block diagram.*

less than 10% of the total. The exact spectral characteristics of the Lear Siegler RM41 were not available and in this size range extinction is a strong function of wavelength. Furthermore, an ideal transmissometer still gains contributions from multiple scattering which were neglected in our treatment. Finally, the soiling of the window resulted in a small but obvious underestimate of particle size and opacity.

The average particle volume (mass) distribution (3rd moment) is given in Figure 16. This is probably the most interesting of all the spectral plots. It reveals several dominant mass modes each being statistically valid. Perhaps most surprising is the dominant mass mode at 0.65 μm. It is more striking when presented with the full resolution of Range 3 as shown in Figure 17. Here there is little doubt that the FPSSS has captured nearly all of the mass. The integrated mass loading is surprisingly low being on the order of only 0.01 to 0.02 g/m$^3$, depending on the assumed density. The known undersizing due to the soiled window should have only resulted in underestimates of mass less than 30%.

We expected mass loadings nearer a tenth of a gram; however, the only way in which higher mass loading values would be compatible with opacity values of less than 20% (regulatory compliance value) would be with an increase in size and decrease in concentration over that observed. A simple increase in size of a factor of two provides an eight-fold mass increase but also a four-fold increase in cross section and opacity. Since the

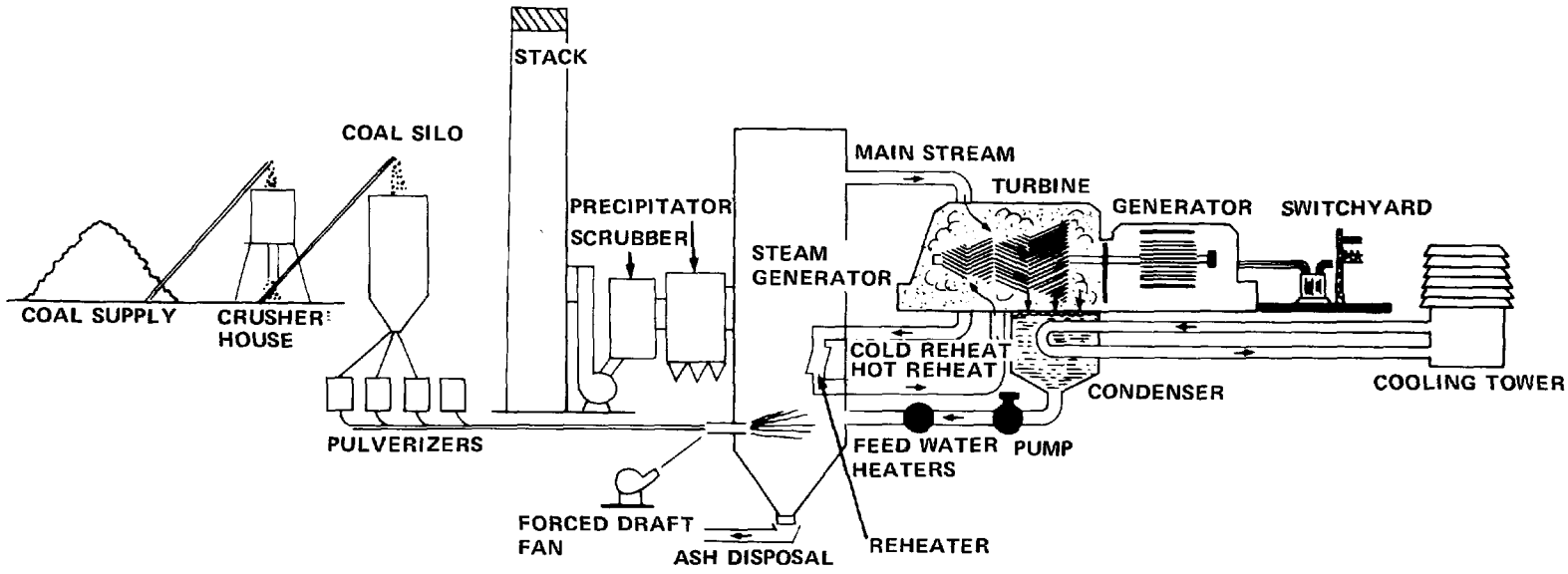


*Figure 13. Schematic drawing of a steam electric generating station.*

mass-to-cross section ratio is proportional to radius, or size, it is necessary to increase size by a factor of ten and decrease concentration by a factor of 100 to maintain the same opacity but a factor of ten higher mass loading. Either of the above is totally unreasonable from an instrumental standpoint. We are thus left to conclude that this particular stack does indeed have a low mass loading characterized by particles of about 1.3 μm diameter.

## FUTURE WORK AND CONCLUSIONS

We are encouraged to believe that the FPSSS will be a satisfactory instrument for making in situ size distribution measurements in a hot stack environment. However, field testing has only begun and final assessment must await much more exhaustive work on other stacks and stationary sources where particulate characteristics may be quite different. Results of measurements ahead of the control devices in the Valmont stack are currently being analyzed. Evaluation of control devices by performing measurements up and down stream is a goal of the FPSSS development. Suffice to say a great deal of work remains.

It is helpful when analyzing the performance of a new instrument to bear in mind the trade-offs made in its design. With regard to the FPSSS two come to mind immediately. One has resulted in the current size limit of 0.4 μm and the other may prove to limit the maximum concentration to a lower level than desirable. These two factors are strongly coupled.

The EPA initially asked for a size range of 0.5 to 5.0 μm. We felt that a 0.3 μm sensitivity could be obtained. Our current instrument has a 0.4 to 10 μm range. The difference between 0.3 and 0.4 μm is about a factor of five in signal. An expansion of the collecting angles from 11 to 20° would pick up the difference. However, as mentioned in the previous section, this would require moving the sample region closer to the prime objective since this objective's size cannot be increased by the rough factor of two required and still allow the FPSSS head to fit in standard 4 in. stack ports. Our wind tunnel results do not preclude moving the sample region closer but it obviously will not be as aerodynamically clean as it currently is. In view of the highly turbulent conditions observed in the Valmont stack, clean aerodynamics may not be a profitable design feature and movement of the sample volume closer could indeed be a better choice. A decision to move the sample region closer must also await tests of a purge air fitting for the window which will cause some reduction in available room.

The current instrument design can handle concentrations up to 50,000/cm$^3$ although coincidence losses must be corrected for. An increase in magnification from 20 to 30X will provide measurements up to a maximum concentration of $10^5$/cm$^3$ --- our

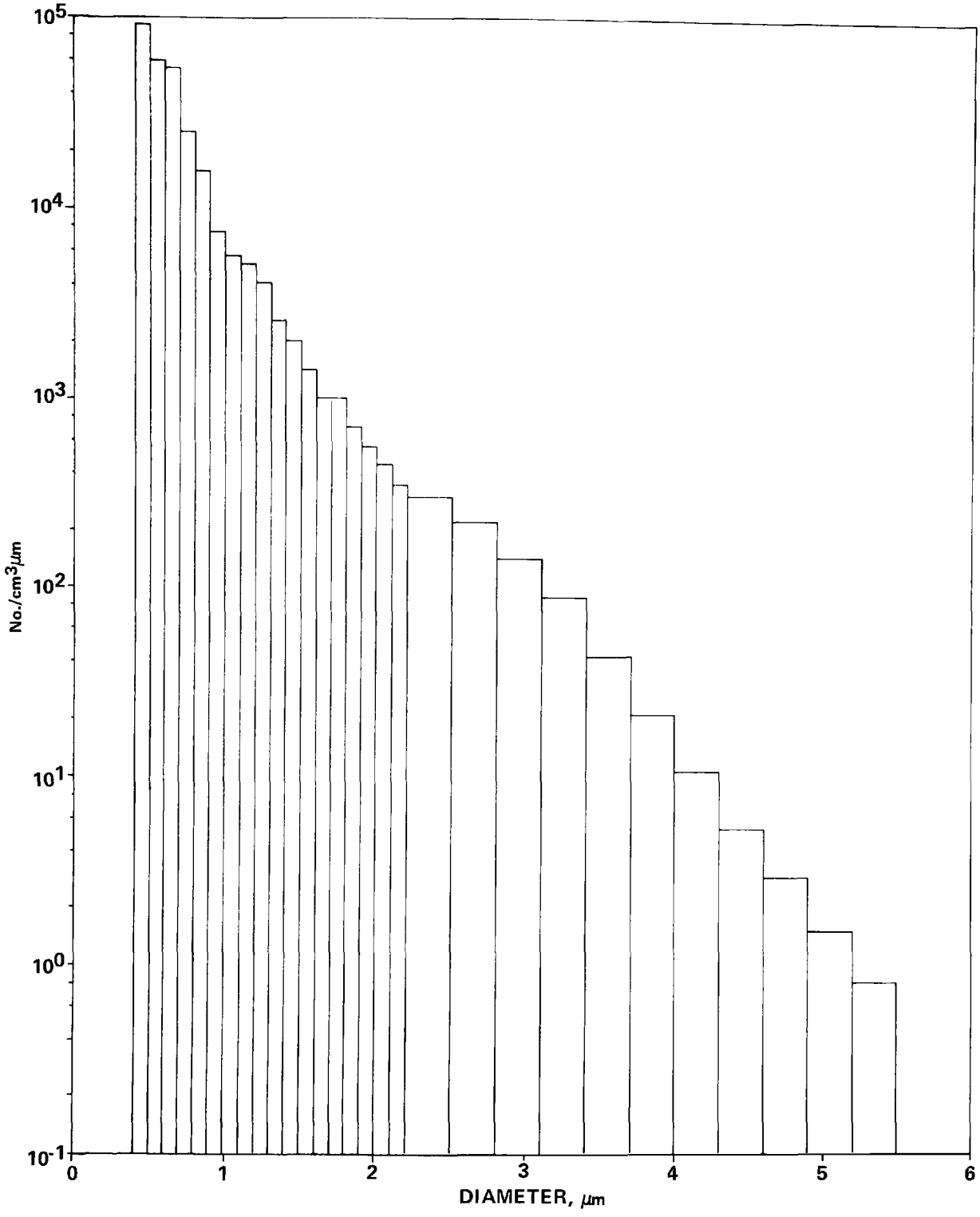


*Figure 14. Average in-stack size distribution. The higher resolution data for size range no. 3 has been summed into 0.1 µm size classes.*

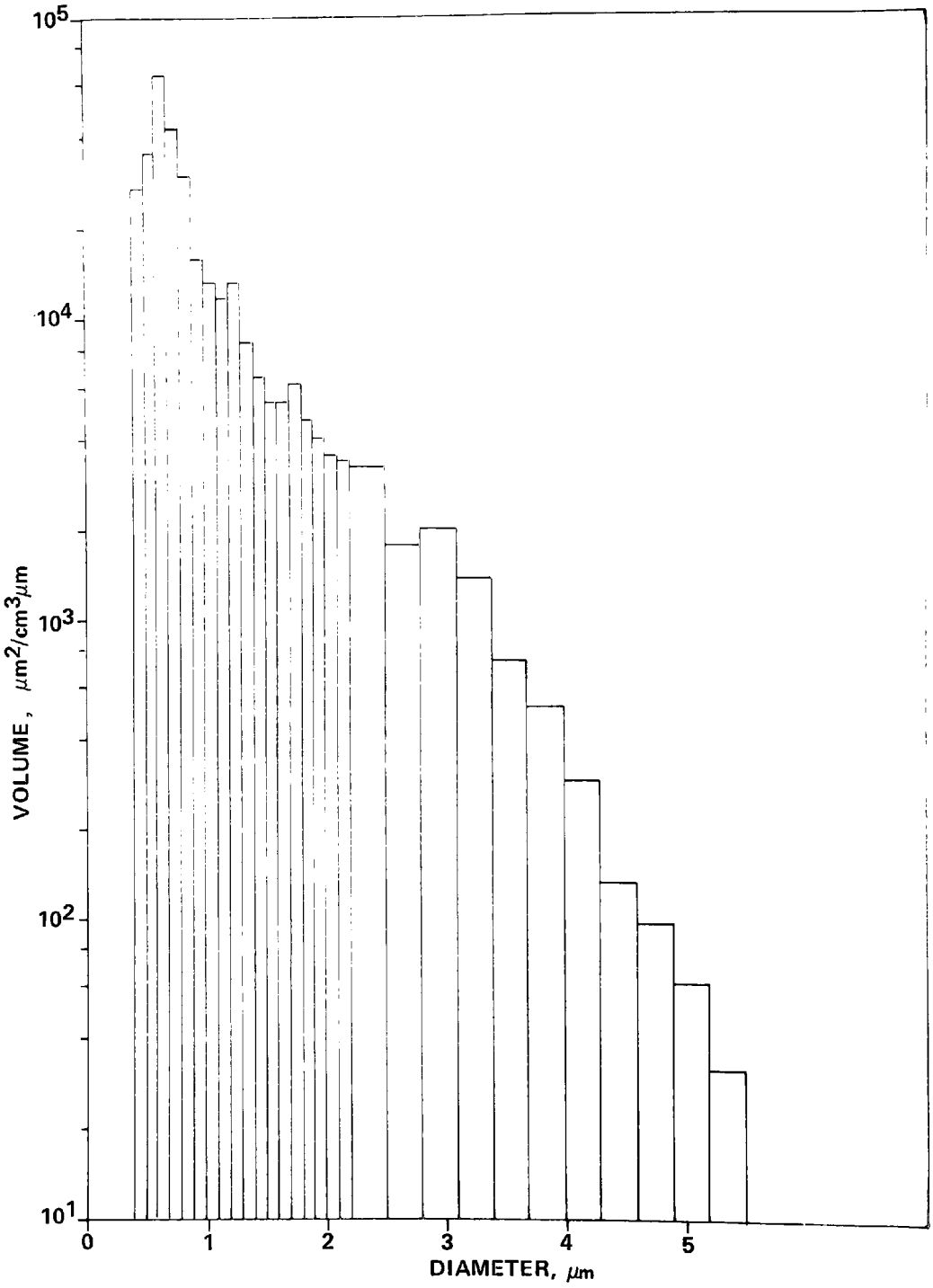


*Figure 15. Average in-stack extinction cross section distribution. The higher resolution data for size range no. 3 has been summed into 0.1 μm size classes. The mean cross section size is 0.79 μm.*

design goal. An increase in the inner collecting angle from 2 to 4° also doubles the maximum concentration where measurements can be made. Halving the laser beam diameter has a fourfold effect.

We previously mentioned that achieving a higher maximum concentration limit and greater sensitivity were strongly coupled. First, from glancing at Figure 14 it is obvious that increasing the sensitivity automatically increases the number of particles viewed and coincidence losses. Conversely, doubling the inner collecting angle reduces the light collected. The overall sensitivity is obviously reduced as well but there is a more subtle effect. The 2° inner angle allows for very accurate measurements out to 10 μm by collecting the diffracted light at small forward scattering angles. A deterioration in sizing performance would result if the inner angle were increased above 6° for 10 μm particles or above 10° for 5 μm particles. Of course, the latter would require enlarging the outer collecting angle to achieve adequate sensitivity. Halving the laser beam diameter aids sensitivity as well as maximum concentration limits. However, here one must be absolutely sure that alignment will be extremely stable. To decrease the beam diameter a factor of two requires either a condensing mirror of half the radius of the current one or doubling the laser beam diameter input.

Probably the easiest and least controversial change would be to increase the magnification to 30X. The only penalty paid is in increasing the detector bandwidth (admitting more noise) to see the relatively shorter pulses which would result. An increase in bandwidth is required because the photodiode is sized to view the full transit of a particle and any increase in magnification will truncate the time a particle is viewed.

Work obviously needs to be done in all of the above areas to determine optimum design; however, progress is complicated by the impact of changes in one area of design or another. Conversely, other areas of continuing work should experience rapid progress. The DAS design should be ready for fabrication in July, 1978. From our field experience with actual stack measurements valuable insight into desired packaging improvements affording better portability and human engineering have been found. For instance, we have found that five foot boom sections could pose a problem when catwalks are narrow and guard rails interfere. Four or even three foot boom sections may be preferable. Anyone who has tried to make measurements around stacks knows of the difficulties that can occur. In designing the FPSSS we have tried to remain fully cognizant of the user's environment and attempted to maximize the usefulness of such an instrument. The real utility of a device such as the FPSSS is not in extending its sensitivity to the smallest particles or its ability to handle the highest concentrations, rather it is in providing

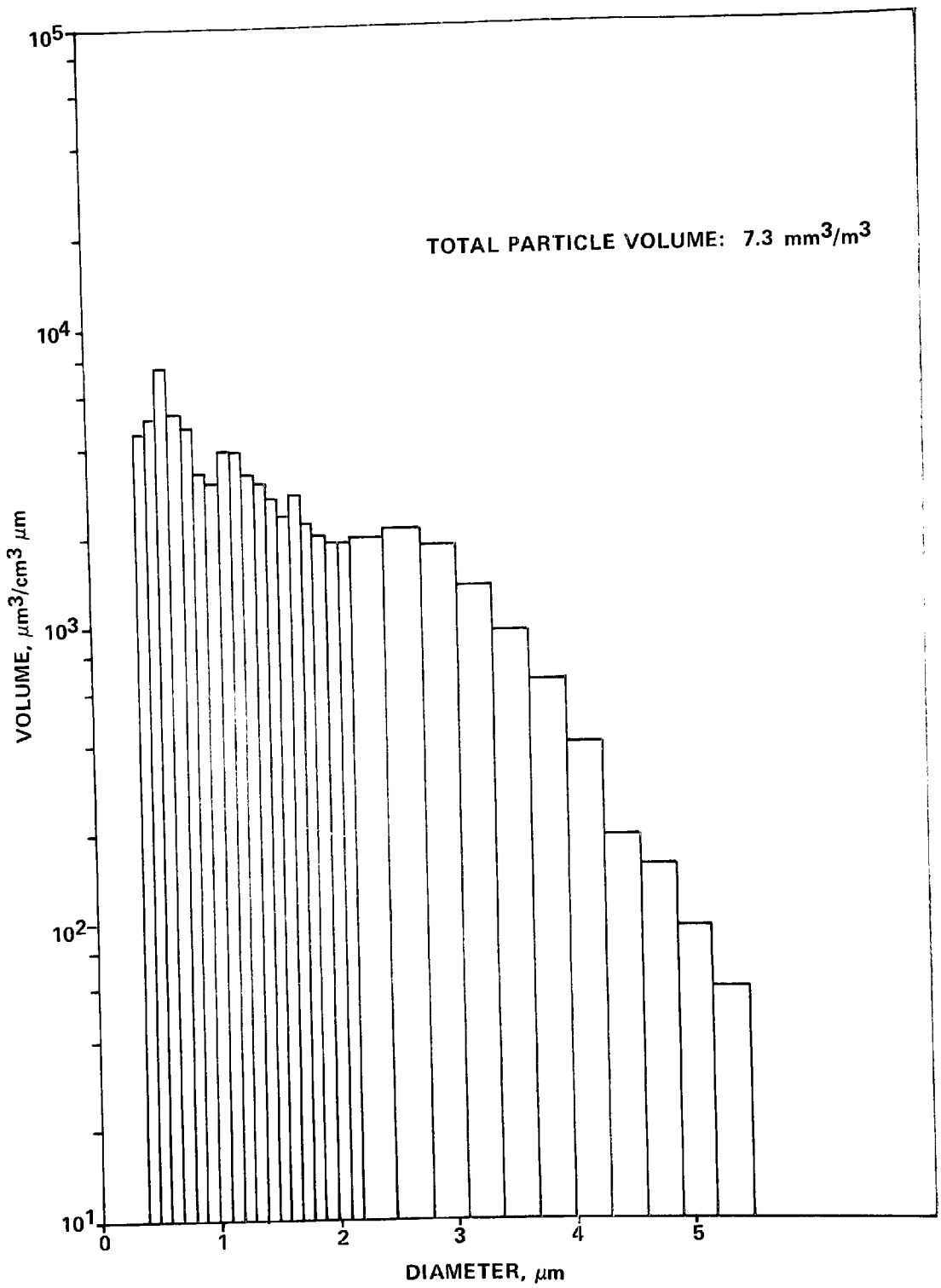


*Figure 16. Average in-stack volume (mass) distribution. The higher resolution data for size range no. 3 has been summed into 0.1 μm size classes. The mean volume (mass) size is 1.31 μm.*

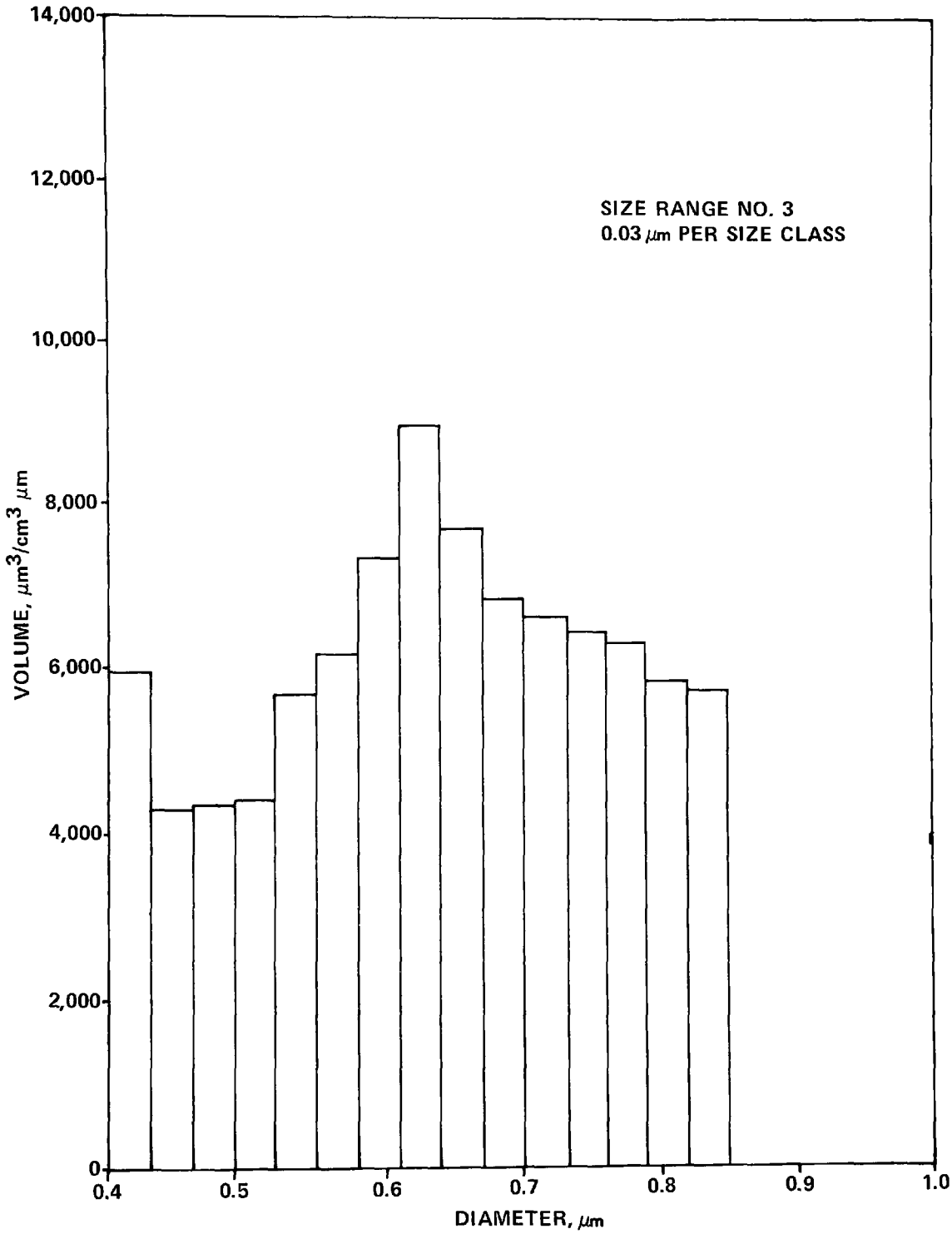


*Figure 17. Average in-stack volume (mass) distribution from 0.4 to 0.85 μm.*

measurements of sufficient spectral quality to gain insight into processes which produce changes in particle size and number density while retaining a reasonable confidence in integrated properties such as mass loading and opacity.

One final remark is directed at the measurements reported in the section on results, above. We reported that the velocity variations were quite large. For the FPSSS this poses little problem; however, it clearly must be problematic for direct samplers using so-called isokinetic intakes. In our view it would be impossible to follow the fluctuations observed with a pumping system and achieve isokinetic sampling conditions. What effect the stack gustiness has on such techniques is not currently known but could possibly be explored by intercomparisons with the FPSSS.

ACKNOWLEDGEMENT

This work was funded by the Environmental Protection Agency (EPA), IERL--Process Measurement Branch.

REFERENCES

1. Knollenberg, R.G., J. Hansen, B. Ragent, J. Martonchik, and M. Tomasko. The Clouds of Venus. Space Sci. Rev. 20:329-354, 1977.

2. Colin, L. The Exploration of Venus. Space Sci. Rev. 20:249-258, 1977.

3. Knollenberg, R.G., and R.E. Luehr. Open Cavity Laser "Active" Scattering Particle Spectrometry from 0.05 to 5 Microns. In: Fine Particles, B.Y.H. Liu, ed. Academic Press, New York, 1976. pp. 669-696.

4. Knollenberg, R.G. Three New Instruments for Cloud Physics Measurements: The 2D Spectrometer, The Forward Scattering Spectrometer Probe, and The Active Scattering Aerosol Spectrometer. Presented at The Cloud Physics Conference July 26-August 6, 1976. Preprint available from the American Meteorological Society.

5. Knollenberg, R.G. The Use of Low Power Lasers in Particle Size Spectrometry. SPIE, Practical Applications of Low Power Lasers, Vol. 92, 1976. pp 137-152.

PAPER 9

# OPTICAL MEASUREMENTS OF PARTICULATE SIZE IN STATIONARY SOURCE EMISSIONS

A.L. WERTHEIMER
M.N. TRAINER
W.H. HART
LEEDS & NORTHRUP COMPANY

## ABSTRACT

A new light scattering instrument is described for in-situ measurements of particulates in the 0.1 to 10.0 μm diameter size range. Two modes of scattering are used, each with two wavelengths of light, to generate five size fractions by volume from a distribution of particulates. One mode measures polarized light scattered in two orthogonal orientations at an angle of 90° to the optical probe beam. The second mode measures light scattered in near forward angles (4 to 11°). Both modes allow the extraction of size data when particles of different sizes are present simultaneously in the sensing region. These principles have been incorporated into a prototype portable stack monitor, consisting of a 1.5 meter long, 9 cm diameter insertable probe capable of withstanding temperatures up to 260°C. The optical signals are carried through fiber optic cables contained in the probe. An arc source and silicon photodetectors are outside the stack at the end of the probe, while a digital microprocessor analyzes the set of measurements and calculates the size fractions. The microprocessor, an air purge system, the lamp power supply, and a digital printer are housed separately from the probe for ease of installation and service.

## INTRODUCTION

Light scattering is ideally suited for measurements of particulates in real time situations. The characteristics of the materials are not disturbed during the course of the measurements, measured sizes can be correlated well with standard optical microscopy, and the technique is rapid and, in general, real time. Frequently it is of interest to measure the mass or volume

of particulates within a given size interval, and recent developments have produced low angle forward light scattering industrial process instruments capable of real time measurements of particle size and volume in either liquid or gases in the 2 to 200 μm diameter range.[1,2] These instruments are also unique for their ability to simultaneously accommodate multiple sizes of particles in the sensing region, so the loading level is considerably higher than is normally possible with single particle counters.

One of the limitations in low angle forward scattering is the difficulty in discriminating sizes much below the 1 μm level with visible light. Prior to this work no comparable instrumentation was available to discriminate mass fractions in the 0.1 to 1 μm size range, the lower decade of the respirable region. This paper discusses a new approach, based on scattering of light at 90° to the direction of an optical probe beam for the generation of volumetric size fractions below the range normally covered by forward light scattering. A combination of 90° and forward light scattering has been incorporated to construct a prototype stack monitor capable of measuring volume in five logarithmically spaced size intervals in the range of 0.1 to 10 μm.

## PRINCIPLES OF OPERATION

Light scattering is classically divided into regions of analysis according to the relationship between size of the particle and the wavelength of light. For particles much larger than the wavelength, scalar diffraction theory is adequate to describe the interaction and define the angular distribution of scattered light.[3] Low angle forward light scattering is commonly discussed using this analysis.

For particles much smaller than the wavelength, the angular light distribution is independent of particle size. Equal amounts of light are scattered into forward and backward lobes. This is referred to as Rayleigh scattering,[4] and is typical of scattering observed in the atmosphere or from suspensions of low and intermediate molecular weight materials.

The most complicated analysis is required when the particle is comparable in size to the wavelength. A full treatment for all size ranges was first performed by Mie,[5] and entire texts have been written using this theoretical approach.[6] The 90° scattering approach described here is based on characteristics of the transition between simple Rayleigh and rigorous Mie scattering, and the analysis is included in the next section.

### Principles of 90° Scattering

Mie theory will be used throughout this paper to describe the angular distributions of flux for particles of different sizes. Tables[7] and computer programs[8] are available to facilitate rapid analysis using Mie theory, thus eliminating the need

to decide if a simpler theoretical treatment would be sufficiently accurate for the particular size and refractive index of interest. Spherical shapes are usually assumed in light scattering theory and have been used for ease of computation.

To illustrate some specific characteristics of light scattering, Figures 1 and 2 were computed for spherical water droplets of refractive index 1.33. A dimensionless size parameter, a, is frequently used where

$$a = \pi D/\lambda, \tag{1}$$

with $\lambda$ the wavelength of light. Figures 1 and 2 cover a range of a = 0.5 to a = 40. Two orthogonal polarizations of incident light are shown, referred to as $i_1$ and $i_2$. The electric field of $i_1$ is in a plane perpendicular to the plane containing the probe beam and the observation point. The log of the flux per particle is graphed, covering a hemisphere from 0° (light returning directly toward the source) through 180° (forward scattering direction).

For a = 0.5 and 1.0, Rayleigh scattering characteristics dominate. Equal intensities are shown in both forward and reverse directions, and no light is scattered at 90° for the incident light designated as $i_2$. As the parameter, a, increases, the null at 90° disappears and the two curves tend to be more alike. For larger values of a, the fine structure of the curves changes slightly as the refractive index varies. However, one of the more stable characteristics of the patterns is the null at 90° for small values of "a" with $i_2$, the light polarized so that the electric field is in the plane defined by the direction of propagation of the incident beam and the point of observation.

Finally, it should be mentioned that these curves describe the light scattered from the individual particles. Suspensions of N identical particles widely separated from each other produce an angular pattern N times as intense as that of the single particle, if no significant shadowing or secondary scattering occurs. This assumption is referred to as single scattering.

For small "a" values the differences between Figures 1 and 2 are greatest in the region of 90°. The relative differences become smaller as the size parameter increases, where the difference in intensity can be calculated by subtracting the two curves at 90°. At this point, it is appropriate to consider the scattered flux per unit volume, since typical particle size distribution curves frequently imply a vastly greater number of small particles than large ones. When the flux difference per particle, $i_1 - i_2$, is divided by the volume of the particle, and plotted against the log of "a", a well-defined peak is observed. Figure 3 shows such a curve, computed for spheres of

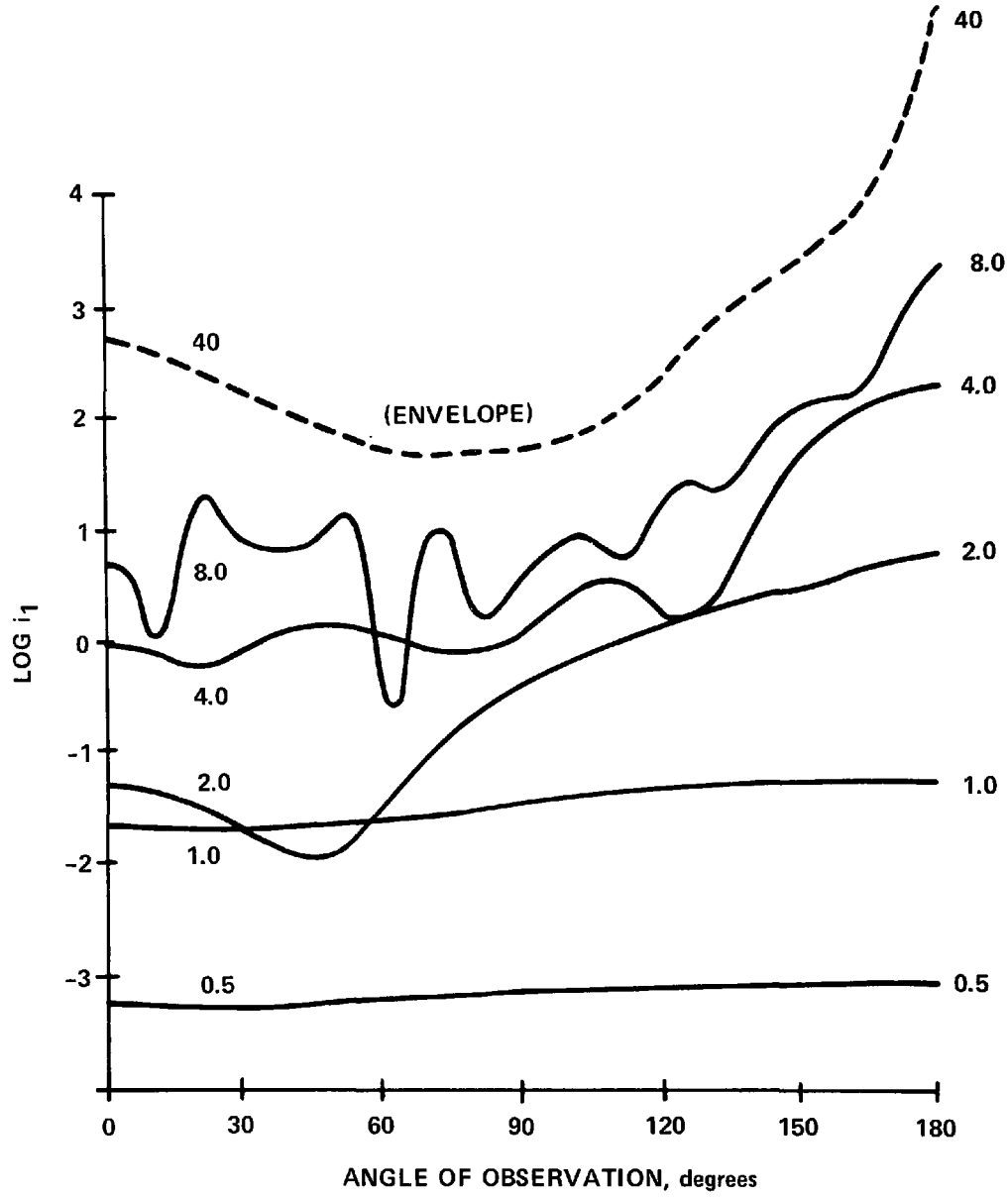


*Figure 1. Log of scattered intensity per particle as a function of observation angle, with forward direction at 180°. Two orthogonal polarizations of incident light are shown, $i_1$ in Figure 1, and $i_2$ in Figure 2.*

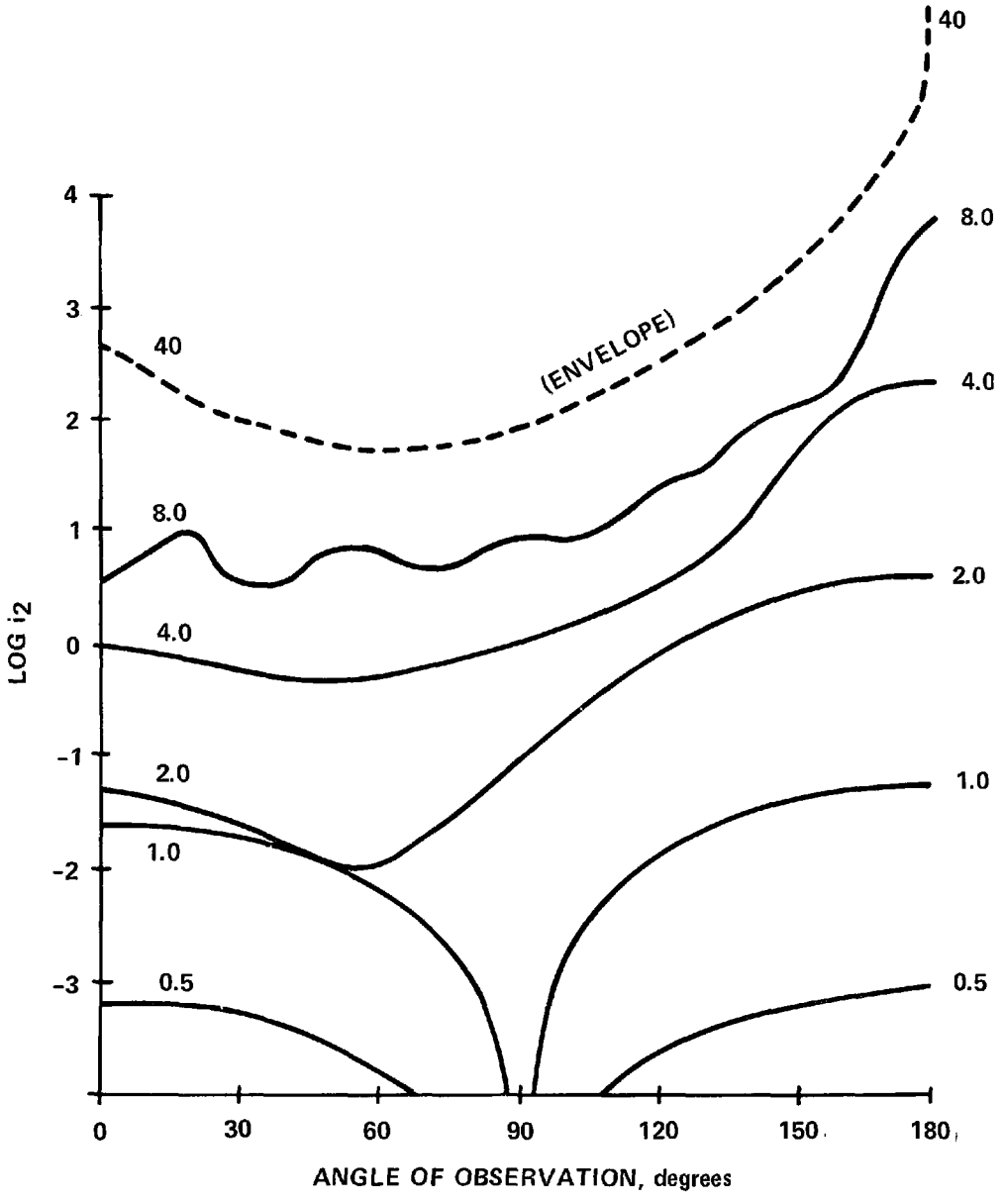


*Figure 2. Log of scattered intensity per particle as a function of observation angle, with forward direction at 180°. Two orthogonal polarizations of incident light are shown, $i_1$ in Figure 1, and $i_2$ in Figure 2.*

index 1.33. In order to simulate a realistic observation angle, the flux difference per unit was computed over an angular collection range of 90° ± 10°.

The curve in Figure 3 has a peak at about a = 1.5, and the width at half maximum covers a range from approximately a = 1 to 2. In order to identify a corresponding particle size, a wavelength must be specified. For a helium-neon laser with $\lambda$ = 0.6328 μm, the half width covers diameters from 0.2 to 0.4 μm, and the peak is located at 0.3 μm. Other wavelengths can be used to measure volume components at other locations, as shown in Table 1.

TABLE 1. VOLUME RESPONSE AS A FUNCTION OF WAVELENGTH FOR 90° SCATTERING

| Wavelength, μm | Particle diameter at peak of response, μm | Diameter range, μm |
|---|---|---|
| 0.45 | 0.21 | 0.14 to 0.3 |
| 0.6328 | 0.30 | 0.2 to 0.4 |
| 0.90 | 0.43 | 0.3 to 0.6 |

These numbers are computed for an index of 1.33. Other indices produce slightly different curves, although the basic characteristics are preserved. The curve for glass spheres, for example (n = 1.55) has its peak at approximately the same value (a = 1.5) and is quite similar in shape to the curve in Figure 3 for the region around a = 1.5.

The approach, then, is quite simple. Scattered light intensities are measured for two orthogonal planes of monochromatic polarized light, at 90° to the probe beam, and the difference is proportional to the volume of particles in the size range where a = 1.5. This value of "a" translates to a size diameter of approximately one half the wavelength of the probe beam, and other size fractions can be defined by using other wavelengths. For the probe described here wavelengths of 0.45 and 0.9 μm were used to generate two submicron channels.

## Principles of Forward Scattering

Forward scattering has been discussed in references 1-3, so only a summary of the techniques and pertinent variations is included here. Low angle forward scattering is most readily treated by using simple diffraction theory. Three discrete scattered flux measurements are made at observation angles of approximately 4, 8, and 11 degrees in two wavelengths, 0.45 and 0.90

μm. The signals are then algebraically combined to produce a response per unit volume of material maximized for particles at a particular size or size range and minimized or reduced to zero for particles far from the size of interest. Since large particle scattered flux is concentrated more toward the forward angles, the largest particle response curves are dominated by flux from the innermost zones. Smaller particles require higher contributions from the outer zones. The nominal size range peaks for the three forward scattering channels are listed in Table 2.

TABLE 2. FORWARD SCATTERING CHANNELS

| Response peak μm diameter, nominal | Wavelength, μm |
|---|---|
| 1.0 | 0.90 |
| 3.5 | 0.45 |
| 7.0 | 0.90 |

After the response shape was defined through scalar diffraction theory, which does not depend on the refractive index of the material, the design was tested using rigorous (Mie) theory. As expected, the two upper channels where the respective size ranges are somewhat larger than the wavelength of the light showed very little shape variation sensitivity to refractive index of the material. The most sensitive peak was in the 1 μm range, with the diameter and wavelength nearly equal. Mie calculations for all five response curves used in the instrument are shown in Figure 4. These were calculated for an index of 1.5, typical of silica particulates, a common stack material. The ripples in the forward scattering curves occur due to resonances of light in the non-absorbing ($n = 1.5 - 0.0i$) material, but will tend to be smoothed if small amounts of absorption are present or if the light is not perfectly monochromatic.

## EXPERIMENTAL VERIFICATION

The performance of the volumetric response functions in the forward channels is based on knowledge and experience with the Leeds & Northrup Microtrac™ Particle Size Analyzer. The use of forward scattering, here, is merely an engineering extension of a previously tested system, so no fundamental testing was required.

Major effort, however, was put into verification of the 90° response curves. Since the response function requires accurate knowledge of signal differences, variations in beam intensity had to be compensated. A ratio of $i_1/I_0$ and $i_2/I_0$ was measured, where $I_0$ was the strength of the probe beam. Then the intensity difference was computed.

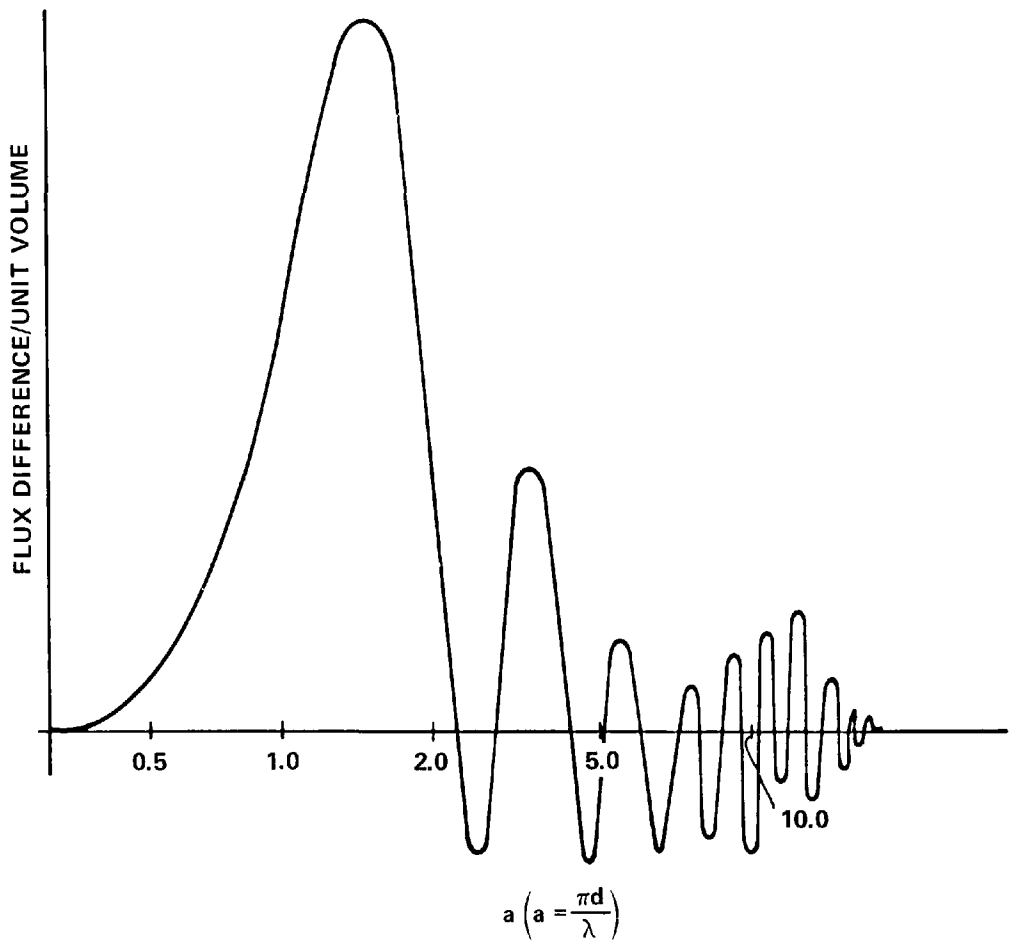


*Figure 3. Intensity difference per unit volume, $(i_1 - i_2)/a^3$, for a scattering angle of 90°. The size parameter, a, is plotted in equal log intervals.*

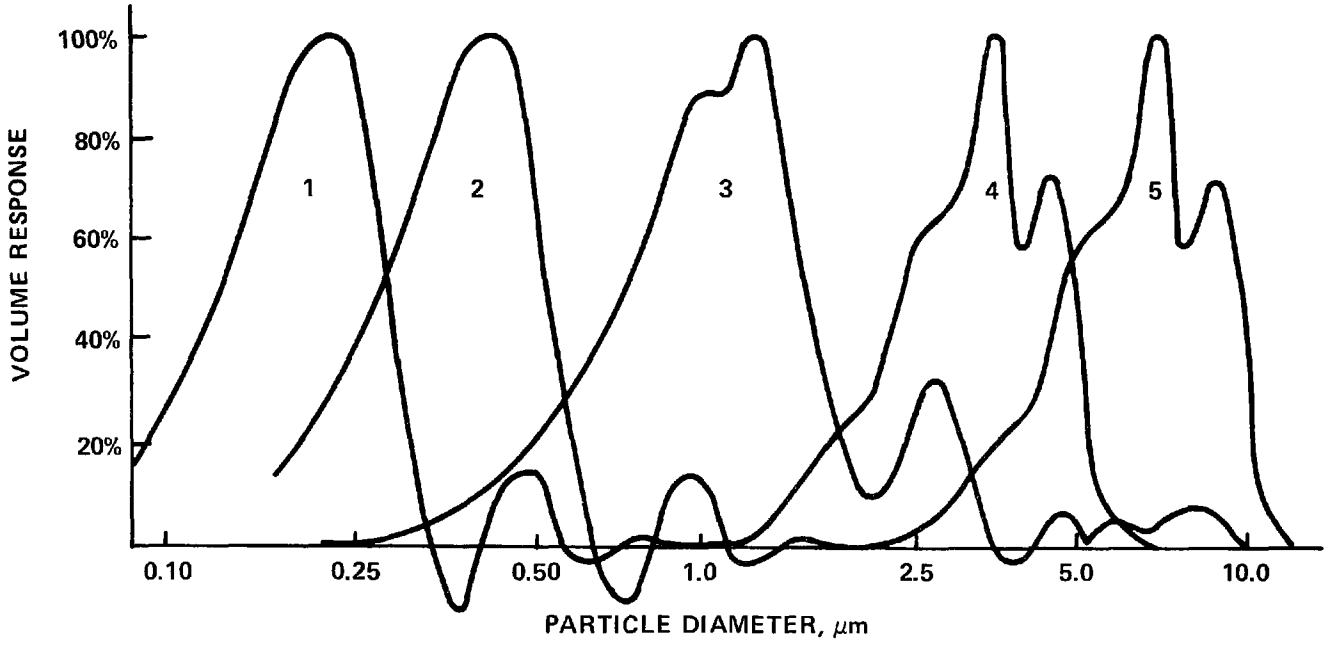


*Figure 4. Volumetric response curves, as a function of particle diameter, for the five channels of the prototype. Curves 1 and 2 are obtained with 90° scattering, and curves 3, 4, and 5 from forward scattering.*

An experimental system was built, incorporating a lock-in amplifier and an electronic ratio circuit, to accurately measure 90° scattering. This system recorded scattering curves for both polarizations, $i_1$ and $i_2$, concurrently. Hence, the response curve for the function $(i_1 - i_2)$ could be generated quite easily and accurately.

The system, shown in Figure 5, consisted of a xenon arc, grating monochromator, and two silicon detectors. The source flux was chopped and a lock-in amplifier used to filter ambient radiation noise from the relatively small 90° scattering signal. The flux passing directly through the sample was focused onto a reference detector. This signal was electronically filtered to present a dc level to an analog divider, which ratioed the scattered and reference signals to correct for variations in source intensity. Therefore, the output of the divider was directly proportional to $i_1$ or $i_2$. While a rotating prism polarizer alternately selected $i_1$ or $i_2$, a synchronous motor scanned the monochromator from 400 nm to 800 nm at a speed chosen so that a pair of measurements, $i_1$ and $i_2$, were recorded once every 5 mm on a chart recorder. Variations in the size parameter, a, were thus accomplished by changing wavelength rather than size. Since the volume of particles remained the same, the flux per unit volume was readily determined.

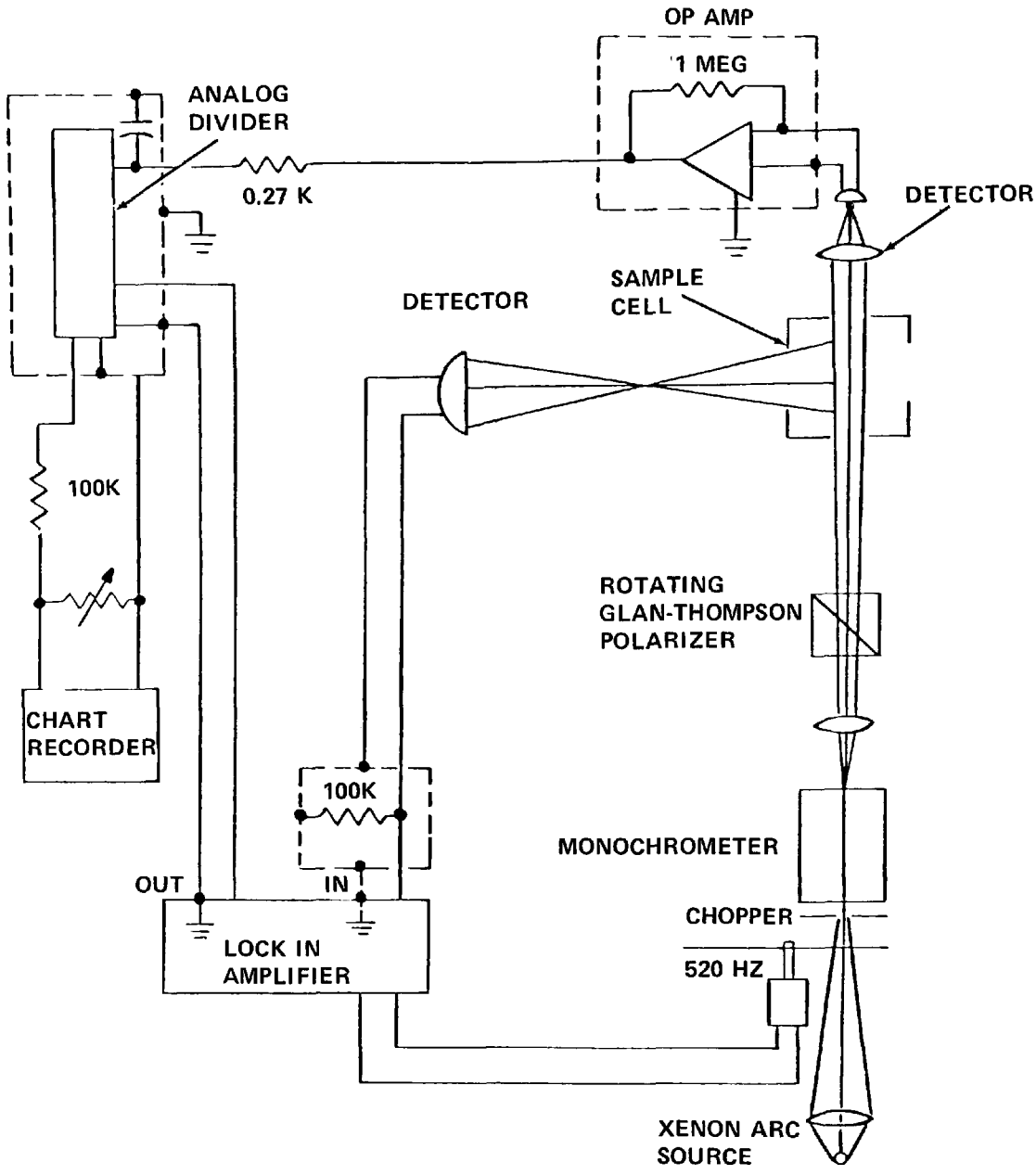


*Figure 5. Schematic drawing of laboratory system used to verify the volumetric response functions for 90° scattering.*

This system was used to record data for 0.234 μm and 0.801 μm polystyrene spheres, dispersed in deionized water at 20 ppm. The relative refractive index of polystyrene to water was 1.20. These two particle sizes generated scattering data for "a" values from 1.22 to 2.44 and 4.18 to 8.37, respectively. The angular scattering field was 20° centered at 90° with respect to the incident beam.

Further theoretical Mie scattering studies indicated that particle absorption should reduce the secondary volume response peaks significantly, but cause negligible changes in the primary response peak. Experiments were then performed to confirm this selective reduction of secondary response peaks. Data at 90° scattering was recorded for dyed (absorbing) polystyrene spheres of 0.234 μm and 0.801 μm diameter. This data is plotted along with a theoretical curve for non-absorbing particles in Figure 6. The primary peak data (d = 0.234 μm) for absorbing and non-absorbing particles are almost identical, but the secondary response peaks (d = 0.801 μm) are greatly reduced for absorbing particles. Notice the excellent agreement between experiment and theory for non-absorbing particles. These experiments confirmed the theoretically generated response curves, and gave us confidence to proceed with the design of the prototype instrument.

## DESIGN OF THE PROTOTYPE

Real time measurements inside an industrial stack create rather unique structural and environmental operation conditions, with typical temperatures as high as 260°C, flow velocities up to 50 feet per second, and atmospheres containing acid vapors. Access to the measuring point is often limited to 10 cm diameter ports, and sampling requirements make penetration well into the stack a highly desirable goal. Anticipated loading levels are in the range of 4 to 40 parts per billion by volume, assuming a specific gravity of 2.5 for stack particulates. For representative sampling, a sensing zone containing a reasonably large volume is required. The prototype design is based on these constraints, and Figure 7 shows a sketch of the instrument with the associated electronics.

### Optical Design

The interior stack temperatures rule out the use of in-situ detectors, so a set of high temperature fiber optic cables is utilized to sense the scattered light at five points (three forward angles and two orthogonal positions at 90° to the probe beam). These cables are installed inside a 1.5 meter long stainless steel tube, whose outside dimension is approximately 9 cm. The active sensing region is towards the end of the probe and is a slot 36 cm long by 3 cm wide. A lens located in the tube tip collects scattered flux for the forward angles, while the

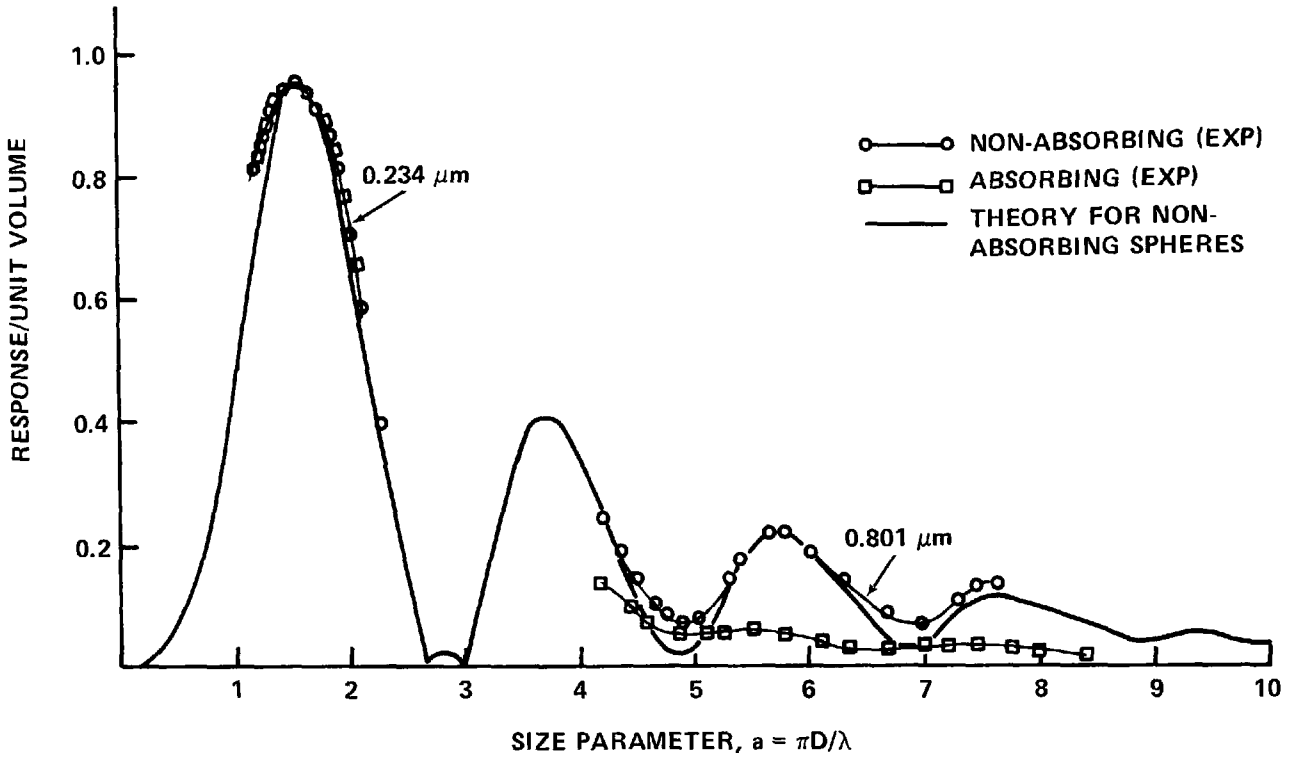


*Figure 6. Theoretical and experimental curves for 90° scattering showing the flux difference, $i_1 - i_2$, per unit volume of material. Two sizes of polystyrene spheres were used, 0.234 and 0.801 μm in diameter, and the wavelength was varied to change the size parameter, a.*

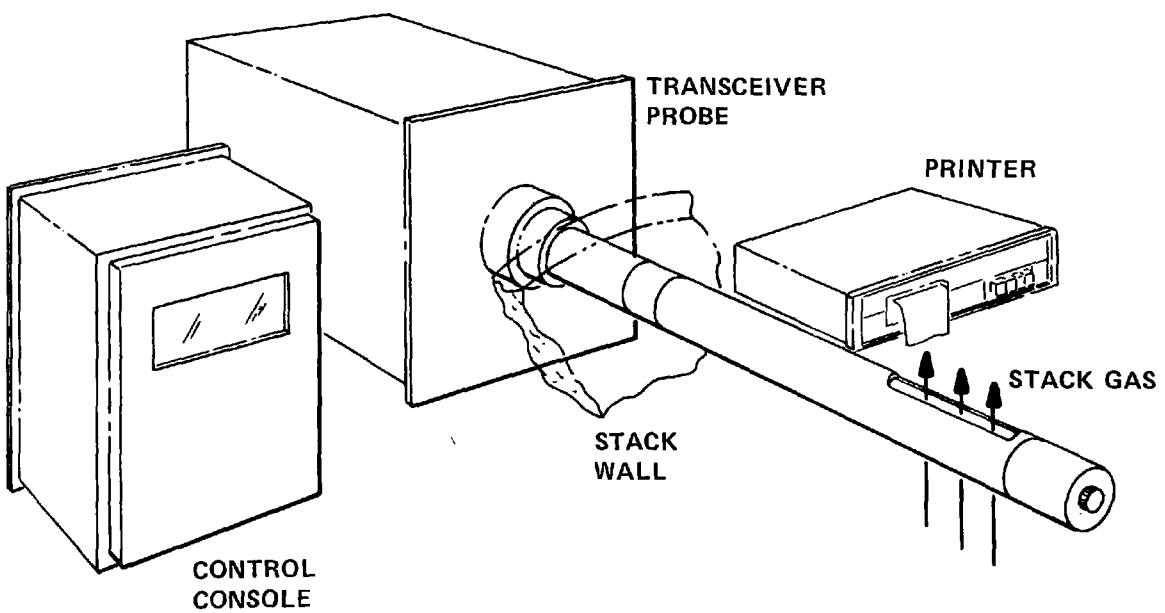


*Figure 7. Prototype system in use in stack, showing control console and printer with transceiver.*

two 90° fibers look directly through protective windows into the sample region. Each fiber cable runs to its own detector, located outside the stack at the end of the probe. A sixth detector is used to monitor beam strength.

The optical probe beam is generated by a xenon arc source, located in the transceiver end of the probe. Thin film interference filters with center wavelengths of 0.45 and 0.90 μm are combined with linear polarizers in a filter wheel. The light is then projected down the center of the tube in a nearly collimated beam of alternating blue or infrared polarized light, with a beam diameter of approximately 1.25 cm at the end. To avoid spurious signals the light is not reflected internally, but exits the probe through a hole at the tip.

## Electrical Design

A digital electronic approach has been taken, similar to the single detector Microtrac system as described in Reference 2. For this system the six detectors generate electrical signals in proportion to the light flux levels incident on them, and after a pre-amplification stage, the electrical signals are fed to an analog-to-digital converter. The microcomputer consists of programmable read-only memories (PROM), random access memories (RAM), and a central processing unit (CPU). Program instructions are inserted in the PROM's, and the CPU carries out the instructions. Interim calculations and the final results are stored in the RAM's until the point in the program where a display command is given to the output.

The cycle time is adjustable, but a full measurement cycle can be completed in as little as four seconds. The digital microprocessor handles twelve resultant input signals, five angular scattering signals and one beam strength signal from each of the two colors. The signals are first combined to produce the volumetric response curves shown in Figure 4, and then a matrix decoupling routine is incorporated to remove most of the effects of the response curve overlaps. A resulting normalized five channel histogram of the volume distribution is displayed on a digital printer. A mean size is also computed from the histogram, as well as a number proportional to the total volume of particulates.

## Mechanical Design

All parts of the insertable section of the probe, except for glass fibers and lens and window material, are fabricated from stainless steel. The probe is mounted to the transceiver with an insulating collar to minimize heat transfer.

To insure cleanliness of the optical surfaces during measurements, and to provide cooling of the enclosed arc lamp, a portable skid-mounted air blower is provided. Air is forced into the probe portion through a set of four tubes running from the transceiver end. These tubes terminate as specially designed air curtains to flush across the faces of the two 90° windows on the sides and the forward scattering lens system at the end of the probe.

## SUMMARY

This paper has described the principles and design of a new light scattering instrument for real time measurements of the size of source particulates. A photograph of the recently completed prototype is included as Figure 8, and the operational characteristics of the unit are defined in Table 3. The instrument offers a method for in-stack analysis of particulate size without dilution or extraction of material, and directly produces a distribution of the particulates by volume fraction. This device thus provides a unique and valuable measurement capability for analysis and monitoring of particulates in source emissions.

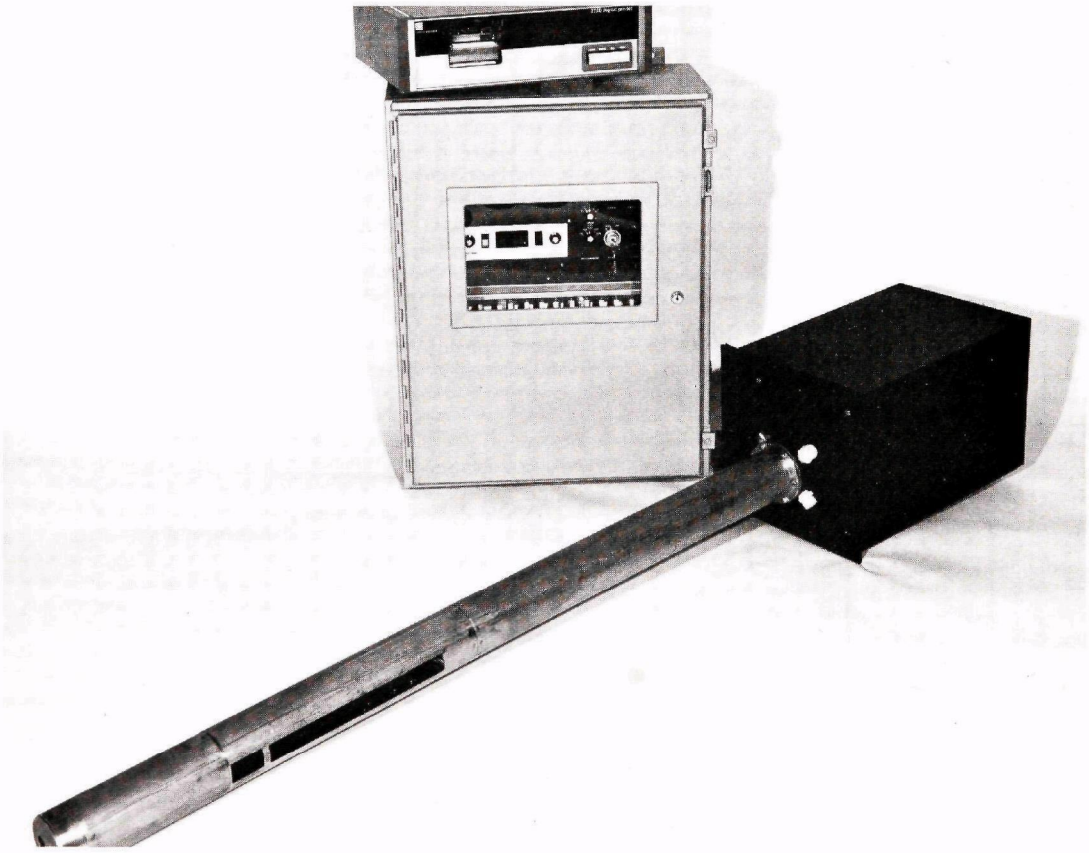

*Figure 8. Photograph of prototype system.*

TABLE 3. CHARACTERISTICS OF PROTOTYPE LIGHT SCATTERING INSTRUMENT

| | |
|---|---|
| Size range (particle diameter) | 0.1 to 10.0 μm |
| Size discrimination | Five volume fractions with centers at 0.2, 0.4, 1.0, 3.5, and 7.0 μm |
| Anticipated loading range | 0.01 to 0.1 grams of material/ $meter^3$ or 4 to 40 parts/billion by volume (with specific gravity of 2.5) |
| Operational range | 4 to 400 parts/billion |
| Mode of operation | Low angle forward scattering and 90° polarization dependent scattering |
| Power requirements | 115 volts, 60 hertz, 45 amps |
| Operational temperature | Probe portion in stack: up to 260°C (500°F) |
| | Transceiver portion and other electronics outside stack: 0° to 43°C (32° to 110°F) |
| Speed of measurement sequence | Integration time selectable from 4 to 256 seconds |

ACKNOWLEDGEMENT

The development, design, and construction of the prototype were funded by the U.S. Environmental Protection Agency, under EPA contract 68-02-2447, "Instrumentation to Measure Particle Size in Source Emissions."

REFERENCES

1. Wertheimer, A.L., and W.L. Wilcock. Appl. Optics 15:1616, 1976.

2. Wertheimer, A.L., et al. Effective Utilization of Optics on Quality Assurance. SPIE Conference Proc. 129:49, 1977.

3. Born, M., and E. Wolf. Principles of Optics, Pergamon, New York, 1959. Chapter 8.

4. Kerker, M. The Scattering of Light and Other Electromagnetic Radiation, Academic, New York, 1969. Chapter 1.

5. Mie, G. Ann. Phys. 25:377, 1908.

6. Van de Hulst, H.C. Light Scattering by Small Particles, Wiley, New York, 1957.

7. National Bureau of Standards. Tables of Scattering Functions for Spherical Particles, Applied Mathematics Series - 4, U.S. Govt. Printing Office, Washington, 1948.

8. Dave, J.V. Subroutines for Computing the Parameters of the Electromagnetic Radiation Scattered by a Sphere. Report No. 320-3237, IBM Scientific Center, Palo Alto, CA, 1968.

PAPER 10

# STUDIES ON RELATING PLUME APPEARANCE TO EMISSION RATE AND CONTINUOUS PARTICULATE MASS EMISSION MONITORING

K. T. HOOD
H. S. OGLESBY
NATIONAL COUNCIL FOR AIR AND STREAM IMPROVEMENT

## INTRODUCTION

The National Council for Air and Stream Improvement has participated in several studies incorporating extensive field work and data analysis in investigations relating plume appearance to continuous mass monitoring and emission rate. Emission sources that have been studied with plume observing panels to date include kraft recovery furnaces, power boilers, and a lime kiln. The experience and results gained through evaluations performed at these sources will be presented in the following discussion.

Continuous particulate monitors have proven to be a valuable tool in the development of relationships between plume appearance and particulate concentration. The utility of these devices has been greatly enhanced by the established linearity of their response to particulate concentration determined through stack sampling. A synopsis of the evaluation of a mass monitor relying on the principle of laser light backscattering is offered as a means of obtaining continuous particulate concentration data in terms of grams per actual cubic meter.

## THE RELATIONSHIP OF PARTICULATE CONCENTRATION AND OBSERVED PLUME CHARACTERISTICS AT KRAFT RECOVERY FURNACES AND LIME KILNS

A study was organized by the National Council in the summer and fall of 1974 to determine the relationship among continuously measured light transmission properties of selected pulp and paper process flue gases, the gravimetrically determined filterable particulate concentration and the appearance of the plumes as judged by certified observers. The entire results of this study

can be found as NCASI Atmospheric Quality Technical Bulletin No. 82. This relationship was derived to establish a scientific basis for adoption of plume opacity regulations.

Previous studies reported on in NCASI Atmospheric Quality Technical Bulletin No. 79 indicated the validity of using a transmissometer as a continuous monitor of flue gas particulate concentration at temperatures above the moisture dew point. This conclusion was based on the instrument's linear optical density response to particulate concentration. The transmissometer enabled the subsequent association of particulate concentration to observer measured opacity determined through field testing at two kraft recovery furnace sites in addition to the data developed on a lime kiln source. The lime kiln and one of the kraft recovery furnaces were sites located in the Northwest United States. The recovery furnace at this site was a non-direct contact evaporator system. The other kraft recovery furnace was located at a Southern site incorporating a direct contact evaporator.

The majority of the observing panel members taking part in the study were technically oriented students complemented by regulatory agency personnel with extensive plume reading experience. A transmissometer was used as an intermediate, and as such opacity or optical density values were simultaneously recorded corresponding to both the observer panel runs and the particulate sampling tests.

The accuracy and reproducibility of observer read opacity was characterized through data analysis that involved the calculation of observations in accordance with EPA Method IX procedures. This entailed the arithmetic average of 25 readings taken at 15-second intervals, which encompassed a six-minute total time span. The result was a data base of approximately 1800 EPA Method IX observations from more than 300 observer panel runs which formed the data base from which to work. The normal size of the observing panel was thus an average of six individuals making and recording plume readings simultaneously.

An observer opacity lower detection limit in terms of particulate concentration was a parameter sought for the non-DCE kraft recovery furnace Northwest site. The transmissometer was used as a reference for the detection level depicted in Figure 1. The dotted lines in this figure encompass a range for the transmissometer opacity response (corrected to a ten-foot path length) where 25% to 75% of the observers reported "non-visible" or zero opacity. Transformation of this range to the transmissometer calibration curve represented in Figure 2 provides a comparison of the percent of observers reading non-visible at the stack exit against the EPA Method V particulate concentration. The dotted lines in this figure indicate 25%, 50% and 75%

of the observers reported non-visible opacity corresponding to particulate concentration levels of 0.041, 0.034, and 0.027 g/DSCM (0.018, 0.015 and 0.012 gr/DSCF), respectively. The conclusion obtained from this exercise was that below this range the observers did not see a plume, while above the concentration range a plume was detected with a great degree of regularity. The point defined as the observer detection limit corresponded to that level where 50% of the observers reported zero opacity. The particulate detection limit for the source studied was approximately 0.034 g/DSCM (0.015 gr/DSCF).

The relationship of plume appearance or opacity (based on a ten-foot path length) to particulate concentration for the Northwest non-DCE kraft recovery furnace site is presented in Figure 3. The total observer member variation is represented by the associated prediction intervals. Single observer opacity is depicted here as a function of particulate concentration based on data generated with clear or blue sky background conditions. Use of the large field collected data bank which was analyzed to derive this relationship indicated that single observer read opacity could vary by ±13% opacity for the range of particulate concentration studied at the 95% prediction interval. The equivalent relationship of observer opacity to particulate concentration is presented in Figure 4 for the Southern site incorporating dark mountain background viewing conditions. Total observer variation was also found to be roughly ±13% opacity over the measurement range of particulate concentration. The particulate concentration that was indicated for the 20% observer opacity level for both of the background conditions presented from the two sites was approximately 0.080 g/DSCM (0.035 gr/DSCF).

Observer opacity depicted as a linear function of transmissometer opacity is shown in Figures 5 and 6 for the Northwest and Southern sites, respectively. The variation in the observer readings when compared to the instrument was ±10 to 15% opacity for the measurement range studied. The second parameter denoted as "B", or particulate concentration, on the X-axis was obtained graphically from transmissometer calibration curves. Figures 3 and 4 presented previously incorporate this parameter to enable their construction through a simple axis transformation.

The lime kiln opacity segment of the NCASI field study was conducted in 1974 at a Northwest site. Two certified observers were used in the nine test runs accomplished. During each test, which ran approximately one hour, each observer recorded one plume opacity reading per minute or 60 per test. Simultaneous particulate sampling provided a comparison of mass concentration to observed opacity. Two lime kilns each equipped with a venturi scrubber operating in excess of 51 cm (20 in.) of water pressure drop were routed to a common stack. The plume was read a few

seconds after stack exit allowing the moisture to dissipate. The plume diameter was judged to be about 6 to 8 stack diameters at the point of observation. The stack was 1.8 m (4.5 ft) in diameter.

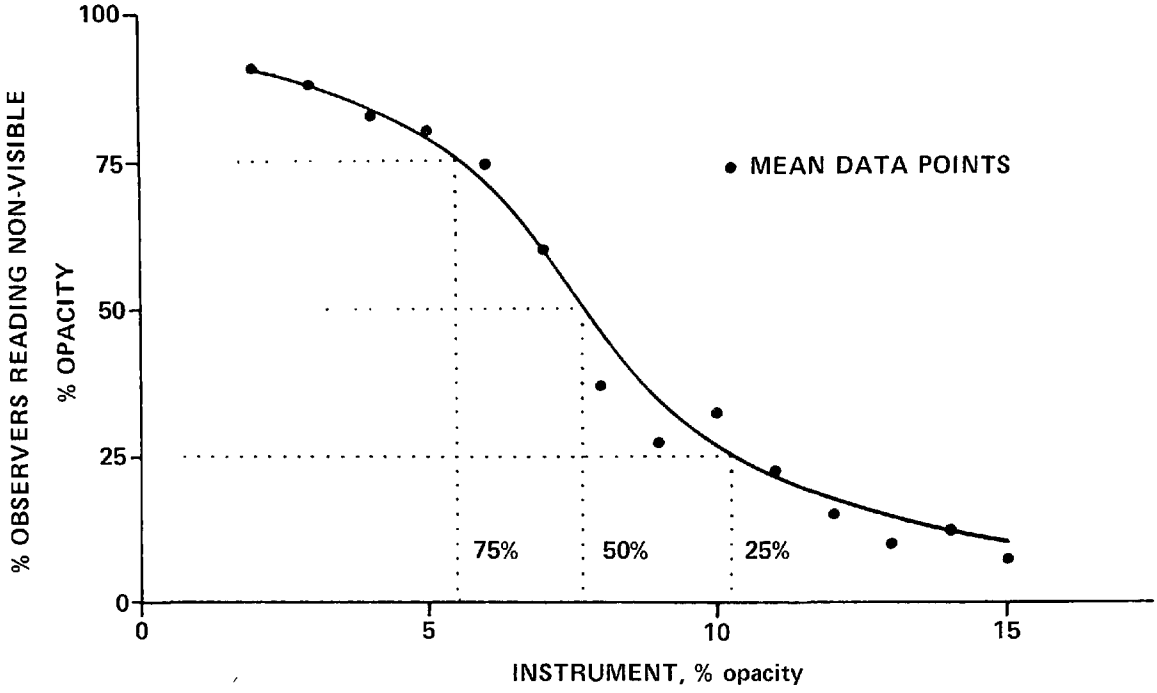


*Figure 1. (NW) All data: relationship between observers reading nonvisible and instrument opacity.*

An exponential regression was assumed from theory to fit the data with the resulting relationship displayed as Figure 7. The small sample size proved to be a limitation in the data and chiefly responsible for the wide confidence interval noted. Each observing run was characterized for plume type and background. The codes for the plume conditions experienced are included in the figure for informative purposes.

The visibility threshold or the particulate level at which 50% of the observations were reported as non-visible was also determined for the lime kiln source. The data indicated a value of roughly 0.041 g/DSCM (0.018 gr/DSCF) for the detection limit on this source. This was relatively close to the level found for the kraft recovery furnace of 0.034 g/DSCM (0.015 gr/DSCF).

## THE RELATIONSHIP OF PARTICULATE CONCENTRATION AND OBSERVED PLUME CHARACTERISTICS AT COMBINATION WOOD AND FOSSIL FUEL-FIRED BOILERS

Another portion of NCASI studies concerning the relationship of observed plume opacity and particulate concentration dealt with combination wood and fossil fuel-fired boiler sources.

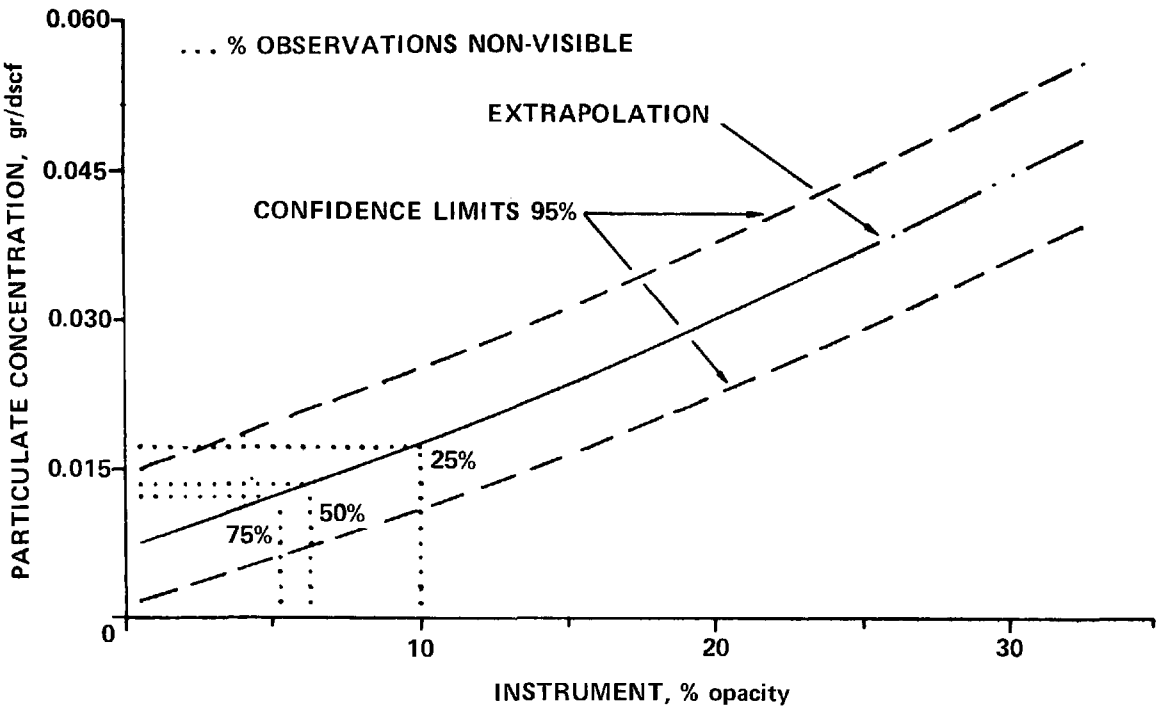


*Figure 2. (NW): Detection range for observers.*

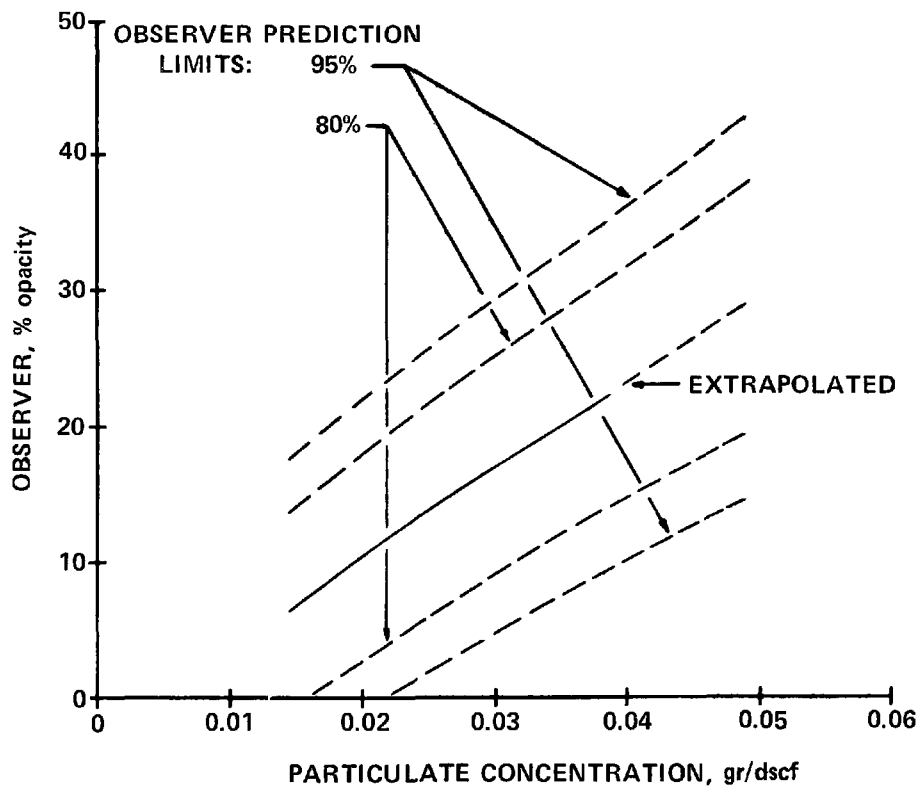


*Figure 3. (NW) Clear data (Std): observer opacity vs. particulate concentration.*

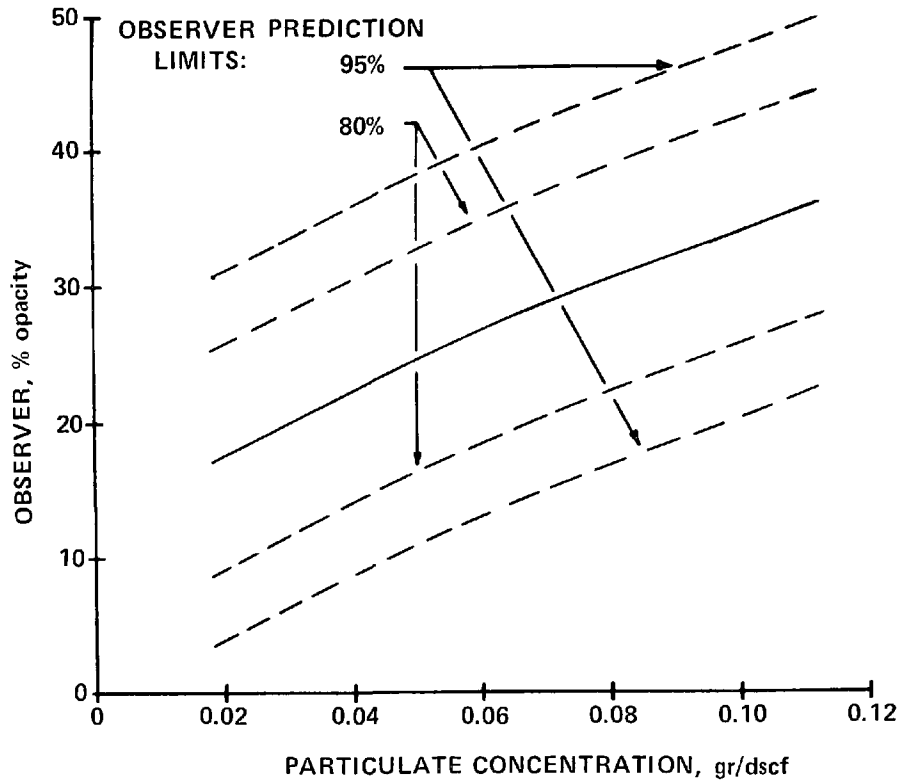


*Figure 4. (S) Dark data (Std): observed opacity vs. particulate concentration.*

The study in its entirety can be found as NCASI Atmospheric Quality Technical Bulletin No. 85. The two types of boilers investigated in this project were a bark and coal combination boiler located at a Middle Atlantic site and a bark and oil combination boiler at a Southeastern United States site. The comparison of predicted single observer opacity and transmissometer opacity for the Middle Atlantic location is shown in Figure 8 with the 80% and 95% confidence intervals. As noted, the observations were accomplished against a generally cloudy and hazy background which contributed to the wide scatter in the data. The values ascribed to the independent variable labeled "A" in the figure are the particulate concentrations in grains per DSCF obtained from the transmissometer's calibration curve. To obtain units of grams per DSCM simply multiply by 2.29.

The relationship of predicted single observer opacity and transmissometer opacity for the Southeastern site is represented in Figure 9. The background described as primarily bright blue sky was judged to result in less observer variation than the cloudy and hazy background conditions experienced at the previously discussed site. Observer variability as denoted by the 95% confidence interval corresponded to approximately ±10% opacity for the Southeastern site as compared to ±22% opacity at the

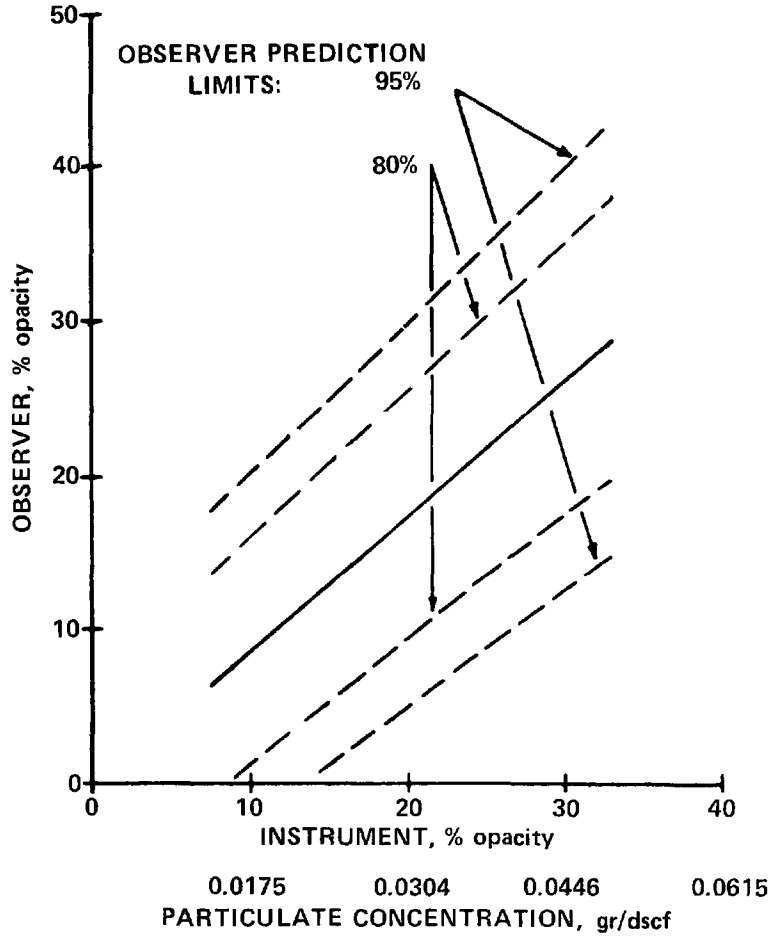


*Figure 5. (NW) Clear data (Std) intermediate for Figure 3.*

Middle Atlantic site over the measurement range studied. As in the previous figure, the independent parameter denoted as "A" in Figure 9 corresponds to particulate concentration in grains per DSCF as obtained from the transmissometer calibration curve for this source.

While the observer variability is relatively small as depicted in Figure 9 underlying the accuracy of the relationship, the slope or change in observer readings was small for large differences in transmissometer opacity response. The field data collected suggested that observer reading only increased by 10% opacity for a transmissometer increase of 45% opacity. The Middle Atlantic site on the other hand reflected a 35% observer opacity increase which corresponded to a 45% transmissometer increase. Particle characteristics and plume background were judged to be the chief contributors to such phenomena.

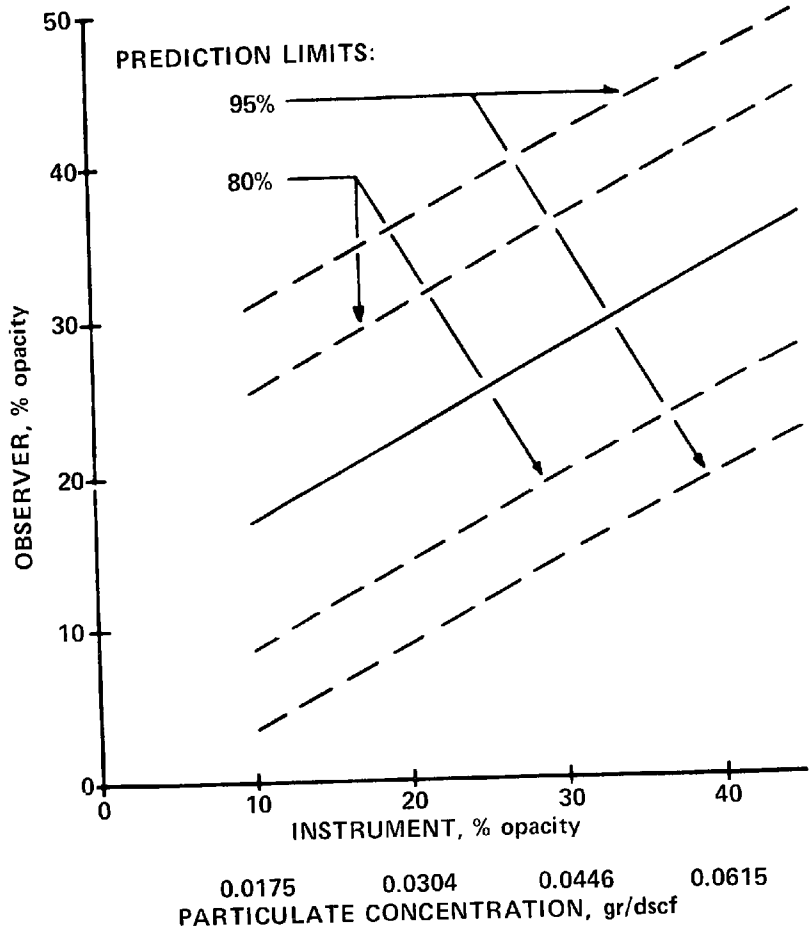


*Figure 6. (S) Dark data (Std) intermediate for Figure 4.*

Fuel combination was one variable expressed by the investigators as responsible for plume appearance changes causing observer response variability. The magnitude of the fuel combination changes at the study sites was indicated by the ratio of steam derived from the coal and bark which varied at the Middle Atlantic site over a range encompassing 1.0 to 2.2 (coal/bark). The ratio for steam derived from oil to that derived from bark fuel was found to vary at the Southeastern site from 1.2 to 2.9 (oil/bark).

Particulate characteristic changes produced as a result of fuel combination variability include particle density and index of refraction. A range of densities between 2.0 and 4.0 $g/cm^3$ were judged by the investigators as possible for coal-fired power plants. In this context particle density, or maybe it would be more accurate to say the physical size of the particle, could have a pronounced effect on the opacity level while being relatively independent of particulate concentration. The particle index of refraction is another parameter which affects plume

opacity but is not necessarily a function of particulate concentration. A small change in this value can lead to a substantial shift in plume opacity.

The appearance or color of the plume is obviously caused by the nature of the particulate matter in the plume. Particulates emitted from an oil-fired boiler can be characterized into three general types: black, white and colored. The black particles are judged to be chiefly carbonaceous material containing traces of white and colored matter. The white portion of the particulate is mainly in the form of irregular crystals or a grouping of spherical particles containing primarily silicon. The colored particles usually consist of a large fraction of metallic elements and sulfur compounds in the form of oxides and salts. The coal-fired boiler particulate emissions range from milk white, yellow, gray, orange, and brown to black. Black spheres found as particles consist of unburned hydrocarbons while a colorless glassy sphere fraction was judged to have been burned more efficiently. All of the particles contained a limited quantity of metallic elements. A sand and char mixture was determined as the major constituent of particulate emitted from bark boilers. While the sand is essentially ash which proceeds through the system unchanged, the char is for the most part satisfactorily described as unburned carbon whose quantity and nature is determined by boiler design and operation.

The background against which the various plumes were viewed was an important factor in plume opacity judgements made by observers. The kraft recovery furnace plumes were reported by the observers at a higher value when viewed against a dark mountain or a blue sky background as compared to a cloudy sky. The maximum contrast for the predominately "white" plume was the controlling factor. The bark and coal combination boiler plume was judged to yield the highest observer response when viewed against a grey cloud background rather than dark mountains or other conditions. The bark and oil combination boiler plume was found to be most detectable with grey clouds or hazy sky as background rather than white clouds or blue sky. Plume contrast was indicated as the major criterion to follow for maximization of observer response resulting in readings comparable to those measured by transmissometers.

## FIELD PERFORMANCE OF A LASER LIGHT BACKSCATTERING SOURCE PARTICULATE MASS MONITOR

A study was recently completed by the NCASI to evaluate the applicability of the P-5A laser light backscattering mass monitor to the measurement of particulate concentration prior to and following control devices. Kraft recovery furnaces and a wood-waste fired boiler were the sources used to determine the monitor's performance by comparison to transmissometer optical density and EPA Method V sampling.

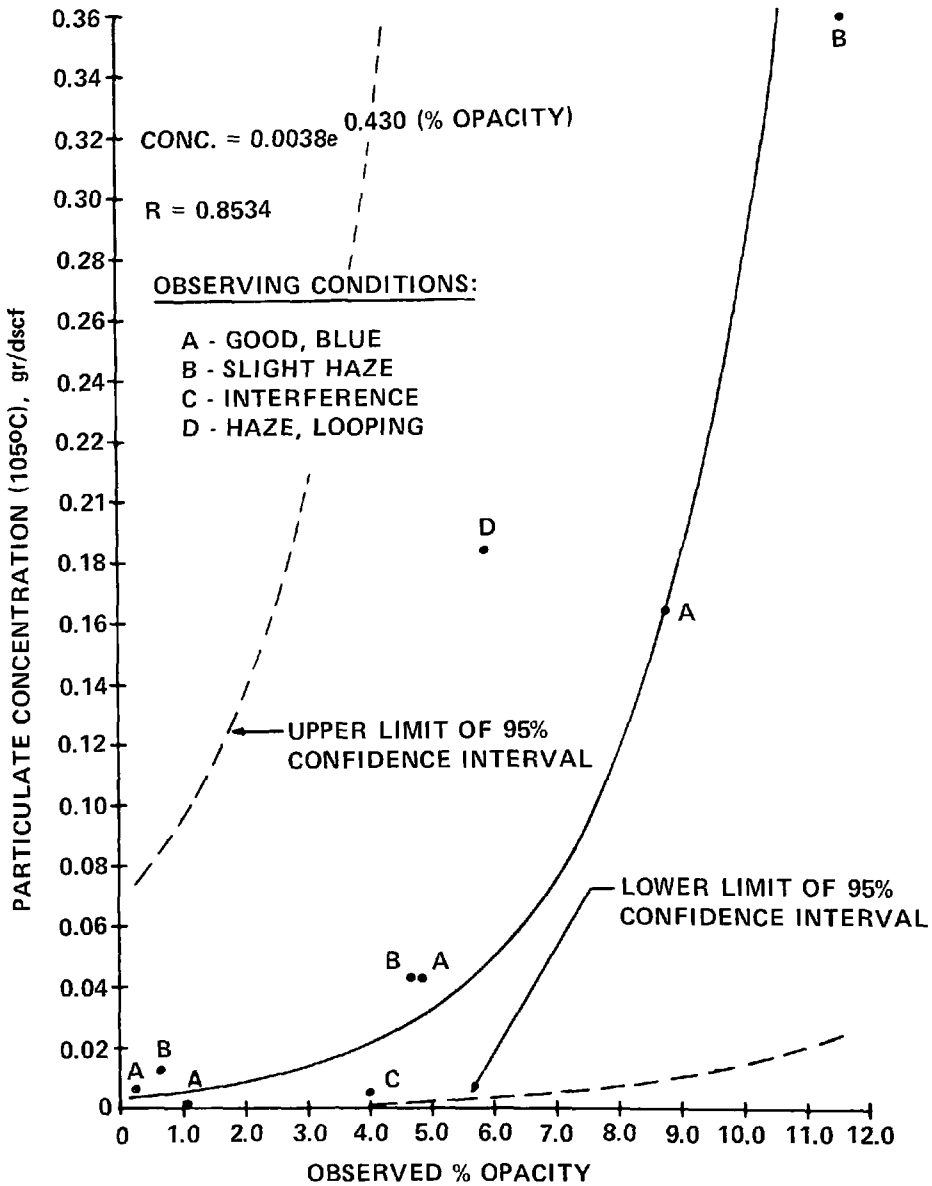


*Figure 7. Particulate concentration vs. observed opacity.*

The operating principles and theory of the laser monitor manufactured by Environmental Systems Corporation can be found in NCASI Atmospheric Quality Technical Bulletin No. 92 and in several other publications. While beyond the scope of this paper, Figure 10 is offered to illustrate the basic operation of the instrument's optics head. Particles passing through the one-ended beam generated by this optical complex causes light scatter in all directions. As shown, the instrument has been designed to allow light to be returned along small incident angles. The light follows a path co-axial to the emitted beam to a light collection lens. This lens serves to focus the light to a solid state detector. Changes in the instrument response due to component aging or temperature variation in the LED output power are compensated for through a ratio of the signal detector response to a reference signal. Interference from ambient light sources is minimized through the use of a specific pulsed frequency. Care must be taken, however, to shield the receptor from artificial light (such as fluorescent) when adjustments for zero and span are performed.

The first site on which the instrument was evaluated consisted of emissions following a non-DCE kraft recovery furnace source equipped with a high efficiency electrostatic precipitator. A comparison at this site of the laser light monitor to an LSI RM-4 transmissometer encompassed a 21-day time interval during which 368 simultaneously hourly averages of measurement response were obtained for each of the monitors. The transmissometer was chosen for the evaluation based on the demonstrated linear instrument response of optical density to gravimetrically determined particulate concentration found at this site and in previous studies. Use of the transmissometer facilitated the compilation of a large data bank to enable the conduct of more accurate and meaningful statistical analysis. The instrument ranges chosen for the transmissometer correspond to a full-scale value of 0.45 optical density while 0.1 g/ACM was selected for the laser light monitor.

The relationship developed for the instrument comparison is depicted in Figure 11 with the 95% confidence interval indicated by the dashed lines. The regression equation corresponded to:

$$\frac{\text{GRAMS}}{\text{ACM}} = 0.00069 + 0.1861 \text{ (OPTICAL DENSITY)}$$

The standard deviation calculated was 0.0018 g/ACM, which along with a correlation coefficient of 0.88 projected a minimal amount of scatter in the data over the range studied. This range encompassed the lower half of the most sensitive setting of the laser monitor with particulate concentration measurements which corresponded to less than 0.229 g/DSCM (0.1 gr/DSCF).

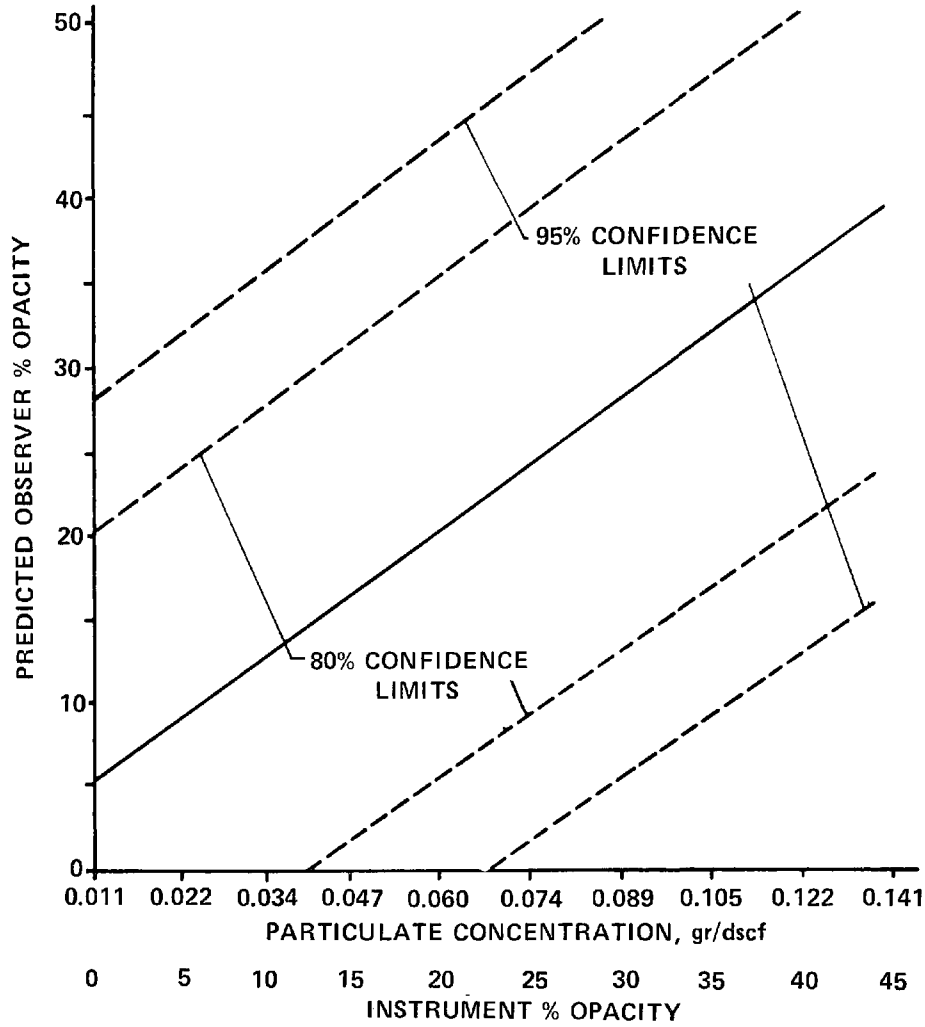


*Figure 8. Bark and coal combination boiler. Mainly cloudy and hazy background.*

The second portion of this study was carried out at a DCE kraft recovery furnace operated under computer control. Evaluation of the mass monitor was undertaken at two locations with characteristic high mass concentrations, i.e., immediately preceding and following the direct contact evaporator. A laser light monitor modified with a high temperature "ceramic" valve assembly in the probe was employed for the testing accomplished at the DCE entrance location to enable both gravimetric sampling and short time interval RM-4 transmissometer comparisons to be made. The laser light monitor was operated on the 2 g/ACM range while the 0.9 optical density range was chosen for the transmissometer which utilized an actual four-inch measurement path length which was mathematically adjusted to ten feet.

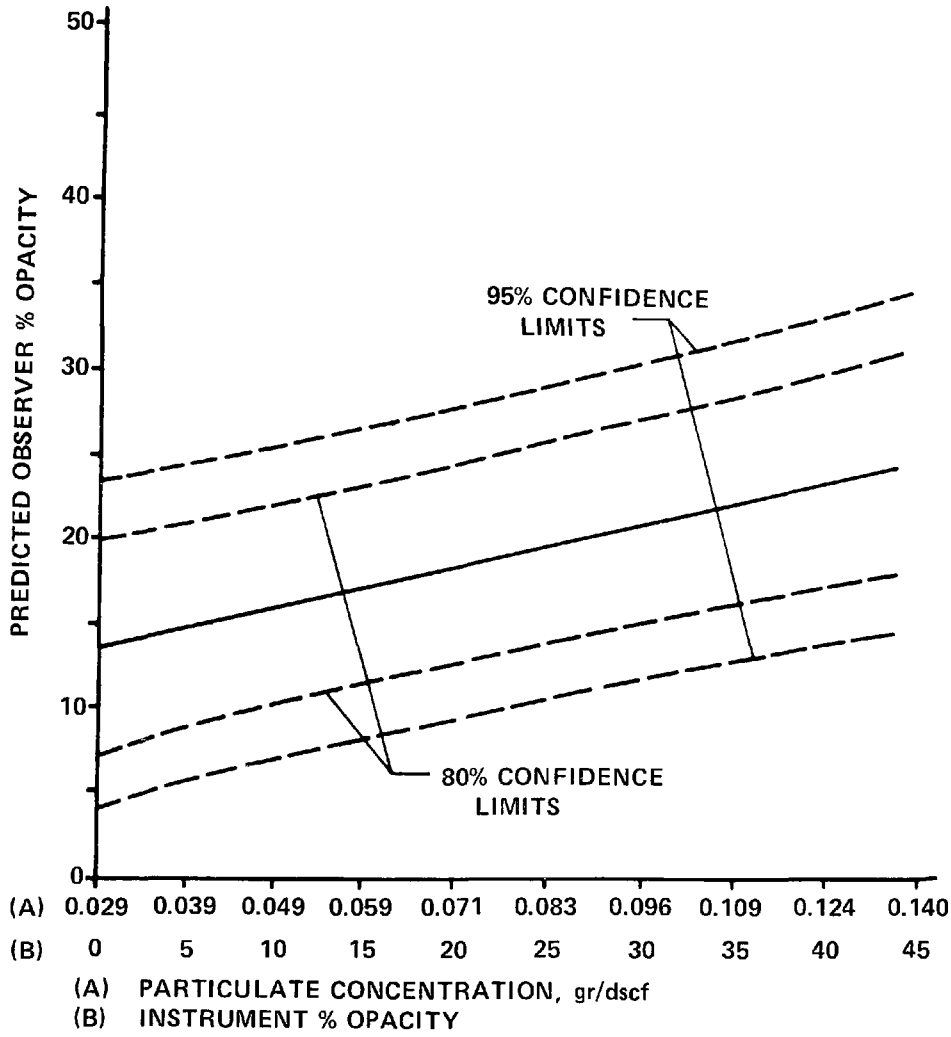


*Figure 9. Bark and oil combination boiler. Mainly bright blue sky background.*

The calibration curve for the laser light monitor developed through particulate sampling at the DCE entrance location is depicted in Figure 12. This relationship corresponds to the following regression equation:

Laser Monitor = 0.038 + 0.334 (Particulate Concentration)

with a standard deviation of 0.076 g/ACM and a correlation coefficient of 0.987.

The corresponding statistical analysis for the modified transmissometer at this site was also calculated with a result similar to that obtained with the mass monitor. A correlation coefficient of 0.978 was found for this analysis. The recorder

trace of the transmissometer visually possessed more noise than that for the mass monitor, only a small portion of which might actually be attributable to actual recovery furnace operation.

The mass monitor required essentially no maintenance over a six-week study time interval. The transmissometer, on the other hand, required daily attention with respect to lens cleaning and removal of particulate build-up in the slotted pipe used to reduce the measurement path length of the instrument. The information compiled at this site indicated the mass monitor would operate satisfactorily in the range of approximately 3.75 g/ACM (5 gr/DSCF) found directly exiting the recovery furnace. In this application the data generated could serve as an aid to the operator in maintaining particulate emissions from the furnace at a minimum.

A third phase of the mass monitor evaluation incorporated a wood-waste fired spreader stoker power boiler site equipped with two-stage multicyclones. The boiler was reported by the mill to be rated at about 500,000 pounds of steam per hour. A total of 142 hourly averages for the mass monitor and RM-4 transmissometer were compared with the resulting statistical analysis represented as Figure 13. The relationship between the two monitors was exceptional with a standard deviation of 0.002 g/ACM and a coefficient of variation of 0.986. The regression equation corresponded to:

$$\frac{\text{GRAMS}}{\text{ACM}} = 0.005 + 0.154 \text{ (OPTICAL DENSITY)}$$

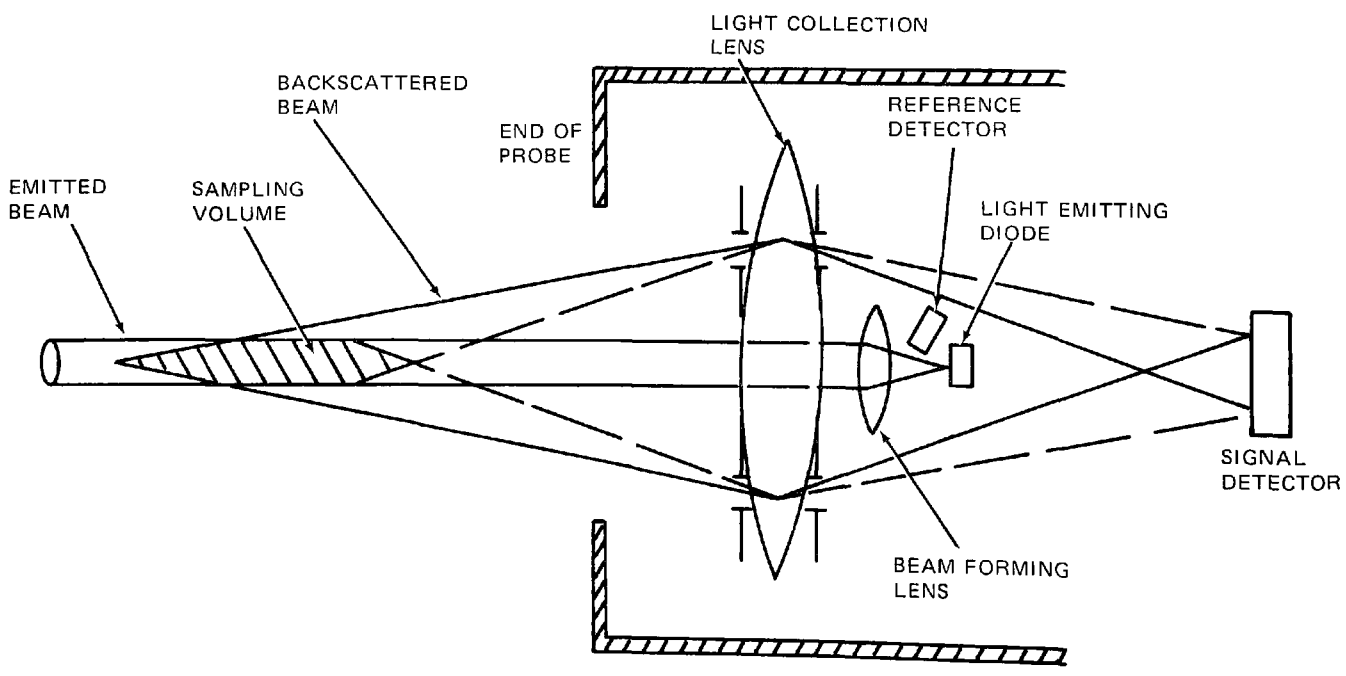


*Figure 10. P-5A optics diagram.*

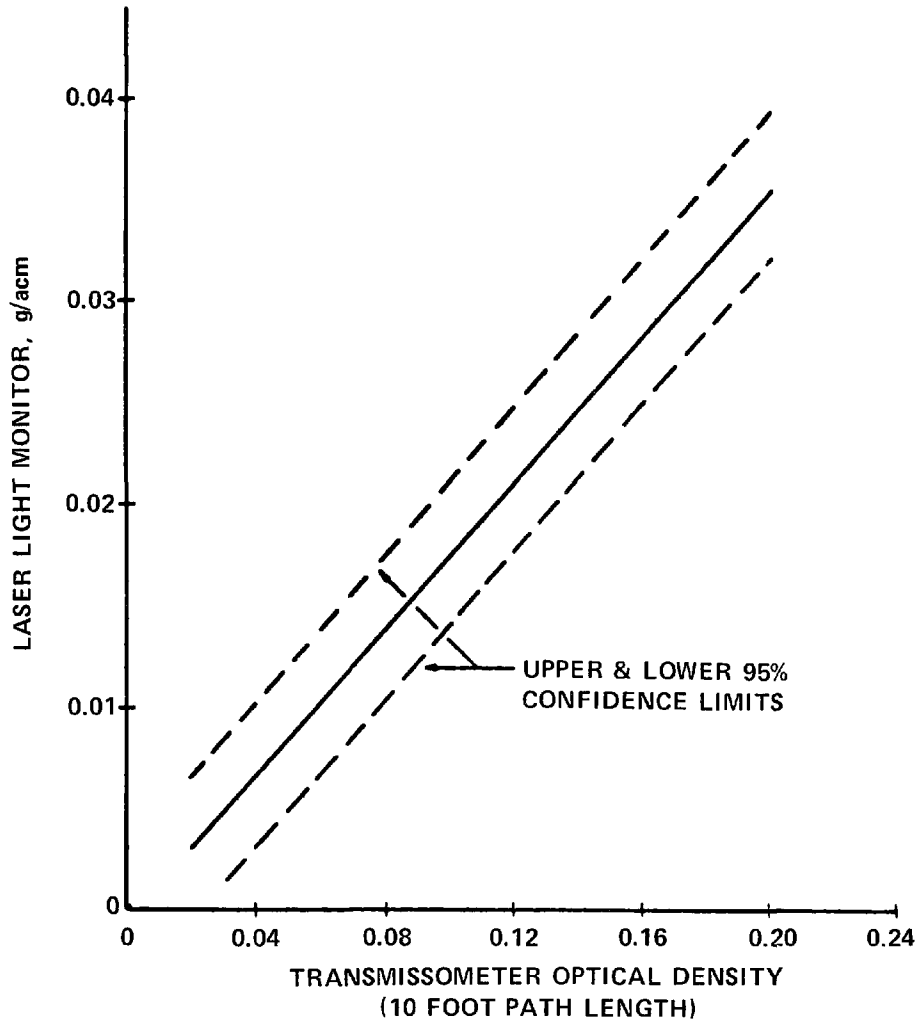


*Figure 11. Non-DCE kraft recovery furnace relationship between ESC laser light monitor and Lear Siegler transmissometer.*

The equation for the statistical relationship determined for the two monitors in this application was found to be surprisingly close to that presented in Figure 11 for the non-DCE kraft recovery furnace equipped with an electrostatic precipitator. This result addresses the similarity of the two monitors in their response to particulate emissions with obviously different particle characteristics.

SUMMARY

The relationships developed between in-stack measured opacity and simultaneous opacity measurements by trained observers have been found to aid in the interpretation of regulations which assume these opacity measurements to be equivalent. The relationship between particulate concentration and opacity was defined

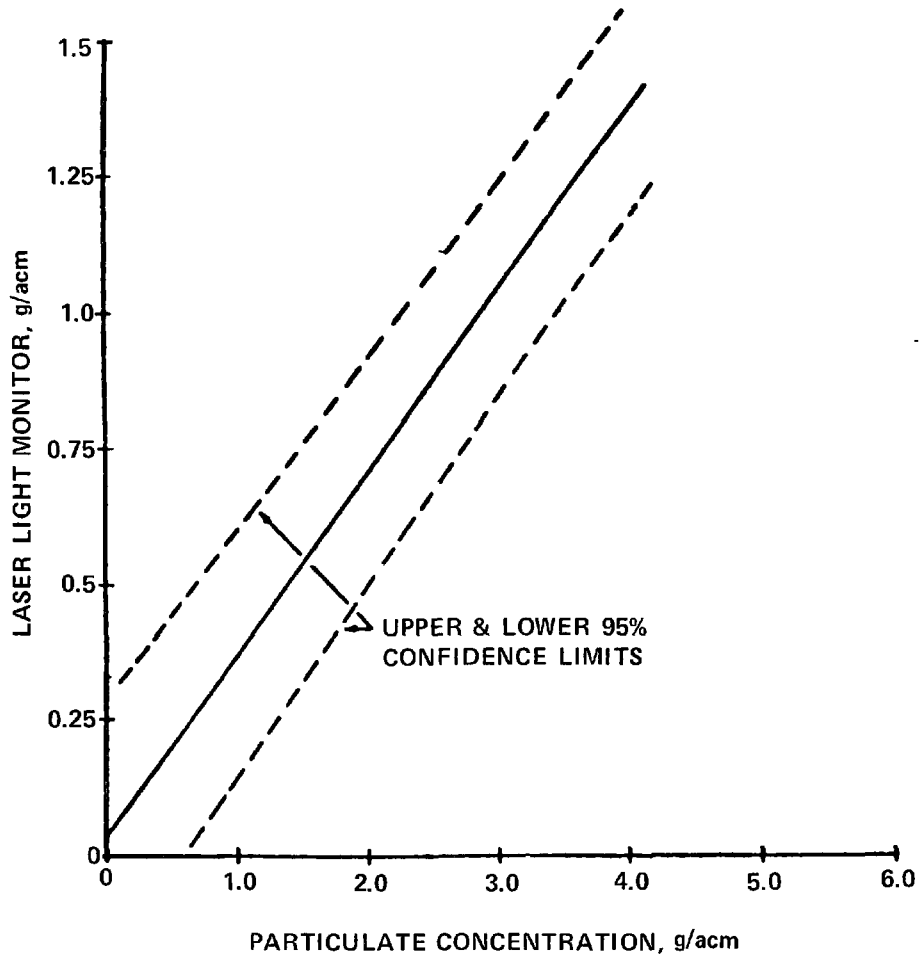


*Figure 12. West cyclone entry: ESC P-5A calibration curve.*

over a practical range of particulate concentrations at the recovery furnaces studied. An additional study was completed to determine the relationship of combination wood and fossil fuel-fired boiler plume appearance, or opacity, and particulate concentration within a spectrum of existing and developing particulate emission regulations. The findings for the fossil fuel-fired boiler paralleled in many respects those made during investigations at the kraft recovery furnace. These include, among others, a well-defined variability in observed plume characteristics by trained observers viewing the same plume, and the need to consider this variation if plume appearance is not to be the controlling feature of comparison plume appearance mass emission rate regulations. The findings differ in that the relationship between plume appearance and particulate concentration is not as precise for wood and fossil fuel combination boilers as for kraft furnaces. Particle characteristics were discussed as forming the probable cause of the lower precision encountered.

An evaluation conducted on a laser light monitor designed to measure particulate concentration as contrasted to opacity monitors which measure the light transmission changes induced by changes in flue gas particulate concentration displayed exemplary results. When monitoring data were compared with simultaneously generated opacity monitoring records on controlled sources from a kraft recovery furnace and a wood residue-fired power boiler the laser monitor was judged to be equivalent in quality of data and performance when used on sources with particulate concentrations of about 0.229 g/DSCM (0.1 gr/DSCF) and less.

The laser light monitor was also found to perform satisfactorily and unattended at particulate concentrations of about 3.75 g/ACM (5 gr/DSCF) found in the flue gas of a kraft recovery furnace preceding an electrostatic precipitator. This application was judged to be particularly attractive as a diagnostic tool for operators in defining reasons for variability in particulate generation within recovery furnaces.

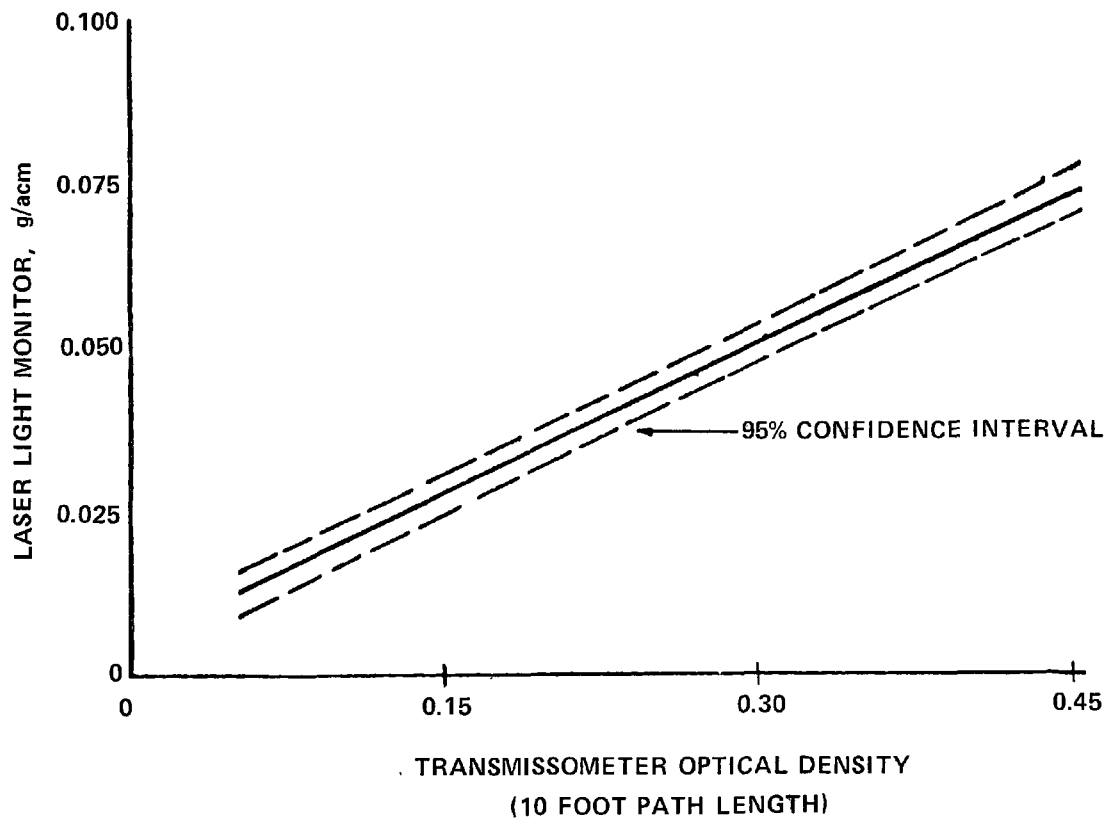


*Figure 13. Relationship between a laser light monitor and transmissometer for a power boiler.*

PAPER 11

# A DATA REDUCTION SYSTEM FOR CASCADE IMPACTORS

J.D. McCAIN
G. CLINARD
L.G. FELIX
J. JOHNSON
SOUTHERN RESEARCH INSTITUTE

ABSTRACT

A computer based data reduction system for cascade impactors has been developed. The system utilizes impactor specific calibration information together with operating conditions and other pertinent information such as stage weights and sampling duration to determine particle size distributions in several forms for individual runs. A spline technique is applied to fit a curve to the cumulative size distribution obtained from each individual impactor run. These fitted curves have forced continuity in coordinates and slopes. Averages of size distributions for multiple runs are made using the fitted curves to provide interpolation values at a consistent set of particle diameters, irrespective of the diameters at which the data points fall in the original individual run data sets. Statistical analyses are performed to locate and remove outliers from the data being averaged, following which averages, variances, standard deviations, and confidence intervals are calculated. The averages and statistical information are available in tabular and graphical form in several size distribution formats (cumulative mass loading, cumulative percentage by mass, differential mass, differential number). The averaged data are stored in disk files for subsequent manipulation. Additional programs permit data sets from control device inlet and outlet measurements to be combined to determine fractional collection efficiencies and confidence limits of the calculated efficiencies. These results are available in graphical form with a choice of log-probability or log-log presentations and as tabular output. The program is set up to handle all commercially available round jet cascade impactors, including common

modifications, which are in current use in stack sampling. Other round jet impactors can be easily substituted and slot type impactors could be accommodated with slight program revision.

## INTRODUCTION

Cascade impactors have gained wide acceptance as a practical means of making particle size distribution measurements. These devices are regularly used in a wide variety of environments, ranging from ambient conditions to flue gas streams at 500°C (950°F). Specially fabricated impactors can be used for more extreme conditions.

Because of their usefulness, the U.S. Environmental Protection Agency has funded research which has explored the theoretical and practical aspects of impactor operation. As part of this research, an effort has been made to design a comprehensive data reduction system which will make full use of cascade impactor measurements.

The cascade impactor data reduction system (CIDRS) described here is designed to automatically reduce data taken with any one of four commercially available round jet cascade compactors: The Andersen Mark III Stack Sampler, the Brink Model BMS-11 (as supplied and with extra stages), the University of Washington Mark III Source Test Cascade Impactor, and the Meteorology Research Incorporated Model 1502 Inertial Cascade Impactor. Provision is not made in this system for reducing data taken with slotted jet impactors. With modification the computer programs can accommodate any round jet impactor with an arbitrary number of stages, and with more extensive revision, can be made to handle data from slotted jet impactors.

The computer programs which comprise this data reduction system are written in the FORTRAN IV language. The plotting subroutines used were written specifically for the Digital Equipment Corporation (DEC) PDP-15/76 computer, and these programs are not compatible with other plotting systems. However, these programs can be used as a guide when revision is made for use with another operating system.

A broad outline of the program fundamentals is given here with sufficient detail for anyone without a specialized knowledge of computers to understand the methods and rationale of the program. The program comprises two major blocks. The first block treats data from individual impactor runs while the second treats data from groups of runs, providing averages, statistical information and fractional penetration (efficiency) results. The six mainline programs which make up the data reduction system are described in the overall program flow shown in Table 1.

TABLE 1. PROGRAM FLOW

BLOCK 1. SINGLE RUN ANALYSIS

I. Impactor Program (MPPROG)

Takes testing conditions and stage weights to produce stage $D_{50}$'s, cumulative and cumulative % mass concentrations $<D_{50}$, geometric mean diameters, and mass number size distributions. Executed for each run.

II. Fitting Program (SPLIN1)

Uses modified spline technique to fit cumulative mass loading points for each plot. Stores fitting coefficients and boundary points on file. Executed for each run.

III. Graphing Program (GRAPH)

Produces individual run graphs with points based on stage weights and impactor $D_{50}$'s. Also superimposes plot based on fitted data, if desired. Graphs include cumulative mass loading, cumulative % mass loading, and mass and number size distributions. Can be executed as desired for each run.

BLOCK 2. GROUPED DATA

IV. Statistical Program (STATIS)

Recalls cumulative mass loading fitting coefficients to produce average cumulative mass loading, average % cumulative mass loading, average mass size distribution, and average number size distribution plots each with 50% or 90% confidence bars. Executed for each group or data to be averaged.

Programs I-IV are used for both inlet and outlet data sets.

V. Efficiency Program (PENTRA) or (PENLOG)

Recalls average mass size distribution values along with 50% confidence limits for inlet and outlet to plot percent penetration and efficiency with 50% confidence bars. Executed once for each pair or groups and used to define a fractional efficiency curve.

INDIVIDUAL RUN DATA ANALYSIS

This portion of the impactor data reduction package utilizes impactor hardware information, particulate catch information, and sampling conditions from single impactor runs to calculate size distributions. The overall distributions are available

in several forms. The run analysis and output presentation are accomplished by three main programs, MPPROG, SPLIN1, and GRAPH. MPPROG and SPLIN1 perform analysis and manipulation while GRAPH is totally devoted to various forms of graphical presentation of the calculated distributions. The routines used in GRAPH are specifically for use on a PDP-15/76 computer and are not compatible with most other computers without modification. However, the general structure of GRAPH should serve as a useful base for programming to achieve similar graphical output from other computing systems.

## MPPROG

In MPPROG, sampling hardware information, sampling conditions and particulate catch information are used to determine the effective cut sizes of the various impactor stages and the concentrations of particles caught on these stages. The output is organized into several tabular forms and stored on a disk file for latter use.

### Input Data to MPPROG--

Because individual impactors, even of the same type, do not necessarily have precisely the same operational characteristics, the program calculates stage cut diameters on an impactor specific basis. Hardware data are stored within the program which include, for each impactor to be used, the number of stages, the number of jets per stage, the jet diameters, the stage calibration constants, and flow-pressure drop relations for each stage.

Run specific input data to MPPROG are listed in Table 2. The maximum particle diameter must be measured by microscopic examination of the particles collected on the first stage. Gas analysis must be made at the same time the impactor is run.

### Output from MPPROG--

Both input information pertaining to individual impactor runs and calculated results are listed on the line printer. A sample of output from MPPROG generated to the line printer is shown in Table 3.

Input information for each run is given in the first five lines of the printout. (Impactor pressure drop in inches of mercury is calculated within the program; gas composition is input as dry fractions and output as wet gas composition by percent.) The mass collected on each stage in milligrams is listed in the tenth line of the table.

TABLE 2. INPUT DATA TO MPPROG

1. Impactor identification (required to call up hardware information)
2. Gas composition ($CO_2$, CO, $N_2$, $O_2$, $H_2O$)
3. Impactor flow rate (acfm at stack conditions)
4. Stack pressure
5. Stack temperature
6. Gas temperature within impactor
7. Duration of sampling
8. True density of particles
9. Maximum particle diameter present in sample
10. Masses of catches by stage

The mass loading is calculated from the total mass of particles collected by the impactor and the total gas volume sampled, and it is listed in four different units after the heading CALC. MASS LOADING. The units are defined as:

GR/ACF - grains per actual cubic foot of gas at stack conditions of temperature, pressure, and water content.

GR/DSCF - grains per dry standard cubic foot of gas at engineering standard conditions of gas. Engineering dry standard conditions in the English system are defined as 0% water content, 70°F, and 29.92 inches of mercury.

MG/ACM - milligrams per actual cubic meter of gas at stack conditions of temperature, pressure, and water content.

MG/DNCM - milligrams per dry normal cubic meter of gas at engineering normal conditions of the gas. Engineering dry normal conditions in the metric system are defined as 0% water content, 21°C and 760 mm of mercury (torr).

TABLE 3. SAMPLE CALCULATIONS

INPUT INFO

HYPOTHETICAL ANDERSEN

IMPACTOR FLOWRATE = 0.500 ACFM  IMPACTOR TEMPERATURE = 400.0 F = 204.4 C  SAMPLING DURATION = 20.00 MIN

IMPACTOR PRESSURE DROP = 0.3 IN. OF HG  STACK TEMPERATURE = 400.0 F = 204.4 C

ASSUMED PARTICLE DENSITY = 1.35 GM/CU.CM.  STACK PRESSURE = 26.50 IN. OF HG  MAX. PARTICLE DIAMETER = 100.0 MICROMETERS

GAS COMPOSITION (PERCENT)  CO2 = 1.94  CO = 0.00  N2 = 76.53  O2 = 20.53  H2O = 1.00

CALC. MASS LOADING = 8.0711E-03 GR/ACF  1.4748E-02 GR/DNCF  1.8470E+01 MG/ACM  3.3748E+01 MG/DNCM

INPUT INFO

| IMPACTOR STAGE | S1 | S2 | S3 | S4 | S5 | S6 | S7 | S8 | FILTER |
|---|---|---|---|---|---|---|---|---|---|
| STAGE INDEX NUMBER | 1 | 2 | 3 | 4 | 5 | 6 | 7 | 8 | 9 |
| D50 (MICROMETERS) | 10.72 | 9.93 | 6.35 | 4.18 | 2.21 | 1.28 | 0.67 | 0.33 | |
| MASS (MILLIGRAMS) | 0.72 | 0.40 | 0.53 | 0.09 | 0.38 | 1.43 | 1.25 | 0.04 | 0.39 |
| MG/DNCM/STAGE | 4.71E+00 | 2.62E+00 | 3.47E+00 | 5.89E-01 | 2.49E+00 | 9.35E+00 | 8.18E+00 | 2.62E-01 | 2.55E+00 |

CUMULATIVE

| | | | | | | | | |
|---|---|---|---|---|---|---|---|---|
| CUM. PERCENT OF MASS SMALLER THAN D50 | 86.23 | 78.59 | 68.45 | 66.73 | 59.46 | 32.12 | 8.22 | 7.46 |
| CUM. (MG/ACM) SMALLER THAN D50 | 1.59E+01 | 1.45E+01 | 1.26E+01 | 1.23E+01 | 1.10E+01 | 5.93E+00 | 1.52E+00 | 1.38E+00 |
| CUM. (MG/DNCM) SMALLER THAN D50 | 2.91E+01 | 2.65E+01 | 2.31E+01 | 2.25E+01 | 2.01E+01 | 1.08E+01 | 2.77E+00 | 2.52E+00 |
| CUM. (GR/ACF) SMALLER THAN D50 | 6.96E-03 | 6.34E-03 | 5.52E-03 | 5.39E-03 | 4.80E-03 | 2.59E-03 | 6.64E-04 | 6.02E-04 |
| CUM. (GR/DNCF) SMALLER THAN D50 | 1.27E-02 | 1.16E-02 | 1.01E-02 | 9.84E-03 | 8.77E-03 | 4.74E-03 | 1.21E-03 | 1.10E-03 |

DIFF

| | | | | | | | | | |
|---|---|---|---|---|---|---|---|---|---|
| GEO. MEAN DIA. (MICROMETERS) | 3.27E+01 | 1.03E+01 | 7.94E+00 | 5.15E+00 | 3.04E+00 | 1.68E+00 | 9.30E-01 | 4.75E-01 | 2.36E-01 |
| DM/DLOGD (MG/DNCM) | 4.86E+00 | 7.93E+01 | 1.78E+01 | 3.24E+00 | 8.96E+00 | 3.95E+01 | 2.94E+01 | 8.56E-01 | 8.47E+00 |
| DN/DLOGD (NO. PARTICLES/DNCM) | 1.96E+05 | 1.02E+08 | 5.03E+07 | 3.35E+07 | 4.52E+08 | 1.18E+10 | 5.18E+10 | 1.13E+10 | 9.12E+11 |

NORMAL (ENGINEERING STANDARD) CONDITIONS ARE 21 DEG C AND 760MM HG.

Below the run condition data summary, the information pertinent to each stage is summarized in columnar form in order of decreasing particle size from left to right. Thus, S1 is the first stage, S8 is the last stage, and FILTER is the back-up filter. If a precollector cyclone was used, a column labeled CYC would appear to the left of the S1 column and information relevant to the cyclone would be listed in this column. Beneath each impactor stage number is listed the corresponding stage index number, which also serves as identification for the stage.

Directly beneath these listings are the effective stage cut diameters. The effective stage cut diameter is assumed to be equal to the particle diameter for which the stage collection efficiency is 50%. This diameter, $D_{50}$, is calculated from an equation of the form

$$D_{50} = k_s \left[\frac{\mu d}{\rho_p C v}\right]^{\frac{1}{2}} \tag{1}$$

where $D_{50}$ = effective cut size,

$k_s$ = stage calibration constant,

$\mu$ = gas viscosity,

$d$ = jet diameter,

$\rho_p$ = particle density,

$C$ = Cunningham slip correction factor, and

$v$ = jet velocity.

Because the particle diameter, $D_{50}$, enters the equation for C, the solution of Equation 1 is obtained by an iterative process. If the particle density, $\rho_p$, is set equal to the true density of the particles, as is the case in the sample output in Table 3, the resulting diameter calculated from Equation 1 is the Stokes diameter, $D_S$. If $\rho_p$ is set equal to 1.0 the resulting diameter is the aerodynamic diameter $D_A$ as defined by the Task Group on Lung Dynamics.[1] If both $\rho_p$ and C are set equal to 1.0, the resulting diameter is the aerodynamic impaction diameter, $D_{AI}$, as defined by Mercer.[2] Unless otherwise specified, MPPROG will automatically provide parallel output in terms of $D_S$ and $D_A$. Parallel results in terms of $D_S$ and $D_{AI}$ or in terms of $D_A$ and $D_{AI}$ are available if called for.

The stage weights, in units of milligrams as input, are likewise listed for the respective stages on the line labeled MASS. The mass loadings from each stage follow and are labeled MG/DNCM/STAGE (milligrams per dry normal cubic meter per stage).

The percentage of the total mass sampled contained in particles with diameters smaller than a particular $D_{50}$ is called the CUMULATIVE PERCENT OF MASS SMALLER THAN $D_{50}$. It is the cumulative percentage of total mass accumulated in the stage j.

The cumulative mass loading of particles smaller in diameter than the corresponding $D_{50}$ is listed in four different units: milligrams per actual cubic meter, milligrams per dry normal cubic meter, grains per actual cubic foot, and grains per dry normal cubic foot. Note that these are the same units used for calculating the total mass loading. They represent both metric and English units and both stack conditions and engineering dry standard conditions of temperature, pressure, and water content.

The geometric mean diameter for the particles collected on each stage is then listed in micrometers. The geometric mean diameter of a given stage may be expressed as the square root of the product of the $D_{50}$ of the given stage and the $D_{50}$ of the previous stage. In calculating the geometric mean diameter of the first stage (or cyclone if applicable), the maximum particle diameter is used instead of the "$D_{50}$ of the previous stage." In calculating the geometric mean diameter of the filter, one-half the $D_{50}$ of the last stage (stage eight, here) is used instead of the "$D_{50}$ of the given stage." (There is no $D_{50}$ for the back-up filter since all remaining particles are captured by this filter.)

Finally, an approximate differential particle-size distribution is listed as DM/DLOGD, in milligrams per dry normal cubic meter, and as number concentration, DN/DLOGD, in number of particles per dry normal cubic meter.

Differential size distributions may be derived two ways:

1. Finite difference methods may be used based on the $D_{50}$'s (abscissa) and the particulate masses on each stage (ordinate). This technique was used to generate the differential size distribution data in Table 3.

2. Curves may be fitted to the cumulative mass distribution from which the differential curves (slope) for each test can be calculated. This method is preferred and is described in the following paragraphs.

SPLIN1

In many, if not most, sampling programs, a number of impactor runs will be made. Frequently, these runs will be made using several impactors, having different performance characteristics. The latter may be true even if the same type of impactor is used throughout a sampling program. This behavior results both from manufacturing variations which cause calibration differences

and run-to-run variations in sampling rates, which cause shifts in the $D_{50}$'s. Averaging results from such testing to obtain a representative composite size distribution requires that the distributions be broken down into like size intervals for all the runs to be averaged. The same requirement for like size intervals also holds for using inlet and outlet data from control device sampling programs to obtain fractional efficiencies. This requires curves to be fit to the data for each run to permit interpolation to obtain values at common diameters for all runs to be compared or averaged.

Before making the final selection of the spline technique for fitting curves to the size distribution data, consideration was given to a number of alternate fitting methods, and several of them were tried. It was concluded that any attempt to fit a predetermined functional form (e.g., log-normal) to the data was generally not proper. Because the slope of the cumulative distribution curve, the differential distribution, is the required quantity for calculating fractional efficiencies, consideration was also given to fitting curves to the $\Delta M/\Delta \log D$ approximations of the true differential distribution, which are estimated directly from the stage loadings and $D_{50}$'s. However, the magnitudes of the steps in $D_{50}$ are large enough in most impactors as to frequently make $\Delta M/\Delta \log D$ a poor approximation to $dM/d\log D$. Moreover, the boundary conditions are more difficult to handle in fitting curves to $\Delta M/\Delta \log D$ than in fitting to the cumulative distributions. It was ultimately concluded, after many trial fitting methods were tested, that the best use was made of the data if the fitting was done to the cumulative distribution curve by means of a spline method.

SPLIN1 operates by fitting a curve which is continuous in X and Y and the first derivative of Y with respect to X to the cumulative mass concentration size distribution data. The resulting fitted curve is similar to that which one would draw through the data points using a "French curve" or mechanical spline. This fitted curve invokes no a priori assumptions as to the shape of the distribution (e.g., power law or log-normal). The manner in which the spline fits are made is described below.

Initial attempts at using the spline technique on the set of points defining the cumulative distribution curve obtained directly from the $D_{50}$'s were not satisfactory. The difficulty occurred as a result of the inability of the method to generate sufficiently rapid changes in curvature when the curve to be generated was defined by a small number of points. A satisfactory fit could be obtained by adding a set of interpolated points between the original data points of the measured cumulative curve. These points are generated by means of a series of parabolas through consecutive sets of three adjacent data points of the original cumulative curve defined by the impactor stage data.

The fitting is done using log (concentration) and log (particle diameter) as variables and begins with the segment containing the smallest $D_{50}$ in the data set.

The sequence of operations by which the interpolated points are generated is shown in Figure 1. A series of parabolas are fit through consecutive sets of 3 data points beginning at the smallest $D_{50}$ as shown in Figures 1a and 1b. In this description, three interpolation points between each pair of $D_{50}$'s will be assumed. However, the program will accommodate up to 5 interpolation points. The use of more points will improve the accuracy of the fitting, but will require more storage capacity. The interpolation points are located along the parabolas, between the lower pair of the three $D_{50}$ points used to generate the parabola. The interpolated points are spaced evenly in log diameter between the pair of original points. A similar process is used to generate interpolated points between consecutive pairs of $D_{50}$'s up to the segment which terminates at the $D_{50}$ of the first collection stage as illustrated in Figures 1c to 1e. A slightly different procedure which will be described later, is used for segments which include the first collection stage $D_{50}$.

Since the fitting is for a cumulative curve, negative slopes are not allowed. Therefore, a check is made for negative first derivatives of the interpolation parabola at the bounds of each segment within which the interpolated points are to be generated. If a negative derivative is found in any segment other than the first (the segment including the smallest $D_{50}$) a straight line interpolation between the segment bounds is used rather than parabolic interpolation. If a negative first derivative is found in the first segment to be fitted, a fictitious point is generated and used to form a parabola which has no negative derivatives in this segment. This fictitious point has the same concentration value as that of the first point on the cumulative curve and has a diameter defined by

$$D_{fictitious} = \frac{(D_{50} \text{ of last stage})^2}{(D_{50} \text{ of next to last stage})}$$

The interpolated values for the segment between the last two $D_{50}$'s on the cumulative curve are then generated from the parabola which passes through this fictitious point, and the points for the last two stages on the cumulative distribution curve.

In the region about the first stage $D_{50}$, three sets of interpolated points are generated. The first are generated by parabolic interpolation using a parabola through DMAX, $D_{50}$ (stage 1) and $D_{50}$ (stage 2) as was done in the case of the previous segments. However, in addition to these, two more points are generated along the parabola above the first stage $D_{50}$. These additional points are spaced evenly in log (diameter) at the same intervals in log (diameter) as the interpolated points between $D_{50}$ (stage

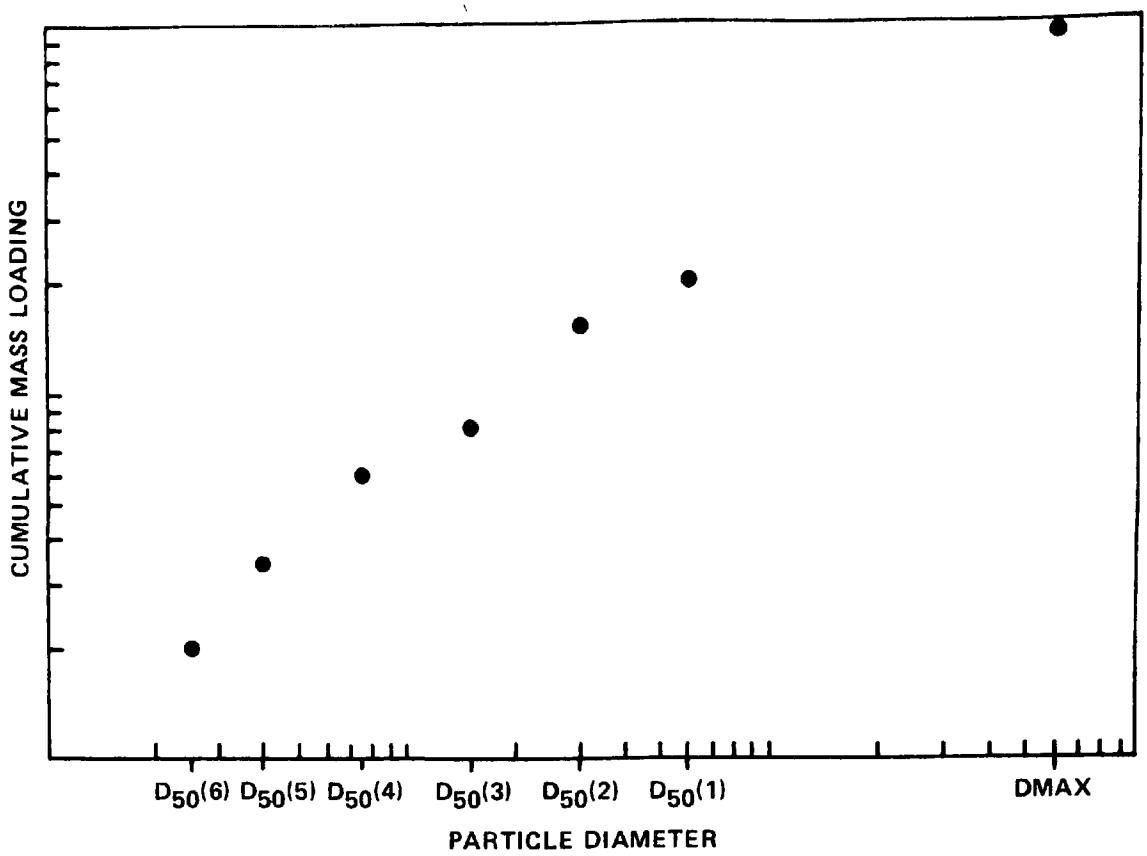


*Figure 1a. Cumulative size distribution from raw impactor data.*

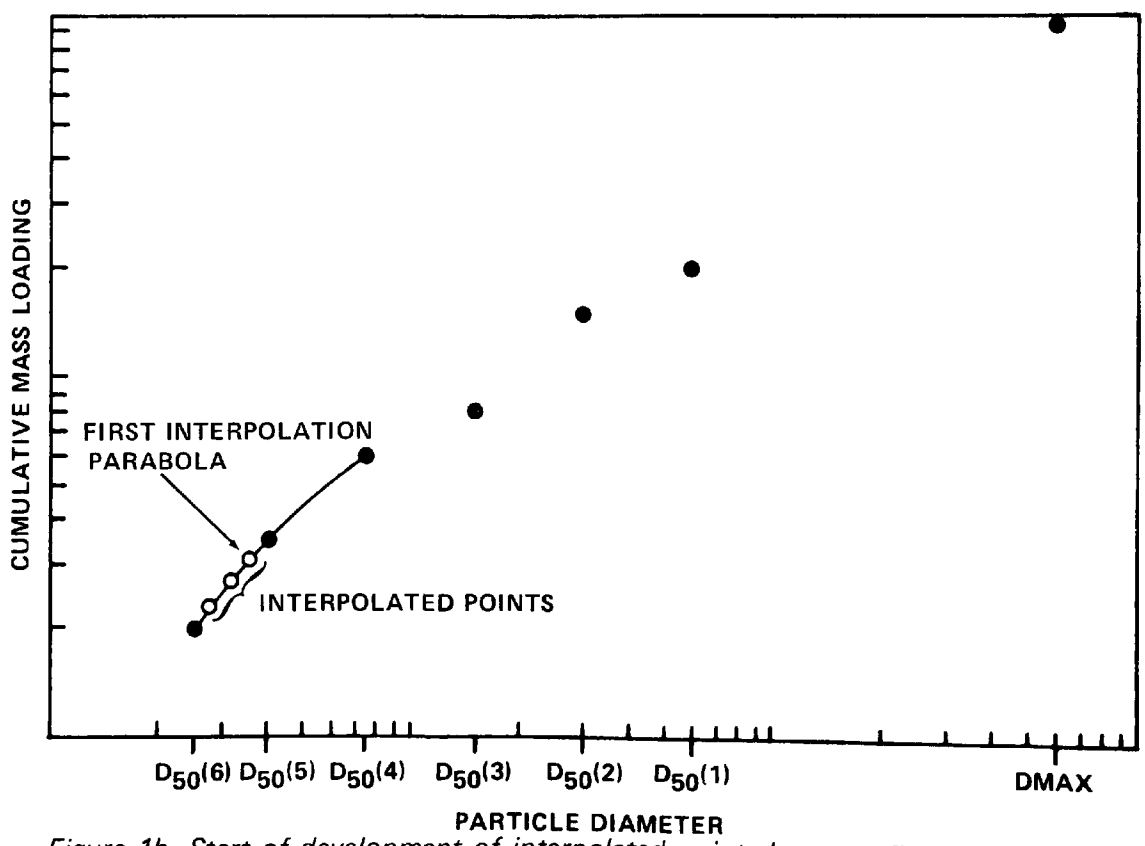


*Figure 1b. Start of development of interpolated points between first and last $D_{50}$.*

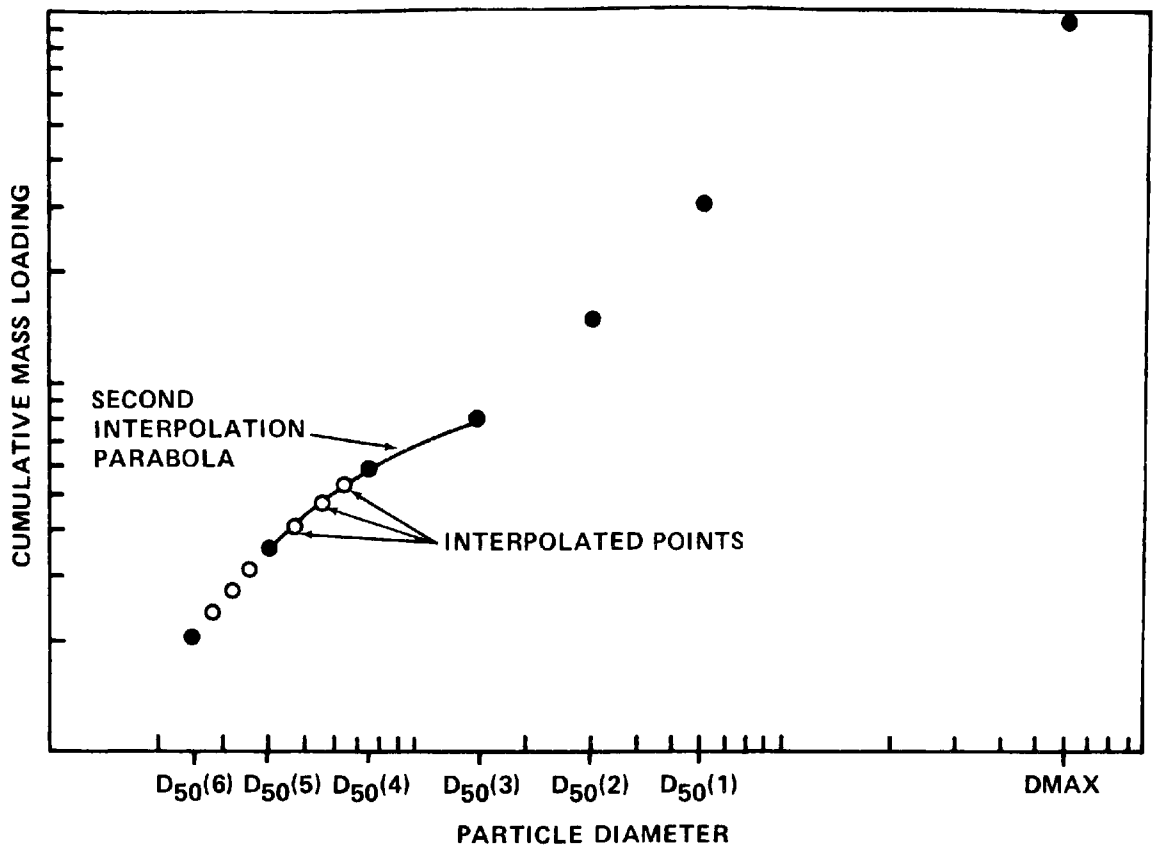


*Figure 1c. Continued generation of interpolated points*

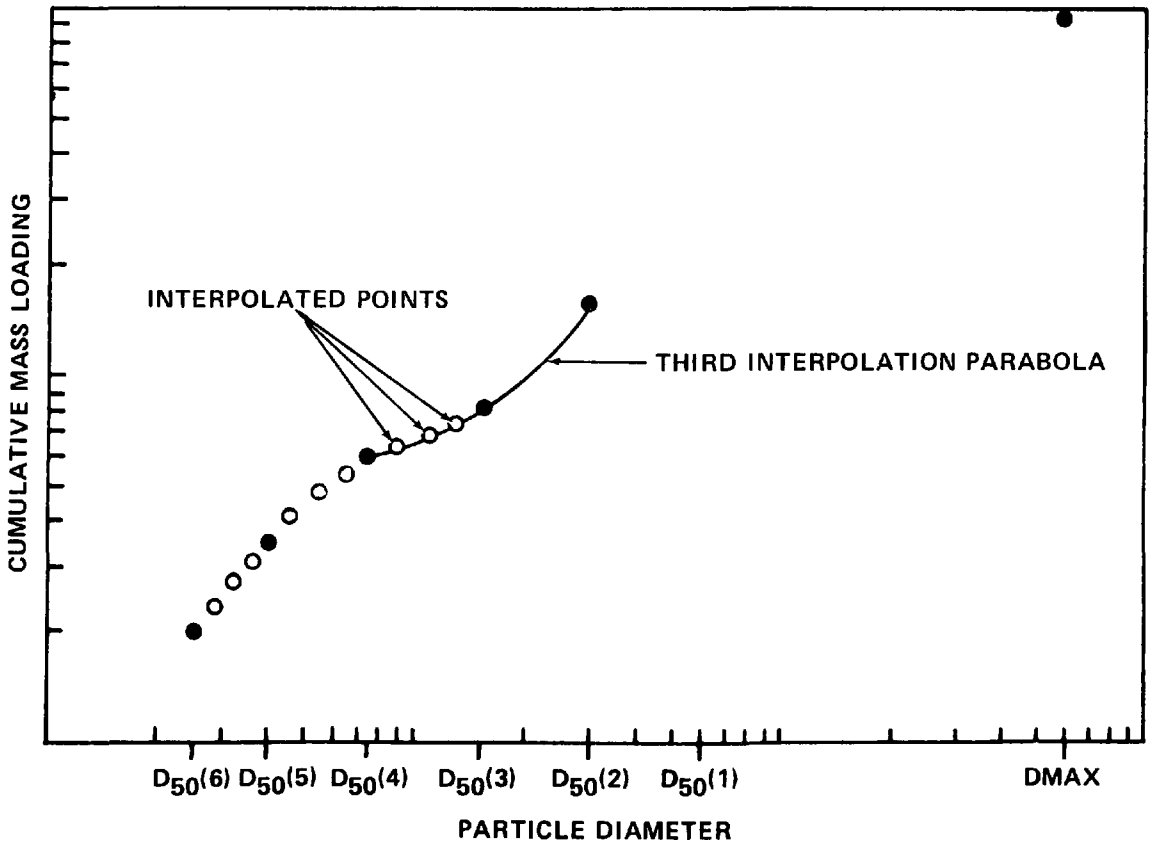


*Figure 1d. Continued generation of interpolated points*

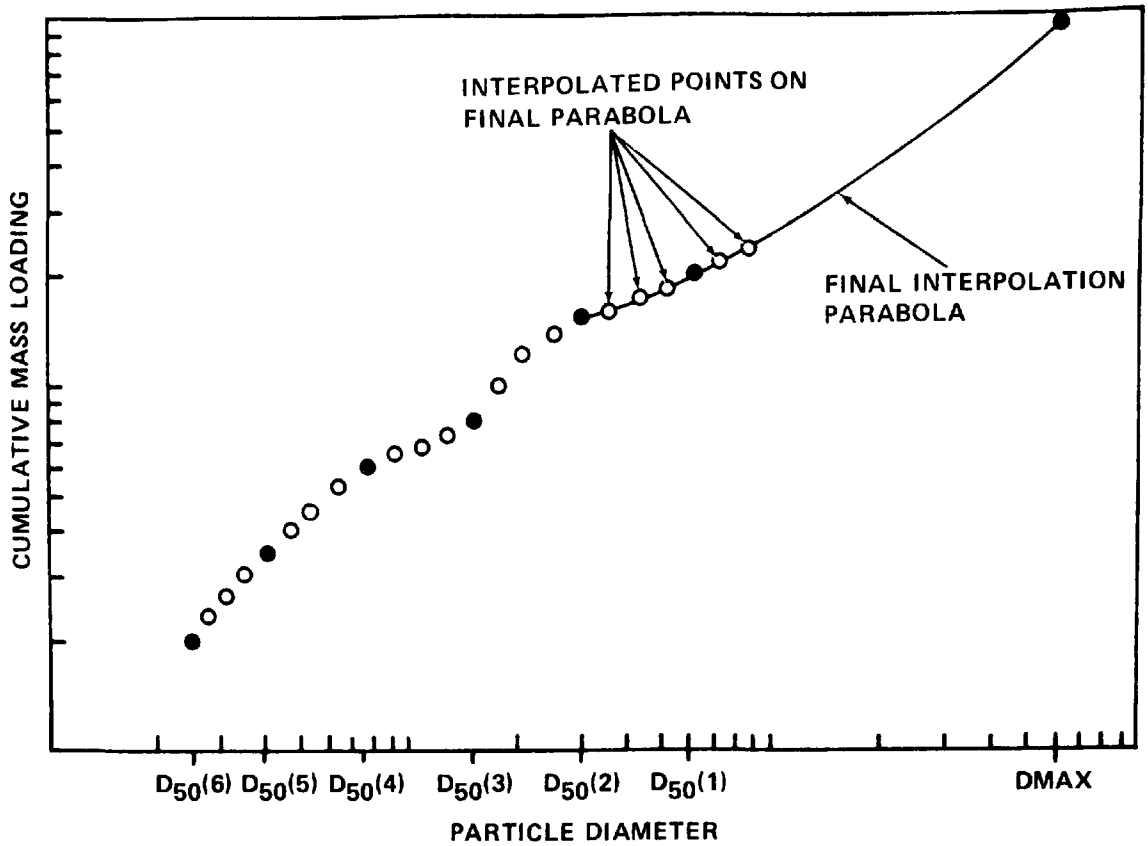


*Figure 1e. Generation of interpolated points on parabola which includes DMAX.*

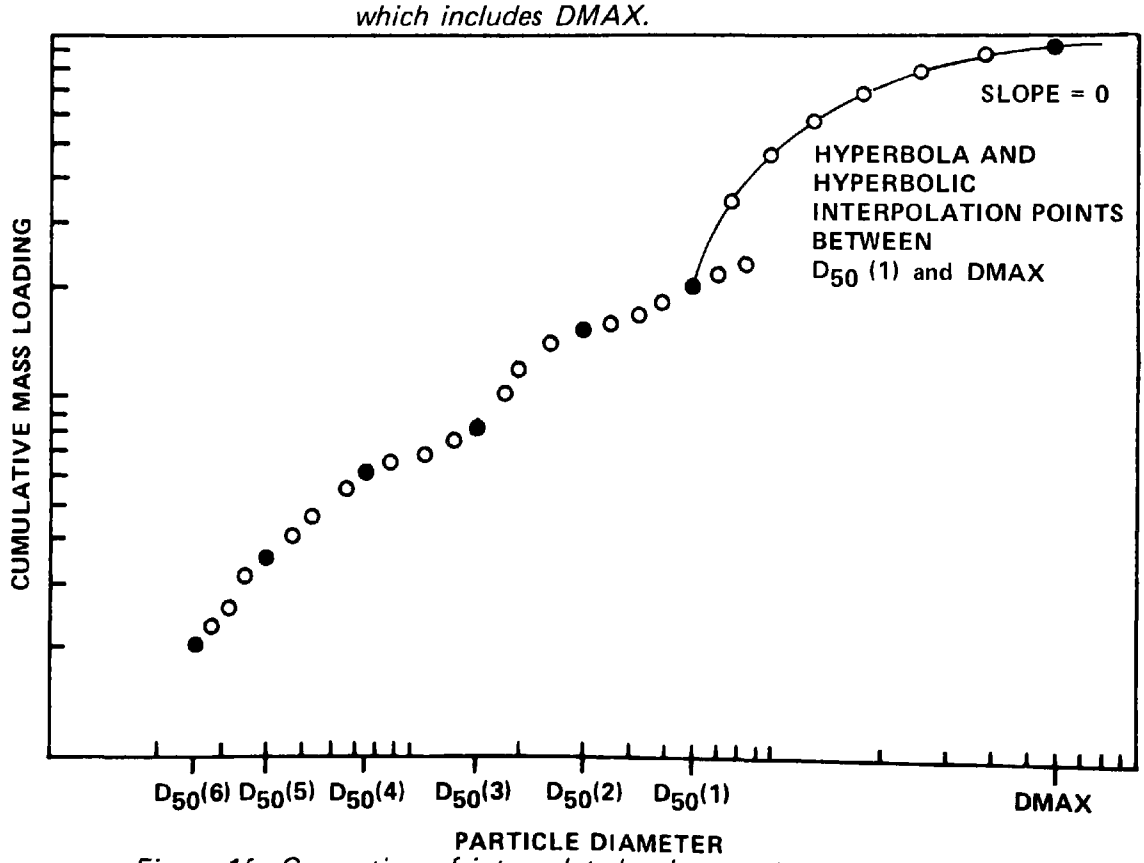


*Figure 1f. Generation of interpolated points on hyperbola through $D_{50}(1)$ and DMAX*

1) and $D_{50}$ (stage 2) as shown in Figure 1e. These points are used in generating the final curve fit up to the point on the cumulative distribution curve defined by the first stage $D_{50}$. The third set of points is illustrated in Figure 1f.

Note that the cumulative mass distribution used in the illustrations of Figure 1 is one in which a large step in concentration occurs between $D_{50}$ (stage 1) and DMAX. This is typical of a cumulative curve for a bimodal distribution in which one mode has a median diameter substantially greater than first stage $D_{50}$. The interpolation parabola through DMAX, $D_{50}$ (stage 1 and $D_{50}$ (stage 2) does not properly represent the shape of the true distribution curve in this region. In particular, the true curve must have zero slope at DMAX. It was empirically determined that a hyperbolic interpolation equation fit in terms of linear concentration and linear diameter between DMAX and $D_{50}$ (stage 1) with the hyperbola asymptotic to the total loading at infinite particle size resulted in acceptable results for the final spline fits. Therefore, a seven point hyperbolic interpolation is used in addition to the previously described parabolic interpolation over this segment of the curve. This hyperbolic interpolation is illustrated in Figure 1f. The use of the two sets of interpolated points in the final interval will be discussed later.

Generation of the Final Spline Fit--

The original data points, defined by the $D_{50}$'s, together with the interpolated points just generated, form a set of points along a continuous curve (if one disregards the two sets of points in the final segment) which has no negative slopes. However, the derivative of the curve in most cases will not be continuous at the $D_{50}$ points. The spline fit to be described is a smoothing technique which generates a series of parabolic segments that approximates a continuous curve through the complete set of points defining the cumulative distribution. The segments to be generated now will pass near or through those points and will have forced continuity in both coordinates and first derivatives. The technique is applied first to cover the interval between the first and last stage $D_{50}$'s and then a second time to cover the interval between the first stage $D_{50}$ and DMAX. From this point on in the discussion, no distinction is made between the original points defined by the $D_{50}$'s and the interpolated values located between them.

The spline fit is generated by joining successive parabolas at locations determined by the X (or log diameter) coordinates of the points which now represent the cumulative distribution curve (original points at the $D_{50}$'s plus the interpolated points). These parabolas have continuity in slope forced by the fitting procedure and are generated in such a fashion as to pass near or through the points on the cumulative distribution curve.

The procedure is illustrated in Figure 2. The spline fit is begun at the lowest point, O, on the distribution curve (at the $D_{50}$ of the last stage). The parabola used to generate the interpolated points between the last two stages is assumed to be the fitted curve up to the first interpolated point. (Point 1 in Figure 2a.) This parabola, a, is followed until the x-coordinate at point 1 is reached. At the point A, located on this parabola by the X-coordinate of point 1, a new parabola is fitted as shown in Figure 2b. This parabola, b, is forced to pass through point A with the same slope at A as the parabola used to define point A, and is forced to pass through the third point above point 1 in the set of points defining the cumulative curve, i.e., point 4. The parabola, b, is followed to the point defined by the X-coordinate of point 2, thus locating a point B. At B a new parabola is fit with forced slope continuity with b passing through the third point ahead of point 2, i.e., point 5, as shown in Figure 2c. From C this process is repeated using point C and 6 to generate a new parabola, d, and termination point D, e, and E, etc., until a termination point at the $D_{50}$ of the first collection stage is reached. The last three points obtained by parabolic interpolation are used in generating the spline fit parabolas up to the first collection stage $D_{50}$. The coefficients of the fitting spline fit parabolas for the segments a, b, c, d, . . etc., are saved for future use. These now represent the smoothed curve and will be used henceforth to define the cumulative curve for that run.

The final spline fit starts by picking up at the point on the fitting parabola which terminated at the $D_{50}$ of the first stage. The same procedure as before is followed, except that the third point ahead determined by the hyperbolic interpolation is now used for fitting, and the fitting parabolas are followed to X-coordinates defined by the hyperbolic interpolation points. The curve generated in this second zone of the spline fit (i.e., between $D_{50}$ (stage 1) and DMAX) is an extrapolation which has been found to be reasonably good to diameters equal to about 2 to 3 times the first stage $D_{50}$. By using the second, third (as illustrated), fourth, etc., point ahead in generating the final parabola segments one can influence the amount of smoothing provided by the program.

The cumulative concentration and slope of the cumulative curve, dm/dlogD, can be calculated for any arbitrary particle size by locating the fitting coefficients for the spline segment containing that size. The boundary locations of each of the parabolic segments, O, A, B, C, . ., and the fitting coefficients for each segment are stored in a disk file for subsequent use by other programs (e.g., GRAPH, STATIS, etc.).

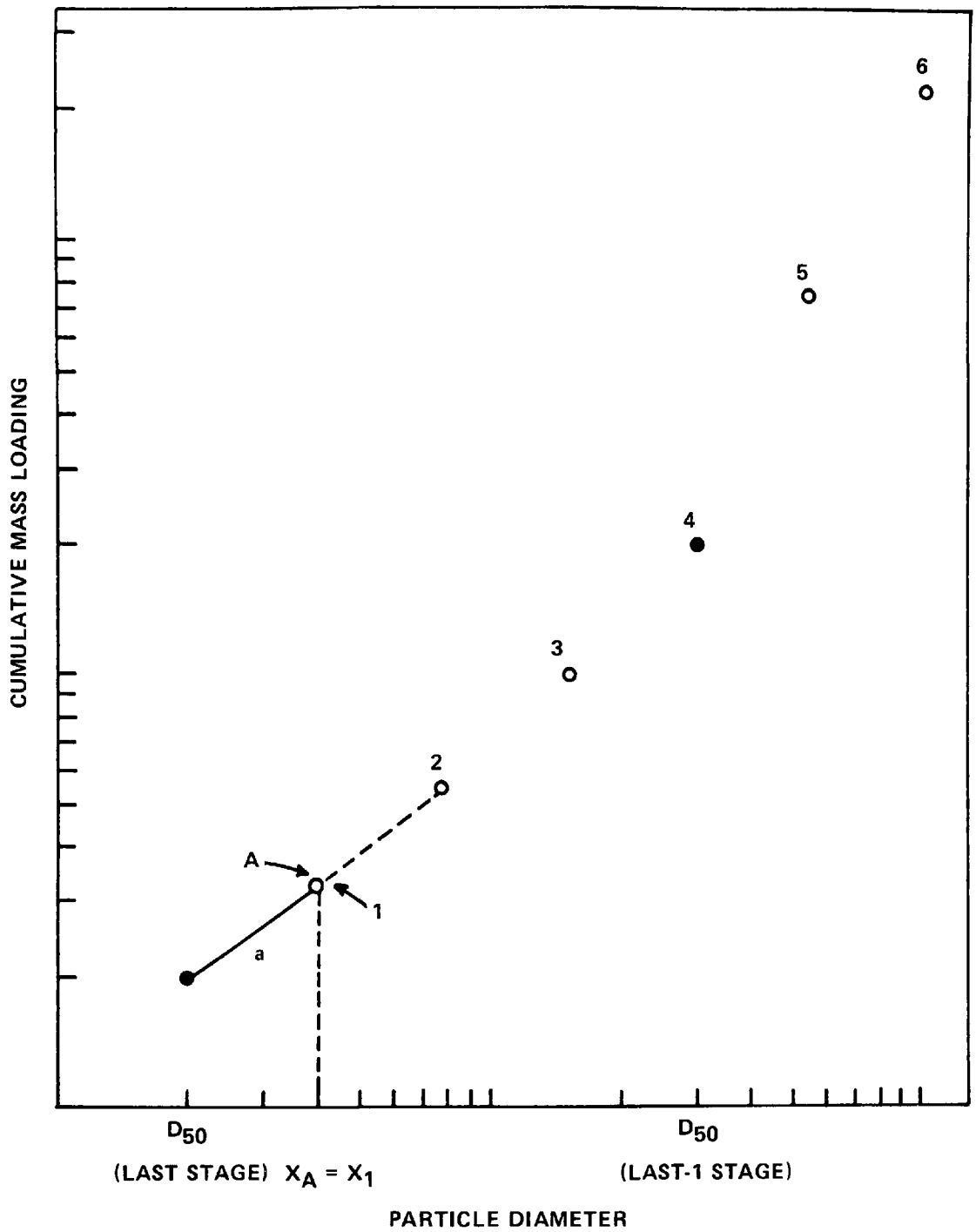


*Figure 2a. Start of the curve fitting procedure. Cumulative mass loadings derived from stage catches are represented by solid circles. Interpolated values are shown with open circles.*

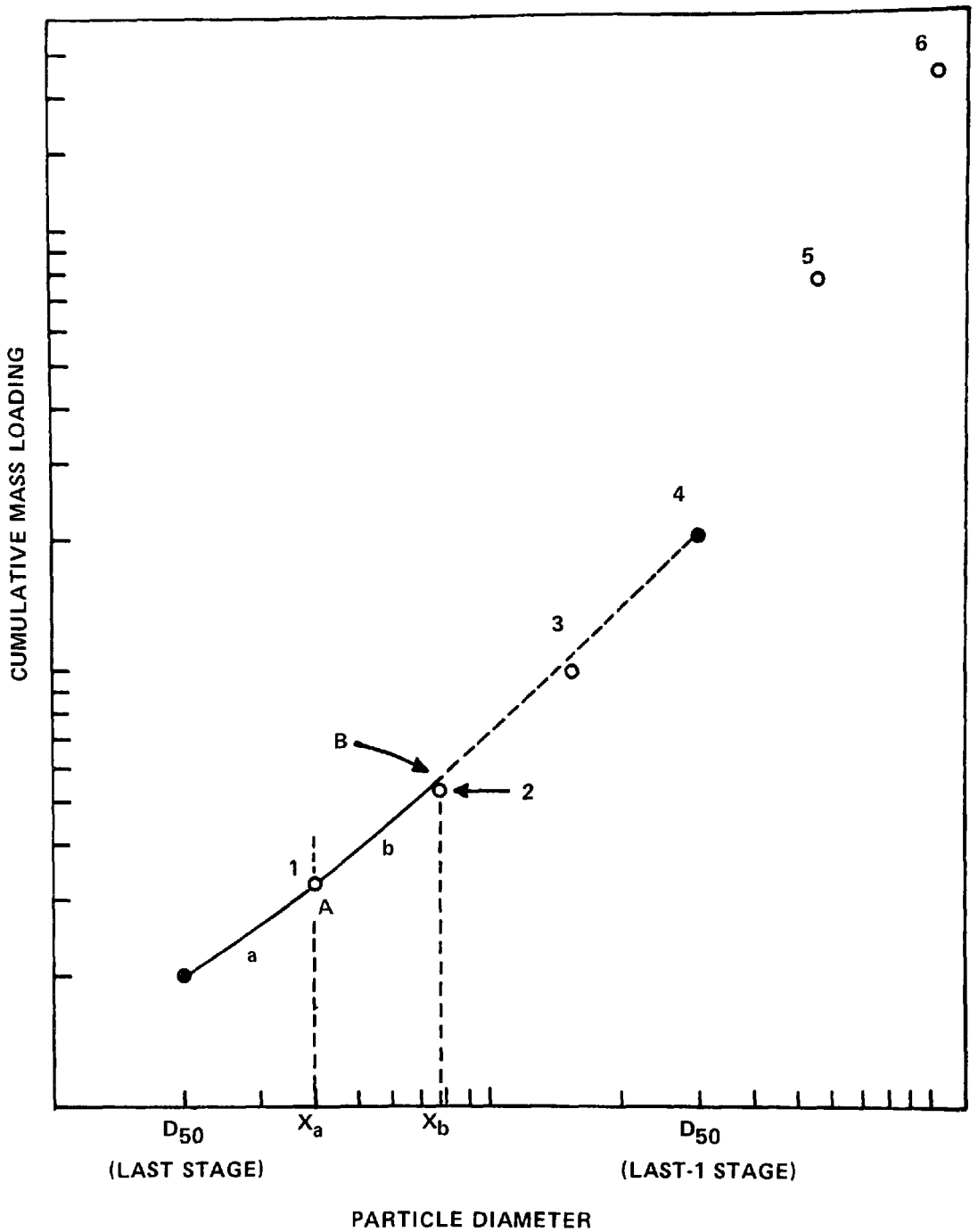


*Figure 2b. Second step in the curve fitting procedure. Cumulative mass loadings derived from stage catches are represented by solid circles. Interpolated values are shown with open circles.*

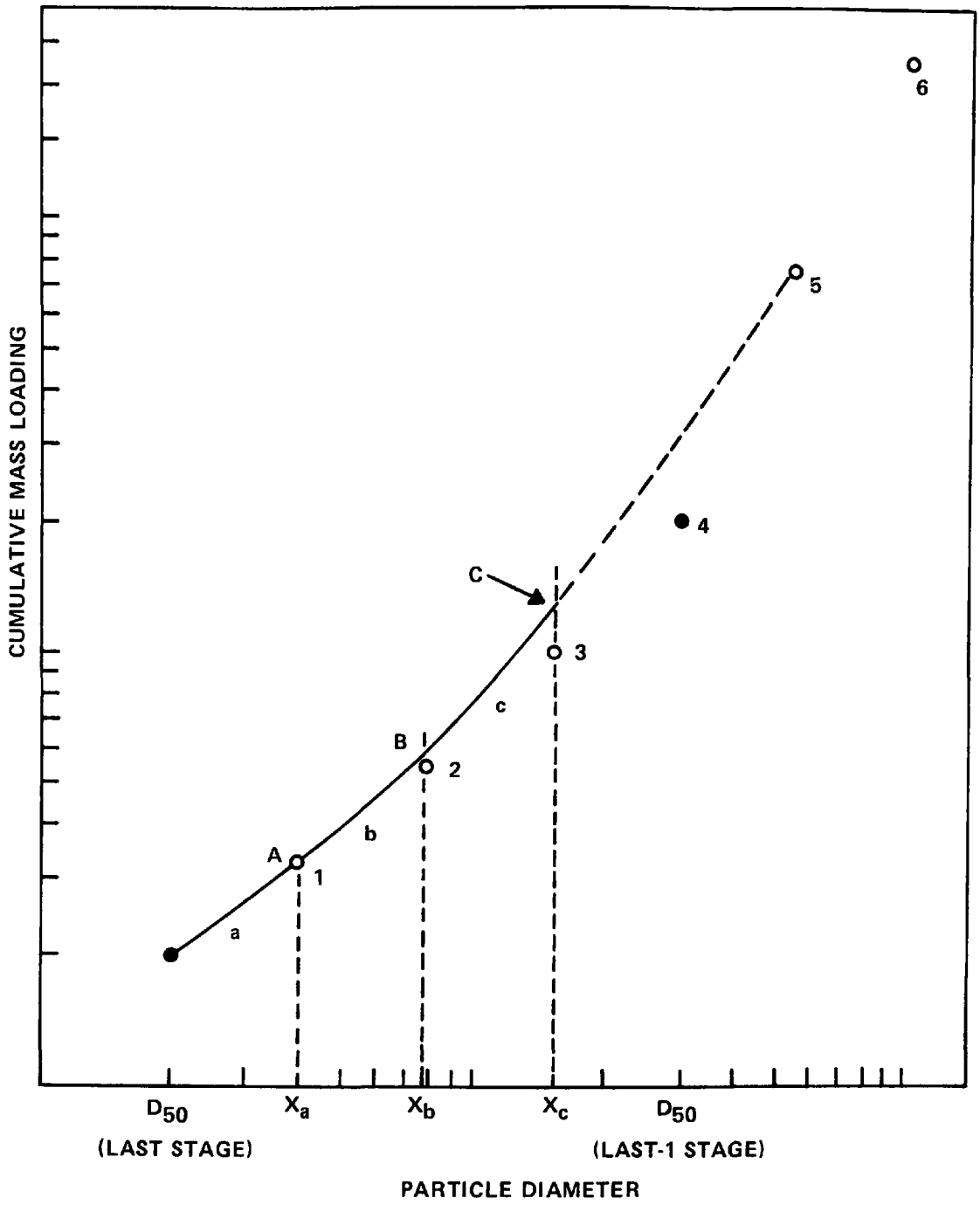


*Figure 2c. Third step in the curve fitting procedure. Cumulative mass loadings derived from stage catches are represented by solid circles. Interpolated values are shown with open circles.*

Problems Resulting from Extremely Close Stage Cut Diameters ($D_{50}$'s)--

When two stages are used on an impactor which differ only slightly in $D_{50}$, the second of the two will collect too much material because of the finite slope of real impactor stage collection characteristics. The simplest example of this effect would be obtained if two identical stages are used sequentially. If that were the case, in an ideal impactor the second stage should collect no material; however, because of the finite slope of the real stage collection efficiency curve, it will collect some particles. This would lead to the formation of a step increase (infinite slope) in the cumulative concentration curve. The severity of the effect is reduced as the spacing between the $D_{50}$'s increases but can be sufficiently severe to cause significant errors in the size distribution curves if it is not properly accounted for. Calibrations indicate that the effective cut diameters, or $D_{50}$'s, at the first two stages of several impactors suffer from this problem. The program MPPROG, because of this, ignores the presence of the second stage of Andersen, MRI, and University of Washington impactors in generating the cumulative mass concentration curve from which the fitted curves will be made by SPLIN1. This procedure effectively nullifies the problem. However, if calibrations of future versions of these impactors do not show the small spacing in $D_{50}$, MPPROG should be modified appropriately so as not to lose good information when the curve fits are made.

GRAPH

Program GRAPH is dedicated entirely to presenting data from single impactor runs. The output forms available on call are cumulative mass loading versus $D_{50}$, $\Delta M/\Delta \log D$ versus geometric mean diameter, and $\Delta N/\Delta \log D$ versus geometric mean diameter as calculated in MPPROG. The latter are available on Stokes aerodynamic and aerodynamic impaction diameter bases. As an option, up to ten runs can be superimposed on a single plot. Plots and tabular output of the fitted curves from SPLIN1 are also available. The fitted curves from SPLIN1 are plotted superimposed on the data points from MPPROG, but only as single run plots. The plots are all made on log-log grids.

The tabular output includes cumulative percent mass loading less than particle diameter generated from the SPLIN1 fitted curves, $dM/d\log D$ versus particle diameter, and $dN/d\log D$ versus particle diameter generated by differentiation of the SPLIN1 fitted curves.

ANALYSIS OF GROUPED DATA

STATIS

STATIS is a program for combining data from multiple impactor runs under a common condition. The program tests data from a series of runs (specified by the user) for outliers, flags and

removes outliers from the set, and then provides output in the form of averaged size distributions with confidence intervals as desired in both tabular and graphical form. The program is set up to provide 50% confidence intervals; however, changes can be made for the calculation of other confidence intervals as desired (e.g., 90% or 95%).

The input data to STATIS are the fitted polynomial segments generated from MPPROG by SPLIN1 which now define the cumulative mass loadings for each run. The particle diameter basis for averaging (i.e., aerodynamic, aerodynamic impaction, Stokes) is user specified on control cards used to execute STATIS.

The fitting equations from SPLIN1 are differentiated at preselected particle diameters to obtain the quantity $(dM/dlogD_i)_j$ where i refers to particle diameter and j refers to the sequence number of a particular run in the set to be averaged. The values, at each particle diameter, $D_i$, are subjected to an outlier analysis based on the deviations of the values of dM/dlogD for individual runs from the mean for all runs.

The outlier test used is that for the "Upper 5% Significance Level". A curve fitted to the tabular list of critical values for excluding an outlier is used to generate the table. The test is based on the quantity

$\frac{|X_i - \bar{X}|}{S}$ being greater than a critical value, $C_n$, which is a function of the number of points in the data set.

$X_i$ = individual value

$\bar{X}$ = mean of all values

S = standard deviation of the data set.

The application of this test requires that there be three or more runs in the sequence to be averaged. This outlier test is repeated after discarding any outliers already identified, provided there are at least three runs remaining in the set of retained points.

After discarding outliers, a final average, standard deviation, and confidence interval are calculated for each $(dM/dlogD_i)$. These values are output on the line printer and are plotted on call by the user.

Cumulative size distributions on a mass basis or percentage basis are derived from the averaged dM/dlogD values by integration of these values. The choice of integrating the dM/dlogD curve rather than direct computation of the cumulative averages from the individual cumulative distributions was based on the

fact that an error in a single stage weight is propagated forward throughout the cumulative curve for all stages subsequent to the one on which the error occurred. This would cause substantial quantities of good data from other stages to be discarded by the outlier analysis. Integration of the averaged differential distribution, on the other hand, allows the data from the remaining, error free, stages to have their proper influence on the averaged cumulative distributions. These cumulative distributions are again output in tabular form and, on call, in graphical form.

The cumulative distributions can be obtained either including or excluding particles smaller than 0.25 μm in diameter. The option of excluding the particles smaller than 0.25 μm is made available because of the fact that in a significant percentage of sampling situations, impactor back up filter catches can be dominated by oversize particles because of bounce and/or reentrainment. This results in a filter weight gain which can be many times higher than the weight of the fine particles, which, ideally, should be the only material present. In those cases, omission of the material which is nominally smaller than 0.25 μm from the cumulative distributions will make the result a much better representation of the true size distribution. This, of course, is true only when the $D_{50}$ of the last impactor stage is about 0.25 to 0.5 μm as is usually the case with the commercially available impactors.

Standard deviations and confidence limits for the cumulative distributions are calculated from the approximation that the variance (and square of a confidence interval) for a sum, A + B, is given by the sums of the variances (and squares of the confidence intervals) for A and B separately, i.e.,

$$\text{Variance}_{A+B} = \text{variance}_A + \text{variance}_B$$

and

$$(\text{confidence interval})^2_{A+B} = (\text{confidence interval})^2_A + (\text{confidence interval})^2_B$$

The averaged differential size distributions generated by STATIS are stored in a disk file for use by the programs PENTRA or PENLOG in calculating control device fractional efficiency curves.

Tabular and graphical output from STATIS includes cumulative mass loading versus diameter, cumulative percentage on a mass base versus diameter, dM/dlogD versus diameter, and dN/dlogD versus diameter. The graphical presentations are made on log-log grids with the exception of the cumulative percentage plot which is made on a log-probability grid. All output forms, graphical and tabular, include confidence limits. The choice of diameter definition used is left to the user. An index of runs which

were rejected through the outlier analysis before averaging is also printed. Rejection at any one particle size does not result in the run being excluded at all particle sizes.

Programs PENTRA/PENLOG

These two programs are virtually identical and provide tabular and graphical output of control device penetration and/or efficiency versus particle size for a preselected series of particle sizes from about 0.25 to 20 μm. The only difference between the two programs is in the form of the graphical output. In the case of PENTRA, the fractional efficiency curves are presented on a log-probability grid while in PENLOG they are presented on a log-log grid.

The calculations are made from averaged sets of inlet and outlet data developed by STATIS. The user identifies the pair of averaged data sets from which the efficiency is to be calculated together with the diameter basis required (i.e., Stokes, aerodynamic, aerodynamic impaction). The program retrieves the appropriate averaged data sets and calculates the fractional efficiency as

$$\text{efficiency}_i(\%) = 1 - \left[\frac{(dm/d\log D_i)_{outlet}}{(dm/D\log D_i)_{inlet}}\right] \times 100$$

where i refers to the $i^{th}$ particle diameter in the preselected diameter sequence. Simultaneously, if both the inlet and outlet data sets included two or more runs, confidence limits are calculated based on a method described by Y. Beers.[4] The confidence level associated with the limits generated by the program as provided are 50% levels; however, other levels can be generated by simply changing values of three constants used to generate the appropriate t-table.

Test Cases and Exemplary Results

Tests of the final fitting process were made by generating fictitious impactor runs having known size distributions. These runs were generated by calculating the $D_{50}$'s associated with several sets of sampling conditions. The stage weights required to produce exact unimodal and bimodal log normal distributions were then generated for these sets of particle diameters. The program was exercised on these artificially constructed runs and results obtained from the fitting procedure were then compared to the original distributions. Figures 3 and 4 show examples of two such tests in the form of differential size distributions. Figure 3 illustrates the input distribution and recovered distribution for an aerosol having a mass median diameter of 4 μm and geometric standard deviation of 3.0. Recovered distributions from the spline fit and approximation results, $\Delta M/\Delta \log D$,

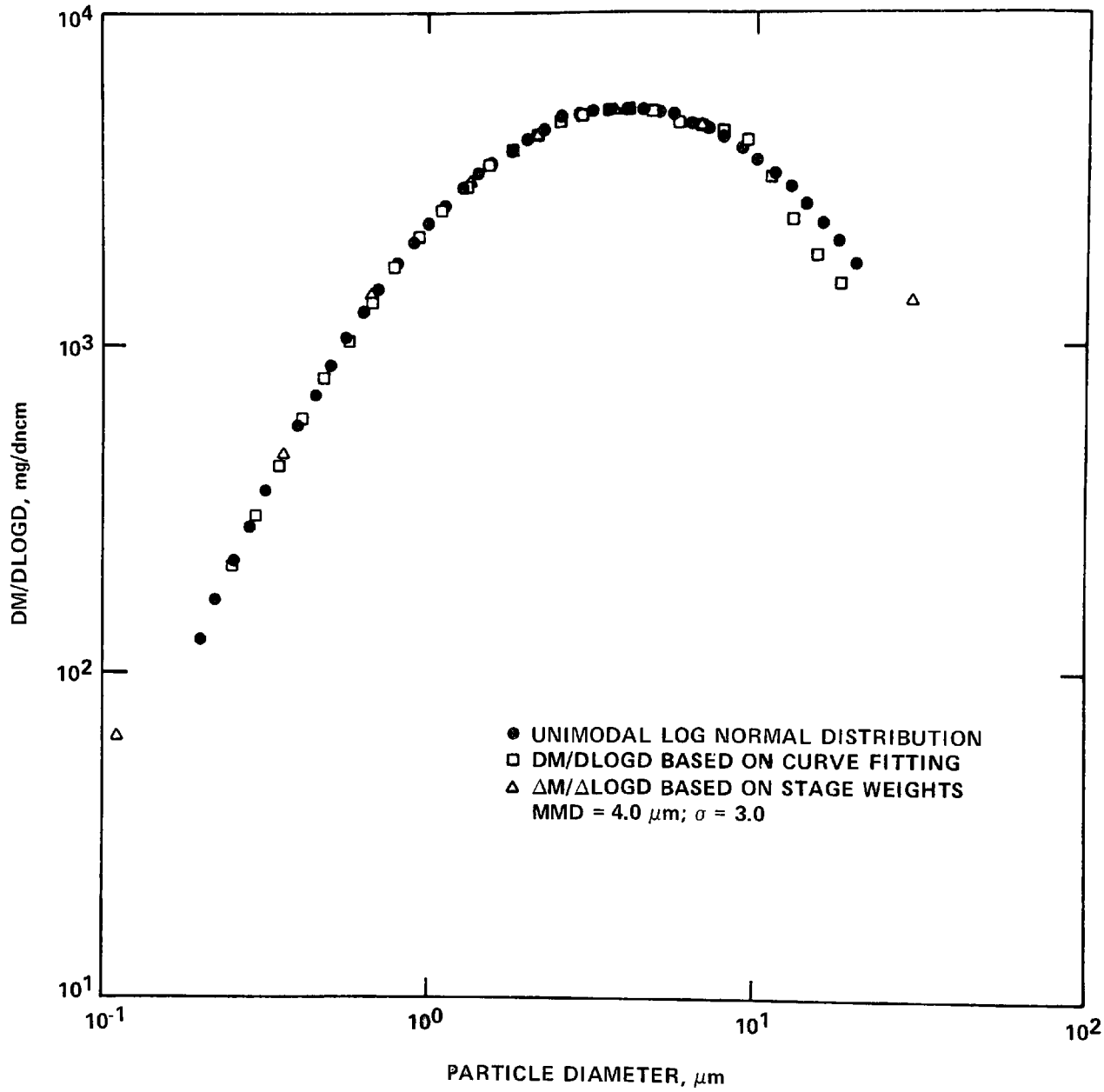


*Figure 3. Approximate differential size distribution based on stage weights and same distribution based on spline fitting are compared to a true unimodal log normal distribution.*

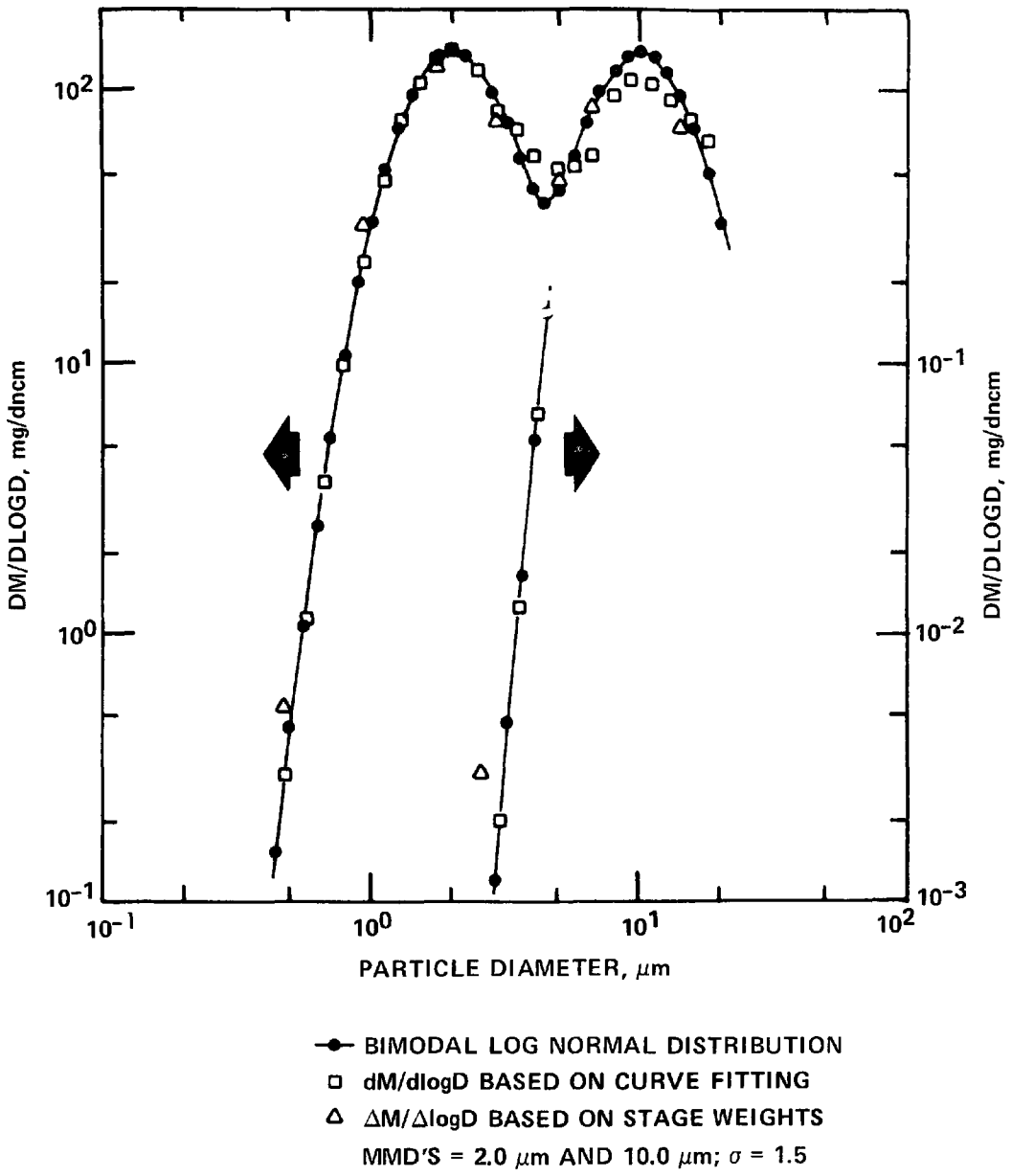


*Figure 4. Approximate differential size distribution based on stage weights and same distribution based on spline fitting are compared to a true bimodal log normal distribution.*

taken directly from the stage weights both show excellent agreement with the input distribution. The fitted results for diameters larger than 7 μm represent an extrapolation to sizes larger than the first stage $D_{50}$. Figure 4 illustrates a similar test for a bimodal distribution having equal amplitude modes, mass median diameters of 2 μm and 10 μm, and geometric standard deviations of 1.5. Again, beyond about 7 μm, the fitted points represent extrapolations. Note that the $\Delta M/\Delta \log D$ approximations derived directly from the stage weights lie very close to the input curve in regions where the slopes are not large but fall significantly above the true curve in regions of high slope. Errors expressed as percentage deviations from true values are shown for two cases each for unimodal MMD = 4, $\sigma g$ = 2, and bimodal MMD = 2, $\sigma g$ = 1.5, and MMD = 10, $\sigma g$ = 1.5 distributions in Figures 5 and 6. Note that the results from the fitted curves generally fall within ±10% or better of the true values in the size interval covered by the impactor stage $D_{50}$'s and are for the most part within ±50% of the true values in the extrapolation region above the first stage $D_{50}$. Much larger errors occur with the $\Delta M/\Delta \log D$ approximations to the differential distributions obtained directly from the stage weights. The errors shown in Figures 5 and 6 result only from the fitting procedure and do not include any effects from non-ideal behavior in the impactors. Errors arising from the latter can be much greater, as described by McCain and McCormack.[5]

Examples of some of the graphical output formats available from the program are shown in Figures 7 through 10. Figure 7 illustrates a single run cumulative mass distribution with the original data points and fitted curve from SPLIN1. Figure 8 shows the differential distribution obtained for the run shown in Figure 7. Figure 9 illustrates a cumulative mass distribution on a percentage basis with confidence limits obtained from the average of several runs similar to that shown in Figures 7 and 8. Figure 10 illustrates a control device penetration curve with confidence limits obtained from sets at averaged inlet and outlet runs.

## SUMMARY AND CONCLUSIONS

CIDRS represents a powerful, versatile tool for reducing and managing data obtained with cascade impactors. It provides the capability for single and multiple run data analysis with varying degrees of smoothing of single run data available and averaging and statistical analysis of multiple runs. Results from the program are not biased by forced fits to arbitrary distribution forms. Finally, the program makes possible a very significant time saving in handling and processing field data obtained with cascade impactors.

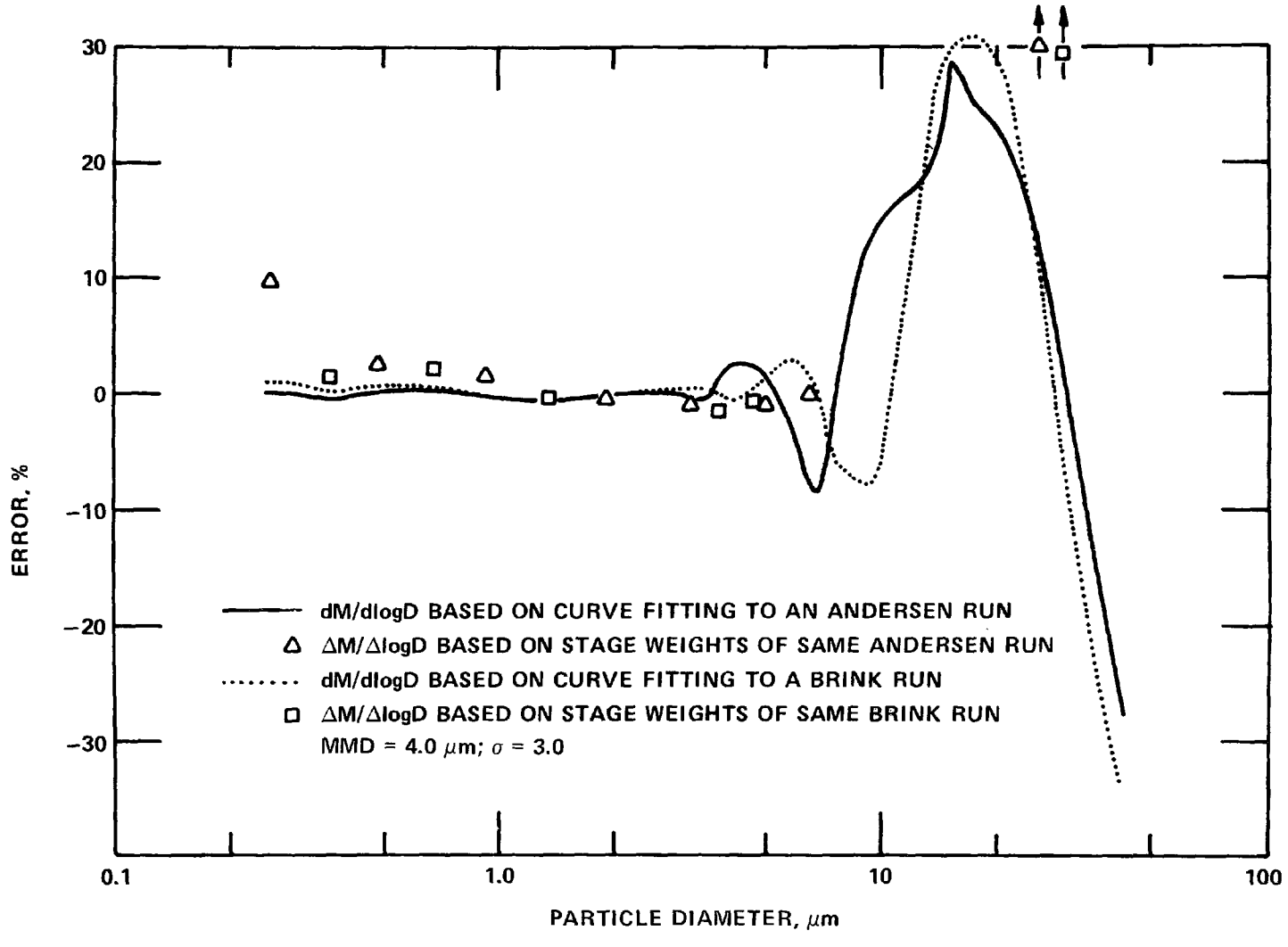


*Figure 5. Percent error of approximate differential size distributions based on stage weights and the same distributions based on spline fitting from a unimodal log normal distribution.*

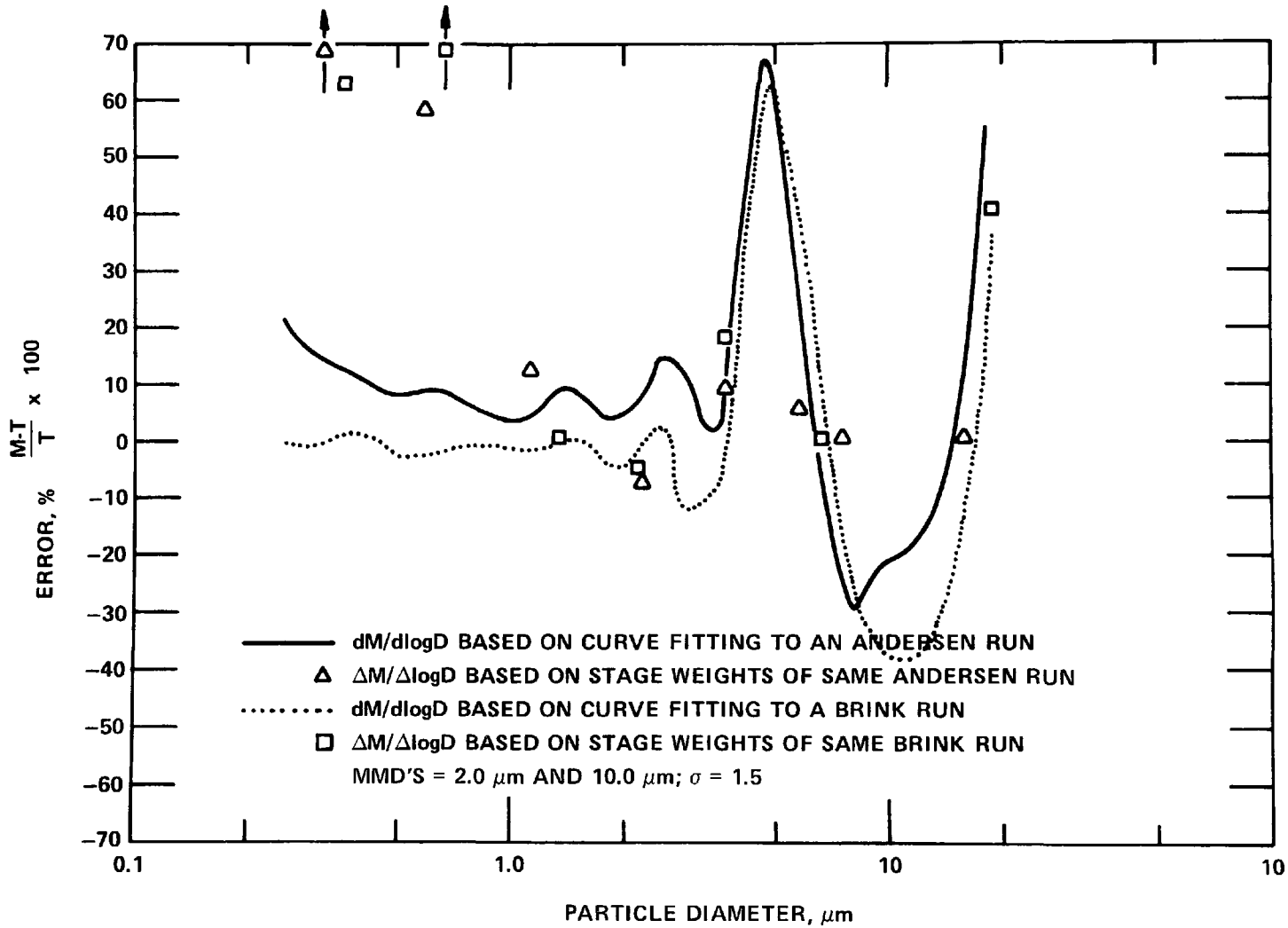


*Figure 6. Percent error of approximate differential size distributions based on stage weights and the same distributions based on spline fitting from a bimodal log normal distribution.*

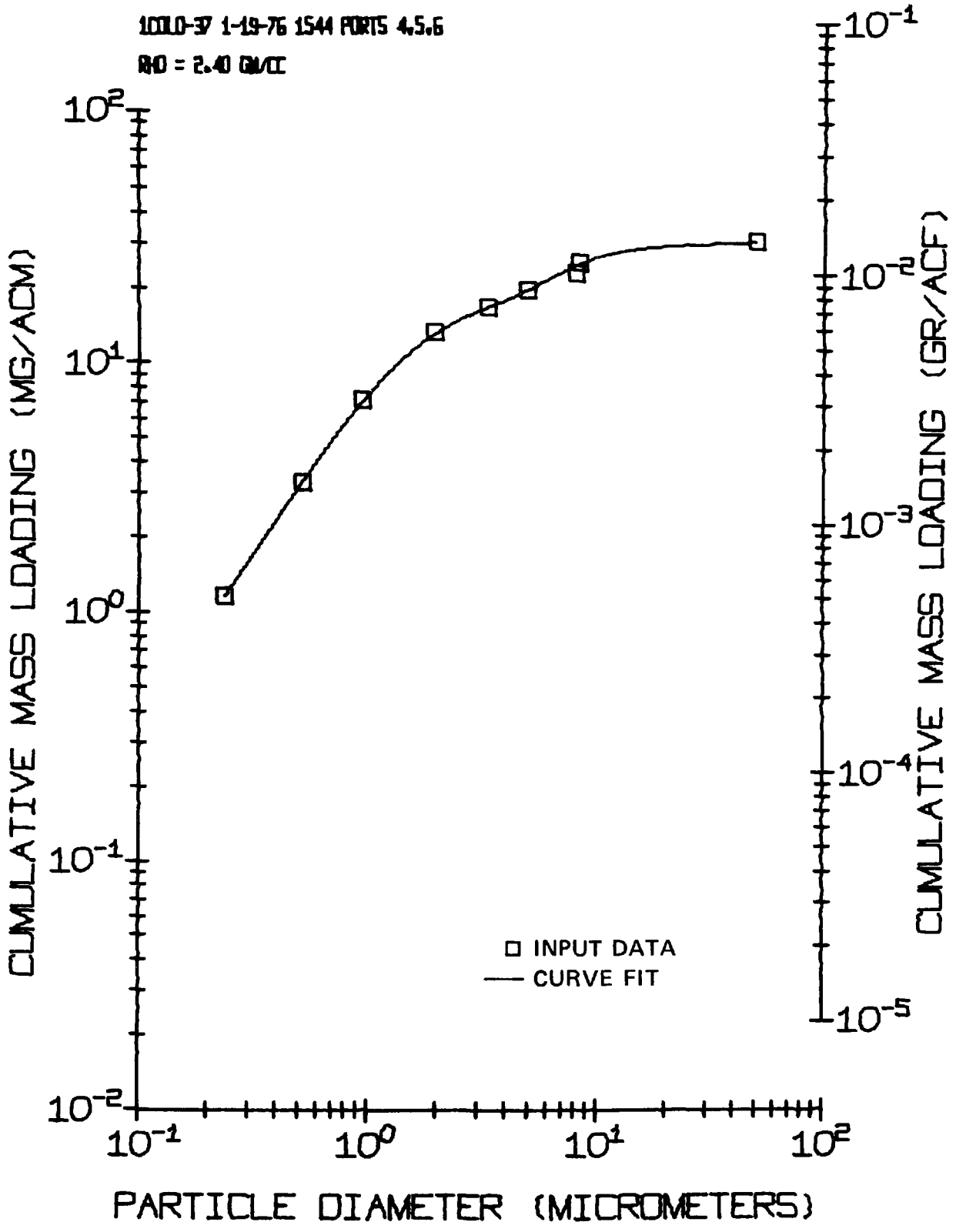


*Figure 7. Single run cumulative mass distribution with original data points based on stage weights and fitted curve from SPLIN1.*

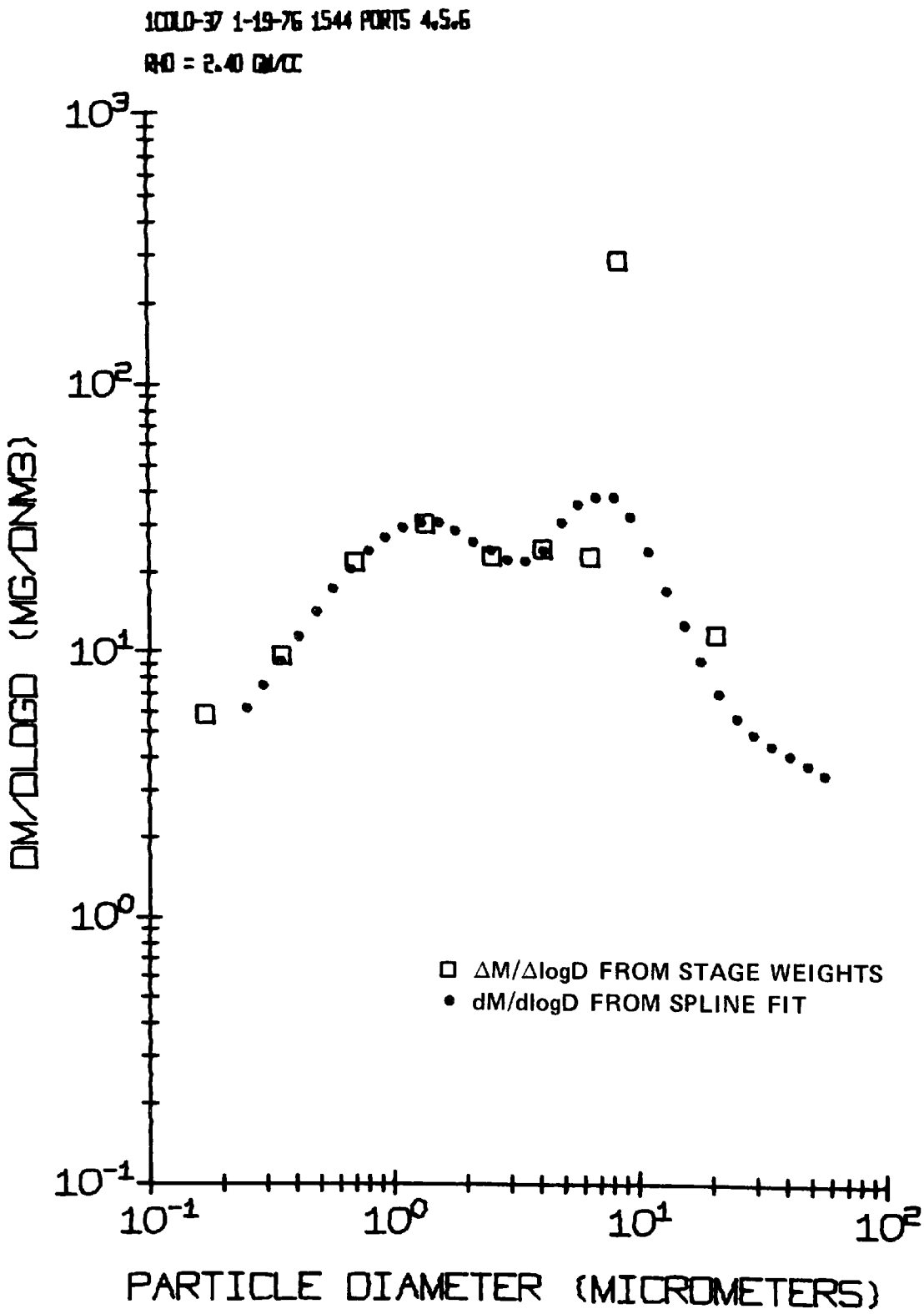


*Figure 8. Differential size distribution obtained for the run in Figure 7 based on stage weights and based on curve fitting.*

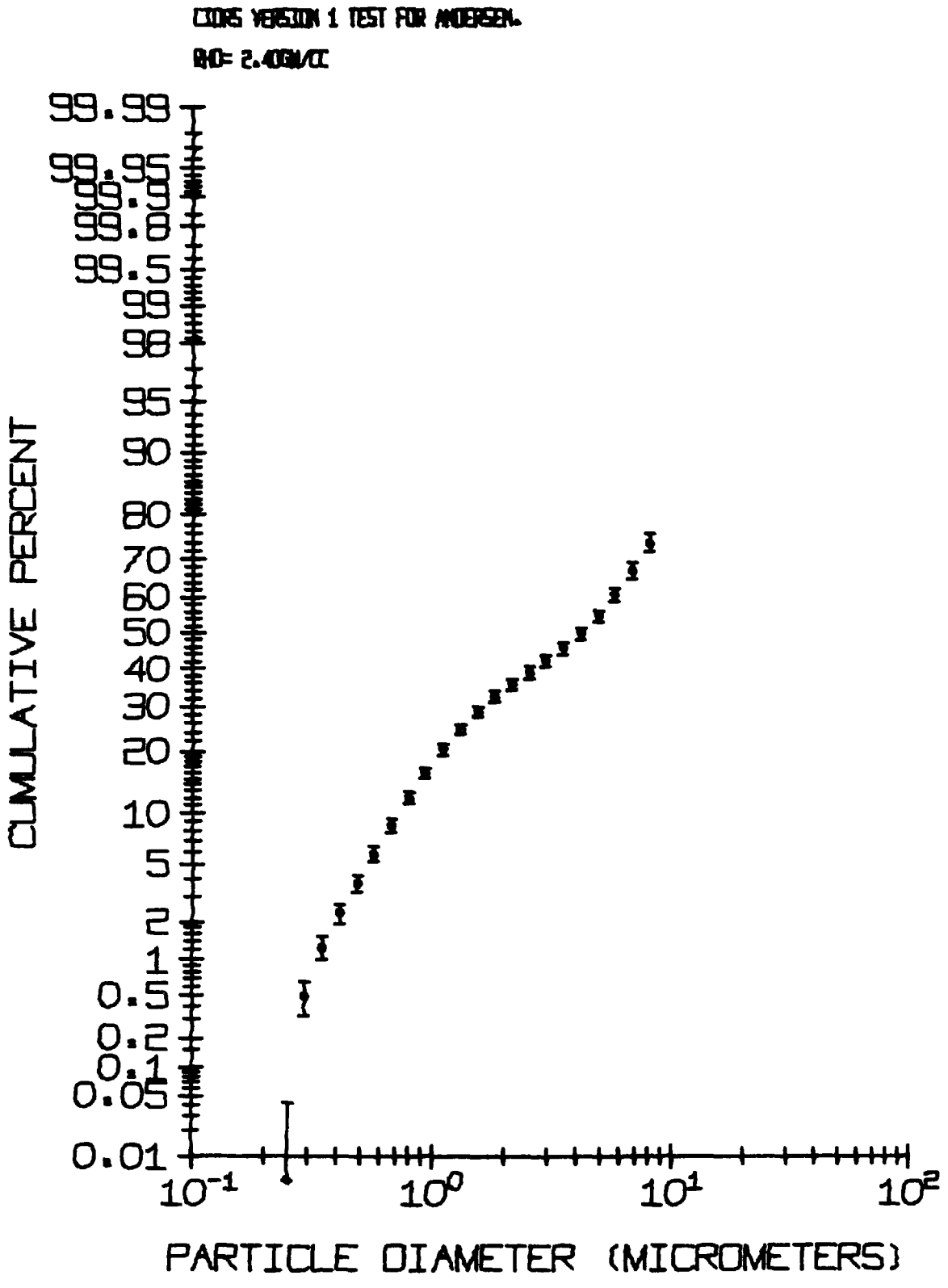


*Figure 9. Cumulative mass distribution on a percentage basis with confidence limits obtained from the average of several runs similar to that shown in Figures 7 and 8.*

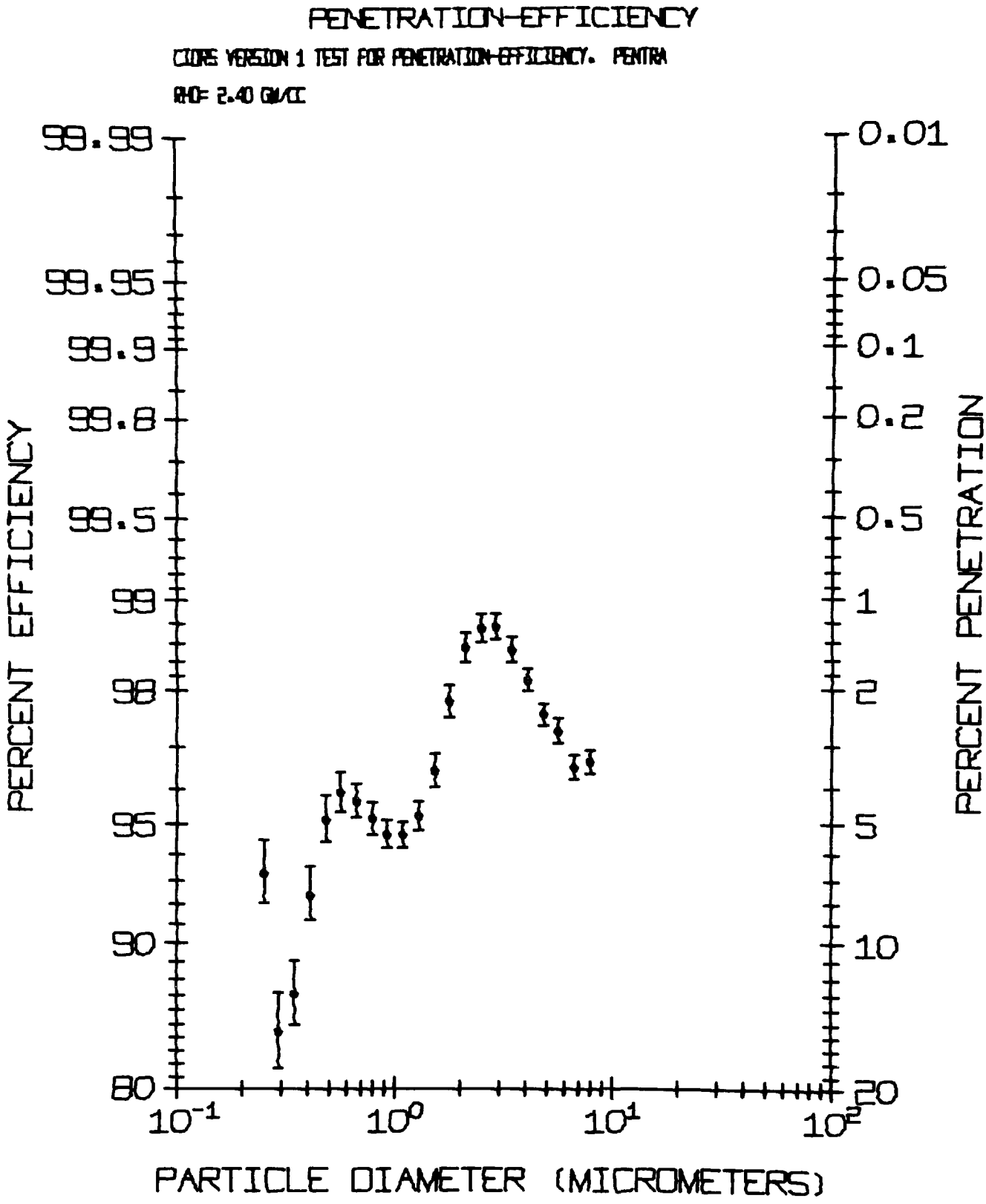


*Figure 10. A control device penetration curve with confidence limits obtained from sets of averaged inlet and outlet runs.*

ACKNOWLEDGEMENTS

This work was conducted under U.S. Environmental Protection Agency contracts 68-02-0273 and 68-02-2131. The continued support and assistance of Dr. D.B. Harris, the EPA project officer on these contracts is gratefully acknowledged. Additional appreciation is also expressed to Mr. B. Gaston and Ms. A. Henry for their assistance with the programs; to Mr. K. Cushing whose earlier program was used as a basis for program MPPROG; and Dr. W.B. Smith for his assistance and guidance during the program development.

REFERENCES

1. Morrow, P.E. Deposition and Retention Models for Internal Dosimetry of the Human Respiratory Tract. Health Phys. 12:173-208, 1966.

2. Mercer, T.T., M.I. Tillery, and H.Y. Chow. Operating Characteristics of Some Compressed Air Nebulizers. J. Amer. Ind. Hyg. Assoc. 29:66-78, 1968.

3. Quality Assurance Handbook for Air Pollution Measurement Systems, Vol. 1. Principles. EPA-600/9-76-005, U.S. Environmental Protection Agency, Research Triangle Park, NC, 1976.

4. Beers, Y. Introduction to the Theory of Error. 2nd Edition. Addison-Wesley, Reading, MA, 1957.

5. McCain, J.D., and J.E. McCormack. Non-ideal Behavior in Cascade Impactors. Paper 77-35.3, 70th Annual Meeting, APCA, Toronto, 1977.

PAPER 12

# AEROSOL GENERATION AND CALIBRATION OF INSTRUMENTS

DAVID Y.H. PUI
BENJAMIN Y.H. LIU
MECHANICAL ENGINEERING DEPARTMENT
UNIVERSITY OF MINNESOTA

## ABSTRACT

Standardization and calibration of aerosol measuring instruments generally require the use of monodisperse aerosols. In this paper, a review is first given of various aerosol generators that can be used for instrument standardization and calibration. The basic principles of several generators are described which can be used for producing monodisperse aerosols of primary standard quality and polydisperse aerosols of high concentration stability. Particular attention is devoted to the aerosol generators developed at the Particle Technology Laboratory, University of Minnesota; these include the vibrating orifice monodisperse aerosol generator, the mobility classifier monodisperse aerosol generator, the ultrafine condensation monodisperse aerosol generator, and the constant output atomizer aerosol generator. With the use of these generators, monodisperse and polydisperse aerosols can be generated from 0.002 μm to 50 μm in diameter at various concentration levels up to $10^6$ particles/$cm^3$ in certain size ranges. Further, the particle size and concentration from the monodisperse aerosol generators are known to a high degree of accuracy (2% for size and 5% for concentration). The accuracy has been verified by using independent microscopic and other particle sizing and counting techniques.

In addition, the paper reviews various aerosol measuring and sampling devices that have been calibrated by means of the monodisperse aerosol standards. These include the diffusion battery, the condensation nuclei counter, the electrical aerosol analyzer, the optical particle counter and the inertial impactor. The calibration procedures, precautions, and results are briefly outlined. In addition, comparative studies for some of the calibrated instruments are described. It is shown that good agreement can be obtained when the instruments are properly calibrated and standardized.

## INTRODUCTION

Recent advances in experimental aerosol science and instrument development have made possible the rapid, in situ measurement of particle size distribution. Instruments are now available for size determination of aerosols from 0.002 to over 50 μm in diameter. The successful application of these instruments to experimental aerosol studies requires that the instrument be properly standardized and calibrated. A well-calibrated instrument is essential for the correct interpretation of experimental data, and for obtaining the highest possible accuracy from a given device.

Standardization and calibration of aerosol measuring instruments can best be accomplished by the use of monodisperse aerosols. The size, and sometimes the concentration, of the calibrating aerosol must also be known to a sufficiently high degree of accuracy. The quality of the calibration is often dependent upon the quality of the calibrating aerosol used and the accuracy to which the particle size and concentration are known. Figure 1 shows the size range of some of the commonly used aerosol size distribution measuring instruments, and the size range and other pertinent characteristics of the monodisperse aerosol generation techniques that can be used for instrument calibration.

## AEROSOL GENERATION

### Monodisperse Aerosol Generation Techniques Available Before 1970

Prior to 1970, the most commonly used techniques for generating monodisperse aerosols for instrument calibration and experimental aerosol studies were the condensation aerosol generator of La Mer and Sinclair[1] and the several variations of this generator as reported by Rapaport and Weinstock,[2] Liu et al.,[3] and others;[4-6] and the spinning disc aerosol generator as originally reported by Walton and Prewett[7] and May,[8] and subsequently by others.[9-13] These aerosol generators are capable of generating aerosols of a moderate degree of monodispersity ($\sigma_g \simeq 1.10$). However, both the size and the concentration of the aerosol must be determined by an independent technique, such as electron or optical microscopy. Therefore, the accuracy of the aerosol particle size and concentration is limited by the accuracy of the size and concentration measuring techniques used, which is often not very high due to the inherent limitation of the technique itself, the tedious nature of the process involved, or the requirement of high operator skill.

A relatively simple technique of generating a monodisperse aerosol of a known size is that based on the use of monodisperse suspensions of polystyrene and other latex spheres available from Dow Diagnostics (P.O. Box 68511, Indianapolis, IN 46268). These spheres are prepared by an emulsion polymerization process

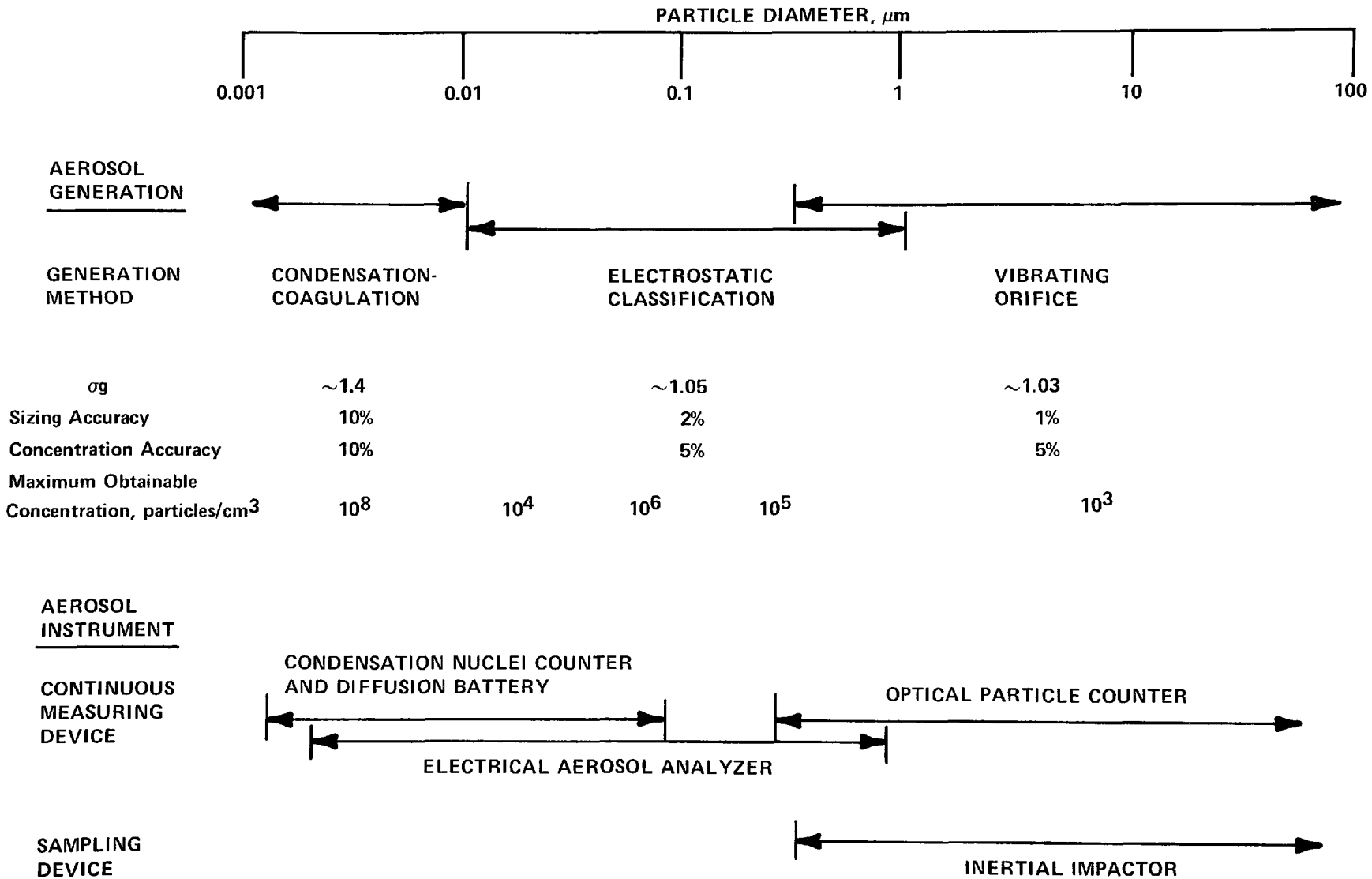


*Figure 1. Size range of aerosol generation, measuring, and sampling devices.*

and are very uniform in size, with $\sigma_g$ generally less than 1.06. Both the size and the $\sigma_g$ of the particles are determined by the manufacturer by electron microscopy. Although these particles are widely used in several applications, for example, in calibrating optical particle counters, there are several problems associated with the use of these particles which are worth pointing out.

One problem results from the fact that the latex particles in liquid suspension must be aerosolized, which is usually done by means of an atomizer. During the atomization process, a large number of empty water droplets are produced, along with those containing the latex spheres. When these empty droplets are evaporated, residue particles are formed from the dissolved impurity in the liquid. The residue particles are usually orders of magnitude higher in concentration than the primary latex spheres (see Whitby and Liu[14]; Langer and Lieberman[15]). Thus, the use of the latex aerosol for instrument calibration is limited to those calibrations for which the presence of the residue particles is unimportant. For example, the latex aerosol can be used for calibrating optical particle counters, which generally do not respond to the residue particles. However, it cannot be used to calibrate the electrical aerosol analyzer or the condensation nuclei counter, both of which are sensitive to the small residue particles present.

For a detailed discussion of the various aerosol generating techniques including those described above, the reader is referred to the review papers by Fuchs and Sutugin[16] and Raabe.[17]

## Modern Techniques for Generating Monodisperse Aerosols--Generation of Monodisperse Aerosol Standards

A new generation of monodisperse aerosol generators has been developed during the past few years, primarily as a result of research at the Particle Technology Laboratory, University of Minnesota. The aim of this research was to develop generators for producing monodisperse aerosols of a known size and/or concentration, which can be used as standards of calibration for aerosol instruments and for general aerosol research. As a result of this research, solid and liquid aerosols of extremely narrow size distributions can now be generated. Further, the size and concentration of the monodisperse aerosol generated can be calculated to a high degree of accuracy from the basic generator operating conditions. The monodisperse aerosols generated by these devices can be referred to as "aerosol standards". The particle size range and other pertinent characteristics of these aerosol generators have been summarized in Figure 1, mentioned earlier.

Vibrating Orifice Monodisperse Aerosol Generator--

For generating monodisperse aerosols in the size range from 0.5 μm to over 50 μm, a vibrating orifice monodisperse aerosol generator has been developed by Berglund and Liu.[18] The generator is based on the instability and uniform break-up of a liquid jet under periodic mechanical disturbance. The generator, shown schematically in Figure 2, is composed of a droplet generation and dispersion system and an aerosol dilution, neutralization, and transport system.

To generate an aerosol with this system, the material to be aerosolized is first dissolved in a suitable solvent, e.g., NaCl in water, or DOP or other oil in alcohol. The solution is then supplied to the droplet generator by a syringe pump. In the droplet generator, the liquid flows through a small (5, 10 or 20 μm diameter) orifice, which is vibrated by a piezoelectric ceramic. The liquid jet is broken up by this vibration into uniform droplets which are then quickly dispersed by a turbulent air jet. The dispersed droplets are then mixed with a much larger volume of filtered dry air to evaporate the solvent from the solution droplets. The monodisperse aerosol formed is then passed through a vertical drying column containing a radioactive $^{85}Kr$ source for neutralizing the particle electrostatic charge. The monodisperse aerosol is then ready for use.

The diameter, $D_p$, of the aerosol produced by the vibrating orifice generator can be calculated from the equation

$$D_p = (6Q_\ell C_v/\pi f)^{1/3} \tag{1}$$

where $Q_\ell$ is the liquid solution flow rate through the orifice, $C_v$ is the volumetric concentration of the non-volatile solute in the solvent, and f is the vibrating frequency. The quantities $Q_\ell$, $C_v$, and f can all be measured accurately. The overall uncertainty of the calculated particle size is about 1%. Further, since the rate of droplet production is equal to the vibrating frequency, the theoretical particle concentration, $N_{th}$, is given by

$$N_{th} = f/Q_a \tag{2}$$

where f is the vibrating frequency and $Q_a$ is the total air flow in the drying column. The actual concentration is slightly less than the theoretical concentration because of particle loss in the system. When the losses are properly determined, the generator can be used as a secondary concentration standard with uncertainty of about 5%. The operating conditions of the generator are summarized in Table 1.

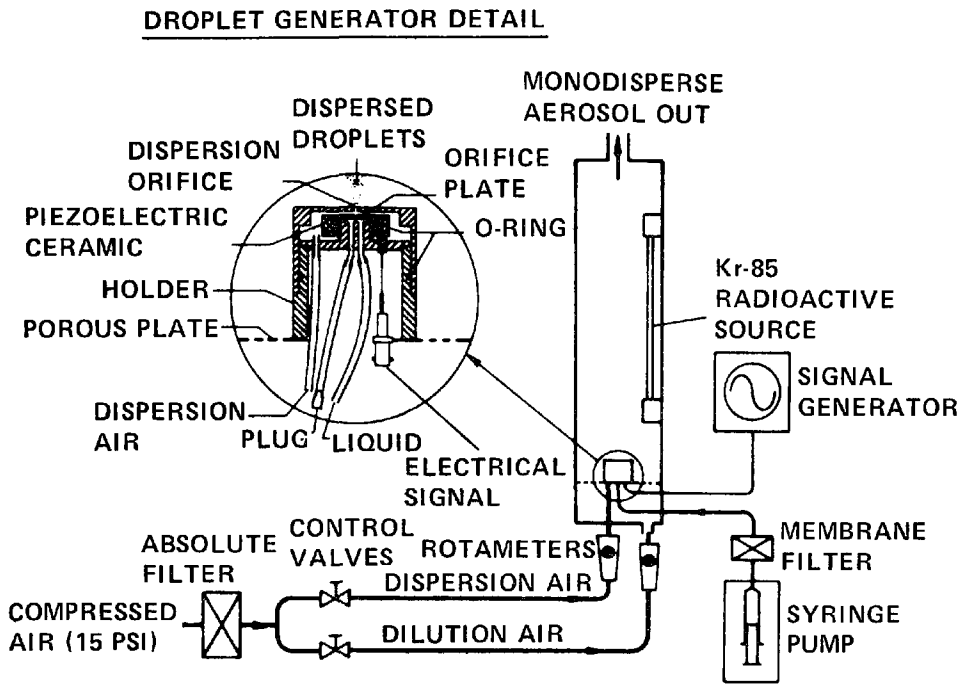


*Figure 2. Schematic diagram of the vibrating orifice monodisperse aerosol generator.*

Some of the operating precautions that must be observed in order to use equation (1) for calculating particle size have been discussed by Liu:[19]

(1) There must be no leak in the liquid flow system;

(2) the solvent used must contain a negligible amount of non-volatile impurity;

(3) the solvent must be completely evaporated from the solution droplets; and

(4) the density of particles must be the same as the intrinsic density of the material.

Generation of Monodisperse Aerosols by Mobility Classification--

For producing submicron monodisperse aerosol standards in the size range between 0.01 to 1.0 μm, a mobility classifier monodisperse aerosol generator has been developed by Liu and Pui.[20] The method is based on the monotonic relationship between the electrical mobility of a singly charged particle and particle size. For particles in the submicron size range, an aerosol in charge equilibrium with bipolar ions will acquire a bipolar charge distribution with most of the particles either electrically neutral or carrying only ±1 elementary unit of charge (see Liu and Pui[21]). By passing this charge equilibrated aerosol through a mobility classifier, a monodisperse fraction can be extracted

TABLE 1. CHARACTERISTICS OF THE VIBRATING ORIFICE MONODISPERSE AEROSOL GENERATOR (MODEL 3050 BERGLUND-LIU MONODISPERSE AEROSOL GENERATOR, TSI, INC., P.O. BOX 3394, ST. PAUL, MN 55165)

| Diameter of liquid orifice, μm | Nominal frequency, kHz | Droplet diameter, μm[a] | Particle diameter, range, μm[b] | Nominal concentration, particles/cm$^3$[c] |
|---|---|---|---|---|
| 5 | 450 | 15 | 0.6 - 15 | 273 |
| 10 | 225 | 25 | 1.0 - 25 | 137 |
| 20 | 60 | 40 | 1.8 - 40 | 36 |

[a] Continuously adjustable over an approximate 25% range by varying the frequency.

[b] Obtainable by the solvent evaporation technique.

[c] Theoretical concentration based on the nominal aerosol output of 100 liters per minute.

according to electrical mobility. The generator, shown schematically in Figure 3, consists of an atomizer, a diffusion dryer, a $^{85}Kr$ "neutralizer", a differential mobility analyzer, and an electrometer current sensor.

To generate a monodisperse aerosol with this system, a polydisperse aerosol is first produced by spraying a liquid solution with the atomizer and drying the particles with the diffusion dryer. The aerosol is then passed through the $^{85}Kr$ "neutralizer" to obtain a Boltzmann equilibrium charge on the aerosol particles.[22] This aerosol is then classified electrostatically by the differential mobility analyzer.

The differential mobility analyzer, described in detail by Liu and Pui[20] and by Knutson and Whitby,[23] is in the form of two concentric metal cylinders. Aerosol and clean air are introduced into the apparatus near the top and flow down the annular gap space between the cylinders in the form of laminar streams. A dc voltage is applied to the inner cylinder--the collector rod--and the outer cylinder is grounded. The applied dc voltage causes particles of the opposite polarity to be attracted to the collector rod, and those that have the correct mobility, and hence the particle size, will be attracted to the

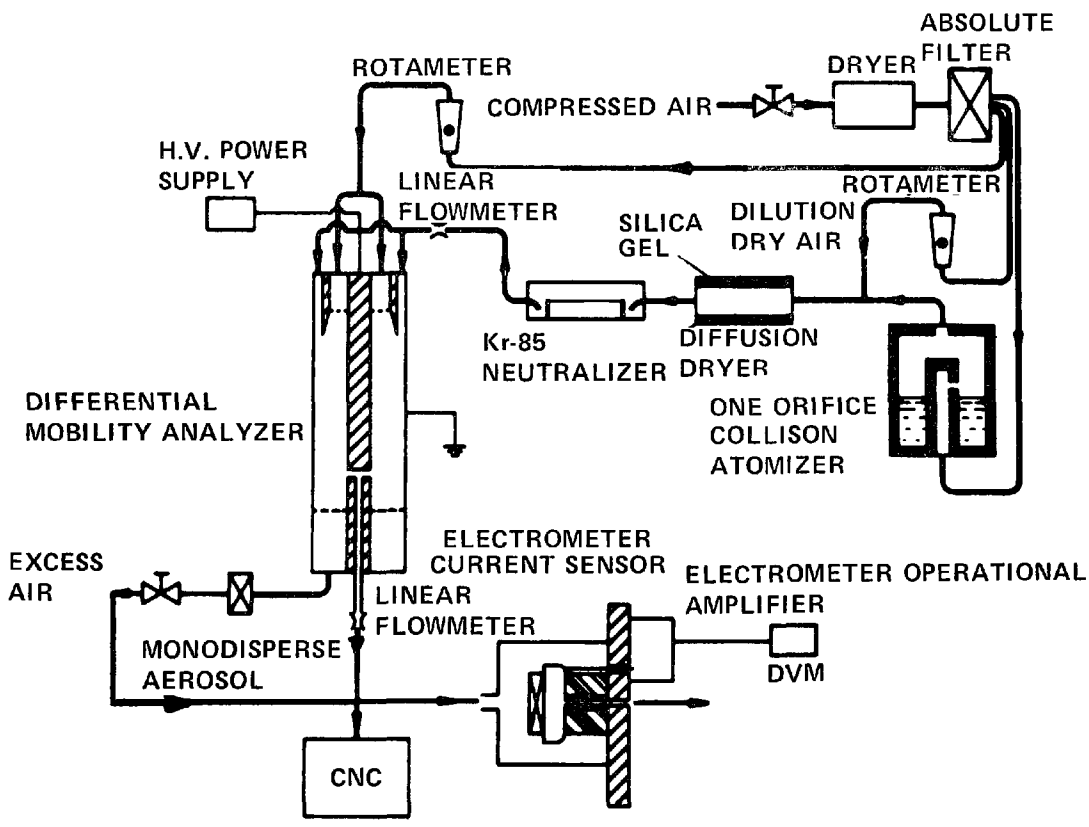


*Figure 3. Schematic diagram of the mobility classifier monodisperse aerosol generator.*

vicinity of the slit where they are swept out by the small air stream flowing through the slit. The mean electrical mobility of the particles extracted by the device, $Z_p$, can be calculated from the operating conditions and the dimensions of the analyzer by the equation

$$Z_p = \left[ q_c + \frac{1}{2}\left(q_a - q_s\right) \right] \frac{\ln(r_2/r_1)}{2 \pi V L} \tag{3}$$

where $q_c$ is the flow rate of clean sheath air in the mobility analyzer, $q_a$ is the flow rate of the polydisperse aerosol entering the analyzer, $q_s$ is the flow rate of the monodisperse aerosol leaving the analyzer, $r_1$ and $r_2$ are the inner and outer radii of the annular gap space in the analyzer, L is the length of the collector rod between the aerosol entrance and the exit slit, and V is the applied voltage on the collector rod. Knowing the aerosol mobility from the above equation, the particle diameter, $D_p$, can then be calculated as follows:

$$D_p = \frac{e\ C}{3\ \pi\ \mu\ Z_p} \tag{4}$$

where e is the elementary unit of charge, C is the slip correction for the particle, and $\mu$ is the gas viscosity. An accuracy of 2% in the calculated particle diameter can be achieved upon carefully measuring the flow rates, the voltage, and the dimensions of the mobility analyzer.

In addition to providing a standard for particle size, the mobility classifier also provides a standard for particle concentration. This is based on the fact that the particles leaving the analyzer are predominantly singly charged. By sampling these particles into a Faraday cup and measuring the corresponding current flow, I, the particle concentration, N, can be calculated as follows:

$$N = (I\ /\ e\ q_e)\ K \tag{5}$$

where $q_e$ is the aerosol flow rate into the Faraday cup (the electrometer current sensor shown in Figure 3) and K is a factor near unity to correct for the presence of multiply charged particles in the output aerosol stream. Using a high sensitivity electrometer (Cary 401 vibrating reed electrometer, Varian Instrument Division, 611 Hansen Way, Palo Alto, CA 94303), currents as small as $10^{-16}$ A can be measured. Using the standard aerosol flow rate of $q_e$ = 22 ℓpm, particle concentrations as low as 2 particles/cm$^3$ can be determined. The accuracy in the measured particle concentration, after making a small correction for the interference effect of multiply charged particles (see the last column of Table 2 for the value of the correction factor, K), is about 5%. Other characteristics of the aerosol generator are summarized in Table 2.

TABLE 2. CHARACTERISTICS OF THE MOBILITY CLASSIFIER GENERATOR FOR PRODUCING SUBMICRON AEROSOL STANDARDS (MODEL 3071 ELECTROSTATIC CLASSIFIER, TSI, INC., P.O. BOX 3394, ST. PAUL, MN 55165)

| Output aerosol | | Input aerosol[a] | | Operating conditions of mobility analyzer | | | |
|---|---|---|---|---|---|---|---|
| Diameter, μm | Nominal maximum concentration, $cm^{-3}$ | Material | Solution concentration, % by wt | Flow rate, $q_c$ ℓpm[b] | Collector Rod voltage, V[c] U of M | TSI | K factor[d] |
| 0.013 | 5,000 | NaCl | 0.005 | 20 | 65 | 71 | 1.0 |
| 0.018 | 10,000 | NaCl | 0.01 | 20 | 123 | 134 | 0.99 |
| 0.024 | 50,000 | NaCl | 0.05 | 20 | 215 | 234 | 0.98 |
| 0.032 | 150,000 | NaCl | 0.1 | 20 | 373 | 406 | 0.96 |
| 0.042 | 300,000 | NaCl | 0.5 | 20 | 624 | 680 | 0.93 |
| 0.056 | 600,000 | NaCl | 1.0 | 20 | 1064 | 1159 | 0.90 |
| 0.075 | 600,000 | NaCl | 1.0 | 20 | 1807 | 1968 | 0.86 |
| 0.10 | 80,000 | DOP | 0.01 | 20 | 2994 | 3260 | |
| 0.13 | 80,000 | DOP | 0.04 | 20 | 4660 | 5075 | |
| 0.18 | 100,000 | DOP | 0.1 | 7 | 2750 | 2995 | |
| 0.24 | 200,000 | DOP | 0.6 | 7 | 4243 | 4620 | |
| 0.32 | 150,000 | DOP | 0.8 | 7 | 6381 | 6949 | |
| 0.42 | 40,000 | DOP | 1.0 | 7 | 9174 | 9990 | |

[a] The input aerosol to the generator is obtained by atomizing an NaCl solution at the indicated concentration with a Collison atomizer operating at 241 kPa, or in the case of the DOP aerosol, obtained by the use of the vaporization-condensation technique described by Liu and Lee.[24] $\sigma_g \simeq 2$ for the NaCl aerosol and $\sigma_g \simeq 1.2$ for the DOP aerosol.

[b] $q_c$ is the clean sheath air flow in the mobility analyzer. Other flows are: $q_a = q_s \simeq 0.1\ q_c$, where $q_a$ = flow rate of the polydisperse aerosol at input and $q_s$ = flow rate of the output monodisperse aerosol.

[c] The collector rod voltage given is based on the following dimensions:

U of M prototype: $r_1 = 0.950$ cm, $r_2 = 1.907$ cm, L = 45.52 cm
TSI Model 3071: $r_1 = 0.937$ cm, $r_2 = 1.958$ cm, L = 44.44 cm

and assuming T = 21°C and P = 1 atmosphere.

[d] K is a correction factor to account for the effect of doubly charged particles in the calibration of condensation nuclei counters. K is the ratio of the actual particle concentration and the nominal concentration calculated by assuming all particles are singly charged.

In order to obtain a monodisperse aerosol with the above stated accuracies in particle size and concentration, several conditions must be met:

(1) The number median diameter of the polydisperse aerosol at the classifier input should be kept equal to or smaller than the desired diameter of the output monodisperse aerosol.

(2) The $^{85}Kr$ "neutralizer" should have sufficient radioactivity and neutralizing volume to insure that the input aerosol is at Boltzmann charge equilibrium.

(3) For generating particles with diameter larger than 0.08 μm, the $\sigma_g$ of the input aerosol should not exceed 1.4.

(4) The flow must be laminar in the mobility analyzer, and the flow ratio, $(q_a+q_s)/q_c$, should be kept small.

(5) Conducting tubing should be used to transport charged particles in the monodisperse output aerosol stream and, in addition, the charged particles must be neutralized before being introduced into the test instruments.

Conditions (1), (2), and (3) are necessary in order to reduce to a minimum the concentration of the multiply charged particles of a larger particle size that have the same electrical mobility as the primary singly charged particles.

Condition (1) can be met by using the proper solution concentration in the atomizer for generating the input polydisperse aerosols. The solution concentrations to be used with the Collison atomizer to obtain the indicated number median diameters are shown in Table 2. In no case should a more concentrated solution be used, since this would lead to a higher proportion of multiply charged particles in the output aerosol.

In the case of condition (2), the criteria described by Liu and Pui[22] can be followed to design the charge neutralizer to obtain Boltzmann equilibrium on the input polydisperse aerosol.

In the case of condition (3), moderately monodisperse aerosols, such as those produced by the condensation aerosol generator can be used.[24]

Condition (4) is necessary in order to reduce the range of mobility, and consequently the range of particle diameters passing through the classifier. To maintain laminar flow in the analyzer, the critical Reynolds number should not be exceeded and the flow rates $q_a$ and $q_c$ must have the proper ratio.

Condition (5) is necessary in order to avoid particle precipitation due to charge build-up on insulating tubing. Preferably, metal tubing should be used to transport the charged particles. If plastic tubing is to be used, the tubing should be rinsed with a detergent or glycerine solution in order to form a conductive layer on the inside surface.

Generation of Ultrafine Monodisperse Aerosols--

An aerosol generator is currently under development at the Particle Technology Laboratory for producing monodisperse aerosol below 0.01 μm in particle diameter.[25,26] The generation method is based on the rapid condensation of NaCl vapor in a cold air stream and the controlled coagulation of the resulting ultrafine aerosol. The aerosol generator, shown schematically in Figure 4, consists of two major components: the droplet generation-vaporization section and the aerosol condensation-coagulation section.

To generate an aerosol with this system, an NaCl solution of known concentration is atomized with the liquid atomizer to form a polydisperse spray. The spray is then passed through the diffusion dryer to evaporate the water from the droplets. The aerosol then enters the evaporating tube in which the NaCl particles are vaporized. The vapor is then injected into the mixing nozzle, where it encounters a cold, primary dilution air supplied to the nozzle from a filtered, dry compressed air source. The rapid mixing of the vapor and the primary dilution air causes a fine NaCl aerosol to be formed. This aerosol is then allowed to coagulate and grow under controlled conditions. It is subsequently mixed with a large volume of secondary dilution air to "freeze" the particle size distribution and to transport the aerosol to the testing instruments. Particles as small as 0.003 μm have been generated with this system.

Aerosol Generators of High Stability

Several aerosol generators of high stability have been developed for use in a variety of aerosol studies. These include the constant output atomizer[24] for filtration, electrostatic precipitation and other laboratory aerosol studies, the sulfuric acid aerosol generator[27] for studying the health effect of sulfuric acid aerosol particles, and the constant-feed fluidized-bed dust generator[28] for generating coal dust and other solid particles for use in instrument calibration and other studies. Only the constant output atomizer described by Liu and Lee[24] will be further considered below.

The constant output atomizer is shown schematically in Figure 5. The generator makes use of a syringe pump to provide a constant flow of liquid to a pneumatic atomizer to achieve a stable aerosol output. In the conventional atomizer, the

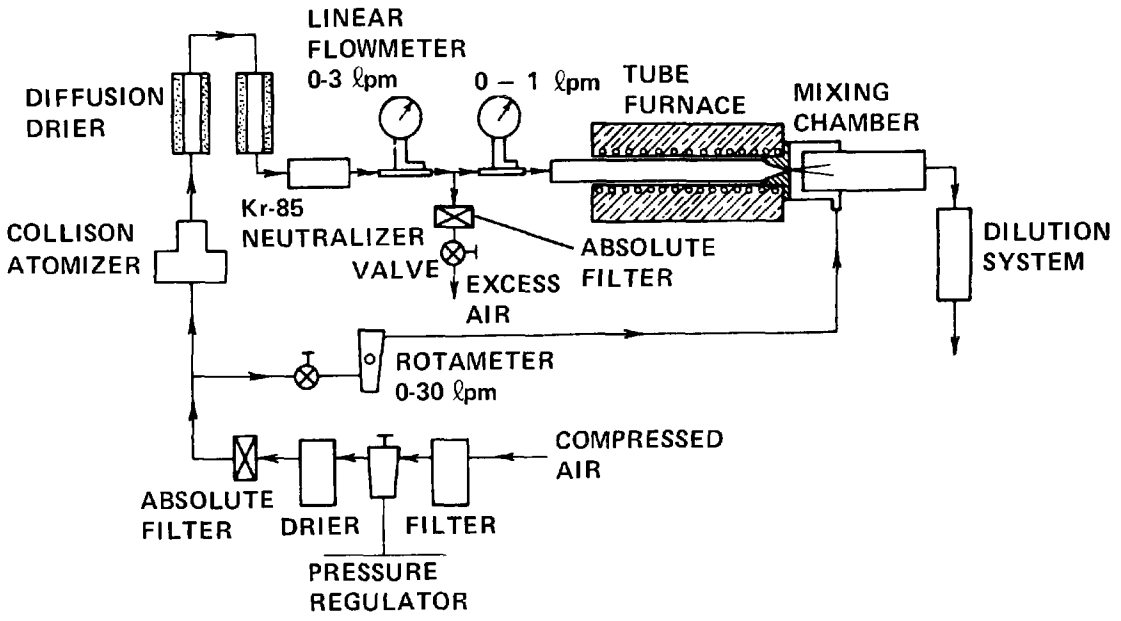


*Figure 4. Schematic diagram of system for generating ultrafine monodisperse aerosols.*

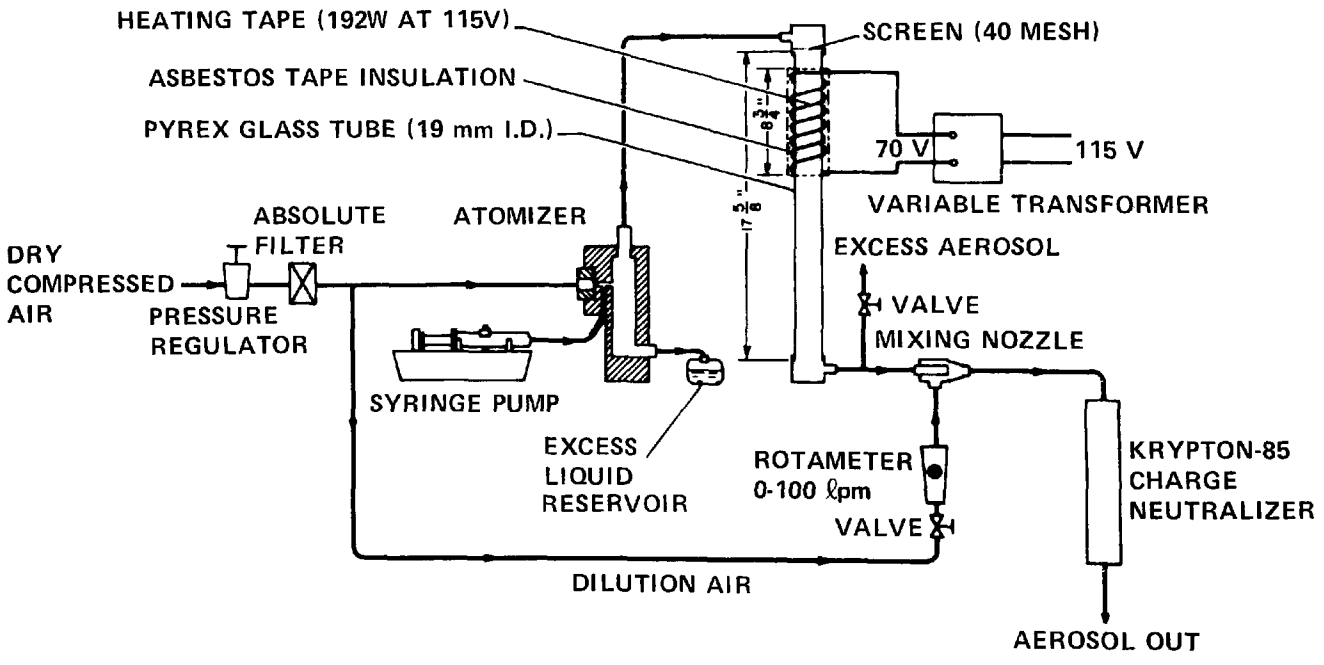


*Figure 5. Schematic diagram of the constant output atomizer and condensation aerosol generator.*

solution being atomized is recirculated and, due to solvent evaporation, the liquid in the atomizer reservoir becomes more concentrated with time, causing the output particle size to increase. In the present device, the liquid is not recirculated. The output particle size consequently remains very stable. The device can also be used to generate monodisperse aerosol of high stability. With the addition of a heater and condenser, monodisperse DOP (di-octyl phthalate) aerosols in the 0.03 to 1.3 μm diameter range can be generated.

Particle Size Accuracy of Monodisperse Aerosol Generators

Among the several aerosol generation techniques discussed above, three are capable of producing particles with a high degree of accuracy in the generated particle size. The monodisperse aerosols from the vibrating orifice generator, the mobility classifier generator, and latex suspensions all have a stated accuracy in particle size of better than 2%. Therefore, it would be of interest to see whether such accuracy in size can be realized in actual practice.

Two types of comparisons have been made in our Laboratory. In one comparison, monodisperse aerosols of DOP were generated by the vibrating orifice generator and their size determined by the differential mobility analyzer using an optical particle counter as the particle detector. The size of the particles was also calculated from the generator operating conditions using equations (1) and (4). This comparison will show whether the vibrating orifice generator and the differential mobility analyzer were operating with the stated accuracy.

In a second comparison, monodisperse aerosols of polystyrene latex (PSL) were generated by aerosolizing the monodisperse latex suspensions using the usual spray-drying technique (see Whitby and Liu[14]). These latex suspensions were sized by their manufacturer (Dow Diagnostics, P.O. Box 68511, Indianapolis, IN 46268) by electron microscopy. By measuring the size of the latex aerosols with the differential mobility analyzer, and comparing it with the size supplied by the manufacturer, one can obtain some ideas as to the reliability of the particle size data supplied by the manufacturer.

The results of the comparisons are shown in Table 3. We found good agreement between the vibrating orifice and the mobility classification methods. The maximum difference between the calculated particle diameters based on these two methods was 1.9%. This difference is well within the combined uncertainties of these two independent methods.

A larger discrepancy was found between the sizes of the polystyrene latex particles supplied by Dow Diagnostics and that determined by the differential mobility analyzer, the maximum

TABLE 3. COMPARISON OF THE PARTICLE DIAMETER MEASURED BY THE DIFFERENTIAL MOBILITY ANALYZER WITH DIAMETERS GIVEN BY THE MANUFACTURER (PSL PARTICLES) AND THOSE GIVEN BY THE VIBRATING ORIFICE MONODISPERSE AEROSOL GENERATOR

| Aerosol | Generation method | Particle diameter, μm | | | % Difference |
|---|---|---|---|---|---|
| | | Given by Dow Co. | Calculated (vibrating orifice) | Measured (differential mobility) | |
| DOP | Vibrating orifice | -- | 0.890 | 0.888 | +0.27 |
| DOP | Vibrating orifice | -- | 1.094 | 1.115 | -1.9 |
| DOP | Vibrating orifice | -- | 1.701 | 1.695 | +0.35 |
| PLS(LS-1010-E) | Spray-drying | 0.357 | -- | 0.338 | +5.6 |
| PSL(LS-061-A) | Spray-drying | 0.365 | -- | 0.345 | +5.8 |
| PSL(LS-1020-E) | Spray-drying | 0.481 | -- | 0.517 | -6.9 |
| PSL(LS-1029-E) | Spray-drying | 0.500 | -- | 0.528 | -5.3 |
| PSL(LS-1117-B) | Spray-drying | 0.79 | -- | 0.820 | -3.7 |
| PSL(LS-1166-B) | Spray-drying | 1.10 | -- | 1.182 | -6.9 |

difference being 6.9%. A large part of the discrepancy can probably be attributed to the error in the particle size data of the latex suspensions supplied by the manufacturer. Several investigators have found similar discrepancies in the particle sizes supplied by Dow and the sizes determined by their independent techniques. Table 4 summarizes these findings. It is interesting to note that most techniques give particle sizes which deviate from the sizes given by Dow Chemical Co. in the same direction (either larger or smaller) as that given by the mobility classification method. Further, the average of the sizes given by these investigators agrees with the size determined by the mobility classification method to about 2%.

Some of the frequently mentioned causes for the possible sizing errors by electron microscopy are:

(1) Due to the use of emulsifier in the latex suspension, a thin layer of the emulsifier is usually present on the surface of the particles. The thickness of the emulsifier shell would vary with the amount of dilution used in preparing the suspension.

(2) The particles, upon continuous electron bombardment in the microscope, have been found to change in size.

Nevertheless, a few percent error in size determination for the PSL particles is usually not too serious for most applications. Consequently, the nominal particle size supplied by the manufacturer can be used in these cases. When more accurate particle size data are needed, the actual particle size should be determined by an appropriate technique capable of giving the required accuracy.

## CALIBRATION OF AEROSOL MEASURING AND SAMPLING INSTRUMENTS

A variety of aerosol measuring and sampling devices have been calibrated by means of the monodisperse aerosol standards described above. These include the condensation nuclei counter, the diffusion battery, the electrical aerosol analyzer, the optical particle counter, and the inertial impactor. The calibration studies have been reviewed in several papers contained in the book, Fine Particles: Aerosol Generation, Measurement, Sampling, and Analysis, edited by Liu.[36] Therefore, only a few of these calibration studies will be reviewed here to illustrate the application of the monodisperse aerosol standards and the precautions in the use of the various aerosol generators for instrument calibration and evaluation studies.

### Condensation Nuclei Counter

Several commercial condensation nuclei counters have been calibrated by means of the mobility classifier monodisperse aerosol generator and the calibration system shown in Figure 3.

TABLE 4. DIAMETERS OF PSL PARTICLES GIVEN BY THE MANUFACTURER (DOW DIAGNOSTICS) AND THOSE MEASURED BY DIFFERENT INVESTIGATORS

| | Particle diameter, μm | | | | | | | | | |
|---|---|---|---|---|---|---|---|---|---|---|
| | | | | Electron microscopy | | | Light scattering | | | |
| PSL I.D. | Dow Co. | Mobility classification | Average of values on right | (1) | (2) | (3) | (4) | (5) | Centrifuge (6) | Optical array (7) |
| LS1010-E | 0.357 | 0.338 | 0.334 | 0.33 | 0.318 | | | | 0.354 | |
| LS061-A | 0.365 | 0.345 | 0.340 | | | 0.336 | 0.342 | 0.339 | | 0.343 |
| LS1020-E | 0.481 | 0.517 | - - - | | 0.488 | | | | | |
| LS1029-E | 0.500 | 0.528 | 0.516 | 0.50 | 0.499 | | | | 0.55 | |
| LS1117-B | 0.79 | 0.820 | - - - | | | | | | | |
| LS1166-B | 1.10 | 1.18 | - - - | | | | | | | |

Investigators: (1) Heard et al.[29] (2) Porstendörfer and Heyder[33] (3) Davidson and Haller[30] (4) La Mer and Plesner[34] (5) Dezelic and Kratohvil[31] (6) Stöber and Flachsbart[35] (7) Davidson and Collins[32]

In this system, the particle concentration can be varied continuously by varying the ratio of aerosol and clean air flows. A critical orifice in a vacuum line is used to draw a portion of the flow (3 ℓpm) through the electrometer. The remaining aerosol flow (20 ℓpm) is then available for delivery to the nuclei counter being calibrated.

Due to the pulsating inlet flow common for most nuclei counters, care must be taken to insure that the flow rate of the calibrating aerosol is larger than the peak suction flow in the counter. Further, in order to minimize precipitation of particles in the sampling line and within the instrument due to the charge on the particles, the test aerosol should be neutralized before being introduced into the counter. The particle loss inside the neutralizer should be evaluated and taken into account in the concentration calculation.

Figure 6 shows the calibration results for an Environment/One condensation nuclei counter.[20] The response of the counter is seen to be linear at concentration levels only up to 130,000 particles/cm$^3$, above which the response becomes non-linear. Further, the indicated concentration of the counter is lower than the true concentration by a factor ranging from 2.5 in the lower linear range to 5.3 at the upper concentration limit, 600,000 particles/cm$^3$, used in the calibration.

Since all commercial nuclei counters have been referenced by their manufacturer to the photoelectric counter of Pollak,[37] the above result suggests that the Pollak counter calibration may be in error. However, in a subsequent study,[38] a Pollak counter was evaluated with the mobility classifier aerosol generator. Figure 7 shows the results of the calibration study. The particle concentration determined by the Pollak counter using the original Pollak calibration is seen to be in good agreement with that determined by the mobility classification method, the maximum discrepancy being 17% at the upper concentration limit of 250,000 particles/cm$^3$ used in the study. The source of error in the Environment/One counter calibration, therefore, must be attributed to the calibration error made at the factory.

The response of the condensation nuclei counters has also been evaluated as a function of particle size. The result for the case of the General Electric counter is shown in Figure 8.[25] The counting efficiency (ratio of indicated concentration to input aerosol concentration) of the GE counter is found to drop rapidly below 0.02 μm, reaching a value of 50% at a particle diameter of 90 Å.

Similar studies on the counting efficiency of the GE and Environment/One counters by Cooper and Langer[39] have resulted in a similar finding. The study by Bricard et al.[40] on the continuous flow counter using alcohol as the working fluid also

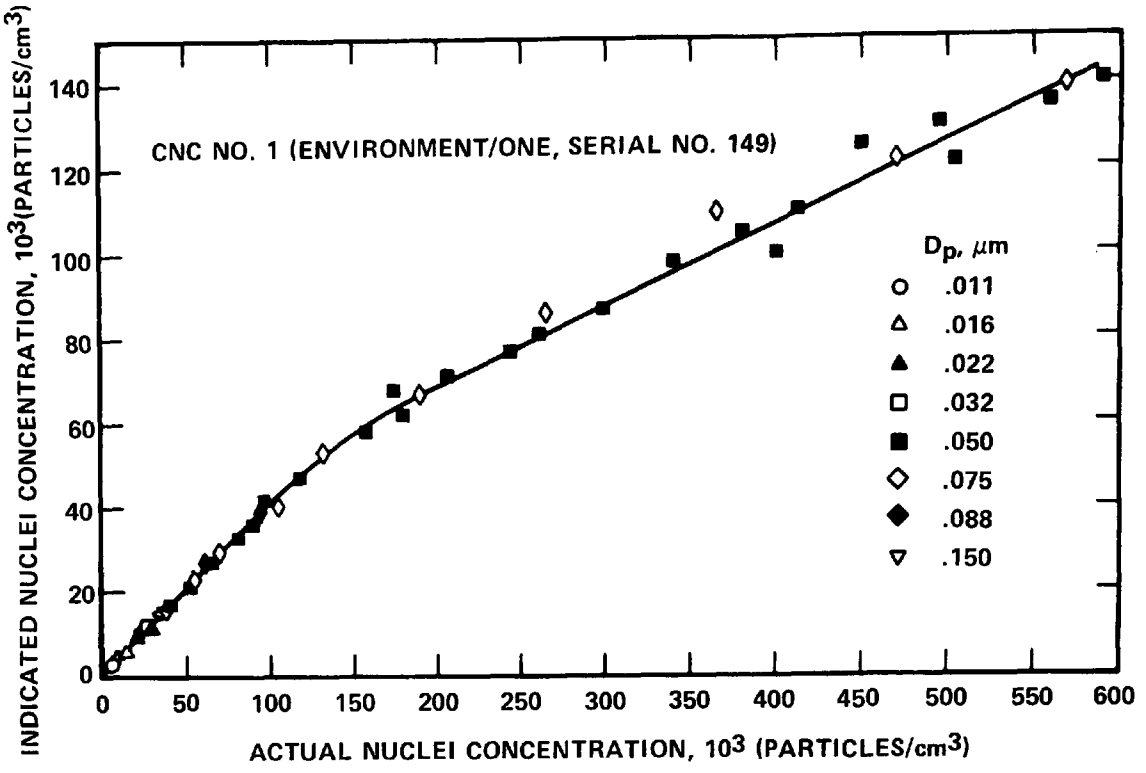


*Figure 6. Response of the Environment/One, Rich 100 condensation nuclei counter to monodisperse aerosols produced by the mobility classifier aerosol generator.*

gives similar results. Recently, Porstendörfer and Soderholm have also found the size dependence of the Environment/One counter using a photographic counting-diffusion battery technique.[41] The cause of this non-ideal behavior has not yet been identified at the present time, but it seems that this non-ideal behavior is an inherent characteristic of most of the automatic condensation nuclei counters.

## Diffusion Battery

The mobility classifier aerosol generator has also been used for calibrating the diffusion batteries described by Sinclair et al.[42,43] In the first calibration study, the diffusion battery comprised of the "collimated holes structures" was used. These are metal discs with uniform size holes. Since the number, the diameter, and the length of these uniform tubular holes can be measured accurately with a microscope, the penetration of a monodisperse aerosol of a known particle size through the battery can be predicted from the diffusion theory. In the calibration study, monodisperse aerosols of various diameters were generated by the mobility classifier generator, and the particle penetration through the battery was measured with a condensation

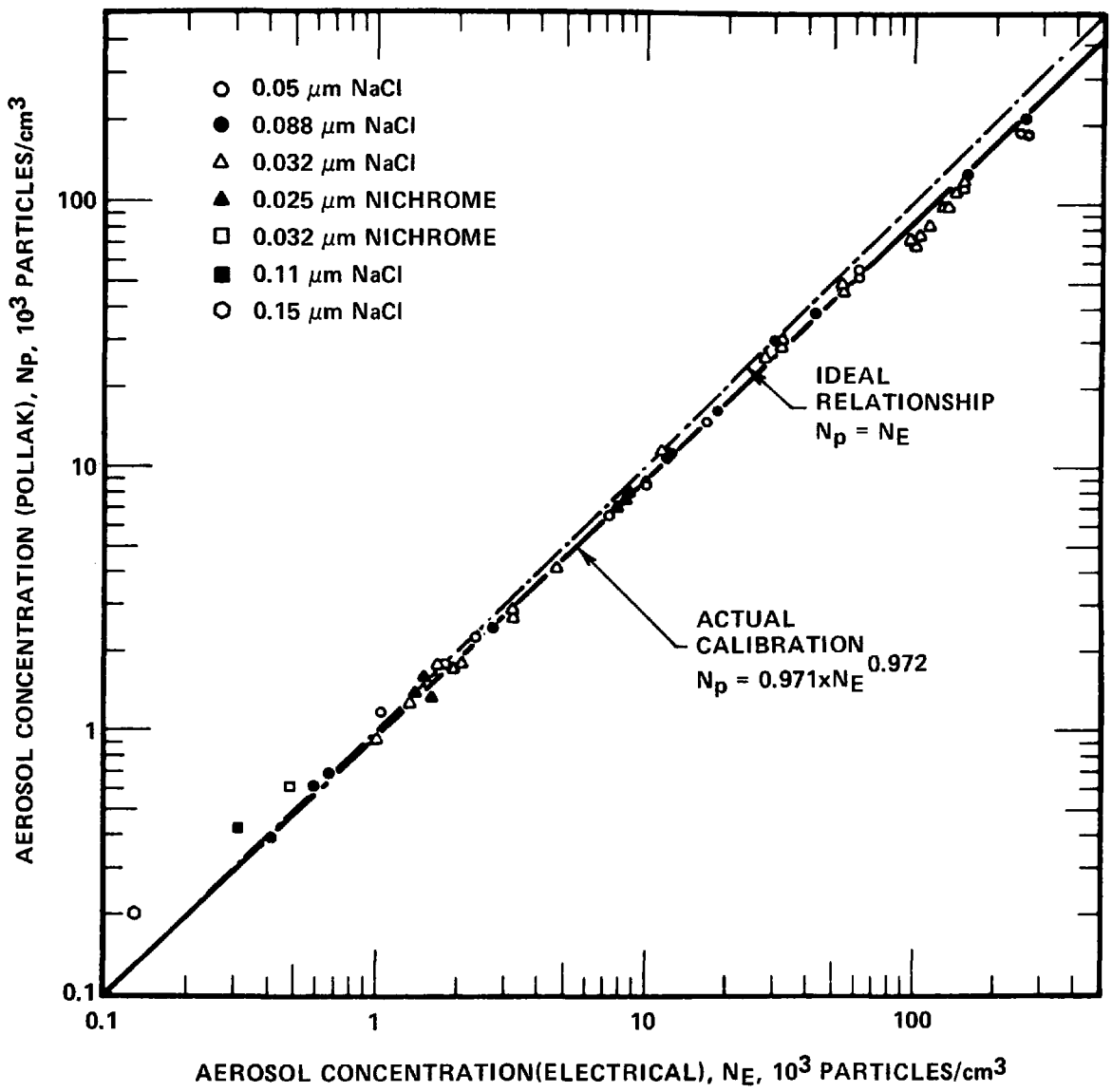


*Figure 7. Calibration of the Pollak counter with the mobility classifier aerosol generator.*

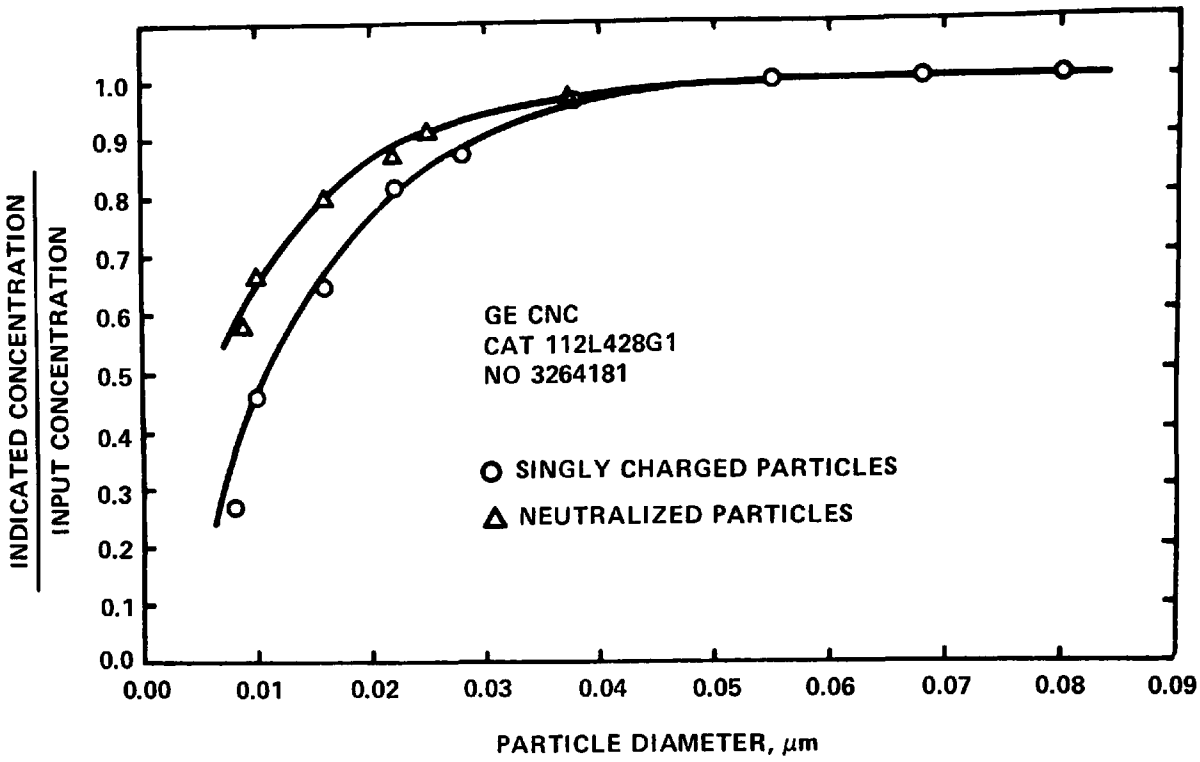


*Figure 8. Counting efficiency of the General Electric condensation nuclei counter as a function of particle size.*

nuclei counter. Figure 9 compares the particle penetration determined experimentally with that predicted from theory. The agreement is seen to be very good in the tested size range from 0.024 μm to 0.110 μm. The good agreement constitutes a direct verification of the theory of diffusion battery.

Electrical Aerosol Analyzer

The electrical aerosol analyzer is an aerosol size distribution measuring device operating on the principle of unipolar diffusion charging and mobility analysis.[44] The analyzer operates by first placing a unipolar charge on the aerosol being measured, and measuring the resulting mobility distribution of the charged particles by means of a mobility analyzer. Although the charge acquired by an aerosol particle under a specific set of charging conditions can be calculated theoretically using the available charging theories,[45] the uncertainties in the theoretical results, particularly that caused by the particle loss in the instrument, require that the instrument be calibrated. In the calibration study reported by Liu and Pui,[44] the mobility classifier generator was used to generate monodisperse aerosols of a known size and concentration for the study.

Some sample results from the calibration are shown in Figure 10. The figure shows the empirical voltage-current for the electrical aerosol analyzer upon exposure to monodisperse aerosols

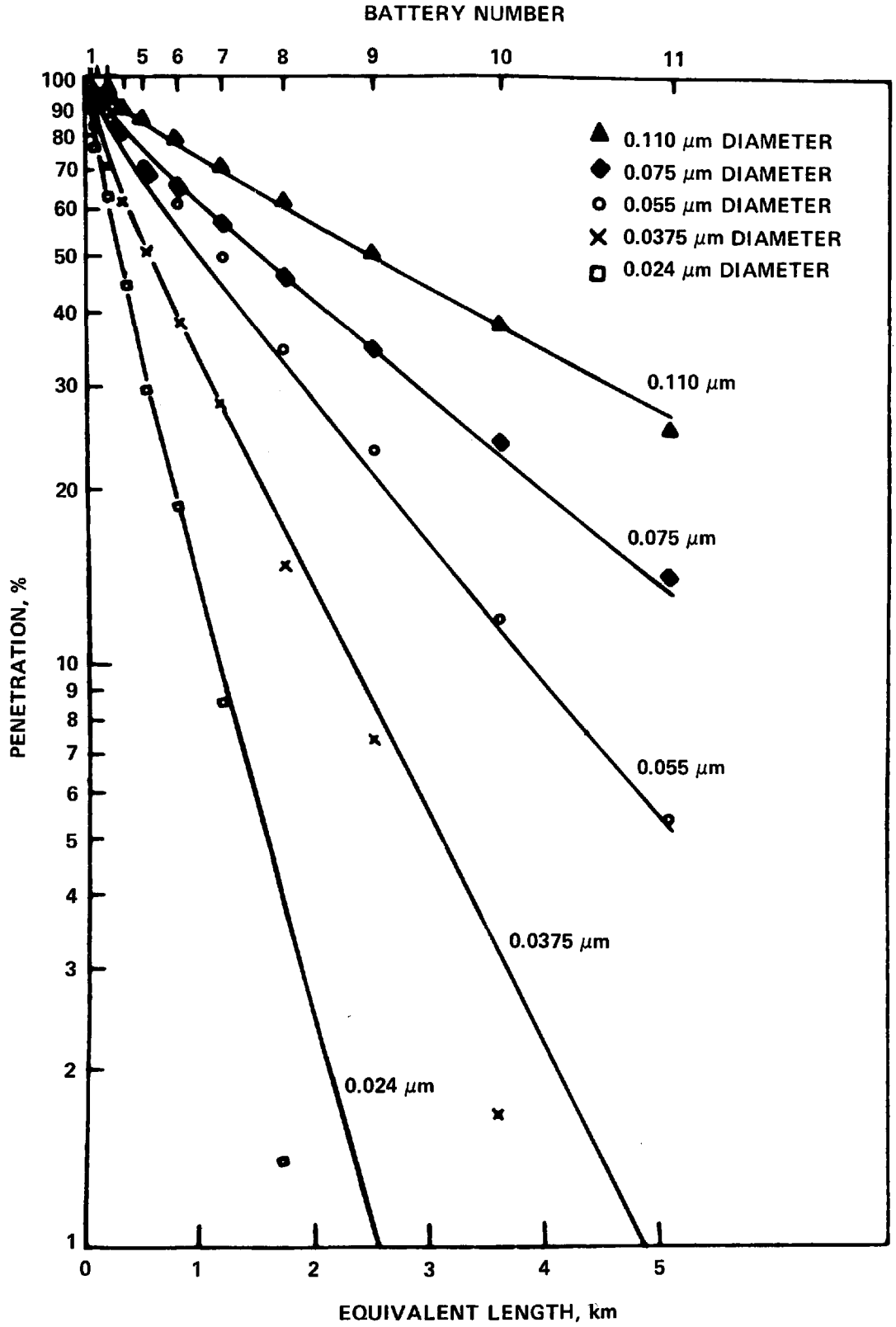


*Figure 9. Comparison of theoretical (solid lines) and experimental penetrations through the Sinclair diffusion battery using monodisperse aerosols from the mobility classifier generator.*

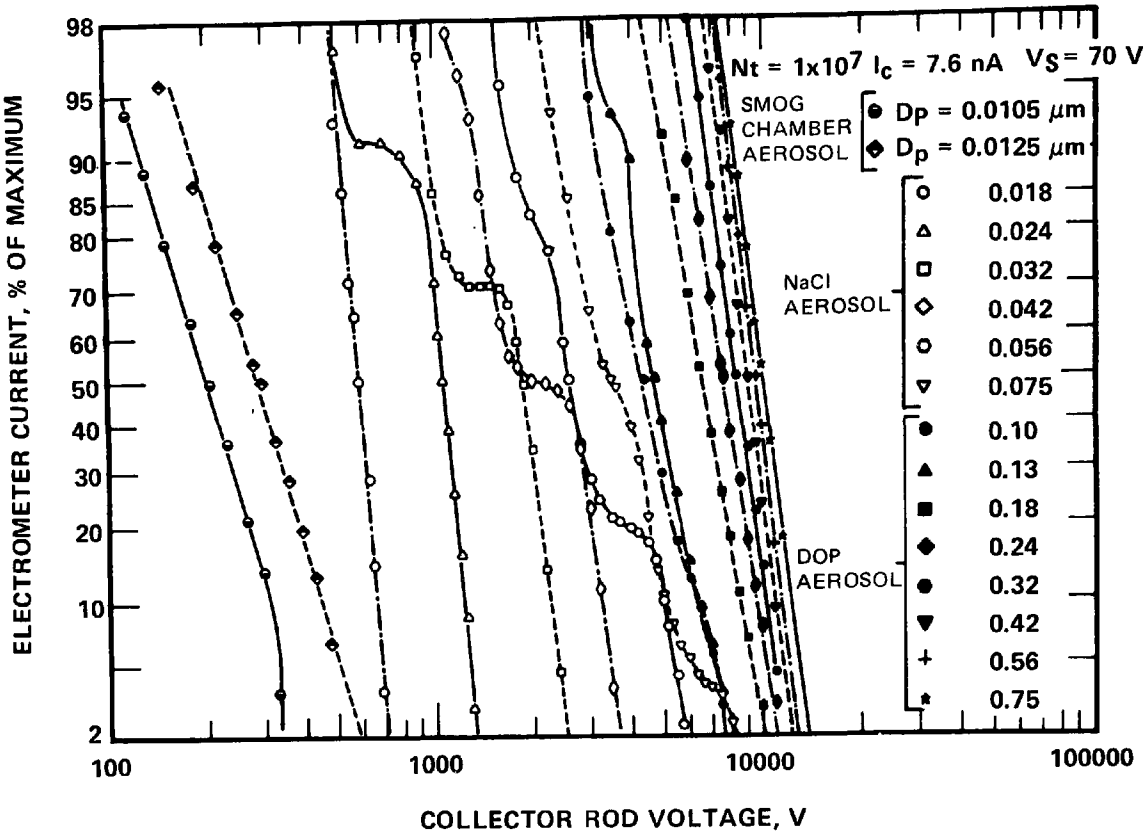


*Figure 10. Response of electrical aerosol analyzer to monodisperse aerosols.*

of various sizes. These curves can be used to construct a calibration matrix which can be used in a data reduction algorithm[46] for the inversion of instrument data to obtain the original size distribution.

## Optical Particle Counter

Several commercial optical particle counters have been evaluated by means of the latex aerosols and aerosols produced by the vibrating orifice generator.[47] Since the response of the optical counter is a function of the size, the refractive index, and the shape of the measured particle, a variety of test aerosols is needed in order to determine the instrument response empirically. The ability of the vibrating orifice generator to generate aerosol from a variety of materials has made this an ideal generator for studying the response of optical counters. Materials with a variety of refractive indices, such as the Cargille index-of-refraction liquids, methylene blue, sodium chloride and India ink, may be dissolved or diluted in a suitable solvent and used in the generator to produce aerosols with the desired optical properties.

Some typical results for the Royco 220 particle counter are shown in Figure 11. The response of the counter is shown as a function of particle size and particle refractive index. Such information can be used for determining the effect of the refractive index on the measurement accuracy of the instrument.

Calibrations of the optical particle counters using irregular particles have also been performed. In one study, coal dust particles obtained by aerosolizing a finely ground coal powder with the fluidized bed were used.[48] The polydisperse coal aerosol generated by the fluidized bed aerosol generator was passed through a differential mobility analyzer to extract a monodisperse fraction, and the resulting monodisperse aerosol was then applied to the optical counter for calibration. In another study, inertial impactors of various cut sizes were placed at the inlet of the optical counter and the response of the optical counter was determined, from which an "aerodynamic" calibration could be obtained.[49]

Inertial Impactor

The inertial impactor has found widespread use in aerosol studies because of its simplicity and well defined operational characteristics. Various designs of impactors are available commercially for different applications.[50,51] An extensive theoretical analysis of the inertial impactor has been performed by Marple[52] and Marple and Liu.[53,54] Although the impaction efficiency can now be accurately predicted by theory, experimental evaluation still must be made in order to characterize the real impactor behavior, including problems due to particle reentrainment and bounce.

Many impactors have been calibrated by means of the vibrating orifice monodisperse aerosol generator. Two different approaches can be used in the calibration. In one approach, an optical counter is used as a particle detector. By counting the particles upstream and downstream of the impactor, the collection efficiency can be obtained. In another approach,the particles are tagged with a fluorescent tracer, and the particles deposited on various stages of the impactor, including the after filter, are measured fluorometrically, from which the impaction characteristics are determined. This latter technique is especially useful for evaluating the multistage impactors, since the wall losses can also be evaluated.

Figure 12 shows the calibration results for a single-stage impactor and a two-stage impactor consisting of two identical impaction nozzles.[49] The experimental results are seen to agree well with the theoretical prediction. The monodisperse aerosols from the vibrating orifice generator have also been used to evaluate the Lundgren impactor, the Andersen impactor, and the Sierra impactor[55-57] as well as the virtual impactor.[51] Using the latex

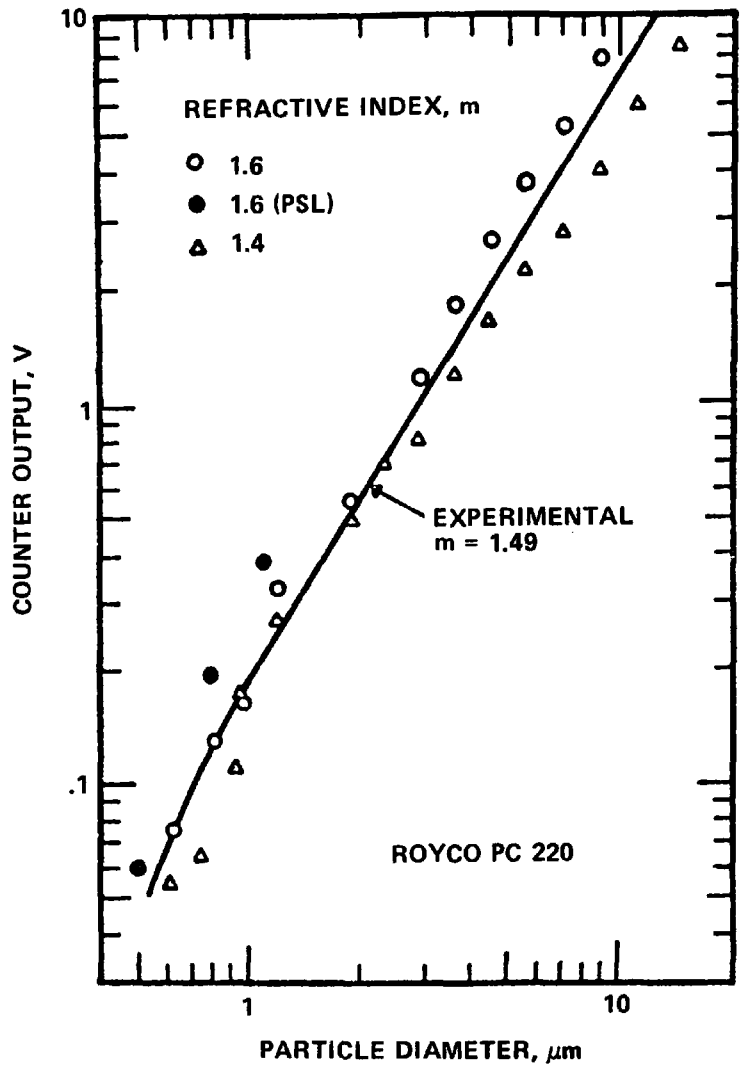


*Figure 11. Experimental calibration curve for the Royco 220 optical particle counter.*

aerosols, Rao and Whitby have also studied the particle bounce phenomena inside impactors.[58,59]

Comparative Studies Between Aerosol Measuring Instruments

In the preceding sections, we have discussed the calibration of various aerosol measuring instruments with monodisperse aerosol standards. If the instruments are properly calibrated and the data properly analyzed, different instruments should give the same measurement results when they are used on the same aerosol. Such comparative studies involving the simultaneous aerosol measurement of the same aerosol by different measuring instruments are the subjects of this section.

The electrical aerosol analyzer (EAA) is capable of measuring particle size distribution in the 0.005 to 1.0 μm diameter

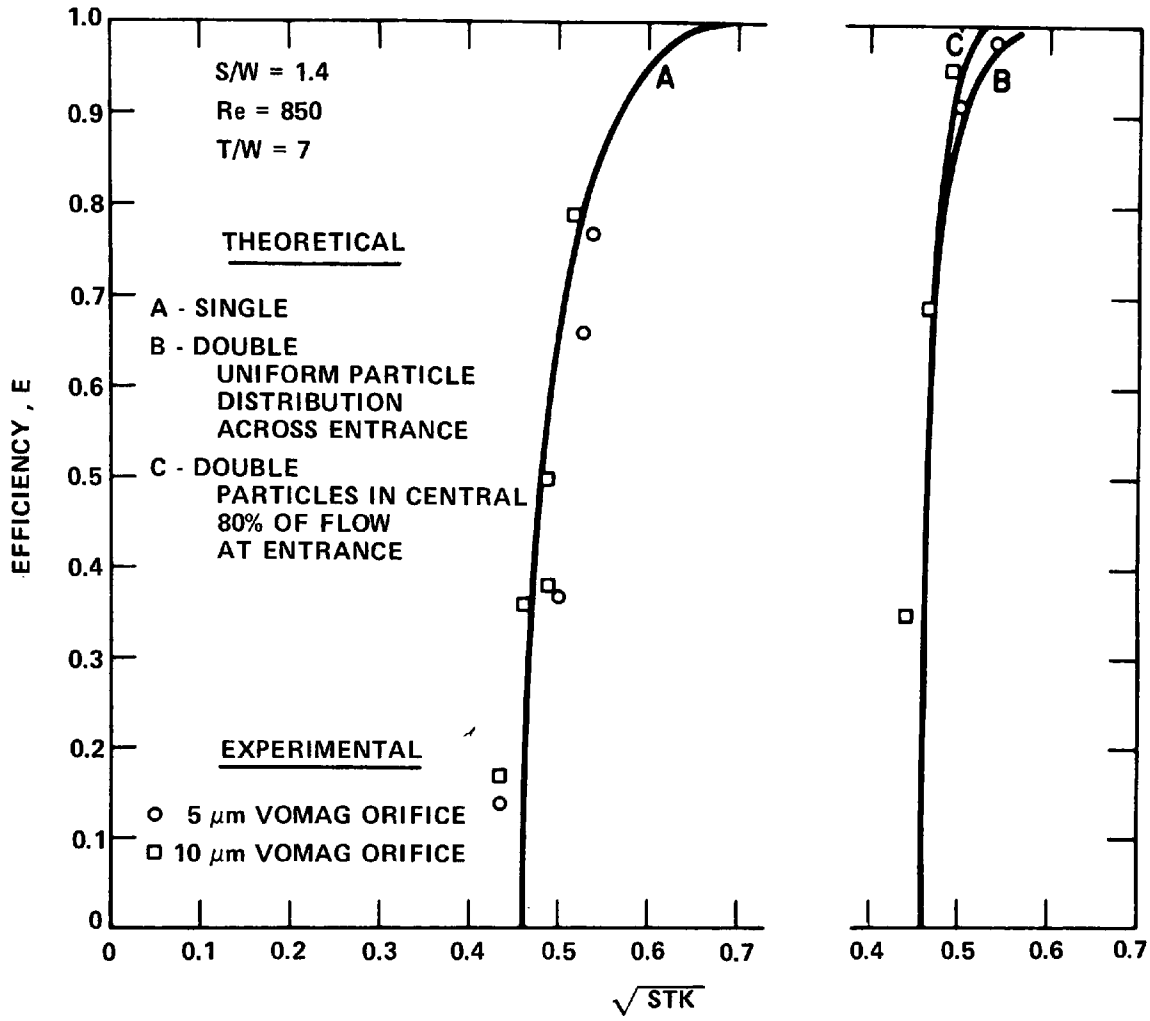


*Figure 12. Comparison of theoretical and experimental efficiency curves for two impactors.*

range. The measured distribution can be integrated to yield the number and volume concentrations. Therefore, the EAA may be compared with a condensation nuclei counter (CNC) and a gravimetric analysis technique for number and volume concentration determinations. Such comparisons have been made, the detail of which will be described in a forthcoming paper by Mulholland et al.[60] Some preliminary results of this study are described below.

For number concentration determinations, polydisperse aerosols of NaCl, $(NH_4)_2SO_4$, DOP, and sucrose were generated by the constant output atomizer and supplied to two EAA's and a GE CNC. In Figure 13, the total number concentrations measured by the EAA's are compared with that measured by the CNC. It is seen that good agreement is obtained between the two different measuring techniques. It should be mentioned that the CNC had been calibrated several months prior to the experiment, and that the

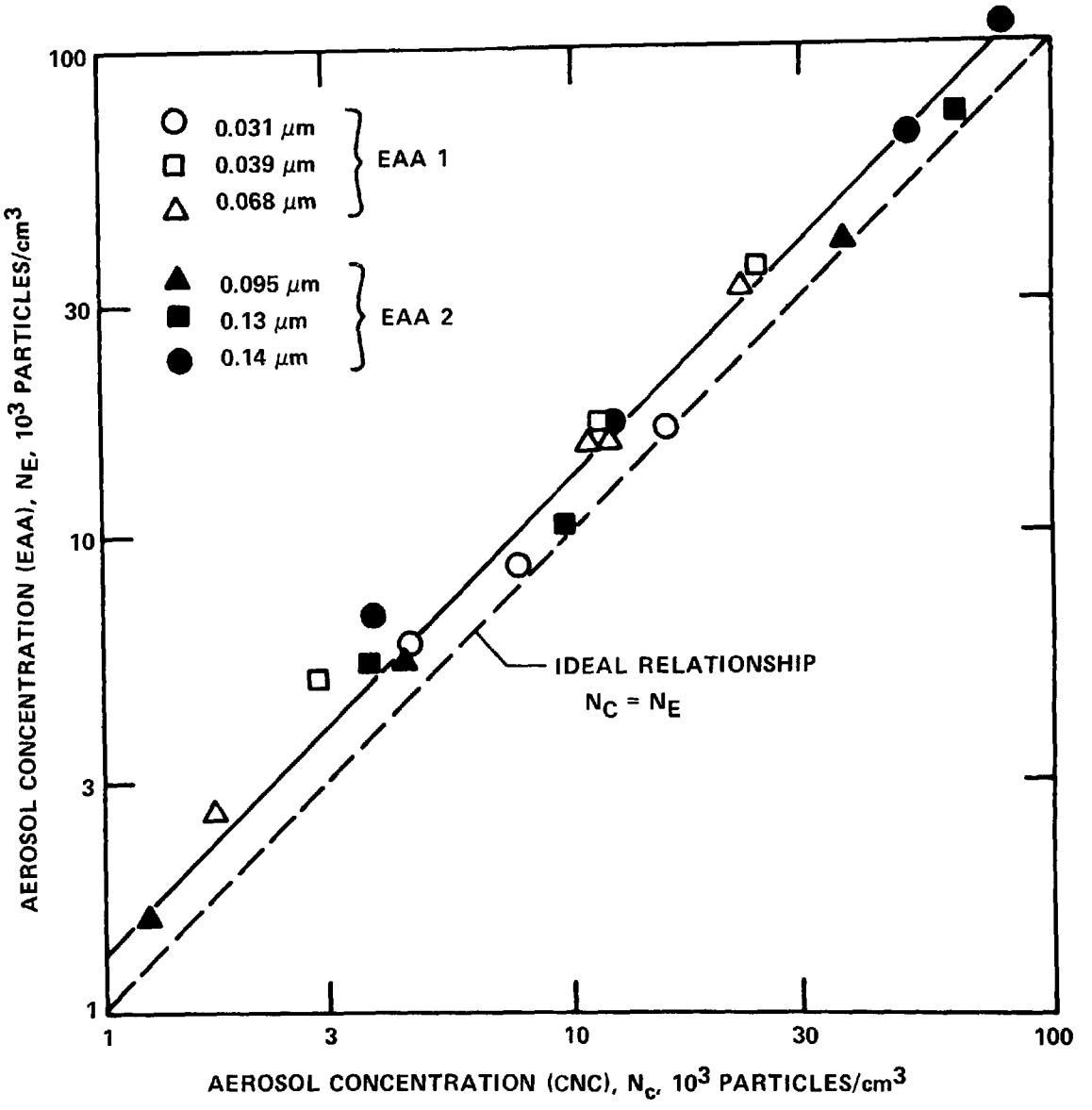


*Figure 13. Comparison of EAA and CNC for total number concentration measurements obtained in the first experimental series.*

EAA concentrations were calculated by the simplified data reduction procedure of Liu and Pui[44] using the instrument sensitivities for monodisperse aerosols.

In the second series of experiments, the CNC was recalibrated, and a simplex minimization program of Liu and Kapadia[61] was used for reducing the EAA data. The results of the comparison are shown in Figure 14. Very good agreement is obtained, the maximum discrepancy being about 10%.

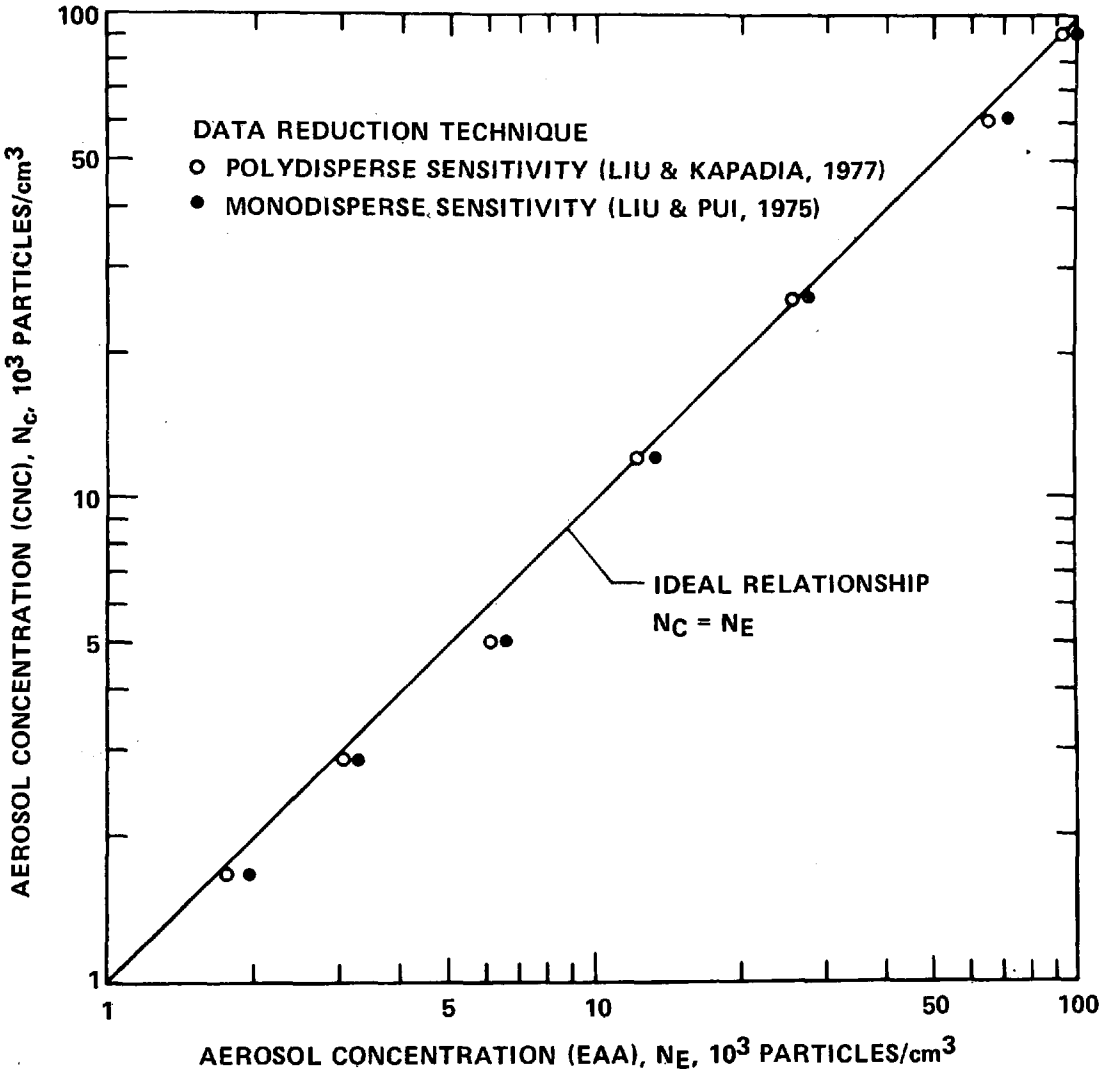


*Figure 14. Comparison of EAA and CNC for total number concentration measurements obtained in the second experimental series.*

## SUMMARY AND CONCLUSIONS

In this paper, we have reviewed the recent developments in monodisperse aerosol generation. Some of the techniques developed, such as the vibrating orifice generator and the mobility classifier generator, are capable of generating monodisperse aerosols of an accurately known particle size and concentration. These aerosols can be referred to as "aerosol standards" since they can be used as standards of measurement or calibration in the field of aerosol science. The application of these monodisperse aerosol standards to instrument calibration and evaluation has also been briefly described and some sample results presented. It is shown that with proper calibration of the instruments used, aerosol measurement can be made with good accuracy as in many other fields of science and technology.

## REFERENCES


1. La Mer, V.K., and D. Sinclair. An Improved Homogeneous Aerosol Generator. OSRD Report No. 1668, Office of Publication Board, U.S. Department of Commerce, Washington, DC, 1943.

2. Rapaport, E., and S.G. Weinstock. A Generator for Homogeneous Aerosols. Experientia 11:363-364, 1955.

3. Liu, B.Y.H., K.T. Whitby, and H.H.S. Yu. A Condensation Aerosol Generator for Producing Monodispersed Aerosols in the Size Range 0.036 μm to 1.3 μm. J. Rech. Atmos. 3:397-406, 1966.

4. Kogan, I., and S. Burnasheva. Zh. Fiz. Khim. 34:2630, 1960.

5. Fuchs, N.A., and A.G. Sutugin. Generation and Use of Monodisperse Aerosols. In: Aerosol Science, C.N. Davies, ed. Academic Press, New York, 1966. pp. 1-30.

6. Espenscheid, W., E. Matijevic, and M. Kerker. J. Phys. Chem. 68:2831, 1964.

7. Walton, W.H., and W.C. Prewett. The Production of Sprays and Mists of Uniform Drop Size by Means of Spinning Disc Type Sprayers. Proc. Phys. Soc. (London) 62:341-350, 1949.

8. May, K.R. An Improved Spinning Top Homogeneous Spray Apparatus. J. Appl. Phys. 20:932-938, 1949.

9. Boshoff, W. Proc. Inst. Mech. Engrs. 166:443, 1952.

10. Schwendiman, L.C., A. K. Postma, and L.F. Coleman. A Spinning Disc Aerosol Generator. Health Phys. 10:947-953, 1964.

11. Whitby, K.T., D.A. Lundgren, and C.M. Peterson. Homogeneous Aerosol Generators. Int. J. Air Water Pollut. 9:263-277, 1965.

12. Lippmann, M., and R.E. Albert. A Compact Electric-Motor Driven Spinning Disc Aerosol Generator. J. Am. Ind. Hyg. Assoc. 28:501-506, 1967.

13. Philipson, K. On the Production of Monodisperse Particles with a Spinning Disc. J. Aerosol Sci. 4:51-57, 1973.

14. Whitby, K.T., and B.Y.H. Liu. Polystyrene Aerosols--Electrical Charge and Residue Size Distribution. Atmos. Environ. 2:103-116, 1968.

15. Langer, G., and A. Lieberman. Anomalous Behavior of Aerosols Produced by Atomization of Monodisperse Polystyrene Latex. J. Colloid Sci. 15:357-360, 1960.

16. Fuchs, N.A., and A.G. Sutugin. Kolloid. Zh. 25:487, 1963.

17. Raabe, O.G. The Generation of Aerosols of Fine Particles. In: Fine Particles: Aerosol Generation, Measurement, Sampling and Analysis, B.Y.H. Liu, ed. Academic Press, New York, 1976. pp. 57-110.

18. Berglund, R.N., and B.Y.H. Liu. Generation of Monodisperse Aerosol Standards. Environ. Sci. Technol. 7:147-153, 1973.

19. Liu, B.Y.H. Standardization and Calibration of Aerosol Instruments. In: Fine Particles: Aerosol Generation, Measurement, Sampling and Analysis, B.Y.H. Liu, ed. Academic Press, New York, 1976. pp. 39-53.

20. Liu, B.Y.H., and D.Y.H. Pui. A Submicron Aerosol Standard and the Primary, Absolute Calibration of the Condensation Nuclei Counter. J. Colloid Interface Sci. 47:155-171, 1974.

21. Liu, B.Y.H., and D.Y.H. Pui. Equilibrium Bipolar Charge Distribution of Aerosols. J. Colloid Interface Sci. 49:305-312, 1974.

22. Liu, B.Y.H., and D.Y.H. Pui. Electrical Neutralization of Aerosols. J. Aerosol Sci. 5:465-472, 1974.

23. Knutson, E.O., and K.T. Whitby. Aerosol Classification by Electric Mobility: Apparatus, Theory and Applications. J. Aerosol Sci. 6:443-451, 1975.

24. Liu, B.Y.H., and K.W. Lee. An Aerosol Generator of High Stability. J. Am. Ind. Hyg. Assoc. 36:861-865, 1975.

25. Liu, B.Y.H., and C.S. Kim. On the Counting Efficiency of Condensation Nuclei Counters. Atmos. Environ. 11:1097-1100, 1977.

26. Kim, C.S. Ultrafine Aerosol Studies: Generation, Measurement and Coagulation. Ph.D. Thesis, Mechanical Engineering Department, University of Minnesota, Minneapolis, MN, 1978.

27. Liu, B.Y.H., and J. Levi. Generation of Sulfuric Acid Aerosols for Health Effects Studies. Report to the U.S. Environmental Protection Agency, Publication No. 341, Particle Technology Laboratory, Mechanical Engineering Department, University of Minnesota, Minneapolis, MN, 1978.

28. Marple, V.A., B.Y.H. Liu, and K.L. Rubow. A Dust Generator for Laboratory Use. J. Am. Ind. Hyg. Assoc. 39:26-32, 1978.

29. Heard, M.J., A.C. Wells, and R.D. Wiffen. A Re-Determination of the Diameters of Dow Polystyrene Latex Spheres. Atmos. Environ. 4:149-156, 1970.

30. Davidson, J.A., and H.S. Haller. Latex Particle Size Analysis. Part V--Analysis of Errors in Electron Microscopy. J. Colloid Interface Sci. 47:459-472, 1974.

31. Dezelic, G., and J.P. Kratohvil. Determination of Particle Size of Polystyrene Latexes by Light Scattering. J. Colloid Sci. 16:561, 1961.

32. Davidson, J.A., and E.A. Collins. Particle Size Analysis. Part IV--Comparative Methods for Polyvinyl Chloride Latex. J. Colloid Interface Sci. 40:437-447, 1972.

33. Porstendörfer, J., and J. Heyder. Size Distribution of Latex Particles. J. Aerosol Sci. 3:141-148, 1972.

34. La Mer, V.K., and I.V. Plesner. J. Polymer Sci. 24:147, 1957.

35. Stöber, W., and H. Flachsbart. High Resolution Aerodynamic Size Spectrometry of Quasi-Monodisperse Latex Spheres with a Spiral Centrifuge. J. Aerosol Sci. 2:103-116, 1971.

36. Liu, B.Y.H., ed. Fine Particles: Aerosol Generation, Measurement, Sampling and Analysis, Academic Press, New York, 1976.

37. Pollak, L.W., and A.L. Metnieks. Intrinsic Calibration of the Photoelectric Nucleus Counter Model 1957, with Convergent Light Beam. Tech. Note 9, Contract AF61 (052)-26, School of Cosmic Physics, Dublin Institute for Advanced Studies, 1960.

38. Liu, B.Y.H., D.Y.H. Pui, A.W. Hogan, and T.A. Rich. Calibration of the Pollak Counter with Monodisperse Aerosols. J. Appl. Meteorol. 14:46-51, 1975.

39. Cooper, G., and G. Langer. Limitations of Commercial Condensation Nucleus Counters as Absolute Aerosol Counters. J. Aerosol Sci. 9(2):65-75, 1978.

40. Bricard, J., G. Madelaine, and M.-L. Perrin. Comparison of the Size Distribution of a Submicronic Aerosol Obtained by the Diffusion Battery Method and Electrical Aerosol Analyzer. Presented at the Ninth International Conference on Atmospheric Aerosols, Condensation and Ice Nuclei, Galway, Ireland, Sept. 21-27, 1977.

41. Porstendörfer, J., and S.S. Soderholm. Particle Size Dependence of a Condensation Nuclei Counter. Atmos. Environ., in press.

42. Sinclair, D., R.J. Countess, B.Y.H. Liu, and D.Y.H. Pui. Experimental Verification of Diffusion Battery Theory. J. Air Pollut. Contr. Assoc. 26:661-663, 1976.

43. Sinclair, D., R.J. Countess, B.Y.H. Liu, and D.Y.H. Pui. Automatic Analysis of Submicron Aerosols. Presented at the Aerosol Measurement Workshop, University of Florida, Gainsville, FL, March, 1976.

44. Liu, B.Y.H., and D.Y.H. Pui. On the Performance of the Electrical Aerosol Analyzer. J. Aerosol Sci. 6:249-264, 1975.

45. Liu, B.Y.H., and D.Y.H. Pui. On Unipolar Diffusion Charging of Aerosols in the Continuum Regime. J. Colloid Interface Sci. 58:142-149, 1977.

46. Liu, B.Y.H., D.Y.H. Pui, and A. Kapadia. Electrical Aerosol Analyzer: History, Principle and Data Reduction. Presented at Aerosol Measurement Workshop, University of Florida, Gainsville, FL, March, 1976.

47. Liu, B.Y.H., R.N. Berglund, and J.K. Agarwal. Experimental Studies of Optical Particle Counters. Atmos. Environ. 8:717-732, 1974.

48. Liu, B.Y.H., V.A. Marple, K.T. Whitby, and N.J. Barsic. Size Distribution Measurement of Airborne Coal Dust by Optical Particle Counters. J. Am. Ind. Hyg. Assoc. 35:443-451, 1974.

49. Marple, V.A., and K.L. Rubow. Aerodynamic Particle Size Calibration of Optical Particle Counters. J. Aerosol Sci. 7:425-433, 1976.

50. Marple, V.A., and K. Willeke. Inertial Impactors: Theory, Design and Use. In: Fine Particles: Aerosol Generation, Measurement, Sampling and Analysis, B.Y.H. Liu, ed. Academic Press, New York, 1976. pp. 411-446.

51. Loo, B.W., J.M. Jaklevic, and F.S. Goulding. Dichotomous Virtual Impactors for Large-Scale Monitoring of Airborne Particulate Matter. In: Fine Particles: Aerosol Generation, Measurement, Sampling and Analysis, B.Y.H. Liu, ed. Academic Press, New York, 1976. pp. 311-350.

52. Marple, V.A. A Fundamental Study of Inertial Impactors. Ph.D. Thesis, Mechanical Engineering Department, University of Minnesota, Minneapolis, MN, 1970.

53. Marple, V.A., and B.Y.H. Liu. Characteristics of Laminar Jet Impactors. Environ. Sci. Technol. 8:648-654, 1974.

54. Marple, V.A., and B.Y.H. Liu. On Fluid Flow and Aerosol Impaction in Inertial Impactors. J. Colloid Interface Sci. 53:31-34, 1975.

55. Rao, A.K., and K.T. Whitby. Non-Ideal Collection Characteristics of Single-Stage and Cascade Impactors. J. Am. Ind. Hyg. Assoc. 38:174-179, 1977.

56. Willeke, K. Performance of the Slotted Impactor. J. Am. Ind. Hyg. Assoc. 36:683-691, 1975.

57. Willeke, K., and J.J. McFeters. The Influence of Flow Entry and Collecting Surface on the Impaction Efficiency of Inertial Impactors. J. Colloid Interface Sci. 53:121-127, 1975.

58. Rao, A.K., and K.T. Whitby. Non-Ideal Collection Characteristics of Inertial Impactors--I. Single-Stage Impactors and Solid Particles. J. Aerosol Sci. 9:77-86, 1978.

59. Rao, A.K., and K.T. Whitby. Non-Ideal Collection Characteristics of Inertial Impactors--II. Cascade Impactors. J. Aerosol Sci. 9:87-100, 1978.

60. Mulholland, G.W., B.Y.H. Liu, A. Kapadia, and D.Y.H. Pui. Aerosol Number and Mass Concentration Measurements: A Comparison of the EAA with Other Measurement Techniques, to be submitted for publication.

61. Liu, B.Y.H. and A. Kapadia. A Computer Data Reduction Program for the Electrical Aerosol Analyzer. Publication No. 325, Particle Technology Laboratory, Mechanical Engineering Department, University of Minnesota, Minneapolis, MN, 1977.

PAPER 13

# SUBSTRATE COLLECTORS FOR CASCADE IMPACTORS AN EVALUATION

D. BRUCE HARRIS
PROCESS MEASUREMENTS BRANCH
INDUSTRIAL ENVIRONMENTAL RESEARCH LABORATORY-RTP
U.S. ENVIRONMENTAL PROTECTION AGENCY

AND

G. CLINARD, L.G. FELIX
G. LACEY, J.D. MCCAIN
SOUTHERN RESEARCH INSTITUTE

The use of cascade impactors to obtain particle size information on process streams has increased dramatically in the past few years. The Process Measurements Branch (PMB) of EPA's Industrial Environmental Research Laboratory-RTP has been involved in investigating their performance and application for almost a decade. Early in this effort we recognized the inherent potential for error caused by the small sample weights on the heavy metal collection stages being used in commercially available impactors, and proposed and implemented the use of light weight substrates. Many problems were met and resolved during the evolutionary development of the methodologies of using cascade impactors.

Substrates have generally been made of filter media (most often fiber glass) and thin metal foils. An early study of substrate usage was included in a test of a then-available commercial impactor at a coal-fired power plant in 1973 and has been reported in detail in EPA report "Field Measurements of Particle Size Distribution with Inertial Sizing Devices," EPA-650/2-73-035 (NTIS No. PB 226292). The advantages of substrates were demonstrated and the method became the one recommended for IERL-RTP use.

Weight loss problems were reported by some users of fiber glass substrates. A detailed study of this problem was made by Southern Research Institute under contract to EPA's PMB. It found that most of the trouble was due to careless handling and suggested procedures to be used to limit the errors to a reasonable level. The detailed report is available: "Andersen Filter Substrate Weight Loss," EPA-650/2-75-022 (NTIS No. PB 240720).

Many investigators opted not to use filter media: instead, thin metal foils, usually aluminum or stainless steel, were used to solve the weight loss problem previously noted with fiber glass. Many found that these solid metal surfaces had a problem which had been observed with the original collection surfaces supplied by the manufacturer – particles tended to bounce off the collection surface. An obvious solution was to increase the stickiness of the surface, usually by coating it with grease. This appeared to solve much of the problem; however, a grease that worked at one source might not work at another test.

In the meantime, people were reporting anomalous weight gains with the fiber glass substrates, including variations with temperature (Figure 1) and between various fiber glass filter types (Figure 2). As the depth of this problem became evident, EPA's PMB again asked SoRI to investigate the whole problem of substrate use in cascade impactors. A detailed laboratory study was conducted, utilizing many fiber glass filter media and metal foil greases.

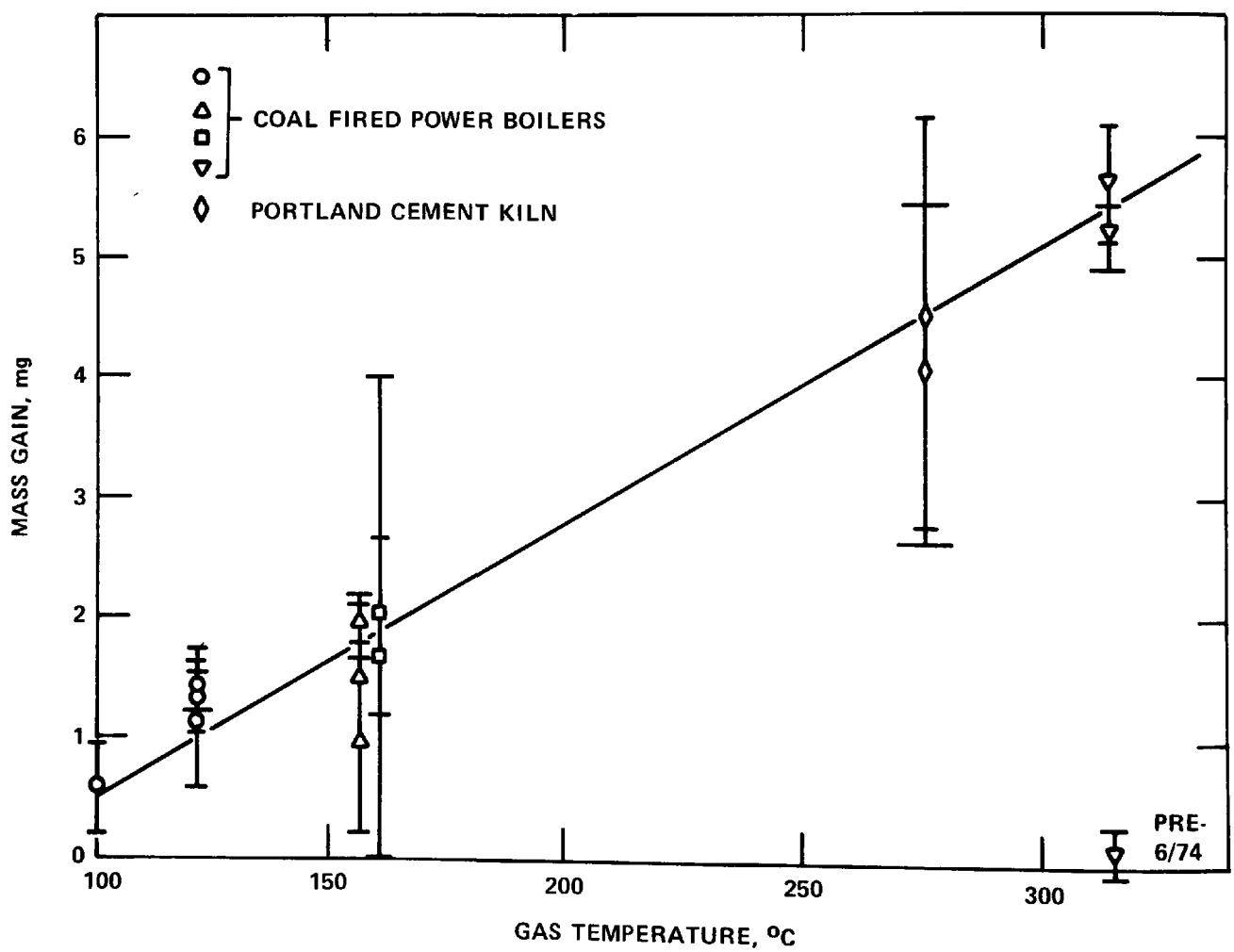


*Figure 1. Anomalous mass increases of Andersen glass fiber impaction substrates at different flue gas temperatures.*

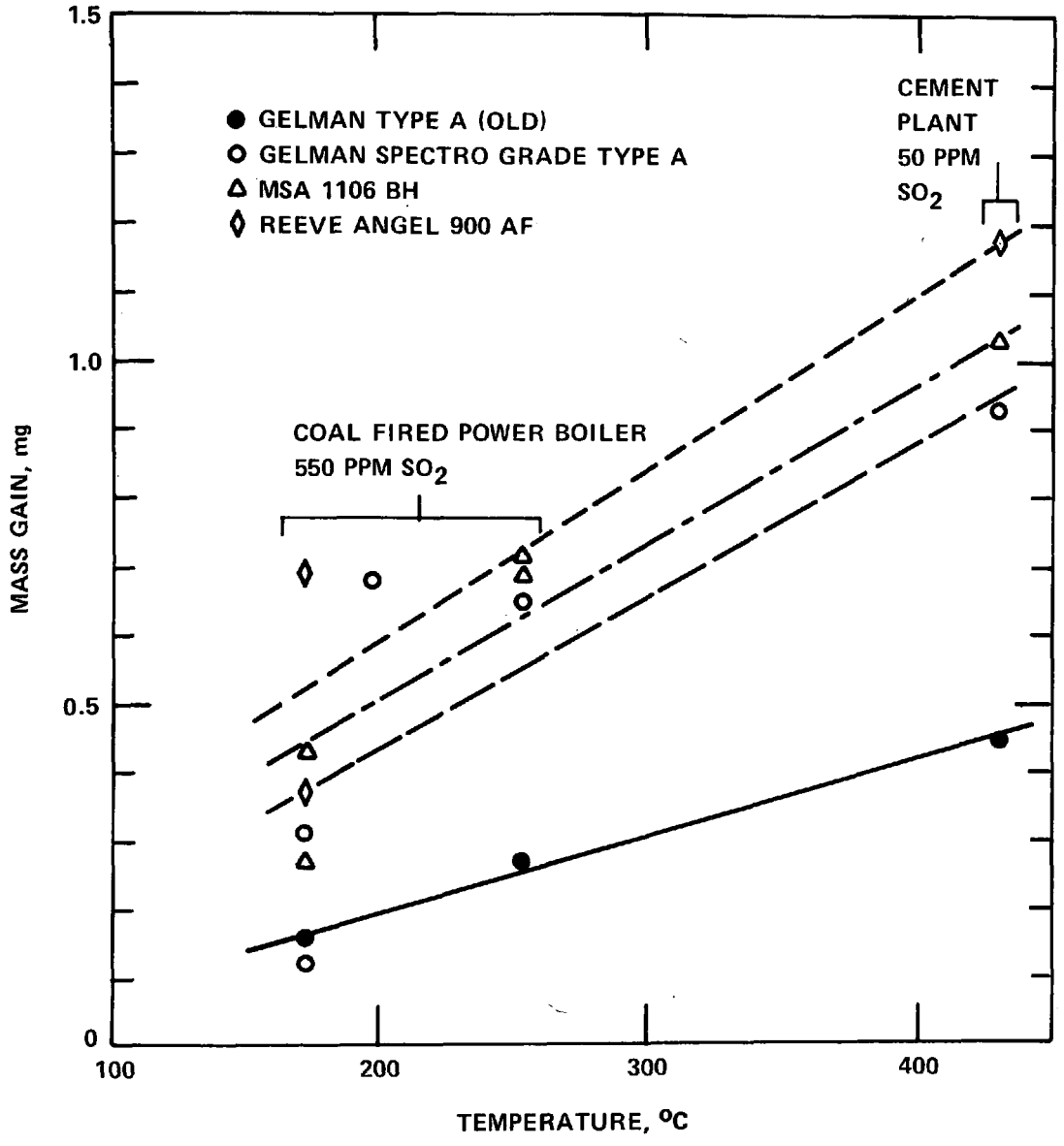


*Figure 2. Anomalous mass gains of various 47 mm diameter glass fiber filters at different temperatures (60 minute samples at flow rates of 0.25 acfm).*

Many investigators had reported extraneous mass gains on ambient filter media due to $SO_2/SO_3$ conversion on the filter to sulfates. The laboratory screening tests were run to understand what occurs during this mass gain and to select a material sufficiently inert for use as instack impactor substrates. A suitable material would be one which has stable low mass characteristics and is mechanically strong enough to resist cutting, tearing, and loss of material. Two laboratory test methods were used: one employed a flow of gaseous $SO_2$ through the filter media (Figure 3); the other involved soaking the material in hot sulfuric acid solution. The results of the gas flow studies are summarized in Table 1, which includes two materials which had been soaked in sulfuric acid. One fiber glass material (Reeves Angel 934AH) stands out for use as substrate media. Since manufacturers sometimes change processes without changing the media name, the substrates should be checked when received for conformity with previous batches. A pH stability test, for long term levels around 7, can be a good indicator.

Control of particle bounce and deposit scouring from metal foil substrates has been demonstrated for a number of grease coatings. The principal difficulty noted has been the deleterious effect of elevated temperature on their physical and chemical characteristics. Changes in viscosity sufficient to remove the grease from the collection surface and chemical breakdown to hard brittle masses have been noted.

A laboratory screening test was used, consisting of heating each grease in an oven for several hours, followed by examination of the material for changes in consistency, color, and mass. Of the many materials tested, Dow Corning silicone and Apiezon greases were the only ones to exhibit sufficient stability to warrant field testing.

The field test was conducted at a coal-fired power plant. Each impactor was loaded with the greased stages and the normal backup filter. A Gelman 47 mm prefilter was attached to the inlet to ensure that only gas (no particulate) would flow through the impactor, which was horizontal in the stack.

The two Dow Corning greases (Molycote III and Silicone High Vacuum) lost measurable weight from the stages and added weight to the backup filter. It was decided that these did not have the stability needed for instack use. The Apiezon tests are summarized in Table 2. The only grease not to lose weight was Apiezon H, which actually gained. Close examination of the stages revealed a fine even layer of dust, probably deposited during loading and unloading of the unit. Jet patterns were barely visible on most stages and a uniform coating of grease remained. No evidence of overflow was noted. An extended test

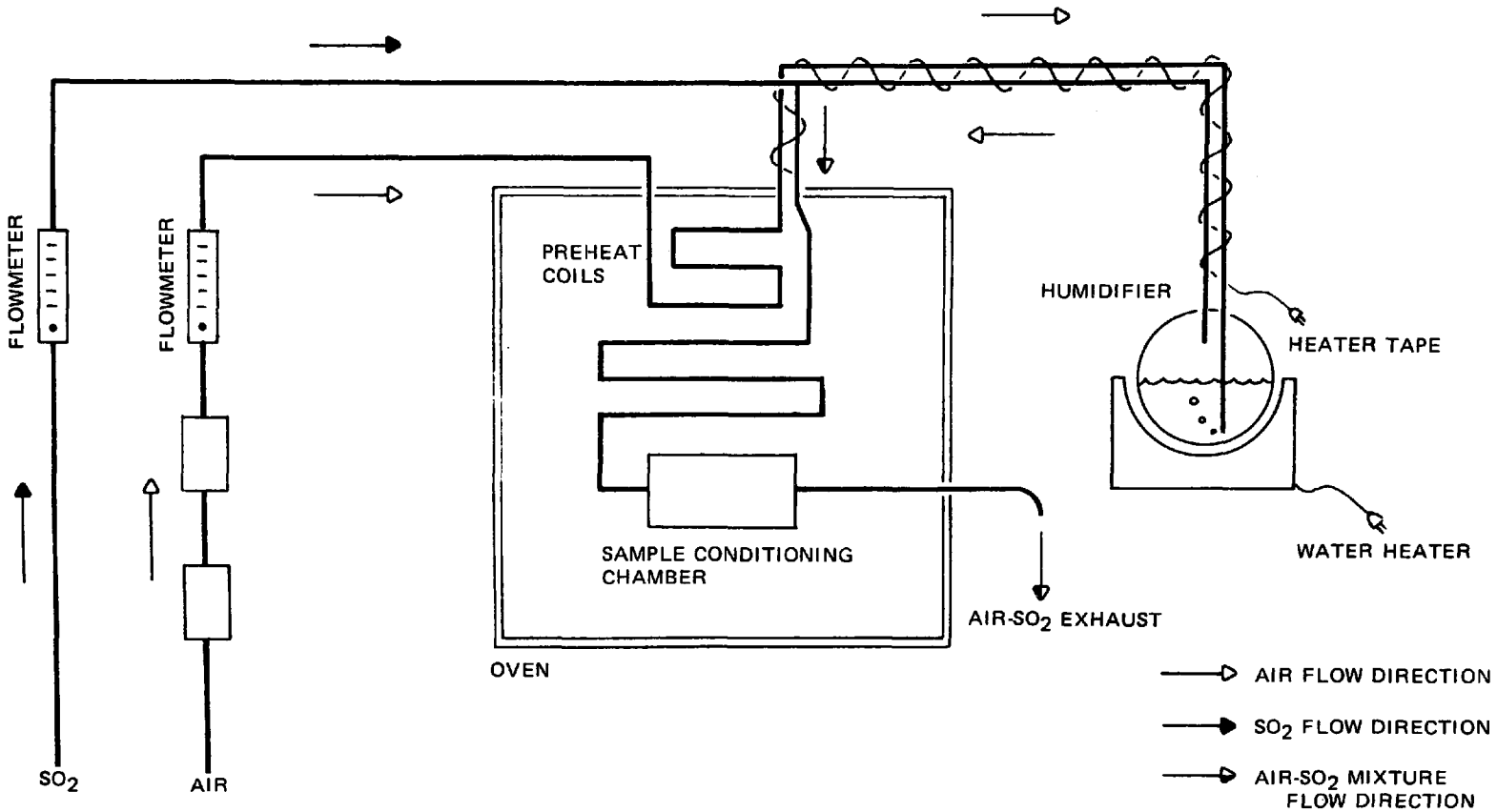


*Figure 3. Diagram of experimental set-up for filter substrate conditioning experiment.*

TABLE 1. MASS GAINS OF 47 mm GLASS FIBER FILTER SUBSTRATE MATERIALS FROM LABORATORY CONDITIONING[a]

| Material[b] | Batch Number | Number of 47 mm Filters Conditioned | Conditioning Time (hours) | Mass Before Conditioning (grams) | Mass After Conditioning (grams) | Mass Gain per Filter (mg) | Mass Gain (percent) |
|---|---|---|---|---|---|---|---|
| Reeve Angel 934AH | 3307 | 20 | 26 | 2.1888 | 2.1881 | -0.04 | -0.03 |
| Gelman AE | 8204 | 20 | 26 | 2.6644 | 2.8735 | 10.46 | 7.84 |
| Gelman Spectro Glass | 8192-20232 | 20 | 26 | 2.6717 | 2.8160 | 7.22 | 5.40 |
| Whatman GF/A | 3563 | 20 | 26 | 1.7695 | 1.8349 | 3.27 | 3.70 |
| Reeve Angel 934AH | 3307 | 20 | 26 | 2.2149 | 2.2166 | 0.09 | 0.08 |
| Gelman AE | 8204 | 20 | 26 | 2.6266 | 2.8375 | 10.55 | 8.03 |
| Gelman Spectro Glass | 8192-20232 | 20 | 26 | 2.6522 | 2.8051 | 7.65 | 5.77 |
| Whatman GF/A | 3563 | 20 | 26 | 1.7361 | 1.8272 | 4.56 | 3.64 |
| Reeve Angel 934AH (Acid Washed) | 4292 | 20 | 18 | 2.0968 | 2.0975 | 0.04 | 0.03 |
| Gelman AE (Acid Washed) | 8206 | 20 | 18 | 2.6939 | 2.7699 | 3.80 | 2.82 |

a. 1% $SO_2$, 3-5 ppm $SO_3$, saturated $H_2O$, 220°C (428°F).

b. Filter materials are listed in order of conditioning in a stainless steel Alundum thimble holder.

TABLE 2. SUMMARY OF FLUE GAS TEST RESULTS. THE FLUE GAS TEMPERATURE AVERAGED ABOUT 149°C (300°F) FOR ALL TESTS. IMPACTOR FLOW RATE WAS 0.7 acfm

| Substrate Set | 1 (Apiezon L) | | | 2 (Apiezon L) | | | 3 (Apiezon M) | | | 4 (Apiezon T) | | | 5 (Apiezon H)[e] | | | 6 (Apiezon N) | | |
|---|---|---|---|---|---|---|---|---|---|---|---|---|---|---|---|---|---|---|
| | Grease on Substrate, mg | Mass Change mg | Mass Change % | Grease on Substrate, mg | Mass Change mg | Mass Change % | Grease on Substrate, mg | Mass Change mg | Mass Change % | Grease on Substrate, mg | Mass Change mg | Mass Change % | Grease on Substrate, mg | Mass Change mg | Mass Change % | Grease on Substrate, mg | Mass Chan mg | % |
| Stage | | | | | | | | | | | | | | | | | | |
| 0 | Blank | +0.23 | - | Blank | +0.18 | - | Blank | +0.08 | - | Blank | +0.04 | - | Blank | +0.01 | - | Blank | +0.03 | - |
| 1 | 25.05 D | -4.96[a] | 19.8 | 35.28 D | -3.25[a] | 9.2 | 21.69 D | -0.02[c] | 0.1 | 23.68 D | -1.10[c] | 4.6 | 41.55 D | +1.56 | 3.8 | 18.19 D | -1.52[c] | 8. |
| 2 | 13.48 P | -7.29[a] | 54.1 | 7.51 P | +0.33 | 4.4 | 3.19 P | +0.04 | 1.3 | 1.89 P | -0.25 | 13.2 | 4.18 P | +0.82 | 19.6 | 4.41 P | +0.05 | 1. |
| 3 | 38.33 D | -27.98[a] | 73.0 | 37.24 D | -26.54[a] | 71.3 | 19.03 D | -7.14[c] | 37.5 | 3.25 P | -0.21 | 6.5 | 3.81 P | +0.80 | 21.0 | 19.00 D | -1.75 | 9. |
| 4 | 11.99 P | -0.64 | 5.3 | 9.14 P | +0.15 | 1.6 | 4.36 P | +0.10 | 2.3 | 24.87 D | -0.61 | 2.5 | 29.04 D | +0.44 | 1.6 | 3.37 P | -0.06 | 1. |
| 5 | 39.36 D | -24.18[a] | 61.4 | 29.28 D | -13.05[a] | 44.6 | 26.09 D | -10.11[c] | 38.8 | 24.78 D | -1.07[c] | 4.3 | 30.13 D | +0.53 | 1.8 | 18.79 D | -1.73[c] | 9. |
| 6 | 12.06 P | -0.35 | 2.9 | 8.69 P | +0.34 | 3.9 | 7.10 P | -0.05 | 0.7 | 3.69 P | +0.09 | 2.4 | 4.87 P | -0.05 | 1.0 | 4.14 P | -0.10 | 2. |
| Back-up | - | +0.15[b] | 0.1[f] | - | +0.17[b] | 0.2[f] | - | +4.40[d] | 3.1[f] | - | +5.13[d] | 3.6[f] | - | +4.36[d] | 3.0[f] | - | +4.74 | 3. |

a. Grease lost to overflow, not recovered.

b. Reeve-Angel 934AH Filter Material, preconditioned.

c. Some grease lost to overflow, most recovered and deposited back on foil.

d. Gelman AE Filter Material, preconditioned. Weight gains may be partially due to flue gas reactions.

e. Substrates contaminated with ambient dust, but probably not enough to alter results significantly.

f. Percent mass change in filter calculated using final filter weight.

Note: D means that the grease-toluene mixture was dropped on with a medicine dropper (20 to 25 drops).
P means that the grease-toluene mixture was painted on with a small camel's hair brush (3 to 4 times).

program of Apiezon H was run at a coal-fired power plant: results are given in Table 3. As a result of these tests, Apiezon H grease was approved for use in IERL-RTP programs for temperatures up to 177°C (350°F).

The complete results of this study can be found in EPA report "Inertial Cascade Impactor Substrate Media for Flue Gas Sampling," EPA-600/7-77-060 (NTIS No. PB 276583).

This paper has briefly reviewed the development of the use of collection substrates in cascade impactors. We will continue to monitor operational procedures for impactors and recommend techniques to satisfactorily use them; such as "Procedures for Cascade Impactor Calibration and Operation in Process Streams," EPA-600/2-77-004 (NTIS No. PB 263623), currently being used by IERL-RTP personnel and contractors.

TABLE 3. APIEZON H BLANK MASS GAINS FOR UNIVERSITY OF WASHINGTON MARK III SOURCE TEST CASCADE IMPACTORS[a]

| Stage | Run 1 5/17/76 | Run 2 5/17/76 | Run 3 5/19/76 | Run 4 5/20/76 | Run 5 5/21/76 | $\bar{X}$ | $\sigma$ |
|---|---|---|---|---|---|---|---|
| 0 | 0.22 | 0.08 | 0.16 | 0.55 | 0.65 | 0.33 | 0.25 |
| 1 | 0.06 | 0.09 | -0.18 | 0.11 | 0.85 | 0.19 | 0.39 |
| 2 | 0.04 | 0.01 | 0.04 | 0.10 | 0.64 | 0.17 | 0.27 |
| 3 | -0.03 | -0.11 | 0.09 | -0.13 | 0.64 | 0.09 | 0.32 |
| 4 | 0.02 | -0.08 | 0.09 | -0.05 | 0.47 | 0.09 | 0.22 |
| 5 | -0.06 | -0.13 | 0.05 | -0.03 | 0.31 | 0.03 | 0.17 |
| 6 | -0.14 | -0.12 | 0.13 | -0.05 | 0.16 | -0.004 | 0.14 |
| Filter[b] | -0.32 | -0.18 | 0.02 | 0.08 | 0.34 | -0.01 | 0.25 |

a. Coal-fired power boiler source, cold side precipitator operating at 107°C (225°F), 30 minute runtime. All masses in milligrams.

b. Reeve Angel 934AH 47 mm disc.

PAPER 14

# PARTICLE SIZE MEASUREMENT FOR THE EVALUATION OF WET SCRUBBERS

SEYMOUR CALVERT
RICHARD CHMIELEWSKI
SHUI-CHOW YUNG
AIR POLLUTION TECHNOLOGY, INC.

## INTRODUCTION

Under the sponsorship of the EPA, A.P.T. has performed performance tests on several industrial scrubber systems to obtain data on the fine particle collection efficiency of air pollution control scrubbers. The scrubber performances in different situations are reported in terms of grade penetration curves and the A.P.T. cut/power relationship.[1] This information was used to evaluate the scrubbers and to verify, improve and develop design equations for the scrubber systems.

The measurement of the size of small wet particles presents unique problems which were not entirely appreciated until recent studies were specifically conducted towards these measurements. This paper presents our experience with this problem including possible errors due to evaporation of water from the particulate as well as a single stage impactor design which has proved satisfactory.

## PARTICLE SIZE DISTRIBUTION MEASUREMENTS

The most important experimental measurements in the performance tests are those regarding particle size and concentration in the inlet and outlet of the scrubber. For accurate determination of particle size distribution, the measuring devices should be able to measure the particles as they exist in the scrubber. The devices should cause neither formation of particles nor breakup of aggregates. Cascade impactors are the most commonly used particle classifier in scrubber performance tests.

In a cascade impactor, particles are classified by inertial impaction according to their mass. The larger ones are collected

on the plate opposite the first stage and smallest on the plate opposite the last stage. Cascade impactors are found to be useful for measuring dry particle size distribution and concentration for particles with diameters from a few tenths to several microns.

In the outlet of a scrubber the particles are usually wet. Even though cascade impactors have been used for particle fractionation at the scrubber outlet, there is doubt whether the measured size distribution is representative of the wet particle size distribution leaving the scrubber. This doubt surfaced when we tried to measure the "grown" particle size distributions in flux force/condensation scrubbers with cascade impactors.

Flux force/condensation (F/C) scrubbers utilize diffusiophoresis, thermophoresis and condensation of water vapor to improve particle collection. A.P.T. has operated an F/C demonstration plant as well as several pilot plants.[2-5] Particle growth due to condensation of water vapor was demonstrated by the improved performance of the scrubbers as well as by observation of condensation clouds.

## Wet Particles

Measurement of the grown particle size distribution with multistage cascade impactors indicated some growth; however, the measured size distributions were not as large as predicted. The particles act as condensation nuclei and are predicted to grow to a size which is dependent upon the amount of water condensed and the number of particles present. In typical applications the problem becomes one of measuring wet particles with an aerodynamic diameter on the order of 1 μmA.

It was suspected that evaporation of water from particles occurred inside the cascade impactor due to the pressure reduction from stage to stage. To study the evaporation from particles within the cascade impactor we used the experimental apparatus shown in Figure 1. A 5% by weight sodium chloride solution was atomized using a Collison atomizer. The gas was mixed with dilution air which passed through a conditioner which either humidified or dried and heated the dilution air. The aerosol was then passed through an impactor to obtain size distribution data. A specific ion probe for Cl was used to determine the mass of salt collected in these experiments.

The first part of the experiment involved drying the aerosol generated by the atomizer by mixing it with dehumidified and heated dilution air. The size distribution obtained was that of the dry residual salt particles. Observation of the substrates indicated that no moisture was present for these runs. Figure 2 shows the size distribution obtained for the dry particles.

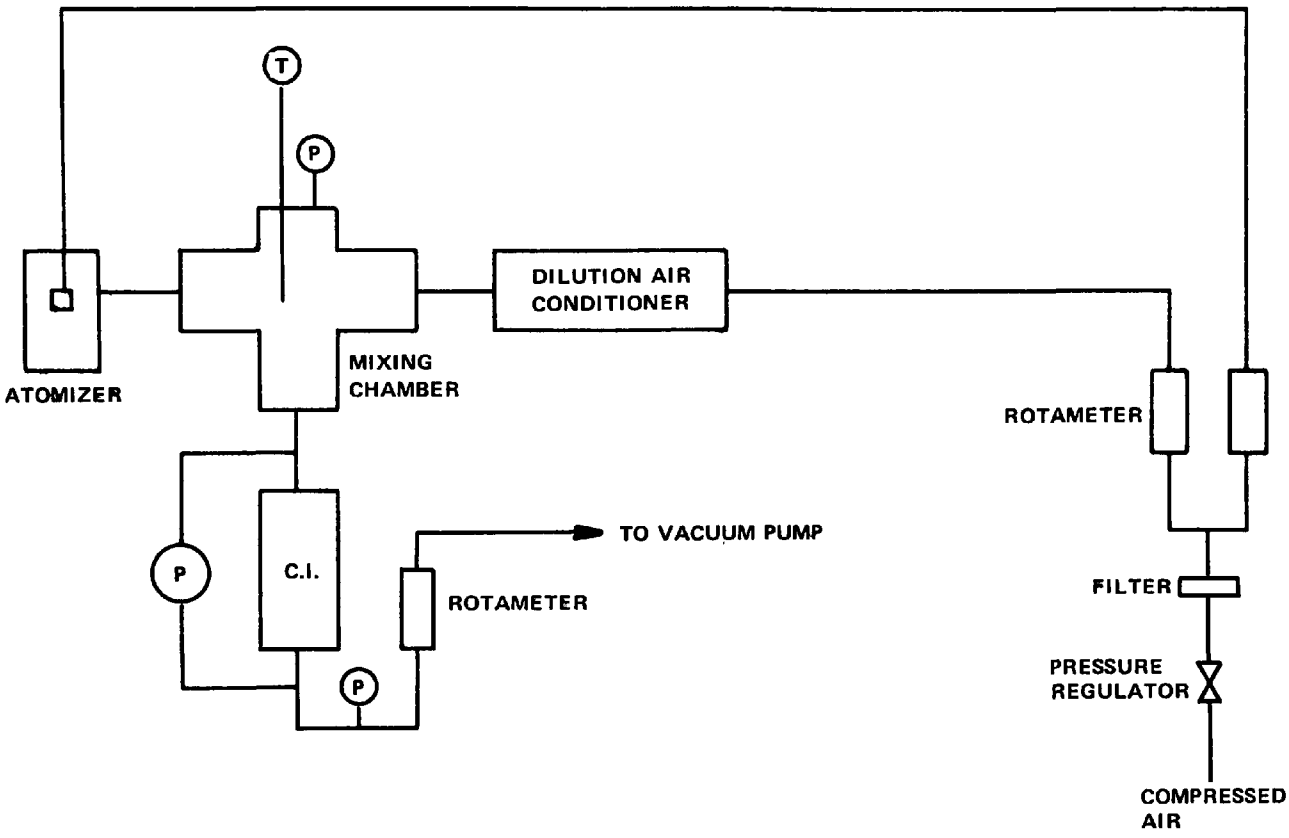


*Figure 1. Sketch of experimental equipment.*

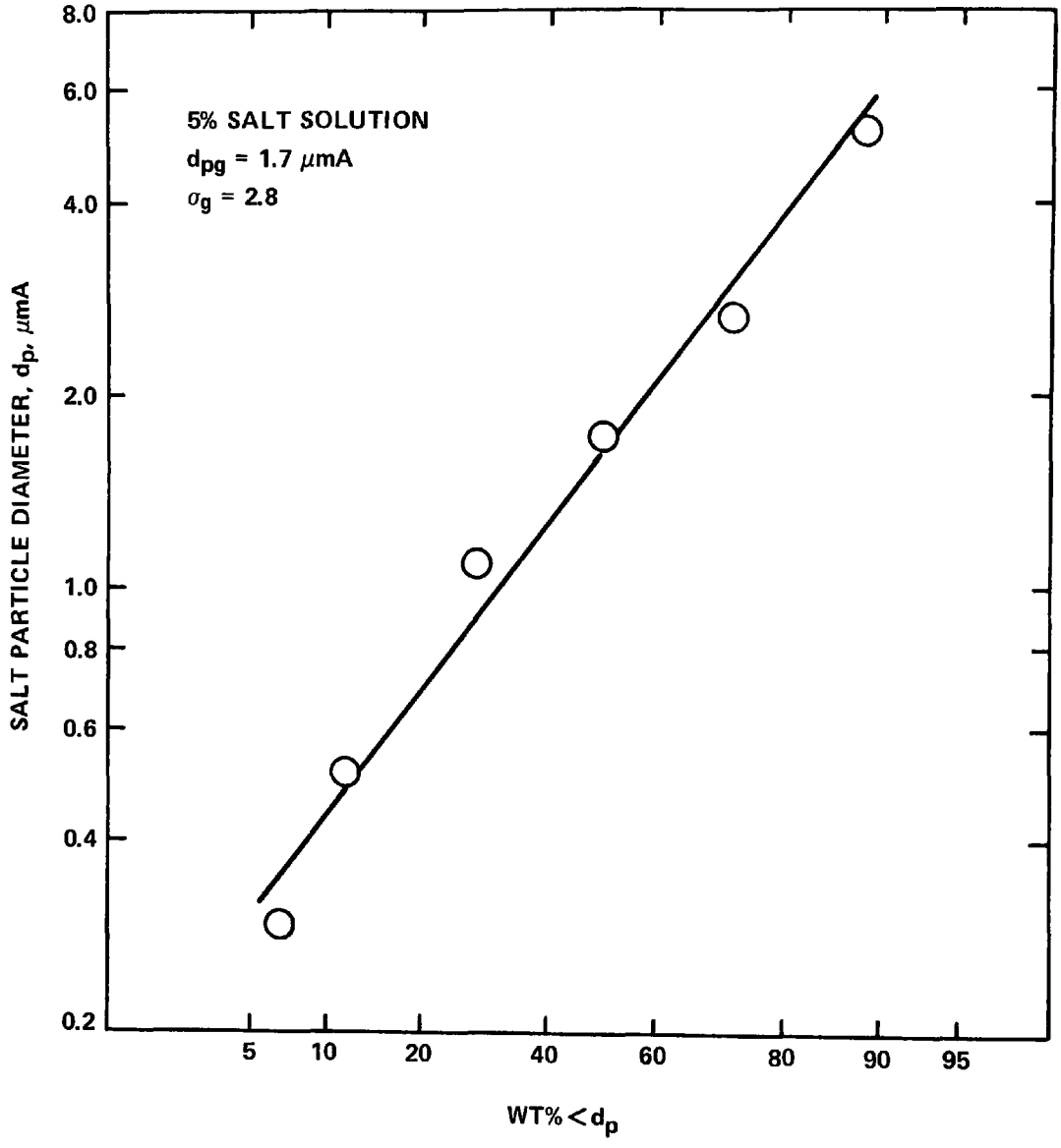


*Figure 2. "Dry salt" particle size distribution.*

The size distribution of the parent wet particles can be obtained from the size distribution of the residual salt particles since the initial salt concentration is known. The initial drop diameter is related to the salt particle diameter by the following equation:

$$d_d = d_p \, (\rho/c)^{1/3} \qquad (1)$$

where: $d_d$ = wet particle physical diameter, μm

$d_p$ = salt particle physical diameter, μm

$\rho$ = salt density, 2.16 g/cm$^3$

$c$ = salt concentration in solution, weight fraction

This equation is good for diluted salt solutions where the density of the solution is close to that of pure water. The predicted wet particle size distribution is shown in Figure 3. Note that the aerodynamic diameter is shown and that conversion to physical diameter is required for application of equation (1). Also shown on this figure are lines which represent size distribution which would exist if a given fraction of the water were evaporated from each of the particles. The upper curve shows the parent wet particle distribution while the lowest curve represents the measured dry size distribution.

Wet Size Measurement

The second part of the experiment involved measurement of the wet drop size distribution. For this case the dilution air was first saturated in a fritted disk bubbler so that particle drying would not occur. The results of several sampling runs with the University of Washington cascade impactor are shown in Figure 4. As can be seen, the wet size distribution, instead of being close to the predicted parent wet particle size distribution, is close to the size distribution of dried salt residues. This indicated that evaporation from particles occurred. Since the air was saturated with water vapor, evaporation from particles could not occur before the cascade impactor. Thus, it could be deduced that evaporation occurred within the cascade impactor.

To verify that evaporation did not occur before the cascade impactor, a second series of experiments were conducted using a series of glass impactors which allowed observation of the jet and impaction plate. Figure 5 shows the experimental setup. Each glass impactor consisted of one jet. By properly selecting the jet diameter, the pressure drop across each stage could be kept at a minimum.

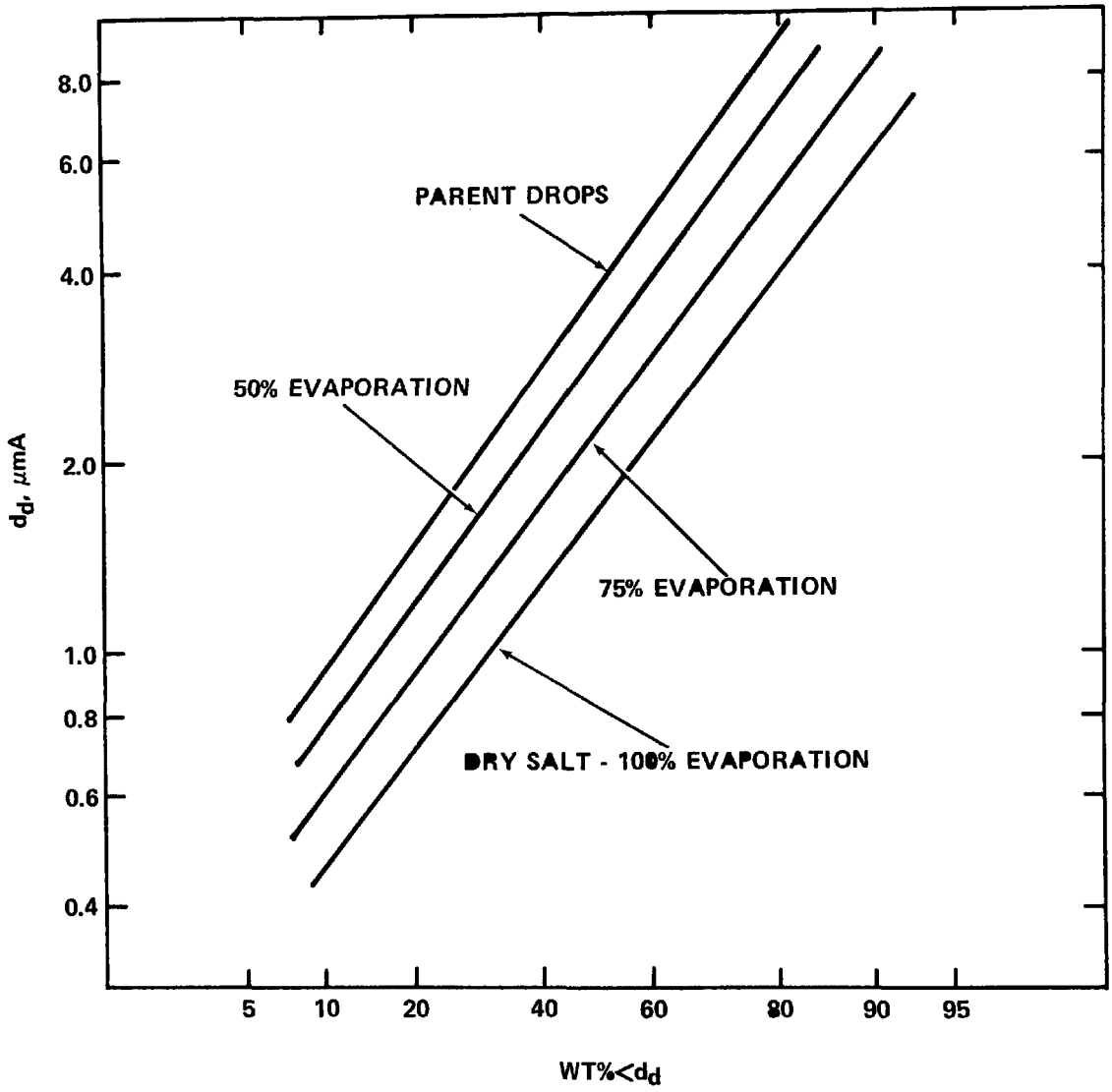


*Figure 3. Predicted drop size distribution as a function of water evaporated.*

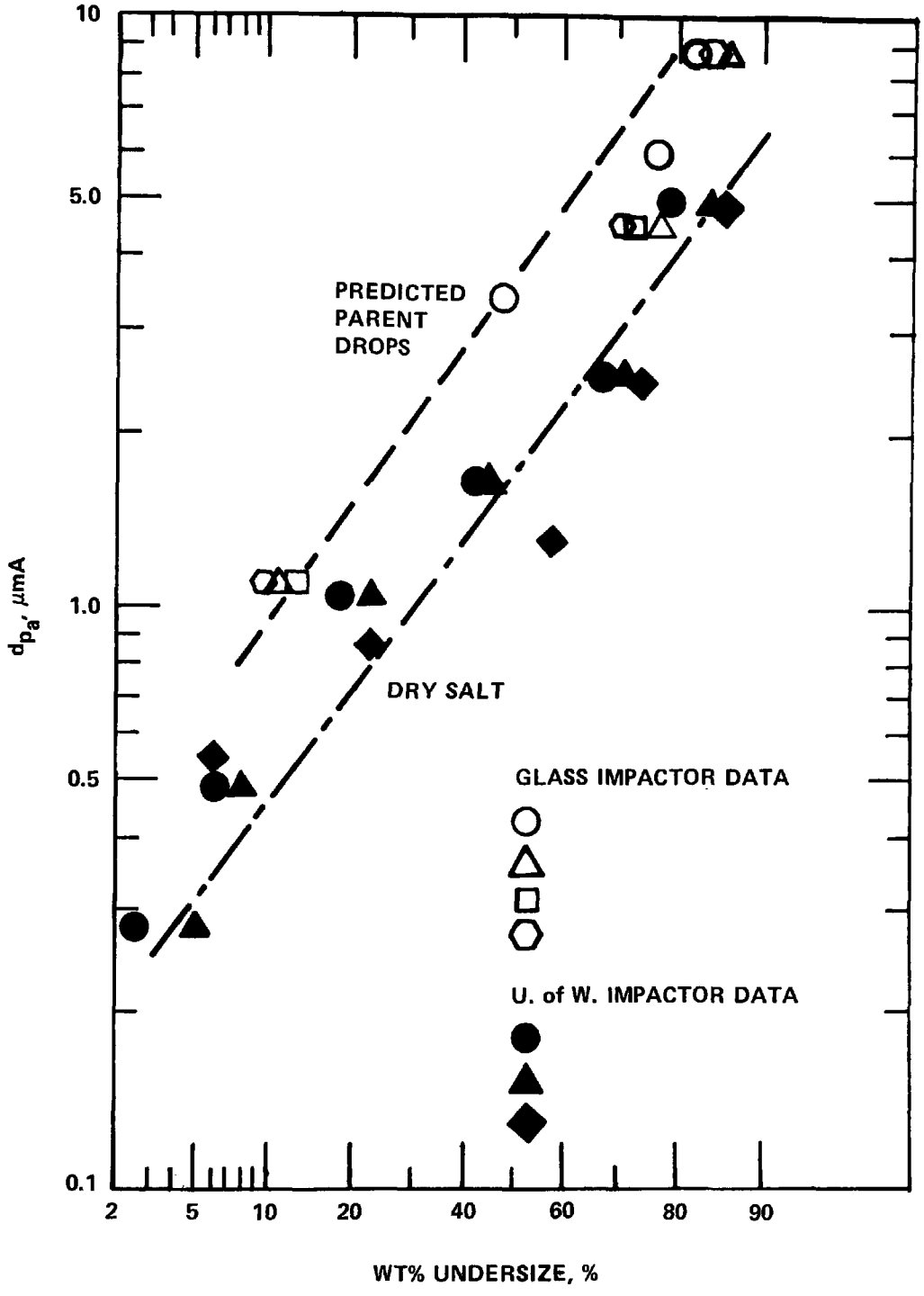


*Figure 4. Measured wet size distribution, U. of W. impactor and series glass impactor.*

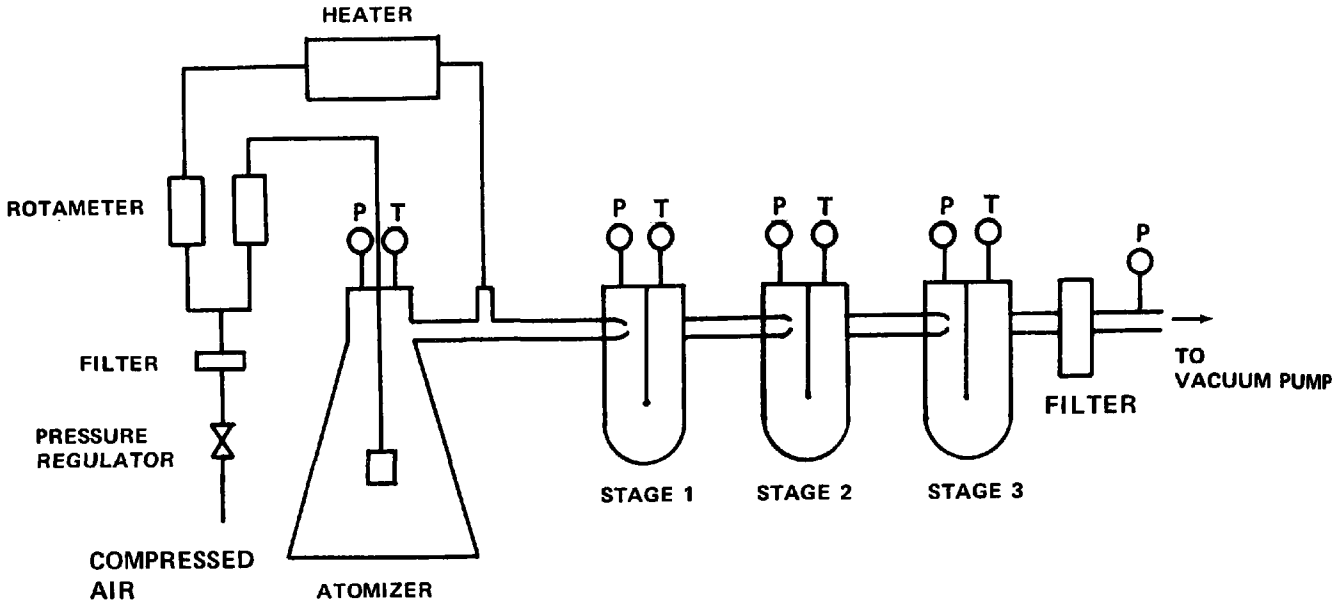


*Figure 5. Experimental setup for glass impactors.*

A solution of 5% by weight salt was atomized. The aerosol was dried by mixing it with heated dilution air. The dry salt size distribution confirmed the previously obtained dry size distribution from the University of Washington cascade impactor.

Several runs were then run without dilution air. The results are shown in Figure 6 along with the predicted wet particle size distribution. As can be seen, there is a reasonably good fit between the glass impactor data and the predicted wet particle size for diameters below 3 μmA. There is slight deviation for drops larger than 3 μmA in diameter. The parent drop size distribution was calculated from the dried salt distribution measured with the University of Washington cascade impactor.

The wet size distribution measured with the University of Washington impactor differs from that of the glass impactors for particles smaller than 3 μmA in diameter. The agreement between the two for larger particle sizes is fairly good. Apparently, significant evaporation from small particles occurred within the University of Washington impactor. The results shown in Figure 4 show that particles of 1 μmA in diameter have their diameters reduced to 0.6-0.7 μmA by evaporation.

The reason for the evaporation from the particles is probably due to the pressure reduction in the cascade impactor. The pressure drop across the glass impactor was relatively low. Therefore, little or no evaporation from particles occurs and the measured wet particle size distribution is close to prediction.

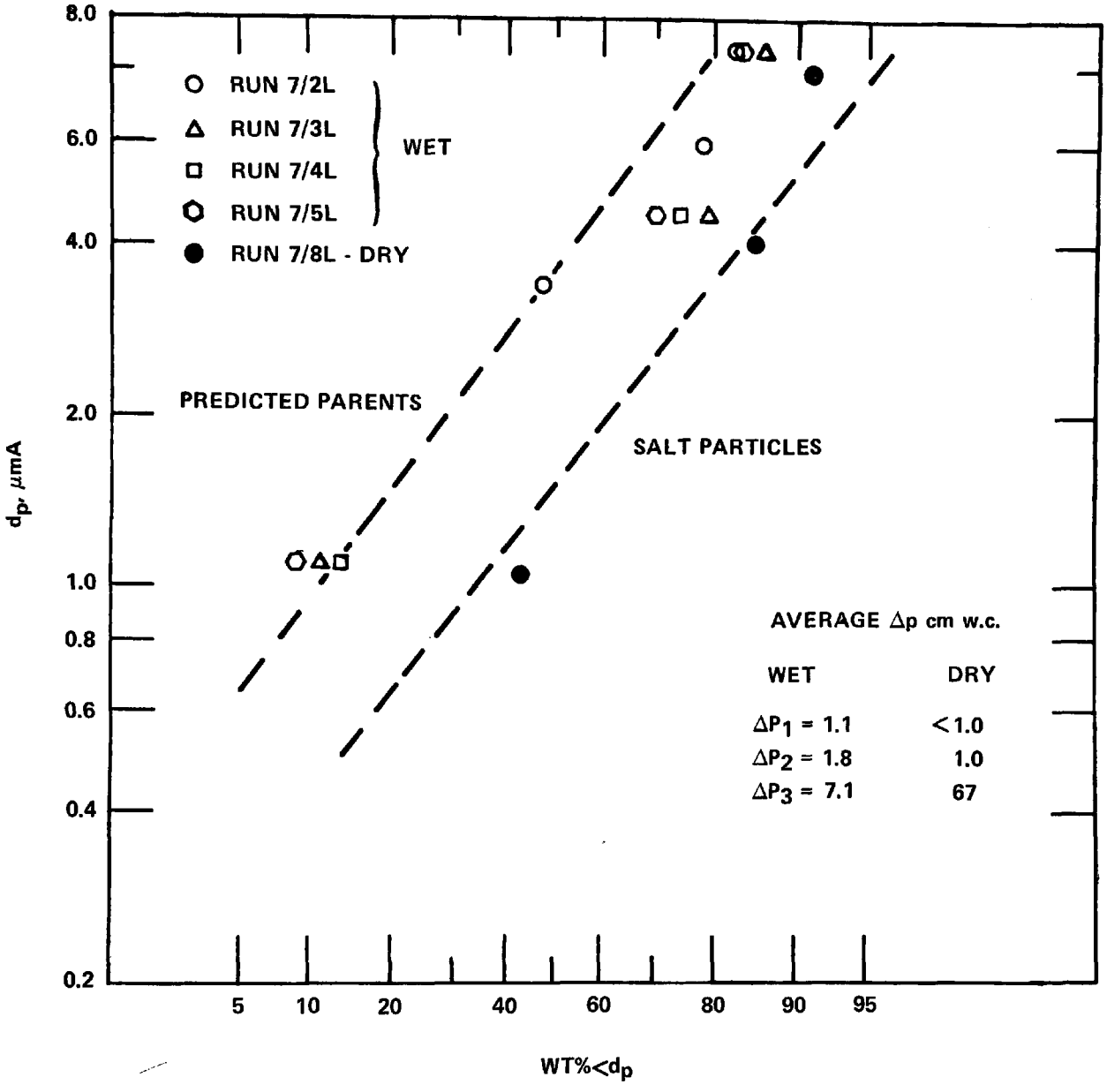


*Figure 6. Wet size distribution obtained with glass impactors.*

## Pressure Drop

Another observation made in the lab and field experiments is that the pressure drop experienced in a cascade impactor is generally larger for wet particles than for dry particles for comparable loading and sampling rates. This is usually attributed to a higher pressure drop across the final filter if water is present. Careful measurement of stage to stage pressure drop in the glass impactor shows a higher pressure drop for wet particles than for dry particles as shown in Figure 6.

The results of these experiments show that the size distribution of small wet particles (>3 μmA) obtained with a cascade impactor can be in error due to evaporation of water from the particles as they experience successive pressure reductions passing through the impactor.

## Single Stage Impactor

A single stage impactor has been used in order to get data on the size of the grown particles in an F/C system. The objective of the single stage device was to minimize the pressure reduction and the evaporation time. The initial sizing system was composed of a Greenburg-Smith impinger with a nozzle size and sample flow rate chosen to provide a cut point in the area of interest. The impinger was followed by a total filter so that a single cut point was obtained.

In one application the predicted grown particle size distribution indicated that a minimum particle diameter on the order of 0.5 μmA should occur with a given amount of condensation. Figure 7 shows the data obtained with the single stage impactor as well as the initial particle size distribution and predicted grown size distribution. These data demonstrate that small wet particles could be measured if enough care is taken and the problems are recognized.

## Entrainment Measurement

A related problem in determining the performance of wet scrubbers is measurement of entrainment. Scrubbing involves the energetic interaction of the gas stream and the scrubbing liquid. Entrained drops containing suspended or dissolved solids can cause excessive particulate emissions. The contribution which liquid entrainment makes to particulate emission can vary widely from system to system. There is no clear cut boundary separating "wet" particulate from entrainment; entrainment will generally be larger in size ranging from about 10 μm to several millimeters in diameter. The advantages and disadvantages of three common methods for measuring entrainment are briefly discussed below.

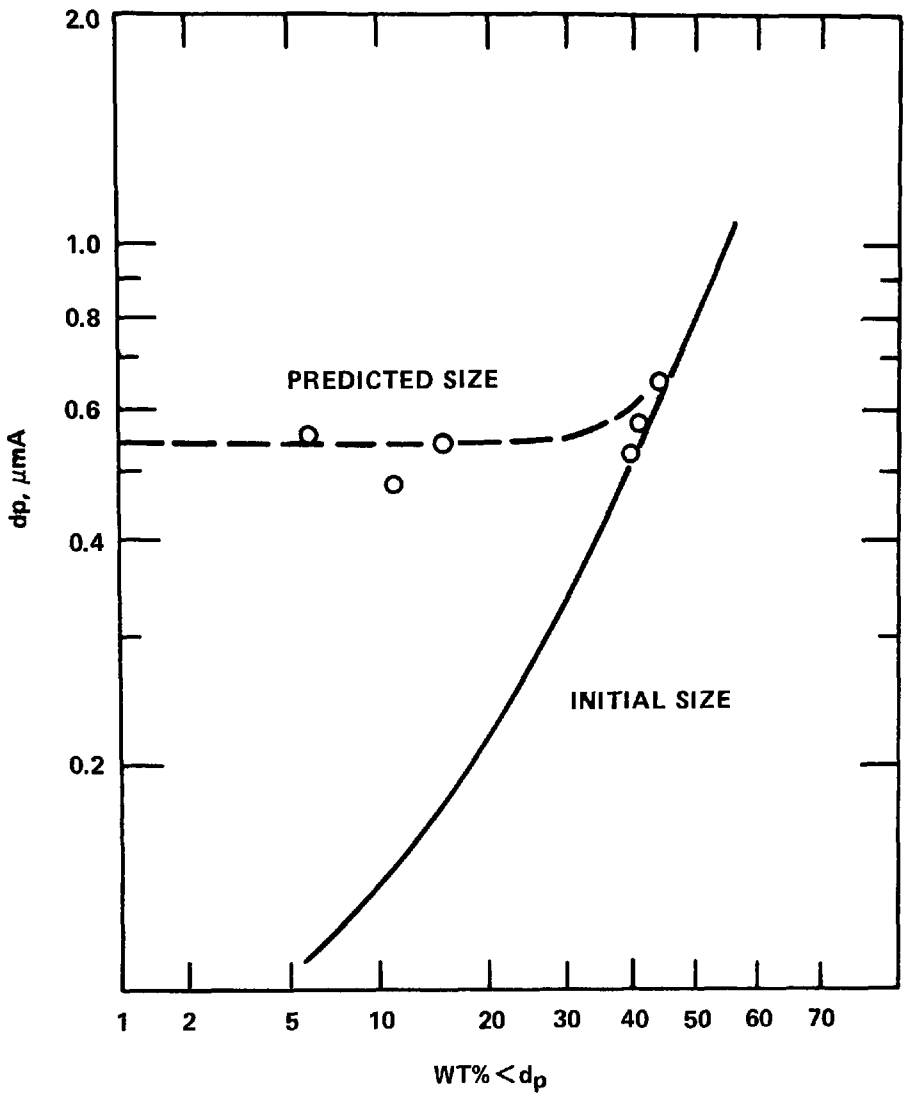


*Figure 7. Predicted and measured size distribution of wet particle with single stage impactor.*

A chemical stain method involving a treated filter paper impregnated with 1% potassium ferricyanide and coated with ferrous ammonium sulfate is one common method. Liquid drops collected on the filter paper make dark blue stains which can easily be counted and measured under the microscope. A correlation given by Chilton[6] is used to convert the blot diameter on the filter paper to the actual drop diameter. This method was found to be unsatisfactory. The main drawbacks are: (1) Due to the grain size of the chemical, it is not suitable for drops with diameters smaller than 20 μm. (2) It only gives the drop size distribution and gives no information on concentration. (3) It is difficult to obtain a representative sample since the impaction efficiency of the drops onto the filter paper will vary with drop diameter, filter size and gas velocity.

The second method is to use a cascade impactor. This can produce correct results for drops larger than a few microns. However, many of the commercially available impactors have cut points which are below the range of interest for entrainment measurement, i.e., for drops with diameters larger than 20 μm.

The third method for entrainment measurement is a hot-wire anemometer. An electrically heated wire is placed in the gas stream. Drops hitting the wire will attach to the wire, evaporate, and cool the wire. The amount of cooling is dependent on the drop size and is detected by monitoring the resistance of the wire. The hot-wire anemometer can yield information on drop size distribution as well as drop concentration. However, we found the hot wire to be very fragile. It could not detect large drops accurately and there were calibration problems.

## CONCLUSIONS

The cascade impactor is useful for measuring dry particle size distribution and concentration. It has a useful range of diameters extending from a few tenths of a micron to several microns. Due to evaporation of liquid from particles it is not generally suitable for measuring small wet particles.

A single stage impactor can provide information on the size of wet particles more accurately than a cascade impactor.

Liquid entrainment drop size distribution and concentration can be measured with hot wire anemometer, impactor and chemical stain methods. None of these techniques gives completely satisfactory results. Better techniques are needed.

## ACKNOWLEDGEMENT

The work upon which this paper is based was performed pursuant to Contracts 68-02-2124 and 68-02-2191 with the Environmental Protection Agency.

## REFERENCES

1. Calvert, S., et al. A.P.T. Field Evaluation of Fine Particle Scrubbers. Presented at the Second Fine Particle Scrubber Symposium, May 2-3, 1977, New Orleans.

2. Calvert, S., et al. Feasibility of Flux Force/Condensation Scrubbing for Fine Particulate Collection. EPA 650/2-73-036, U.S. Environmental Protection Agency, Research Triangle Park, NC, 1973. NTIS PB 277307.

3. Calvert, S., et al. Study of Flux Force/Condensation Scrubbing of Fine Particles. EPA 600/2-75-018, U.S. Environmental Protection Agency, Research Triangle Park, NC, 1975. NTIS PB 249297.

4. Calvert, S., et al. Improved Design Method for Flux Force/Condensation Scrubbing. Presented at the Second Fine Particle Scrubber Symposium, May 2-3, 1977, New Orleans.

5. Chmielewski, R., et al. Flux Force/Condensation Scrubbing. Presented at the Engineering Foundation Conference, November 1977, Monterey, CA.

6. Chilton, H. Elimination of Carryover from Packed Towers with Special Reference to Natural Draught Water Cooling Towers. Tr. Inst. Chem. Eng. 30:235, 1952.

PAPER 15

# EVALUATION OF PERFORMANCE AND PARTICLE SIZE DEPENDENT EFFICIENCY OF BAGHOUSES

D.S.ENSOR
R.G. HOOPER
G. MARKOWSKI
METEOROLOGY RESEARCH, INC.

AND

R.C. CARR
ELECTRIC POWER RESEARCH INSTITUTE

ABSTRACT

Baghouses have several operational characteristics which should be considered during field testing. These factors are high collection efficiency, variation in pressure drop and outlet concentration due to bag cleaning, integrity of the bags, and the operation of the emission source. Real time aerosol instrumentation at both inlet and outlet, gas monitors and pressure transducers, all logged on a common time base, are used to track the dynamic behavior of both baghouse and source. Any effect of mismatch in sampling times between inlet and outlet manual sampling trains can be evaluated with the real time data. A light scattering detector installed at the outlet is also useful in detecting operational problems, such as bag leaks and valve malfunctions. Experience has shown that a systems approach, including both source and baghouse, is required for a meaningful evaluation.

## INTRODUCTION

### Background

Baghouses are capable of unusually efficient collection of particulate matter. Compared to other types of gas cleaning

equipment, baghouses are relatively independent of the composition and size distribution of the material collected. As emission particulate mass limitations become more stringent and "clear stack" opacities are required, baghouses will have greater application.

In the past there has been little incentive to study the details of fabric filtration because of the more than adequate collection efficiency. However, with the potentially large scale application to electric power utilities, the basic data needed to optimize baghouses on full scale units must be obtained in an effective manner.

### Objectives of Paper

The objectives of this paper are to describe test techniques and approaches used to measure the detailed performance of full scale baghouses. The major emphasis is on measuring particle size dependent penetration or collection efficiency. The actual test methods for particle sizing may vary depending on site specific problems. The details of organization and management of a large test group using state-of-the-art methods in a remote location will not be discussed.

The techniques described in this paper have evolved in projects performed by Meteorology Research, Inc. for the Electric Power Research Institute. The objectives of these studies have been the complete evaluation of specific gas cleaning equipment. A systems approach utilizing continuous monitoring instrumentation during the field testing and a parallel engineering study of costs and maintenance problems has resulted in an integrated analysis of the technology for specific installations.

## TEST STRATEGY

### Description of Baghouse

Baghouses have unique aspects when compared to other gas cleaning equipment. A cut away drawing of a baghouse is shown in Figure 1. The dirty air enters through a duct at the hopper level. The gas is filtered through the bags and the cleaned gas exists through ducts at the top of the baghouse. The bags are attached to the cell plate. Baghouses are usually arranged in individual compartments. Each compartment has valves allowing isolation for cleaning with a reverse flow of air or mechanical shaking of the bags. The compartments may be cleaned on a timed cycle or when a limiting pressure drop is reached. Bags are typically 20 to 35 feet long and 12 inches in diameter. A wide variety of fabrics may be used for bag material. Fiberglass fabric coated with graphite or Teflon to reduce wear is the usual choice for utility boiler bags.

Other designs of baghouses include filtration of the gas on the outside of the bags or the use of fabric panels instead of bags. However, baghouses have in common the removal of particulate matter by filtration of the gas through a fibrous material and provision for cleaning the filtering material when the pressure drop becomes excessive.

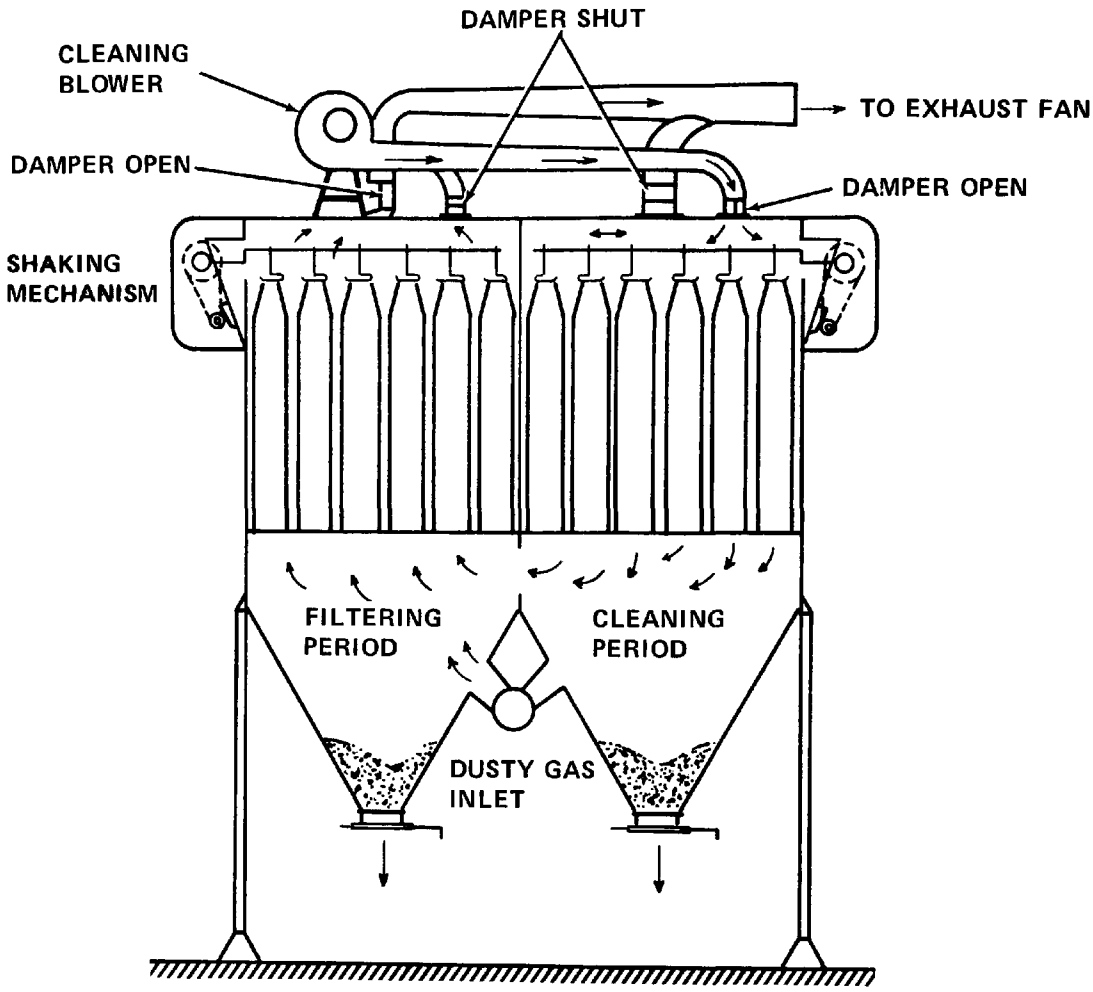


*Figure 1. Typical baghouse.*

## Test Considerations

There are several aspects of baghouse behavior which should be considered during a field test of a baghouse. Failure to consider the following items during the development of a test plan may yield misleading data.

Inspection--The integrity of the bags and cell plate is monitored for interpretation of the test results. For example, leaks could mask effects of bag cleaning and gas flow in a full scale unit. Samples of new and used bags should be obtained for laboratory testing.

High efficiency--The very efficient collection capabilities of fabric filtration place a heavy demand on the ability to measure gas streams with a 10,000 fold difference in particulate concentration. The outlet concentration of a baghouse can be as low as 0.0001 grains/ft$^2$. Thus, long sampling times with high flow rate test equipment and very sensitive instrumentation are required. Also special test and data reduction schemes are required to compute particle size dependent penetration under these conditions.

Batch process--Baghouses effectively behave similar to a "batch process" because of the need to clean the collected particulate matter from the fabric when the pressure drop becomes excessive. The outlet emissions will vary as compartments are removed from service and cleaned. During the test program, the cleaning cycle must be verified.

Time constants--The response of a baghouse is not instantaneous and in some cases several days could be required to obtain steady operation. The slowest changing parameters are those dependent on the ash layer in the bags. New bags require several weeks of conditioning to reach a stabilized collection efficiency and pressure drop. Process changes will introduce a time lag before steady conditions in pressure drop and collection efficiency are reached.

## Effects of Fabric Particulate Matter Loading on Baghouse Performance

The basic filtration parameters are the pressure drop and collection efficiency as a function of particle size. Both of these are dependent on the properties of the collected ash cake and the supporting fabric. The pressure drop mechanisms are best understood and will be used here for illustration of the effects of ash loading on the filter.

The pressure drop through a fabric filter is usually described by the following equation

$$\Delta P = S\ Q/A$$

where $\Delta P$ is the pressure drop through the supporting fabric and ash layer, S is the drag, Q is the volumetric flow rate, and A is the filter area. The parameter Q/A is often called the air-to-cloth ratio, or face velocity. The drag is usually related to the fabric areal loading w by a number of equations, including the linear form suggested by Robinson et al.,[1]

$$S = S_E + K_2 w$$

where $S_E$ is the effective filter drag and $K_2$ is the specific resistance coefficient for the dust. A nonlinear model has also been proposed by Davis et al.[2] for the cake formation zone with the form

$$S = a\ w^b$$

where a and b are regression coefficients.

A drag versus loading curve is shown in Figure 2. An explanation of the linear-nonlinear behavior has been advanced by Dennis et al.[3] from laboratory studies. The drag behaves in two stages depending on the history of the filtration cycle. Nonlinear drag and the cake formation occur during the stage where the particles deposit within the fabric. When the fabric is saturated and the cake forms on the surface, then a linear drag is observed. The nonlinear section is not truly a "cake repair" behavior as described in the earlier literature.[1] Dennis et al.[4] have developed a pressure drop model using the laboratory observation that ash tends to break off in sheets or slabs during cleaning. Therefore the filter cake is not homogeneous and has areas with behavior in both Zones A and B.

There are a considerable number of expressions for the specific resistance, $K_2$. One is the Kozeny-Carman equation

$$K_2 = (25/6)\ \mu\ (1 - \varepsilon)\ S_p{}^2/\ell_p\varepsilon^3 \qquad (1)$$

where $\mu$ is gas viscosity, $\varepsilon$ is the filter cake porosity, $S_p$ is the surface-to-volume ratio and $\ell_p$ is the particle density. $K_2$ could be expected to be a sensitive function of particle size. However, the determination of $K_2$ from experimental data indicated a different dependence on particle diameter than predicted above and a dependence on face velocity.[5]

At the present time, the areal dust concentration cannot be directly measured in the field without shutting off the baghouse and removing a bag. An indirect method to estimate the bag loading is to estimate the loading from the inlet concentration and cleaning frequency.

## Measurable Parameters

The measurable parameters are listed in Table 1. In the typical full scale field test as many of these parameters are measured as possible.

The fabric measurements which are performed in the laboratory are difficult to relate to the operation of the full scale baghouse.

TABLE 1. MEASURABLE PARAMETERS

| |
|---|
| Baghouse: |
| Pressure drop |
| Cleaning cycles |
| Gas flow rate |
| Temperatures |
| Fabric: |
| Permeability |
| Weight |
| Weave |
| Material |
| Flow Stream Properties, IN/OUT |
| Particulate concentration |
| Particulate size distribution |
| Opacity |
| Gas composition |
| Particulate composition |

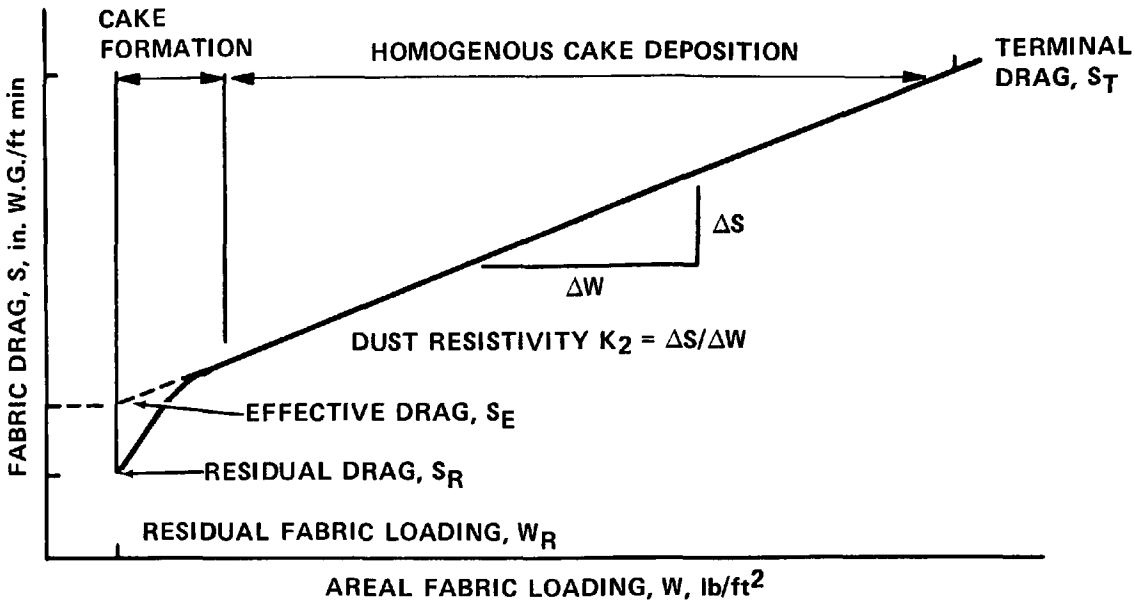


*Figure 2. Fabric filter resistance curve.*

## MEASUREMENTS

### Pressure Drop

Pressure drop is one of the fundamental variables describing the operation of the baghouse. During the fabric cleaning cycles, the pressure drop can be quite variable as shown in Figure 3. The pressure drop across individual modules during the operating/cleaning cycle is useful to trouble shoot and interpret operations. Two items may complicate pressure drop data:

- The overall pressure drop data reported for full scale baghouses is the flange to flange value. The overall pressure drop includes the pressure drop through the ducts and valves in addition to the pressure drop through the fabric. Although the flange to flange pressure drop is significant in the design of the process, it cannot be related to laboratory studies without assumptions or independent measurements of the pressure drop through the baghouse due to the components other than the bags.

- Often only the peak pressure drop for the baghouse is easily obtainable. Although this pressure drop is important for the fan designer, it is not descriptive of the pressure drop through the filtering bags and depends on the design of the baghouse.

For pressure drop data to be useful, the gas volume throughput and the part of the operating cycle during measurement must be specified. Most modern baghouses are well instrumented for

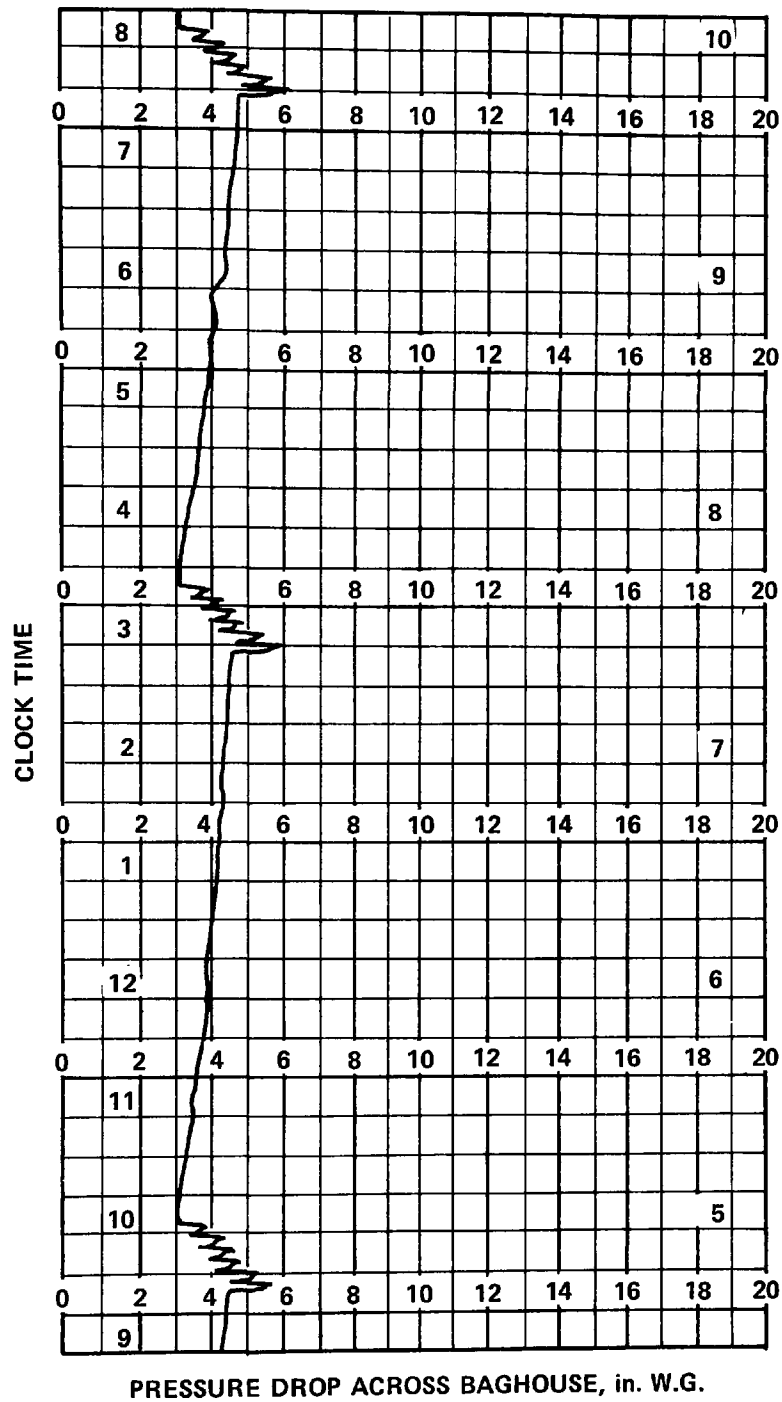


*Figure 3. Typical pressure drop trace.*

pressure drop measurement and additional transducers can often be added if needed.

Mass Concentration and Gas Velocity

Flue gas velocity and mass concentration are typically measured using EPA Methods 2 and 5, respectively.

Particles Larger than 0.5 μm

Cascade impactors have been used for source testing to characterize particles larger than 0.5 μm for a number of years. An example of early work was reported by Pilat, Ensor and Bosch.[6]

The impactor designed at MRI to facilitate sampling of particulate matter in stacks is shown in Figure 4. The design is a simple annular arrangement of jet and collectors reported by Cohen and Montan.[7] The simple jet-collection plate geometry has been thoroughly studied by many investigators (for example, Marple and Liu[8]). The use of a collection disc allows flexibility in choice of substrates. For example, either a greased surface or a filter mat can be used to enhance particle collection. "O" rings under compression seal the jet plates and body sections.

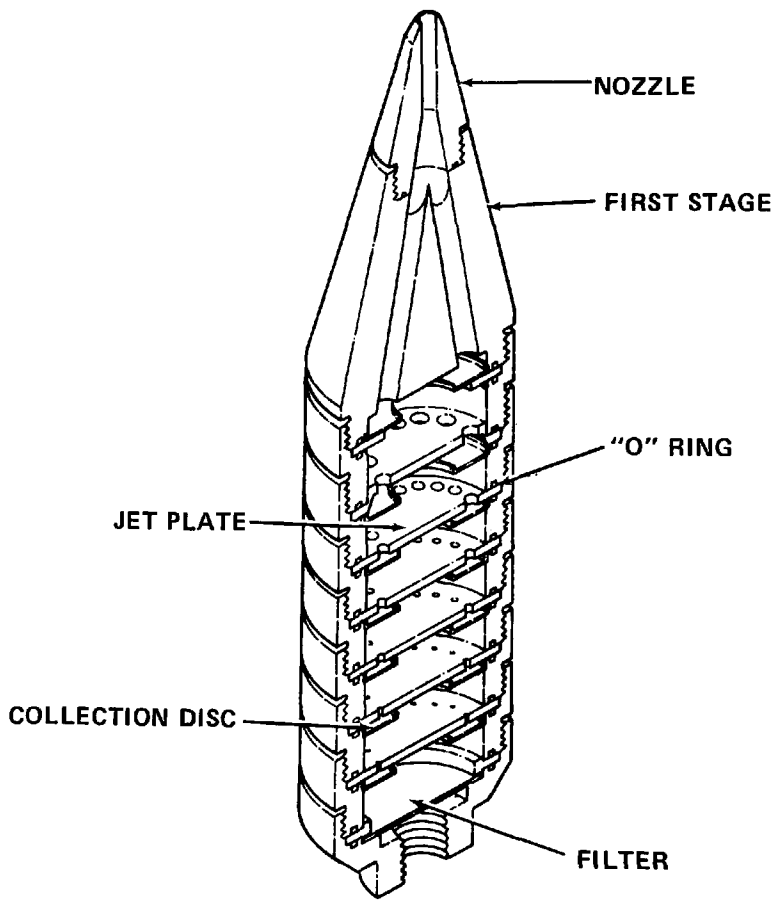


*Figure 4. Cascade impactor.*

The performance of a cascade impactor is strongly dependent on the surface on which the particles are collected. The two most popular substrates have been glass fiber filter mats and greased surfaces. A greased surface is preferable because glass fiber filter mats sometimes react with stack gases (Smith et al.[9]) Also, Rao reported that filter mats have poor collection efficiency.[10]

A large number of materials have been screened as coatings to enhance particle collection. Apiezon-L high-vacuum grease, a high-molecular weight hydrocarbon, had the best properties of the materials tested in terms of stability and particle adhesion and it has been used in tests less than 300°F.

The discs are then weighed on a Cahn 4100 analytical balance to 0.01 mg. Typical weights of the discs are approximately 630 mg. Weighing by substitution is used to improve the accuracy of the weighing. The discs are stored in labeled 15 x 60 mm petri dishes.

Quality control for the impactor tests include blank runs where filtered stack gas is sampled through the impactor to detect chemical reactions with the collection surface. In addition, field controls are used to verify the precision of the weighing.

The weighing precision of the discs is consistently within 0.01 mg. The weight changes of the substrates when subjected to filtered stack gas are typically less than 0.05 mg for flue gas from the combustion of low sulfur coal.

The wide mismatch in inlet and outlet concentrations (a factor of typically $10^4$) precludes simultaneous impactor testing. The approach used is a series of inlet tests a few minutes each within the time period, several hours, of two outlet tests. Blank tests at the inlet and outlet are also conducted.

The data is analyzed with a procedure reported by Markowski and Ensor.[11] The cumulative size distributions are fitted with a numerical interpolation technique. Differential size distribution curves are used to compute penetration. Error bounds on both differential size distribution and penetration are calculated.

## Submicron Particle Sampling

### Electrical Aerosol Size Analyzer--

The Model 3131 Electrical Size Analyzer (EASA) manufactured by Thermo-Systems, Inc., St. Paul, Minnesota, is the only commercially available instrument capable of measuring aerosol par-

ticle size distribution in the 0.01 - 1.0 μm diameter range. The EASA consists of two inter-connected modules: a flow module and a control module. It was commercially introduced in 1973 and is a greatly improved version of the Model 3000 which was commercially introduced in 1967. The EASA is described in detail by Liu, Whitby, and Pui[12] and by Liu and Pui.[13]

The EASA, shown schematically in Figure 5, consists of a charger, an electrical mobility analyzer which removes particles smaller than a selectable size, and an electrometer which measures the electrostatic charge carried by the particles which pass through the mobility analyzer.

Aerosol is drawn into the EASA at a flow rate of 50 ℓpm, of which 4 ℓpm is measured by the instrument, 1 ℓpm is filtered for use as charger sheath air, and 45 ℓpm is filtered for the mobility analyzer core air. The diffusion charger exposes the aerosol to positive ions, which charge the particles as a function of particle size. The charger sheath air prevents particles from entering the ion source chamber where they can acquire excessive charges. The 5 ℓpm of charged aerosol (4 ℓpm aerosol + 1 ℓpm charger sheath air) enters the mobility analyzer through an annular opening near the outer wall of the mobility analyzer, separating the charged aerosol stream from the negatively charged central rod.

The particles are attracted toward the central rod, the smaller ones with high mobility depositing near the entrance. Particles smaller than a certain size are collected, while larger particles pass through. The cutoff size depends on the voltage on the central rod. A high efficiency filter collects the larger particles and the associated current is measured by an electrometer.

By cycling the central rod voltage through a number of programmed steps, each of which represents a factory precalibrated particle size, one obtains a series of electrometer current measurements. The higher current values occur with low central rod voltages and small particle cutoff sizes. The difference of electrometer current between two consecutive central rod voltages is a measure of the particle concentration within the corresponding particle size range.

For field operation, the operator manually or automatically steps the voltage of the mobility analyzer collector rod through eleven internally programmed steps and records eleven corresponding electrometer current values, a procedure which requires about two minutes. Liu and Pui describe the calibration of the instrument, including aerosol sensitivity as a function of size and the collector voltage-particle size relationship.[13]

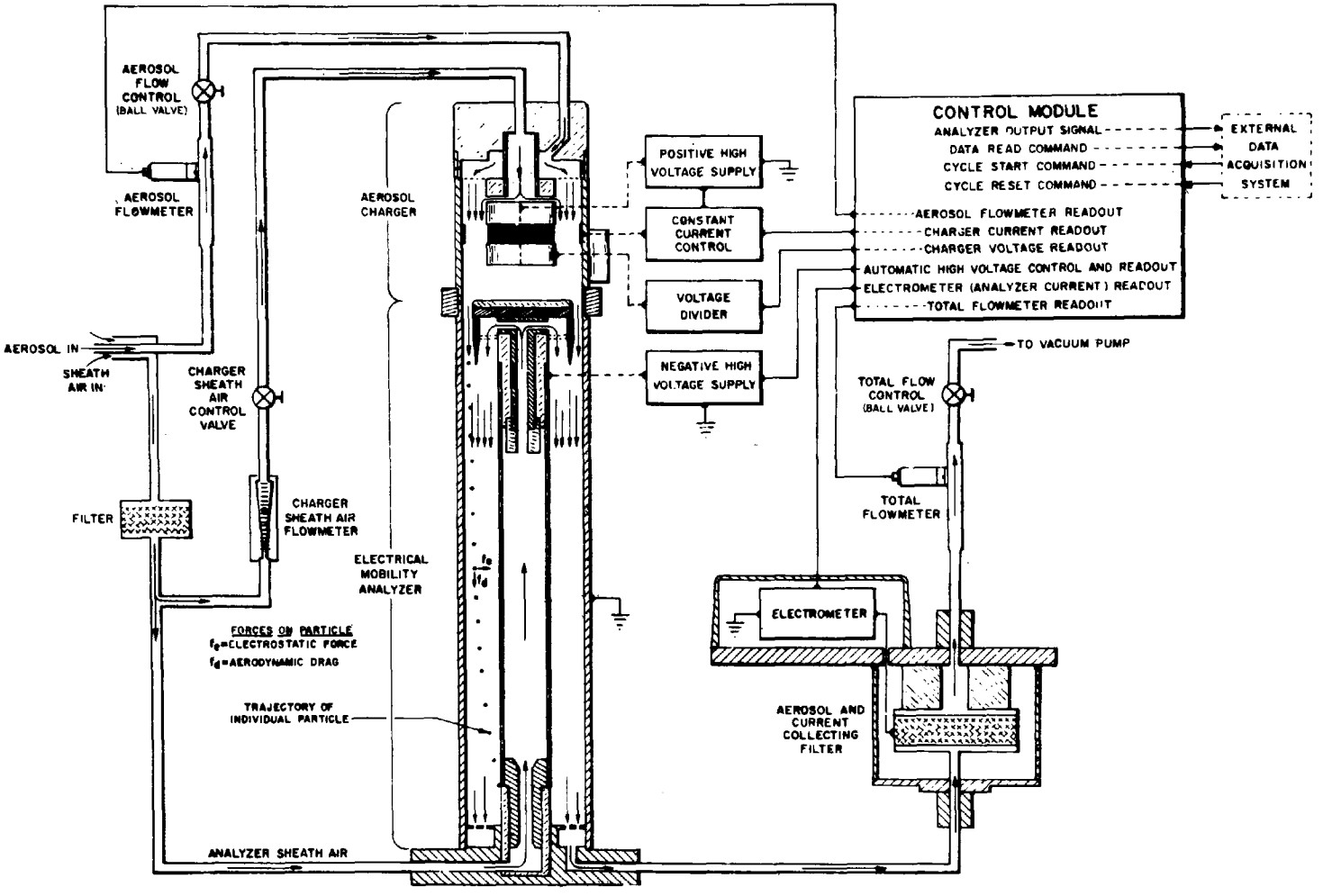


*Figure 5. Flow schematic and electronic block diagram of the electrical aerosol size analyzer.*

Extractive Sampling--

MRI uses dilution systems to precondition the stack aerosol to allow measurements with the EASA. Inlet aerosols to a baghouse may require dilutions from 10 to 5000:1. A coal-fired utility boiler emission usually requires from 100 to 200:1. In a typical system the aerosol is sampled through an impactor precutter through a heated line into a three-stage diluter. Each diluter consists of a venturi meter for the aerosol, an orifice meter for the dilution air and an orifice plate dilution chamber. An in-stack diluter is used at the outlet of a control device where dilutions of up to 20:1 may be required. The emissions from a baghouse may be so dilute that only a diffusional dryer may be used to remove the water from the emissions to prevent condensation in the particle measuring instrument.

Opacity

Plant Process Visiometer--

The real time measurement of the inlet and outlet opacity is very useful to monitor the operation of the baghouse. The outlet opacity is a sensitive indication of problems such as broken or leaking bags or valve leaks. Also the outlet opacity is important from a regulations standpoint.

It has been our experience that the emissions from a properly operating baghouse are so dilute that the opacity may be a few tenths of a percent, which is below the detectability of a stack transmissometer. A Plant Processing Visiometer, a hardened integrating nephelometer, is used instead.

A diagram of the instrument is shown in Figure 6. The aerosol is removed from the stack with a stainless steel probe and transported into the measurement chamber. The aerosol particles in the chamber are illuminated by a flash lamp with an opal glass filter. The scattered light is detected by a photomultiplier tube at approximately right angles to the flash lamp. The optics have been designed so that the output of the photomultiplier tube is proportional to the extinction coefficient due to scattered light. The instrument is a physical analog of the following equation:

$$b_{scat} = 2\pi \int_0^{\pi} \beta(\theta) \sin\theta \, d\theta$$

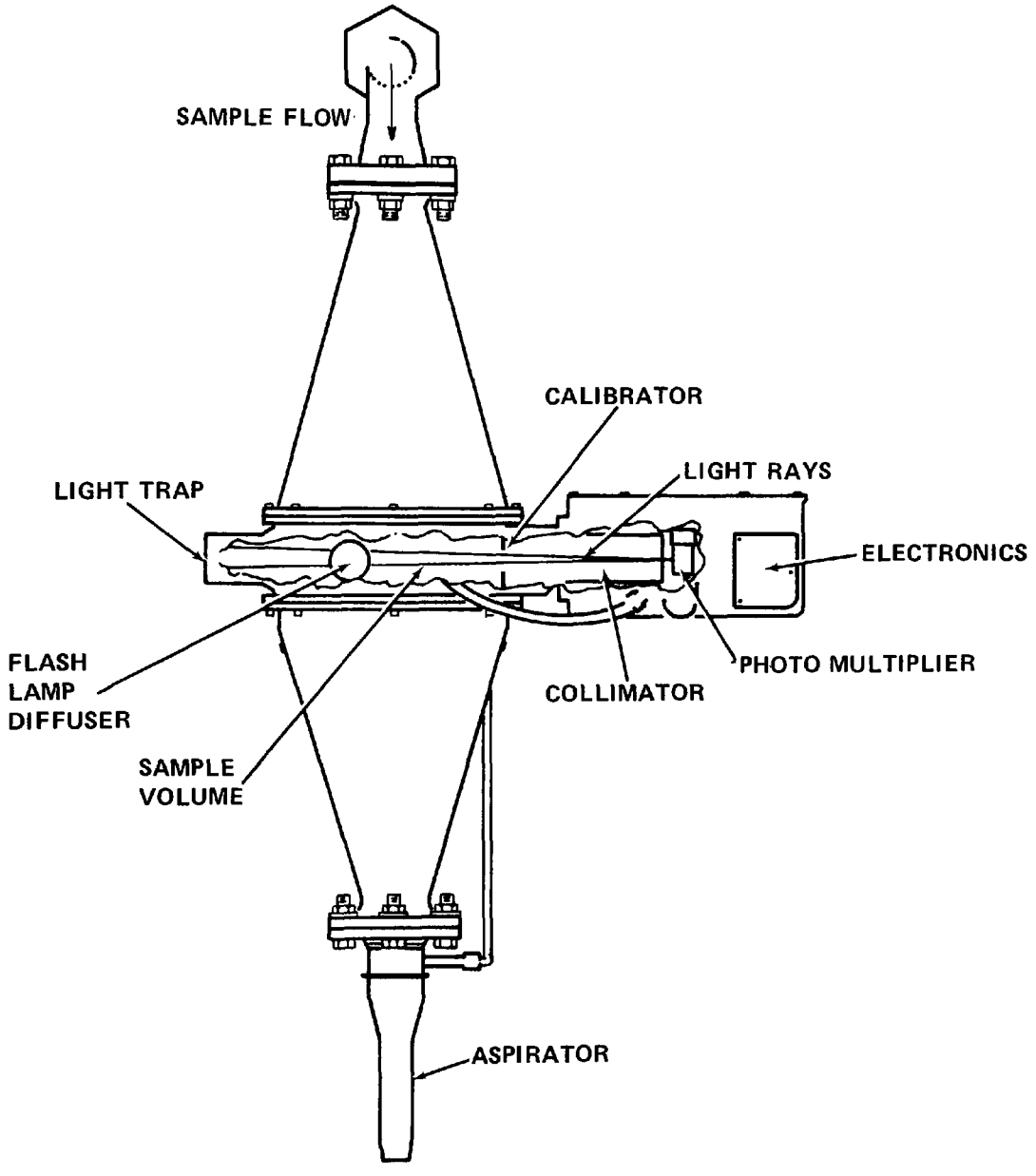


*Figure 6. Diagram of the plant process visiometer (PPV).*

where

$b_{scat}$ = the scattering coefficient due to scattered light

$\beta(\theta)$ = volume scattering function

$\theta$ = scattering angle

If there is no light absorption, the scattering coefficient is identical to the extinction coefficient. The extinction coefficient is related to plume opacity with Beer's Law.

$$\text{Opacity (percent)} = \left[1 - \exp\left(-b_{ext}L\right)\right] 100$$

where

$b_{ext}$ = extinction coefficient, $m^{-1}$

L = stack diameter, m

The instrument is spanned with an internal calibrator consisting of an opal glass lens of known scattering coefficient. The lens is mechanically placed in the view of the detector for calibration and retracted into a sealed chamber between calibrations. The PPV is described in detail by Ensor et al.[14]

Two aspects of the PPV performance are shown in Figure 7. The ability to adjust the gain over a wide range permits the use of two units: one to characterize the incoming ash and one to monitor the outlet of the baghouse. The outlet data indicates the sensitivity possible with the unit. The Freon 12 calibration point corresponds to a scattering coefficient of $3.6 \times 10^{-4} m^{-1}$ (8 mile visibility, 0.036 percent opacity on a 1-meter diameter stack).

Gas Sampling

Continuous gas analyzers are preferred to manual sampling for monitoring utility boilers because of the ability to detect upset conditions. The flue gas must be conditioned before introduction to the instruments. The gas is withdrawn from the stack with stainless steel probes with in-stack filters. The condensate is removed in a chilled dropout jar. Polypropylene tubing is used to transport the gas to the analyzers. Multiple probes at different locations in the duct are used to obtain a representative sample of stack gas and to sample for stratification. On site span and zero gas are used to calibrate the analyzers. Typically, $O_2$, $SO_2$, NO and CO are measured. Orsat samples are used to check the $O_2$, $CO_2$ and CO determinations.

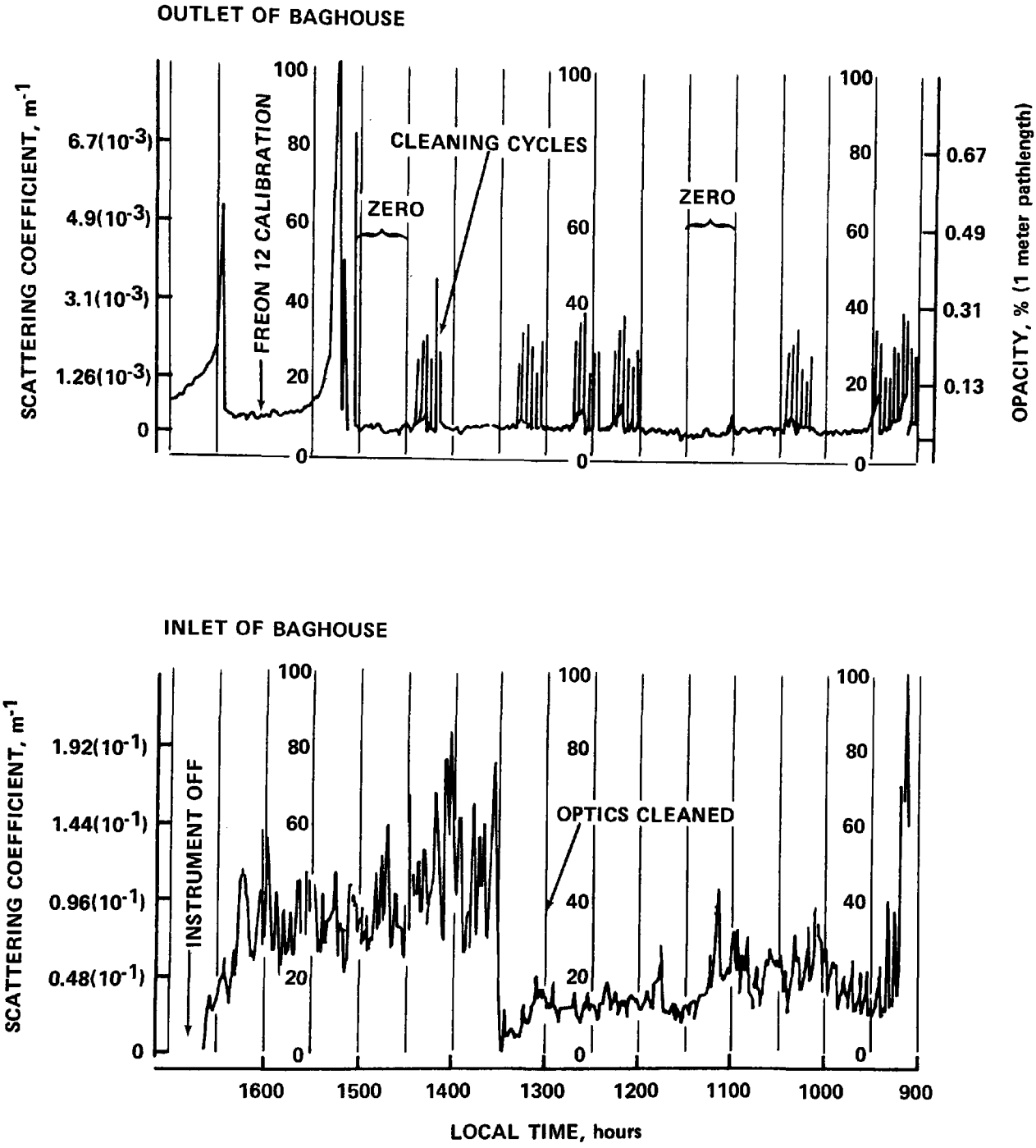


*Figure 7. Example of PPV data taken at Nucla baghouse.*

The Goksoyr/Ross (G/R) controlled condensation method is used to measure $SO_3/H_2SO_4$. The stack gas is pulled through a glass probe maintained at 450°F. The particulate matter is removed from the gas by filtration through a quartz filter maintained above 450°F. At this temperature the $SO_3$ is all in vapor phase and only particulate matter is removed. A quartz filter is used to reduce conversion of $SO_2$ to $SO_3$. The $H_2SO_4$ is then removed in a condenser maintained at 140°F. The condensate is titrated with NaOH to determine the acid concentration. The method is accurate to 16 percent.[15]

## Data Integration

The numerous and diverse measurements performed on a baghouse pose some problems in assembling the information. Our approach to reduce difficulties in data analysis is to data log all continuous output on a magnetic tape data logger. The single time base allows correlation of the various parameters. A schematic of such an arrangement is shown in Figure 8. In this scheme a central data logger is used with backup strip charts. This arrangement allows a field test control room where the test parameters can be monitored from one location.

# EXAMPLES OF DATA OBTAINED

## Process Charts

Process charts of the main parameters plotted on a common time basis are useful to determine the effects of process changes or upsets on the baghouse. An example is shown in Figure 9.

## Efficiency as a Function of Operating Parameters

Ideally the test should include some variation of air-to-cloth ratio and the cleaning cycle to develop the limits of operating parameters. An example of variation of emission with air-to-cloth ratio is shown in Figure 10. This information is useful for engineering design.

## Penetration

The cascade impactor and EASA data are used to compute the particle size dependent penetration through the baghouse. The data reduction technique reported by Markowski and Ensor[11] is used for the cascade impactors. The EASA data is reduced by computing an inlet and outlet size distribution and dividing the outlet by the inlet distribution. An example of penetration data obtained at a baghouse is shown in Figure 11.

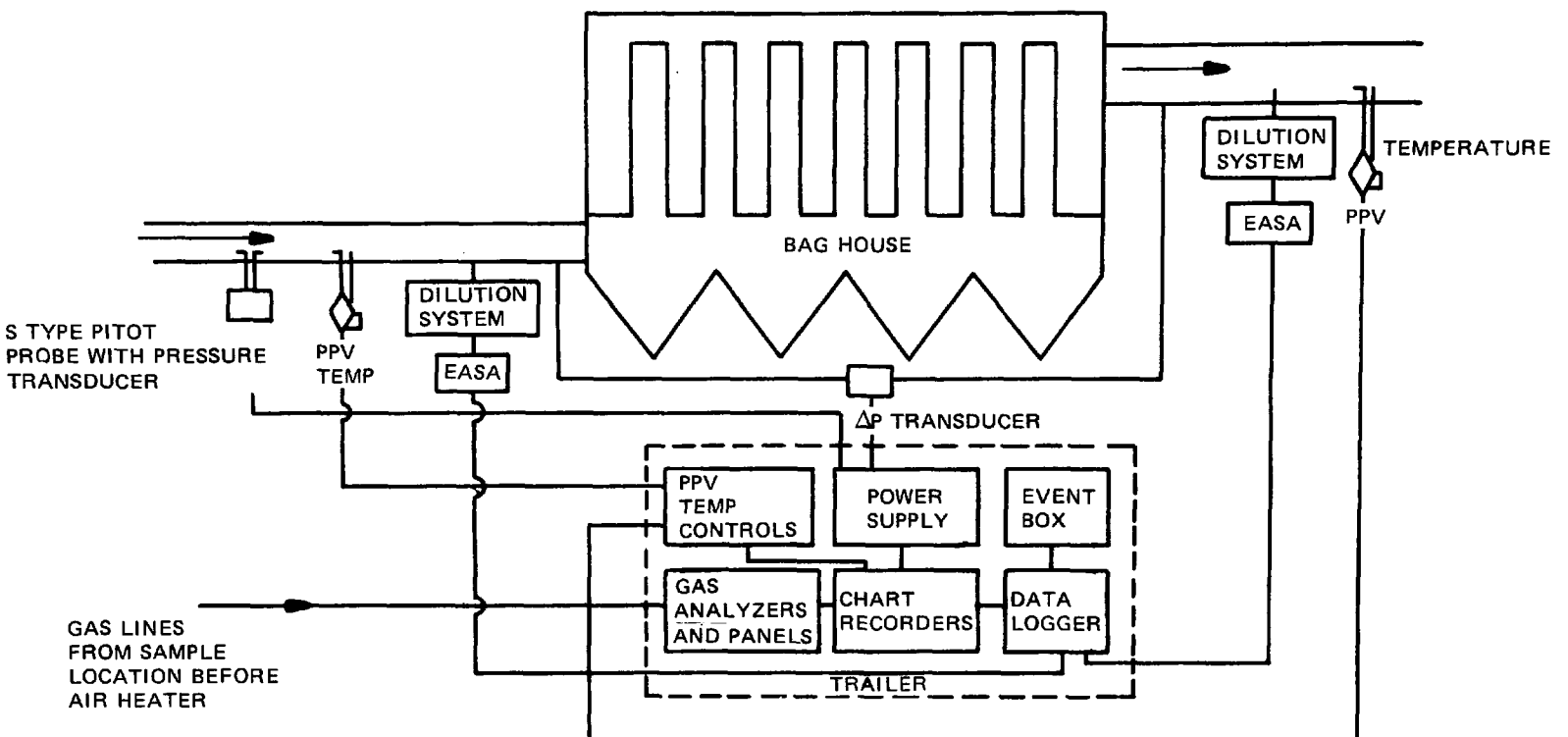


*Figure 8. Integrated baghouse sampling system.*

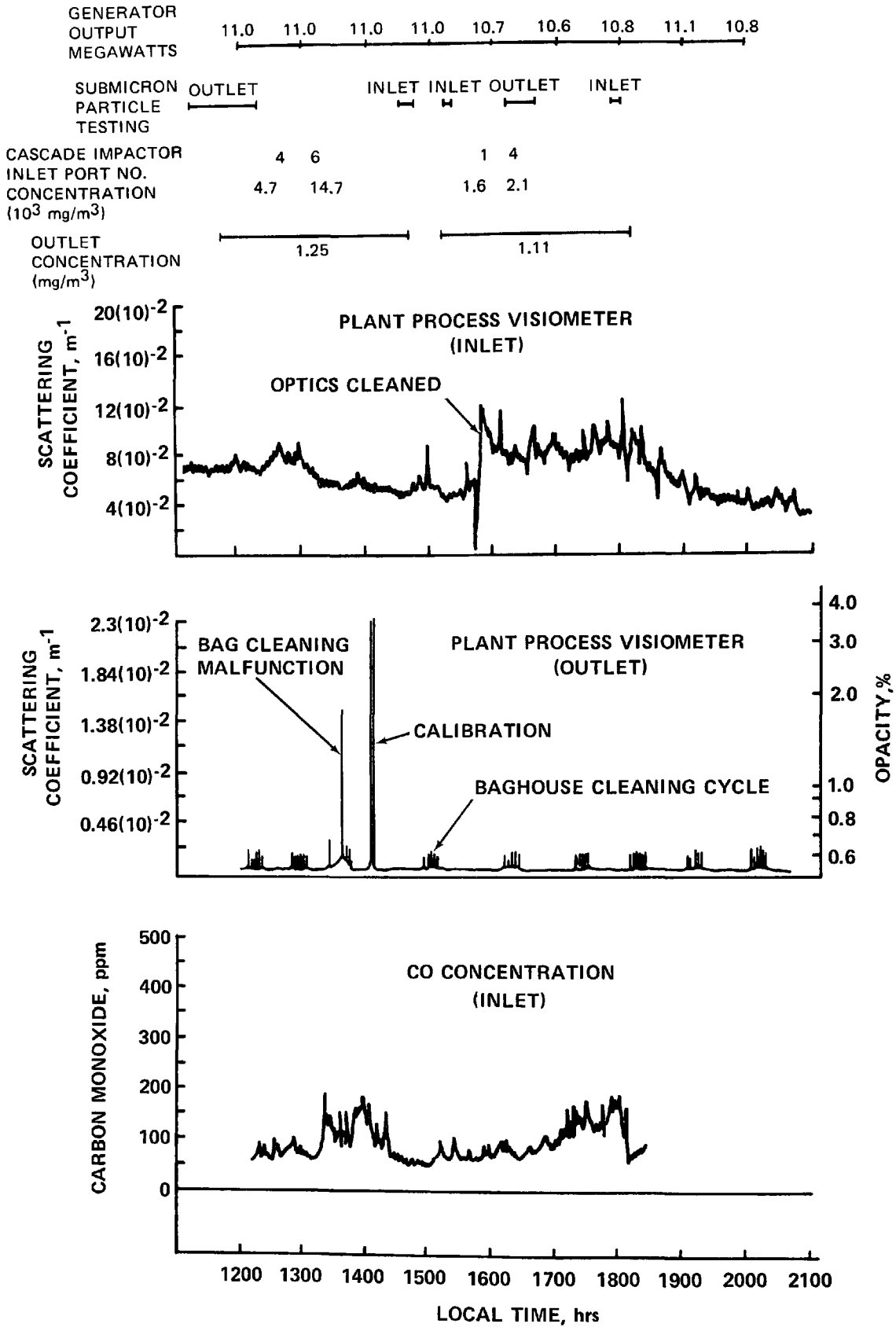


*Figure 9. Process variation during November 12, 1975 (Ensor et al.[16]).*

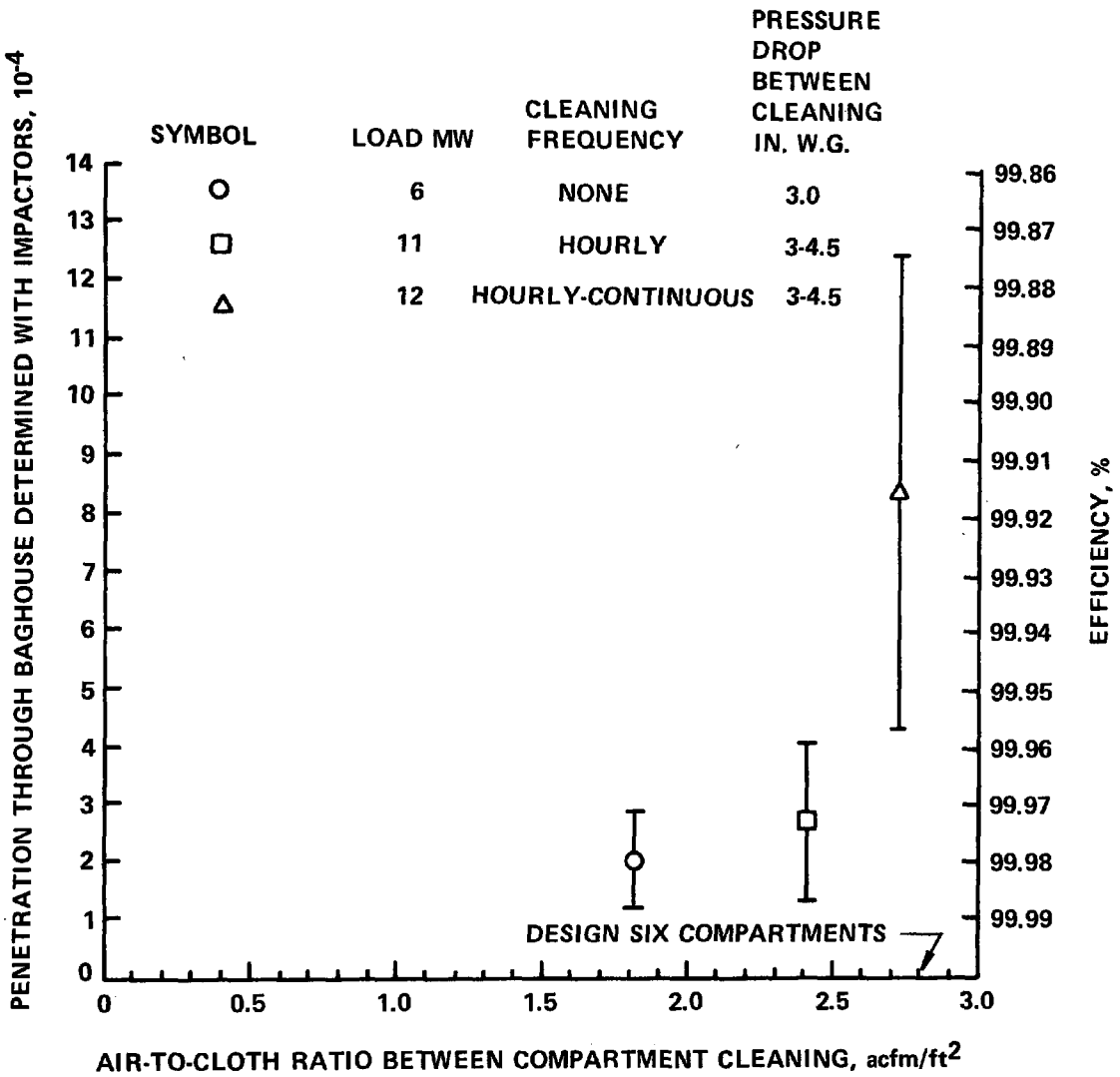


*Figure 10. Penetration as a function of air-to-cloth ratio with one standard deviation limits (Ensor et al.[16]).*

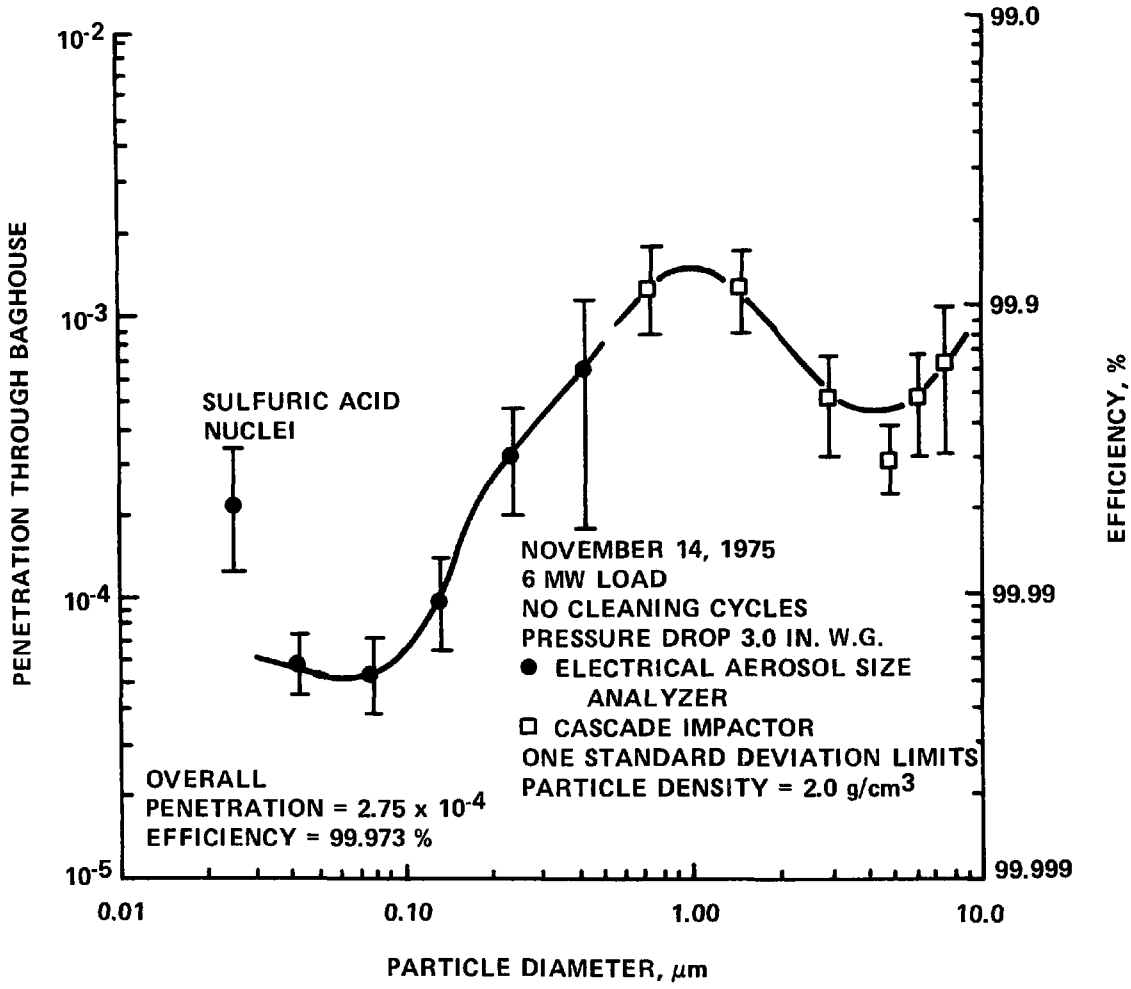


*Figure 11. Fractional penetration through baghouse (Ensor et al.[16]).*

## SUMMARY

The field measurements are complicated by the variability of the outlet particulate concentrations, the dilute emissions, the time required to obtain stable conditions, and the conditions of the bags. The testing of baghouses is facilitated with the use of continuous instruments for both particulate matter and trace gases, and data logging.

## REFERENCES

1. Robinson, J.W., R.E. Harrington, and P.W. Spaite. Atmos. Environ. 1(11):499-508, 1967.

2. Davis, W.T., D.E. Noll, and P.J. LaRosa. A Predictive Performance Model for Fabric Filtration Based on Pilot Plant Studies. In: Proceedings, User and Fabric Filtration Equipment II, Specialty Conference of the Air Pollution Control Association, Niagara Falls, 1975.

3. Dennis, R., R.W. Cass, and R.R. Hall. Observed Dust Dislodgment from Woven Bags and its Measured and Predicted Effect on Filter Performance. Paper No. 77-32.3, presented at the 70th Annual Meeting of the Air Pollution Control Association, Toronto, Canada, June, 1977.

4. Dennis, R., R.W. Cass, D.W. Cooper, R.R. Hall, V. Hampl, H.A. Klenn, J.E. Langley and R.W. Stern. Filtration Model for Coal Flyash with Glass Fabrics. EPA-600/7-77-084, U.S. Environmental Protection Agency, Research Triangle Park, NC, 1977.

5. Cooper, D.W., and V. Hampl. Fabric Filtration Performance Model. In: Proceedings, Conference on Particulate Collection Problems in Converting to Low-Sulfur Coals. G.B. Nichols, ed. EPA-600/7-76-016, U.S. Environmental Protection Agency, Research Triangle Park, NC, 1976. pp. 149-185.

6. Pilat, M.J., D.S. Ensor, and J.C. Bosch. Source Test Cascade Impactor. Atmos. Environ. 4:671-679, 1970.

7. Cohen, J.J., and D.M. Montan. Theoretical Considerations, Design, and Evaluation of a Cascade Impactor. J. Am. Ind. Hyg. Assoc. 28:95-104, 1967.

8. Marple, V.A., and B.Y.H. Liu. Characteristics of Laminar Jet Impactors. Environ. Sci. Technol. 8:648-654, 1974.

9. Smith, W.B., K.M. Cushing, and G.E. Lacey. Andersen Filter Substrate Weight Loss. EPA-650/2-75-022, U.S. Environmental Protection Agency, Research Triangle Park, NC, 1975.

10. Rao, A.K. Sampling and Analysis of Atmospheric Aerosols. Particle Technology Laboratory, Mechanical Technology Department, University of Minnesota, Publication 269, 1975.

11. Markowski, G.R., and D.S. Ensor. A Procedure for Computing Particle Size Dependent Efficiency for Control Devices from Cascade Impactor Data. Presented at the 70th Annual Meeting of the Air Pollution Control Association, Toronto, Canada, June, 1977.

12. Liu, B.Y. H., K.T. Whitby, and D.Y.H. Pui. A Portable Electrical Analyzer for Size Distribution Measurement of Submicron Aerosols. J. Air Pollut. Contr. Assoc. 24:1067, 1967.

13. Liu, B.Y.H., and D.Y.H. Pui. On the Performance of the Electrical Aerosol Analyzer. J. Aerosol Sci. 6:249, 1975.

14. Ensor, D.S., L.D. Bevan, and G. Markowski. Application of Nephelometry to the Monitoring of Air Pollution Sources. Paper No. 74-110, presented at the 67th Annual Meeting of the Air Pollution Control Association, Denver, June, 1974.

15. Maddalone, R.F., and N. Garner. Process Measurement Procedures-Sulfuric Acid Emissions. TRW Report 28055-6004-RU-00 to Environmental Protection Agency, Contract No. 68-02-2165, February 1977. 36 pp.

16. Ensor, D.S., R. Hooper, and R.W. Scheck. Determination of the Fractional Efficiency Opacity Characteristics, and Engineering and Economic Aspects of a Fabric Filter Operating on a Utility Boiler. MRI Final Report No. FR-1411 to Electric Power Research Institute, Contract RP534-1, 1976.

PAPER 16

# EVALUATION OF THE EFFICIENCY OF ELECTROSTATIC PRECIPITATORS

WALLACE B. SMITH
JOHN P. GOOCH
JOSEPH D. McCAIN
JAMES E. McCORMACK
SOUTHERN RESEARCH INSTITUTE

## INTRODUCTION AND SUMMARY

A system is described that can be used to measure the particle-size distribution in process streams at control device inlets and outlets to evaluate their collection efficiency. The fractional efficiency is determined from 0.01 to 10 μm and real-time systems are used to discriminate transient events and nonideal behavior.

Typical results are shown illustrating particle size distributions and collection efficiency with and without rapping. It was found in a series of tests that rapping emissions may constitute up to 80 percent of the total emissions; the higher emissions are observed at hot precipitators.

## EQUIPMENT AND PROCEDURES

Figure 1 is a schematic illustrating the operating principle of electrostatic precipitators. Ions, created near the high voltage corona electrode, attach themselves to the aerosol particles which in turn are collected on the grounded plates by electrostatic forces as they pass nearby. Ideally, the collection efficiency of a precipitator can be made arbitrarily high by increasing the residence time of the aerosol (the precipitator dimensions).

As a layer of collected particles accumulates on the grounded plate, the plates are periodically "rapped" to dislodge the layer, which falls into the hoppers below. Sometimes a fraction of

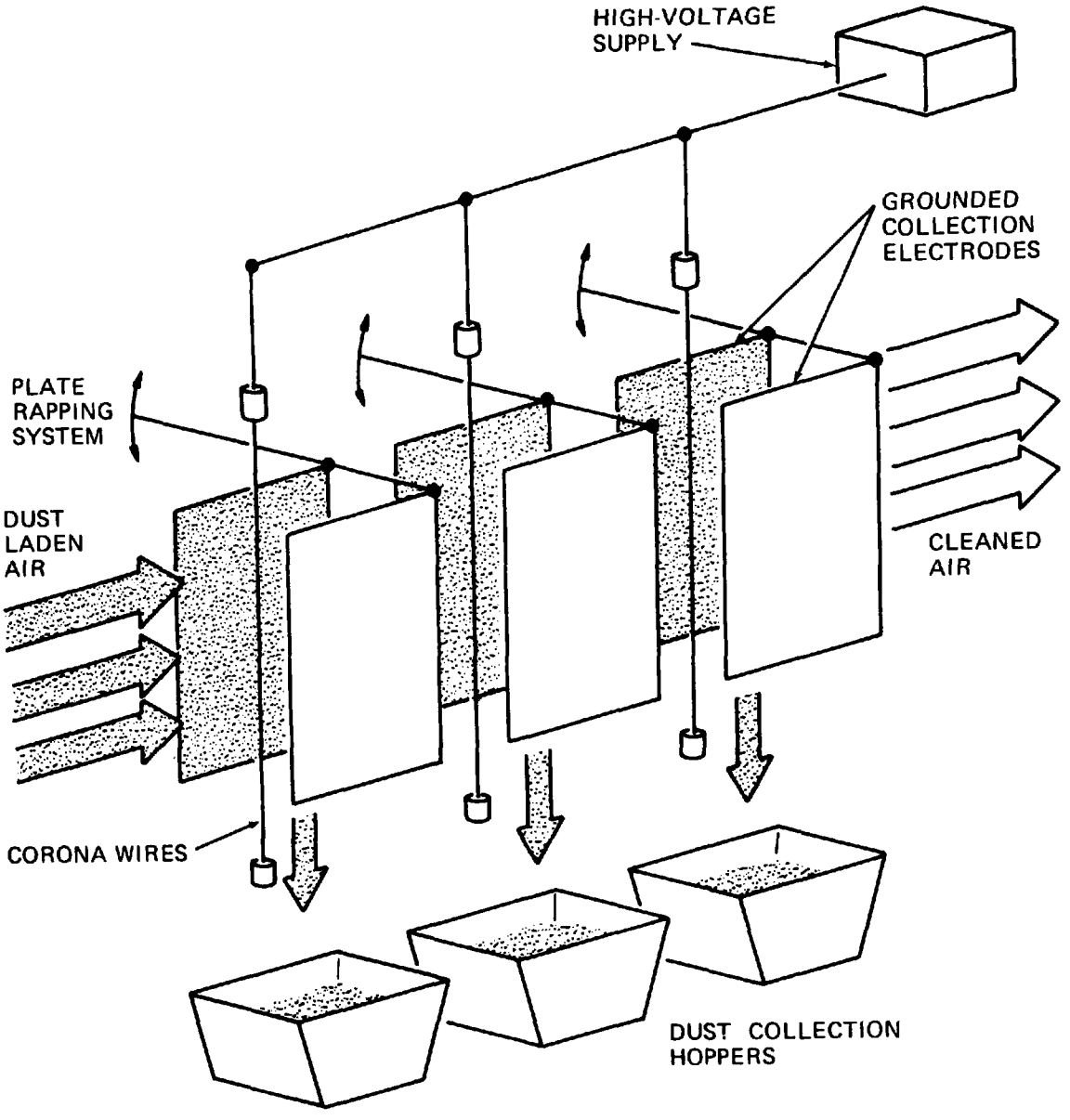


*Figure 1. Schematic drawing of the electrostatic precipitation process.*

the previously collected dust is reentrained into the aerosol stream to be recollected or to escape into the atmosphere. The rapping frequency and power are adjusted to minimize such losses; but, rapping reentrainment is an important factor in limiting precipitator performance.

A second, nonideal factor that influences precipitator performance is "sneakage" or passing of a part of the aerosol stream through areas where the particles are not charged, such as through the hoppers, or the electrode suspension areas. Sneakage is minimized through the precipitator design.

Figure 2 shows curves illustrating the nature of precipitator fractional efficiency; i.e., efficiency vs. particle diameter. Because of the relative electrical mobility of particles of different sizes, the collection efficiency is highest for very fine and very large particles with a minimum value for particles of approximately 0.5 μm diameter. The curves also show how sneakage and rapping reentrainment degrade the performance of the precipitator. Sneakage allows particles of all sizes to penetrate the precipitator, while rapping puffs contain primarily large agglomerates of particles that were collected. Thus, rapping reentrainment should not be considered penetration of the primary aerosol, but rather the creation of a different aerosol. For proper evaluation of a precipitator performance, it is desirable to isolate and identify the emissions due to normal penetration, sneakage, and reentrainment. Other, more subtle nonideal effects exist but are generally less important.

Figure 3 shows the main objectives of precipitator evaluation tests and the requirements to achieve these objectives. For even the most rudimentary diagnostic tests it is necessary to acquire knowledge of the gas velocity distribution, the main gas constituents, and characteristics of the dust such as approximate size distribution, concentration, and electric resistivity. Also, the electric operating parameters must be noted and an assessment of the mechanical condition made. Tests designed to acquire data for research generally require more tests and better accuracy and resolution.

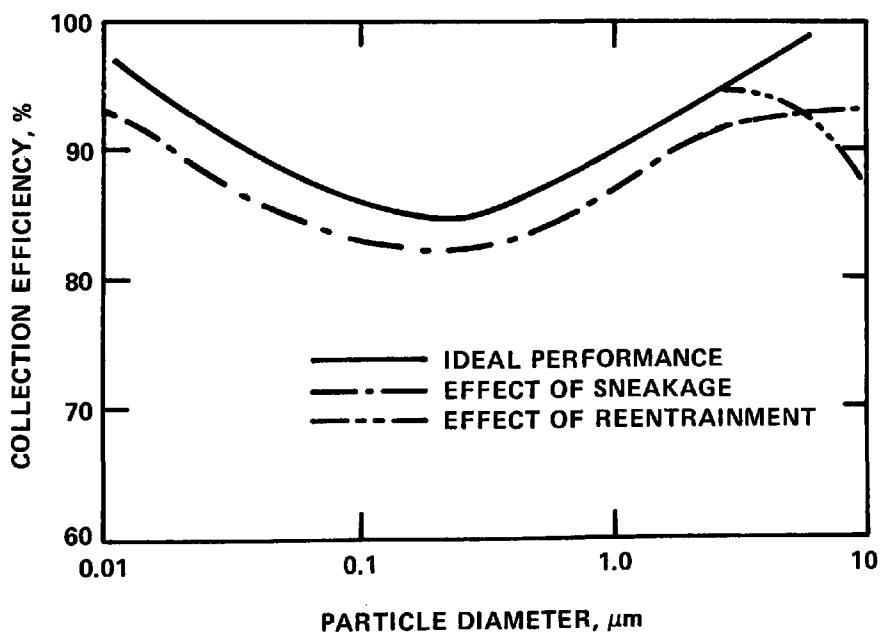


*Figure 2. Typical precipitator performance curve showing negative effects of sneakage and reentrainment.*

| Objective of Tests | Assure Compliance with EPA Regulation | Optimize Performance of Control Device | Obtain Design Data for Control Device | Obtain Data for Modeling Studies | Systems Studies Process and Control Device |
|---|---|---|---|---|---|
| **Tests Required** | | | | | |
| Mass Concentration | O | O | I | I,O | I,O |
| Opacity | O | O | | | O |
| Gas Composition | O | O | I | I,O | I,O |
| Gas Temperature | | | I | I,O | I,O |
| Gas Volume | O | | I | I,O | I,O |
| Pressure | | | I | I,O | I,O |
| Velocity Distribution | | C | C | X | X |
| Particle Size Distribution | | | I | I,O | I,O |
| Dust Composition | | | Qualitative | Qualitative | I,O* |
| Dust Resistivity | | | | ESP only | X |
| Control Device Data | | | | | |
| Operating | | | | X | X |
| Design | | | | X | X |
| Maintenance | | | | | X |
| Plant Process Data | | | | D | D |
| Economic Data | | | | Optional | X |
| **Technical Considerations (Decisions/Problems)** | | | | | |
| Adequate Space, Electric Power | O | O | I | I,O | I,O |
| Laboratory Space | X | X | X | X | X |
| Number of Tests Required | 3 | D | D | D | D |
| Isokinetic Sampling | X | X | X | X | X |
| Condensible Vapors/ Volatile Particles | | C | C | C | C |
| Mass Concentration/ Sampling Time | C | C | C | C | C |
| Traverse Strategy | O | O | O | O | O |
| Aerosol Gas Velocity | C | C | C | C | C |
| Process/Emission Variations | C | C | C | C | C |
| Select Particle Sizing Methods | | | I,O | I,O | I,O |
| Select Mass Train Type | O | O | I,O | I,O | I,O |
| Select Gas Analysis Methods | | D | D | D | D |
| Real-Time Monitors Needed | | D | D | D | D |
| Filter Mass Stability | | C | C | C | C |
| Sample Preservation | | D | D | D | D |

Key:
- O - Outlet
- I - Inlet
- X - Required
- D - Decision based on specific site or test objectives
- C - Must be considered
- * vs. Particle Diameter

*Figure 3. Objectives of precipitator performance evaluations and tests required for completion.*

In Table 1, the particulate sampling methods used by Southern Research for precipitator analysis are listed. Cascade impactors are used more than any other type of sampling device for measuring particle-size distributions. Modified Brink impactors are used when particle concentration is high (inlet) and Andersen or University of Washington impactors are used when the concentration is lower (outlets). Greased foils are preferred as collection substrates, but for temperatures above 300°F, glass fiber filter material is used.

If larger samples are required for analysis, cyclones can be used in a series arrangement to obtain sized particulate fractions in quantities of several tens of milligrams to several grams. The EPA/Southern Research cyclone system has five small cyclones with $D_{50}$'s of 0.3, 0.6, 1.2, 2.5, and 5.6 μm.

Cascade impactors and cyclones yield samples that are accumulated over periods of time ranging from several minutes to several hours; thus, the size distributions measured with these devices are time averaged. Optical particle counters may be used to yield real time or instantaneous data on particle concentration and size. Disadvantages of these counters are: 1) They are designed for laboratory use, and the samples must be diluted and cooled. 2) They do not yield aerodynamic particle size; consequently, some knowledge (or assumptions) of the optical properties of the dust must be known to calculate the aerodynamic sizes from optical data. Alternately, the optical particle counters may be calibrated for the particles of interest to yield aerodynamic sizes. Marple[1] has designed special impactors for calibration of optical particle counters, while McCain[2] has used sedimentation to perform calibrations. We have used the Climet 207 and Royco 225 optical particle counters in our field test programs.

Figure 4 shows schematically an optical particle sizing system for large particles that is used to count particles from 1-30 μm in five size fractions. In the diluter, the particles pass from the inlet jet, through a turbulent zone, toward the outlet jet. Small particles are deflected more than the larger particles; thus a larger fraction of the large particles is counted. It is necessary to dilute the small particles to a number that is within the range suitable for the counter, but the large particles require little or no dilution. Figure 5 shows a special plugin unit designed by Southern Research for use with optical particle counters. It is a five channel pulse height analyzer. The data are seen as analog readings on the front of the plugin, and also analog recorder outputs are provided for each channel. Linear or logarithmic responses are chosen by means of toggle switches on the front of the device. The unit will plug directly into the Royco 225 optical particle counter, or can be used in a special chassis with any optical counter with which it is compatible.

TABLE 1. MAIN COMPONENTS OF THE SOUTHERN RESEARCH PARTICLE SIZING SYSTEM

| Method | Size range (diameter, μm) | Remarks |
|---|---|---|
| Impactors | 0.5 - 10 | Time-averaged sample |
| Cyclones | 0.3 - 6 | Time-averaged larger samples |
| Optical particle counter[a] | 0.3 - 1.5<br>1 - 30 | Real-time data, not aerodynamic sizing |
| Electrical mobility analyzer[a] | 0.01 - 0.5 | Time-averaged sample |
| Diffusion batteries and condensation nuclei counters[a] | 0.01 - 0.2 | Time-averaged size distribution; some time resolution possible |

[a] Sample extraction and dilution required.

For the ultra-fine particle size range (0.01-0.5 μm) electrical aerosol analyzers (TSI Model 3030) or diffusion batteries with condensation nuclei counters are used. Again, these are laboratory instruments and sample dilution and cooling is required. The diffusion batteries are the parallel plate type, and are of our own design. We have used General Electric, Gardner, and Environment One condensation nuclei counters.

A more detailed description of the procedures used to develop and implement precipitator evaluation programs has been given elsewhere.[3]

## QUALITY ASSURANCE AND CONTROL

Three important problems related to quality control of particulate sampling data have been addressed as part of our sampling program. Harris et al. have discussed the first problem, the selection of suitable impactor substrates, in an earlier paper of this symposium. A second problem has been the formation of a sulfuric acid fume in our sample extraction and dilution system. The formation of the fume is detected by a very nonlinear increase in submicron particles as the dilution factor is reduced. This phenomenon is observed at sites when the $SO_3$ concentration is high and when low dilution factors are used.

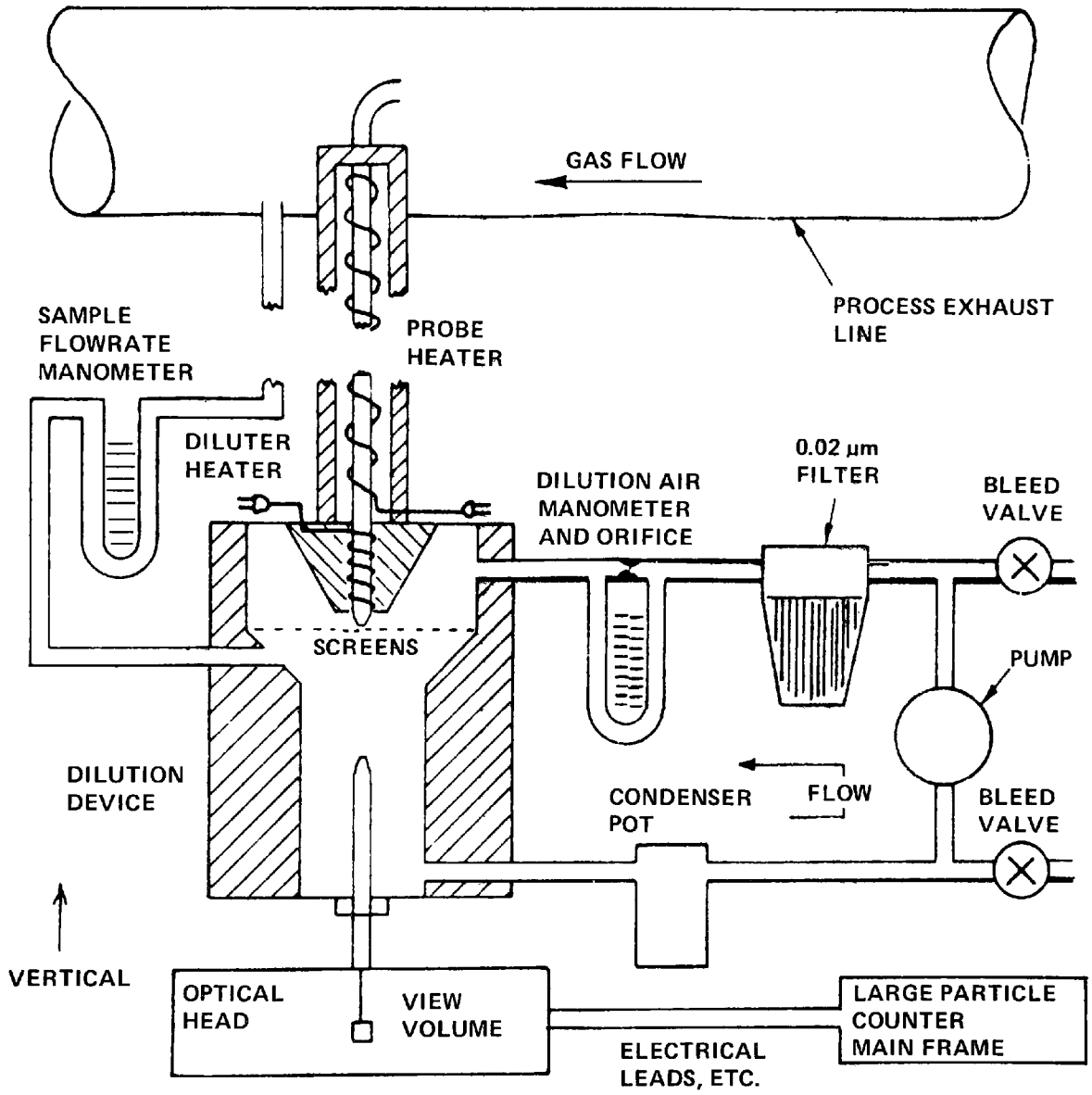


*Figure 4. The large particle sampling system.*

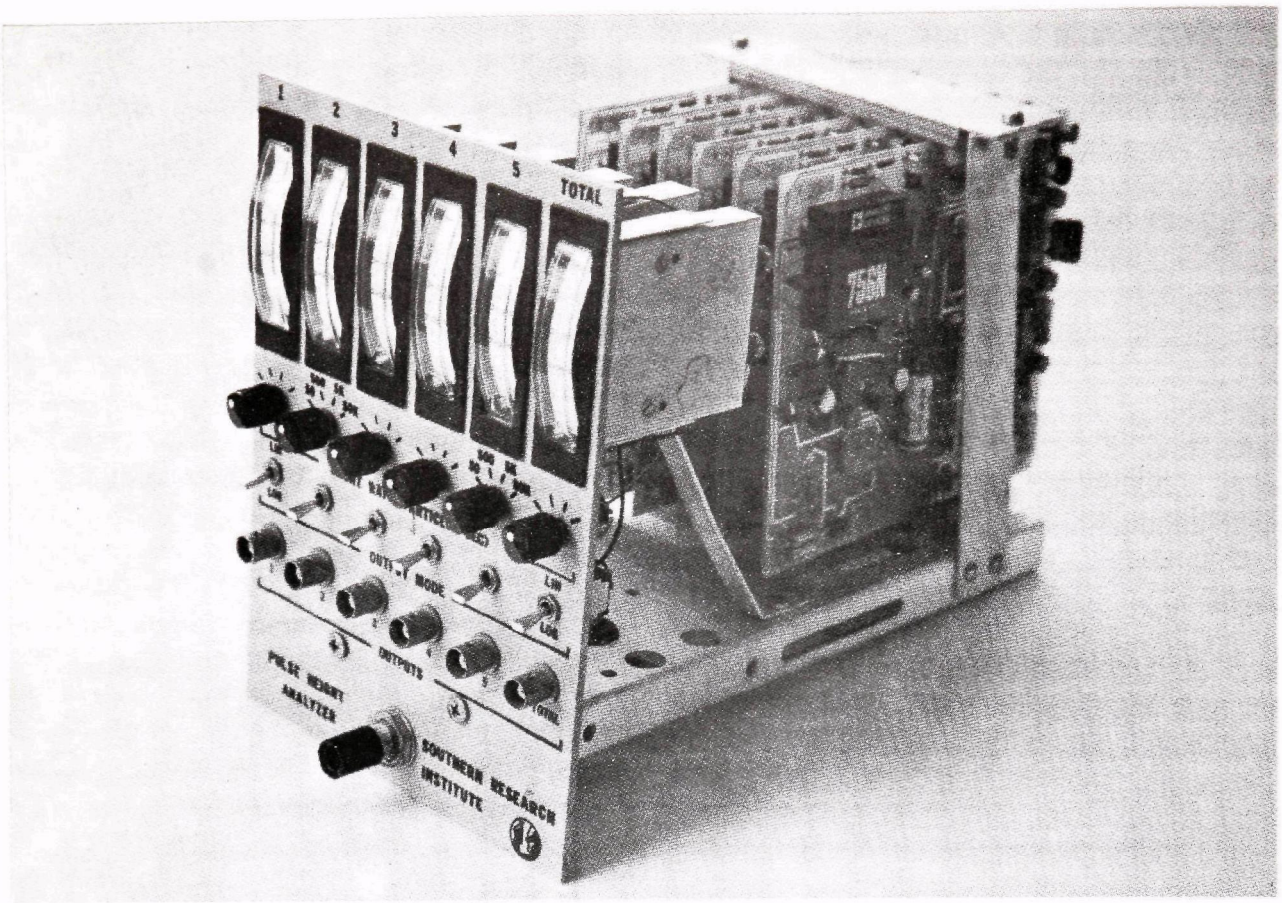


*Figure 5. A special pulse height analyzer plugin developed by Southern Research Institute.*

Figure 6 shows our sample extraction-dilution system with diffusion absorbers for condensible gases. The absorbers consist of stainless steel cylinders, with a smaller, screen cylinder inside. The void between the cylinders is filled with granular, activated charcoal and the aerosol sample passes through the inner cylinder. This technique has been very successful at eliminating the formation of fumes at sources when the $SO_3$ concentrations are quite high.

A third potential problem is the distortion of particle size distributions by electric charges that exist on the particles, particularly at the outlet of precipitators. An extensive study of this problem has been made and the results will be published later. Typical results, however, are shown below.

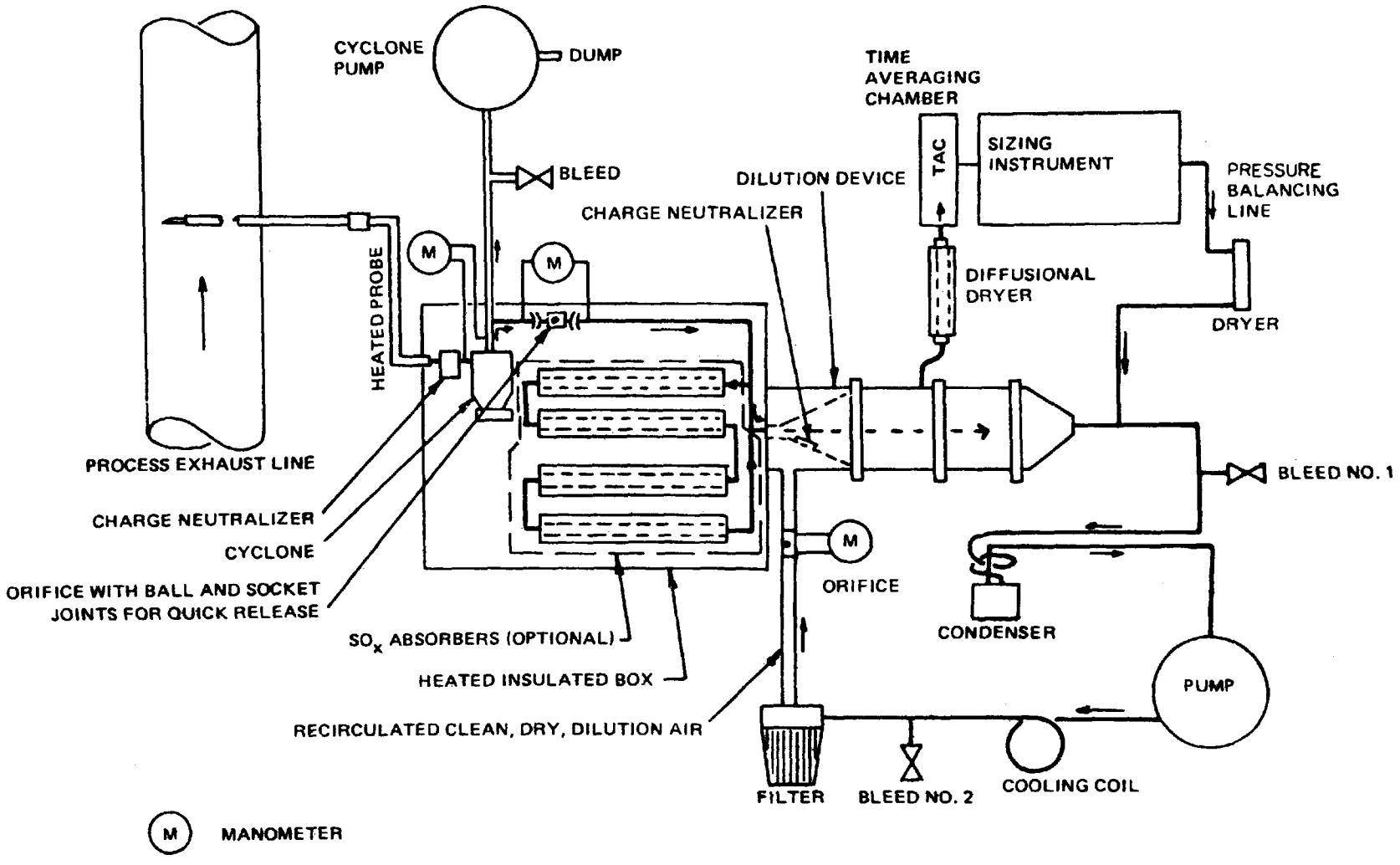


*Figure 6. The sample extraction-dilution system.*

Figure 7 shows one of the experimental setups used for the charged particle experiments. Aerosols of 1.3, 0.69, and 1.0 μm mass median diameter were generated in concentrations that were comparable to those found in process streams by nebulization. The particles were passed through an electric corona charging device, and into the test impactors (Andersen impactors with glass fiber substrates). Polonium-210 devices were used to discharge the particles in one aerosol stream and low voltage ion precipitators were used to remove ions. The cascade impactors were used as Faraday cages and the charge accumulated was measured by electrometers. Care was taken to insure that the aerosol was properly split between the impactors and that losses in the sampling lines were minimal. In all of the experiments the results were extremely reproducible, indicating a high degree of precision.

Typical results from the charged particle experiments are shown in Figures 8 and 9. In Figure 8 a 1.01 μm mmd aerosol was charged to approximately the value that would be acquired in a conventional electrostatic precipitator. The level of charge relative to a precipitator is indicated in the figure. Very little difference was found between the charged and uncharged particle distributions.

A highly charged aerosol was sampled and the results plotted in Figure 9. In this experiment, a much larger, and significant, difference was found in the charged and uncharged aerosols. Experiments were performed with different impactors, different substrates, grounded and ungrounded impactors, monodisperse particles, and different charge levels. Analysis of the results is complete and a report is now being written (EPA Contract No. 68-02-2131).

The results of the charged particle experiments indicate that for moderate levels of charge, and where using glass fiber substrates, the interferences due to electrostatic charges are small. When sampling highly charged aerosols, however, the size distribution can be distorted significantly. Unfortunately no suitable charge neutralizing device is available for in-stack use.

## TYPICAL RESULTS OF PRECIPITATOR EVALUATIONS

Figures 10 through 13 show results from field test measurements illustrating the type of data that is obtained using the systems described and their application to precipitator evaluations and source characterization.

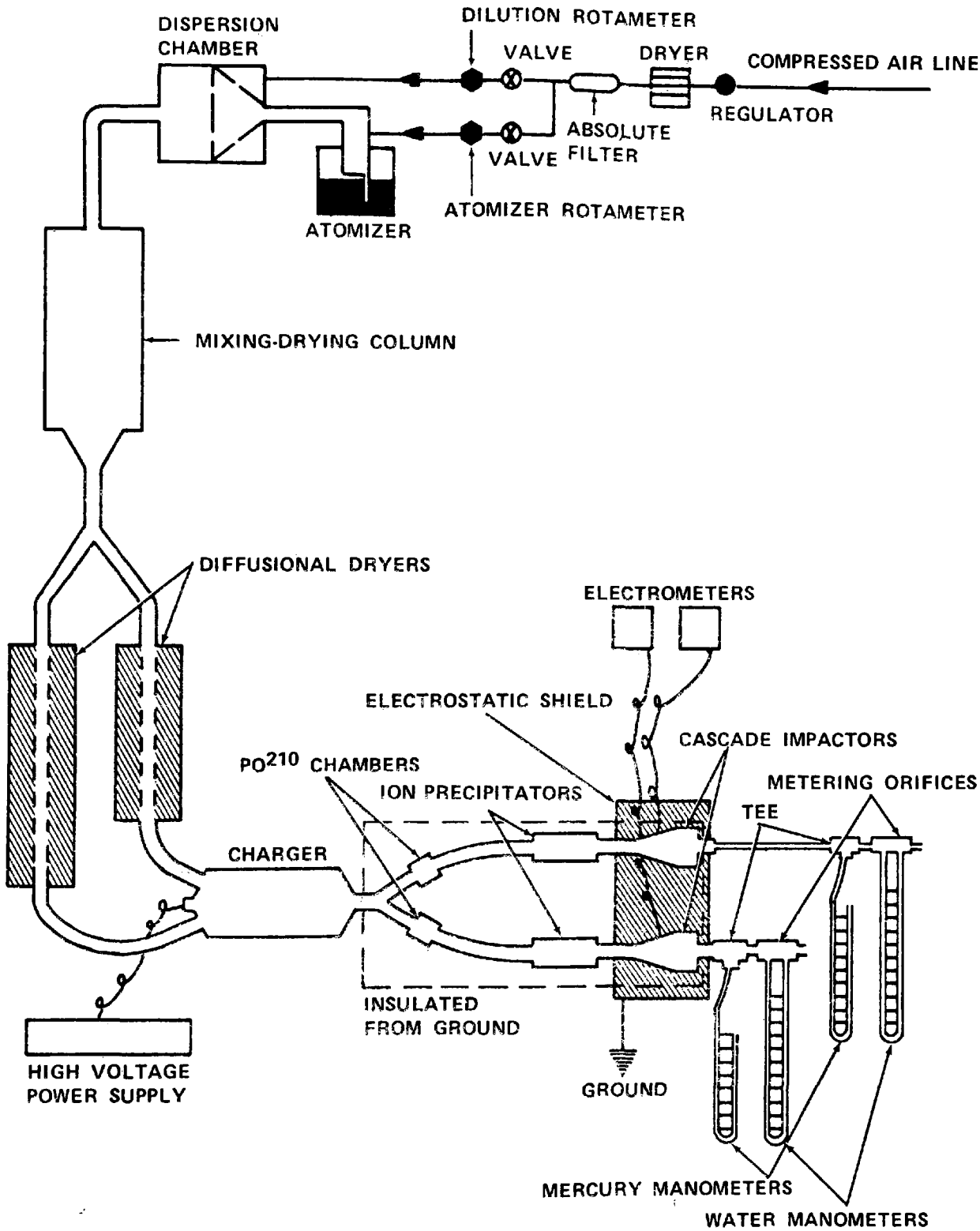


*Figure 7. Experimental setup for the charged particle investigations.*

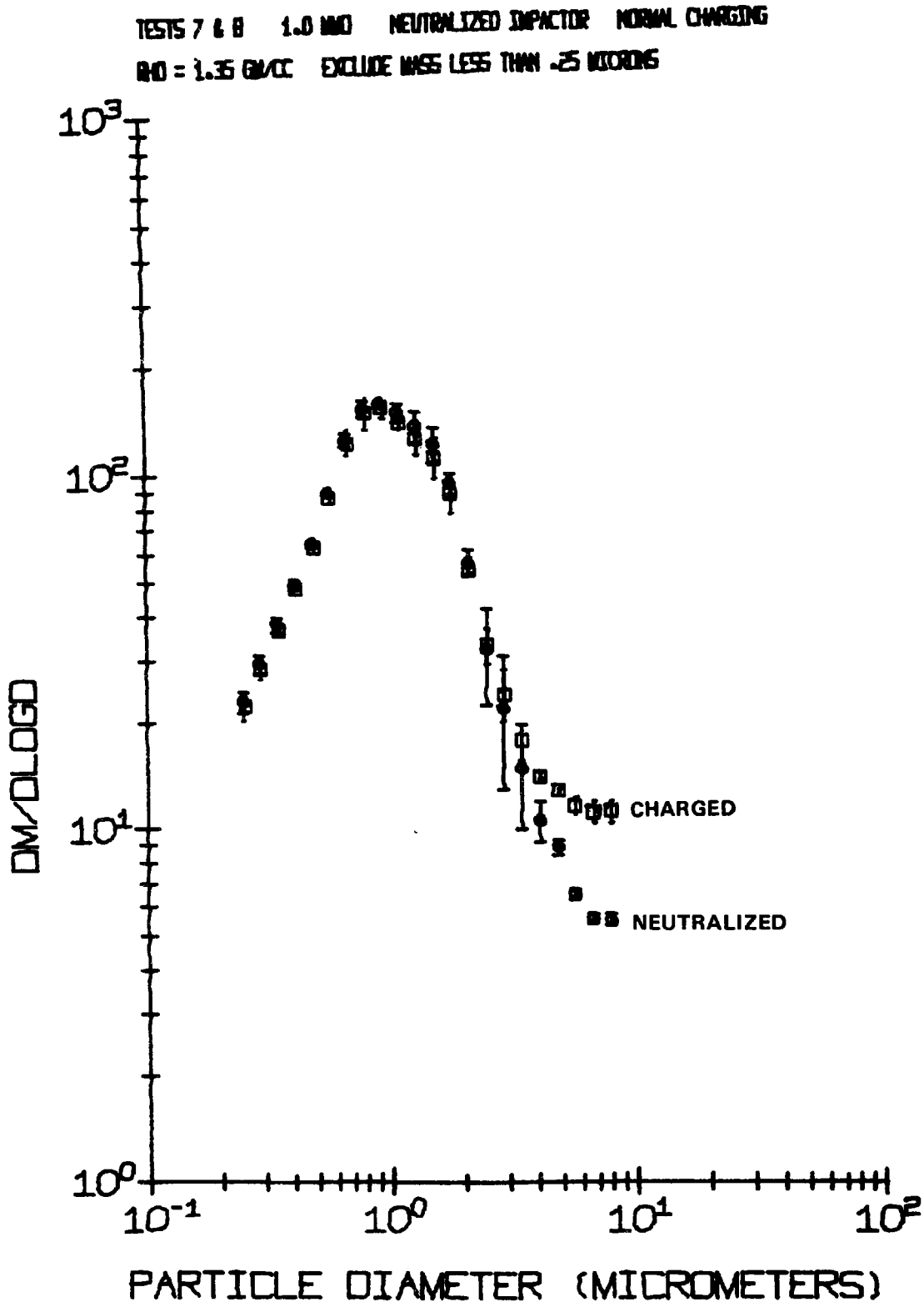


*Figure 8. Particle size distribution for moderate charging conditions for a mass median diameter of 1.02 μm.*

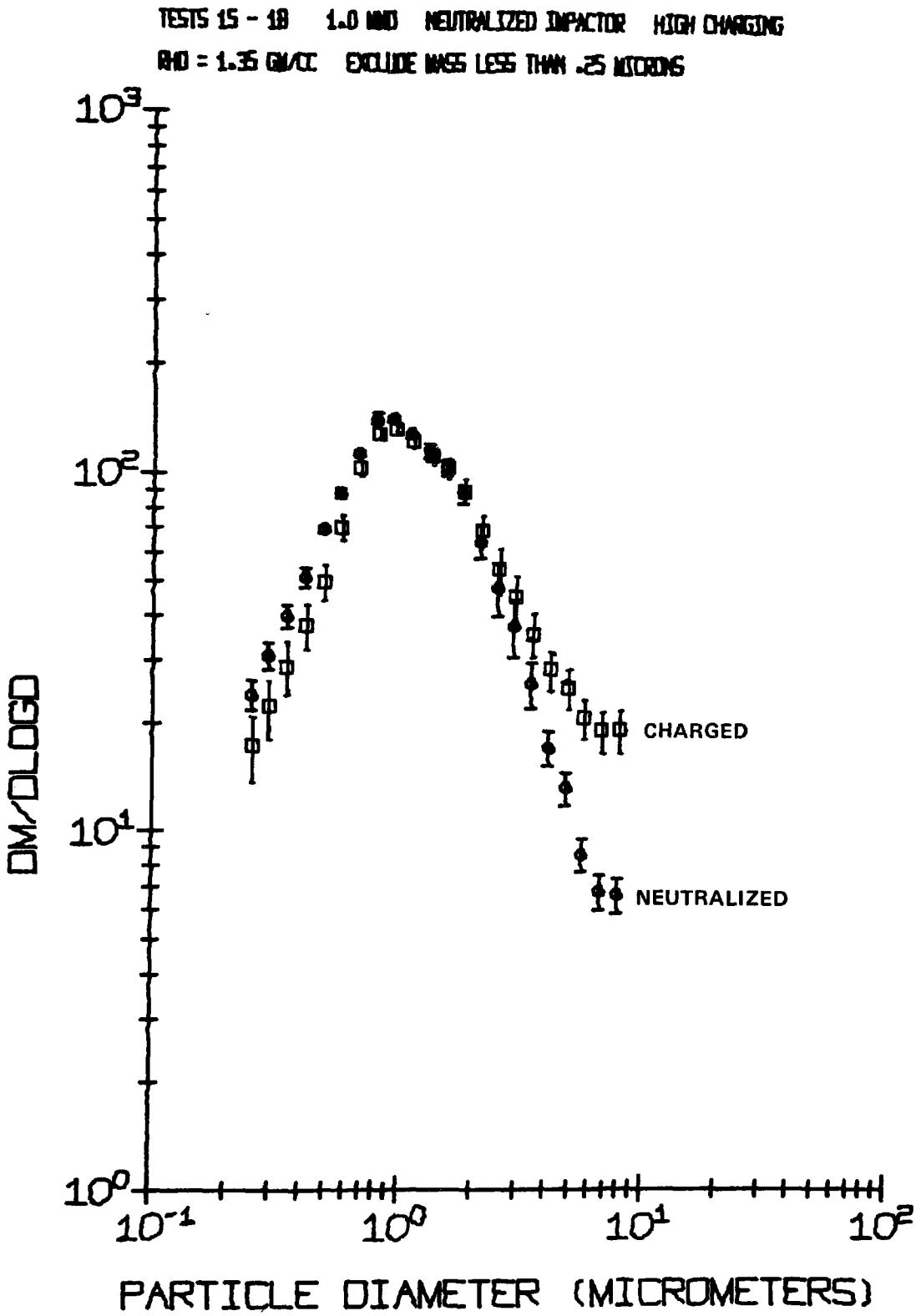


*Figure 9. Particle size distribution for high charging conditions for a mass median diameter of 1.01 μm.*

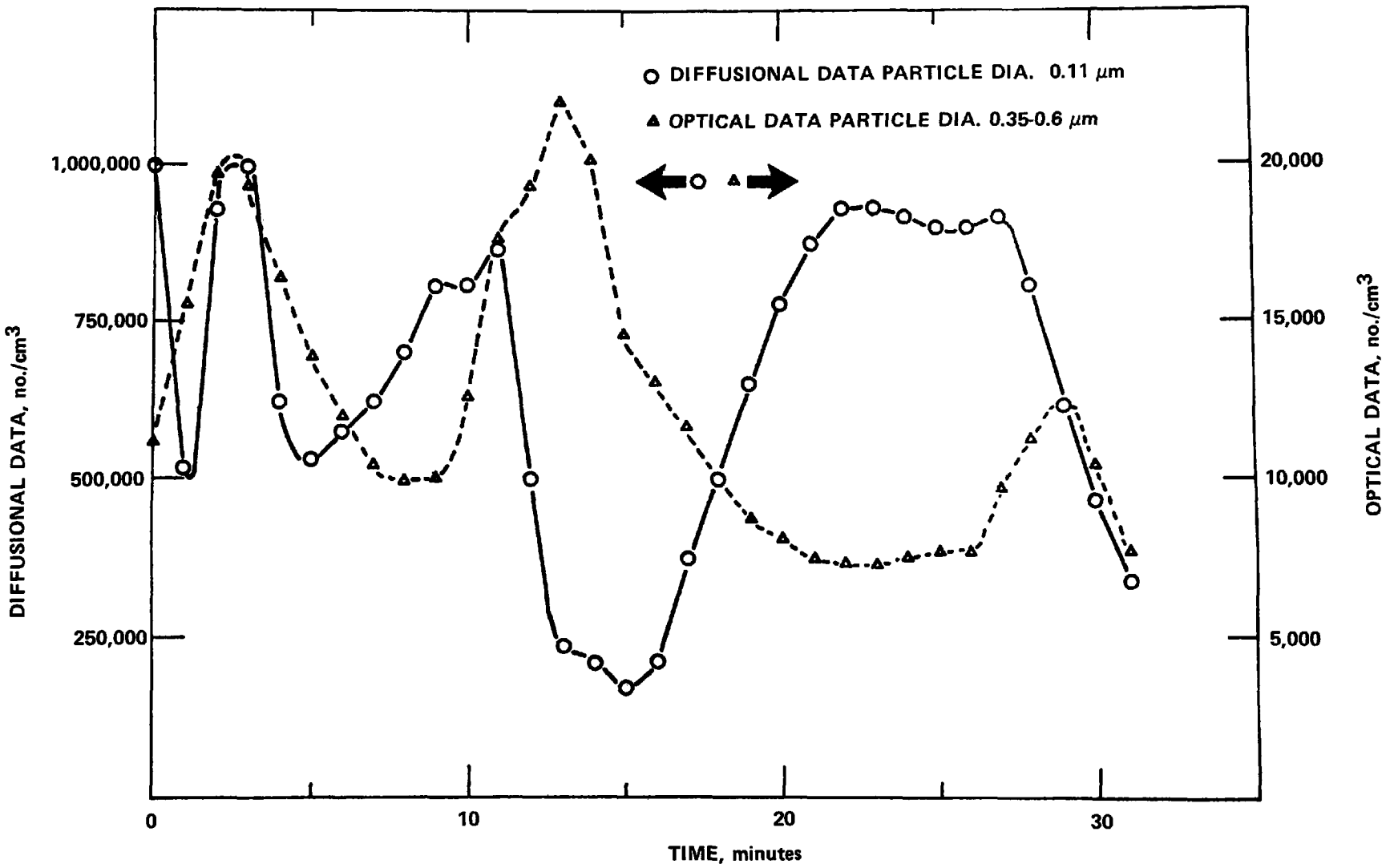


*Figure 10. Particle concentration versus time in the effluent from an asphalt batching process.*

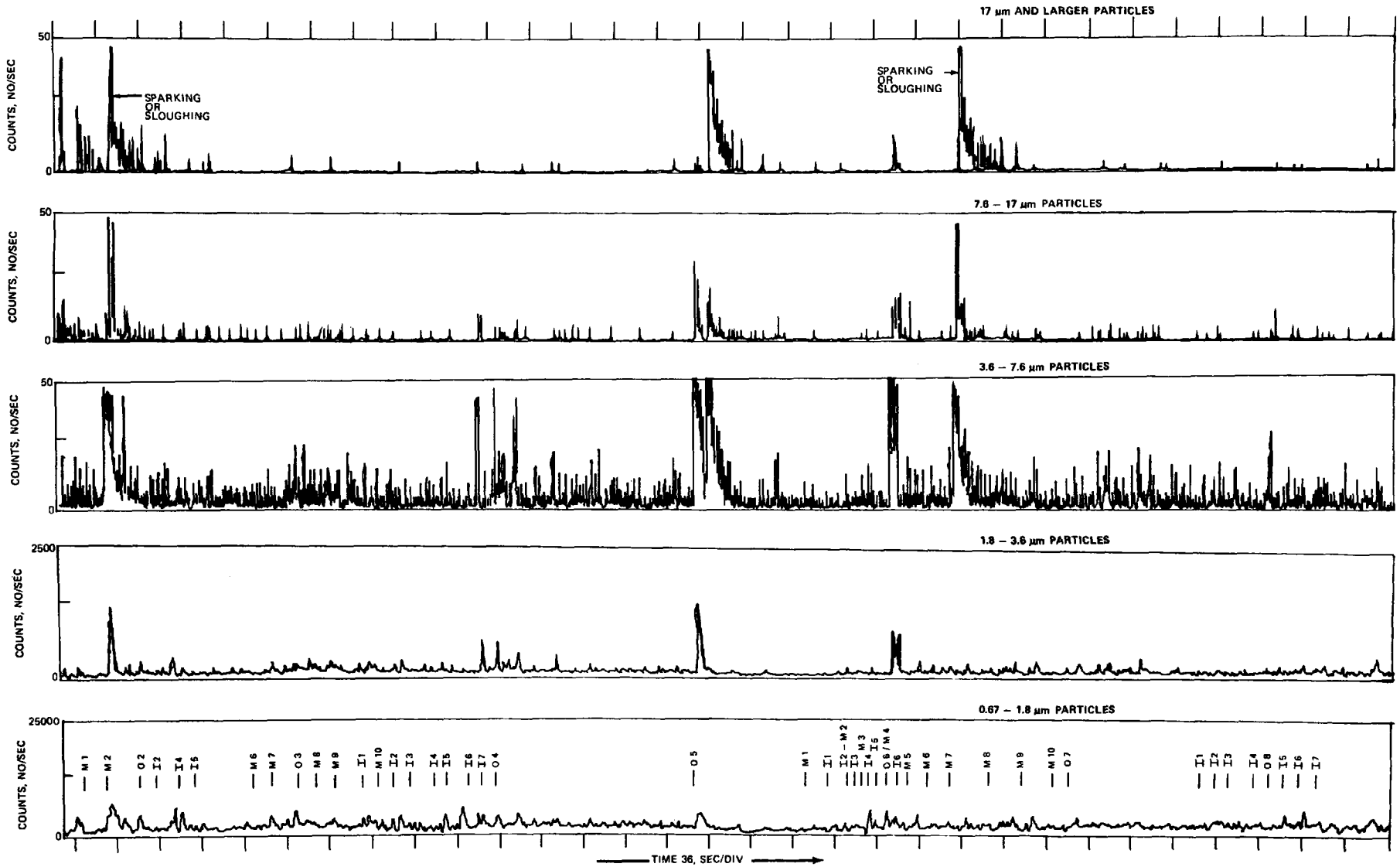


*Figure 11. Chart recordings from the large particle sampling system.*

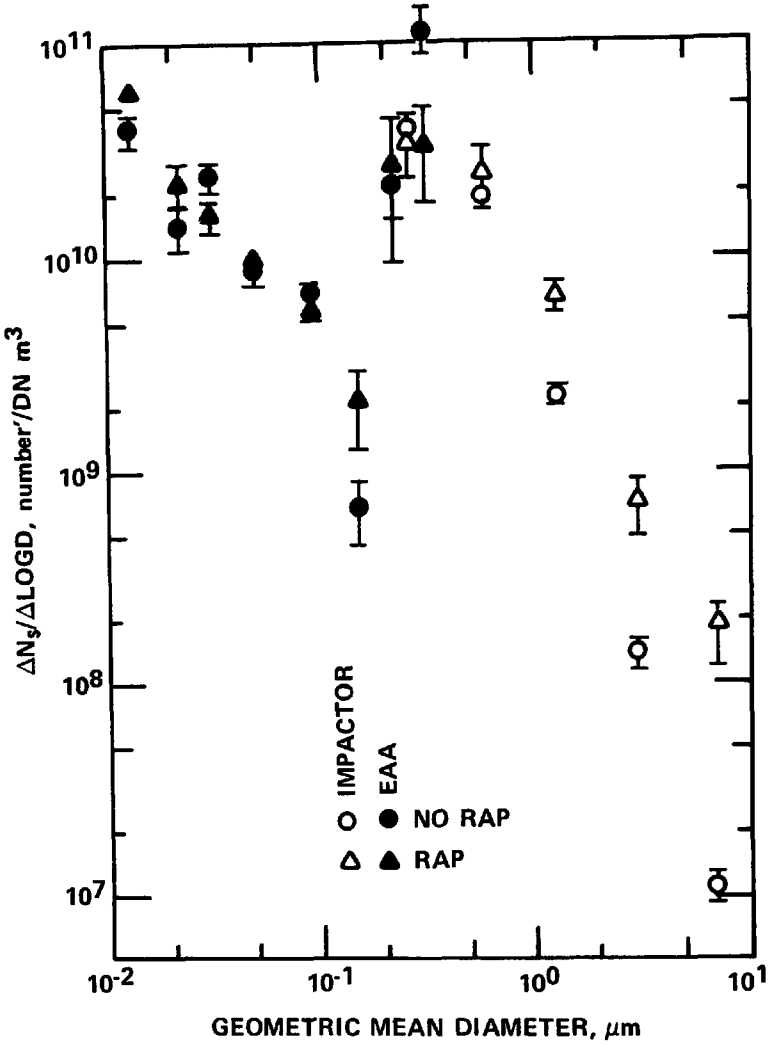


*Figure 12. The size distribution of the effluent from a precipitator installed on a pulverized-coal fed boiler. Measurements were taken with and without rapping.*

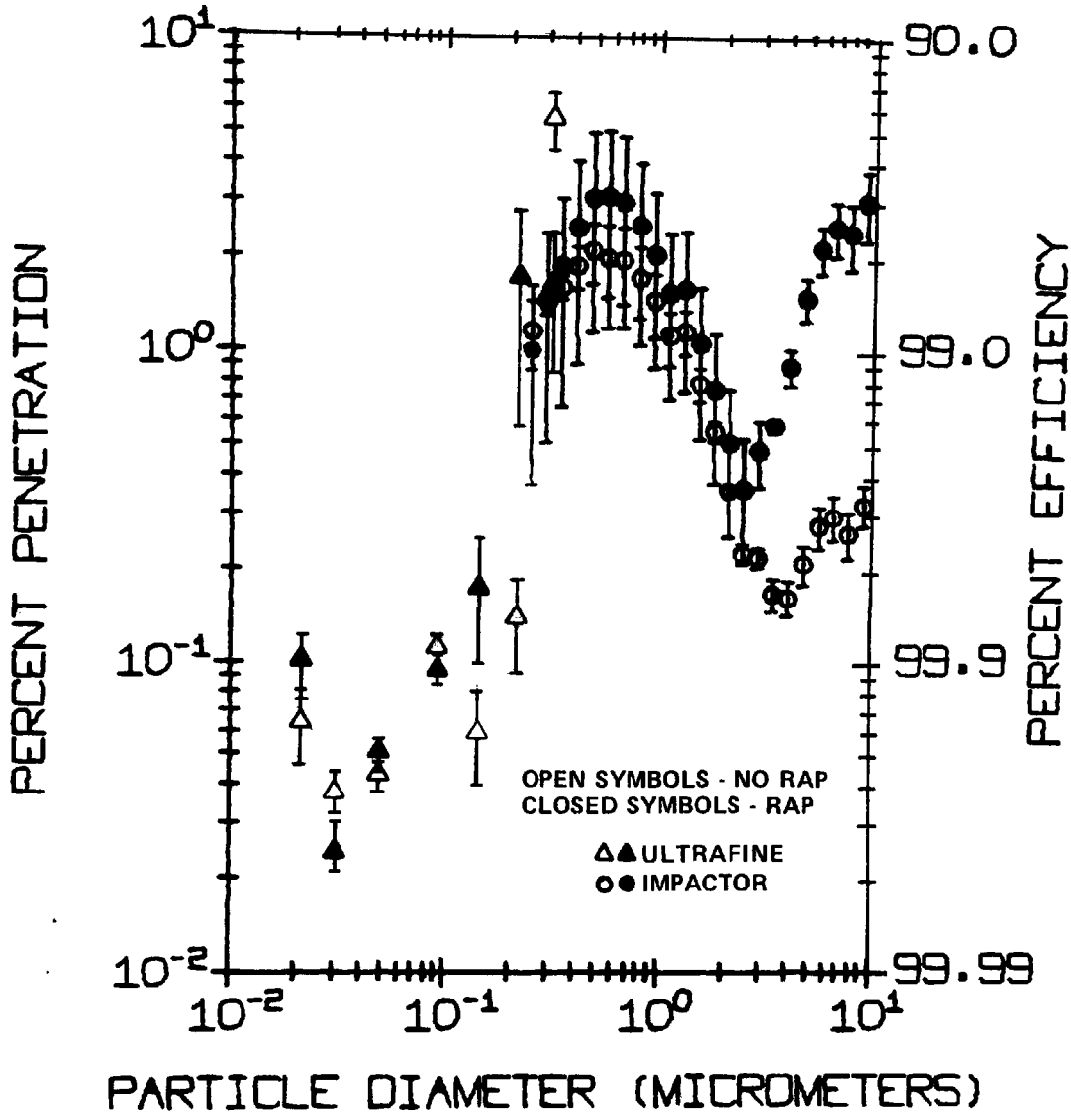


*Figure 13. Fractional efficiency of an electrostatic precipitator showing the negative effects of rapping reentrainment.*

Figure 10 shows data obtained with the sample extraction-dilution system and the optical and diffusional sizing systems in the effluent stream from an asphalt batching process. The need for size resolution in real time is clearly illustrated as the two size fractions fluctuate in concentration, sometimes in phase and sometimes out of phase.

Figure 11 shows particle size and concentration recordings from the large particle sampling system. Emissions are shown in real time for 5 discrete size ranges. From these data, it was possible to identify and analyze the contribution of the rapping puffs to the total emissions.

In Figure 12, the size distribution measured at the outlet of a precipitator installed on the effluent stream from a coal-fired boiler is shown. Measurements were made with cascade impactors and an electrical aerosol analyzer, with and without rapping. Rapping emissions can be seen to constitute a large part of the total emissions in the size range from 1 to 10 μm diameter.

Data of the type illustrated in Figure 12 are taken at precipitator inlets and outlets to determine the collection efficiency versus particle diameter (fractional efficiency). The collection efficiency of one precipitator is shown in Figure 13. The classical dip in efficiency near 0.5 μm is clearly shown. Also, the increase in penetration from rapping reentrainment is seen to be quite large in the 1 to 10 μm size range.

Particle sizing measurements are a valuable tool in control device evaluations, and yield necessary data for diagnoses of poor performance, model development, and for design purposes. Efforts are continuing to refine the techniques in order to improve accuracy and to reduce their complexity and cost.

## REFERENCES


1. Marple, V.A. The Aerodynamic Size Calibration of Optical Particle Counters By Inertial Impactors. Part. Tech. Lab. Publication 306, University of Minnesota, 1976.

2. McCain, J.D., K.M. Cushing, and W.B. Smith. Methods for Determining Particulate Mass and Size Properties: Laboratory and Field Measurements. J. Air Pollut. Contr. Assoc. 24(12):1172-1176, 1974.

3. Smith, W.B., K.M. Cushing, and J.D. McCain. Procedures Manual for Electrostatic Precipitator Evaluation. EPA-600/7-77-059, U.S. Environmental Protection Agency, Research Triangle Park, NC, 1977.

PAPER 17

# SOME STUDIES OF CHEMICAL SPECIES IN FLY ASH

L.D. HULETT
J.F. EMERY
J.M. DALE
A.J. WEINBERGER
H.W. DUNN
C. FELDMAN
E. RICCI
ANALYTICAL CHEMISTRY DIVISION
OAK RIDGE NATIONAL LABORATORY

AND

J.O. THOMSON
THE UNIVERSITY OF TENNESSEE

ABSTRACT

Fly ash specimens from coal fired steam plant precipitators and sluice ponds have been studied. In precipitation ashes from two different plants the distributions of trace elements in the matrix materials that make up the ashes have been found to be the same. Alkali, alkaline earths, and rare earths are more concentrated in the mullite phase; transition metals such as V, Mn, Cr, Co, and Mo are more concentrated in the magnetic phase; carbon and sulfur are enriched in a cinder-type phase. Ash samples extracted from sluice ponds had brown iron-rich phases that were highly concentrated in As and Mo and enriched in other elements. The brown phase was not found in the precipitator ash, so we speculate that a transformation of the ash has occurred in the pond. Some initial results of a glow discharge spectroscopy technique for arsenic speciation are reported. Mössbauer spectroscopy has been used to determine iron chemical states in both the precipitator ash and the pond ash. Engineering studies of a fly ash treatment process that would generate iron compounds to scavenge and fix trace elements in sluice ponds are recommended.

## INTRODUCTION

Because of increased dependence on coal as a source of energy the disposal of ash from its burning presents an increasingly difficult problem. The amount of fly ash generated in the United States is estimated to be in excess of $4 \times 10^7$ tonnes per year. One can visualize a quantity such as this as a pile one meter high, covering an area approximately 4½ km square. Many schemes for the disposal of this material are under study. A primary concern is whether or not trace elements such as arsenic, lead, and many others will be leached from the ash and contaminate the environment. The detection of the trace elements, both in the ash and its effluent, and the determination of their concentrations is rather easily done, but the determining of their chemical species (valence, compound form) is not worked out at all. A knowledge of the chemical species of elements in fly ash is considered very important in order to predict toxicities and the manner in which they will react with the environment. For example, it is believed that arsenic in the +3 state is much more toxic than that in the +5 form. The determination of valences and compound forms of trace elements in fly ash is the subject of this study. The results and conclusions that we will present should be considered rather tentative. Our study is less than one year old and our ash samples have been taken from only two TVA steam plants, Bull Run and Kingston, in the immediate vicinity of Oak Ridge National Laboratory.

The chemist has made some rather impressive accomplishments in molecular spectroscopies capable of determining chemical species: infrared, ultraviolet, x-ray photoelectron spectroscopy (XPS), x-ray diffraction, and many others. All of these are available to our efforts, but in very few cases are sensitivities sufficiently high to be able to determine chemical states directly in fly ash. XPS, for example, is capable of determining valence states, but it is a surface method, and surface concentrations must be in excess of 0.1 monolayer for most elements to be detected. Most of the trace elements in fly ash are more dilute than this. There is no "magic spectroscopy" to which we can expose fly ash and determine chemical states without disturbing the specimen. This leads to the necessity of performing chemical and physical separations on fly ash, which immediately opens up the criticism that the system is being disturbed and probably altered. We argue that with present analytical capabilities there is no alternative to this.

Fly ash is a complicated mixture composed mostly of aluminum, silicon, iron, titanium, alkali and alkaline earths, and oxygen. These elements are present in the form of both amorphous glasses and crystallized minerals. The authors suspect that when the chemical species problem of trace elements is eventually solved it will be found that the "chemical state" of a trace element will be defined by the matrix in which it is dissolved. We do not think that it is likely, for example, that lead will occur in an isolated pure form of PbO or $PbO_2$ or that Cu will

be found as $CuSO_4$. It is for these reasons that we are directing a lot of our efforts toward studying matrix types. We are attempting to determine if certain trace elements are preferentially associated with certain matrices.

## EXPERIMENTAL PROCEDURES

Ash specimens from two TVA steam plants, Bull Run and Kingston, located near Oak Ridge National Laboratory, have been collected for study. Both of these plants use the tangential firing method which requires that the coal be pulverized to a fine particle size. The pulverizing step effects the removal of a large percentage of the sulfur-containing pyrites. The flue gas from the furnaces is passed through cyclone and electrostatic precipitators. The ash that is produced is sluiced to ponds. Specimens from the cyclones and precipitators of both of these plants have been collected. No attempt to collect the submicron material that escapes from the stack has been made at this point. Some specimens from the uppermost strata of the Bull Run plant sluice pond have also been collected.

Mössbauer spectroscopy measurements were made by means of a specially designed spectrometer located at the University of Tennessee Physics Department. Another specially adapted analytical instrument is the glow discharge spectrometer developed by Feldman.[1] This method involves the excitation of the optical spectrum of arsine ($AsH_3$) under very low background conditions. Arsenic in solutions as low as 0.1 ppb can be detected. By adjusting the pH of the solution being analyzed, one can cause arsine to be evolved from arsenic in the $As^{+3}$ state only or from both the $As^{+3}$ and $As^{+5}$ forms. At pH less than 1.5, both the +3 and +5 states are reduced to arsine. At pH above 5, only the $As^{+3}$ form is reduced. We thus have a method of differentiation between $As^{+3}$ and $As^{+5}$.

We have adapted a special oxalate extraction method for removing iron, and those elements associated with it, from the work of Williams, et al.[2] It appears that this will allow us a method of speciating arsenic on fly ash surfaces. Arsenic is displaced from the fly ash surfaces into solutions by the oxalate extraction. The solutions are then analyzed by glow discharge spectroscopy. Oxalate does not appear to interfere with the method, but one must use deaerated solutions to prevent oxidation of the arsenic.

Most of the quantitative elemental analyses performed on the specimens of this study were done by neutron activation analyses, but x-ray fluorescence analysis was also used for many qualitative and semiquantitative measurements. Carbon and sulfur analyses were done by means of the Leco analyzer.

## EXPERIMENTAL RESULTS

When we examine the Bull Run and Kingston cyclone and precipitator ashes by the optical microscope and test their magnetic

properties we are able to distinguish at least three types of matrices. Their gray colors are due to white transparent and translucent particles interspersed with black magnetic and non-magnetic particles. We have separated some of the black particles from the white ones by individual "particle picking" and by magnetic extraction.

X-ray diffraction patterns of the white phase indicated that quite a bit of material had mineralized into a crystal structure of the mullite type. Mullite is a ceramic having a highly variable composition ($3\ Al_2O_3 \cdot 2\ SiO_2$-$2\ Al_2O_3 \cdot SiO_2$). Its diffraction pattern closely resembles sillimanite: $Al_2O_3 \cdot SiO_2$. Mullite exists in the glass as well as the crystalline form. In our specimens most of the white matrix material is probably glass, but the crystalline mullite is quite prominent. Throughout this paper we will refer to both the glass and crystalline forms of the white matrix material as the "mullite" phase. X-ray diffraction patterns of the non-magnetic black particles also indicate a mullite structure, but in addition, there is an intense, broad-lined background due to elemental carbon in a very finely divided state. Diffraction patterns of the magnetic phase show it to have a well-known spinel structure which is usually assigned to $Fe_3O_4$.

Mössbauer spectra were taken of the white matrix and magnetic material. For the white material the spectra suggest that iron in both the $Fe^{+2}$ and $Fe^{+3}$ forms is present; two sets of broadened quadrupole-split doublets were found, one narrow doublet characteristic of $Fe^{+3}$ and one with larger splitting similar to what is found for $Fe^{+2}$, but with a smaller isomer shift than usual. The peaks corresponding to the magnetic phase were analyzed in terms of two six-line hyperfine splittings with fields characteristic of magnetite, as would be expected for the spinel structure of this phase. There is a slight departure, however, of our spectra from that of high purity magnetite. Figure 1 is a Mössbauer spectrum of some as-received fly ash, showing peaks of both the magnetic and non-magnetic phases. Those peaks corresponding to the magnetic phase are labeled $Fe_3O_4$ and those of the non-magnetic are labeled $Fe^{+2}$ and $Fe^{+3}$.

Table 1 shows that trace elements in the alkali, alkaline earths, and rare earths are higher in concentration in the mullite phase than in the magnetite phase. These data are averages of three measurements on different size fractions from a Kingston plant sample. Table 2 shows an identical trend for these elements for a Bull Run fly ash sample. The level of concentrations for the trace elements in the Bull Run sample is lower than for Kingston. The elements V, Mn, Cr, Co, Mo and U appear to be enriched in the magnetic phase, but only by a factor of 2. Table 3 shows the composition of the black cinder phase for both the Kingston and Bull Run plants. This phase is unique in its enhanced concentrations of both carbon and sulfur.

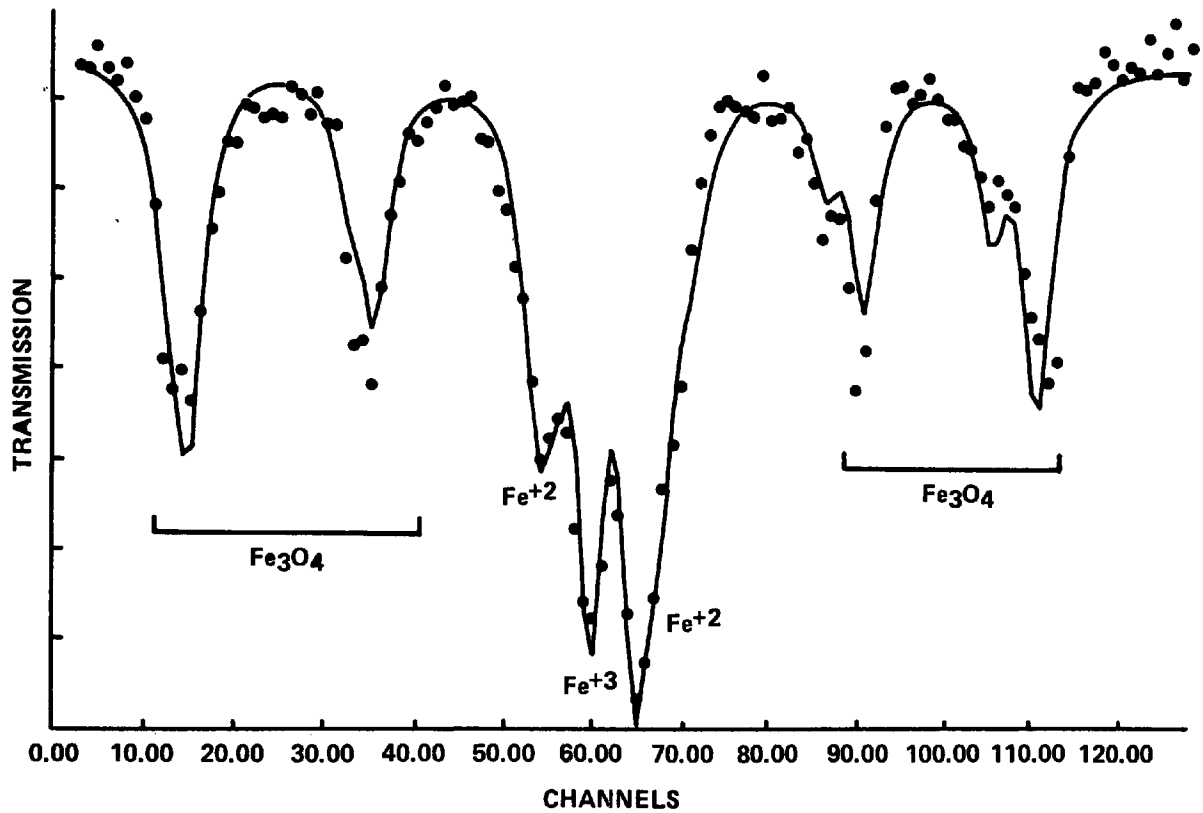


*Figure 1. Mössbauer spectrum of Allen Steam Plant fly ash.*

TABLE 1. DISTRIBUTION OF ELEMENTS IN MULLITE AND MAGNETIC PHASES OF KINGSTON STEAM PLANT FLY ASH, CONCENTRATIONS IN PPM

| Preferential Distribution in Mullite Matrix | | |
|---|---|---|
| Element | Mullite Matrix | Magnetic Matrix |
| Al | 153,000 | 64,000 |
| C | 50,000 | 4,800 |
| K | 24,800 | 4,200 |
| Mg | 13,300 | 6,000 |
| Ti | 9,240 | 3,586 |
| Ca | 9,300 | 4,600 |
| Na | 2,073 | 355 |
| S | 1,900 | 1,500 |
| Ba | 1,236 | 425 |
| Sr | 1,050 | 443 |
| Ce | 173 | 68 |
| La | 100 | 33 |
| Nd | 89 | 0 |
| Sc | 36 | 17 |
| Th | 26 | 12 |
| Sm | 18 | 10 |
| Dy | 14 | 8 |
| Cs | 10 | 4 |
| Hf | 7 | 3 |
| Eu | 3 | 1 |
| Lu | 3 | 2 |

| Preferential Distribution in Magnetic Matrix | | |
|---|---|---|
| Element | Mullite Matrix | Magnetic Matrix |
| Fe | 3,200 | 430,000 |
| V | 295 | 445 |
| Mn | 179 | 473 |
| Cr | 148 | 439 |

(continued)

TABLE 1 (continued)

| Preferential Distribution in Magnetic Matrix (continued) | | |
|---|---|---|
| Element | Mullite Matrix | Magnetic Matrix |
| Co | 45 | 115 |
| Mo | 0 | 23 |
| U | 15 | 22 |
| Random Distribution | | |
| Element | Mullite Matrix | Magnetic Matrix |
| Rb | 196 | 175 |
| Ga | 67 | 62 |
| As | 214 | 283 |
| Se | 18 | 17 |
| W | 7 | 0 |
| Ta | 2 | 2 |

TABLE 2. DISTRIBUTION OF ELEMENTS IN MULLITE AND MAGNETIC PHASES OF BULL RUN STEAM PLANT FLY ASH, CONCENTRATIONS IN PPM

| Preferential Distribution in Mullite Matrix | | |
|---|---|---|
| Element | Mullite Matrix | Magnetic Matrix |
| Al | 155,000 | 62,700 |
| K | 20,100 | 5,100 |
| Mg | 11,800 | 5,300 |
| Ti | 9,475 | 3,300 |
| Ca | 2,500 | 1,900 |
| Na | 1,225 | 370 |
| Ba | 515 | 260 |
| Sr | 360 | 142 |
| Ce | 150 | 63 |
| La | 84 | 33 |
| Nd | 32 | 0 |
| Sc | 30 | 18 |
| Th | 24 | 11 |
| Sm | 15 | 8 |
| Dy | 10 | 6 |
| Cs | 10 | 2 |
| Hf | 6 | 2 |
| Eu | 3 | 2 |
| Lu | 2 | 1 |
| **Preferential Distribution in Magnetic Matrix** | | |
| Element | Mullite Matrix | Magnetic Matrix |
| Fe | 17,600 | 465,000 |
| V | 206 | 304 |
| Mn | 82 | 270 |
| Cr | 170 | 260 |

(continued)

TABLE 2 (continued)

| Preferential Distribution in Magnetic Matrix (continued) | | |
|---|---|---|
| Element | Mullite Matrix | Magnetic Matrix |
| Co | 28 | 230 |
| Mo | 0 | 100 |
| U | 9 | 13 |
| **Random Distribution** | | |
| Element | Mullite Matrix | Magnetic Matrix |
| Rb | 160 | 160 |
| Ga | 27 | 31 |
| As | 25 | 47 |
| Se | 16 | 15 |
| W | 3 | 7 |
| Ta | 2 | 2 |

TABLE 3. CONCENTRATION OF ELEMENTS IN CINDER MATRIX OF KINGSTON AND BULL RUN STEAM PLANTS, CONCENTRATIONS IN PPM

| Element | Kingston Plant | Bull Run Plant |
|---|---|---|
| C | 450,000 | 241,200 |
| Al | 78,600 | 60,200 |
| K | 7,833 | 5,550 |
| S | 3,000 | 4,150 |
| Mg | 5,800 | 3,880 |
| Ti | 4,466 | 3,510 |
| Ca | 7,300 | 1,050 |
| Na | 753 | 378 |
| Ba | 426 | 155 |
| Sr | 435 | 250 |
| Ce | 93 | 65 |
| La | 52 | 35 |
| Nd | 41 | 0 |
| Sc | 15 | 13 |
| Th | 17 | 10 |
| Sm | 10 | 7 |
| Dy | 7 | 5 |
| Cs | 3 | 4 |
| Hf | 4 | 3 |
| Eu | 2 | 2 |
| Lu | 1 | 1 |
| Fe | 9,223 | 6,850 |
| V | 92 | 90 |
| Mn | 48 | 24 |
| Cr | 185 | 180 |
| Co | 11 | 13 |
| Mo | 2 | 7 |
| U | 6 | 4 |
| Rb | 59 | 75 |

(continued)

TABLE 3 (continued)

| Element | Kingston Plant | Bull Run Plant |
|---|---|---|
| Ga | 10 | 6 |
| As | 64 | 20 |
| Se | 12 | 35 |
| W | 3 | 2 |
| Ta | 3 | 1 |

Samples were collected from the Bull Run sluice pond by careful core drilling of the surface so as not to disturb the stratification. A specimen six centimeters deep was extracted and divided into four strata. The uppermost stratum was tan in color. The tan color was less for the second stratum. The lower two strata were slate gray. The data in Table 4 show quite clearly why the color changed from tan to gray; the iron concentration decreased with depth of the strata. Note that the aluminum concentration, and some other elements common to mullite, increased slightly with depth. Since these data were taken by neutron activation analysis, we do not have a direct measure of silicon content. There is a remarkable regularity in the manner in which certain trace elements change in concentration as a function of stratum depth. As, Se, Br, Mo, Sb, Ba, Ga, W, and Mn decreased uniformly with depth, while Sc, Cs, La, and Nd increased slightly.

Oxalate extractions were done on the stratified samples of Table 4. Most of the iron was removed, leaving the residues gray in color. Essentially all of the arsenic and molybdenum were removed from the specimens by the iron extraction process. Figure 2 shows x-ray fluorescence spectra of the oxalate extract and the residue of the uppermost stratum. The arsenic and molybdenum peaks of the residue are not measurable, but in the dried oxalate extract they are quite prominent.

Mössbauer spectra showed the $Fe^{+3}$ is the species most readily removed when fly ash is treated with oxalate. Figure 3 shows a spectrum, after oxalate extraction, of the same sample used for Figure 1. Note the decrease in the $Fe^{+3}$ peak. The specimens for Figures 1 and 3 were taken from the Allen Steam plant in Memphis, Tennessee. We chose this sample, rather than the Kingston or Bull Run sample, because of the higher proportion of magnetic phase.

TABLE 4. DISTRIBUTION OF ELEMENTS IN STRATIFIED SLUICE POND ASH. BULL RUN PLANT, CONCENTRATIONS IN PPM

| Element | Top Stratum | 2nd Stratum | 3rd Stratum | Bottom Stratum |
|---|---|---|---|---|
| Al | 128,000 | 137,000 | 147,000 | 157,000 |
| K | 17,000 | 22,000 | 23,000 | 23,000 |
| Mg | 14,800 | 16,300 | 17,200 | 17,500 |
| Ti | 5,900 | 6,400 | 7,100 | 7,500 |
| Ca | 5,700 | 5,000 | 5,400 | 3,500 |
| Na | 1,600 | 1.800 | 1,750 | 1,300 |
| Ba | 780 | 700 | 680 | 350 |
| Sr | 400 | 540 | 530 | 217 |
| Ce | 120 | 130 | 135 | 140 |
| La | 69 | 76 | 72 | 74 |
| Nd | 87 | 84 | 102 | 123 |
| Sc | 25 | 27 | 30 | 32 |
| Th | 19 | 20 | 21 | 23 |
| Sm | 12 | 13 | 13 | 13 |
| Dy | 9 | 9 | 9 | 9 |
| Cs | 9 | 8 | 10 | 10 |
| Hf | 4 | 4 | 5 | 5 |
| Eu | 3 | 3 | 3 | 3 |
| Lu | 4 | 4 | 5 | 5 |
| Fe | 88,000 | 64,500 | 46,000 | 17,500 |
| V | 277 | 269 | 269 | 248 |
| Mn | 248 | 240 | 223 | 104 |
| Cr | 135 | 133 | 125 | 125 |
| Co | 53 | 53 | 47 | 44 |
| Mo | 129 | 59 | 15 | 12 |
| U | 15 | 14 | 12 | 10 |
| Rb | 134 | 200 | 71 | 220 |
| Ga | 80 | 70 | 64 | 46 |
| As | 395 | 267 | 125 | 30 |
| Se | 33 | 33 | 18 | 11 |
| W | 11 | 9 | 7 | 8 |
| Ta | 1 | 1 | 2 | 2 |

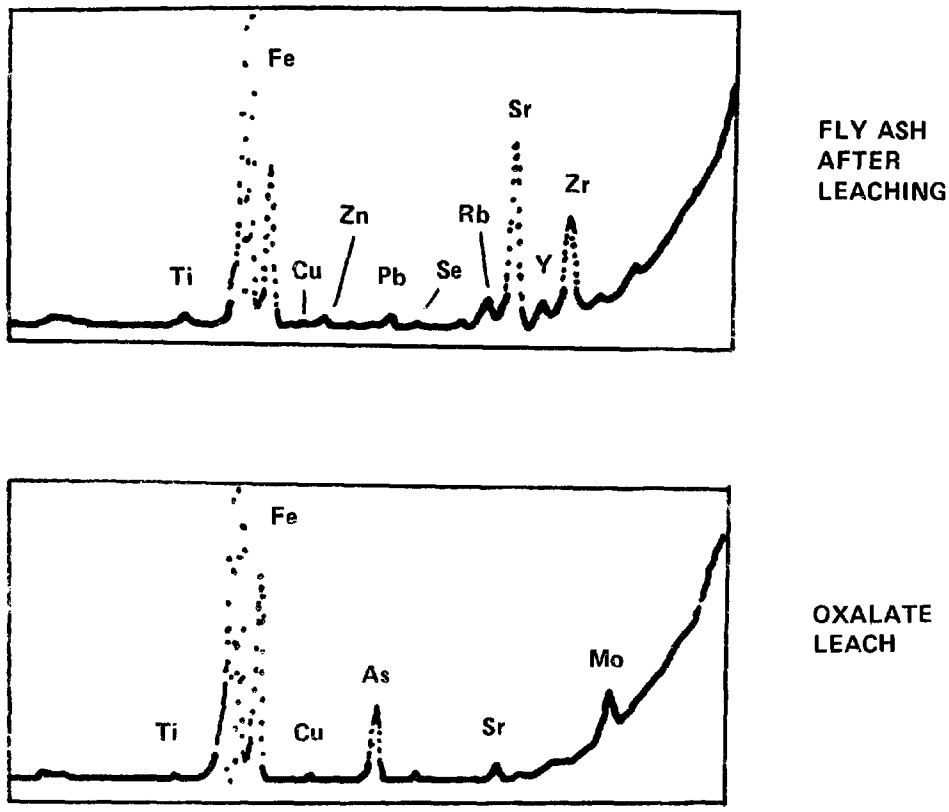


*Figure 2. Oxalate extraction studies of fly ash. Lower spectrum: x-ray fluorescence spectrum of dried oxalate extract. Upper spectrum: x-ray fluorescence spectrum of fly ash residue after extraction.*

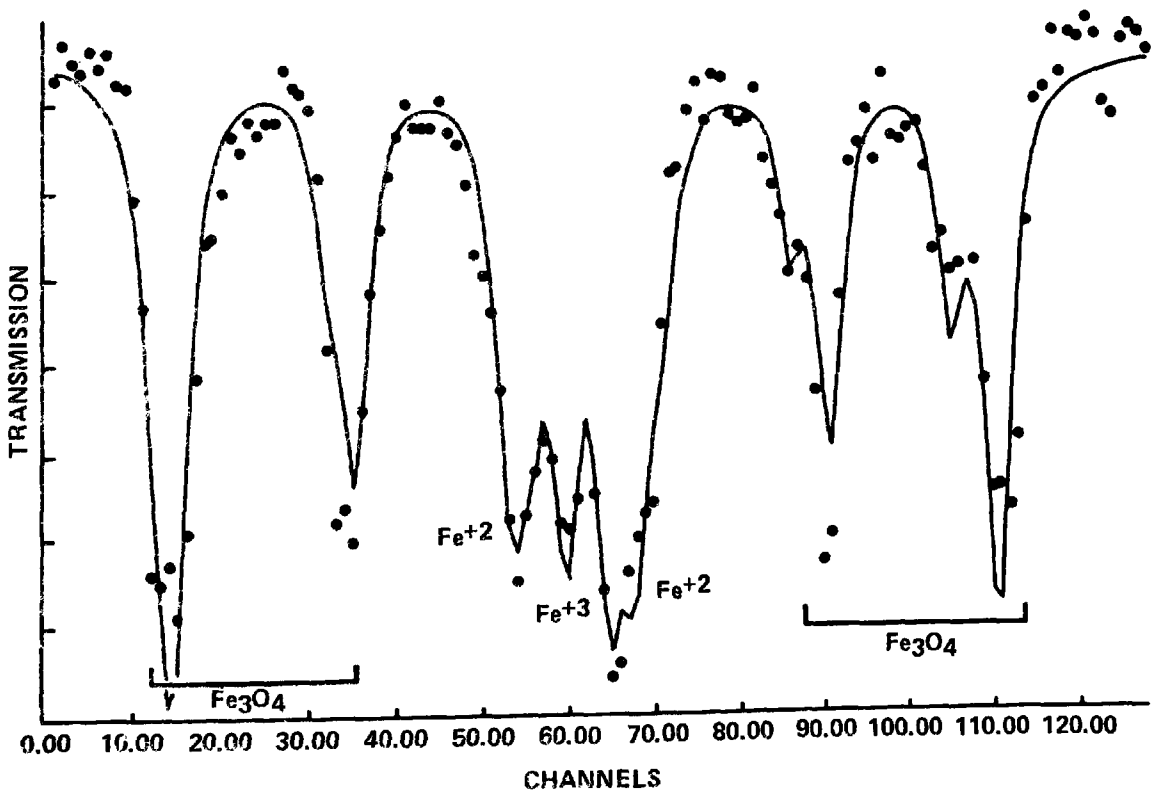


*Figure 3. Mössbauer spectrum of Allen Steam Plant fly ash after oxalate extraction.*

Glow discharge spectroscopy measurements of oxalate extracts from Bull Run ash before and after it contacted the sluice pond have been made. The ratio of $As^{+3}/As^{+5}$ for the precipitator ash, before pond contact, was 0.020. After pond contact (upper stratum, Table 4) the ratio was 0.030.

Another sluice pond specimen, very rich in the brown iron-containing component, was acquired. Using sedimentation techniques, the finely divided brown component was concentrated into a fraction relatively free of the coarser, gray material. X-ray fluorescence showed again that this iron-rich component had high concentrations of As and Mo. This component was examined by Mössbauer spectroscopy at room temperature and liquid nitrogen temperature. No appreciable change in the spectrum at the lower temperature was observed, indicating that the material was probably not a simple hydrated ferric oxide. Hydrated ferric oxide becomes magnetic at liquid nitrogen temperatures and exhibits multiplet splitting in its Mössbauer spectrum.

We suspect that the iron-rich component in the sluice pond is produced by a transformation of the fly ash, possibly the oxidation of $Fe_3O_4$. We have separated some ash into a magnetic and a non-magnetic component and subjected both to aeration in a water extract of fly ash in the laboratory. The pH of the water extract is 4-5. After about five weeks of aeration, the solution exposed to $Fe_3O_4$ is acquiring a slight tan color. The solution exposed to the non-magnetic material is still colorless.

## SUMMARY AND CONCLUSIONS

Our thesis that we stated in the introduction of this paper, that "chemical species" of trace elements in fly ash might be determined by the matrices that contain them, is given a great deal of support by our data. There does appear to be a preference for the mullite matrix over $Fe_3O_4$ for the trace elements Ba, Sr, Ce, La, Nd, Sc, Th, Sm, Dy, Cs, Hf, Eu, and Lu. It is true that the magnetic phase also has appreciable concentrations of these elements, but is is not completely free of mullite, and we think that this might actually be the carrier of the trace elements instead of the $Fe_3O_4$ matrix. Table 1 shows that there is quite a bit of aluminum in the magnetic fraction which we assume is associated with mullite. The data in Table 2 are from a totally different steam plant, but they are remarably similar to those of Table 1. This suggests that there may be a common pattern in the way trace elements speciate themselves in fly ash matrices. Perhaps solubilities play a role. The above trace elements are members of the alkali, alkaline earth, and rare earth families. Since these are soluble in glasses it is not surprising that they concentrate in the mullite matrix.

Since the mullite phase is by far the largest component of fly ash, it is obviously very important to determine more

specifics about how trace elements are contained in it. Linton, Evans, Williams, and Natusch[3] have shown that many of them occur in the outer surface layers of the particles. This should be explored further. Also, studies should be done on how trace elements are distributed between the amorphous and crystalline portions of mullite. These are now in progress in our laboratory.

Transition elements such as V, Cr, Mn, Co, Ni, Cu, and Mo are known to be soluble in iron oxides and many are capable of forming solid solutions in $Fe_3O_4$. The mixed spinel, $NiFe_2O_4$, for example, is also magnetic and has an x-ray diffraction pattern very similar to $Fe_3O_4$. This led us to speculate that some of the transition elements may seek the magnetite matrix in preference to the mullite. The data for V, Cr, Mn, Co, and Mo support this (our analyses for Cu and Ni are not complete), but the enrichments are only by a factor of 2. It appears that the transition elements do favor the magnetite matrix, but they are not exclusively associated with it. The fact that the Mössbauer spectrum of the magnetic phase departs slightly from that of pure $Fe_3O_4$ suggests that solid solutions may have occurred.

The cinder phase that we isolated was very rich in carbon and sulfur. Perhaps the sulfur was adsorbed on the surfaces of the carbon; our x-ray diffraction patterns showed that it was finely divided. In past work, we have shown that sulfur is associated with fly ash surfaces.[4] We could find no clear cut evidence of other trace elements being preferentially concentrated in the cinder phase. At the Asheville meeting, where this paper was presented orally, we stated that the cinder phase appeared to be rich in Se and Br; but since that time, we have examined other cinder specimens and found Se and Br to be much lower.

Fly ash researchers may have a lucky break with regard to arsenic speciation. Previous work by ourselves[4] and others show that arsenic is primarily associated with fly ash surfaces. Treatment of fly ash with oxalate appears to elute a large portion of the arsenic. Feldman's glow discharge spectroscopy method is capable of distinguishing $As^{+3}$ and $As^{+5}$. Another ORNL group is also using the glow discharge spectroscopy method to speciate arsenic in runoff waters from ash disposal sites. The ratio of $As^{+3}/As^{+5}$ was found to be slightly greater for ash from precipitators than for ponded ash, but this does not appear significant to us. Since the ratio in both cases is rather small, we tentatively conclude that most of the arsenic is oxidized to +5 before it contacts the pond.

We think that in sluice ponds fly ash can undergo transformations such that a new iron-rich phase is generated. Arsenic and molybdenum can be translocated to this phase. The color of the Bull Run pond ash samples was considerably different from

that of the precipitator specimens. The upper strata of the pond samples were deep tan because of high iron concentrations, and there was a definite correlation of the concentrations of As, Mo, and other trace elements with iron concentrations. The fact that As and Mo are removed simultaneously with iron, when it is extracted with oxalate, suggests strongly that they are located on the surface of the iron-rich phase. There is a correlation of other elements, Se, Br, Sb, Ba, Ga, W, and Mn with iron concentration in the stratified pond samples, but we have not yet shown a definite association with iron, as for As and Mo. Theis has also reported correlations of certain trace elements with both iron and manganese.[5]

More work should be done to determine the exact nature of the iron-rich material formed in sluice ponds. Our Mössbauer data show that is is not "hydrated iron oxides." Also, engineering studies should be considered for the processing of fly ash to promote the formation of iron compounds that are efficient in fixing trace elements in sluice ponds and disposal sites. Rather than allow the magnetite and other oxidizable iron compounds to lie useless in the pond, perhaps it would be practical to transform them into trace element scavengers.

ACKNOWLEDGEMENT

The authors would like to express their sincere appreciation to the Electric Power Research Institute, Palo Alto, California, for the funding of this work. We are especially indebted to Dr. Ralph Perhac of that Institute for directing our attention to the importance of fly ash chemical speciation. Professor Roger Minear of the University of Tennessee Chemistry Department has also contributed to our overview of the fly ash problem. Dr. Perhac and Dr. Minear have worked together to facilitate contacts between many individual researchers.

REFERENCES

1. Feldman, C. Annual Progress Reports, 1975, 76, 77, Analytical Chemistry Division, Oak Ridge National Laboratory, ORNL 5100, ORNL 5244, ORNL 5360. Improvements in the Arsine Accumulation-Helium Glow Detector Procedure for Determining Traces of Arsenic, submitted to Analytical Chemistry.

2. Williams, J.D.H., J.K. Syers, S.S. Shukla, R.F. Harris, and D.E. Armstrong. Environ. Sci. Technol. 5(11):113-1120, 1971.

3. Linton, R.W., Peter Williams, C.A. Evans, and D.F.S. Natusch. Determination of the Surface Predominance of Toxic Elements in Airborne Particles by Ion Microprobe Mass Spectrometry and Auger Electron Spectroscopy. Anal. Chem. 49:1514, 1977.

4. Hulett, L.D., T.A. Carlson, B.R. Fish, J.L. Durham. Studies of Sulfur Compounds Adsorbed on Smoke Particles and Other Solids by Photoelectron Spectroscopy. In: Determination of Air Quality, G. Mamantov and W.D. Shults, eds. Plenum Press, New York, 1972; L.D. Hulett, H.W. Dunn, J.M. Dale, J.F. Emery, W.S. Lyon, P.S. Murty. The Characterization of Solid Specimens from Environmental Pollution Studies Using Electron, X-ray and Nuclear Physics Methods. Measurement Detection and Control of Environmental Pollutants, International Atomic Energy Agency Conference (IAEA SM-206/1) Vienna, Austria, 1976.

5. Theis, Thomas L., and J.L. Wirth. Sorptive Behavior of Trace Metals on Fly Ash in Aqueous Systems. Environ. Sci. Technol. 11(12):1096-1100, 1977.

## SUMMARY

# ADVANCES IN PARTICLE SAMPLING AND MEASUREMENT

WILLIAM FARTHING
SOUTHERN RESEARCH INSTITUTE

The technology for particulate sampling in process streams has been expanded and improved over the last several years. New instruments have been developed, traditional devices and methods have been refined, and standard procedures have been established. The Process Measurement Branch of the Environmental Protection Agency's Industrial Environmental Research Laboratory sponsored a symposium in Asheville, NC, on recent developments and related research.

The symposium began with papers concerning inertial effects of sampling and sizing by inertia. C.N. Davies reviewed theoretical and experimental work concerning the aspiration coefficient of sampling tubes and presented some new findings. His primary emphasis was on the inability of the existing theory to account for all of the effects of a finite wind velocity on the aspiration of particles with finite inertia by a sampling tube with finite diameter. An experimental test of one expression, a quadratic equation of the Stokes number, was presented for tubes sucking at right angles to the wind. The comparison showed that the level of aspiration predicted by the quadratic was too high and there was evidence that at least a cubic equation is necessary. A potentially useful criterion was also given for accurate sampling at low wind speeds relative to the sampling velocity.

In a paper presented by Koichi Iinoya, the observed and calculated effects of anisokinetic sampling were presented for round and slit probes. It was suggested that the results presented could be used to estimate sampling errors. The concentration errors were smaller at extremely high sampling velocities, so super high speed sampling could be a simple method without the tedium of isokinetic sampling. The amount of particles deposited in the probe and sampling tube was found to be minimized when the Reynolds number was between 2000 and 3000. In a study

of the effect of probe diameter on sampling errors with isokinetic sampling, it was found that the reproducibility, measured in terms of the standard deviation of the deduced concentration from many tries, of sampling experiments decreases as the probe diameter decreases. In those experiments the average deduced concentration increased as the probe diameter decreased.

Other work described by Dr. Iinoya concerned particle impaction efficiencies on ribbons suspended at different orientations across a pipe and impactors with different clearance ratios, defined as the ratio of the nozzle to plate distance over the nozzle diameter. In the ribbon study, calculations based upon a discontinuous potential flow model agreed well with observed efficiencies over a wide range of particle Reynolds numbers extending from the Stokes to Newton regions. (These velocities are somewhat higher than employed in typical impactors for sampling process streams.) The purpose of the work concerning impactors was to theoretically account for the effects of the velocity boundary layer at the nozzle outlet of impactors using a potential flow model. Good agreement with measured efficiencies was claimed at ratios of 2, 1, 0.5, 0.33, and 0.25.

The performance of cyclone collectors and samplers was described by Morton Lippmann. Traditionally used for control devices, cyclones are now being routinely used for sampling of "respirable" aerosols for assessment of health effects. More recently, cyclones have been introduced for in-situ classification of aerosol size distribution. Cyclones have been designed with sharp collection efficiency versus size curves comparable to impactors down to particle diameters of 0.5 μm while offering several advantages such as no deterioration in performance with large samples and much simpler operation than with dichotomous samplers. The major problem is the lack of an accurate theory to be used for design purposes. One important point of this paper was the evidence that caution must be exercised in coupling cyclones in series because it may affect flow and thus the behavior. An empirical relation for efficiency was presented in this paper with four constants. The constants have been evaluated for eleven cyclones for which reliable calibrations exist covering a range of particle sizes from 0.3 to 10 μm and gas flow rates from 0.1 to 2700 ℓ/min.

Recently developed systems for particle sizing by impactors were described by Michael Pilat. The University of Washington Mark 4 Cascade Impactor utilizes low absolute gas pressure resulting in large Cunningham correction factors permitting inertial sizing of particles from 0.02 to 0.2 μm in diameter. In conjunction with the University of Washington Mark 3 Impactor, two systems, one with 0.5 acfm and another with 1.8 acfm flow rate, have been assembled and tested which size particles from 0.02 to 20 μm. A new impactor for high concentrations, using many stages (28) to reduce overloading, has also been constructed for sizing particles from 0.05 to 30 μm.

Recent work with the Sinclair diffusion battery was described by Earl Knutson. It has been coupled to a data processing system which enabled unattended runs of several days with hourly sampling. The penetration of particles through the battery was measured with a new continuous flow condensation nuclei counter. Experience has revealed several improvements in operating procedures. An iterative mathematical technique was studied and chosen to calculate size distributions from the data obtained. Nearly 1000 size spectra of New York City urban aerosol have been analyzed showing typical geometric mean diameters from 0.025 to 0.050 μm with geometric standard deviations from 1.8 to 2.0.

Although in-situ sizing of particles is available, many instances still arise when laboratory sizing is desirable. Ronald Draftz described the instruments available for such work. Such measurements can be very sophisticated and can include shape measurements in short times. The electronic image analyzers are extending the practicality of the many useful measurements possible with a light microscope. The problem of particle agglomeration remains unsolved.

A recent field evaluation (at a Canadian lead smelter) of five real time particulate monitors, all commercially available, was described by A.W. Gnyp. Two transmissometers, a mass monitor based on the backscattering of light, a charge transfer monitor, and a beta radiation attenuation device were rated according to accuracy, reliability, and maintenance over a one year period. Accuracy was based upon the proportionality of the instrument signal to aerosol mass concentration determined as a reference by a manual sampling train. The sensitivity of the monitor output to particle size distribution and composition was evaluated using impactors and laboratory analysis of samples as references. The overall conclusion was that reliable continuous mass monitoring is now possible in stacks if the aerosol physical and chemical properties are approximately constant, as found in process streams that have passed through efficient control equipment.

A real time in-situ particle sizing probe utilizing small angle light scattering is being developed under the sponsorship of the Process Measurement Branch of USEPA/IERL. The field prototype of the instrument exhibited at the symposium is now being tested. Robert Knollenberg described the operation principle and some preliminary results from a coal-fired power plant. The instrument covers a 0.3 to 10.0 μm size range with 60 channels resolution. The major uncertainty in sizing spherical particles with the instrument, performed by relating size to flux scattered at small forward angles by single particles, is the particle refractive index giving at most an error of ±20% and normally within ±10% of actual size. The concentration range for accurate measurements limited by coincidence counting in the present model is $5 \times 10^4/cm^3$. Normally, the main effect

of higher concentrations is to decrease the effective size range. An optical velocimeter is also designed into the instrument. The present design permits temperatures up to 250°C and velocities up to 30 m/sec. The results of an initial in-stack test at a coal-fired power plant with an electrostatic precipitator and a scrubber were reasonable. Calculated opacity from the measured particle size distribution was about 15% while measured opacity was 17%. The calculated mass loading was 0.01 to 0.02 $g/m^3$ with a volume average diameter of about 1.3 μm. It appears that the instrument was capable of resolving several size modes in this test.

Another in-situ portable light scattering instrument being developed under EPA sponsorship to determine size distribution was described by A.L. Wertheimer. This device measures flux scattered from many particles simultaneously at three small angles relative to the forward direction, 4°, 8°, and 11°, and at a range of large angles of 80°-100°. Each measurement is performed at two wavelengths, 0.45 and 0.9 μm, and the large angle scattering is measured at two orthogonal polarizations. The instrument relates the small angle signals dominated by Fraunhofer diffraction to the volume of particles in three size ranges, centered at 1.0, 3.5, and 7.0 μm. For the lower end of the size distribution, the difference in the two 90° signals at two orthogonal polarizations obtained with the 0.9 μm (0.45 μm) wavelength is related to the volume of particles in a size range centered about 0.4 μm (0.2 μm). The size range, mass loading, and temperature range are 0.1 to 10 μm, 4 to 400 ppb by volume, and 0° to 260°C. The prototype had just been delivered to EPA to be tested in a wind tunnel facility.

Kenneth T. Hood reported the results of studies performed by the National Council for Air and Stream Improvement concerning the relationships of plume opacity, in-stack opacity, and continuous mass monitors to mass emission rate as defined by filter samples. A previous study had indicated the validity of an in-stack transmissometer to monitor particulate concentrations in flue gas, and calibration curves had been obtained for each site to provide mass concentrations from transmissometer opacities. In these studies observer opacity was frequently related to particulate concentration through use of simultaneous transmissometer measurements and their calibration curves. The opacity studies involved five different sites: a lime kiln, two kraft recovery furnaces (one with a direct contact evaporator, and one without), and two wood and fossil fuel-fired boilers (one with coal and another with oil). The observer opacity under good contrast conditions (dark or blue sky background) was found to vary between ±10 and ±15% opacity from the average. The relationships of plume opacity to in-stack opacity were generally found to be linear; however, the slopes were not one as might be expected and varied from site to site, and the curves did not intercept the origin. At the non-direct contact evaporator system, 75%, 50%, and 25% of the technically trained observers

read a non-visible plume at instrument opacity levels of 6%, 8%, and 10%, respectively. In tests of the mass monitor based upon backscattering of light, it was compared to transmissometer behavior at two kraft recovery furnaces and a wood-waste fired spreader stoker boiler. The mass monitor was found to be equivalent to the transmissometer in quality of data and performance except that the former required less attention at high loadings (3.76 g/acm) at which the latter required frequent cleaning.

After three sessions on instruments for sampling and measuring aerosols, the topics of the meeting turned toward procedures for using the data and quality control. A computer based data reduction system for cascade impactors, developed under EPA sponsorship, was described by Joseph D. McCain. The system of programs, becoming available for general use, utilizes calibration information for each impactor with operating conditions, time, and stage weights to determine particle size distributions in any one of several forms for individual runs or averages thereof. The first program in the series utilizes a spline technique, described as an "automated French curve", to fit a curve to the cumulative size distribution. If differential mass or differential number size distributions are desired, these are obtained from the cumulative curves which are forced to be continuous in coordinates and slopes. Statistical analyses, including the location of outliers, are performed on the data. Additional programs permit data sets from inlet and outlet measurements of control devices to be combined to determine fractional efficiencies. The program in its present form handles all commercially available round jet cascade impactors, including common modifications, which are in current use in stack sampling. Other round jet and slot type impactors could be accommodated with slight program revision.

In the area of instrument calibration, D.Y.H. Pui described various aerosol generators now available. Three instruments provide monodisperse aerosols for primary standards over a broad range of sizes: the vibrating orifice aerosol generator for diameters of 0.5 - 50 μm, the mobility classifier monodisperse aerosol generator for diameters of 0.01 - 0.5 μm, and the ultrafine condensation monodisperse aerosol generator for smaller sizes. The constant output atomizer aerosol generator provides polydisperse aerosols of high concentration and stability. In addition, some calibration measurements of various aerosol measuring and sampling devices were reviewed, and comparative studies showed good agreement between different types of instruments.

Quality control work by EPA was presented by D. Bruce Harris and Gene Tatsch. Particle bounce or blow off is perhaps the major problem associated with particle sizing with cascade impactors. The use of substrates on collection plates such as grease or glass fiber filter material has been employed to reduce bounce. Tests were performed to ascertain which of the available substrates are most suitable for flue gas sampling. Of nineteen

greases tested, only Apiezon H grease was found to perform satisfactorily at temperatures above 149°C (300°F). At higher temperatures glass fiber material appeared to be more stable. However, large mass changes, induced by reactions related to $SO_x$ concentrations, were observed with glass fiber and to a lesser extent with grease. After various laboratory and field tests, a treatment procedure for glass fiber was identified which significantly reduces mass gains. This treatment involves washing the substrates in $H_2SO_4$, followed by rinsing, drying, baking and in-situ conditioning before use in impactors. Reeve Angel 934AH glass fiber filter material performed best among those tested. It was pointed out, however, that filter materials change from batch to batch. The details of the results of this study are available in a recent report.

In another area of quality control, Mr. Tatsch described problems which have arisen because different procedures are presently utilized to reduce and present data, specifically that from impactors. Methods are being sought to alleviate such problems. It is hoped that the computer programs described in the paper by Mr. McCain will be a practical means for uniform data reduction and presentation with the required versatility.

The last session of the symposium contained three papers concerning the procedures by which the available technology is utilized to evaluate particulate control devices: scrubbers, baghouses, and electrostatic precipitators. The first paper, by Richard Chmielewski, was concerned with identification and solutions of problems which arise in sizing wet particles. It was suspected that because of the pressure reduction from stage to stage, evaporation of water from particles occurred inside cascade impactors. This was indicated by disagreement between measured size distributions and those predicted from scrubber theory. Laboratory experiments with a University of Washington cascade impactor and a series of glass impactors verified this suspicion. The jet diameter of the glass impactors could be adjusted to minimize pressure drop. It was also found that pressure drop across a stage is higher for wet particles than dry ones. Based on the laboratory results a single stage impactor usable in the field with a variable cut point was constructed using a Greenburg-Smith impinger to minimize pressure reduction and evaporation time. In one application the measurements agreed with the prediction that the condensed particle size distribution should have a minimum aerodynamic diameter on the order of 0.5 μm. Also discussed were problems which arise in measurements of entrainment where particles above 10 μm are involved. None of the attempted techniques---hot wire anemometer, cascade impactor, and chemical stain methods---give completely satisfactory results.

A presentation of the measurements necessary for evaluation of fabric filter control devices by D.S. Ensor stressed the importance of a systems approach and real time monitors for a meaningful evaluation. The overall mass loading is normally very low and cleaning processes cause large fluctuations in loading---at some units one compartment per minute receives a burst of air in the reverse direction. This is accompanied by large changes in the velocity distribution of the stream. Other aspects causing variations are bag integrity, bag conditioning time, and valve malfunctions. The problems of matching data sets obtained at different locations with different instruments are reduced with a mobile control room containing an automatic data logging system with a common time base. Sizing instruments utilized in evaluations are diffusion batteries, optical particle counters, electrical mobility analyzers, and cascade impactors. In addition, gas monitors, pressure transducers, and a light scattering nephelometer are used to track the dynamic behavior of both the baghouse and the source.

The presentation concerning electrostatic precipitators by Wallace B. Smith also stressed the importance of monitoring transient events. Rapping reentrainment of short duration has been found in many installations to be responsible for most of the total emissions. If, for diagnostic purposes, collection efficiency due to electrostatic behavior is sought, the measurement program must differentiate between the different types of emissions: simple penetration, rapping reentrainment, sneakage around the collection fields, and boil up from the hoppers. A measurement system was described which determines collection efficiency for particles from 0.01 to 10 μm diameter. It includes cascade impactors, mass trains, electrical mobility analyzers, diffusion batteries, and optical particle counters. A specially designed extraction-dilution apparatus is used to condition the aerosol for compatibility with the latter three instruments. Laboratory experiments were performed to determine the effects of particle charge upon impactor behavior. The experiments showed that, at high charge levels, size distributions determined with impactors are significantly skewed toward larger sizes. However, at charge levels produced in electrostatic precipitators on process streams (where fields of 4 - 8 x $10^3$ V/cm are employed), the effect of particle charge was not significant.

Research into the chemical state of fly ash was the last topic on the program. L.D. Hulett reported some results from a program to develop methods for trace element analyses in fly ash and in waters with which it has been in contact. The samples studied came from a precipitator hopper and a sluice pond disposal site at a coal-fired power plant. The analytical procedures discussed were x-ray fluorescence, scanning electron microscopy, optical microscopy, x-ray diffraction, x-ray photoelectron spectroscopy, Mössbauer spectroscopy, flow discharge spectroscopy, and chemical separation. None of these techniques can discriminate chemical states of trace elements from fly ash matrix, so the indirect approach of oxalate leaching was utilized. This treatment separated iron in the +2 and +3 valence states accompanied by nearly all of the arsenic and molybdenum present especially after exposure to the pond. It appears that these were associated with the iron on the fly ash surfaces. Most of the lead was found in a phase, termed "mullite", consisting mainly of ferroaluminosilicate glass. Selenium was concentrated in a black cinder phase consisting of a combination of carbon and "mullite". A phase, termed "magnetite", was identified as relatively free of trace elements. A method was developed using glow discharge spectroscopy to determine the ratio $As^{+3}/As^{+5}$ in water exposed to fly ash. Other trace elements observed on the surfaces were zinc, copper, selenium, and bromine. A search for the valence states of other elements will be continued.

## METRIC CONVERSION FACTORS

| To convert from: | To: | Multiply by: |
|---|---|---|
| lb | kg | 0.454 |
| $gr/ft^3$ | $g/m^3$ | 2.29 |
| $ft^3/min$ (cfm) | $m^3/sec$ | 0.000472 |
| $lbs/in.^2$ | $kg/m^2$ | 703. |
| °F | °C | (°F-32) x 5/9 |
| $ft^2/1000$ cfm | $m^2/(m^3/sec)$ | 0.197 |
| in. WG | mm Hg | 1.868 |
| gallons | liters | 3.785 |
| ft | m | 0.3048 |
| in. | m | 0.0254 |
| tons | kg | 908. |
| $in.^3$ | $cm^3$ | 16.39 |
| $ft^3$ | $m^3$ | 0.028 |
| gal/min | l/sec | 0.0631 |
| $ft^2$ | $m^2$ | 0.0929 |
| $in.^2$ | $cm^2$ | 6.452 |
| gal/1000 $ft^3$ | $l/m^3$ | 0.135 |
| grams | grains | 15.43 |
| ft/min | cm/sec | 0.508 |
| ounces | grams | 28.34 |
| $oz/yd^2$ | $g/m^2$ | 33.89 |
| grains | grams | 0.0647 |
| $gr/ft^2$ | $g/m^2$ | 0.698 |
| lb force | dynes | $44.44 \times 10^5$ |
| $lb/ft^2$ | $g/cm^2$ | 0.488 |
| in. $H_2O$/ft/min | cm $H_2O$/cm/sec | 5.00 |
| Btu | calories | 252 |

## TECHNICAL REPORT DATA
*(Please read Instructions on the reverse before completing)*

| | | |
|---|---|---|
| 1. REPORT NO. EPA-600/7-79-065 | 2. | 3. RECIPIENT'S ACCESSION NO. |
| 4. TITLE AND SUBTITLE Proceedings: Advances in Particle Sampling and Measurement (Asheville, NC, May 1978) | | 5. REPORT DATE February 1979 |
| | | 6. PERFORMING ORGANIZATION CODE |
| 7. AUTHOR(S) W.B. Smith, Compiler | | 8. PERFORMING ORGANIZATION REPORT NO. |
| 9. PERFORMING ORGANIZATION NAME AND ADDRESS Southern Research Institute 2000 Ninth Avenue, South Birmingham, Alabama 35205 | | 10. PROGRAM ELEMENT NO. INE623 |
| | | 11. CONTRACT/GRANT NO. 68-02-2131, Task 21306 |
| 12. SPONSORING AGENCY NAME AND ADDRESS EPA, Office of Research and Development Industrial Environmental Research Laboratory Research Triangle Park, NC 27711 | | 13. TYPE OF REPORT AND PERIOD COVERED Proceedings; 1/77 - 9/78 |
| | | 14. SPONSORING AGENCY CODE EPA/600/13 |

15. SUPPLEMENTARY NOTES IERL-RTP project officer is D. Bruce Harris, MD-62, 919/541-2557.

16. ABSTRACT The proceedings consist of 17 papers on improved instruments and techniques for sampling and measuring particulate emissions and aerosols; e.g., cascade impactors, cyclone collectors, and diffusion-battery/nuclei-counter combinations. Transmissometers and instruments for measuring scattered light were used for continuous monitoring of emissions from a secondary lead smelter and from three pulp and paper mill sources (a wood-waste-fired power boiler, a kraft recovery furnace, and a lime kiln). Also discussed were: computer-based data reduction for plotting curves of particle size distribution; equipment for generating aerosols and its use in calibrating instruments; analysis for trace elements in fly ash; and sources of sampling errors. Applications of improved techniques for evaluating emission control devices included: a wet impingement technique for measuring particle sizes in wet scrubbers; use of real-time instruments in studying the dynamic behavior of baghouses; and measurement of fractional collection efficiency and detection of fly ash entrainment in electrostatic precipitators.

17. KEY WORDS AND DOCUMENT ANALYSIS

| a. DESCRIPTORS | | b. IDENTIFIERS/OPEN ENDED TERMS | c. COSATI Field/Group | |
|---|---|---|---|---|
| Pollution | Diffusion | Pollution Control | 13B | |
| Dust | Transmissometers | Stationary Sources | 11G | |
| Aerosols | Light Scattering | Particulate | 07D | 20N,20F |
| Sampling | Lead | Cascade Impactors | 14B | 07B |
| Measuring Instruments | Smelters | Nuclei Counters | | 11F |
| Impactors | Paper Industry | Lime Kilns | 13I | 11L |
| Cyclone Separators | Wood Wastes | Baghouses | 07A | |

| | | |
|---|---|---|
| 18. DISTRIBUTION STATEMENT Unlimited | 19. SECURITY CLASS *(This Report)* Unclassified | 21. NO. OF PAGES 390 |
| | 20. SECURITY CLASS *(This page)* Unclassified | 22. PRICE |

EPA Form 2220-1 (9-73)